Earthquakes and sea-level change in Hokkaido, north-east Japan

THOMSON, KATIE,HANNAH

Earthquakes and sea-level change in Hokkaido, north-east Japan

Katie H. Thomson

Department of Geography

Durham University

Thesis submitted for the degree of Doctor of Philosophy

2009

I confirm that no part of this material presented in this thesis has previously been submitted for a degree at this or any other institution. In all cases the work of others, where relevant, has been fully acknowledged.

Katie Thomson
August 2009

This thesis details the results of an investigation into the pattern of relative sea-level (RSL) changes in north-east Hokkaido, Japan. The aim of the research is to better understand the importance of seismic and non-seismic processes in controlling spatial patterns of vertical land motions over a range of timescales. The main focus is on using salt-marsh sediments as a source of data to reconstruct RSL change during the current interseismic period, since *c*. 300 calibrated years before present (cal. yr BP). Previous research on the Pacific coast of Hokkaido suggests that this period is characterised by subsidence caused by strain accumulation on the locked part of the Pacific/North American plates.

I apply foraminiferal-based methods of palaeoenvironmental reconstruction to develop, using transfer functions, quantitative reconstructions of RSL change at five sites in north-east Hokkaido. Contemporary foraminifera are zoned with respect to elevation and tidal inundation, and my preferred transfer function (a model that contains 87 samples and 24 taxa) has a prediction r^2 of 0.75 and a root mean squared error of prediction of ± 0.32 m. I apply this transfer function to shallow fossil sediment sequences at five salt marshes and use a combination of ^{210}Pb, ^{137}Cs and tephra chronology to establish age models for the sequences. The reconstructions are consistent in demonstrating little net RSL change during the last 300-100 cal. yrs, with the exception of data from one site, Sarfutsu-toh, located on the northern tip of Hokkaido. Chronologies from two profiles developed on the Pacific coast record strong evidence for recent RSL rise since the mid-1980s, but during earlier periods of the 20th century reconstructed RSL was stable or falling.

I compare my reconstructions with other direct and proxy records of land and sea-level motions. Previously published GPS and repeat levelling data indicates subsidence in south-east Hokkaido during the 20th century, although the spatial patterns and rates of change have varied. An unknown amount of this subsidence at the Kushiro tide gauge likely reflects anthropogenic activities associated with sediment compaction as well as mining-induced subsidence. An analysis of the tide-gauge records from Hokkaido show a more varied pattern of land motions, although they also confirm subsidence on the Pacific coast, close to the Kuril trench. A database of Holocene sea-level index points provides insights into longer-term millennial-scale trends in RSL. Data from six regions of Hokkaido demonstrate stable RSL close to present during the mid- and late Holocene; only the northern tip of Hokkaido (around Sarubetsu) is there evidence for a small mid-Holocene highstand of 1-3 m above present.

Finally, a review of Pleistocene raised marine terrace data shows net uplift over the last *c*. 330 k yr, with two areas of particularly high uplift at Abashiri and on the Pacific coast near Kushiro.

The evidence presented in this research demonstrates that it is incorrect to infer that the current interseismic period is characterised by subsidence. Overall, RSL has changed little in the last 300-100 cal. yrs. The subsidence recorded in the mid- and late 20th century on the Pacific coast of Hokkaido is not typical of the full interseismic period, nor can it have been sustained over Holocene or Pleistocene timescales. Limited data from previous earthquake cycles indicate that RSL was stable, rising or falling during previous interseismic intervals. These observations suggest that a representative 'Hokkaido earthquake deformation cycle' may not exist. Future research should better understand the controls of Quaternary volcanic activity on regional deformation patterns, and apply microfossil-based techniques to multiple earthquake cycles at sites to help define the spatial extent of land motions associated with different events.

In loving memory of Barrie Stuart Thomson
31st December 1943 – 9th February 1997

This PhD thesis has been the culmination of a number of years of work, and the help of so many people. To say the road has been difficult would be an understatement. The highs have been amazing, travelling to places I never dreamed I would visit, making lifelong friends, and working in such a stimulating department on a topic I still find fascinating has been a blast. However like any long project, somewhere in the middle I got very lost, and notwithstanding the amazing support of my three supervisors and the friends I have made throughout my time in Durham, this long road on which I have been travelling would not finally be drawing to a close.

Firstly, I am indebted to the support of my supervisors. Professor Antony Long as my only Durham supervisor has been without doubt the single most important driving force behind my thesis, helping me wrestle my intellectual and personal demons and produce a thesis that I am as proud of its content as its aesthetic beauty. From this project's conception, Dr Benjamin Horton has been a pillar of strength providing constant support and advice throughout my thesis, and I am truly indebted to his patience and encouragement. Finally, Dr Yuki Sawai has been incredibly helpful, guiding me on my fieldwork, and providing a window for me to gain insight into the academic and cultural idiosyncrasies of the Land of the Rising Sun.

This PhD was made possible by financial support from the Durham University Doctoral Award, however funds provided by the Quaternary Research Association, the British Sedimentological Research Group, Durham Geographers Graduates Association, the Dudley Stamp Memorial Fund (Royal Society), the Trevelyan College Travel Bursary and the Geological Survey of Japan have enabled me to undertake the fieldwork, for which I am extremely grateful.

Special thanks to Hiroo Nasu, Yushiro Fujii, Than Tin Aung, and Takanobu Kamataki for help in the field. Thanks also to the laboratory staff in the department, Frank Davies, Neil Tunstall, Martin West, Mark English, Alison Clark, Eddie Million, Kathryn Melvin and Chris Longley for helping me at every stage. Notably thanks also to Dr Sarah Woodroffe for her friendship and help throughout the duration of this thesis. I can never repay your kindness helping and supporting me throughout my time in Durham. Thanks also to all the many postgraduates which have passed through the department during my time in Durham, particularly Matthew Brain, Katie Oven and Rob Dunford. I am grateful for all of the support and encouragement you have provided me over the years. Special thanks go to Michael Lim for providing me accommodation, driving practice and a lot more besides. You have seen me at my lowest and each and every time you pick me up and make me a stronger, better person.

Finally I am indebted to the help of my family for providing me with the emotional support enabling me to finish this momentous project. To my sister Lucie for understanding the turmoil which I have been going through for the past few years, and to my mum for listening to me during my darkest days. This thesis is without doubt a group effort, and I thank you both from the bottom of my heart for your continued love, assistance and guidance. One person whom I would dearly love to thank personally, but was cruelly taken away is my dad. You sculpted me into the person I am. Your dedication, hard-working ethos and commitment to excellence should have been a guiding light in my times of trouble. I am only sorry I waivered and let you down. Rest assured I have discovered so much about myself over the duration of my thesis. Thank you for inspiring me and making me strive to do better. I'll love and miss you always.

TABLE OF CONTENTS

Title page i
Declaration ii
Abstract iii
Dedication v
Acknowledgments vi
Table of Contents viii
List of Figures xii
List of Tables xvii
List of Appendices xviii

1. INTRODUCTION 1

1.1 Background 1
1.2 Tectonic deformation and sea-level change 6
1.3 Research rationale 8
1.3.1 Research aim 8
1.3.2 Research approach 8
1.3.3 Outline of thesis 9

2 RESEARCH CONTEXT 10

2.1 INTRODUCTION 10
2.2 RSL CHANGE ON ACTIVE PLATE BOUNDARIES 10
2.2.1 The earthquake deformation cycle 11
2.2.2 Earthquake magnitude and elastic dislocation modelling 15
2.2.3 Tidal-wetland stratigraphies as recorders of seismic land-level changes 17
2.3 RSL CHANGE AND PALAEOSEISMICITY IN JAPAN 19
2.3.1 Holocene sea-level changes in Japan 19
2.4 HOKKAIDO 21
2.4.1 Palaeoseismicity in Hokkaido 22
2.4.2 The Sawai *et al*. (2004b) elastic dislocation model 26
2.5 CONCLUSIONS 29

3. RESEARCH METHODS AND STUDY SITES 31

3.1 INTRODUCTION..... 31
3.2 RECONSTRUCTING FORMER SEA LEVELS..... 34
3.2.1 Definition of sea level..... 34
3.2.2 Interpretation of former sea levels..... 35
3.2.3 Lithostratigraphical methods..... 36
3.2.4 Biostratigraphical methods..... 39
3.2.5 Sources of error in sampling..... 47
3.2.6 Statistical methods..... 51
3.2.7 Chronostratigraphical methods..... 53
3.3 OTHER METHODS OF SEA-LEVEL RECONSTRUCTION..... 56
3.3.1 Pleistocene sea-level index points..... 56
3.3.2 Holocene sea-level index points..... 61
3.3.3 Tide-gauge data..... 64
3.4 SITE SELECTION..... 74
3.4.1 Geological setting of Hokkaido..... 74
3.4.2 The geological evolution of Hokkaido..... 75
3.4.3 Environmental setting..... 76
3.4.4 Rationale for site selection..... 78
3.5 CONCLUSIONS..... 87

4. RESULTS I – CONTEMPORARY SALT-MARSH DATA.....89

4.1 INTRODUCTION..... 89
4.2 CONTEMPORARY ENVIRONMENTS..... 89
4.3 PHYSICAL PROPERTIES OF THE HOKKAIDO SALT MARSHES..... 92
4.4 CONTEMPORARY FORAMINIFERAL ASSEMBLAGES FROM THE MARSHES OF HOKKAIDO..... 98
4.4.1 The salt marshes of Hokkaido..... 98
4.4.2 Elevation-dependent ecological zones on Hokkaido..... 106
4.4.3 Canonical correspondence analysis (CCA)..... 119
4.4.4 Infaunal foraminifera..... 124
4.5 NUMERICAL ANALYSES..... 127
4.5.5 Local versus regional training sets..... 128
4.5.6 Species response curves..... 129
4.5.7 Transfer function development..... 130
4.5.8 ‘Pruned’ Model..... 132

4.6 CONCLUSION 135

5. RESULTS II – FOSSIL ENVIRONMENTS AND RELATIVE SEA-LEVEL RECONSTRUCTION 137

5.1 INTRODUCTION 137
5.2 THE FOSSIL ENVIRONMENTS AND RSL HISTORY OF THE HOKKAIDO SALT MARSHES 137
5.2.1 Mochiruppu 138
5.2.2 Furen-ko 145
5.2.3 Tohoro 151
5.2.4 Tofutsu-ko 156
5.2.5 Sarfutsu-toh 161
5.3 CONCLUSION 163

6. DISCUSSION 165

6.1 INTRODUCTION 165
6.2 RSL CHANGES IN HOKKAIDO DURING THE CURRENT INTERSEISMIC PERIOD 166
6.2.1 Intra-site variability in interseismic RSL change 166
6.2.2 Comparison with the Kushiro and Hanasaki tide gauge records 169
6.2.3 Salt marsh trends in RSL change recorded in Hokkaido 172
6.2.4 Assessment of the viability of the transfer function technique in microtidal environments and back barrier environments 174
6.3 COMPARISON OF SALT MARSH RSL RECORDS WITH OTHER GEODETIC TIMESERIES 175
6.3.1 Tide-gauge data 175
6.3.2 Repeat levelling and GPS record 180
6.4 HOLOCENE RSL RECORDS FROM HOKKAIDO 185
6.5 PLEISTOCENE RSL RECORDS FROM HOKKAIDO 193
6.6 RATES OF RSL CHANGE IN HOKKAIDO OVER DIFFERENT TIMESCALES . 197
6.6.1 Land motions during the interseismic period in Hokkaido 198
6.7 CONCLUSIONS 202

7. CONCLUSIONS 204

7.1 CONTEMPORARY FORAMINIFERA AND RSL IN HOKKAIDO 204

7.2 RECONSTRUCTING CHANGE IN RSL IN THE CURRENT INTERSEISMIC PERIOD 205
7.3 COMPARISONS WITH OTHER TIMESCALES..... 206
7.4 IMPLICATIONS FOR MODELS OF RSL CHANGE IN HOKKAIDO..... 208
7.5 LIMITATIONS OF THE CURRENT STUDY..... 209

8. REFERENCES 212

LIST OF FIGURES

Figure 1.1 Schematic diagram illustrating the factors affecting changing sea levels in space and time, with typical range in metres. 2
Figure 1.2 Plate tectonic setting around the Japanese Islands. 4
Figure 1.3 Schematic diagram illustrating the techniques for recording or estimating land deformation over differing timescales used by this thesis to understand earthquake-related land-level change in Hokkaido. 6
Figure 1.4 Schematic diagram showing the development of peat-silt couplets following coseismic submergence together with associated tsunami deposits 7
Figure 1.5 Schematic diagram showing the earthquake deformation cycle interpreted from the stratigraphies on Hokkaido's eastern coast. 8
Figure 2.1 Schematic diagram illustrating the use of different sea-level indicators to document tectonic displacement on tropical coastlines……..11
Figure 2.2 Schematic diagram showing the earthquake deformation cycle associated with a subduction-zone thrust fault beneath a coast: 12
Figure 2.3 Earthquake deformation model for Alaska. 13
Figure 2.4 Four models of earthquake recurrence, after Shimazaki and Nakata (1980) and Satake and Atwater (2007). 14
Figure 2.5 Generic elastic slip dislocation model. 16
Figure 2.6 Schematic diagram of lithostratigraphical and biostratigraphical responses to the earthquake-related deformation cycle in Alaska, modified from Hamilton (2003). 18
Figure 2.7 Holocene RSL changes for the Japanese Islands, modified from Pirazzoli (1991). 21
Figure 2.8 Photo of Shari-dake volcano, Hokkaido, with the Tofutsu-ko salt marsh studied in this thesis visible in the foreground. 22
Figure 2.9 Box and whisker plot showing earthquake magnitudes for the Hokkaido/Kuril Trench area 23
Figure 2.10 Source regions of the great interplate earthquakes along the southern Kuril Trench (after Satake, 2004). 24
Figure 2.11 Vertical displacement computed by elastic dislocation modelling of fault slip. 27
Figure 2.12 Schematic diagram showing the differential development of tidal marsh stratigraphies along the eastern Hokkaido coastline according to the proposed elastic dislocation model (Savage, 1983) of fault slip. 28
Figure 3.1 A summary of the thesis methodology used to understand vertical land movements on the Hokkaido coastline. 31
Figure 3.2 Schematic diagram illustrating the components of indicative meaning. 36

Figure 3.3 Photographs illustrating the use of a Geoslice corer. 37
Figure 3.4 Schematic diagram of post-earthquake changes in accumulation and land level following the 1964 Alaska earthquake. 48
Figure 3.5 Subtidal sampling at Akkeshi-ko. 50
Figure 3.6 Transfer function methodology (after Birks, 1995). 52
Figure 3.7 ^{238}U radioactive decay series, showing the production of ^{210}Pb via the decay of ^{226}Ra and its short-lived daughters. 54
Figure 3.8 Marine terraces in northern Japan, after Okumura (1996; http://home.hiroshima-u.ac.jp/kojiok/hokkaido.htm). 56
Figure 3.9 Late Pleistocene widespread marker tephras and neotectonic framework of eastern Hokkaido (Okumura, 1996). 57
Figure 3.10 Space-time diagram for marker tephras in Hokkaido (after Okumura, 1996). Vertical line for the age is not to scale. Revised ages of marker tephras taken from Koaze *et al.* (2003) 58
Figure 3.11 Profiles of former shoreline altitude along the Pacific Ocean and Okhotsk Sea. 59
Figure 3.12 Uplifted terraces along the coastline of eastern Hokkaido (after Koike and Machida (2001)). 60
Figure 3.13 Modern oyster beds in a quiet water location in Tofutsu-ko. 63
Figure 3.14 Location map and showing tide-gauge data used in northern Japan and the north Pacific 65
Figure 3.15 Length of record for tide-gauge stations around Hokkaido. 66
Figure 3.16 An example of the steps used to process tide-gauge records around Hokkaido, using records from Petropavlovsk-Kamchatsky and Abashiri 70
Figure 3.17 RLR record from Urakawa showing coseismic offset following the 2003 Tokachi-oki earthquake. 71
Figure 3.18 Method showing the eustatic correction used in this thesis 72
Figure 3.19 Idealised model of a subduction zone (arc-trench system) 75
Figure 3.20 Geological map of Hokkaido 76
Figure 3.21 Climate variability for Nemuro, on the north-eastern coastline of Hokkaido in 2004. 77
Figure 3.22 Location of marshes in north and north-eastern Hokkaido. 78
Figure 3.23 Location maps of northern (1) and eastern (2) Hokkaido coastline showing the location of salt marshes with details of the study locations. 79
Figure 3.24 Location map of Ikuraushi salt marsh, Akkesko-ko with photo detail 81
Figure 3.25 Location map of Mochiruppu salt marsh with photo detail 82
Figure 3.26 Site map and photos of Furen-ko marsh. 83
Figure 3.27 Site map and photo of Tofutsu-ko showing a photo across the study marsh, ... 85

Figure 3.28 Site map and photo of Kerochi marsh, Saroma-ko. The white dashed lines are the locations of the contemporary transects. 86
Figure 3.29 Site map and photo of the marsh at Sarfutsu-toh 86
Figure 4.1 Variations in loss on ignition across the six contemporary marshes……93
Figure 4.2 Intersite variability in environmental variables across at Mochiruppu. 94
Figure 4.3 Variations in grain size across the six contemporary marshes..... 96
Figure 4.4 Variations in salinity across the six contemporary marshes. 97
Figure 4.5 Variations in pH across the six contemporary marshes..... 98
Figure 4.6 Foraminiferal distributions (in %) for the dominant species at Akkeshi-ko. 99
Figure 4.7 Foraminiferal distributions (in %) for the dominant species at Mochiruppu (transects A, B, and C)……...101
Figure 4.8 Foraminiferal distributions (in %) for the dominant species (> 5%) at Furen-ko. 103
Figure 4.9 Foraminiferal distributions (in %) for the dominant species at Tofutsu-ko..... 104
Figure 4.10 Foraminiferal distributions (in %) for the dominant species at Saroma-ko. ... 105
Figure 4.11 Foraminiferal distributions (in %) for the dominant species at Sarfutsu-toh. . 106
Figure 4.12 (A) Summary of foraminiferal distributions and unconstrained cluster analysis based on unweighted Euclidean distance, (B) DCA zones and (C) summary of elevation-dependent zones using cluster analysis results from contemporary transects from Akkeshi-ko. 107
Figure 4.13 Intrasite variability of foraminifera at Mochiruppu. 109
Figure 4.14 (A) Summary of foraminiferal distributions and unconstrained cluster analysis based on unweighted Euclidean distance, (B) DCA zones and (C) summary of elevation-dependent zones using cluster analysis results from contemporary transects from Furen-ko. 111
Figure 4.15 (A) Summary of foraminiferal distributions and unconstrained cluster analysis based on unweighted Euclidean distance, (B) DCA zones and (C) summary of elevation-dependent zones using cluster analysis results from contemporary transects from Tofutsu-ko. 112
Figure 4.16 (A) Summary of foraminiferal distributions and unconstrained cluster analysis based on unweighted Euclidean distance, (B) DCA zones and (C) summary of elevation-dependent zones using cluster analysis results from contemporary transects from Saroma-ko. 113
Figure 4.17 (A) Summary of foraminiferal distributions and unconstrained cluster analysis based on unweighted Euclidean distance, (B) DCA zones and (C) summary of elevation-dependent zones using cluster analysis results from contemporary transects from Sarfutsu-toh. 114

Figure 4.18 Summary of foraminiferal zonation for marshes of Hokkaido plotted against metres TP. 115
Figure 4.19 The CCA biplots of the Hokkaido site data showing (A) foraminiferal sample-environment and (B) species-environment. 121
Figure 4.20 Pie chart showing the total variation (in %) of the Hokkaido foraminiferal training set in unexplained and explained portions. 122
Figure 4.21 Relative abundance of taxa comprising greater than 5% in low-marsh core at Akkeshi-ko, eastern Hokkaido. 125
Figure 4.22 Relative abundance of taxa comprising greater than 5% in high-marsh core at Akkeshi-ko, eastern Hokkaido. 126
Figure 4.23 Summary vegetation zones from the six sites investigated in this study. 127
Figure 4.24 Observed versus predicted elevation and elevation residuals (predicted-observed) using the ‘‘All data’’ model. 131
Figure 4.25 Optima and tolerances of foraminiferal species in ‘‘All data’’ model predicted by WA-PLS component 1 (with bootstrapping). 132
Figure 4.26 Observed versus predicted elevation and elevation residuals using the ‘Pruned B’ model. 134
Figure 5.1 Site map of Mochiruppu, showing locations of transects completed in this and previous studies. 138
Figure 5.2 Litho- and biostratigraphy recorded by Sawai *et al*. (2004b) at Mochiruppu. .. 139
Figure 5.3 Litho-bio-, and chronostratigraphical analysis at Mochiruppu North. 141
Figure 5.4 Core stratigraphy for Mochiruppu South. 143
Figure 5.5 Litho-bio-, and chronostratigraphical analysis at Mochiruppu South. 145
Figure 5.6 Site map showing location of transects studied at Furen-ko during this study 146
Figure 5.7 Stratigraphy at three lithostratigraphic transects known as Yausubetsu (north and south) and Kimura at Furen-ko (Atwater *et al*., 2004). 147
Figure 5.8 Core stratigraphy for Furen-ko. 149
Figure 5.9 Litho-bio-, and chronostratigraphical analysis at Furen-ko. 151
Figure 5.10 Site map showing location of transects studied Tohoro during this study. 152
Figure 5.11 Stratigraphy at Tohoro (transect 1) in relation to tidal frame (Yuki Sawai *pers. comm*.). 153
Figure 5.12 Stratigraphy at Tohoro, transect 2. 154
Figure 5.13 Litho-, bio-, and chronostratigraphical analysis at Tohoro 156
Figure 5.14 Site map showing location of transects studied Tofutsu-ko during this study. 157
Figure 5.15 Stratigraphy at Tofutsu-ko. 158
Figure 5.16 Litho-, bio-, and chronostratigraphical analysis at Tofutsu-ko 160

Figure 5.17 Site map showing location of transects studied Sarfutsu-toh during this study. 161
Figure 5.18 Stratigraphy at Sarfutsu-toh. 161
Figure 5.19 Litho-, bio-, and chronostratigraphical analysis at Sarfutsu-toh..... 163
Figure 6.1 Comparison of salt marsh reconstructed RSL from the six study sites in Hokkaido……168
Figure 6.2 Kushiro tide gauge record from 1947-2008. 169
Figure 6.3 Hanasaki I and II tide gauge records from 1957-1977 and 1983-2008. 170
Figure 6.4 RSL records from the Mochiruppu North and South salt marsh cores alongside the raw tide gauge records from Kushiro and Hanasaki II. 171
Figure 6.5 Tide-gauge stations around Hokkaido showing a rate of RSL rise between 1979-2007..... 176
Figure 6.6 Tide-gauge analysis showing RSL and RSL attributable to tectonic movement. 177
Figure 6.7 RSL and tectonic residuals around Hokkaido..... 180
Figure 6.8 Land subsidence (in cm) in south-east Hokkaido derived from repeat levelling between 1900-1950 (Yokoyama, 1987). 181
Figure 6.9 Horizontal rates of land motion in north-east Japan and Hokkaido based on GPS data from Ito *et al*. (2000). 182
Figure 6.10 Vertical land motions based on analysis of GPS data (Ito *et al.*, 2000). 183
Figure 6.11 Rates of vertical land motion inferred from GPS data 184
Figure 6.12 Map showing location of sites used for Holocene RSL reconstruction and GIA model predictions 185
Figure 6.13 Age/altitude plots of Holocene RSL change from Hokkaido. 186
Figure 6.14 Holocene sea-level index points from the six study areas in Hokkaido, with GIA model prediction 190
Figure 6.15 Holocene sea-level index points from Akkeshi/Mochiruppu and Sarubetsu, with GIA model prediction..... 192
Figure 6.16 The elevation of the three main Late Pleistocene marine terraces identified in north-east Hokkaido plotted by coast (from Okumura, 1996). 193
Figure 6.17 The elevation of the three main Late Pleistocene marine terraces identified in north-east Hokkaido plotted against distance from the coastline at Mochiruppu (from Okumura, 1996)..... 194
Figure 6.18 Uplift rate (and variance) for MIS 5e interglacial terrace identified in north-east Hokkaido..... 195
Figure 6.19 Quaternary volcanoes of north-east Hokkaido..... 196
Figure 6.20 The 1,500 m high Shari-Dake volcano of north-east Hokkaido. 201

LIST OF TABLES

Table 2.1 Land deformation in eastern Hokkaido associated with selected 20th century earthquakes illustrates direction of land movements (i.e. uplift or subsidence). 25
Table 3.1 Techniques employed in this thesis……33
Table 3.2 Factors affecting the distribution of foraminifera on salt marshes..... 41
Table 3.3 Present tidal range on the northern coastline of Hokkaido. 47
Table 3.4 Estimated errors accumulated during modern and fossil sampling in this thesis (after Woodroffe, 2006)..... 50
Table 3.5 Summary dates and sea-level variability relating to MIS 5e. 61
Table 3.6 Data classes used in this thesis, after Brooks and Edwards (2006). 63
Table 3.7 Reference water levels and indicative meanings used in this thesis. 64
Table 3.8 List of tide-gauge data used in this thesis 67
Table 3.9 GIA model predictions for RSL change over the last 100 years in Hokkaido. 73
Table 3.10 Tide levels (m TP) for Hokkaido. 79
Table 4.1 Summary of CCA results from foraminiferal assemblages taken from six salt marshes on Hokkaido……120
Table 4.2 Comparison of CCA and partial CCA results between this and other microfossil-based studies..... 123
Table 4.3 Examples of training set numbers, with approximate area over which training function encompasses. 129
Table 4.4 DCA axis 1 gradients for training sets developed in this thesis. 130
Table 4.5 Summary statistics for all models in this thesis using a WA-PLS transfer function with three components..... 133
Table 5.1 Lithostratigraphy of the sample core from Mochiruppu North described using the Troels-Smith (1955) scheme of stratigraphic notation. 140
Table 5.2 Lithostratigraphy of the sample core from Mochiruppu South described using the Troels-Smith (1955) scheme of stratigraphic notation. 144
Table 5.3 Lithostratigraphy of the sample core from Furen-ko described using the Troels-Smith (1955) scheme of stratigraphic notation..... 150
Table 5.4 Lithostratigraphy of the sample core from Tohoro described using the Troels-Smith (1955) scheme of stratigraphic notation..... 155
Table 5.5 Lithostratigraphy of the sample core from Tofutsu-ko described using the Troels-Smith (1955) scheme of stratigraphic notation..... 159
Table 5.6 Lithostratigraphy of the sample core from Sarfutsu-toh described using the Troels-Smith (1955) scheme of stratigraphic notation. 162

LIST OF APPENDICES

Appendix A Foraminiferal taxonomy 248
Appendix B Modern foraminiferal data 252
Appendix C Fossil lithostratigraphic data (on CD) 261
Appendix D Fossil foraminiferal data 262
Appendix E Fossil Sea-level database 268

CHAPTER ONE

Introduction

1.1 BACKGROUND

The significance of relative sea level (RSL) during the Quaternary is recognised by disciplines across the Earth sciences. Sea-level histories are important for calibrating and constraining geophysical models of Earth's rheology and glacio-isostatic adjustment (e.g. Peltier, 2004). Furthermore, sea level is crucial to any study of coastal evolution as it serves as the ultimate baseline for continental denudation (Summerfield, 1991). For human populations, sea levels during the late Quaternary have been an important factor in sustaining coastal communities and may even have profoundly influenced the initiation of human civilization (e.g. Turney and Brown, 2007). Reports from the Intergovernmental Panel on Climate Change (IPCC, 2007) have re-emphasised the importance of sea level as a barometer of climate and drawn attention to the potentially devastating consequences of future climate change (e.g. Rahmstorf, 2007). However, the IPCC also highlighted the uncertainty with which the driving mechanisms of recent sea-level change are understood and the disconnection between long-term geological records and recent observational trends.

Sea levels vary over a variety of different spatial and temporal scales. Over short timescales (hours to days), atmospheric and astronomic factors dominate the small magnitude, high-frequency signals within the sea-level record. Over longer timescales and over wider spatial settings, geological and glaciological factors primarily affect sea level. These changes are manifestations of RSL, a term which reflects the uncertainty in separating the often simultaneous contributions from movements of the ocean surface and land (Figure 1.1). RSL changes record transfers of mass between oceans and continents during expansion and contraction of great ice sheets (e.g. Lambeck *et al.*, 2002) and incorporate extreme events such as storm surges (e.g. Donnelly and Woodruff, 2007) and tsunamis (e.g. Jankaew *et al.*, 2008). Further, RSL changes document vertical movements in the Earth's crust over a wide range of timescales, from uplift and subsidence during great plate boundary earthquakes (e.g. Nelson *et al.*, 2008), through to century- and millennial-scale movements driven by glacial isostatic adjustment (e.g. Milne *et al.*, 2005).

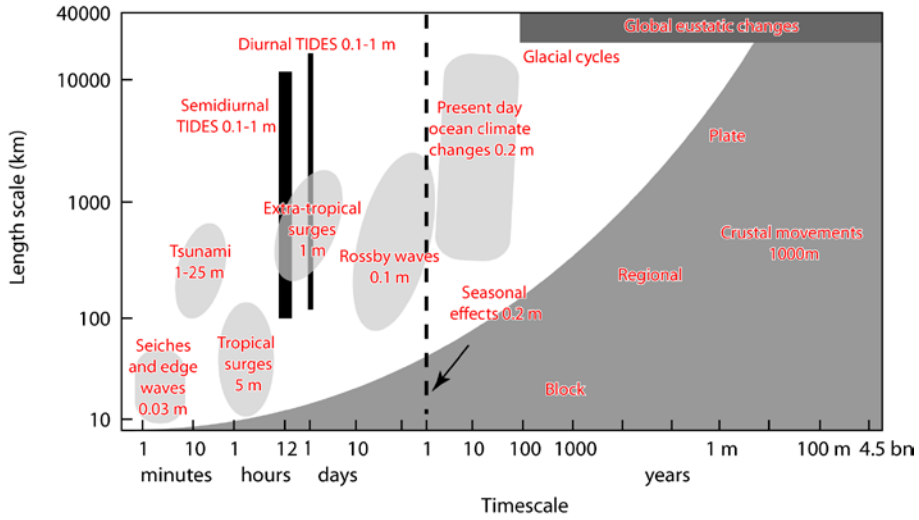

Figure 1.1 Schematic diagram illustrating the factors affecting changing sea levels in space and time, with typical range in metres. Small magnitude, high frequency changes occupy the bottom left-hand corner, whereas high magnitude, low frequency events are situated toward the top, right-hand corner. Adapted from Pugh (2004).

Globally, we can separate coastlines into active and passive coastal margins. On passive coastal margins, such the Atlantic coasts of north-west Europe, the tectonic component is minimal and the dominant controls on Holocene RSL are the interaction of global changes in ocean volume, regional scale changes in the loading of the earth's crust by water and ice in addition to the effects of changes in the Earth's gravity field caused by ice mass variations (Mitrovica *et al.*, 2001).

Since the Last Glacial Maximum (LGM) approximately 50 million km^3 of ice melted from the land-based ice sheets, raising RSL in passive margins distant from the major glaciation centres (far-field sites) by *c*. 120 m (Lambeck *et al.*, 2002). In contrast, RSL has dropped by many hundreds of meters in regions once covered by the major ice sheets as a consequence of the isostatic rebound of the solid Earth (e.g. Shaw *et al.*, 2002). Such rapid changes in RSL are part of a complex pattern of interactions among eustatic, isostatic (glacio- and hydro-) and local factors, all of which have different response timescales.

The eustatic contribution to sea-level change during deglaciation averaged 10 mm year; however peak rates potentially exceeded 50 mm year during 'meltwater pulses' at 19,000 and 14,500 cal. yr BP (calibrated radiocarbon years before present, AD 1950) (Alley *et al.*, 2005). Empirical and glacial isostatic modelling studies suggested a significant reduction in the eustatic contributions to relative sea-level change at *c*. 7000 cal. yr BP and the Earth entered into a period of sea-level stability during which ocean volume, on average, changed only by a few meters (Milne *et al.*, 2005).

Large plate boundary earthquakes and corresponding tsunamis and landslides affect one-third to one-half of the Earth's marine coast (Lajoie, 1986; Nelson, 2007) and the corresponding populations they support. Records of RSL change on active margins archive the response of the Earth's surface to the earthquake deformation cycle, volcanic processes and isostatic tectonic processes (Nelson, 2007). For example, coasts above subduction-zone faults slowly rise or fall (recording displacement from strain accumulation above the fault) for hundreds of years between great earthquakes on the subducting plate boundary, and then are suddenly offset vertically, by a similar amount during earthquakes. Following each earthquake, strain again accumulates during the interseismic period between the previous and the next earthquake on the fault (Nelson, 2007). Patterns of solid Earth deformation accompanying past earthquakes have been documented in association with several great historical earthquakes, including Chile (see for example Plafker and Savage, 1970), Alaska (e.g. Plafker, 1972), south-western Japan (e.g. Thatcher, 1984; Savage and Thatcher, 1992), and most recently Sumatra (e.g. Vigny *et al.*, 2005; Boschi *et al.*, 2006; Pollitz *et al.*, 2006b).

Although there are several kinds of geological faults, large earthquakes that occur along subduction zones are some of the most powerful. These interplate earthquakes often arise as a result of the sudden release of accumulated strain at the boundary between a subducting and an overriding plate. To reduce the uncertainty associated with these devastating earthquakes, and allow governments to evaluate building codes and evacuation plans, a long-term perspective on earthquake hazard is required.

Over the late Quaternary, the position of former marine terraces and associated deposits record deformation patterns attributable to seismic and non-seismic RSL change. Subduction plate boundaries commonly form raised shorelines that extend many hundred of metres above present sea level that indicate long-term net uplift associated with crustal shortening (Lajoie, 1986; Nelson, 2007).

Approaches to Holocene RSL research are based on well established research protocols that typically entail the careful collection and analysis of litho-, bio- and chronostratigraphic data at local to regional scales (e.g. Rongved and Frasier, 1958; Shennan *et al.*, 1983; Long *et al.*, 1998; Shennan and Horton, 2002; Gehrels *et al.*, 2004). The latter have tended to focus on the analysis of transgressive and regressive contacts, representing the stratigraphic transition between a semi-terrestrial and marine environment and vice versa. More recently transfer function techniques, using microfossils (such as foraminifera and diatoms), are used to calibrate fossil sediments from a wide range of intertidal (and potentially subtidal) environments and provide more continuous sea-level reconstructions

through fossil sediment sequences (e.g. Horton *et al.*, 1999; Woodroffe *et al.*, 2005; Edwards and Horton, 2006).

Stratigraphic investigations on the active coastal margins chronicle abrupt coseismic movements associated with plate-boundary earthquakes that are followed by longer intervals of gradual, interseismic deformation of the land surface. The use of litho-, bio- and chronostratigraphic techniques, originally developed over many decades on passive coastal margins, have only recently been applied to these coastal settings (Long and Shennan, 1994). For example, in the most intensively studied area of the Pacific Northwest (USA) and Alaska, sea-level research using passive coastal margin methods only began 20 years ago (e.g. Atwater, 1987; Shennan *et al.*, 1995; Nelson *et al.*, 1996; Shennan *et al.*, 1999).

In contrast to the Pacific Northwest sites, research using these techniques on the tectonically active coastline of Japan is still in its infancy. However, the geological setting of Japan and the configuration of the study site, Hokkaido, which trends orthogonal to the Kuril subduction zone (Figure 1.2), provides an excellent natural laboratory to reconstruct patterns of RSL change over different timescales on an active plate boundary.

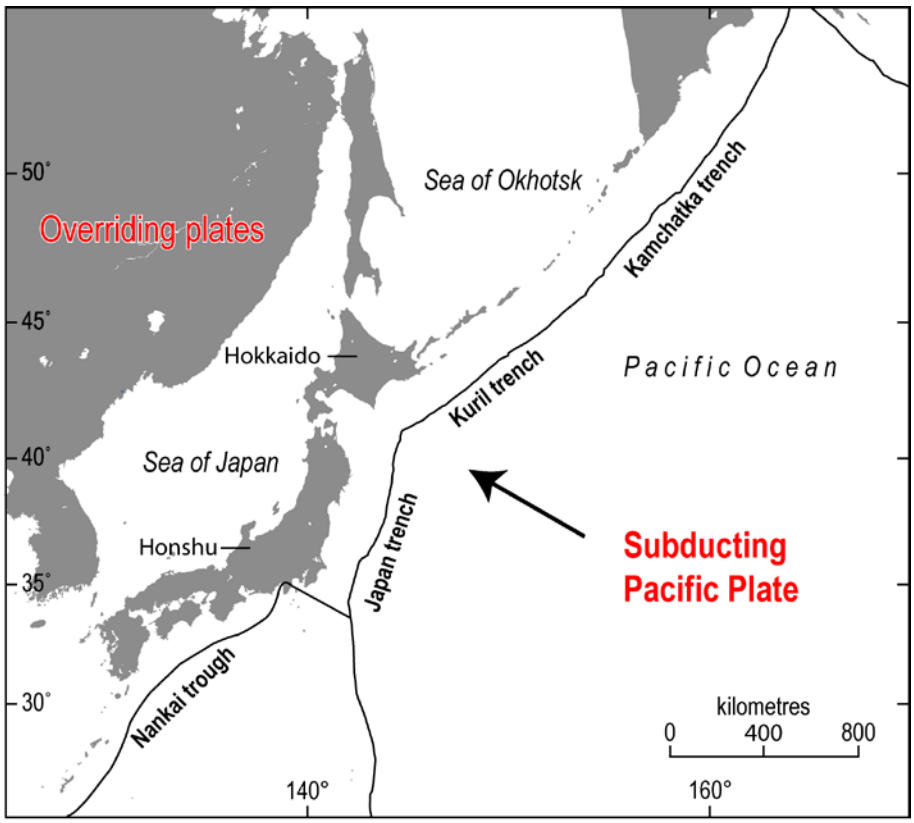

Figure 1.2 Plate tectonic setting around the Japanese Islands. The Pacific Plate is sinking below the overriding continental plate(s) along a subduction zone which is identified by the Kamchatka, Kuril and Japan trenches.

Computer modelling is an increasingly powerful tool for understanding and predicting the mechanisms and consequences of earthquakes on subduction zone coasts. Elastic dislocation theory (Rongved and Frasier, 1958; Steketee, 1958) infers the geometry of faults from the inversion of coseismic surface observations. This inversion process assumes relatively simple models of a dislocation embedded in an isotropic, uniform elastic half-space. Following the Indian Ocean earthquake and tsunami in 2004, observed rates of deformation using short-term GPS and repeat levelling surveys have been used by elastic dislocation models to constrain coseismic slip on the megathrust[1] (Briggs *et al.*, 2006).

The nature with which plate-boundary faults accumulate and release crustal strain is difficult to model because many model parameters are inadequately constrained by measurements (e.g. Wang *et al.*, 2007). Estimates of crustal deformation are spatially limited or imprecise over complete earthquake cycles (Thatcher, 1989; Sieh, 1996). Almost two decades of GPS instrumentation at plate boundaries, coupled with increasingly sophisticated modelling, has identified new patterns of fault deformation (e.g. Dragert *et al.*, 2001; Melbourne *et al.*, 2002; Mazzotti *et al.*, 2003; Wang *et al.*, 2003; Yagi *et al.*, 2003; Hsu *et al.*, 2006; Pollitz *et al.*, 2006a). But because GPS measurements span only fractions of most earthquake cycles, many aspects of ongoing plate deformation lack a satisfactory interpretation (Wang *et al.*, 2007). Subduction-zone megathrusts are an obvious target for improving our understanding of plate-boundary deformation because the scale of crustal deformation during earthquake cycles is greater, and therefore easier to measure, than for other faults (Flück *et al.*, 1997; Long and Shennan, 1998). Forward elastic dislocation modelling has been successfully applied to the AD 1700 Cascadia earthquake in the Pacific Northwest (Leonard *et al.*, 2004) to more reliably assess seismic hazard. In Japan modelling work of this type has begun (Sawai *et al.*, 2004b), but constraining these preliminary elastic dislocation models is limited by the paucity of data regarding past land and sea-level motions over the most recent (*c*. AD 1700) and older earthquake deformation cycles.

To understand the models of land movement in Hokkaido, there is a need to evaluate crustal movements over a variety of temporal and spatial scales. Accordingly, in this thesis I develop new RSL records from sites that occur at increasing distances from the Kuril trench to allow a comprehensive analysis of land movements. A broader consideration of short-term (10^1 - 10^2 yr) and longer-term (10^5 - 10^6 yr) models of land movement offers complementary insights into the nature of subduction zone behaviour and an opportunity to explore the significance of long-term versus short-term patterns of land and sea-level movements on this coast (Figure 1.3).

[1] The contact surfaces between the two plates.

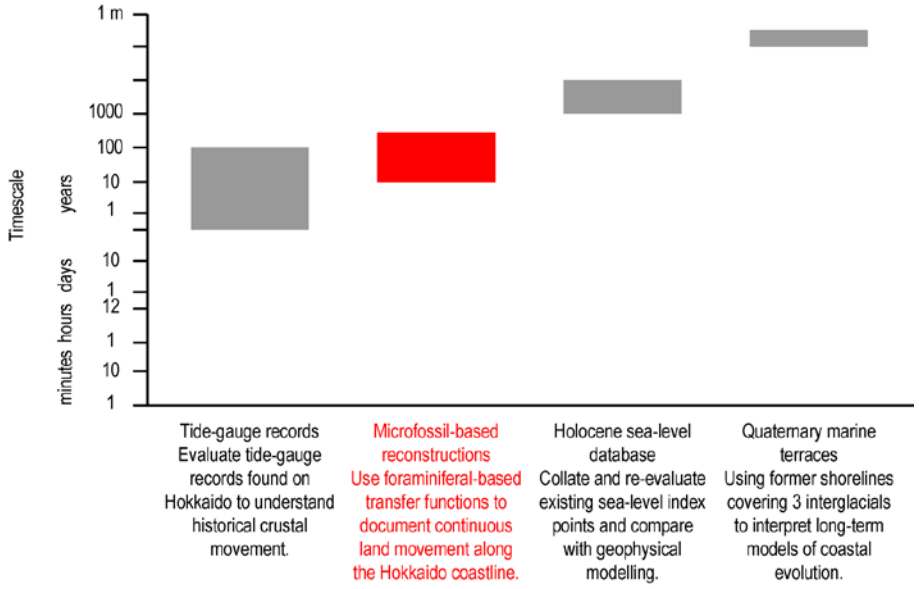

Figure 1.3 Schematic diagram illustrating the techniques for recording or estimating land deformation over differing timescales used by this thesis to understand earthquake-related land-level change in Hokkaido.

1.2 TECTONIC DEFORMATION AND SEA-LEVEL CHANGE

As noted above, subduction plate boundaries often experience long periods (centuries to millennia) of gradual stress accumulation on the locked part of the interface between two converging plates, followed by sudden earthquakes that abruptly release this accumulated energy (Thatcher and Rundle, 1984; Savage and Thatcher, 1992). This simple 'earthquake deformation cycle' is locally more complex, as will be discussed later, but provides an obvious starting point from which to develop models of RSL change on subduction-zone coasts.

Estuarine sequences throughout the coastlines of the Pacific Northwest and Alaska contain intercalated sequences of brackish-marine mud with brackish to freshwater peat, which reflect RSL changes associated with multiple earthquake cycles in the late Holocene. Atwater (1987) was the first to describe a repetitive sequence of alternating peat and mud couplets, the former often possessing a sharp upper boundary to the overlying mud, sometimes with a small intervening sand deposit. He proposed that these stratigraphies reflected multiple episodes of coseismic subsidence (and associated RSL rise) during large earthquakes (Figure 1.4A) followed by gradual interseismic stress accumulation (and RSL fall). The thin sand deposits that sometimes blanket former coastal lowland deposits in the Pacific Northwest and other examples (Figure 1.4B) are interpreted as being of tsunami origin (see for example Clague and Bobrowsky (1999); Williams *et al*. (2005)).

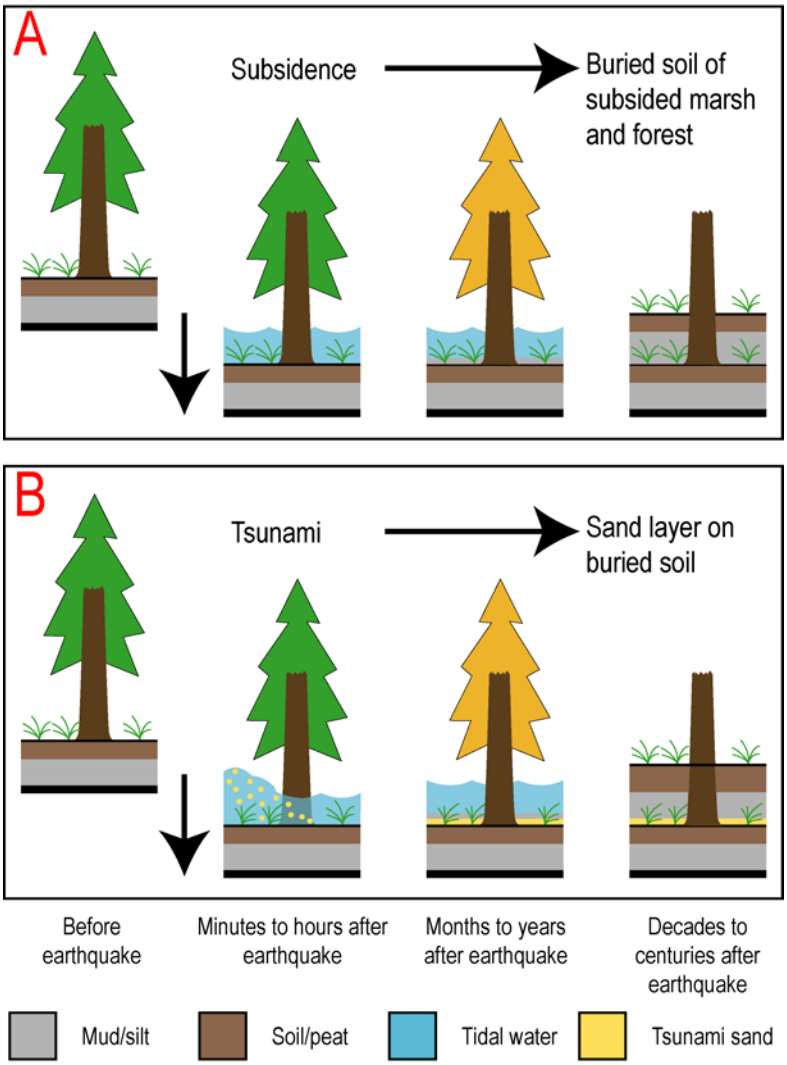

Figure 1.4 Schematic diagram showing the development of peat-silt couplets following coseismic submergence together with associated tsunami deposits (Atwater and Hemphill-Haley, 1997).

The proximity of a sample site to the subduction zone provides a strong influence on the patterns of land- and sea-level motions experienced on subduction coastlines. In the Pacific Northwest, the earthquake deformation cycle causes coseismic subsidence along the coast followed by interseismic uplift. In contrast, recent research in Hokkaido indicates that coseismic uplift (and RSL fall) accompanies strain release during great earthquakes, recorded in the coastal marsh stratigraphy by an upwards change from tidal mudflats to freshwater swamp and forest (e.g. Sawai, 2001; Sawai *et al.*, 2002; Sawai *et al.*, 2004b; Sawai and Nasu, 2005). Palaeoenvironmental studies using diatom-based reconstructions demonstrate repeated late Holocene emergence events that accompanied plate-boundary earthquakes, which were followed by centuries of interseismic subsidence (Figure 1.5) (Sawai, 2001; Sawai *et al.*, 2004b). The attributes of this simple model are discussed more fully in the following Chapter.

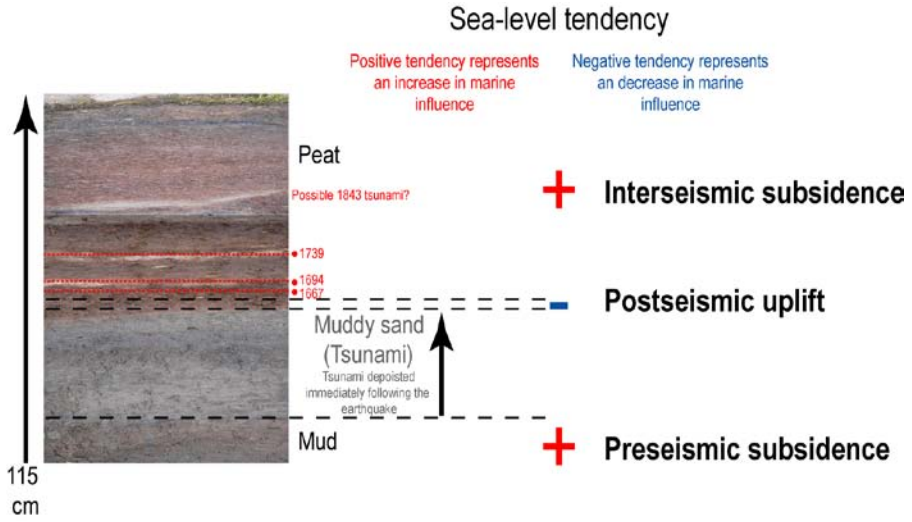

Figure 1.5 Schematic diagram showing the earthquake deformation cycle interpreted from the stratigraphies on Hokkaido's eastern coast. The stratigraphy shows the sedimentological evidence for postseismic coastal uplift followed by interseismic subsidence as recorded at Mochiruppu (Sawai *et al.*, 2004b).

1.3 RESEARCH RATIONALE

1.3.1 Research aim

The overarching aim of this thesis is to improve our understanding of the controls of seismic and non-seismic factors in determining sea-level change in Hokkaido, northern Japan. To address this aim, I focus on evaluating the evidence for RSL change over a variety of spatial and temporal scales using a combination of proxy and direct measurement methods. Of particular interest is the detailed pattern of RSL change recorded during the last 300 yrs or so of the current interseismic interval, a period of time widely thought to be associated with subsidence.

1.3.2 Research approach

To address these questions, I structure my research in the following manner:

I. I start by reviewing previous research into the evidence for land and sea-level movements in the study area of Hokkaido, Japan;
II. I then review methods for reconstructing past RSL change, focusing in particular on methods associated with developing a microfossil-based transfer function using foraminifera;
III. I apply this methodology to reconstruct RSL change and determine land deformation over the last earthquake cycle (the last *c*. 500 years) from a number of carefully selected sites in Hokkaido that are aligned orthogonal to the Kuril subduction zone;

IV. I then compare relative land-level changes over a variety of temporal scales using tide-gauge data, GPS and repeat-levelling data, Holocene sea-level index points and Quaternary marine terraces to understand RSL patterns over different timescales;
V. Lastly, I evaluate the implications of this new research for our understanding of earthquake processes and RSL change in Hokkaido, consider the limitations to the current work and identify future directions for research.

1.3.3 Outline of thesis

In *Chapter Two* I review the mechanisms by which seismic deformation and sea level are related and evaluate the existing evidence for coupled sea-level change and palaeoseismicity in Japan. I introduce models and observations in order to understand patterns of RSL change and constrain earthquake parameters.

In *Chapter Three* I describe the research methodology I employ in this thesis and introduce the study sites selected for contemporary and fossil studies.

In *Chapter Four* I present the results of my research into the contemporary salt-marsh environment of Hokkaido, including the development and application of a foraminiferal-based transfer function.

In *Chapter Five* I present the results of lithostratigraphic analyses, culminating in the development of a new series of local records of RSL change from five study sites.

In *Chapter Six* I discuss these findings in the context of other datasets that relate to recent (GPS, tide gauge and repeat levelling) Holocene and Pleistocene RSL changes and evaluate the implications of the work for our understanding of the patterns and processes associated with land deformation over different periods.

Finally, in *Chapter Seven* I summarise the main findings of the thesis, assess limitations to the work and identify future research directions.

CHAPTER TWO

Research Context

2.1 INTRODUCTION

This Chapter provides a review of previous relevant research regarding the reconstruction of past earthquake activity using RSL data. It provides a context for the new research conducted in this study on the Hokkaido coast of Japan. I start by reviewing the methods used on active plate boundaries for reconstructing land- and sea-level movements, over Pleistocene and Holocene timescales. I then review previous attempts to model these patterns using elastic dislocation models, before concluding by elaborating on the thesis research questions introduced in Chapter One.

2.2 RSL CHANGE ON ACTIVE PLATE BOUNDARIES

Tectonic processes contribute to the morphology and evolution of coastlines on active plate boundaries by driving both gradual and abrupt changes in RSL, including the destructive effects of tsunamis that can accompany local or far-field earthquakes. These processes are in addition to the normal array of mechanisms that control coastal and RSL change on passive coastal margins. The resultant complexity requires the development of well-defined models of RSL change and coastal response to be developed and validated.

The patterns of RSL change and associated coastal response on active-plate boundaries vary over space and time. In the short term, the most dramatic changes in RSL are those linked to the coseismic vertical displacements associated with earthquakes or volcanic eruptions (Lajoie, 1986; Berryman, 1987). Over long-term periods of decades to centuries, vertical tectonic motions will usually include long-lasting slower deformation following plate-boundary earthquakes that affect hundreds of kilometres of coastline.

Over multiple earthquake cycles a component of the simple two-stage deformation cycle, which comprises of coseismic subsidence/uplift and interseismic strain accumulation, can result in a net upwards or downwards trend in RSL. In Hokkaido, abundant raised marine terraces of Pleistocene age (Okumura, 1996) provide evidence of long-term uplift.

Unravelling the cumulative effect of multiple earthquake cycles on long-term trends in RSL over Holocene and Pleistocene timescales is a critical challenge; any attempt to address this research problem requires the potential contribution of global and regional non-seismic processes such as changes to RSL caused by 'eustasy' and the processes of glacio- and hydro-isostatic adjustment to be identified.

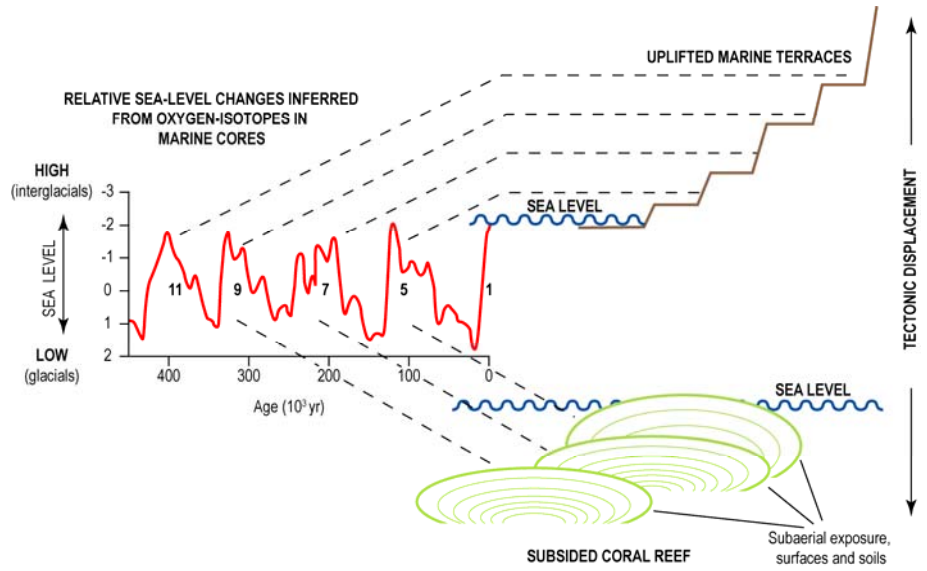

Figure 2.1 Schematic diagram illustrating the use of different sea-level indicators to document tectonic displacement on tropical coastlines. The highstands in the oxygen-isotope record from deep-sea foraminifera correspond with uplifted interglacial marine shorelines while the lowstands formed during glacial periods relate to subsided coral reef records (after Muhs *et al*. (1994) and Nelson (2007)).

2.2.1 The earthquake deformation cycle

Land-level movements associated with large plate-boundary earthquakes commonly display predictable deformation patterns that vary with distance from any particular geological fault. Observations associated with the California earthquake of April 1906 formed the basis for our current scientific understanding of plate-boundary earthquake deformation. Reid (1910) used the patterns of land motion associated with this event to develop his theory of elastic rebound, which remains the basic tenet of current earthquake models.

Reid's (1910) theory predicts that elastic strain accumulates across a fault during the interseismic period and is then released suddenly during the earthquake. Between earthquakes relatively steady interseismic motions, where the shallow part of the subduction zone is locked and the coastline rises, comprise the majority of the cycle ('A', Figure 2.2). Coseismic deformation accompanies the earthquake itself as the previously locked section of the seismogenic zone slips ('B', Figure 2.2).

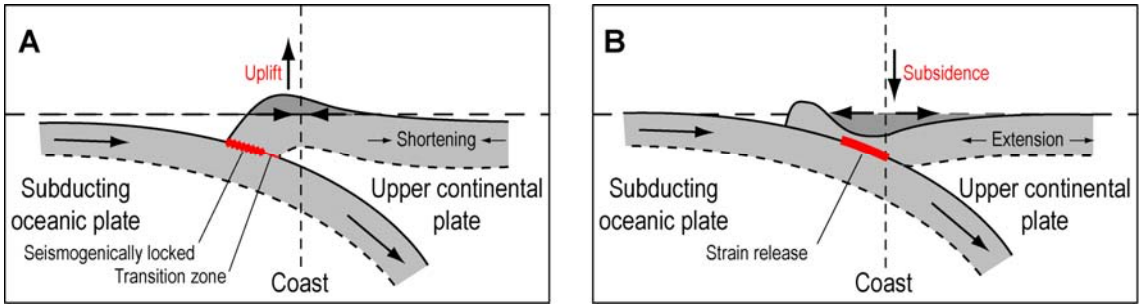

Figure 2.2 Schematic diagram showing the earthquake deformation cycle associated with a subduction-zone thrust fault beneath a coast: (A) the interseismic strain accumulation, and (B) the coseismic fault slip and strain release. Modified from Nelson *et al.* (1996).

In response to strain accumulation and slip, coastlines adjacent to subduction zones record predictable patterns of deformation that are related to their distance from the fault. Thus, during the interseismic period the coastline above the fault experiences maximum uplift, with areas further from the trench experiencing down-warping in response to shortening of the continental plate. This may continue for hundreds of years, but when the frictional strength of the fault is exceeded and the built-up strain is released, coastlines suddenly readjust. The uplifted region quickly subsides, while the offshore region undergoes rapid uplift, possibly triggering a tsunami wave.

Since Reid's (1910) seminal paper, research using geodetic observations and high-resolution palaeo data has demonstrated this two-stage earthquake deformation model is too simplistic to account for the complexity of deformation patterns that accompany plate-boundary earthquakes. For example, research in Washington and Oregon, and more recently in Alaska, suggests that the rate of RSL change accelerates prior to and immediately after earthquakes, resulting in a four-stage deformation cycle (Shennan *et al.*, 1999). The two new stages of the earthquake deformation cycle are; i) a period of pre-seismic RSL change, in the time immediately prior to an earthquake, and; ii) a period of immediate postseismic adjustment. The cause of the pre-seismic signal is debated but it may be due to 'slow earthquakes' along a deeper part of the subduction zone. This suggests warning signs may be detectable before great subduction-zone earthquakes, although at present evidence for a consistent pre-seismic signal is equivocal (Bourgeois, 2006). The postseismic adjustment records the immediate readjustment of the plate boundaries following strain release, and in Washington and Oregon, for example, is associated with a period of rapid rebound that is followed by slower interseismic recovery (e.g. Nelson *et al*., 2008). The immediate postseismic adjustment can include uplift, as observed following the 1960 Chile earthquake (Hu *et al*., 2004) and also inferred from bio- and lithostratigraphic grounds in Hokkaido (e.g. Sawai *et al.*, 2004b).

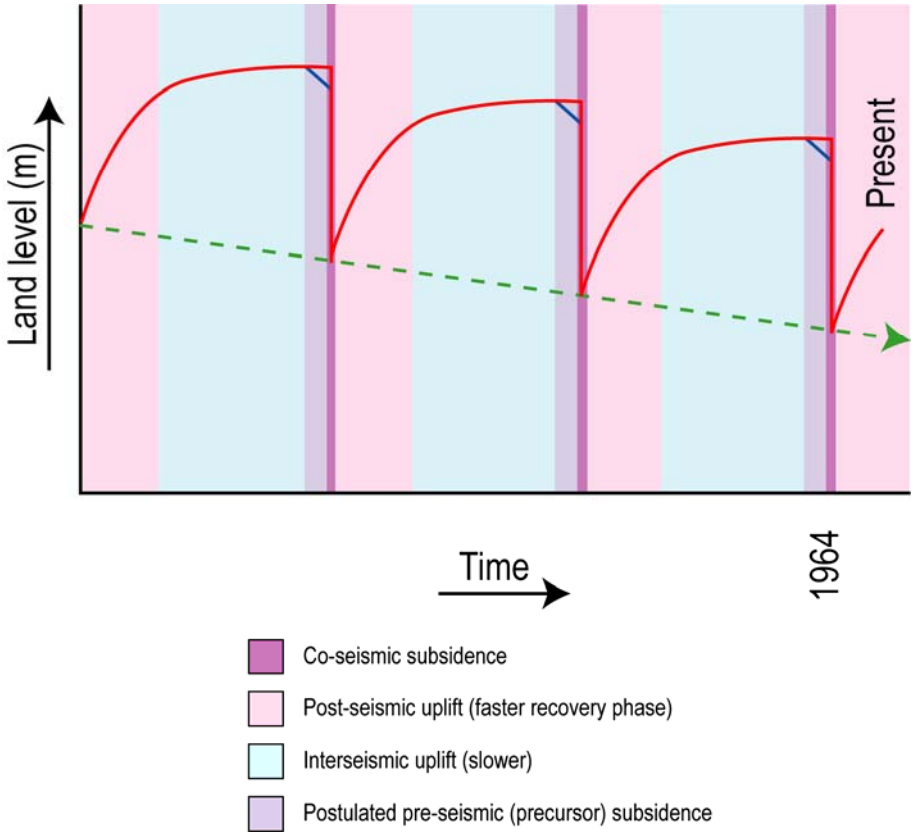

Figure 2.3 Earthquake deformation model for Alaska. The red line shows a simple cycle of the rise and fall of land, the blue line shows the small-scale subsidence that is postulated to precede great earthquakes, and the dashed green line shows net subsidence over time. The period between the earthquakes is on the order of centuries, with the end of the series showing the present elevation of the Alaska coast following the 1964 earthquake (Bourgeois, 2006).

If one assumes that the Earth is a perfectly elastic medium, with no memory of previous ruptures, and that rates of plate movements remain constant, then it is reasonable to expect that a given fault will produce earthquakes of a similar size, at regular intervals. However, direct observation and palaeo-reconstructions demonstrate that sometimes there is a mismatch between inter-earthquake strain accumulation and coseismic strain release. Such a mismatch causes permanent deformation to occur which, although small in magnitude (perhaps only a few decimetres) can, over many earthquake cycles, cause significant uplift or subsidence of active plate boundaries which may amount to tens to hundreds of meters over successive millennia.

Over Quaternary timescales, vertical deformation on active coastal margins may appear to be continuous, although successive earthquake cycles may vary significantly in style, magnitude and frequency. Such differences can be characterised by four different models (A-D) (Figure 2.4):

- In a periodic, characteristic model (A) stress levels before and after the earthquake are known and the slip and recurrence of the earthquake is predictable.

- In a time dependable model (B) a more realistic scenario assumes that the stress prior to an earthquake is known, the interseismic rate is constant and that the recurrence interval can be predicted even though the amount of slip is not unknown.

- In a slip-predictable model (C), the lower stress limit following an earthquake is assumed to remain constant, allowing the amount of slip to be predicted even though its recurrence is not.

- Perhaps the most realistic of all is the non-predictable and non-characteristic model (D), for which the amount of slip and recurrence interval varies.

The Cascadia subduction zone displays an earthquake history most akin to that predicted by model D. The geological data from this region suggests plate-boundary ruptures of varying length (and hence magnitude), with recurrence intervals that average *c*. 500 years, yet which range from a few centuries to a millennia (Nelson *et al*., 2006).

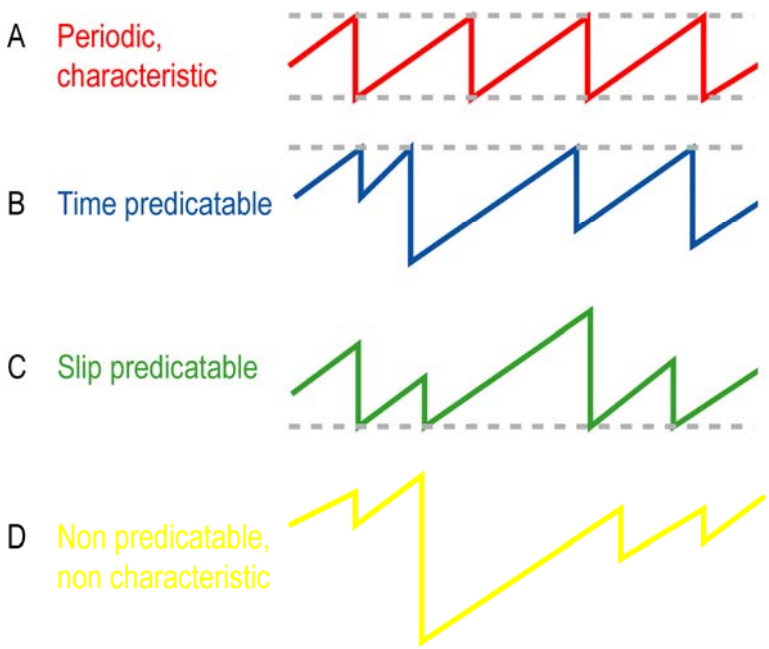

Figure 2.4 Four models of earthquake recurrence, after Shimazaki and Nakata (1980) and Satake and Atwater (2007).

Understanding deformation patterns, even over multiple cycles during the Holocene period, may be insufficient to characterise a subduction zone over Pleistocene timescales. Successive earthquakes may induce changes to the fault plane properties over time (Nelson, 2007) and 10,000 years may be too short to document the cumulative effects of

several seismic cycles. For example, in southern Italy, late Holocene deformation rates are 64-124% higher than those predicted from the elevation of the MIS 5e shoreline, although it is not certain whether the latter indicates a true change in regional tectonic processes or simply the result of only partial elastic strain release during earthquakes (Antonioli *et al*., 2006).

2.2.2 Earthquake magnitude and elastic dislocation modelling

The maximum seismic moment (M_0) defines the earthquake potential for a subduction zone and is calculated from seismogenic parameters associated with the fault (and is measured in Nm):

$$M_0 = \mu AD \qquad \text{Equation 2.1}$$

Where;

μ = a product of the rigidity (shear modulus);

A = the total fault area;

D = average displacement across a fault.

The moment magnitude (M_w) is based on seismic moment and is computed as:

$$M_w = \frac{\log M_0 - 9.1}{1.5} \qquad \text{Equation 2.2}$$

Where;

M_0 = seismic moment (as above).

The nature of the seismogenic zone governs the moment magnitude of earthquakes. Rupture length is a critical parameter for palaeoseismic studies to quantify. According to a recent comparison of radiocarbon ages for coseismic subsidence and tsunamis along the Cascadia subduction zone (Nelson *et al*., 2006), approximately two thirds of great earthquakes along the Pacific Northwest coastline in the past 5,000 years were likely to be associated with full-length ruptures or a smaller series of shorter ruptures. Other, smaller magnitude earthquakes during this interval also produced palaeoseismological records, but these are restricted to individual segments of the northern, central, or southern part of the Cascadia subduction zone.

The three largest earthquakes since 1900 ruptured along a fault length of at least 800 km, the largest being the Chilean earthquake of May 1960. Palaeoseismic analysis of tsunami deposits suggests much of the fault dislocation that accompanied this event stemmed from

a release of energy that had remained 'locked' since AD 1575; that is, the earthquakes that occurred between those dates had expended comparatively little of the accumulated stress (Cisternas *et al*., 2005).

The amount of slip on the thrust fault is also fundamental in controlling the magnitude of earthquakes. In particular, the thermal properties of the thrust as well as other structural features (such as the nature of the intersection of the subduction thrust with the fore-arc mantle) govern the width (or the updip and downdip limits of rupture) during great subduction-thrust earthquakes (Hyndman and Wang, 1993; Hyndman and Peacock, 2003).

Patterns of land motions during plate-boundary earthquakes can be modelled using elastic dislocation theory (Rongved and Frasier, 1958; Steketee, 1958) in which faults are considered as displacement discontinuities or dislocations in an otherwise continuous elastic medium modelled as a uniform elastic half-space.

Figure 2.5 shows a simple elastic dislocation model that assumes the surface movements cease as soon as the movement on the fault stops and that can be used to predict crustal deformations associated with different phases of the earthquake-related deformation cycle. In this example, during the interseismic period the portion of the upper plate overlying the locked subduction interface is gradually dragged downwards, while the region landward of the locked fault zone bows upward. During an earthquake the region above the up-dip portion of the rupture recovers the elastic strain stored during the interseismic phase and experiences sudden coseismic uplift, whereas the downdip end of the rupture and adjacent regions subside.

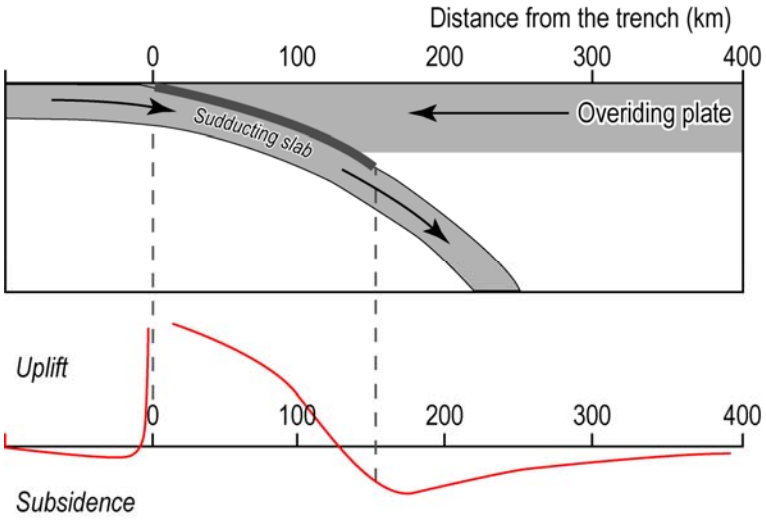

Figure 2.5 Generic elastic slip dislocation model. The thick line represents the locked interface, which slips during the earthquake. Hypothetical pattern of coseismic uplift and subsidence and its geometrical relationship to slip on the locked interface are shown by the red line (Meltzner *et al*., 2006).

The application of sea-level observations to constrain elastic dislocation models on active margin coasts is in its infancy. Where such work has been attempted, studies have focussed on using recent observations, such as tide gauges (Larsen *et al*., 2003) or GPS/repeat levelling surveys (Verdonck, 2005) for model development and testing. Proxy records are occasionally used although there tends to be a bias toward the recent historical past, for example the deformation of coral microatolls following the Sumatra Nias-Simeulue earthquake (Briggs *et al*., 2006) in 2005. Long and Shennan (1998) used mid- and late Holocene RSL data from Washington and Oregon to test competing models of current deformation patterns in Washington and Oregon. However, the paper of Leonard *et al*. (2004) was arguably the first attempt to test the consistency of the dislocation models for the AD 1700 Cascadia earthquake using estimates derived from analyses of coastal marsh sediment sequences. Although a similar approach has been explored in Hokkaido by Sawai *et al*. (2004b) research has not so far rigorously tested elastic dislocation models in this region.

2.2.3 Tidal-wetland stratigraphies as recorders of seismic land-level changes

Sedimentary records from tidal wetlands adjacent to subduction zones document repeated Holocene earthquakes and also help distinguish between earthquake-related and non-earthquake processes (Long and Shennan, 1994; Nelson *et al.*, 1996; Atwater and Hemphill-Haley, 1997; Clague and Bobrowsky, 1999; Sawai *et al.*, 2004a; Cisternas *et al.*, 2005; Shennan and Hamilton, 2006). Nelson *et al*. (1996) propose five criteria to identify coseismic subsidence in tidal-wetland stratigraphic sequences at the Cascadia subduction zone from other non-seismic controls of RSL; (i) the suddenness of submergence; (ii) the amount of submergence; (iii) the lateral extent of peat-silt couplets with sharp upper contacts; (iv) the presence of tsunami deposits; and (v) the synchronicity of submergence.

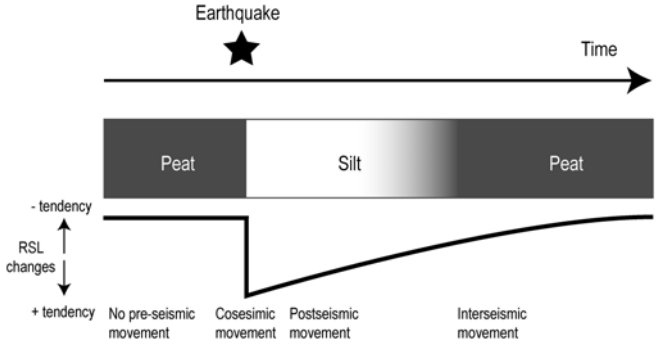

Seismic process	Lithostratigraphical and biological response
Pre-seismic movement	Slight change in organic content, or particle size distribution of the sediments during pre-seismic subsidence (RSL rise). Increase in agglutinated taxa, or those species prefering high-marsh conditions.
Cosesimic movement	Rapid switch to deposition of clastic material following submergence, giving rise to sharp, erosive contact. Peat rapidly buried by tidal-flat mud or tsunami-deposited sand.
Postseismic movement	Sudden drop in organic content, and general increase in size of minerogenic particles. Calcareous foraminifera become dominant in assemblage, with rapid grading into the next peat bed, with corresponding increase in agglutinated taxa.
Interseismic movement	Slower increase in organic matter, and fining of material as marsh vegetation redevelops on uplifted tidal flats. Agglutinated taxa, indicative of higher marsh environments become prevalent in foraminiferal assemblages.

Figure 2.6 Schematic diagram of lithostratigraphical and biostratigraphical responses to the earthquake-related deformation cycle in Alaska, modified from Hamilton (2003).

Research at accessible estuarine outcrops has used suddenly buried plant macrofossils within tidal wetland soils to infer sudden coseismic subsidence (e.g. Atwater, 1987), but the broad elevational range of macrofossil species limited estimates of the amount of subsidence to > ±0.5 m (Nelson *et al*., 1996). Microfossils, such as foraminifera, diatoms and pollen, superseded these analyses by providing quantitative estimates of RSL change (Figure 2.6). For example, diatoms in buried soils along the Washington and Oregon coastline have been used to estimate subsidence during seven great Holocene earthquakes (Hemphill-Haley, 1995; Nelson *et al.*, 1996; Shennan *et al.*, 1996; Atwater and Hemphill-Haley, 1997; Nelson *et al.*, 1998; Shennan *et al.*, 1998). In other work, Sherrod *et al*. (2000) and Sherrod (2001) have analysed diatoms to infer earthquake-induced uplift and subsidence in coastal marshes of Puget Sound, Washington State. Dramatic changes in diatom assemblages across mud/peat stratigraphic contacts confirmed rapid emergence and submergence, which modern analogues indicated to be about 7 m (Sherrod *et al*., 2000) and 1-3 m (Sherrod, 2001), respectively.

Some of the initial diatom research in Washington and Oregon applied numerical techniques to relate contemporary diatom distributions to past changes in RSL, using correspondence analysis (e.g. Shennan *et al.*, 1995). Recent developments in the use of the transfer-function technique in sea-level studies, first applied to passive coastal margin salt marshes but equally applicable to active coastal settings, provide more sophisticated

statistical approaches for reconstructing continuous records of RSL change during multiple earthquake cycles (e.g. Zong *et al.*, 2003; Shennan and Hamilton, 2006).

2.3 RSL CHANGE AND PALAEOSEISMICITY IN JAPAN

The Japanese archipelago is located in an area where several continental and oceanic plates meet (see Figure 1.2; pg 4), and as a result, is one of the most seismically active areas of the world. Pleistocene coastal deposits provide extensive evidence of tectonic movements, at rates and directions that reflect the local or regional tectonic setting. The majority of sea-level data comprise uplifted shorelines and the deposition of marine sediments, although archaeological information and borehole analysis has also been instrumental in documenting the RSL history of the Japanese islands.

2.3.1 Holocene sea-level changes in Japan

According to the GIA modelling work of Clark (1978), Japan is located in a region of the earth that is characterised by a continually rising RSL during the Holocene, with an inflection, or slow-down, during the mid-Holocene at *c*. 5 k cal. yr BP when RSL was within *c*. 2 m of present. However, empirical observations suggest that patterns of RSL change in Japan are in fact much more varied, with different areas experiencing continuous RSL rise or a mid-Holocene highstand that reaches up to 5 m above present (Ota and Machida, 1987; Pirazzoli, 1991).

An important objective of this thesis is the development of a new, validated database of Holocene sea-level index points from Hokkaido, which I use to construct new RSL histories from the region. The method of database construction and the results of the work are detailed in Chapter Three. Here, I provide a brief summary of the general patterns of Holocene RSL change in Japan, which provides a context for the current study on Hokkaido.

A summary of the varied Holocene RSL history of Japan is provided in Figure 2.7 based on the compilation by Pirazzoli (1991). Almost all of the records indicate a rising RSL following the LGM lowstand, which recent ^{230}Th, ^{234}U and AMS dating from the Ryukyu Islands (south-west Japan) suggests was *c*. -126 m between *c*. 22-30 ka BP (Sasaki *et al*., 2006). In older literature, this initial rise in RSL is termed the 'Jomon transgression', after the presence of early Jomon middens associated with shorelines developed under this transgression (Ota and Machida, 1987; their figure 6.15).

Many regions of Japan record evidence for a mid-Holocene RSL highstand. Comparisons of observations and recent GIA models suggest this is a product of hydro-isostatic loading of the Japanese continental crust (e.g. Maeda *et al*., 1992; Yokoyama *et al*., 1996). The magnitude of the highstand varies; it reaches a maximum of *c*. 6 m at 5,500 cal. yr BP in the Kyushu region of southwest Japan (Yokoyama *et al*., 1996). Recent ground penetrating radar surveys and sedimentological investigations of the raised beaches at Kujukuri (south Japan) also record a 5 m RSL fall since *c*. 6 ka cal. yr BP (Tamura *et al.*, 2007; Tamura *et al.*, 2008).

The fall in RSL from the mid-Holocene highstand is in many regions represented by a smooth RSL curve whereas detailed sedimentological analyses suggest that the fall has been associated with several abrupt changes. For example, dating or raised mid- and late Holocene corals on the Ryukyu Islands indicated at least four episodes of uplift dated to 6.3, 4.3, 3.1 and 1.4 ka cal yr BP (Sugihara *et al.*, 2003). Ota and Machida (1987) summarise the evidence for the most recent fall in RSL, termed the 'Yayoi regression', including evidence for several fluctuations in RSL during the overall fall to present.

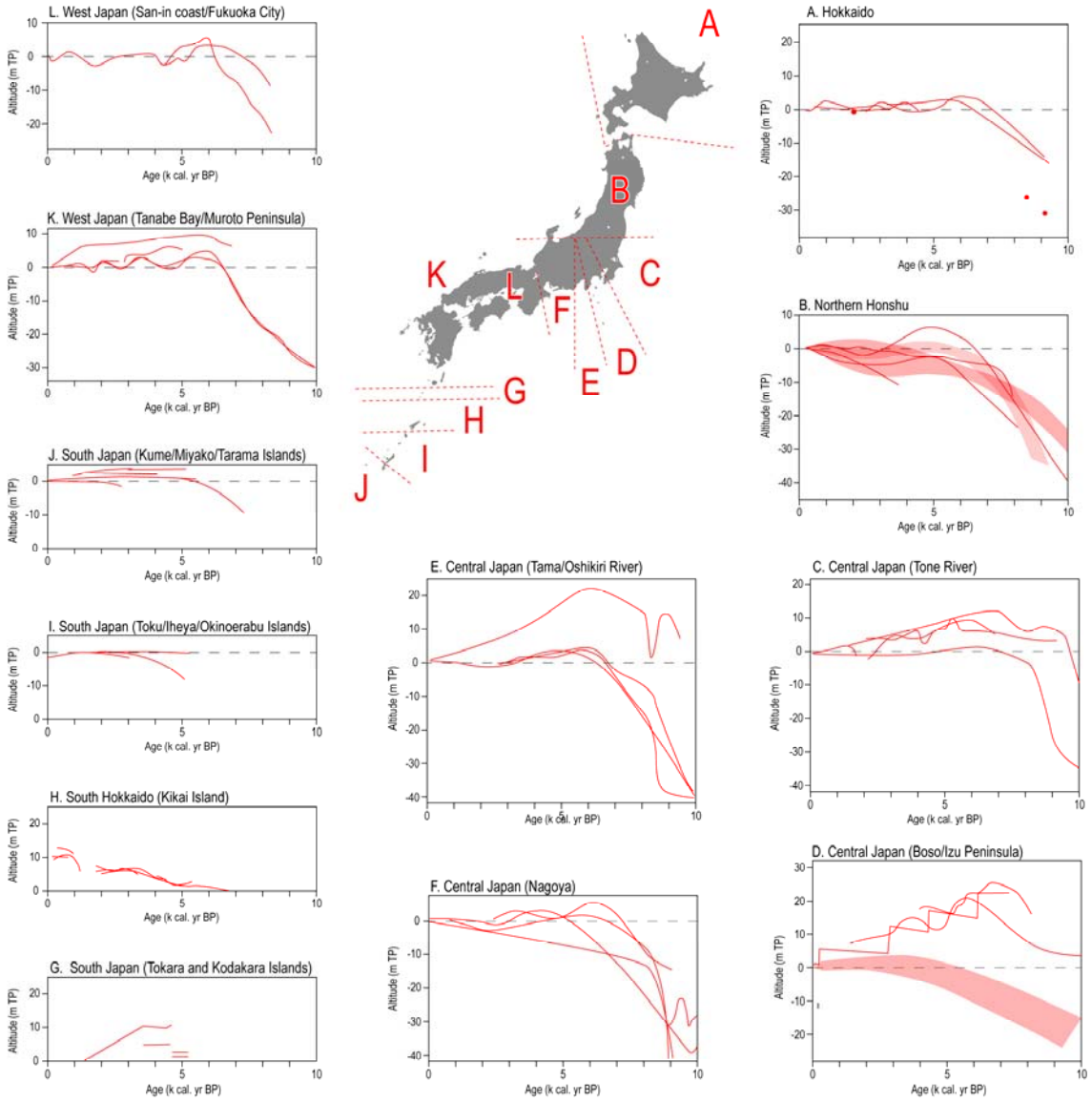

Figure 2.7 Holocene RSL changes for the Japanese Islands, modified from Pirazzoli (1991).

2.4 HOKKAIDO

The Kuril Trench is a deep submarine depression in the western Pacific Ocean, situated on the east side of the Kamchatka Peninsula, the Kuril Islands and Hokkaido. The trench extends for about 2,900 km north-south and has a maximum depth of *c*. 10,500 m. This is a critical element of the tectonic infrastructure of the Hokkaido study area and has a dominant influence on patterns of past and current land motions and associated RSL change.

2.4.1 Palaeoseismicity in Hokkaido

Hokkaido ('North Sea Province') is the northernmost of the four main islands of Japan, bordered by the Sea of Japan (west), the Sea of Okhotsk (north), and the Pacific Ocean (east and south) and has an area of 77,978 km^2. The Kuril continental margin along the eastern coast of Honshu/Hokkaido and the Kuril archipelago, where the Pacific Plate presently descends beneath the continental Eurasian Plate at a rate of 8-9 m per century (Demets, 1992), shows features typical of a subduction zone, including a chain of active volcanoes (e.g. Shari-dake; Figure 2.8) and thrust earthquakes.

Figure 2.8 Photo of Shari-dake volcano, Hokkaido, with the Tofutsu-ko salt marsh studied in this thesis visible in the foreground.

Recent survey observations and studies of Pleistocene geology show conflicting patterns of land motions. Raised marine terraces from the last interglacial provide unequivocal evidence of long-term net uplift, at an average rate of 0.1-0.4 mm yr for the past 125,000 years (Ota and Omura, 1991; Okumura, 1996; Koike and Machida, 2001). However, during the historic period for which detailed geodesy (e.g. Shimazaki, 1974) and tide-gauge measurements (e.g. Shimazaki, 1972; Kasahara, 1975; Kato, 1983; Ozawa *et al.*, 1997) are available a steady submergence is reported that has not been reversed by 20th century earthquakes. A consequence of subsidence during the last century (at least) is that estuaries throughout the Hokkaido region have expanded into fringing forests, with visible reminders left in the form of 'ghost' forests.

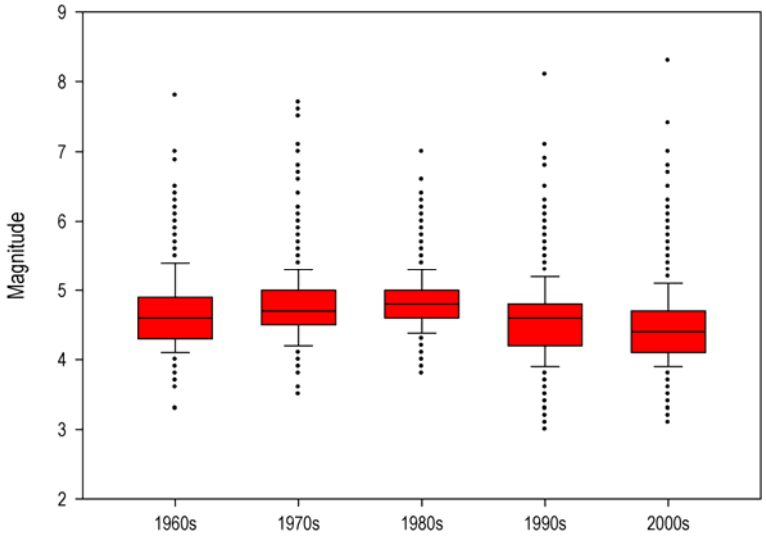

Figure 2.9 Box and whisker plot showing earthquake magnitudes for the Hokkaido/Kuril Trench area (latitude 41°32 - 45°31; longitude 139°45 - 149°00) from the 1960s to the present day (May, 2007). The data were sourced from the Advanced National Seismic System (ANSS) Worldwide Earthquake Data Center (http://quake.geo.berkeley.edu/anss).

Earthquakes in Hokkaido are numerous and up to 1,300 (> Mw 3) have occurred in the last five decades (Figure 2.9 and 2.10). Plate-boundary earthquakes in the range of Mw 7.8 to 8.2 are the largest known from the region's 200 years of written records. Tokachi-oki earthquakes (off the Tokachi coast) occurred in 1843, 1952 and 2003, whilst Nemuro-oki earthquakes (to the east, off Nemuro) occurred in 1894 and 1973 (Figure 2.10). Coastal land-level changes known to have accompanied these earthquakes are limited to subsidence that amounts to a few decimetres at most (Table 2.1).

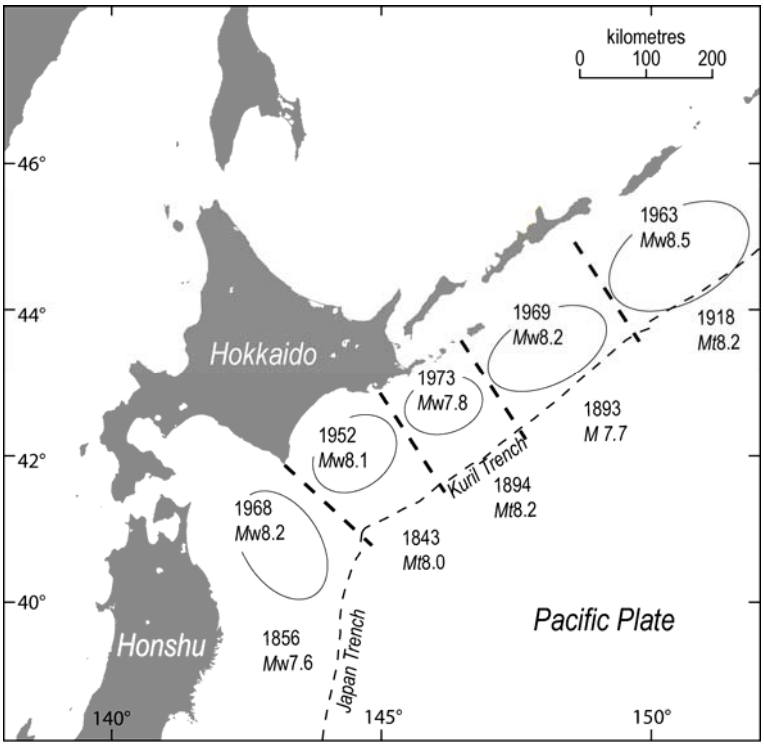

Figure 2.10 Source regions of the great interplate earthquakes along the southern Kuril Trench (after Satake, 2004).

The land deformation that has accompanied some of the earthquakes recorded in the last few decades in eastern Hokkaido are detailed in Table 2.1. These relatively minor patterns of land motion are in contrast to the reconstructions made by several palaeoseismic studies in the region that suggest that successive plate-boundary earthquakes along the Kuril trench have caused vertical movements of a metre or more (Sawai, 2001; Sawai *et al.*, 2002; Atwater *et al.*, 2004; Sawai *et al.*, 2004a; Sawai *et al.*, 2004b).

Table 2.1 Land deformation in eastern Hokkaido associated with selected 20th century earthquakes illustrates direction of land movements (i.e. uplift or subsidence).

Year	M[1]	Region	Fault geometry			Deformation (cm)[4]		References
			L[2]	D[3]	Slip (m)	Offshore	Onshore	
1843	8.0	Tokachi-oki	100-200?					Satake *et al*. (2005; 2006)
1894	8.2	Nemuro-oki	200					Satake *et al*. (2006); Tanioka *et al*. (2007)
1952	8.2	Tokachi-oki	150?	45	<8	+200 to -80	-10 to -20 (Tokachi Lowlands)	Central Meteorological Observatory; Hirata *et al*. (2003); Satake *et al.* (2006)
1973	7.8	Nemuro-oki	80	40	3	+100	5-10 (Hanasaki)	Japan Meteorological Agency; Shimazaki (1974); Kasahara (1975); Kasahara and Kato (1981); Kato (1983); Satake *et al*. (2005); Tanioka *et al*. (2007)
2003	8	Tokachi-oki	160	42	4.3	>1 <90	<60	Japan Meteorological Agency; Honda *et al*. (2004); Miura *et al*. (2004); Miyazaki *et al*. (2004); Tanioka *et al*. (2004); Baba *et al*. (2006)

[1] M – Magnitude;
[2] L – Rupture length (in km);
[3] D – Rupture depth (in km);
[4] Deformation in red represents offshore geodetic and GPS data used to estimate afterslip distribution following the 2003 Tokachi-oki earthquake (Baba *et al.*, 2006).

The study of tsunami deposits provides a valuable archive for investigating the recurrence of earthquakes in Hokkaido. In the eastern coastal lowlands, for example, Sawai *et al*. (2009) describe evidence for 15 tsunamis that were deposited between 200 and 6,000 cal. yr BP, based on stratigraphic studies of sediment sequences of between 2 and 4 m thick. The intervals between the inferred tsunamis average nearly 400 years and range from as little as a century to a millennium. This analysis assumes that each tsunami layer is associated with a distinct, locally-generated plate-boundary earthquake. However, it is known from several data sources that Japan is also occasionally struck by tsunamis generated from far-field earthquakes (e.g. Satake *et al.*, 1996), or such layers may even represent possible tsunamis from submarine landslides (c.f. Storrega Slide; Dawson *et al*. (1988)). The recurrence intervals described by Sawai *et al*. (2009) are therefore maximum estimates.

There is widespread evidence for raised Pleistocene marine terraces on Hokkaido that provide clear evidence for long-term uplift and RSL fall (Okumura, 1996). However, this uplift contrasts with the geological data from the late Holocene that record only minor coseismic uplift (at best) and in many instances negligible uplift or even subsidence during recent earthquakes. The long-term uplift is also in conflict with the chronic subsidence recorded in recent tide gauge and GPS data archives referred to above. It has been suggested that apparent contradictions can be explained by a two-phase earthquake cycle in which large multi-segment earthquakes offshore cause a deep slip on the down-dip extension of the plate boundary that causes postseismic crustal uplift and RSL fall (Sawai *et al.*, 2004b; Kelsey *et al.*, 2006).

This model is developed based on detailed investigation of the sedimentary changes associated with the most recent large plate-boundary earthquake on the Hokkaido coast, dated using tephra and radiocarbon methods to *c*. AD 1650. Diatom data from a core collected from Mochiruppu by Sawai *et al*. (2004b) suggests that a period of pre-seismic RSL was followed by the deposition of a tsunami, preceding a 30-year period of uplift that saw a former tidal environment transformed into a freshwater wetland. This transient uplift is estimated to have been >1 m but less than 2 m (Atwater *et al.*, 2004) and was followed by subsidence that has also been reported from the 20th century tide-gauge records.

This particular pattern of RSL changes has thus far only been reconstructed for the AD *c*. 1650 event in eastern Hokkaido (Atwater *et al.*, 2004; Sawai *et al.*, 2004b). Micro- and macro-fossil analysis of other, older events, suggests patterns of land motions were potentially different to that associated with the AD *c*. 1650 event (e.g. Sawai and Nasu, 2005). Moreover, almost no biostratigraphic investigations exist for the period between *c*. AD 1700, when the aseismic uplift ended, and the start of tide-gauge records. It is not known, therefore, whether the assumed chronic subsidence of the 20th century is a persistent feature of the current interseismic period.

2.4.2 The Sawai *et al*. (2004b) elastic dislocation model

Sawai *et al*. (2004b) hypothesised that the 17th century earthquake ruptured the plate-boundary offshore, which then gave rise to unusual amounts of postseismic slip further down the plate boundary. These estimates of fault slip were incorporated into the elastic dislocation model of Savage (1983) to develop a predicted model of vertical displacement of the ground surface (Figure 2.11). This predicts that shallow coseismic rupture of the interseismic locked zone is followed by deep postseismic after-slip, down-dip from the zone of full interplate coupling.

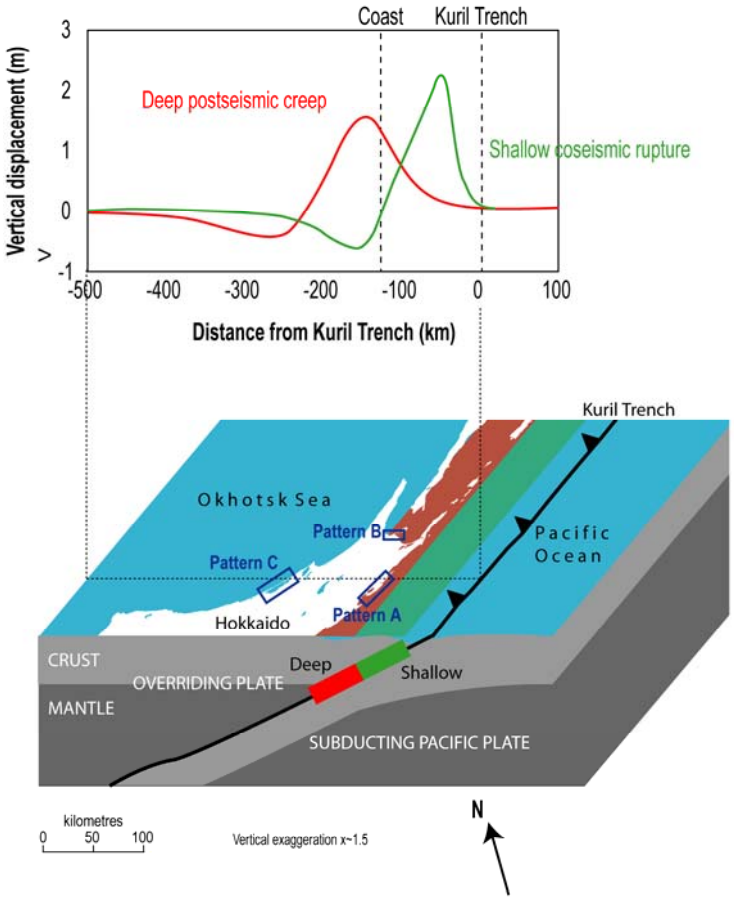

Figure 2.11 Vertical displacement computed by elastic dislocation modelling of fault slip (after Sawai *et al.*, 2004b) with a map illustrating locations of predicted different land movements referred to in the text. Red indicates the shallow seismic rupture of the interseismic locked zone (Mazzotti *et al*., 2000) at 15 to 55 km depth. Blue denotes areas of deep afterslip at 55 to 85 km, downdip from the zone of full interplate coupling.

The Sawai *et al*. (2004b) model suggests that sites along the Hokkaido coast should record different patterns of land movement that vary as a function of distance from the Kuril trench. Thus, for sites closest to the trench no coseismic movement is predicted as the fault (the ruptured plate boundary) does not reach beneath location A (e.g. pattern 'A'; Figure 2.11 and Figure 2.12). Such earthquakes may be responsible for the deposition of tsunami deposits that are not associated with significant coseismic deformation. Following plate rupture, however, the model predicts that metres of plate-boundary creep beneath eastern Hokkaido should raise the coast, since these areas are located directly above the area of slip on the thrust fault (as predicted by Savage (1983)). The coastline then readjusts further through slower interseismic subsidence.

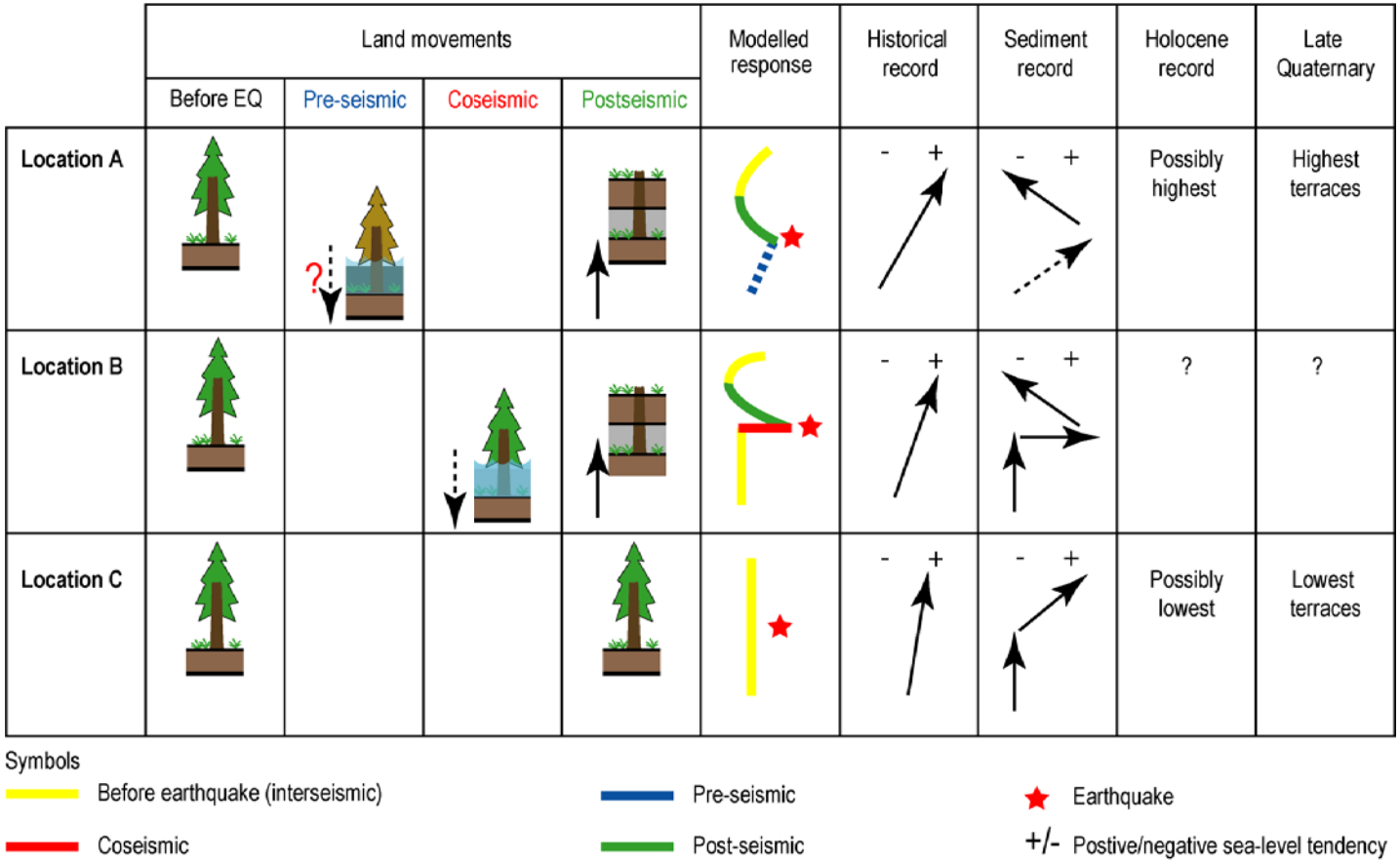

Figure 2.12 Schematic diagram showing the differential development of tidal marsh stratigraphies along the eastern Hokkaido coastline according to the proposed elastic dislocation model (Savage, 1983) of fault slip. Patterns A, B and C are associated with increasing distance from the Kuril Trench. RSL changes illustrated with associated sea-level tendencies. A positive sea-level tendency represents an increase in marine influence and a negative sea-level tendency represents a decrease in marine influence.

At Notsuke, no land-level changes prior to the earthquake are predicted since this area is located further away from the locked zone (pattern 'B', Figure 2.11 and Figure 2.12). Here the model predicts coseismic subsidence due to the elasticity of the continental plate, which follows a period of gradual uplift caused by postseismic creep. Finally, following an interplate earthquake, sites furthest from the trench should experience no coseismic tectonic movement because the plate boundary beneath this area is deeper than the interseismic locked zone (pattern 'C'). The model predicts land subsidence in this region because the zone of uplift is restricted to being above the area of slip on the thrust fault (e.g. patterns 'A' and 'B').

Testing the Sawai *et al*. (2004b) model requires comparison of geological and geodetic observations against measurements of the actual deformation measured during co- and interseismic intervals. Estimates of the coseismic displacement associated with the AD *c*. 1650 event are well constrained by micro- and macrofossils as well as lithostratigraphic evidence (e.g. Atwater *et al.*, 2004). However, direct observational data for the current interseismic period in Hokkaido are only available for the historic period. An alternative source of data for this interval is to use quantitative reconstructions of land movements generated by microfossil transfer functions developed on salt-marsh sediments.

2.5 CONCLUSIONS

This chapter provides a context for the research presented in this thesis by reviewing the evidence for land- and sea-level changes in passive and active coastal margins, focussing in particular on the processes operating to influence RSL change in Japan and Hokkaido. The main conclusions from this Chapter are as follows:

- A lengthy history of research on passive coastal margin coasts has developed an established methodology for RSL investigation that has, until relatively recently, not been rigorously applied to active coastal margins. In Japan, for example, palaeoseismic studies using salt-marsh RSL reconstructions have only recently been undertaken (Sawai *et al*., 2004a).
- Elsewhere, especially in Cascadia and Alaska, the application of detailed litho-, bio- and chronostratigraphic methods has enabled the development of new models of land- and sea-level changes that have helped develop new understanding of the so-called 'earthquake deformation cycle'. These methods enable analysis of multiple cycles of land motions throughout many earthquake cycles during the late Holocene.

- Tidal wetlands are ideal sedimentary environments for recording both the high energy tsunami as well as the more subtle changes in RSL change recorded during the interseismic period.
- A review of RSL change in Hokkaido and Japan more widely indicates considerable variability in the patterns observed. There is extensive evidence in the form of raised beaches, many dated by tephra chronology, for long-term uplift of the Hokkaido coastlines by several hundreds of metres. This provides evidence for long-term net uplift. Following the LGM lowstand, RSL rose in Japan as elsewhere in mid- and low-latitude regions unaffected by glacio-isostasy. This rise culminated in a highstand in many parts of Japan dated to the mid-Holocene, after which RSL fell to present.
- Changes in RSL in Japan and Hokkaido are characterised by abrupt steps associated with earthquakes. In Hokkaido, historical records suggest that land motions associated with large earthquakes have been minor, only a few decimetres at most. This contrasts with the evidence recorded from palaeoseismic research that suggests metre-scale changes in RSL accompanied large earthquakes.
- Elastic dislocation models provide a method of reconstructing land- and sea-level movements during the earthquake deformation cycle. However, a key weakness to current models of RSL change is a lack of detailed data from the current interseismic period, particularly between *c*. AD 1700 and the present. The interval of time is spanned by near-surface salt-marsh deposits that are potentially ideal recorders of tide-level changes that can complement the direct tide gauge and other geodetic observations from the 20th century.

CHAPTER THREE

Research Methods and Study Sites

3.1 INTRODUCTION

The primary aim of this thesis is to collect new information on RSL changes in Hokkaido over a range of temporal and spatial scales, paying particular attention to patterns during the current interseismic period. The main focus for the new data collection is the use of salt-marsh sediments as archives of recent RSL change over the last earthquake cycle, from *c*. 1700 to present. In addition, these new data are combined with analysis of other datasets that relate to both recent and longer-term RSL histories and land movements, including tide-gauge and GPS records, as well as Holocene and Pleistocene sea-level records (Figure 3.1).

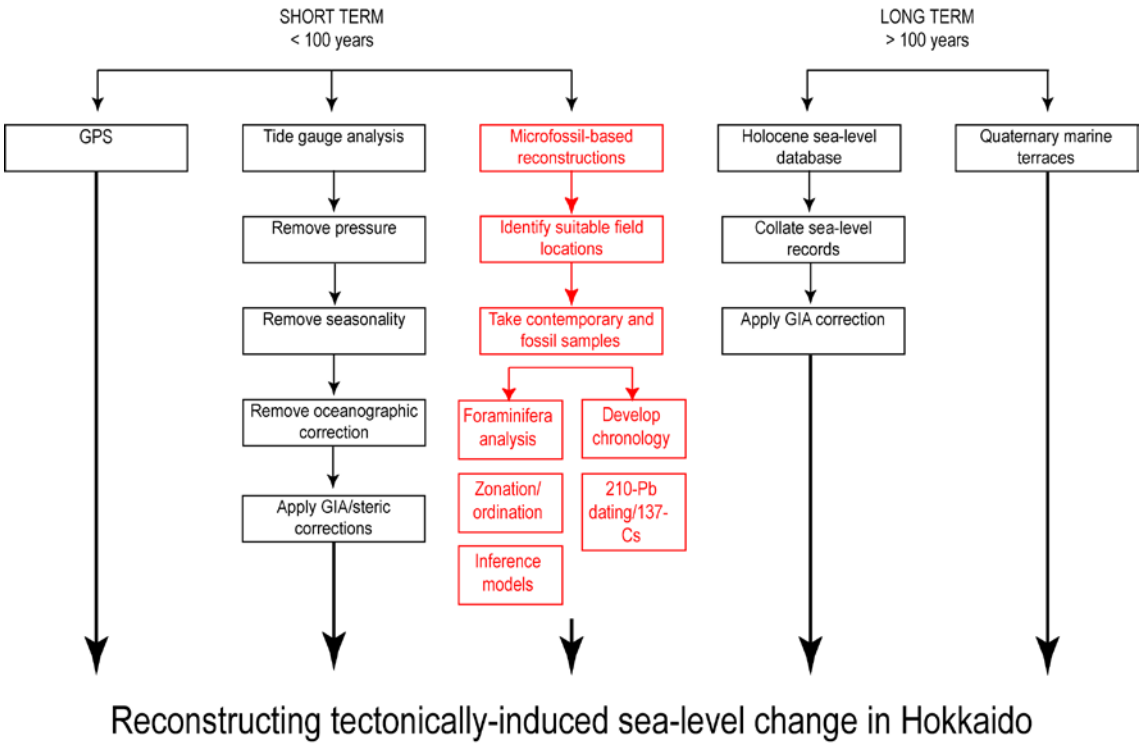

Figure 3.1 A summary of the thesis methodology used to understand vertical land movements on the Hokkaido coastline.

The aim of this chapter is to explain the methods used in my research and to outline the study area and the specific sites chosen for this study. I begin with a brief overview of the terminology used in sea-level research, before providing a summary of the litho-, bio- and chronostratigraphical approaches used (Table 3.1). I have selected the study sites to provide information on the spatial pattern of RSL changes, taking advantage of the fact that the east coast of Hokkaido is oriented perpendicular to the Kuril Trench. In introducing the field sites I provide an overview of the tectonic, geological and geomorphological characteristics of Hokkaido, before describing the specific sites visited during three field seasons (October, 2004; May, 2005; May, 2006).

Table 3.1 (overleaf) Techniques employed in this thesis**.**

Technique	Purpose	Sampling	Methodology	Output	Interpretation	Benefits	Constraints	References
Drilling/coring	Provide complete sedimentary sections through late Holocene sequences.	Study sites determined with respect to the existing elastic dislocation modelling in Hokkaido (Sawai *et al.*, 2004). Coring sites on the marsh identified from the inspection of existing maps and drilling holes.	Hand-gouge sampler used to quickly assess lithostratigraphy on marsh. Geoslice sampler[1], hand auger and Russian corer employed to collect samples for laboratory analysis.	Hand-gouge sampler – 2 cm core. Geoslice – rectangular sediment section (10 x 2 x 30 cm, width, depth and height). Hand auger – 5 cm diameter cores. Russian corer – 5 cm x 50 cm.	Drilling stopped after capturing the last earthquake cycle (typical sedimentary sequences are *c.* 1 m).	Penetrates clays to gravels. Usually good core recovery. In the case of a geoslice sampler, a 'peel' of the sediment gives a permanent record of the core.	Compaction of near-surface fine-grained sediments and peats. Some disturbance particularly of sands and gravels. Penetration and recovery affected by water-table in sands and gravels. Relatively imprecise depth measurements.	Ridgeway *et al.* (1998), Nakata and Shimazaki (1997), Takada and Atwater (2004)
Levelling	Provide precise heights of borehole tops with respect to national datum in Japan (m TP).	All borehole sites and modern foraminiferal and environmental sampling locations.	Nikon Totalstation levelling system used to relate core and modern sampling locations to benchmarks.	Altitude of borehole tops and modern sampling locations in relation to m TP.		Accurate altitudes to relate other measurements to.	Availability of benchmarks. Frequency of surveying.	Ridgeway *et al.* (1998)
Logging	Provide a basic sedimentological description of each core.	Assessed in the field, or the laboratory.	Visual inspection and measurement of core recovery, thickness of lithologies, depth of boundaries etc.	Interpreted core logs.	Lithologies based on Troels Smith scheme. Colours based on Munsell chart scheme.	Minimum of equipment required. Non-destructive.	Objective, but may vary with logger.	Troels-Smith (1955), Ridgeway *et al.* (1998), Long *et al.* (1999)
Particle size analysis (PSA)	Detailed sedimentological characterization.	Sub-samples from cores.	Particle size based on laser diffraction.	Particle size found between 0.04 and 2000 microns.	Folk classification of samples.	Quantitative classification from clay to sand.	Destructive of cores, time consuming, quality control difficult.	Ridgeway *et al.* (1998)
Loss on ignition (LOI)	To determine the organic content of salt marsh sediments.	Sub-samples from cores.	Oven drying, and then burning to ash at 550°C.	Organic content, as a percentage.		Quick, relatively cheap.	Sensitive to amount of sediment used. At higher temperatures water crystallation occurs which may influence results.	Ball (1964)
Foraminiferal analysis	To help define palaeoenvironment and validate sea-level index points.	Sub-samples from cores.	Wet sieving followed by identification and counting using an optical microscope.	Counts of identified species.	Classification into intertidal and subtidal environments using cluster analysis and detrended correspondence analysis.	Semi-quantitative palaeoenvironmental reconstructions.	Not suitable for freshwater environments. Subject to post-depositional changes.	Scott and Medioli (1980; Scott, 1986) (Horton *et al.*, 1999; Horton and Edwards, 2006) (Gehrels, 1994, 2000)
Radiometric dating	To provide an independent chronology for the most recent sediments.	Sub-samples from cores (average mass is typically 1 to 10 g, depending on the amount of ^{210}Pb expected).	Lead (^{210}Pb) and caesium (^{137}Cs) are measured using gamma spectrometry. The samples are freeze-dried and ball milled before analysis. Lead concentration is calculated using cumulative dry mass using dry bulk density.	Gamma radiation occurs at the high-energy, short wavelength end of the electromagnetic spectrum. For ^{210}Pb dating, the supported and unsupported components are recorded, and caesium activity is used as an independent method, providing activity levels at 1958, 1963 and 1986 can be identified in the record.	Because ^{210}Pb is produced both in the atmosphere and in sediments, it is necessary to make basic assumptions about the origin of ^{210}Pb in the sample of interest. The 'Simple' model, Constant Initial Concentration, and Constant Rate of Supply models are used where appropriate.	Facilitates correlation of events and processes between cores.	Possible early diagenetic movement of ^{210}Pb. Theoretically applicable to sediments that are younger than 250 years old. The optimum range for this method is 5 to 100 years.	Noller (2000), Goldberg (1963), (Appleby, 2001), Appleby and Oldfield (1978)

[1] The geoslice comprises a sample tray and a shutter plate. The sample tray is first pushed down, and then the shutter plate, and then both tray and shutter are pulled up having attached a bar for leverage.

3.2 RECONSTRUCTING FORMER SEA LEVELS

Existing approaches to the reconstruction of RSL on active coastal margins uses methodological protocols developed on the passive continental coastal lowlands of north-west Europe and the east coast of North America from the 1970s onwards (reviewed in Long and Shennan, 1994; Nelson *et al.*, 1996). These techniques, where applied appropriately, are able to distinguish between the signals of local and regional sea-level change in the stratigraphies of tidal wetlands, in addition to those changes associated with earthquakes and other, non-seismic processes (Nelson *et al.*, 1996). Sea-level research has its own particular vocabulary and hence I define below the key terms used in this thesis.

3.2.1 Definition of sea level

Sea level is often synonymous with Mean Sea Level (MSL). This represents the 'still water level' (with high frequency motions such as wind waves averaged out) taken over a period of time (usually a month or a year). Mean Tide Level (MTL) is the mean calculated from the mean high water and mean low water levels and is the most commonly used datum in the construction of sea-level curves. This is not synonymous with MSL because of the presence of higher frequencies in the tidal constituents. The use of MTL as the standard reference datum enables the comparison of data from different sites.

The mean high water spring tide (MHWST) level is an ecologically more important reference level than MTL and is used more frequently (Kidson and Heyworth, 1978; Shennan, 1982; Kidson, 1986; Shennan, 1986; Long, 1992; Shennan and Woodworth, 1992). This is because many sea-level indicators are derived from certain salt-marsh plants that normally accumulate around or above MHWST and are found beneath or above clastic sediment deposits. Estuaries, such as those on Hokkaido have mixed semi-diurnal tides; meaning two low and two high tides occur every day, resulting in a considerable difference in water levels. As such, up to seven tidal levels[1] are used for sea-level research for Hokkaido. From the lowest water-level elevation to the highest these are:

- **Lowest Astronomical Tide (LAT):** The lowest level that can be predicted to occur under average meteorological conditions and under any combination of astronomical conditions.
- **Mean Lower Low Water (MLLW):** The mean of the lower of the two daily low waters over a long period of time.

[1] When only one high/low tide occurs, these values are omitted in order to indicate the tide is diurnal at these stations.

- **Mean Higher Low Water (MHLW):** The mean of the higher of the two daily low water levels over a long period of time.
- **MSL** (as above).
- **Mean Lower High Water (MLHW):** The mean of the higher of the two daily low water levels over a long period of time.
- **Mean Higher High Water (MHHW):** The mean of the higher of the two daily high water levels over a long period of time.
- **Highest Astronomical Tide (HAT):** The highest level that can be predicted to occur under average meteorological conditions and under any combination of astronomical conditions.

3.2.2 Interpretation of former sea levels

A sea-level index point (SLI) is a sample of material with a known age, elevation, location and tendency that contains information about the altitude and direction of MTL at a particular point in time. The concept was developed during the International Global Correlation Programme (IGCP) Projects 61 and 200, and is described in '*The Manual of Sea-level Research*' (van de Plassche, 1986) as well as in a number of earlier papers (Preuss, 1979; Shennan, 1982; Tooley, 1982; Shennan *et al.*, 1983). A group of sea-level index points plotted on an age-altitude graph provides the basis for reconstructing a sea-level graph with individual data points possessing a defined age and altitude errors.

An index point must possess a tendency that describes whether the index point records an increase or a decrease in the proximity of marine conditions at a given point in time. A local positive tendency may, for example, be indicated by an up-core replacement of a semi-terrestrial freshwater deposit by a brackish-water salt-marsh deposit. The reverse constitutes a negative tendency. At the local scale, tendencies should not be confused with vertical changes in RSL, since a change in the proximity of marine conditions may reflect variations in sediment supply or a change in coastal configuration. However, where there is widespread evidence for synchronous changes in sea-level tendency at a given time, then the probability of such a change reflecting a vertical change in sea level becomes significantly higher. On tectonically active coastal margins, widespread coseismic movements can cause regional changes in sea-level tendency.

The terms transgression and regression have been used in a wide variety of contexts and, as identified by Shennan (1982) and Tooley (1982), inconsistencies in the use of the terms have led to much confusion. Transgression and regression refer to a change in sediment type recorded in coastal marsh stratigraphy associated with positive or negative tendency respectively. A transgression refers to a change in lithology up-core from a semi-terrestrial

to a shallow marine deposit and a regression represents the replacement up-core of a shallow marine deposit by a semi-terrestrial deposit.

The indicative meaning of a coastal sample describes the vertical relationship of the local environment in which it accumulated and a contemporaneous reference tide level (van de Plassche, 1986). The indicative meaning, which can vary between different indicators, comprises of the indicative range and a reference water level (Figure 3.2). The indicative range specifies the height range in which the coastal sample formed, expressed with reference to local water-level conditions such as HAT and MHHW.

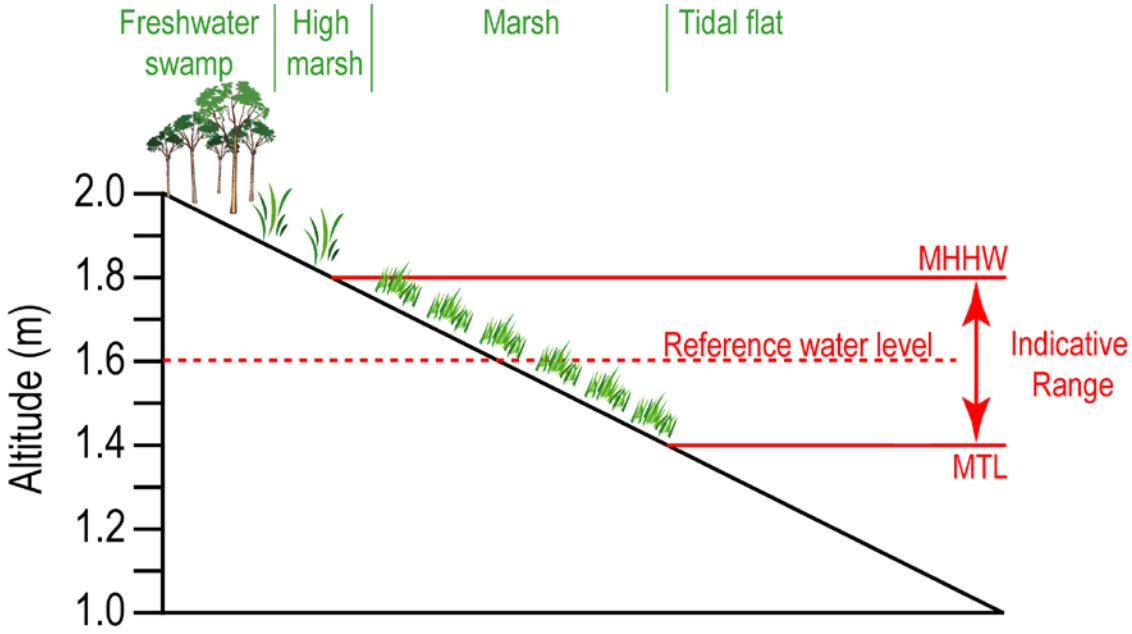

Figure 3.2 Schematic diagram illustrating the components of indicative meaning. In this example, a marsh peat forms between MHHW and MTL (the indicative range) and therefore its associated reference water level is equal to the midway point between the two tide levels (e.g. 1.6 m).

3.2.3 Lithostratigraphical methods

Stratigraphic survey

I used a combination of hand gouge corers (2 cm in diameter) and natural outcrops in tidal creeks to survey the stratigraphy along levelled cross sections at each study site. The lithostratigraphy was recorded using the Troels-Smith (1955) scheme of sediment notation (see Long *et al.*, 1999). The Troels-Smith (1955) scheme is widespread amongst sea-level scientists. The scheme is based on a set of clearly specified guidelines and, although the technique is subjective, the method provides a relatively simple, quick and accurate portrayal of the different components of any sediment unit.

Stratigraphic plots are presented in a simplified form using a stratigraphic scheme to aid visual interpretation. All elevations are plotted relative to MTL (m TP; metres Tokyo Peil). Sample cores were collected using different methods depending on the thickness of the sequence under study. In most cases, a large diameter (50 mm diameter) gouge corer was used to collect overlapping sequences of undisturbed sediment but I also used samples collected using a hand operated Geoslicer sampler (see Figure 3.3).

Figure 3.3 Photographs illustrating the use of a Geoslice corer. After the initial sampling tray is hammered into the sediment, a shutter plate is attached (A) and hammered into place. A handle is then screwed onto the Geoslice and is used to extract the sediment (C) ready for its lithostatigraphic description (D).

Once collected in the field, samples were carefully cleaned to remove any possible contamination and transferred from the gouge sampler or the Geoslice sampler into half-cut plastic piping or a plastic sealed wooden box and returned to Durham University for analysis. Samples at Durham were stored in refrigerated conditions at 4ºC prior to sampling.

Grain-size Analysis

Grain size is a fundamental property of sediment particles, affecting their entrainment, transport and deposition. Grain-size data provide important information regarding sediment provenance, transport history and depositional conditions (Friedman, 1979; Sheridan *et al.*, 1987; Allen and Thornley, 2004; Pye and Blott, 2004). For particle-size analysis, sub-samples of sediment between 0.5 - 8 g (depending on original organic content) were oxidised using 20 mls of 20% hydrogen peroxide (H_2O_2) in a hot water bath (*c*. 80°C) for 2-4 hours. The removal of all plant material, which frequently involved multiple H_2O_2 treatments, was followed by centrifuging (for 4 minutes at 4,000 rpm) and rinsing of samples in distilled water prior to adding of 2 mls of the dispersant sodium hexametaphosphate ($NaPO_3$; 3.3 wt %) buffered with sodium carbonate (0.7 wt %). For clay-rich sediments, samples were immersed into an ultrasonic bath for 30 minutes prior to analysis to further aid disaggregation. Analysis of the samples used a Coulter™ LS 230 laser granulometer with PIDS (polarisation intensity differential scattering) at Durham University. Laser grain-size analysis is based on the interaction between light and particles, and generates rapid and accurate sizing of particles over the size range 0.04 – 2000 μm. To further aid particle dispersion, samples were sonicated during loading. Grain size divisions are defined according to British Standards and analysed in Gradistat (Blott and Pye, 2001).

The digestion process removes the organic component of the sediment, reducing the samples analysed through laser granulometry to a common basis. Although widely practised, treatment by H_2O_2 removes all plant material indiscriminately. This organic matter includes detritus that constitutes a co-deposited part of the sediment matrix. Allen and Thornley (2004) argue from their study of estuarine silts of the Severn Estuary, UK, that H_2O_2 digestion removes valuable indigenous material as well as less valuable extraneous debris (stems of prior plants and post-depositional root matter). These authors advocate hand picking of visible extraneous plant material; however this approach is not common in sea-level studies, partly because deciding on which material to remove or leave can be a somewhat arbitrary process.

Loss on ignition

Loss on ignition (LOI) data provides a measure of the organic content of samples. This technique involves oven drying a sediment sub-sample (approximately 5 g) to a constant mass (typically at a temperature of 105ºC for an average of 12 hours) and then placing samples in a muffle furnace pre-heated to 550°C for 4 hours. During this time, the organic content is combusted to ash and carbon dioxide. A dessicator cools the samples and crucibles between stages, to prevent moisture loss. The mass loss of each sample is proportional to the organic-matter content of the soil and LOI is determined as follows:

$$LOI_{550} = \frac{(DW_{105} - DW_{550})}{DW_{105}} x100 \qquad \text{Equation 3.1}$$

Where;

LOI_{550} = loss on ignition at 550ºC (%);

DW_{105} = the dry mass (g) of the sample before combustion;

DW_{550} = the dry mass (g) of the sample after combustion;

Measuring LOI is a relatively rapid method for quantifying the organic content of coastal sediments but the conversion of the organic matter to a carbon content may be difficult. This is because at the temperatures used, carbonates can remain stable and are thus are not measured by the LOI method (Rabenhorst, 1988; Schulte and Hopkins, 1996; Wright *et al.*, 2008).

3.2.4 Biostratigraphical methods

Foraminiferal studies

Microfossils such as diatoms, pollen, foraminifera or testate amoeba found within estuarine or salt-marsh sediments are widely used as sea-level indicators. Their value centres on them possessing a quantifiable vertical relationship to a reference water level. Previous work on the Hokkaido coast has made extensive use of diatoms as a sea-level indicator, but prior to this PhD only one published study had explored the potential of foraminifera (Scott *et al.*, 1995). Through my Master's thesis (Thomson, 2004), I demonstrated the potential of foraminifera as complementary sea-level indicators to previous diatom work (e.g. Sawai *et al.*, 2004a).

Foraminifera are prokaryotes (single-celled organisms) that construct their tests from detrital sediment grains (agglutinated foraminifera), or through the secretion of calcium carbonate (calcareous foraminifera). A suite of widespread agglutinated taxa typify

foraminiferal species found on temperate salt marshes (Phleger, 1970; Murray, 1971; Phleger, 1977; Sen Gupta, 1999). These include *Ammotium salsum*, *Arenoparrella mexicana*, *Jadammina macrescens*, *Miliammina fusca*, *Tipotrocha comprimata*, and *Trochammina inflata*. Calcareous taxa including *Ammonia beccarii* are also present.

Previous work shows that species dominance can be used to distinguish low-marsh foraminiferal assemblages from high-marsh ones. The high-marsh zone is particularly useful for reconstruction purposes since the zonation of individual species in this area of the intertidal zone can be particularly well defined. Significantly, a near ubiquitous, monospecific assemblage of *Trochammina macrescens* (or *J. macrescens*) is often reported just below the level of MHHW, above which all foraminifera rapidly disappear. Scott and Medioli (1978; 1980b) suggested that this assemblage zone could be used to locate former MHHW with a precision of ± 0.05 m. Since their seminal paper, other vertical assemblage zones have been identified across a wide range of marsh environments (e.g. Gehrels, 1994; Horton *et al.*, 1999a; Edwards and Horton, 2000), although variations in salinity and tidal regime may influence their precise composition and elevation (de Rijk, 1995a; de Rijk and Troelstra, 1997).

In addition to their almost ubiquitous nature throughout salt-marsh environments, foraminifera are normally well preserved and can be identified to the taxa level in fossil-marsh deposits (Scott and Medioli, 1980b; Scott, 1986). Although diatoms are commonly used as a quantitative proxy for sea level (e.g. Zong and Horton, 1999; Horton *et al.*, 2006; Szkornik *et al.*, 2006), particularly on seismically active coastlines (e.g. Hemphill-Haley, 1995; Hamilton and Shennan, 2005; Cochran *et al.*, 2007) foraminifera are the chosen proxy used in this study.

Many palaeoseismic studies have used foraminifera successfully for earthquake (Guilbault *et al.*, 1996; Cundy *et al.*, 2000; Hayward *et al.*, 2004a; Hawkes *et al.*, 2005) and tsunami research (Hawkes *et al.*, 2007). A few investigations on foraminifera from the western Pacific exist, including at the sites of Hiritappu and Mochiruppu (Hada, 1936), Akkesh-ko (Morishima and Chiji, 1952), and Saroma-ko (Yoshida, 1954; Takata *et al.*, 2006), whilst Scott *et al*. (1995) have demonstrated their potential use in sea-level reconstruction on Hokkaido's eastern marshes. Furthermore, the availability of high-quality diatom analysis from the same area offers the possibility of comparing and contrasting reconstructions by different microfossil groups, offering the potential for more robust reconstructions.

Quantitative reconstructions using microfossils

Improvements in microfossil-based reconstructions of RSL have increased the accuracy of indicative meanings and expanded the range of sediments that can be employed in sea-

level studies. Quantitative sea-level reconstructions using microfossils involve making inferences from contemporary data that are then applied to fossil sequences (Birks and Birks, 1980). This relationship may be quantified using a transfer function approach. In the late 1990s, application of transfer function analysis, widely used on foraminifera from deep marine cores to reconstruct climate change, revitalised studies of Holocene sea-level change on many low energy sedimentary shorelines (e.g. Guilbault *et al.*, 1995; Horton *et al.*, 1999a; Gehrels *et al.*, 2001). The term 'transfer function' is used to describe the set of regression equations that is developed from modern relations between relative abundance of microfossil species and environmental data, such as elevation (Gehrels, 2007). Calibration is then used to reconstruct past elevation from microfossil assemblages in cores or outcrops with decimetre precision.

Ample scope exists for improving the reliability, accuracy and precision of the reconstructions. In terms of modern training sets, these include questions such as: is there an optimum sample size; what constitutes a geographic 'region'; and at what elevation does the vertical relationship between foraminifera and the tidal frame become insignificant? The distribution of foraminifera is affected by various factors other than elevation that can affect the distribution of species within the intertidal zone (Table 3.2). In terms of the application of transfer functions to fossil material, important questions still surround the nature and extent of the various taphonomic processes that act to alter the composition of subsurface foraminiferal assemblages, as well as ways to assess the integrity of a sedimentary sequence and its accumulation history.

Table 3.2 Factors affecting the distribution of foraminifera on salt marshes.

Factor	Explanation
Elevation	The differing extent to which foraminifera can tolerate exposure, or, alternatively, the frequency of tidal submergence, results in a vertical zonation of distinct foraminiferal assemblages.
Salinity	The balance between evaporation and infiltration of seawater controls the level of salinity across the intertidal zone. Species have their own tolerance level, and morphological variations will occur if foraminifera live outside this critical range. Salinity may not be directly related to elevation.
Organic content	Foraminifera live as epifauna or infauna between the roots of salt marsh vegetation. Variations in surface and near-surface organic content can influence assemblages in the contemporary environment.
pH	For survival, it is critical that foraminifera are constrained to a narrow pH since exceeding these limits impacts both the protoplasm cell and the calcareous test. pH can be influenced by several factors, including groundwater, organic matter content, as well as local geology.
Sediment texture	Agglutinated foraminifera use sediment particles between 2-20μm as building material for their tests (de Rijk and Troelstra, 1997). An absence of these particles can limit the occurrence of agglutinated foraminifera.

Sample collection

To asses the modern foraminifera and environmental characteristics over the marshes of Hokkaido, I established stations along transects that run from the freshwater swamp to the mudflat, spanning the intertidal zone from above HAT to LAT (where possible) in order to record the full range of contemporary environments that I expected to encounter in the interbedded peat- and mud-sediment sequences described by previous authors from Hokkaido (e.g. Atwater *et al.*, 2004; Sawai *et al.*, 2004a). Sampling took place at a 0.05 m

vertical resolution for all transects, with additional stations located where there were marked changes in topography and vegetation. I levelled stations to national datum (m TP) using a Leica (TCR307) total station with enhanced distance measurement (EDM) and a survey staff.

Sampling at each station involved the collection of a standard volume of 10 cm^3 (10 cm^2 by 1 cm thick) sediment for foraminiferal analysis. The protein stain Rose Bengal was added to samples in the field to enable subsequent identification of living versus dead foraminifera (Walton, 1952). Tests identified under the microscope that contained protoplasm within the last few chambers were considered living at the time of collection (following Murray and Alve, 1999). To understand the controlling environmental parameters on foraminiferal distribution, a further 15 cm^3 (15 cm^2 by 1 cm thick) of sediment was collected from the same site and returned to the laboratory for LOI and grain-size analysis. Sample pH and salinity were measured in the field using a Eurotech PC10 Waterproof Handheld pH/Conductivity Metre and a Handheld Salinity Refractometre[2].

In the laboratory, foraminiferal sample preparation followed standard procedures (Scott and Medioli, 1980b; de Rijk, 1995a; Scott *et al.*, 2001; Horton and Edwards, 2006). On return to the laboratory, each sample was wet sieved through 500 and 63 µm sieves and decanted. The >500 µm fraction was scanned before being discarded to ensure no foraminifera were present. I counted tests wet under a binocular microscope at typical magnifications of x40 and x50. Counts of approximately 250 specimens were obtained for most stations (following Phleger, 1960).

Taxonomy

Salt-marsh foraminiferal assemblages are typically dominated by less than 10 benthic species, reflecting the marginal-marine nature of intertidal environments. A taxonomic list and plates of the key salt marsh taxa recovered are presented in Appendix A.

Prior to this research there has only been one previous study of contemporary salt-marsh foraminifera on Hokkaido around Nemuro Bay on the east coast (Scott *et al.*, 1995). Therefore, the taxonomy used here follows a variety of publications from Japanese marsh environments (Nomura and Seto, 1992; Scott *et al.*, 1995; Takata *et al.*, 2006), and further afield on temperate marshes in north-western Europe and north America (Murray, 1979; Horton and Edwards, 2006; Vance *et al.*, 2006) and elsewhere (Brönnimann and Whittaker, 1988; Brönnimann *et al.*, 1992; Woodroffe, 2006).

[2] Salinity refractometres measure concentrations of dissolved solids (e.g. salt) in aqueous solutions. Light passing through the liquid causes the refracted angle to be shown on a scale.

Unlike other temperate marshes, calcareous foraminifera are almost completely absent from the Hokkaido marshes and were limited to a small number of live specimens in tidal flat samples. Consequently, I group some minor taxa at the genus level (e.g. *Elphidium* spp.), especially where species or ecophenotypes may be prevalent (e.g. *Ammonia* spp.). Recent DNA sequencing has identified the morphological distinction of molecular types of Ammonia (Hayward *et al.*, 2004b), with limited geographical range. The most likely molecular type of Ammonia common to the northern Japanese archipelago is *Ammonia aomoriensis*[3] (Asano, 1951), however, without more detailed analysis all *Ammonia* taxa are grouped as one.

Scott *et al*. (1995) combined *J. macrescens*, *Jadammina polystoma* and *Balticammina pseudomacrescens* into a single *Trochammina macrescens* group. Here, I split this group into *B. pseudomacrescens* and *J. macrescens* on the basis that the former has a straight suture, an open umbilicus a large umbilical cavity, whereas the latter has a curved suture and a smaller and closed umbilicus (de Rijk, 1995b; Gehrels and van de Plassche, 1999: 90). In Maine, Gehrels and van de Plassche (1999) note that *J. macrescens* occurs in high abundances near the upper edge of the marsh, while numbers of *B. pseudomacrescens* are more spatially variable. These two distinct foraminifera have also been found in Oregon, on the west coast of the United States (Hawkes *et al.*, In Press), so their presence in marshes of the Pacific is already recognised.

Some species or ecophenotypes are more recognisable than others. The genus *Haplophragmoides* is notable for its relatively subtle distinction between *H. wilberti* and *H. manilaensis* and consequently whilst some studies combine the different species at genus level (Gehrels *et al.*, 2001; Massey *et al.*, 2006; Horton and Culver, 2008), others sub-divide the taxa (Vance *et al.*, 2006; Horton and Culver, 2008) in an attempt to obtain greater ecological information. For some individual specimens, which display an intergradational series between *H. wilberti* (with the outline of its test rounded), and *H. manilaensis* (with its test scalloped) identification can be problematic. In this study, where it was not possible to definitively assign an identification to species level, *Haplophragmoides* spp. is used. Indeed, de Rijk (1995a) noted strong similarities between the two forms because of interspecific variability.

It is worth noting that the taxonomic issues surrounding the differentiation of genus, species or ecophenotype identified above do not influence the use of foraminifera as modern analogues for fossil studies, providing these species or forms are identified consistently in both contemporary and fossil samples.

[3] *Ammonia aomoriensis* is characterised by an elongated, pointed folium, with weak imperforate secondary calcite. Often one or more small umbilical bosses are visible, and the radial sutures are perpendicular to the spiral suture on the spiral side (Hayward *et al*. 2004).

Factors affecting the ecological and statistical reliability of sea-level reconstructions

Many factors affect the ecological and statistical reliability of sea-level reconstructions. These include (i) the assemblage constituents; (ii) infaunal foraminifera; and (iii) spatial and temporal factors affecting foraminiferal assemblages. Sampling strategy plays an integral role in improving the likelihood of 'good' reconstructions of former sea levels through the accurate quantification of individual taxa and their relationship to elevation.

To address these issues, I assessed the spatial variation in microfossil assemblages by completing three contemporary transects at one of the salt-marsh sites (at other sites I use a single transect). I also assessed the infaunal component of the fossil records by collecting two cores through the upper 20 cm of sediment from one salt marsh and counting the depth to which live foraminifera occur.

Live, dead and total foraminifera

The choice of assemblage used for palaeoecological studies remains controversial. The integration of seasonal and temporal fluctuations are considered by some authors (Buzas, 1968; Scott and Medioli, 1980a; de Rijk, 1995b; Jennings *et al.*, 1995; Scott *et al.*, 2001) to warrant the choice of total foraminiferal population (live and dead) as the preferential choice for palaeoecological research. However, Murray (1982; 1991; 2000) argues the total assemblage combines data on living assemblages that have yet to undergo post-mortem taphonomic change. Only a long-term monitoring study of life assemblages over time is able to characterise the life cycle of populations of foraminifera (Buzas, 1968). In this study, I use the dead assemblage for my reconstructions, following the identification of only limited infaunal foraminifera in near-surface sediments (see Chapter Four).

Infaunal foraminifera

In this study I will use the commonly collected sampling depth for studies of the modern distribution of foraminifera, as the uppermost one or two centimetres of sediment (Scott and Medioli, 1980b, a; Jennings and Nelson, 1992; Gehrels, 1994; de Rijk, 1995b, a; Horton, 1999; Horton *et al.*, 1999c, a; 2003; Edwards *et al.*, 2004b; Duchemin *et al.*, 2005; Horton *et al.*, 2005; Tobin *et al.*, 2005). This sampling procedure assumes that intertidal foraminifera are primarily epifaunal. However, infaunal foraminifera have been reported in a variety of salt marshes. Infaunal occurrences may change the composition of dead assemblages that accumulate in sub-surface sediments (Akers, 1971; Goldstein and Harben, 1993; Kitazato, 1994; Goldstein *et al.*, 1995; Ozarko *et al.*, 1997; Goldstein and Watkins, 1998; Saffert and Thomas, 1998; Patterson *et al.*, 1999; Hippensteel *et al.*, 2000; Culver and Horton, 2005; Duchemin *et al.*, 2005). Goldstein and Harben (1993) found the

infaunal *A. mexicana* to be virtually absent in surface sediments but abundant in sub-surface assemblages.

Spatial and temporal factors affecting foraminiferal assemblages

The differences in environmental variables over short lateral distances can cause variations in the assemblage composition of foraminifera and their elevational ranges between and within sites (Scott and Medioli, 1980b; Scott and Leckie, 1990; Jennings and Nelson, 1992; Gehrels, 1994; de Rijk, 1995b). Furthermore, the contemporary training set should also be sufficiently comprehensive that fossil samples have contemporary analogues.

The slowly subsiding coastlines prevalent throughout eastern Hokkaido today may provide poor analogues for the uplifting coasts implied by the fossil record. Furthermore, the contemporary environments that prevailed prior to, and immediately after the earthquake event, cannot be sampled directly and this may reduce the reliability of reconstructions during this period of the earthquake cycle. Temporal variations in microfossil distribution can also be significant. For example, Horton and Edwards (2003) concluded that the variations of contemporary foraminiferal distribution across the intertidal zone during an annual cycle may modify the elevations of the zonal boundaries by as much as 0.9 m.

Because of these reasons, and of the time limitations in this thesis, I choose to develop a regional transfer function based on a compilation of contemporary data from each of my sample sites, rather than attempting to develop local transfer function models for each field site. I recognise that this is a potential limitation to my study, but the advantages of this approach in terms of covering a wide range of environments took precedent, especially given the large changes in environment that have occurred in the last 200 yrs or so, based on previous RSL research in Hokkaido.

Standardising water levels

Elevation is used in this thesis as a proxy for flooding frequency and hydroperiod/duration resulting in subaerial exposure (Horton and Edwards, 2006: 35). Whereas in the open ocean, the tidal constituents comprise a limited number of well-defined astronomical frequencies, in coastal regions this spectrum becomes more complex with the non-linear interaction of the astronomical, diurnal and/or semidiurnal constituents. These distortions are invariably incorporated into the geological record and, although often acknowledged by sea-level scientists, their significance on the resulting record is largely ignored (van der Molen, 1997).

Tidal distortion may however invalidate the assumption that the level of Mean High Water (MHW) approximates the elevation of a peat sample at the time of deposition. From his research on the Great Marshes of Massachusetts, van der Molen (1997) observed significant temporal and spatial variability in MHW. Observed differences resulted in up to 0.20 m (6.67% of the tidal range) and 0.55 m (18.3% of the tidal range) in his temporal and spatial dataset. The tidal parameters that are typically available for Hokkaido (and elsewhere) are based on data collected (or predicted) for open-coast sites. However, tidal distortion occurs as tides propagate into the confinement of estuaries. Tidal distortion is an important process on low energy environments, causing the compression of tidal constituents and consequently affecting water chemistry, sediment accretion rates, and the amount of organic matter deposited on the marsh. To accurately quantify the tidal cycle at each marsh, local tide gauges and data loggers should be employed, but in their absence, repeated levelling to sea level (particularly around high tide) helps to quantify the uncertainty with the tidal-gauge derived parameters available from the open coast.

In Hokkaido, only nine tide gauges are calibrated with reference to the Japanese national datum, including just three (Kushiro, Monbetsu and Wakkanai) on the eastern and northern coastlines. The paucity of tide gauges, particularly along the north-eastern coastline, is compounded further by a complicated tidal regime reflecting large differences in tidal amplitude between the Japan Sea and the Okhotsk Sea (Odamaki and Iwamoto, 1999). An amphidromic point exists in the Soya Strait (between the northern tip of Hokkaido and Sakhalin) and consequently tidal amplitude increases away from the Soya Strait. Although the tide-gauge station of Monbetsu is sufficiently close to be used for the eastern sites located around Abashiri, the most western site, Sarfutsu-toh is more complicated. The tidal harmonic constants increase progressively as you travel away from the amphidromic point in the Soya Strait and therefore the tide-gauge stations of Monbetsu and Wakkanai fail to capture the shape and pattern of the tidal cycle at Sarfutsu-toh. Fortunately, the secondary port of Hama-Onishibetsu is located just 2 km away from the salt marsh. Although not levelled to Japanese national datum, by assuming the amplitude of MHHW remains constant along the northern coastline (as is the case at the gauges of Wakkanai and Monbetsu), Hama-Onishibetsu can also be assigned an elevation of 0.36 m TP for MHHW. The tidal range of Hama-Onishibetsu (between MHHW and MLLW) is 0.5 m generating MLLW at an elevation of -0.14 m TP (Table 3.3). By assigning a MLLW and MHHW in relation to national datum, Sarfutsu-toh can be brought into a regional training set.

Table 3.3 Present tidal range on the northern coastline of Hokkaido. Data from Japanese Hydrographic and Oceanographic Department (2006). All altitudes in black with reference m TP.

Location	Station No.	Position		MHHW	MLLW	Tidal range (MHHW-MLLW)
		Lat	Long			
Wakkanai	60	45 24	141 41	0.36	0.16	0.2
Monbetsu	53	44 21	143 22	0.36	-0.44	0.8
Hama-Onishibetsu	56	45 20	142 10	0.6	0.1	0.5
Sarfutsu-toh		45 18	142 11	0.36	-0.14	0.5

The development of regional transfer functions requires combining data from different sites with different tidal ranges. This necessitates a correction process that converts all local elevations to a standardised water-level index (SWLI), which scales each sample against its local tidal constituents (based on Zong and Horton, 1999) :

$$X_{ab} = 100\left(\frac{A_{ab} - MTL_b}{MHHW_b - MTL_b}\right)$$

Equation 3.2

Where,

X_{ab} = the SWLI of station/tide level *a* at site *b*;

A_{ab} = is the measured altitude (m TP) of station/tide level *a* at site *b*;

MTL_b = is the mean tide-level (m TP) at site *b*;

$MHHW_b$ = is the mean higher high water at site *b*.

Other studies use alternative variants of SWLI by incorporating different tidal parameters to improve the correlations with samples at lower ends of the environmental gradient (Horton *et al.*, 1999c; Horton *et al.*, 1999b, 2000; Horton and Edwards, 2006). In this study, my focus is on quantifying sea-level change over the last earthquake cycle through analysis of short cores comprising (mainly) high-marsh sediments, thus a SWLI based on MTL and MHHW as the key tidal datums is the most appropriate for this investigation.

3.2.5 Sources of error in sampling

Fossil sampling errors

A series of largely unavoidable errors arise when using a hand-operated corer including the angle of borehole, the measurement of depth and compaction (Shennan, 1982). Sampling density is an additional factor. Unconsolidated sediments in intertidal environments are prone to compaction and consolidation processes that result in volumetric reductions of sediment, altitudinal displacement of strata and surface subsidence. On seismic coastlines, these problems are compounded further by ground shaking that may, depending upon the nature of postseismic recovery, result in an over or under estimation of land movements.

On 27 March 1964, an earthquake of moment magnitude 9.2 was felt along the south coast of Alaska causing ground shaking for approximately 300 seconds. This local seismic shaking added to the coseismic subsidence by causing local unconsolidated deposits to settle (Plafker, 1969; McCulloch and Bonilla, 1970). Following the subsidence, Atwater *et al*. (2001) concluded that post-earthquake aggradation quickly filled the space made available from the subsidence of the 1964 earthquake, including that created by compaction (*c*. 10 cm). Figure 3.4 illustrates this process schematically based on the observations from Alaska.

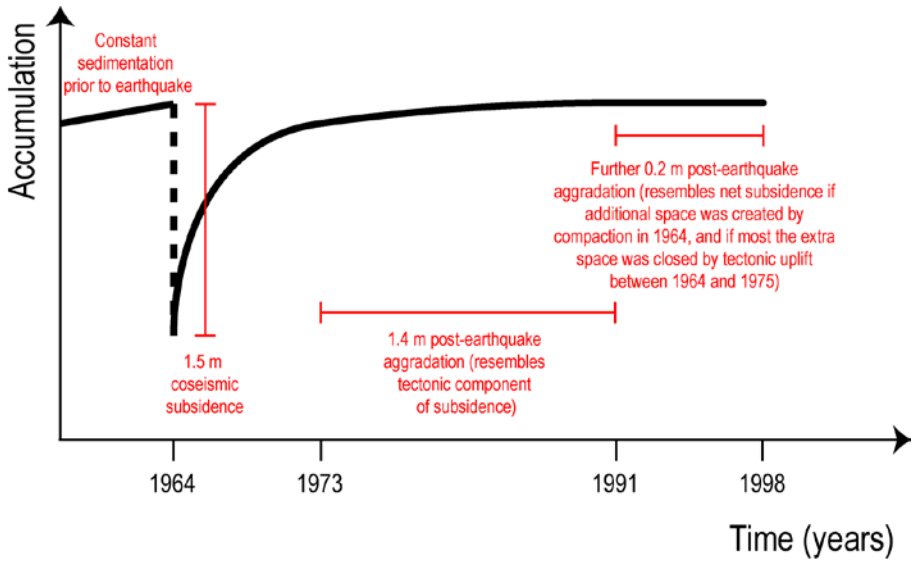

Figure 3.4 Schematic diagram of post-earthquake changes in accumulation and land level following the 1964 Alaska earthquake. Text taken from Atwater *et al*. (2001).

Compaction is strongly dependent upon the nature of the substrate; samples with high organic content are likely to be affected far more than those deposits with a high sand content (Shennan *et al.*, 2000b). Clastic deposits are less affected by post-depositional displacement in altitude, potentially just *c*. 10% of their height may be lost (Paul and Barras, 1998). Since one of my aims is to reconstruct interseismic RSL following the most recent 17th century AD event, the focus on shallow sequences limits (but does not entirely remove) potential compaction errors. Over the short-time period of interest I assume no such changes in palaeotidal range. It is possible that local changes in tidal inlet and tidal basin configuration caused by reclamation and sediment infilling may have influenced tidal range but quantifying this potential effect is beyond the scope of this thesis.

Modern sampling errors

For all marshes except Mochiruppu (which had been previously levelled to sea level), nearby benchmarks are available that enable elevations to be expressed as a function of national datum. The survey error is a product of levelling error and the difference between

the elevation of the benchmark and the national datum. This is subject to slight deformation in the interseismic phase of the earthquake deformation cycle, however this is considered to be included in the levelling error.

It was more difficult to relate subtidal sample elevations to Tokyo Bay datum because I was unable to survey these sites to a local benchmark. In these cases, I used hourly readings of tidal height at Kushiro to relate time-still water levels to the national datum (Figure 3.5). Akkeshi-ko is located nearly equidistant between the tidal stations of Kushiro and Hanasaki (located 60 km northeast). My own levelling survey results located close to high tide indicate that the Kushiro tide gauge better represents tidal levels at Akkeshi. The tidal distortion in Akkeshi Bay is not known. However, based on local survey of time-still water level, I observed a 19 minute delay between the low tide at Kushiro and Akkeshi[4] on the 24 May 2005. To estimate error and check accuracy, the elevations of the landward samples collected using the time-still water method were compared with the elevations calculated using the local benchmark. For the six samples where both methods were applied the maximum deviation was 7.9 cm and the average was 1.7 cm. To provide conservative estimates, a larger vertical error is introduced when collecting these samples from a boat in order to reflect the additional complexities associated with measuring the depth of the water column (see Table 3.4).

[4] Based on predictions at Kushiro and Akkeshi Wan. Admiralty EasyTide http://easytide.ukho.gov.uk/EasyTide/EasyTide/index.aspx

Figure 3.5 Subtidal sampling at Akkeshi-ko. (A) Sampling in Akkeshi-ko, with Ekman Bottom Grab sampler. At each location, the sampler is used to extrude the bay sediments and the depth of time-still water is noted to be used to calculate the elevation of the sample using the nearby Kushiro tidal-gauge station. (B) The grab sampler is emptied into a shallow tray, and the uppermost sediment is scraped for bio-, and lithostratigraphical analysis (C).

Table 3.4 Estimated errors accumulated during modern and fossil sampling in this thesis (after Woodroffe, 2006).

Source of error	Estimated total elevation error (cm)
Modern sampling in intertidal environments:	
Levelling error	5
Benchmark to national datum	5
Total root squared error	7.07
Modern sampling in subtidal environments:	
Angle of staff in water when measuring depth	3
Measuring depth of water column due to waves	2
Variation in timed-still water due to waves	5
Variation in tidal time and height between Kushiro tide gauge and field site	5
Total root squared error	7.94
Core sampling:	
Measuring depth using hand corer	1% of core depth
Angle of borehole	4
Sampling density	14
Levelling error	5
Benchmark to national datum	5
Total root squared error	16.22[1]

[1] Represents the total error of a core sample taken at 1 m depth. For the short sample cores used in this study, the error associated with measuring the depth using a hand corer is negligible.

Sampling errors are calculated using the formula for total root square error:

$$RMSE = \sqrt{e_1^2 + e_2^2 + e_3^2 + ...e_n^2}$$ Equation 3.3

For subtidal sampling the RMSE is calculated using the following constituents:

e_1 = Angle of staff in water when measuring depth;

e_2 = Measuring depth of water column due to waves;

e_3 = Variation in timed-still water due to waves;

e_4 = Variation in tidal time and height between Kushiro tide gauge and field site.

Where sampling errors are combined with other errors (e.g. transfer-function model errors and sample-specific errors), Equation 3.3 is still valid, however, each category of error is combined as $e_1 \ldots e_n$ and fitted into the equation above.

3.2.6 Statistical methods

Zonation

I use two multivariate techniques to detect, describe and classify the vertical distribution of foraminifera at each site: unconstrained cluster analysis and detrended correspondence analysis (DCA). Unconstrained cluster analysis is used to classify modern samples into more-or-less homogeneous faunal zones based on unweighted Euclidean distance and using no transformation or standardisation of the percentage data. DCA is an ordination technique and is used to represent samples as points in a multi-dimensional space, with similar samples located together and dissimilar samples apart. Birks (1974; 1986; 1992) suggests that the two methods complement one another insofar as a single profile gives information that zonation alone does not because it illustrates variation within as well as between zones.

Ordination

I calculated ordinations using the software CANOCO Version 4.5 (ter Braak and Šmilauer, 2002). I selected the regression and calibration models on the basis of the gradient length of DCA Axis 1 using all the modern foraminiferal data (detrended by segments, non-linear rescaling). Canonical correspondence analysis (CCA) relates community composition to known variations in the environment (ter Braak, 1986, 1987; ter Braak and Verdonschot, 1995) and was used to extract synthetic environmental gradients from ecological datasets. Analysis was performed with inter-species distances, biplot scaling and no data transformation. Partial CCAs (Borcard *et al.*, 1992) were run to determine the independence and relative strength of the major environmental gradients. I determined the statistical significance ($p<0.05$) of the partial CCAs using a Monte Carlo permutation test (449 permutations).

Development of inference models

Work by Imbrie and Kipp (1971) revolutionised the field of Quaternary research by developing, for the first time, a procedure for the quantitative reconstruction of past environmental variables from fossil assemblages (Birks, 1995: 161). A wide range of models are now available to express elevation as a function of foraminiferal assemblages, although some are more suited to quantifying the relationship between biological assemblages and lithostratigraphic criteria than others. Model selection is dependent upon the underlying taxon-environment response model (Birks, 1995). I use Detrended Canonical Correspondence Analysis (DCCA: detrending by segments and non-linear rescaling) with elevation as the only constraining variable to determine the amount of biological compositional turnover. Using the program C2 (Juggins, 2006), various methods are able to quantify the fauna-environment relationship. In this study I follow Edwards *et al.* (2004a) and Horton and Edwards (2005) by applying weighted averaging partial least squares (WA-PLS) to the foraminiferal data.

WA-PLS is a modification of the unimodal method of weighted averaging, which considers the variance along a single environmental gradient such as elevation. Where an additional environmental variable (e.g. salinity) influences the composition of assemblages, fauna-elevation relationships may be distorted and cause estimated elevations to differ from their observed values. WA-PLS improves predictions by using any structure present in weighted averaging residuals and, in effect, considers the influence of additional environmental variables such as salinity or pH (ter Braak and Juggins, 1993).

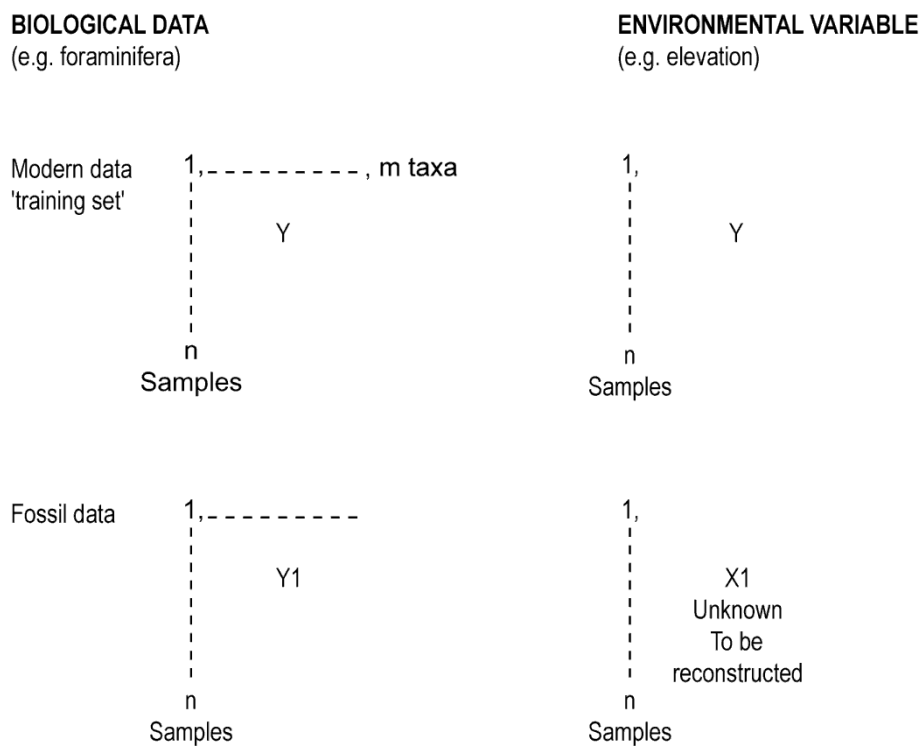

Figure 3.6 Transfer function methodology (after Birks, 1995).

In order to effectively assess the predictive abilities of the transfer function it is important to use cross-validated performance indices since the 'apparent' measures, coefficient of determination (r^2) and root mean squared error (RMSE), use the whole dataset to develop the transfer function and test its performance. Computer intensive methods of cross-validation such as jack-knifing or bootstrapping (ter Braak and Juggins, 1993; Birks, 1995) are used to generate independent test sets from the original training set. Jack-knifed or 'leave-one-out' measures (ter Braak and Juggins, 1993) are a simple cross-validation approach where the reconstruction procedure is applied *n* times using a training set of (*n* - 1). Bootstrapping is a more a rigorous method of data analysis by removing the biased circular inference involved in using a single training set (Reavie *et al.*, 1995).

There is a choice of models within WA-PLS, each with different model components. Component 1 is identical to WA regression and calibration with inverse deshrinking. Further components may be added that utilise the residual structure in the species data to improve the species coefficients (ter Braak and Juggins, 1993). The final model that I use is the one that provides the lowest RMSEP, the highest coefficient of determination (r^2_{boot}) and the lowest mean and maximum bias.

Modern Analogue Technique

The precision of transfer function reconstructions may be assessed in relation to their predictive statistics as detailed above. A firm understanding of the ecology and taphonomy of salt-marsh foraminifera remains central to the development and application of transfer functions (Woodroffe, 2008). Non-analogue situations may occur if an environment recorded in the fossil sequence is not sampled in the training set, or alternatively post-depositional changes (e.g. decalcification) have preferentially depleted certain taxa (Edwards and Horton, 2000). Measuring dissimilarity uses the modern analogue technique (MAT), whereby a measure of faunal dissimilarity is used to compare down-core samples to each reference sample in the modern training set (Birks, 1995).

I calculate the dissimilarity between each fossil sample and the ten most similar modern samples, taking a squared chord distance as the dissimilarity coefficient (Prentice, 1980; Overpeck *et al.*, 1985). Using the maximum dissimilarity coefficient from the modern data, I am then able to isolate any dissimilarity coefficients greater than the maximum, which may be considered poor analogues. The program C2 (Juggins, 2006) is used for the MAT

3.2.7 Chronostratigraphical methods

Precise chronological control is critical for identifying subtle changes in RSL and accurately estimating rates. Radiocarbon dating is the mainstay of Holocene sea-level studies on

passive and active coastal margins. However, the use of this method is unsuitable for dating sediments deposited since *c*. AD 1700 because of a prominent plateau in atmospheric radiocarbon production from this time onwards which means that when calibrated, radiocarbon ages from this interval have multiple-age solutions that may span several centuries. Because of this, I do not use the radiocarbon dating method for the salt-marsh component of this study; instead I employ two widely used radionuclides to develop age-depth models, lead-210 (^{210}Pb, half-life 22.26 years) and caesium-137 (^{137}Cs, half-life 30 years). The combination of lead and caesium dating has proved previously to be potentially useful in dating colluvial deposits associated with recent earthquake activity (Cundy, 2004), showing the usefulness of radionuclide to palaeoseismological studies. I combine these methods with an established tephra chronology to generate a chronology over the last earthquake cycle.

^{210}Pb is a natural radioactive decay product, part of the uranium-238 (^{238}U) series (Figure 3.7). ^{210}Pb reaches sediments in two forms: as a 'supported' (background) component arising from the presence in the sediment of its parent isotope, radium-226 (^{226}Ra), which precedes ^{210}Pb in the decay series, and as an 'unsupported' rainout component derived from atmospheric ^{210}Pb. In using ^{210}Pb for dating recent sediments, both the total ^{210}Pb component and the supported activity must be determined. Subtraction of the supported component from the total ^{210}Pb activity allows calculation of the unsupported ('excess') ^{210}Pb content in the sediment. Under ideal conditions, the ^{210}Pb excess declines with depth below present surface in accordance with a negative exponential function derived from the short half-life of the radioisotope. This depth profile is then used as input for various dating models, which provide chronologies, mass fluxes, and sedimentation rates.

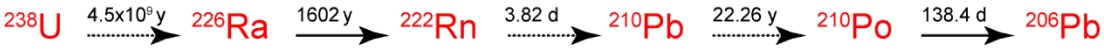

Figure 3.7 ^{238}U radioactive decay series, showing the production of ^{210}Pb via the decay of ^{226}Ra and its short-lived daughters.

The calculations of ages are derived from one of either three models:

I. ***Constant Rate of Supply (CRS)****:* This model is based on the assumption that there is a constant rate of supply of unsupported ^{210}Pb to the sediment, regardless of background sedimentation. Therefore, a higher rate of background sedimentation will lead to a lower ^{210}Pb concentration (Goldberg, 1963).

II. ***Constant Initial Concentration (CIC)****:* This model is based on the assumption that the dilution of ^{210}Pb through the period of deposition is assumed to be constant. Therefore, the initial activity of unsupported lead per gram dry weight is assumed to have remained unchanged throughout the deposition of the core (Goldberg, 1963;

Robbins, 1978). This model requires an excess reservoir of ^{210}Pb to be available at all times, and is particularly useful where sedimentation rates have remained relatively constant through the study period.

III. ***The Simple Model****:* The simple model assumes constant sedimentation, which is modelled from the slope of the least squares fit for the natural log of the $^{210}Pb_{excess}$ activity plotted against depth.

The use of ^{210}Pb in developing age models is not without its problems. Deviations from the exponential decay profile may include a flattening of the profile near the surface, or breaks in the exponential decay trend. Many factors may give rise to a flattened profile, including bioturbation of the upper sediments, increases in background sedimentation, diagenetic mobilization into pore waters and out of the sediment and changes in lead supply rates (Binford *et al.*, 1993).

^{137}Cs is an artificially produced radionuclide, present in the environment because of atmospheric fallout from nuclear weapons testing and reactor accidents, as well as deliberate discharges from nuclear facilities. Following the initial widespread release of ^{137}Cs from high-yield nuclear weapons testing in 1954, significant maxima in atmospheric fallout of ^{137}Cs has occurred in the Northern Hemisphere in 1958, 1963 (from nuclear weapons testing) and 1986 (from the Chernobyl accident). The fallout of ^{137}Cs was rapid and strongly absorbed by soil and sediment particles. In an accumulating sediment column, periods of peak ^{137}Cs fallout provide discrete subsurface activity maxima which can be used to date the sediment column (Ritchie and McHenry, 1990; Cundy and Croudace, 1996).

As with ^{210}Pb dating, ^{137}Cs dating also has its problems. Downcore migration of caesium has been observed in Germany, following the Chernobyl disaster. The proportion of ^{137}Cs occurring in the upper 5 cm of terrestrial cores was showed to have dropped from 90% in 1986 to 50-70% in 1996 (Luise and Heinz, 1997). As such careful consideration is necessary when constructing age models. As tephra is less susceptible to migration compared with the use of radionuclides, the resulting chronologies used in this thesis rely primarily on the two most recent tephra layers (where possible). Two key tephra horizons are found on Hokkaido. The Ko-c2 tephra erupted from Mount Komagatake (AD 1694), and the Ta-a tephra (AD 1739) derives from Mount Tarumai (Tokui, 1989; Furukawa *et al.*, 1997; Sawai, 2001, 2002; Sawai *et al.*, 2002). These key tephra isochrones are then added to if there is a clear and dependable ^{137}Cs peak, and finally further improved if reliable ^{210}Pb profiles are available. The fallout zone of the tephra varies as a consequence of the direction and strength of the prevailing wind. The Ko-c2 and Ta-a ash layers fell primarily on the eastern side of Hokkaido, and traces can only be identified as far west as

Tofutsu-ko. Where tephra has not been identified, the chronology of these cores is primarily associated with the peak in caesium, with supporting evidence from the lead profile.

For radiometric analysis, samples from sediment cores were freeze-dried and ground to a fine powder in a ball mill. Well-type germanium detectors in the Department of Geography (Durham University) are used for ^{210}Pb and ^{137}Cs analyses. The excess ^{210}Pb activity was determined from ^{226}Ra where excess ^{210}Pb equals the total ^{210}Pb minus ^{226}Ra. Similarly, ^{137}Cs activity was determined using gamma spectrometry. Count times of 70,000 seconds were used and errors were typically 4% (1σ). Detection limits of 0.04 Bq/g were obtained.

3.3 OTHER METHODS OF SEA-LEVEL RECONSTRUCTION

3.3.1 Pleistocene sea-level index points

Along the coastlines of northern Japan, a staircase of wave-cut platforms of Middle and Upper Pleistocene record sea-level highstands (Figure 3.8). These coastal landforms provide an opportunity to determine the tectonic and eustatic influences on the morphogenisis of this region, and provide a long-term context for the interpretation of models of land movement during the Pleistocene and recent periods.

Figure 3.8 Marine terraces in northern Japan, after Okumura (1996; http://home.hiroshima-u.ac.jp/kojiok/hokkaido.htm).

The marine terraces of Hokkaido have been extensively studied. Initial research in late 1950s by Sakaguchi (1959) sought to correlate terraces on geomorphological grounds, whilst later work applied local tephrostratigraphy and other marker horizons to develop relative chronologies for their formation (Machida *et al.*, 1987; Okumura, 1996). For example, the widespread tephras known as Spfa-1, KSr, Aso-4, Toya and KHb were deposited across all of Hokkaido and provide marker horizons for the Late Quaternary.

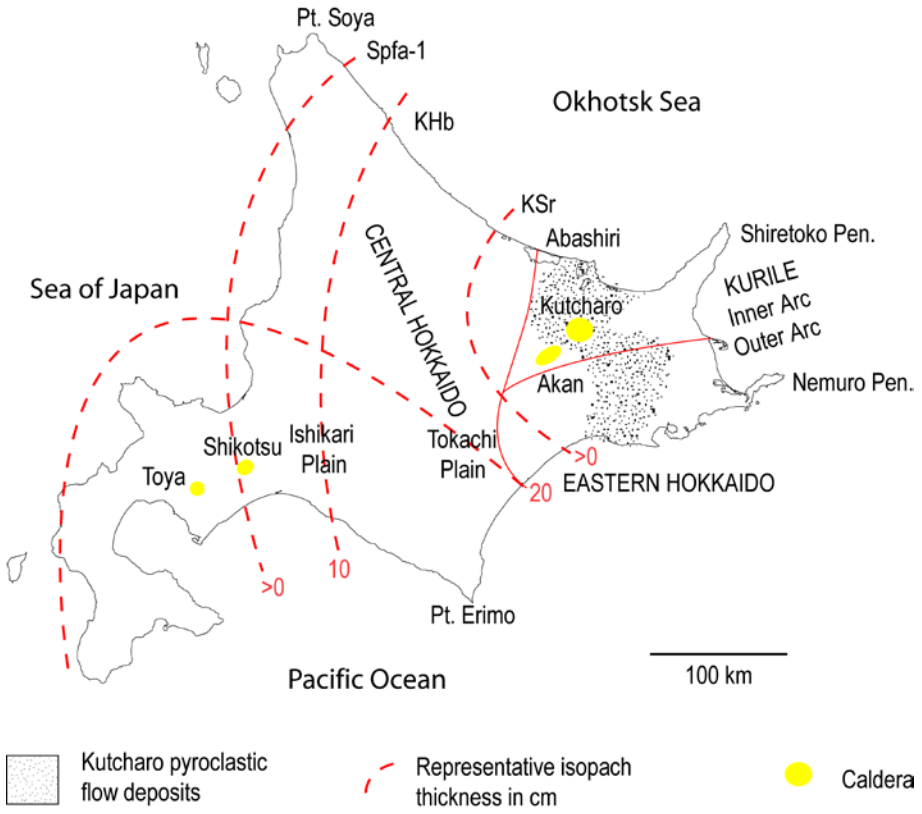

Figure 3.9 Late Pleistocene widespread marker tephras and neotectonic framework of eastern Hokkaido (Okumura, 1996).

Okumura (1996) proposed approximate ages on the basis of key tephra-marker horizons, applying the method to shoreline platforms along the eastern and northern coastlines of Hokkaido. He determined the altitudes of the paleoshorelines using a hand-held barometric altimeter and from a 1/25,000 topographic map, with maximum errors considered to be ± 5 m. Unlike other areas (e.g. Rostami *et al.*, 2000; Barreto *et al.*, 2002; Ferranti *et al.*, 2006; Hearty *et al.*, 2007), there has been no absolute dating on Hokkaido, which limits the precise correlation of the marine deposits to specific highstands. Instead, correlation must be based on the superposition of adjacent tephras that have been dated elsewhere (see Figure 3.10). The lowest of the terraces (M1) postdates the Toya Ash (MIS 5d; 112-115 ka) and KP IV (MIS 5d; 115-120 ka), and predates the KP V and AUP pyroclastic flows which are both attributed to MIS 6 (Okumura, 1996; Koaze *et al.*, 2003). Furthermore, no 5c and 5a terraces have been identified in eastern Hokkaido, except for the area around the Shiretoko promontory (K. Okumura, *pers. comm.*). Consequently, the M1 terrace is confidently assigned to MIS 5e.

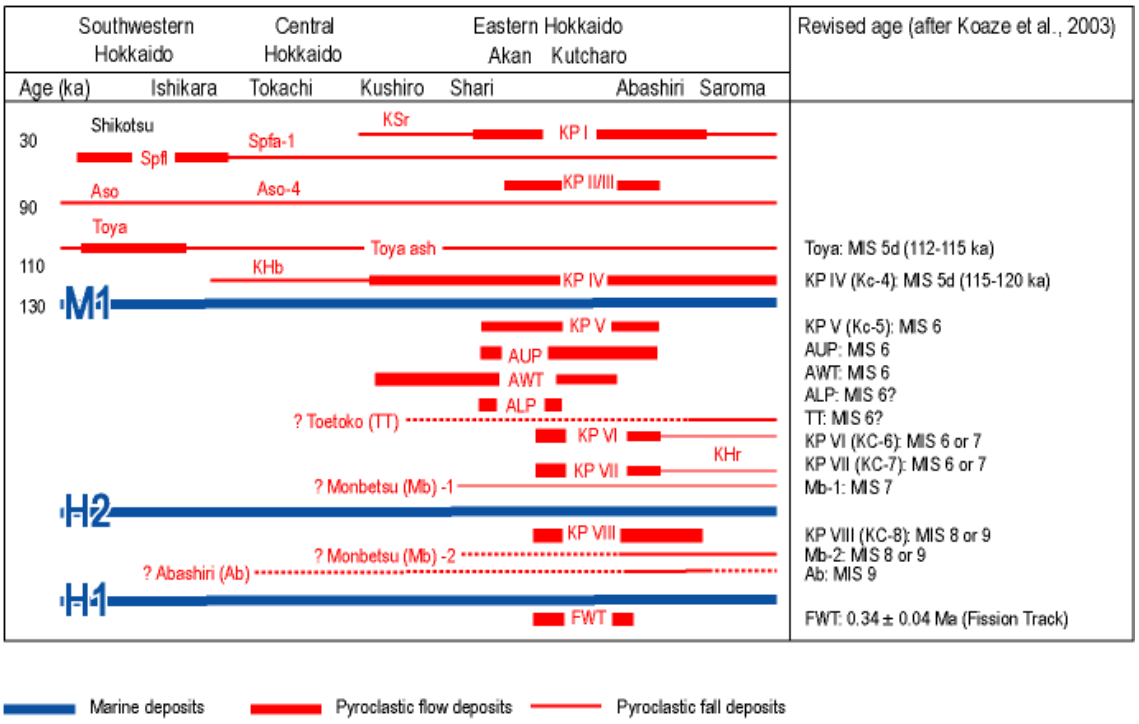

Figure 3.10 Space-time diagram for marker tephras in Hokkaido (after Okumura, 1996). Vertical line for the age is not to scale. Revised ages of marker tephras taken from Koaze *et al.* (2003)

Correlation becomes more problematic with the older terraces. The H2 terrace lies below the KP VII (MIS 6 or 7) and Mb-1 (MIS 7) pyroclastic flow deposits, and above the KP VIII and Mb-2 tephras (MIS 8 or 9). Therefore, the H2 terrace is associated with the MIS 7 highstand. The H1 terrace is likely to be MIS 9 as it lies between the Ab tephra (MIS 9) and the FWT tephra, which has been independently dated by fission track to 0.34 ± 0.04 Ma (Koshimizu and Ikushima, 1989). For both highstands, a number of substages have been observed. During MIS 7, the penultimate interglacial (250–195 ka), elevated marine terraces of selected areas from around the world show two or three main highstands (Zazo, 1999; Dutton *et al.*, 2009), which were separated by a marked sea-level fall around 230 ka (Shackleton *et al.*, 1990). During MIS 9 (310-290 ka) there appears to have been three distinct interstadials based on forest development characteristic of deglacial substages in Southern Europe (e.g. Tzedakis *et al.*, 1997). Without absolute dating of the marine terraces of Hokkaido it is impossible to assign H2 and H1 to a specific substage of MIS 7 or 9, and therefore a corresponding eustatic sea level. Furthermore, sea-level estimates for interglacial substages are uncertain, especially for those predating MIS 5e (e.g. Rohling *et al.*, 2009). The age error associated with these terraces makes the possible range of uplift estimates exceed a threshold that would be reasonable. Due to these uncertainties, the following analysis of uplift rates uses only the most recent MIS 5e terrace. A summary of the height and age distribution of the terraces described by Okumura (1996) is listed overleaf:

- M1 terrace, 6 - 80 m asl (above sea level), approximately 125,000 years, corresponding to MIS 5e;
- H2 terrace, 15 -120 m asl, corresponding to MIS 7.
- H1 terrace, 35 – 160 m asl, corresponding to MIS 9.

The cascade of terraces (Figure 3.11) found along the coastline is interpreted to result from tectonic deformation because: (1) a clear elevational gradient in deformation of the marine terraces is consistent with a Kuril Trench origin; and (2) the tephra ages from the higher terraces are always significantly older than the lower ones.

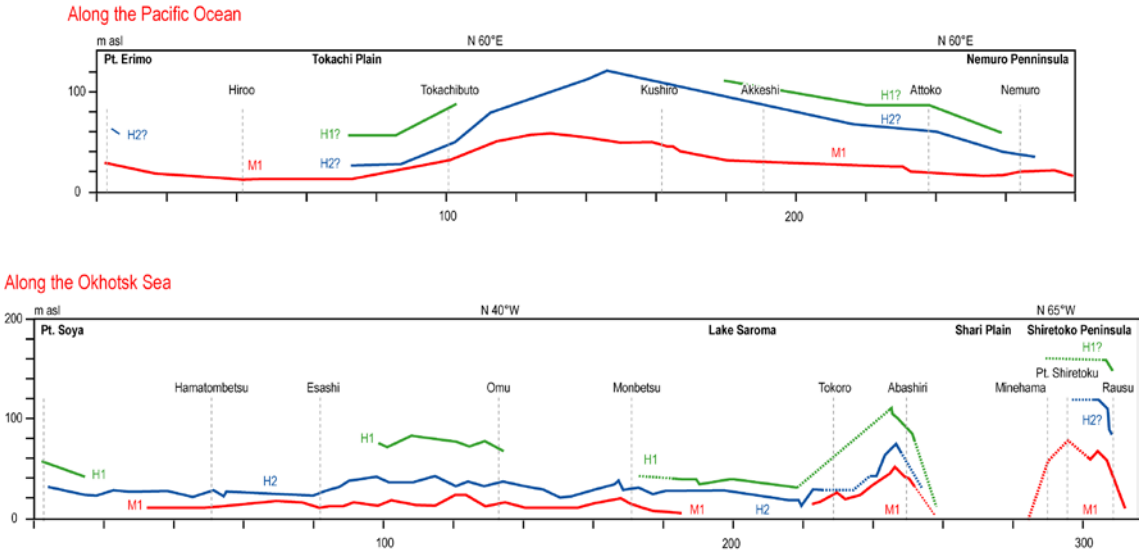

Figure 3.11 Profiles of former shoreline altitude along the Pacific Ocean and Okhotsk Sea. After Okumura (1996).

The vertical displacement of the Hokkaido terraces along the Okhotsk Sea is interpreted by Okumura (1996) as reflecting two uplift zones at Abashiri and Shiretoko separated by an area of subsidence in the Shari Plain (Figure 3.11). The maximum height of the H1 (MIS 9) is *c*. 100 m asl at Abashi and *c*. 120 m asl at Pt. Shiretoko. The terrace elevations in the north of Hokkaido are less deformed, although there is a suggestion of greater uplift in the extreme north at Point Soya relative to other sites on the Okhotsk Sea. In a more recent interpretation of these data, Koike and Machida (2001) present the shorelines in plan form, draped over the topography of Hokkaido, although the basic patterns observed by Okumura (1996) remain essentially the same (Figure 3.12).

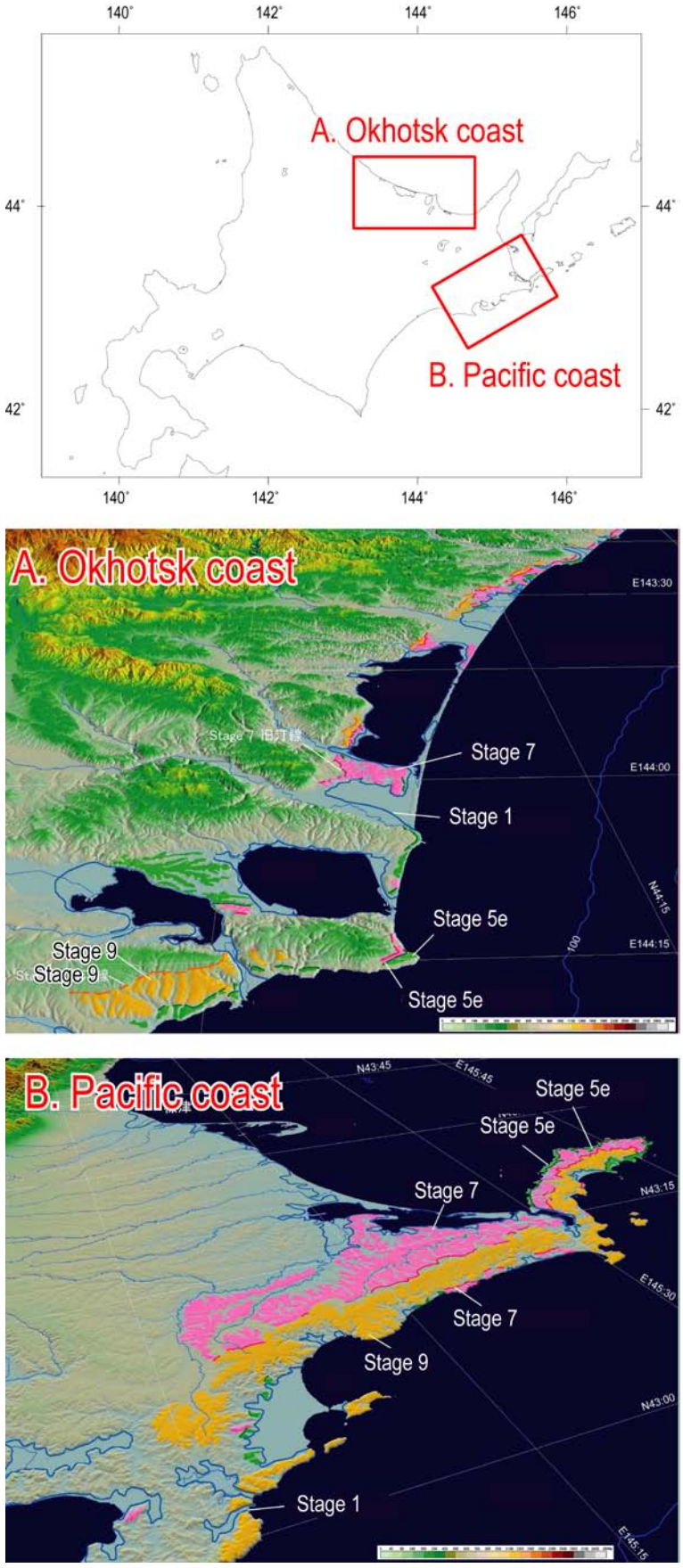

Figure 3.12 Uplifted terraces along the coastline of eastern Hokkaido (after Koike and Machida (2001)).

Uplift rate calculation

Following Lambeck *et al.* (2004), the uplift rate *u* and its variance σ_u^2 are determined using the following equations:

$$u = \frac{\Delta H}{T_{5e}} \quad \text{Equation 3.4}$$

$$\sigma_u^2 = \frac{\sigma_{\Delta H}^2}{T_{5e}^2} + \left(\frac{\Delta H}{T_{5e}^2}\right)^2 \sigma_{T5e}^2 \quad \text{Equation 3.5}$$

With eustatic and glacio-hydro isostatic compensation given by:

$$\Delta H = H_{5e} - \delta H_{5e} \quad \text{Equation 3.6}$$

Where,

H_{5e} = the height of the observed MIS 5e shoreline above MSL;

δH_{5e} = the height of this shoreline in areas of tectonic stability;

T_{5e} = the age of MIS 5e;

σ_{T5e} = the uncertainty in the age of MIS 5e;

$\sigma^2_{\Delta H} = \sigma^2_{H_{5e}} + \sigma^2_{\delta H_{5e}}$ (represents the variance in tectonic uplift).

I adopt the following values; T_{5e} = 125 ka, σ_{T5e} = 5 ka, δH_{5e} = 3m (see Table 3.5 for details; 3m is an average of the data presented), $\sigma_{\delta H5.5}$ = 5m; the latter being the measurement error from Hokkaido, after Okumura (1996).

Table 3.5 Summary dates and sea-level variability relating to MIS 5e.

MIS stage and SPECMAP age	Sea-level	Evidence (reference)
MIS 5e, 125* ka BP	+2 to +4 m	Fossil corals from a tectonically stable part of western Australia (Stirling *et al.*, 1998).
	+0 to +6	Re-evaluation of Barbados uplift rates and fossil coral reef evidence (Schellmann and Radtke, 2004).

* 125 ka (and its associated error of ± 5 m) based on eustatic sea-level estimates from coral estimates (Bard *et al.*, 1990; Szabo *et al.*, 1994; Stirling *et al.*, 1995; Eisenhauer *et al.*, 1996; Stirling *et al.*, 1998; Gallup *et al.*, 2002; Thompson *et al.*, 2003; Siddall *et al.*, 2006; Thomas *et al.*, 2009).

3.3.2 Holocene sea-level index points

An important aspect of this thesis is the development of a new database of Holocene RSL data from Hokkaido. The full results of this are presented in Appendix E, together with a detailed explanation of the database fields, including the datum used as well as the radiocarbon calibration methods used for terrestrial and marine samples.

Over the past three decades, the sea-level history of Hokkaido has been relatively well studied. However, a rigorous assessment of the relationships of the dated material to tide levels has largely been ignored, and studies have tended to be limited to specific geographic areas. The studies tend to focus on glacio-isostatic processes, particularly quantifying the mid-Holocene highstand, with little or no attention paid to earthquake-related movements.

My approach to database construction follows that described by Shennan *et al*. (1989) and Shennan and Horton (2002), who developed a database of sea-level index points from Great Britain. The emphasis in these publications is on providing a screened, standardised database of sea-level data that are categorised depending on their value as sea-level indicators. The best data are from transgressive or regressive contacts and have a defined altitude with respect to a former tidal datum. Less useful data provide limiting observations that simply demonstrate that sea level was above or below the observed elevation of the sample at the time of formation (see below).

The database comprises many of the standard categories incorporated in previous database studies, such as geographic information; a description of the dated material; elevation relation to the national datum in Japan (m TP); details of the radiocarbon age estimate (including the laboratory reference code); indicative meaning and range of the indicator; and the tidal information relating to each study site (Preuss, 1979; Shennan, 1989). The location of samples is given in latitude and longitude within the database. For the purposes of modelling, distinct regional areas are identified, governed by the availability of data and siphoned into distinct geographic areas to permit more meaningful comparisons between relative sea-level observations and predictions. Six key regions are identified, these include (1) Akkesh-ko and Mochiruppu; (2) Furen-ko; (3) Abashiri and Saroma-ko; (4) Sarubetsu Lowlands; (5) Sapporo; and (6) Isikara Lowlands.

Following Brooks and Edwards (2006), index points and limiting dates are divided into primary and secondary tiers, reflecting the accuracy at which the indicative meaning of a sample can be quantified. Table 3.6 details a description of the index points and limiting dates used in this thesis.

Table 3.6 Data classes used in this thesis, after Brooks and Edwards (2006).

Name	Description
Index Points	
Primary Index Points	These index points comprise detailed information about the deposit, including information on its age, altitude and relationship to tidal parameters (the indicative meaning).
Secondary Index Points	These index points comprise less detailed information about the sea-level indicator, with data poorly quantified or associated with uncertainty. Examples include poor elevational or chronological, control, a hiatus, or limited microfossil analysis which making the relationship between the dated material and sea level unclear.
Limiting Dates	
Primary Limiting Dates	These are samples with good chronological control, although there is no quantifiable vertical relationship with sea level. Instead they provide a maximum (or minimum) limit for sea-level at a given time.
Secondary Limiting Dates	These are limiting dates which may have experienced post-depositional movement, having possibly been deposited and reworked prior to burial.

Both index points and limiting dates provide important constraints for sea-level reconstruction. Figure 3.13 shows oyster beds in a quiet water location in Tofutsu-ko (one of my study sites). Oyster beds (*Crassostrea gigas*), as well as other bivalves and molluscs found in samples must have formed below MTL. Sea-level curves should pass through sea-level index points, and remain within the constraints dedicated by limiting dates (Brooks *et al.*, 2006). However, such reconstructions are only valid providing that these index points (and limiting dates) remain at the altitudes at which they formed (Shennan and Horton, 2002).

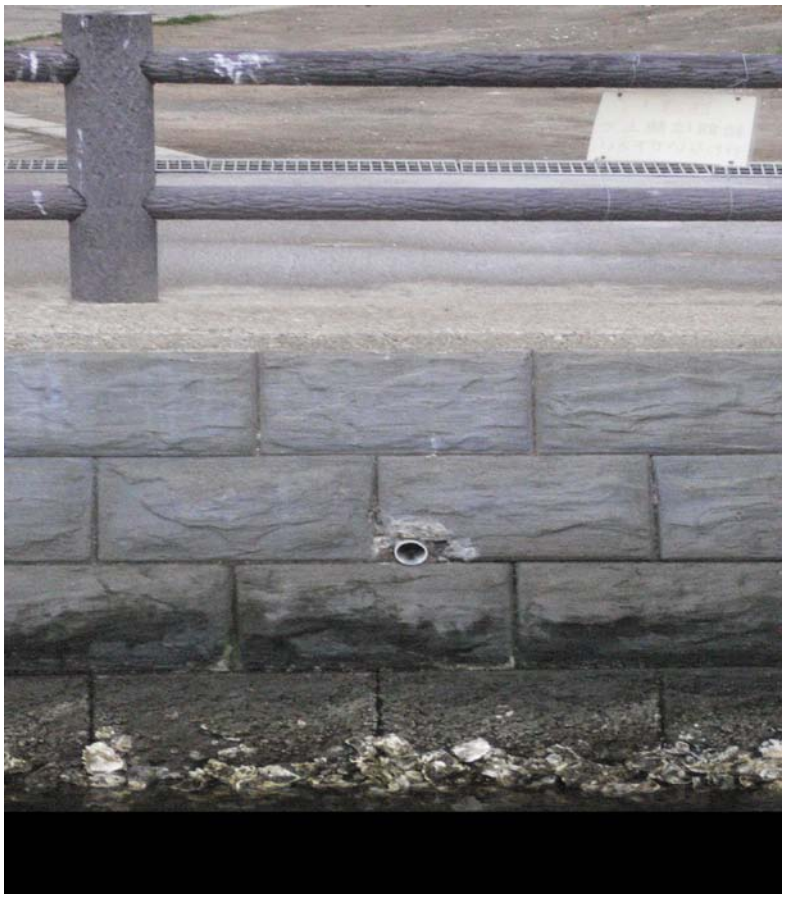

Figure 3.13 Modern oyster beds in a quiet water location in Tofutsu-ko.

Index points are defined by their relationship to tidal levels, which are modelled (and modified) from their present ranges. This assumption is invalid if tidal ranges change over Holocene timescales, introducing error into reconstructions (e.g. Hinton, 1995). Research modelling the western North Sea palaeogeographies show tidal ranges smaller than present in the early Holocene, with only minor changes since 6 ka BP (Shennan *et al.*, 2000a). The analysis of the database assumes a constant tidal range through time. Hokkaido has micro-tidal ranges that limit the extent of coastal geometry changes over Holocene timescales.

Standard ports (levelled into the national datum) are limited around Hokkaido; therefore, site-specific tidal parameters are interpolated from the closest available record. For those areas that have not been surveyed, this extrapolation is more tenuous and introduces error within the records. The indicative meanings defined for Hokkaido are based on previous work on temperate coastlines and modified according to field evidence of the range of the indicator's distribution across the marshes studied during the completion of this thesis (Table 3.7).

Table 3.7 Reference water levels and indicative meanings used in this thesis.

Contact	Dated material	Reference water level	Indicative range	Reference
1a	High marsh peat	MHHW	+ (HAT+MHHW)/2 - (MHHW+MTL)/2	Tooley (1978); Shennan *et al*. (1982; 1986; 1994); Brooks and Edwards (2006)
1b	Marsh peat	(MHHW+MTL)/2	+ MHHW - MTL	Shennan (1982; 1986); Brooks and Edwards (2006)
2	Limiting (undifferentiated peat)	> MTL		
3	Limiting	Freshwater - > MTL		Shennan and Horton (2002); Shennan *et al*. (2002); Peltier *et al*. (2002)
4	Limiting	Marine - < MTL		Shennan and Horton (2002); Shennan *et al*. (2002); Peltier *et al*. (2002)

3.3.3 Tide-gauge data

Tide gauges provide a direct method to record changes in vertical-land movements relative to the sea. In comparison to GPS or satellite observations, which are currently limited to the last decade or so, tide-gauge observations bridge much of the gap between these other forms of direct observation and the proxy records of estuarine stratigraphy that are the main focus of this thesis.

Japan supports numerous tide-gauge stations including several that are located close to the sample areas analysed in this thesis (Figure 3.14). The data used for the analysis presented here are derived from the Permanent Service for Mean Sea Level database compiled by the Proudman Oceanographic Laboratory (www.pol.ac.uk). The database

compiles monthly and annual mean sea-level values for sites related through a common datum. For this study, I use the Revised Local Reference (RLR) data which is a superior subset of the POL catalogue that has been reduced to a common datum using the benchmark history provided by the supplying authority.

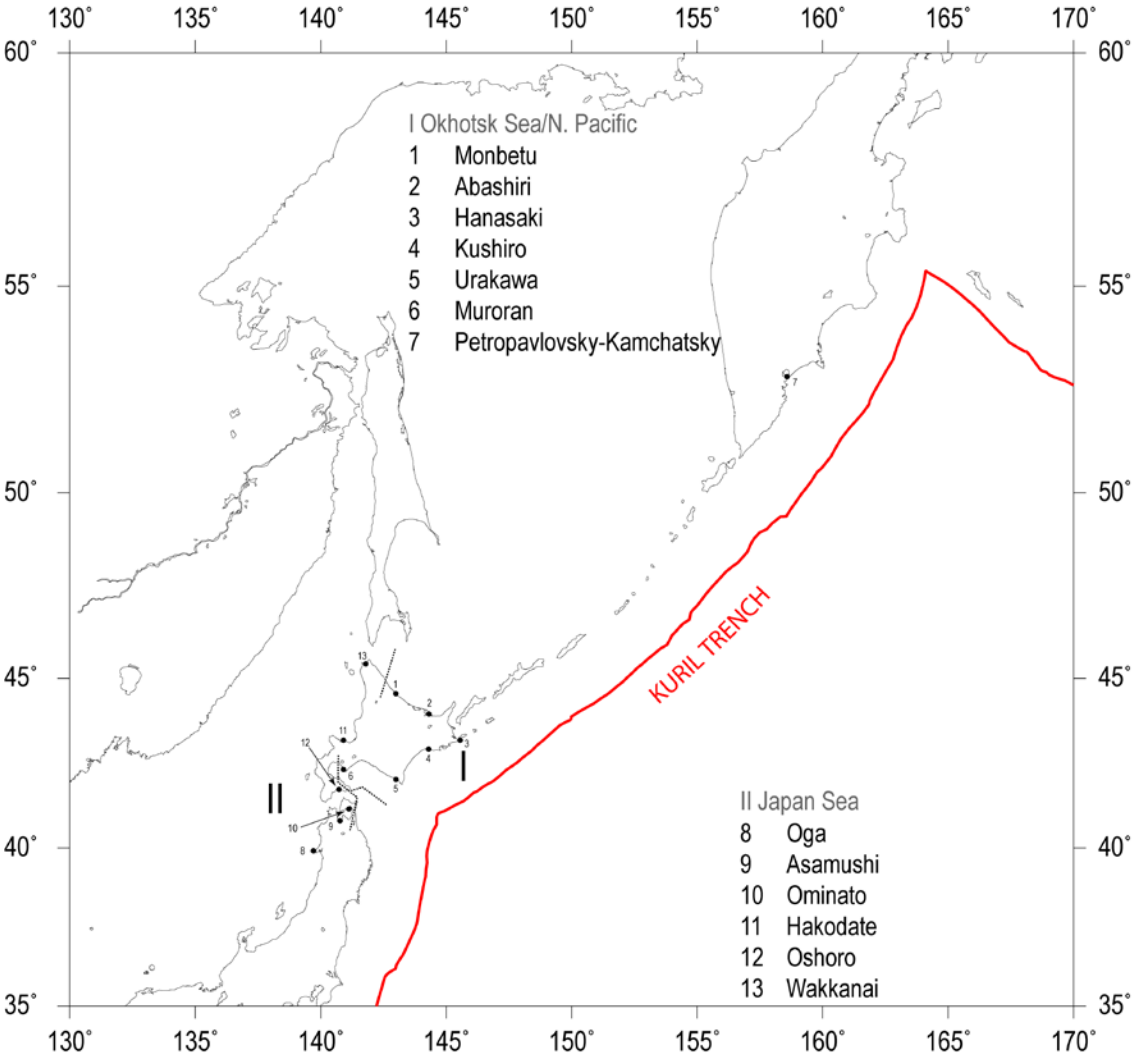

Figure 3.14 Location map and showing tide-gauge data used in northern Japan and the north Pacific, arranged into two oceanographic areas, (I) Okhotsk Sea/Northern Pacific and (II) Japan Sea.

The Japan Oceanographic Data Center, the Japan Meteorological Agency and the Geographical Survey Institute are responsible for the tide-gauge records of Hokkaido and northern Honshu. The stations chosen for the analyses are from Hokkaido to allow comparison with the salt-marsh sample sites studied in this thesis; however other records from northern Honshu and the Pacific West are also used to gain a wider understanding of oceanographic variability across northern Japan. These additional 'control stations' (see below for explanation) are fundamental to detrend the RLR tide-gauge record for oceanographic variability. The Hokkaido stations alone are insufficient in number to understand the changing nature of the oceanographic regimes of Hokkaido (Okhotsk Sea/North Pacific and Japan Sea).

The time series often vary in length, comprise one or two stations operational over different periods and relate to local (arbitrary) datum. For this reason it is impossible to reliably combine all of the records and thus the longest RLR records only date from the 1950s and more commonly the mid-1970s.

In selecting tide-gauge records for analysis, there is a trade off between having a small number of (relatively) long records and a larger number of records that provide shorter record lengths (28 years) from a common time interval. To help inform this decision, I plot the available stations and their record lengths in Figure 3.15 and from this select the time interval 1979-2007 as the focus for study. This maximises the number of tide stations from around Hokkaido available for constraining the spatial variability in RSL movements. The resulting subset of records serves to further eliminate any bias in the analysis that would otherwise be a function of record length and hence unrelated to earthquake-deformation processes.

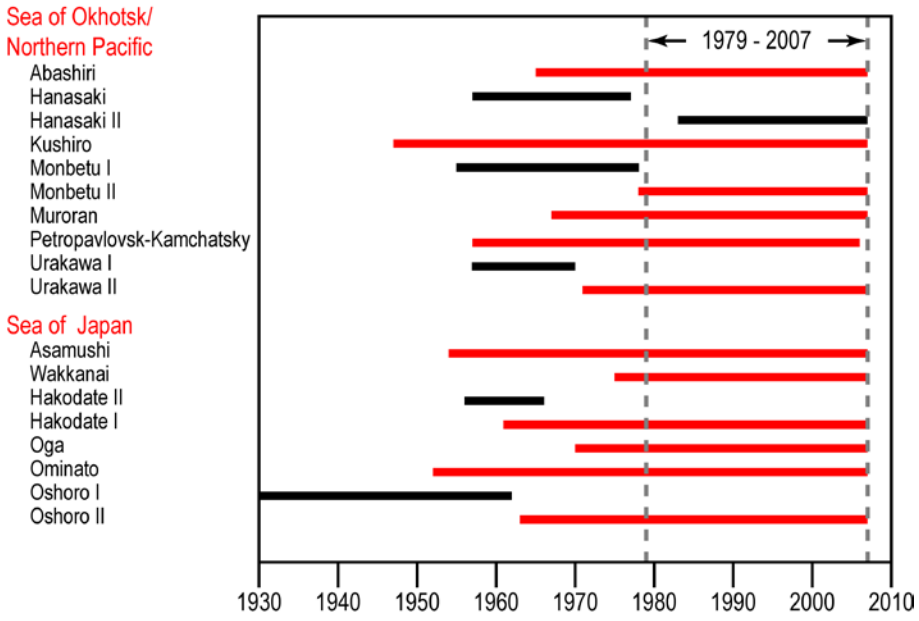

Figure 3.15 Length of record for tide-gauge stations around Hokkaido. Records in red are used in this study and encompass the period 1979 to 2007 inclusive, a minimum interval of 28 years.

Having selected the tide gauges that contain suitable records for analysis (see Table 3.8) for full details), I now make several corrections to remove the contaminating effects of changes in local and regional air pressure, including seasonal effects, as well as a correction for 20th century 'eustatic' sea-level change. The latter correction is not necessary when comparing the tide-gauge trends to the salt-marsh records, since the salt marshes record an integrated sum of oceanic and crustal factors, but the correction is useful for attempting to derive an absolute value for crustal uplift/subsidence and for comparison to GPS data.

Table 3.8 List of tide-gauge data used in this thesis, arranged into two oceanographic areas, (I) Okhotsk Sea/Northern Pacific and (II) Japan Sea

Tide gauge station name	Code No.	Lat. (N)	Long. (E)	From	To	No. of months	No. of missing months
Okhotsk and North Pacific							
Abashiri	641/003	44 01	144.17	1979.042	2007.958	345	3
Hanasaki II	641/012	43 16	145 34	1983.042	2007.958	300	0
Kushiro	641/021	42 58	144 23	1979.042	2007.958	345	3
Monbetu II	641/002	44 21	143 22	1979.042	2007.958	341	7
Muroran	641/029	42 21	140 57	1979.042	2007.958	348	0
Petropavlovsk- Kamchatsky	630/021	52 59	158 39	1979.042	2006.958	322	14
Urakawa II	641/027	42 10	142 46	1979.208	2003.625	281	13
Japan Sea							
Asamushi	647/121	40 54	140 52	1979.042	2007.958	330	18
Esashi	641/035	41 52	140 08	1984.042	1994.078	156	2
Hakodate II	641/032	41 46	140 43	1979.042	2007.958	348	0
Oshoro II	641/042	43 12	140 52	1979.042	2007.958	336	12
Oga	647/096	39 56	139 42	1979.042	2007.958	327	21
Ominato	647/111	41 15	141 09	1979.042	2007.958	345	3
Wakkanai	641/061	45 24	141 41	1979.042	2007.958	347	1

Dealing with data gaps

Tide-gauge records are often discontinuous, typically because of instrument malfunction or relocation. Because of this, prior to analysis it is helpful to interpolate between the missing months. Simply averaging values is too simplistic because some records omit complete years, necessitating a more complex approach. To make such corrections I use sine and cosine terms as predictors for modelling these periodic time series (Cox, 2006). In tectonically active environments such as Japan, sea level is a function of time as well as tidal cycles (estimated using trigonometric functions) and therefore I added time as a predictor variable to generate missing values. These predicted values are removed from subsequent analysis once the initial corrections are applied.

Pressure corrections

The RLR data from POL (termed $MMSL_i$, where the subscript refers to the ith month in a multiple year record) was first corrected for barometric pressure variations. For stations in Japan, the nearest monthly mean sea-level air pressure (P_i) for corresponding POL stations was supplied by the Japan Meteorological Agency (www.data.jma.go.jp/obd/stats/data/en). For those stations not in Japan, the Met Office Hadley Centre's mean sea-level pressure (MSLP) dataset, HadSLP2, is used (Allan and Ansell, accepted). This is a unique combination of monthly globally-complete fields of land and marine pressure observations on a 5 degree latitude-longitude grid from AD 1850. To access the pressure for stations up to the end of AD 2007, I use the updated form using NCEP/NCAR reanalysis fields which gives the near real time product (HadSLP2r).

At each station, the mean barometric pressure ($\overline{P}$) over the 28-year period is calculated. Assuming 1.0 cm sea-level change per mbar, the sea-level variations due to pressure variations about *P* are:

$$PC_i = MMSL_i - 1.0\frac{cm}{mbar} * \left(P_i - \bar{P} \right)$$

Equation 3.7

Where;

MMSLi = the *ith* month in a multiple year record;

Pi = the monthly mean sea-level air pressure;

$\bar{P}$ = the mean barometric pressure at each station.

Removal of seasonal signals

Tide-gauge records record seasonal signals the product of a number of related effects; including seasonal variations in air and water temperatures, predominant wind direction, and the supply of freshwater influx resulting in local density variations (Larsen *et al.*, 2003). One method to correct for these effects is to use meteorological data, but here I use a more straightforward approach that involves applying an average seasonal signal at each station, and removing this from the record (Kato, 1983; Larsen *et al.*, 2003).

I calculate the average seasonal signal by running a high-pass filter (Chebyschev type II, 10 year cutoff) on each station's pressure corrected record. This produces a 10-year smoothed record, which is then subtracted from the pressure corrected record to produce monthly sea-level deviations. An average deviation of each month ($\overline{D_m}$; m = 1 to 12) for the length of the record is then calculated (N years of data for month m):

$$\overline{D_m} = \sum_{j=0}^{N-1} \frac{D_m}{N}$$

Equation 3.8

The average deviation of each month is then subtracted from the pressure corrected record from each matching month throughout the record, giving 'seasonally corrected' values:

$$SC_{(j-1)*12+m} = PC_{(j-1)*12+m} - \overline{D_m}$$

Equation 3.9

Where;

j = year, from 1979 to 2007;

m = month, 1 to 12.

Removal of common mode oceanographic signal

Tide-gauge data from specific oceans often show similar patterns of variability owing to the changing nature of the particular oceanographic regime within which a particular station is located. Removing these patterns is the final stage in correcting the records for meteorological variability. The first stage of this analysis involves dividing up the tide-gauge stations into one of two oceanographic sections; one for the Japan Sea, another for the North Pacific/Okhotsk Sea (following Kato, 1983). For each of these stations, a linear

sea-level trend is determined, and monthly residuals about these trends quantified ($[R_s]_I$, where s = site and i = month). These monthly residuals are then combined to form an average residual for each month, approximating regional sea-level variations that are common to all sites (Kato, 1983; Davis *et al.*, 1999; Cohen and Freymueller, 2001). At each station for each month (i), OC_i is subtracted from the SC_i to obtain the fully corrected record. Each H_i is found using those stations in each oceanographic group (s = 1 to k) as described below:

Equation 3.10

$$OC_i = \frac{\left[\sum_{s=1}^{k} R_s\right]_i}{k}$$

This 'oceanographic correction' (OC) is then subtracted from the SC to leave fully corrected sea level (H_i).

$$H_i = SC_i - OC_i$$

Equation 3.11

The oceanographic correction is derived from as many stable 'control stations' as possible within the complete 28-year period. This approach assumes that sea-level change is linear over the last few decades, a reasonable assumption given the paucity of major plate-boundary earthquakes during this period (and the lack of obvious coseismic offsets visible in the tide gauge record, with one exception: see below). Consequently, a large number of control stations minimises strong local sea-level variations that may be present at one station only (Larsen *et al.*, 2003) and better resolves the variations common to all sites.

These steps are followed in turn to detrend the RLR records from meteorological factors. By identifying and removing changes in the sea-level record associated with pressure, seasonality and ocean-basin responses, I derive a 'cleaned' record of tide-level variability comprising eustatic, isostatic and tectonic processes (Figure 3.16).

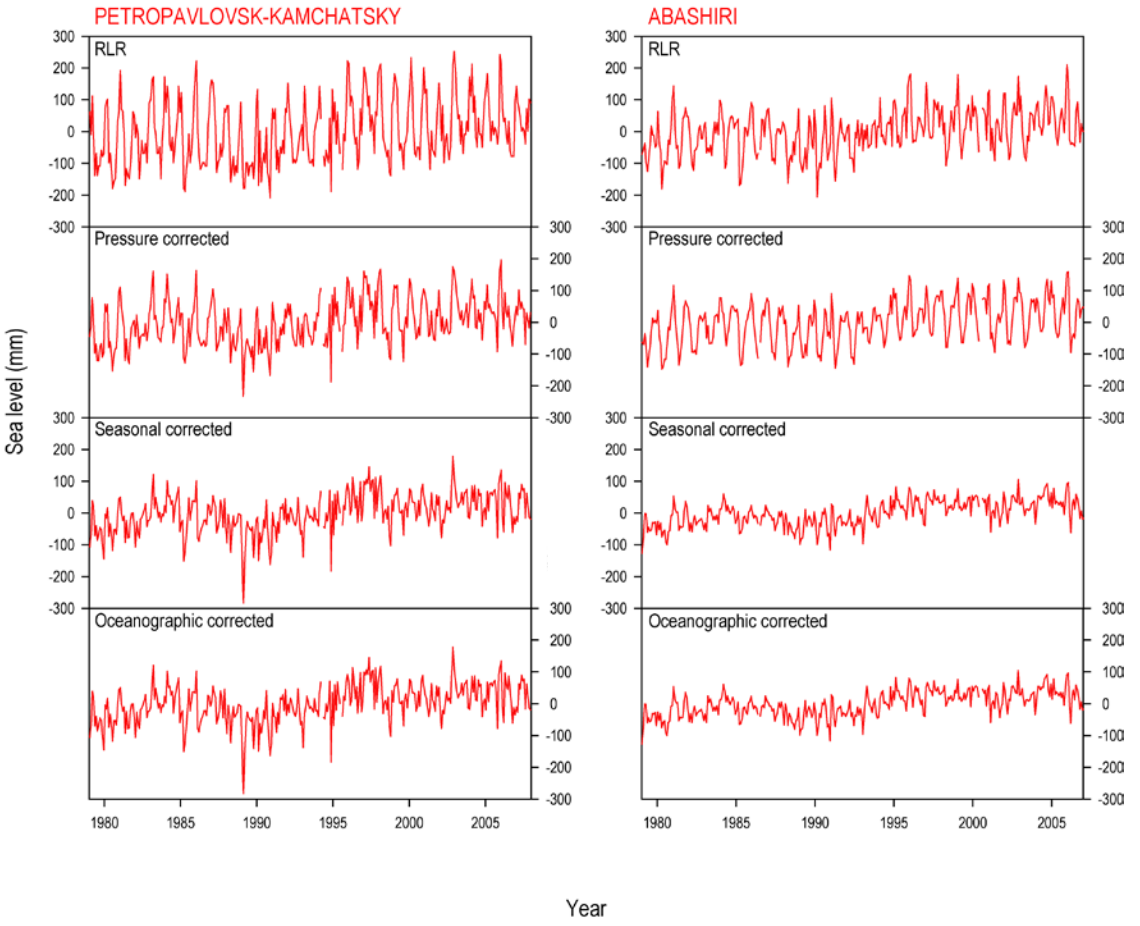

Figure 3.16 An example of the steps used to process tide-gauge records around Hokkaido, using records from Petropavlovsk-Kamchatsky and Abashiri (see Figure 3.14 for locations).

Coseismic offsets

Earthquake-related vertical land movements cause sudden shifts in the tide-gauge record, which are not representative of long-term trends. They appear as a step change in sea-level and can contaminate the oceanographic corrections applied to the each ocean basin. Only one site, Urakawa, displayed this pattern following the 2003 earthquake. Urakawa is on the Pacific east coast (Site 5 in Figure 3.14 above) and was closest to the earthquake epicentre which was located offshore. The earthquake occurred toward the end of the time series (Figure 3.17) so I disregard the most recent section of this record. Urakawa series is no longer a complete record and so I do not include is as a control station for the oceanographic correction.

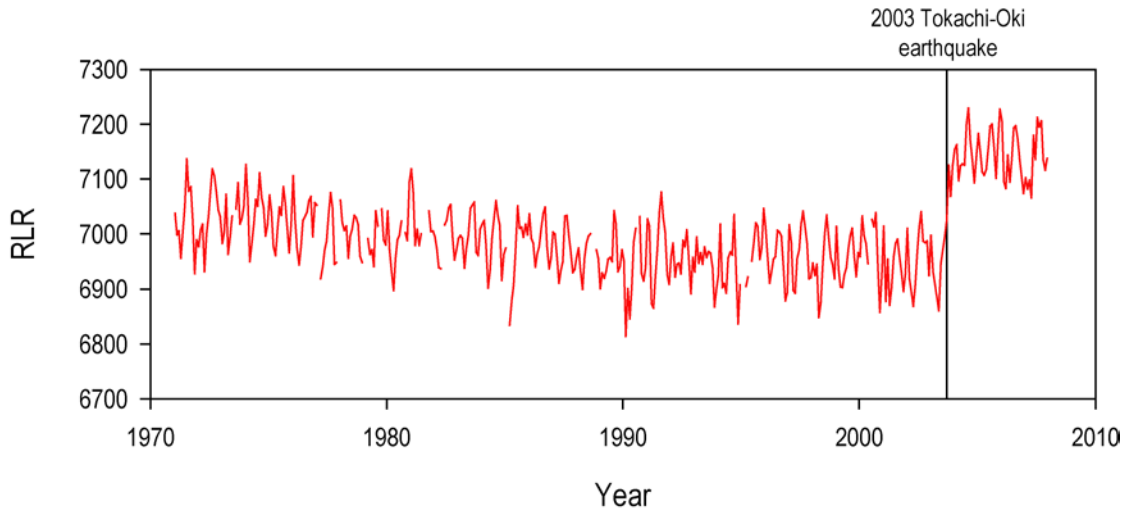

Figure 3.17 RLR record from Urakawa showing coseismic offset following the 2003 Tokachi-oki earthquake.

Eustatic corrections

Over the 20th century, global sea level has risen in the order of 1.7+/- 0.5 mm/yr (IPCC, 2007), which is attributable to changes arising from thermal expansion of the oceans, as well as ice-equivalent sea-level rise due to the melting of continental ice reservoirs. From a recent analysis of global sea-level calculated from tide-gauge records, this acceleration appears to have started at the end of the 18th century and constitutes a rise equal to 0.01 mm/yr (Jevrejeva *et al.*, 2008).

From a global and regional perspective, the effects of eustatic sea-level rise are spatially and temporally variable. To correct for these variations, I use regional estimates of eustatic sea level provided by Aslak Grinsted (*pers. comm.*) following the methods detailed in (Jevrejeva *et al.*, 2006). In brief, the approach involves using West Pacific tidal-gauge data (excluding Japan given its tectonic setting) that has been corrected for local datum offsets and GIA and then stacked to calculate a mean annual rate for a given month over a whole year. Figure 3.18(A) shows the stations used in the analysis, and (B) displays the amount of eustatic sea-level rise has occurred. Sea level was relatively stable until the 1940s after which it rose rapidly. For the 28-year period over which the tide gauges are being detrended in this thesis, sea level has remained relatively flat.

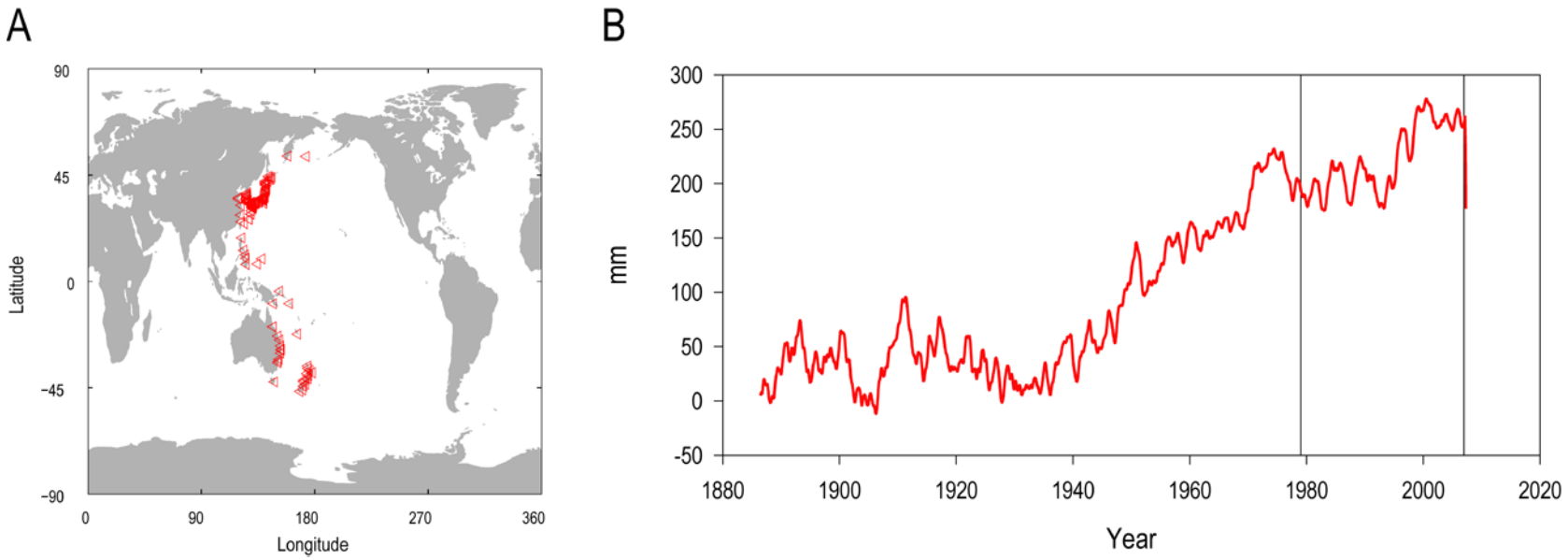

Figure 3.18 Method showing the eustatic correction used in this thesis including (A), map showing all tide-gauge stations used in the West Pacific dataset, and (B) graph showing the amount of eustatic sea-level rise predicted over the last century (highlighted zone represents period of tide-gauge analysis used in this thesis).

Only coseismic offsets are excluded from the record. Therefore, to limit the longer-term tectonic component the eustatic function is derived from stations in the West Pacific area (excluding Japan). Obviously, other circum-Pacific countries will have experienced tectonic deformation but the large Japanese dataset included in the analysis would otherwise mask the eustatic signal in the record. Finally, it is important to note that a three-year trend is computed to encompass the variability arising from El Niño-Southern Oscillation that would otherwise contaminate the record.

Glacio-isostatic corrections

The field sites are located a considerable distance from the former and current ice sheets, although it is likely that they are influenced by on-going isostatic effects associated with water and/or ice-load change. To assess for the significance of this effect, I use the data provided by Professor Dick Peltier accessible from the Permanent Service for Mean Sea Level website (http://www.pol.ac.uk/psmsl/peltier/index.html). The ice-model used throughout is ICE-5G v1.2 (VM2) with a 90 km lithosphere. The values listed for the rate of RSL change for each of the tide-gauge stations analysed are provided in Table 3.9

Table 3.9 GIA model predictions for RSL change over the last 100 years in Hokkaido.

Station Name	Rate of sea level change for past 100 years (mm/yr)
Okhotsk and North Pacific	
Abashiri	-0.82
Kushiro	-0.8
Hanasaki	-0.75
Monbetsu II	-0.83
Muroran	-0.78
Urakawa II	-0.83
Wakkanai	-0.76
Japan Sea	
Hakodate II	-0.77
Oshoro I	-0.77

GPS and repeat levelling data

The Geographical Survey Institute has been running over 1,200 continuous GPS stations throughout Japan for up to 10 years. These provide a unique opportunity to investigate high-resolution land deformation over a wide spatial setting (Ito *et al.*, 2000; Aoki and Scholz, 2003). For example, Takahashi (2004) investigated the postseismic crustal deformation associated with the 2003 Tokachi-oki earthquake and found no evidence of vertical deformation suggesting the afterslip occurred in and around the coseismic fault rather than at the downdip extension. Furthermore, Miura (2004) used GPS data to conclude that the maximum coseismic slip roughly accounted for the slip-deficit accumulated in the past 51 years. In addition to GPS data, there have been several repeat levelling surveys of benchmarks in Hokkaido over the last 100 years (e.g. Yokoyama, 1987).

In this analysis I incorporate only the previously published analyses of these data, especially that by Yokoyama (1987) and Aoki and Scholz (2003).

3.4 SITE SELECTION

3.4.1 Geological setting of Hokkaido

The geological setting of the Japanese archipelago (Figure 3.19) can be divided into distinct geological and geomorphological zones:

- **Forearc basin**: a sedimentary basin in the sea floor located between a subduction zone and a volcanic arc;
- **Outer arc (outer zone):** a non-volcanic and sluggish uplift area;
- **Inner arc (inner zone):** an active volcanism and crustal movement area;
- **Backarc basin**: an ocean basin behind an arc, marginal sea;
- **Collision zone**: a zone in which arcs meet.

Hokkaido sits on a continental plate that is being subducted by the Pacific Plate westward from the Kuril Trench at a rate of 8-9 m per century (Demets, 1992). During this process, sediment is scraped off the top of the descending plate and accumulates as an accretionary prism at the leading edge of the overriding plate. Sediments derived from continual underthrusting overlie previous prisms. Under high pressure, the bases of the accretionary prisms are dragged into the deeper parts of the crust and become metamorphosed. At depth, the resulting magma rises to the surface due to its relative buoyancy and either solidifies to form plutonic rocks in the lower crust, or rises to the surface where it erupts to form volcanoes. Magma is only able to form at sufficient temperatures (corresponding to depths of *c.* 150 km), resulting in a volcanic front forming within the inner arc.

The continuing process of subduction at the Kuril and Japan Trench and the Nankai Trough has resulted in a volcanic arc from the Kuril Islands, north-east of Hokkaido, which stretches throughout the Japanese archipelago. In Hokkaido, active and Quaternary volcanoes run from the Shiretoko Peninsula to the Iburi prefecture in the south-west.

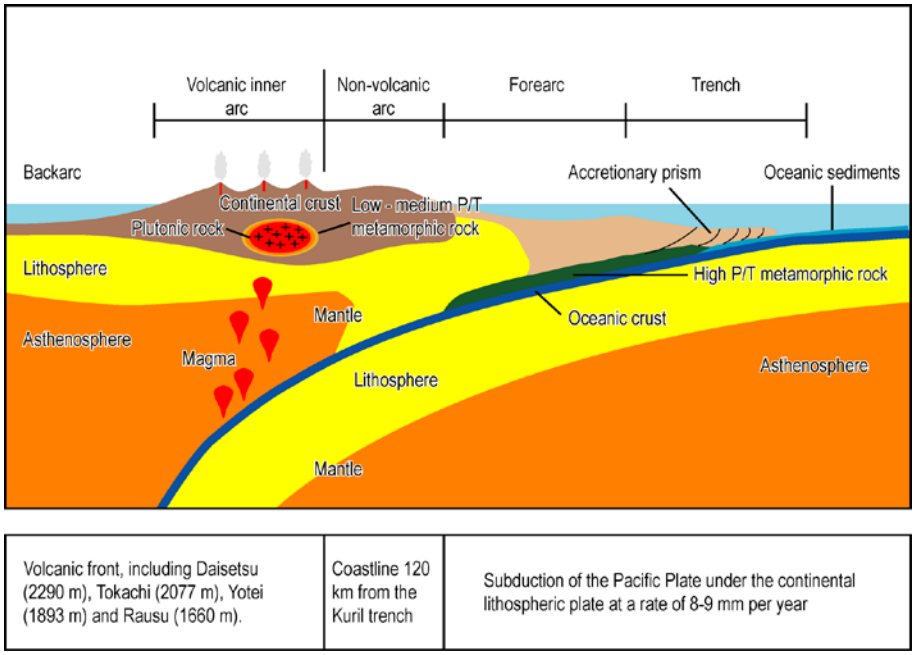

Figure 3.19 Idealised model of a subduction zone (arc-trench system), with additional details on the subduction zone features found on the Hokkaido coastline.

3.4.2 The geological evolution of Hokkaido

The geology of Hokkaido (and Japan more widely) is complex and reflects the range of processes operating on a subduction zone. From the late Jurassic to the present, accretion and collision processes have shaped the crustal evolution of Hokkaido (Maeda, 1986; Niida and Kito, 1986; Sakakibara *et al.*, 1986; Kimura, 1994), and its central and eastern area can be divided into two main geological provinces:

Central area (Collision Zone)

The central part of Hokkaido comprises several North-South trending tectonic units. From west to east, the Sorachi-Yezo Belt is characterised by ophiolite sequences, with Cretaceous forearc basin sedimentary rocks and intrusions of high-P metamorphosed rocks (Kamuikotan Metamorphic Belt). The Hikada Belt was created by an older collision between palaeo-North American and Eurasian Plates initiated in the Eocene (Komatsu *et al.*, 1983; 1989). During the Miocene, westward migration of a fore-arc sliver of the Kuril arc gave rise to a second, younger period of collision (Kimura and Tamaki, 1985), which caused enhanced uplift of the Hidaka Mountains and crustal shortening of *c.* 60 km (Kazuka, 2002). Between such events, Kuril and Japan back-arc basins began to spread (Lallemand and Jolivet, 1986) leading to the rotation and rearrangement of Hokkaido (Itoh *et al.*, 2005).

Eastern area

Eastern Hokkaido represents the south-western margin of the Kuril arc that evolved as an oceanic island arc. The Konsen plateau and the Kushiro plain characterise the outer arc lowlands whereas the Shiranuku Hills, which lie to the west, reflect uplift caused by collision resulting from the westward advance of the Kuril Arc. The Tokachi Plain represents a subsiding basin between the Shiranuku Hills and Hidaka Mountains. Within the inner arc, Hokkaido's volcanic ridges (Akan volcanoes, the Shiretoko Peninsula, Kunshiri Island and the Etorofu Island) are arranged in an echelon caused by the continuing oblique subduction of the Pacific Plate into the Kuril Trench.

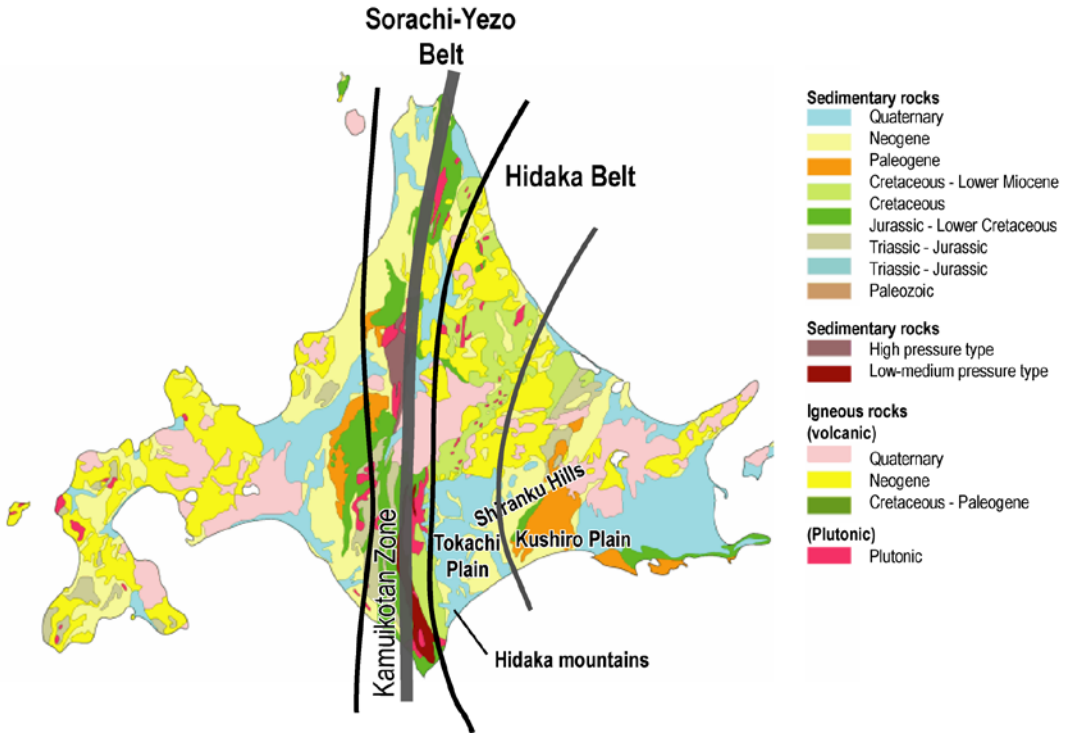

Figure 3.20 Geological map of Hokkaido, showing the main structural zones and areas of interest mentioned in text. Modified from the National Atlas of Japan (Geographical Survey Institute, 1997).

3.4.3 Environmental setting

Hokkaido has a temperate climate with low humidity (Figure 3.21). Summer and winter temperature ranges are generally between 18°C to 22°C and -12°C to -4°C respectively, depending on elevation and latitude. The western side of the island receives particularly heavy snowfall arising from the cold seasonal winds from the Sea of Japan, which are associated with high atmospheric pressure over eastern Siberia. The vegetation of Hokkaido is dominated by boreal, mixed broad-leaved deciduous and coniferous forests of *Picea jezoensis*, *Abies sachalinensis*, *Quercus mongolica* ssp. *Crispula*, and *Acer mono* (Haemet-Ahti *et al.*, 1974; Kojima, 1979). The island was the native home of the aboriginal

Ainu peoples, until the settlement by the Japanese in 1869, when the territory name was renamed from Yezo *dō* (province) to Hokkaido (North Sea Province).

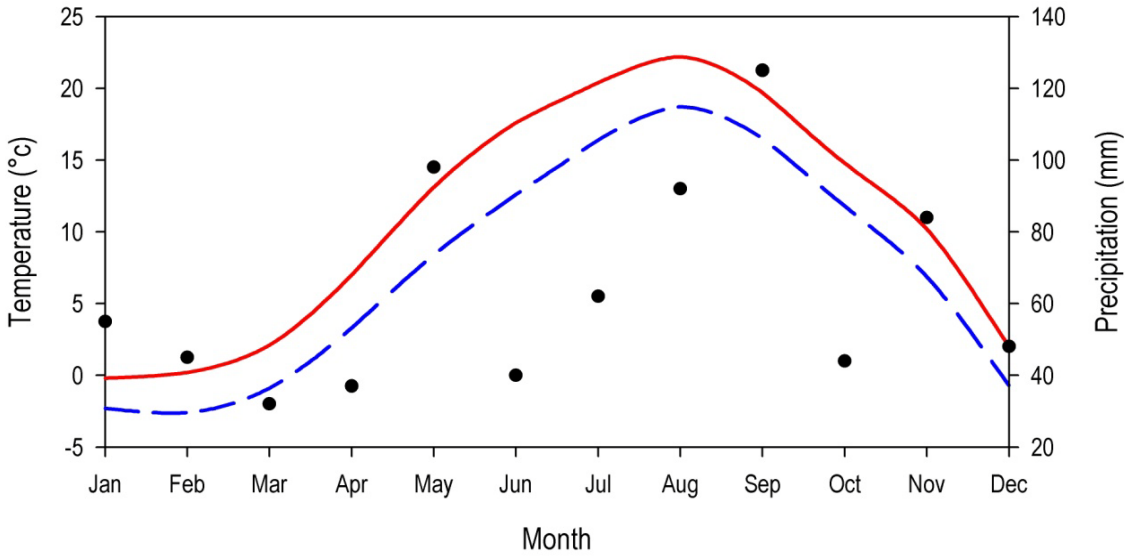

Figure 3.21 Climate variability for Nemuro, on the north-eastern coastline of Hokkaido in 2004. Red and blue lines represent maximum and minimum temperature respectively, and dots indicate precipitation values for individual months. Data sourced from the Climate Data Online system, accessible via http://cdo.ncdc.noaa.gov/CDO/dataproduct.

The cool, temperate climate of Hokkaido has facilitated the formation of a variety of wetland habitats, the majority comprising of peat-forming mires. The lowland mires develop at altitudes below 20 m and are thought to have been influenced by the Joman transgression that peaked *c*. 6,000 years BP (Sawai and Mishio, 1998). The largest mires formed after the sea retreated and are generally younger than 3,000 yrs BP. Compared with Honshu, the salt marshes of Hokkaido are relatively intact, owing to the lower human population density and comparatively short history of land reclamation. According to a recent evaluation of the wetland areas on the Hokkaido coastline, four major salt-marsh areas exist on the northern and eastern coastlines (Saroma-ko, Notoro-ko, Akkeshi-ko and Shunkunitai) as well as eleven smaller ones (Fujita *et al.*, 2009).

Hokkaido contains many of the marshes of Japan, which are specially protected by the government although between 1928 and 1996 salt-marsh areas have decreased from 62,419 ha to 42,876 ha (Sawai *et al.*, 2004b). The section below details the rationale for site selection.

3.4.4 Rationale for site selection

Site selection

Sampling in the marshes of eastern Hokkaido has been established by Dr Yuki Sawai and his colleagues at the Geological Survey of Japan and forms the basis for determining the location of sampling for the fossil material used in this study. Previous research has tended to focus on sites nearest to the trench, on the north-eastern Pacific coastline (e.g. Atwater *et al.*, 2004; Kelsey *et al.*, 2006; Sawai *et al.*, 2009) but less is known about patterns from sites further from the trench. Obtaining data across the full length of the Hokkaido coast was a key objective to test the full pattern of deformation predicted by recent dislocation models (Figure 3.22).

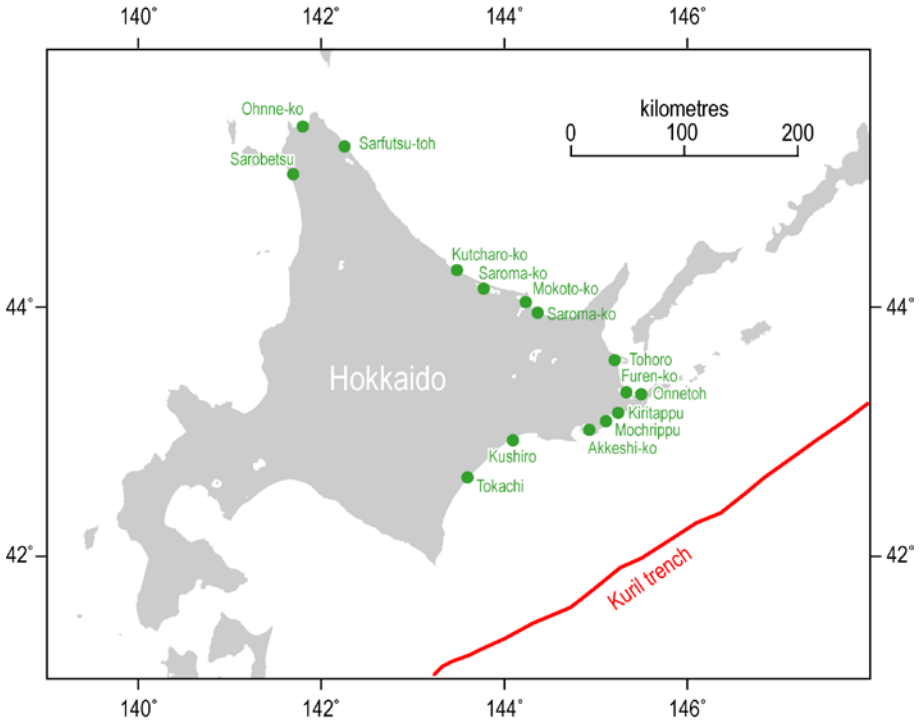

Figure 3.22 Location of marshes in north and north-eastern Hokkaido. Green circles shows areas of marsh.

Reconstructing RSL change in Hokkaido can be approached in two ways. The first is to examine a single event at several sites, to see whether the spatial pattern of uplift/subsidence occurs as predicted by the model. The most appropriate target for this is the 17th century event which is widely recorded and present in the near surface for ease of sampling. A second approach is to assess how typical the 17th century event is of other events. This can be achieved by looking at multiple events in a single core.

Since my main thesis aim is to document deformation patterns during the current interseismic period, I chose to focus solely on the RSL record since the 17th century event.

Site selection followed a review of previous research, an assessment of sites based on preliminary site visits, analysis of remotely sensed data (e.g. Google Earth) and researching the expert local knowledge provided by colleagues from the Japanese Geological Survey. My main objective was to identify low-energy depositional sites with well developed salt marshes (Figure 3.23), containing an undisturbed record of sedimentation since *c.* AD 1700. Where possible I sought to avoid sites significantly influenced by human impact, storm surges or freshwater discharge.

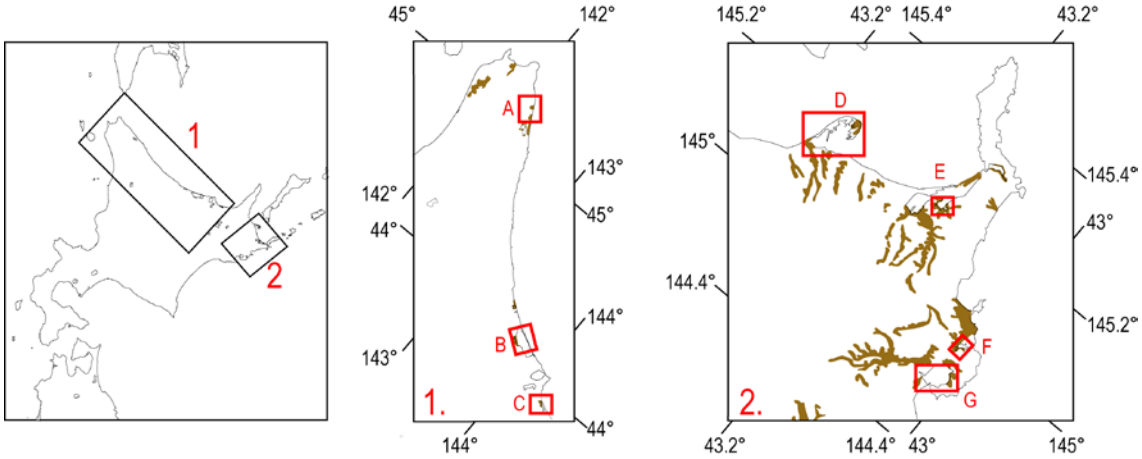

Figure 3.23 Location maps of northern (1) and eastern (2) Hokkaido coastline showing the location of salt marshes with details of the study locations. Brown shading denotes coastal salt marshes and associated freshwater wetlands. Where A: Sarfutsu-toh; B: Saroma-ko (modern samples only); C: Tofutsu-ko; D: Tohoro (fossil analysis only); E: Furen-ko; F: Mochiruppu and G: Akkeshi-ko.

In the following I provide a brief introduction to each of the study sites, including a review of the site's geomorphology as well as reference to previous research. Tide levels vary between the six key study sites as detailed in Table 3.10.

Table 3.10 Tide levels (m TP[1]) for Hokkaido. Source: Hydrographic and Oceanographic Department (2006) with additional information regarding levelling to national datum provided by the Japan Hydrographic Association (*pers. comm.*).

Station name	LAT	MLLW	MLHW	MSL	MHLW	MHHW	HAT
Monbetsu	0.73	0.36	0.06	-0	-0.04	-0.44	-0.87
Wakkanai	0.5	0.36	*	0.24	*	0.16	-0.04
Otaru	0.49	0.26	0.26	0.22	0.26	0.06	-0.07
Hakodate	0.44	0.22	0.02	-0.1	-0.18	-0.48	-0.78
Muroran	0.59	0.19	-0.01	-0.3	-0.31	-0.81	-1.38
Urakawa	0.68	0.32	0.22	-0.1	-0.08	-0.58	-1.12
Kushiro	0.64	0.4	0.2	-0	0	-0.6	-1.08

[1] From observational data up to 1 March 2005.

* Tide is predominantly diurnal.

Akkeshi-ko

Akkeshi-ko (literately Lake Akkeshi) is a coastal embayment on the east coast of Hokkaido (43º01, 144º53) and is the closest study site to the Kuril Trench, at a distance of 120 km. Akkeshi-ko is the largest estuary on the Pacific coast of eastern Hokkaido, at 30 km^2 in size,

and has one major tributary (Bekanbeushi River) that enters the embayment from the north. According to 1:10,000-scale bathymetric maps produced by the Geographical Survey Institute (published in 1979 and 1981), the embayment is approximately 2 m deep (Sawai, 2001). Because of its size, a large tidal prism produces strong tidal currents and maintains a bay-mouth channel (Sawai *et al.*, 2009: 239-40). Akkeshi-ko is connected to a marine embayment at Akkeshi town.

Well developed salt marsh occurs throughout much of the Akkeshi-ko's embayment. The Ikuraushi salt marsh is located on the southern shore and comprises a tidal flat, storm beach deposit, back swamp, high marsh and freshwater swamp. The marsh is dominated by a *Glaux maritima* v. *obtusifolia*, *Triglochin maritimum* and *Atriplex gmelinii* with *Phragmites australis* dominating the high-marsh area. Rich freshwater swamp vegetation characterises the back of the marsh and is dominated by *Alnus japonica*, *Spiraea salicifolia*, Cacalia *auriculta* var. *bulbifera* and *Veratrum album* subsp. *oxysepalum.* In the tidal flat, tree stumps are evident, which are hypothesised to have died following the subsidence event that occurred after the 17th century AD earthquake (Y. Sawai, *pers. comm*.).

A 400 m transect across the Ikuraushi salt marsh has been used to collect contemporary subtidal foraminiferal samples with two additional short-core samples collected to study the infaunal nature of foraminifera on Hokkaido (Figure 3.24).

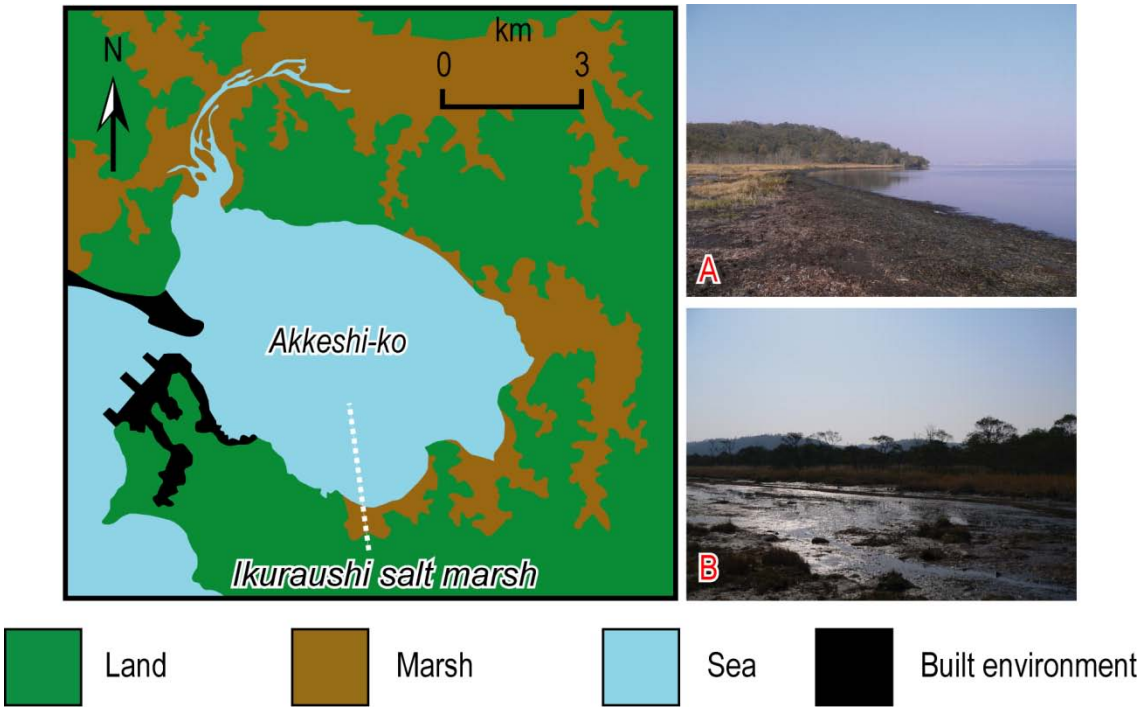

Figure 3.24 Location map of Ikuraushi salt marsh, Akkesko-ko with photo detail, showing A; berm and out to sea, and B; backmarsh. A former interglacial shorelines can be seen in the background as a distinct terrace. The white-dashed line is the location of the contemporary transect. Sampling extended from LAT to the middle of the embayment.

Mochiruppu

Lake Mochiruppu is a small, 1 km^2 brackish estuary along the Pacific coast of eastern Hokkaido (43º, 145º). Mochiruppu is only 9 km from Akkeshi-ko and both should record a similar sea-level history. A small tidal creek several metres wide and over a metre deep maintains saline conditions in the lagoon. The channel was dredged and widened a few years ago according to eye witness accounts (Atwater *et al.*, 2004). Salt marshes border the estuary, particularly established on its south-eastern and western edges. Three transects (A-C) were studied for this thesis.

The low marsh is dominanted by *Carex subspathacea, Spergularia marina, Triglochin asiatica, Glaux maritima var. obtusifolia,* and *Spergularia marina,* with *Veratrum album, Carex* sp., *Spiraea salicifolia, Alnus hirsuta* occupying a higher marsh position. The freshwater swamp at the back of the marsh displays a diverse fauna comprising *Veratrum album, Carex* sp., *Spiraea salicifolia, Alnus hirsuta, Phragmites australis, Betula platyphylla* var. *japonica, Salix* sp. and other species such as *Umbelliferae* sp. and ferns.

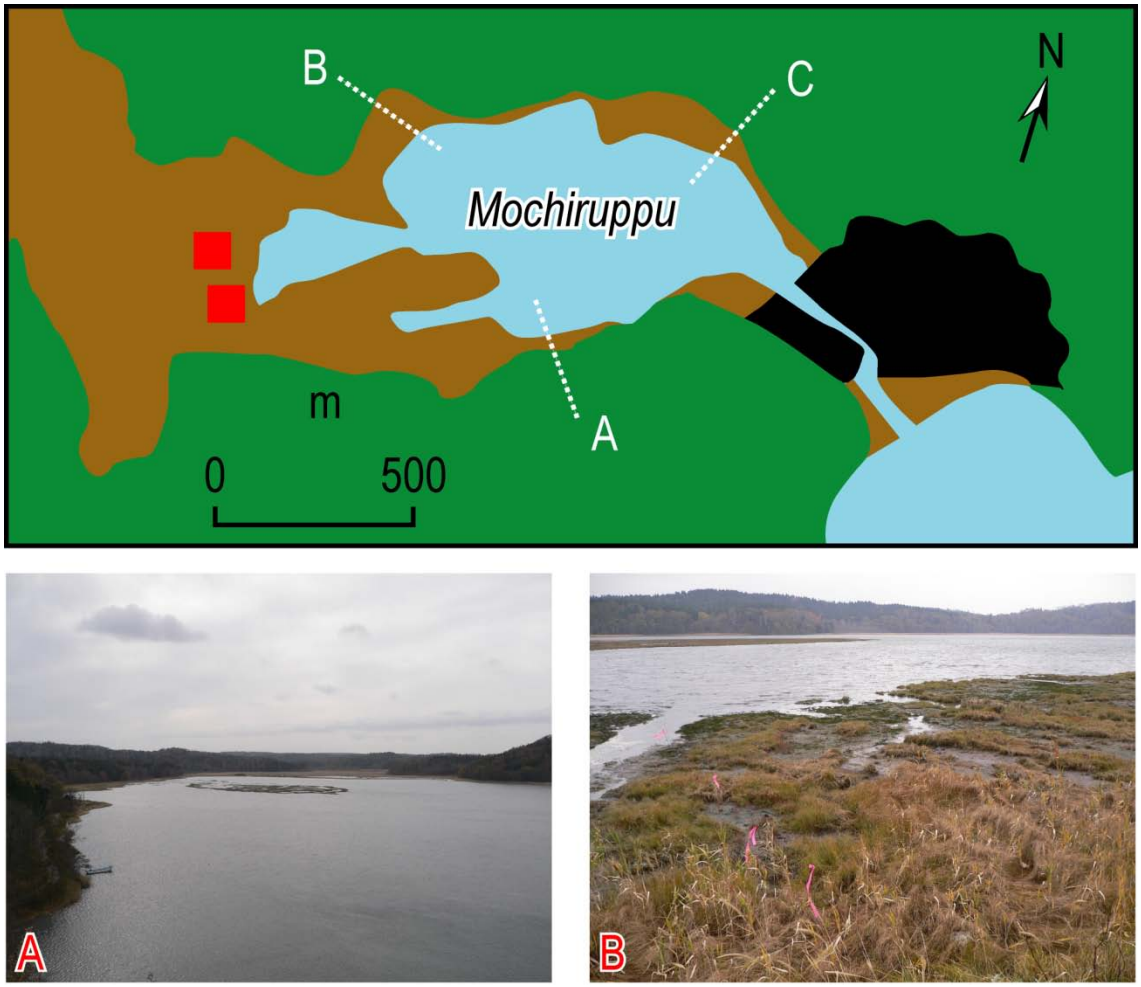

Figure 3.25 Location map of Mochiruppu salt marsh with photo detail showing A; an overview of the site and B; one of the contemporary transects studied for this thesis. Each stick with a (pink) flag represents a 0.05 m cm change in vertical resolution running from tidal flat to freshwater swamp. The white dashed lines are the locations of the contemporary transects, and the red squares represent the temporary benchmarks established at this site by Yuki Sawai.

Furen-ko

Furen-ko is a large (*c.* 40 km^2) lagoon on the Nemuro gulf, close to the Nemuro Peninsula in eastern Hokkaido (43º19, 145º17). The sandbars of Shunkuni-tai extend from the south and Hashirikotan stretches from the north, allowing seawater to flow through two waterways. Furen-ko extends 20 km from east to west and with its circumference of 65 km is one of the largest wetland environments on Japan, giving rise to a rich fauna and flora. Water depths are less than 2 m according to 1:10,000 bathymetric maps produced by the Geographical Survey Institute published in 1979 and 1981 (Atwater *et al.*, 2004). Five major rivers transport freshwater to the lagoon, the largest of which gives its name to the area, the Furen River. Bay-mouth channels may reach 13 m at their deepest parts (Atwater *et al.*, 2004).

Salt marshes fringe a number of the river mouths that terminate in the estuary, although they are particularly extensive along the bank of the Furen. Numerous tree stumps killed by historic submergence occur within the marsh area. Salt marsh extends over the lower reaches of the Furen-gawa (river), which flows into Furen-ko. The marsh is divisible into a low and high marsh zone; *Glaux maritima* v. *obtusifolia*, *Triglochin maritimum* and *Atriplex gmelinii* characterise the low marsh with *Phragmites australis* the dominant species in the high-marsh area. Marsh flora give way to a diverse freshwater swamp characterised by *Alnus japonica*, *Spiraea salicifolia*, Cacalia *auriculta* var. *bulbifera* and *Veratrum album* subsp. *Oxysepalum* with sand dune forests of *Picea glehnii* (The Ministry of the Environment, 2002; http://www.sizenken.biodic.go.jp/pc/wet_en/23/23.html). Pleistocene interglacial shorelines surround Furen-ko (Ohira *et al.*, 2004).

Ohira *et al.* (1993; 1994; 2004) have studied the sediments of Furen-ko extensively. Atwater *et al*. (2004) demonstrate that the stratigraphies at Furen-ko are similar to other eastern Hokkaido marshes showing evidence that intertidal or subtidal flats became well-vegetated late in the 17th century, however dead tree stumps suggest persistent subsidence over the historical period (Moriwake, 2005).

I have collected one transect for contemporary sampling from the south-east part of the Furen-ko embayment (Figure 3.26).

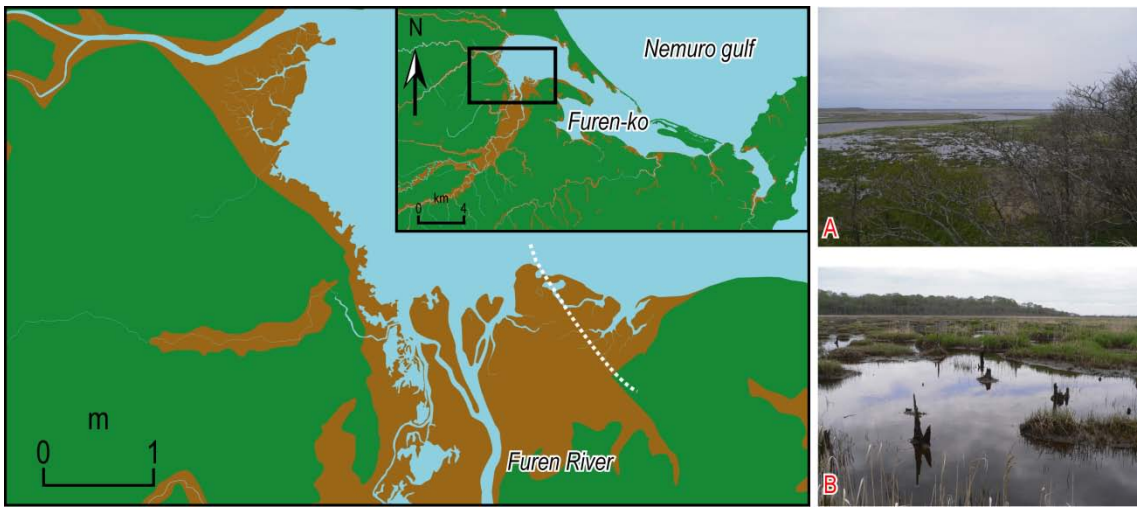

Figure 3.26 Site map and photos of Furen-ko marsh. A; Photo looking north over the salt marsh beside the Furen River and B; looking landward over the low marsh species and dead tree stumps towards the forested swamp and the Pleistocene terraces behind. The white dashed line is the location of the contemporary transect.

In comparison with the other sites the macrophyte vegetation zones (and foraminiferal assemblages, see next Chapter) are found at high elevations within the tidal frame. In particular, high marsh environments extend to above HAT (0.69 m TP) to a maximum of

1.46 m TP. This is a significant difference when considered in the context of the small tidal range in this area and the survey methods used. These datum were surveyed using a Total Station relative to a permanent benchmark that forms part of the national Geological Survey of Japan TP network. It was not practical to use closure to assess the survey data, which was located 4 km from the bench mark and consequently it is possible that errors may exist. Moreover, a survey of time-still-water (TSW) during the field work indicated an elevation difference of precisely 1 m between the predicted TSW and observed water level. The TSW survey work at Akkeshi-ko yielded a predicted value that was within 1 cm of that predicted by tide tables. For this reason, in the following analysis I use the datum determined by the TSW method for the Furen-ko site. This brings the height range of the macrophytes and foraminifera within the range observed at adjacent sites.

Maruman marsh, Tofutsu-ko

Tofutsu-ko is a 20 km^2 lagoon on the eastern Okhotsk Sea (44º00, 144º21; see Figure 3.27), approximately 10 km from the city of Abashiri. Tofutsu-ko is a lake formed by development of sandbar. Its catchment area includes part of the northern area of Mokoto-yama mountain system and connected hills and flatland. Six main rivers flow into the embayment, but the embayment's only outflow is to the east, through the town of Kitahama. The embayment is generally shallow, 1.1 m on average and 2.5 m at its maximum depth (Soeda, 2002). Salt marshes fringe different sections of the embayment and are particularly developed along the Maruman River, at the far eastern end of Tofutsu-ko. The embayment is surrounded by a terrace, which Soeda (2006) interpreted as a pyroclastic flow deposit from a Pleistocene volcanic eruption.

The Maruman salt marsh comprises a low and high marsh fauna; the low marsh is characterised by *Carex lyngbyei*, *Carex subspathacea*, *Stellaria humifusa*, *Eleocharis kamtschatica f. reducta* and *Glaux maritima v. obtusifolia*, which gives rise to a small high marsh zone characterised by *Carex lyngbyei*, *Stellaria humifusa* and *Phragmites australis*. The freshwater swamp is particularly diverse, dominated by *Alnus japonica*, *Prunus* sp., *Veratrum album* subsp. *Oxysepalum* and *Lysichiton camtschatcense*.

I have collected one transect for contemporary sampling from the western part of the Tofutsu-ko embayment (Figure 3.14).

Figure 3.27 Site map and photo of Tofutsu-ko showing a photo across the study marsh, taken from the location of the red square looking south across the embayment. The white dashed line is the location of the contemporary transect.

Kerochi marsh, Saroma-ko

Saroma-ko is a brackish water lagoon (44 6ºN, 143 44ºE) on the north-eastern coastline of Hokkaido. It is 149.2 km^2 in area and comprises two basins, an eastern and central one, both of which exceed 10 m in depth. The central basin is the deeper of the two with water depths of 19.6 m (Tada and Nishihama, 1988). Two main rivers (the Barou and Saromabetsu) outflow to the lagoon, as well as a number of smaller rivers, including the Kerochi. The lagoon connects to the sea through two inlets. The majority (90%) of the total seawater inflow enters through the western inlet opened in 1929, while the remainder comes via the eastern inlet built in 1978 (Shirasawa *et al.*, 2005). During winter the lagoon freezes over, typically to depths of 35-60 cm in the deeper eastern area (Takata *et al.*, 2006).

Previous analysis of the foraminiferal assemblages in the lagoon (Takata *et al.*, 2006) suggest three faunal types; (i) a lagoon-bottom fauna dominated by *Haynesina* spp.; (ii) a shallow-water fauna dominated by *Trochammina* cf. *japonica*; and (iii) a river-mouth fauna dominated by *Elphidium excavatum*. In combination with existing studies of the lagoon (subtidal) species (Takata *et al.*, 2006), (Troels-Smith, 1955)the marshes of Saroma-ko offer the possibility of using intertidal foraminifera as sea-level indicators in this crucial area *c*. 300 km from the Kuril Trench. Whilst the inclusion of these samples may have improved the quantity of the subtidal samples collected at Akkeshi, the collection methods involving surveying to significant water depth is too inaccurate for inclusion in my training set.

Kerochi marsh lies near the town of Yubetsu in Saroma-ko. The marsh lies at the estuary head at Kerochi-gawa (Kerochi River) in the southwest end of the Saroma-ko lagoon. The marsh comprises distinct faunal zones ranging from *Phragmites australis* and *Triglochin asiaticuma* dominating the low marsh areas, to *Phragmites australis*, *Potentilla egedei* v. *groenlandica*, *Carex subspathacea* and *Glaux maritima* var. *obtusifolia* becoming more established in the high marsh zone. I completed the modern sampling along a 130 m

transect located in the Kerochi marsh, with an additional small transect established perpendicular to the marsh to confirm the local stratigraphy.

Figure 3.28 Site map and photo of Kerochi marsh, Saroma-ko. The white dashed lines are the locations of the contemporary transects. Photo looking northwest from the *Phragmites australis* dominated low marsh to the tidal flat and towards the lagoon, with a ranging pole for scale.

Sarfutsu-toh

Sarfutsu-toh is a small marsh covering approximately 1 km^2 near the northern tip of Hokkaido on the Okhotsk Sea coast (45 18 ºN, 142 11ºE). Few salt marshes exist along the northern Hokkaido coastline, making this marsh particularly important for testing models of RSL change *c.* 500 km from the trench. The Sarfutsu River flows through the small estuary as it meanders to the open coast. Interglacial marine terraces lie parallel to and above the contemporary shoreline. Marsh vegetation surrounds a tidal basin and is particularly developed along its eastern shore. The salinity of the marsh is low (< 2 psu) and the macrophyte vegetation is weakly zoned, consisting predominantly of *Phragmites australis* with additional *Chenopodiaceae* sp.-2 characterising the low marsh zone. A 220 m long transect extends from the middle of the estuary (which was very shallow, 1-2 m deep) to a freshwater swamp at the back of the marsh.

Figure 3.29 Site map and photo of the marsh at Sarfutsu-toh, Photo (A) looking from an interglacial marine terrace (unknown age, presumed MIS 5e) over toward the marsh, with the dotted line showing the transect location; and (B) looking west over the *Phragmites australis* to the estuary.

Sampling design

Having studied the lithostratigraphy of each salt marsh in detail using the Troels-Smith scheme of sediment notation, careful consideration of the most appropriate location for coring followed. This study focuses on using foraminifera present in recent sediments to document interseismic sea-level change, and therefore it was essential foraminifera were present at the surface of the core to allow reconstruction up to the present day. Preferably, cores taken from the high marsh are desirable as the microfossils in these locations tend to be more sensitive to changes in sea level, compared to those on the low marsh or tidal flat.

3.5 CONCLUSIONS

This Chapter provides a review of the methods used to collect data in this thesis and an introduction to the study sites where data has been collected. The main conclusions are:

- The focus of my field-based studies is the collection of contemporary and fossil data from a set of salt marshes from Hokkaido, Japan. The methods involved in data collection relate to field and laboratory techniques, as well as some aspects of data processing.
- Field methods entail detailed surveys of contemporary environments relative to a common reference datum to enable between site comparisons. Macrophyte vegetation zones provide a simple zonation of the salt marshes, which can generally be divided into a low and a high marsh, bordered by tidal flat and freshwater swamp respectively, although variations occur as a result of variable freshwater inflows.
- Contemporary surface sediment samples were collected from transects at each site to enable the development of a regional foraminiferal-based transfer function, detailed in the following chapter. The number of sites considered, precluded the development of local training sets for each marsh. The range of palaeoenvironments expected in the fossil sequences also made a regional training set intuitively more attractive, compared to the use of a local training set because of the greater range of contemporary environments sampled.
- Contemporary samples are also analysed using standard methods for grain size, loss on ignition, as well as pH and salinity.
- Lithostratigraphic studies use a hand gouge to sample the sediments associated with the last earthquake cycle, focussing on the upper few metres of unconsolidated sediment at the sample sites. In some instances existing lithostratigraphic data has been used to guide sample core collection, in others a

gouge core survey with either a Russian type sample, a modified piston corer, or a Geoslice sediment corer directed sample collection.

- Radiocarbon dating is not appropriate for dating these recently deposited Hokkaido salt-marsh sediments and instead I use a combination of ^{210}Pb and ^{137}Cs, as well as a prominent tephra to develop local chronologies for RSL change at each sample site.
- A brief introduction is also provided to the other methods used in this thesis that relate to the study including tide-gauge, GPS and repeat levelling data, as well as Holocene and Pleistocene RSL changes.
- Site selection has been designed to enable targeted testing of the spatial variations in RSL change associated with the last earthquake cycle in Hokkaido. Taking advantage of the orientation of the north-east coast of Hokkaido, I sampled sites that, when combined, comprise a transect that extends from close proximity to the Kuril subduction zone (minimum distance *c.* 150 km) to a maximum distance away of *c.* 500 km (where the seismic effect may be thought to be negligible).
- At each site I collected a minimum of one transect of contemporary samples as well as at least one sample core for fossil investigations. All cores and samples are surveyed to a common datum and their elevations standardised using the SWLI methodology.

CHAPTER FOUR

Results I – Contemporary Salt-marsh Data

4.1 INTRODUCTION

This chapter presents the results from the analysis of the contemporary data collected for this thesis from the salt marshes of Hokkaido. First, I present data regarding the contemporary environments of the six study sites, detailing loss-on-ignition, grain size, salinity, pH and the distribution of contemporary foraminifera. I then explore these datasets using various numerical techniques, including the development of transfer function models that I then apply to my fossil sediment sequences in Chapter Five.

4.2 CONTEMPORARY ENVIRONMENTS

Analysing foraminiferal assemblages to determine former sea level requires their contemporary distributions and controlling environmental variables to be established. This is particularly important because differences between rates of sea-level rise and sedimentation will cause shifts in the altitudinal and spatial distribution of foraminiferal zones. With respect to each environmental variable there are five critical limits for foraminifera: lowest level for survival; lowest level for successful reproduction; optimum level; maximum level for reproduction; and maximum level for survival. Variations in the number and type of foraminifera, and the factors that influence their distribution across the intertidal zone, were sampled on the six present day salt marshes on Hokkaido (Figure 3.23). A brief discussion on the importance of each factor in relation to foraminiferal abundance follows below.

Elevation

The salt-marsh elevation relative to MSL has been previously identified as a primary influence on foraminiferal distributions and has been employed to define vertical zonations within the intertidal zone (1980). Contemporary foraminiferal assemblages commonly reflect the same major marsh zones indicated by the distribution of vascular plants (Murray, 1971; Phleger and Walton, 1950; Scott and Medioli, 1980), although many local habitat

factors have the potential to influence the exact composition of individual foraminiferal assemblages. Scott *et al.* (1990) illustrated that foraminiferal assemblage zones in the northern hemisphere mirror those of the southern hemisphere. Moreover, studies from North America (Edwards *et al.*, 2004; Gehrels, 1994; Scott and Leckie, 1990), South America (Jennings *et al.*, 1995; Scott *et al.*, 1990) and Europe (Horton and Edwards, 2006; Massey *et al.*, 2006a; Petrucci *et al.*, 1983) have indicated that distinct low- and high-marsh foraminiferal assemblage zones can be recognised worldwide. The high-marsh zone is dominated by agglutinated species such as *J. macrescens* and *Trochammina inflata* whereas *Miliammina fusca* (also agglutinated) dominates the low marsh zones.

Scott and Medioli (1980) stated that the duration and frequency of tidal exposure are the most important variables controlling the distribution of foraminifera within the intertidal zone with salinity the next most significant variable. However, Jonasson and Patterson (1992) found that the effect of salinity is much more pronounced where there is considerable mixing with freshwater such as at the landward margins of a salt marsh. Furthermore, foraminiferal assemblages may be controlled by a number of variables (e.g. salinity, temperature, dissolved oxygen, etc.), which may have no direct relationship to altitude within the tidal frame (de Rijk, 1995; Murray, 1971; Patterson, 1990).

The depth of water overlying the foraminiferal habitat is a direct function of elevation. There have been many observations of the relationship between foraminiferal distributions and water depth (Bandy, 1960). Murray (1968) stated that the range of depths encountered in intertidal zones are too small to be significant.

pH

The pH variations within the intertidal environment are greater than in any other marine environment (Bradshaw, 1968). The pH has an effect on both the protoplasm cell and the calcareous test of foraminifera. The cell must remain between relatively narrow pH limits for survival. Experiments have shown that *Ammonia beccarii* cannot survive for more than 75 minutes at a pH of 2.0, or more than 37 hours at a pH of 9.5 (Bradshaw, 1968). Low pH creates a stress situation for calcareous foraminifera: specimens must spend considerable energy recalcifying their tests (Boltovskoy and Wright, 1976). Phelger (1970) found a high correlation between low pH and low foraminiferal abundance and diversity. Boltovskoy and Wright (1976) found evidence of dissolution (etching) of the calcium carbonate tests where the pH of the environment was below 7.8. Alve and Nagy (1986) reported dissolution of tests under a pH range of 6.5 to 7.2. Maximum dissolution typically occurs during winter when the solubility of calcium carbonate increases (Arnal, 1961).

Salinity

Salinity within the intertidal zone varies with time as a result of alternating periods of tidal inundation, desiccation, evaporation and heavy rain. The effect of continual increases and decreases in salinity upon foraminifera is unknown (Boltovskoy *et al.*, 1991). However, each foraminifer has specific limits of tolerance to salinity. The minimum and maximum salinity ranges for successful reproduction are small compared to those for survival (Bradshaw, 1968; Murray, 1968). Morphological variations will occur if a given species exists outside its salinity limits for growth. Numerous observations suggest that low salinities result in species becoming smaller and thin walled with their ornamentations decreased or absent (Boltovskoy *et al.*, 1991). Limited information is available on the effects of high salinities on test morphology. Scott and Medioli (1980) suggested that the development of the two ecophenotypes of *T. macrescens* (forma *macrescens* and forma *polystoma*) are the result of differing salinities: forma *polystoma* develops at higher salinities (> 20‰); and forma *macrescens* at lower salinities.

Substrate

Foraminiferal species live in a variety of substrates with sediment being the most common. Some foraminifera live on the firm surfaces of plants, although not all plants are suitable. For example, Codium and Fucus rarely support foraminifera (Matera and Lee, 1972). Foraminifera can be subdivided into those that live on the substrate (epifaunal) and those that live within the sediment (infaunal). Furthermore, species can be either free living and are able to move using their pseudopodia, or attached, either by their pseudopodia (clinging) or by cementation (sessile).

Previous observations of the relationship between sediment and foraminiferal distributions have concentrated on agglutinated species. Agglutinated foraminifera use specifically sized sediment particles (2 to 20 µm) for building their tests (de Rijk, 1995), an absence of which may limit their distribution. However, much of the literature concerning the relationship between sediment and foraminiferal distributions is contradictory. For example, Jones and Ross (1979) and Dublin-Green (1992) found that sediments with silt-clay substrates supported the largest numbers of *M. fusca*. Conversely, no such relationship was observed in similar sediments by Murray (1968) in Christchurch Harbour, England or by de Rijk (1995) in the Great Marshes, Massachusetts.

The influence of organic matter within the substrate on foraminiferal distributions is variable (Boltovskoy and Wright, 1976). High concentrations of organic matter can produce acidic conditions that are detrimental to foraminifera. Conversely, such high concentrations may enhance the nutritive content of the substrate and consequently favour survival, growth and reproduction (Boltovskoy and Wright, 1976).

Vegetation

Vegetation interacts chemically and physically with environmental variables. The interactions include: lower temperature ranges produced by shading beneath vegetation and algal mats; protection against desiccation; and the maintenance of air haloes around root material providing micro-organisms can remain in an aerobic environment (de Rijk, 1995; Dublin-Green, 1992; Murray, 1991).

4.3 PHYSICAL PROPERTIES OF THE HOKKAIDO SALT MARSHES

At each of the six studied sites I have collected data on organic content (expressed by percentage LOI), grain size, salinity and pH. Typically, samples have been collected from one transect across each marsh, which extended from the freshwater 'upland' or swamp across the high and then low marsh and onto the tidal flat. In addition, at one site (Akkeshi-ko) I collected samples from subtidal environments and at Mochiruppu I collected three transects of data in order to assess an extended zonation and intra-site variability in foraminiferal populations respectively. In general, samples from the contemporary environment were collected at fixed 0.05 m vertical intervals.

In general, the organic content of the contemporary Hokkaido salt marshes follows trends observed on other temperate and low latitude salt marshes, with amounts of organic material positively correlated with elevation (e.g. Horton and Edwards, 2006; Woodroffe and Long, 2009). Typical upland values are >80% LOI, high marsh 70-80% LOI, low marsh 40-80% and tidal flat <40% LOI (Figure 4.1). The shape of the curve is typically sigmoidal or 's' shaped, whereby LOI rises rapidly between 0 and 100 SWLI units and is generally flat at both ends of the environmental gradient.

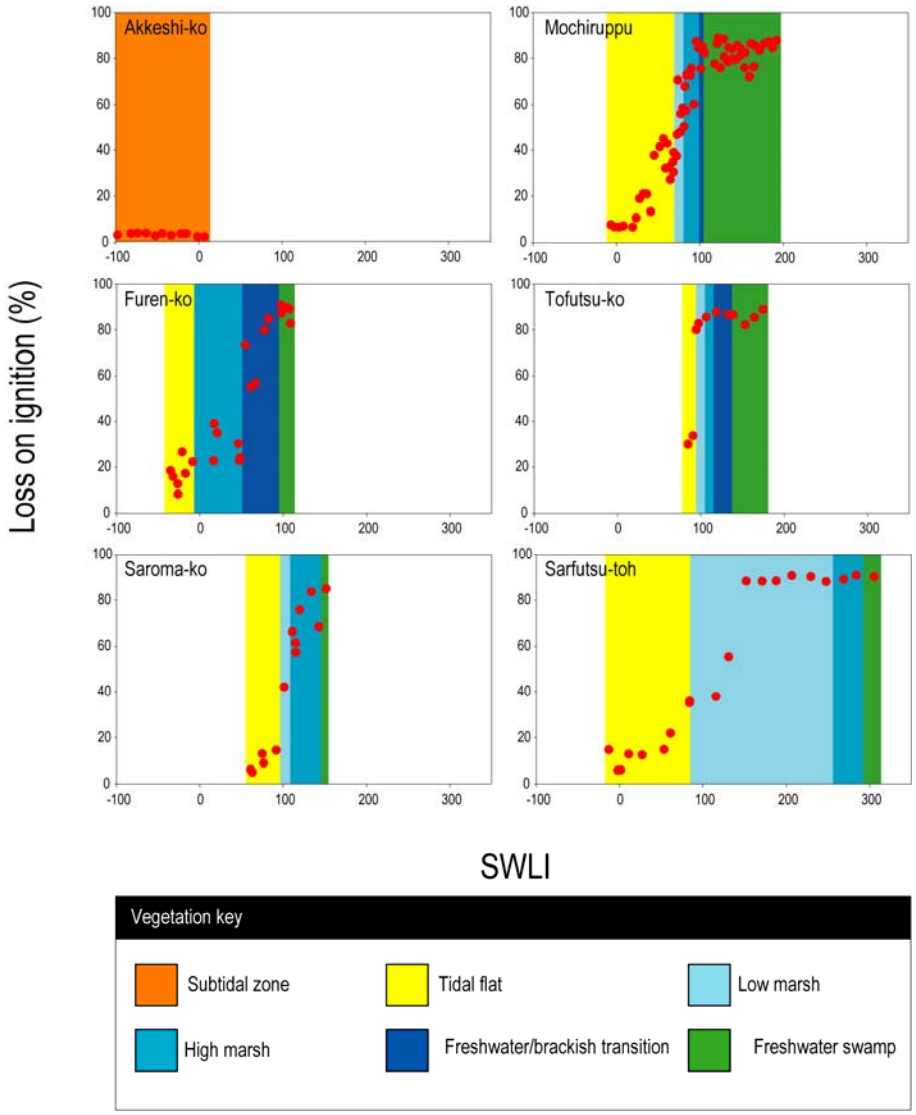

Figure 4.1 Variations in loss on ignition across the six contemporary marshes. In this and other diagrams elevation is displayed in Standardised Water Level Index (SWLI units), where MHHW at each site is 100 SWLI units, and MLLW at each site is 0 SWLI units. Colours on each plot represent different sections along the intertidal zone on the basis of vegetation data.

Data from the three transects at Mochiruppu provides an indication of within site variability. The percentage of LOI changes within this site are similar to the trends identified in the other field sites, showing overlap of the different transects at similar elevations (Figure 4.2).

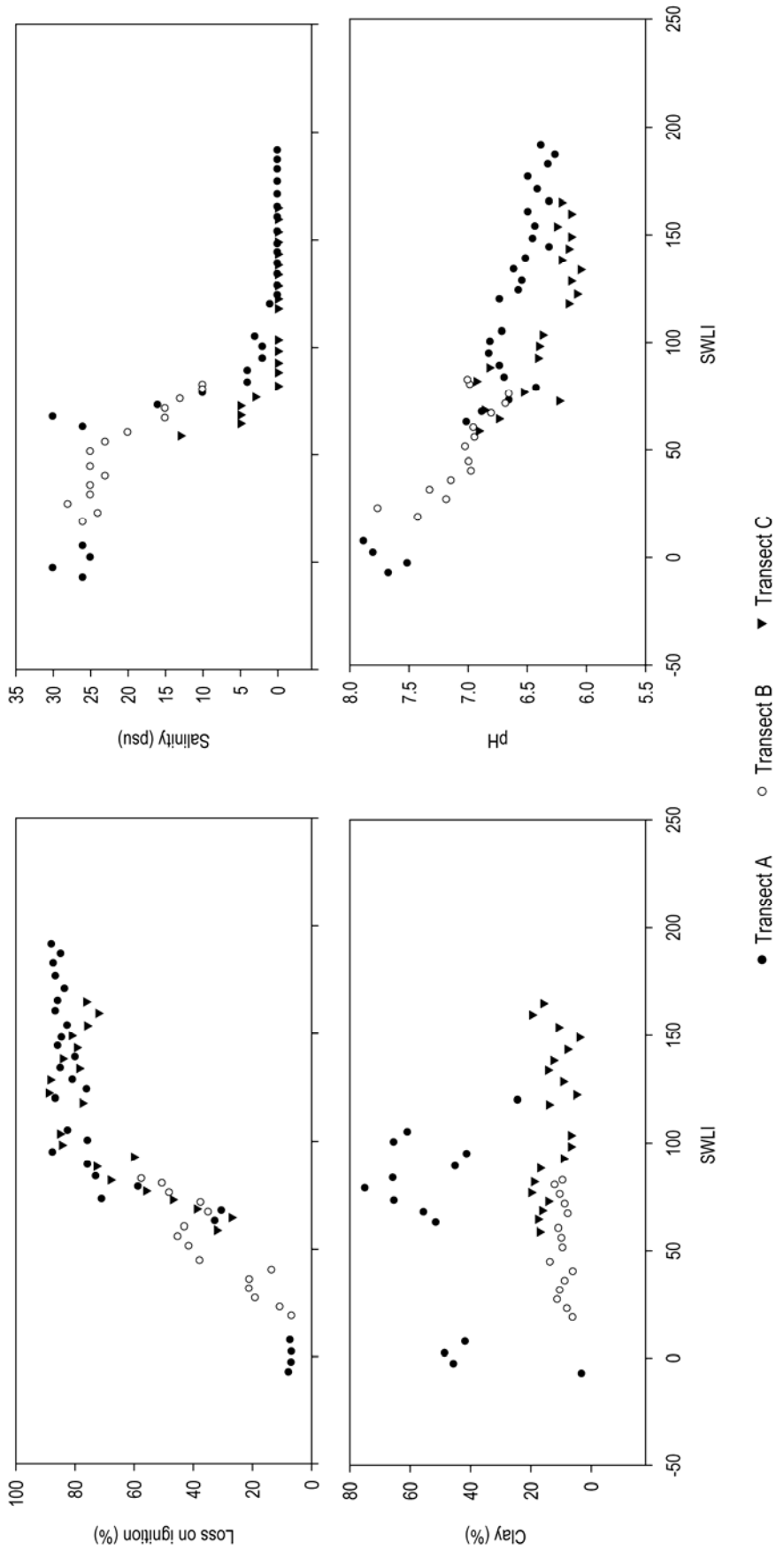

Figure 4.2 Intersite variability in environmental variables across the Mochiruppu salt marsh.

Grain-size measurements are more variable between the study sites (Figure 4.2 and 4.3). This reflects local variations in site exposure, including the presence of sandy barriers, as well as differences in the proximity of sample sites to tidal creeks. Care needs to be taken in interpreting grain-size data from the high marsh where abundant organic material makes interpretation of data problematic. The Hokkaido salt marshes are typically made up of silty clays with comparatively small amounts of sand. Clay content is generally limited in all of the six marshes, usually to < 20%. The three transects of Mochiruppu have the highest levels of clay, with levels typically between 60-80% on the marsh. Amounts of clay decrease across the tidal flat/low marsh transition (from 10% to 0%) in most sites and this is an important change in the contemporary environment that is also seen in fossil sediment sequences associated with a stratigraphic change from tidal flat to low marsh. Sand content varies along the intertidal zone, and is generally highest in the freshwater swamp areas toward the back of the marsh. Whilst this may represent the effect of trapping of sand by tidal-marsh vegetation (e.g. Li and Yang, 2009), as discussed above, it is more likely to represent fine organic fragments that did not fully dissolve during the hydrogen peroxide treatment in the particle size preparation. Excluding the freshwater swamp areas, sand is generally found in small quantities in the lower intertidal zone, with typical amounts varying between 20 and 40%. The quantity of silt recorded on the marshes of Hokkaido fluctuates between marshes. Akkeshi-ko, Tofutsu-ko, Saroma-ko and Sarfutsu-toh record higher levels of silt in the tidal flat and low marsh areas, and lower levels of silt in the upper sections of salt marsh. Mochiruppu and Furen-ko display the opposite trend, recording lower levels of silt in the tidal flat and generally higher levels on the marsh surface.

There appears to be considerable variation in the amount of clay between the three transects at Mochiruppu (Figure 4.2). Whilst transects B and C plot in similar locations, recording generally low levels of clay (between 0-20%), transect A records much higher levels of clay (between 40-80%) reflecting the local variability in environmental conditions.

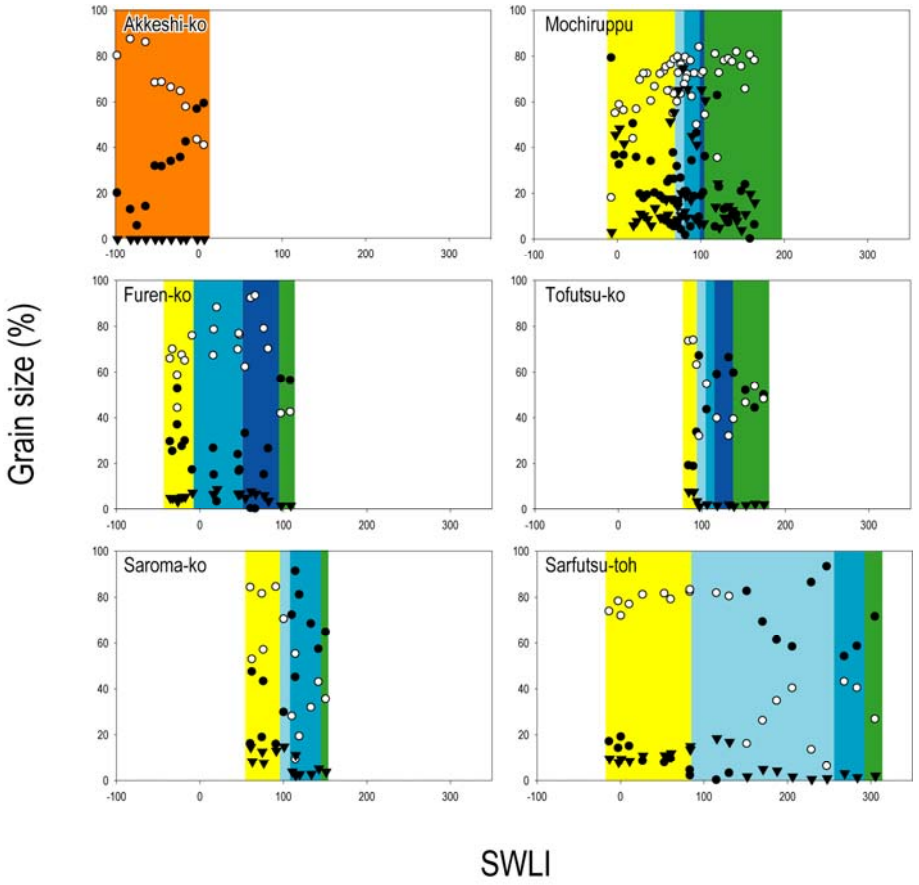

Figure 4.3 Variations in grain size across the six contemporary marshes, where sand = closed circles; silt = open circles; and clay = triangles.

Salinity in four of the six sites is inversely related to elevation and hence tidal immersion (Figure 4.4). Typical salinity values in subtidal and tidal flat environments are 34-35 psu and 25-30 psu, respectively. Salinity values start to decrease strongly above the tidal flat/low marsh transition, declining from 10-20 psu on the low marsh to 0-10 psu on the high marsh. Two of the sample sites have substantially lower salinity values compared to these values and require explanation. At Sarfutsu-toh and Tofutsu-ko, tidal flat salinity values are only *c*. 2 and *c*. 5 psu respectively. It is not clear what the cause is for these low salinity values. It is unlikely that they reflect measurement error, since the results from Sarfutsu-toh were replicated on two occasions in the 2005 and 2006 field seasons. Freshwater snow melt might provide an explanation, but sampling was completed in the summer, well after any snow melt effects might be expected. A more likely explanation is that each of the sites is affected by a combination of high freshwater discharge and a small tidal inlet. These factors, combined with the relatively small tidal range that affects all sites, mean that tidal mixing in both systems is probably lower than at the other, more open sites. Despite the low salinity at these two sites, each marsh and tidal flat support foraminifera in contemporary samples that, as I explain below, are broadly comparable to what I find elsewhere on more saline sites.

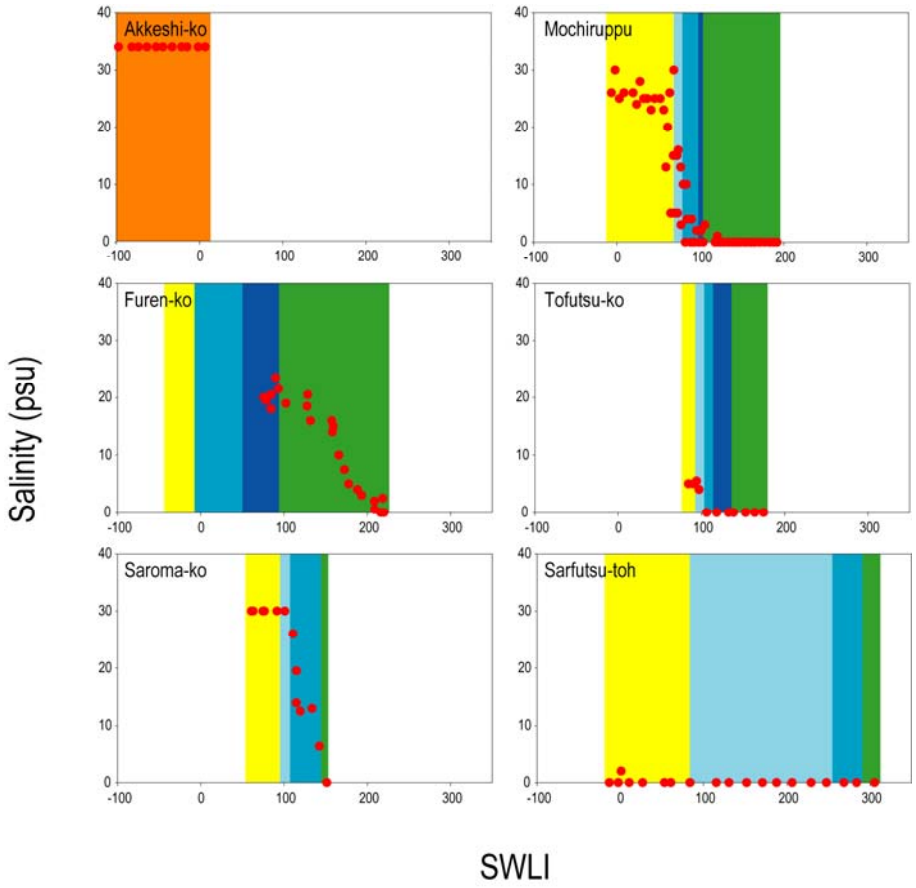

Figure 4.4 Variations in salinity across the six contemporary marshes.

There appears to be little variability of salinity between the three transects at Mochiruppu (Figure 4.2). All transects show a sigmoid-shaped curve, with flat tails at the extreme elevations. Transect A is slightly more saline than transect B at lower elevations, and transect C is more fresh when compared to transect A at higher elevations.

In this study, pH values vary between a minimum of *c*. 5 on the high marsh and upland to a maximum of 8 on the tidal flats (Figure 4.5). There is little variability in these overall trends between the six sample sites, except that Furen-ko and Saroma-ko have typically reduced pH at the freshwater swamp compared with the other transects. Data from the three transects at Mochiruppu (Figure 4.2) are also similar. The higher values are consistent with a lack of calcareous foraminifera in most contemporary and fossil samples from the salt marshes studied.

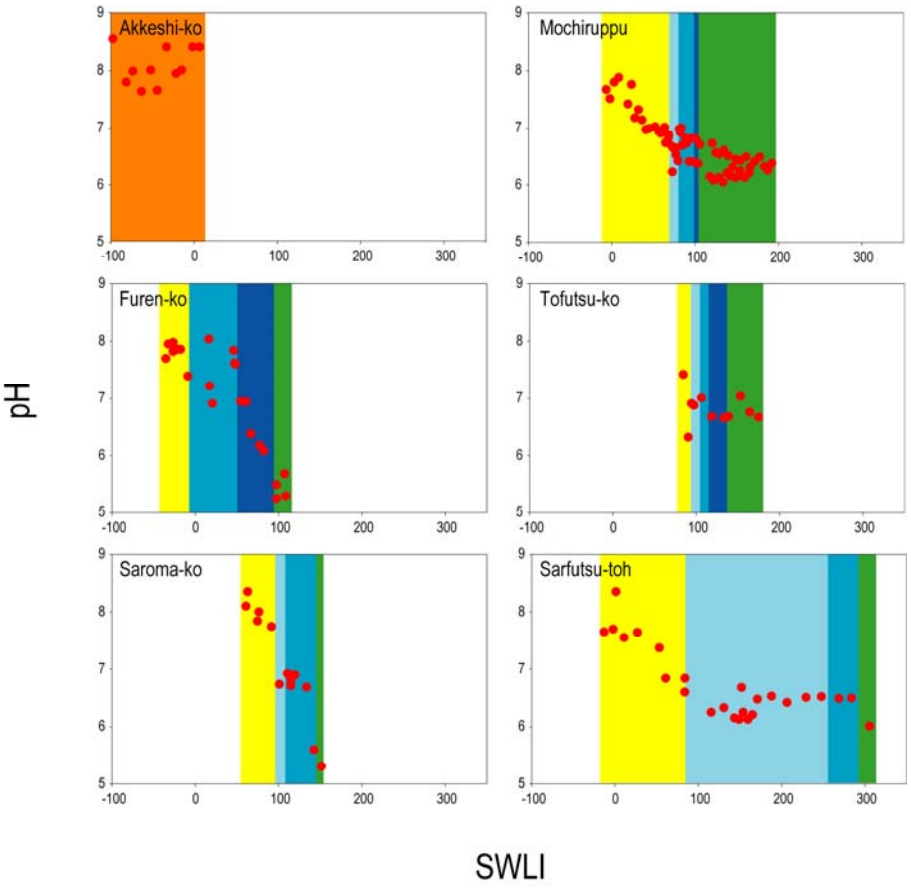

Figure 4.5 Variations in pH across the six contemporary marshes.

4.4 CONTEMPORARY FORAMINIFERAL ASSEMBLAGES FROM THE MARSHES OF HOKKAIDO

I have collected contemporary foraminifera from each of the six field sites from the tidal flat to high marsh/upland. At one site, Akkeshi-ko, I used a small boat to collect samples from subtidal environments. As noted above, at Mochiruppu I collected three transects of contemporary foraminifera to assess intra-site variability in distributions. As detailed in Chapter Three, I counted both living and dead tests and classify the data as such. Overall, I identified 27 species from 95 modern samples.

4.4.1 The salt marshes of Hokkaido

Research on the east coast of Australia has shown the importance of sampling the full environmental range of individual taxa to be used in transfer function models (Horton *et al.*, 2007; Woodroffe, 2009). The only research prior to this study on Japanese foraminifera, conducted by Scott *et al*. (1995), sampled only low- and high-marsh settings. As a result, it

was important that I determined whether there was an elevation control on foraminiferal assemblages that extends to subtidal environments.

Akkeshi-ko (Figure 4.6)

At Akkeshi-ko I collected 16 contemporary samples from subtidal stations, between -1.9 m and -0.5 m TP (LAT = -1.08 m TP). The 1.5 km long transect extended into the middle of the sheltered bay and contained a total of 13 taxa. In contrast to the Australian work referred to above, the subtidal assemblages at Akkeshi-ko are comprised almost exclusively of agglutinated foraminifera and only rare calcareous taxa (*Ammonia* spp., live specimens) are recorded (in the uppermost two samples). In most of the samples, >90% of the foraminiferal assemblages were found to be dead at the time of collection, however a slight increase the numbers of alive specimens were found in the middle of the transect.

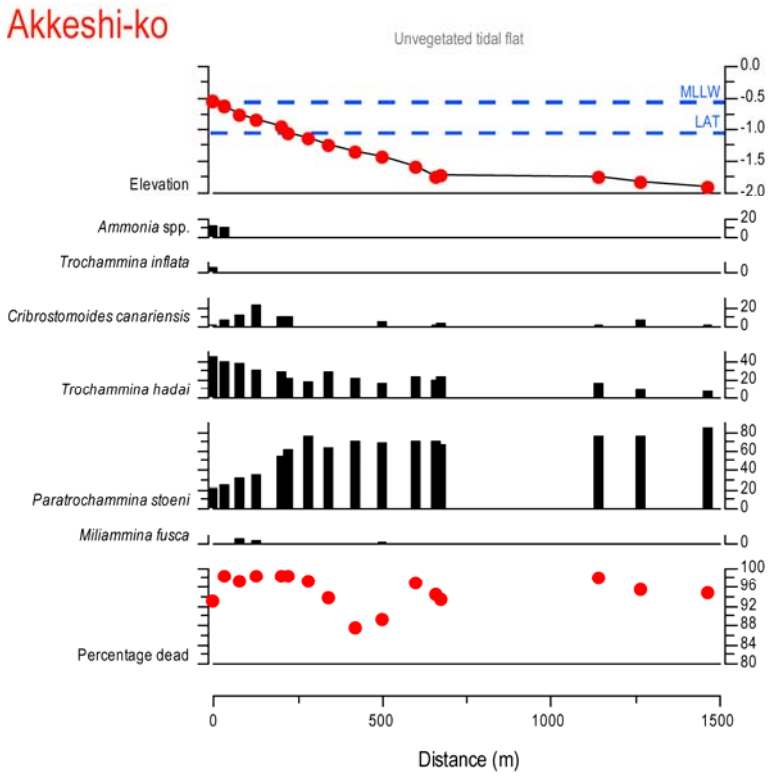

Figure 4.6 Foraminiferal distributions (in %) for the dominant species at Akkeshi-ko. In this and other diagrams, also shown are the tide levels (from the closet tide gauge to the study site), the percentage of dead specimens in a count of approximately 250 and dominant species are those which represent > 5% of the dead assemblage.

The Akkeshi-ko transect has a relatively diverse foraminiferal assemblage dominated by *Paratrochammina stoeni*, *Trochammina hadai* and to a lesser degree *Cribrostromoides canariensis*. The seaward edge of the transect has a near mono-specific *P. stoeni* assemblage (86.3%). The relative abundance of *P. stoeni* declines rapidly above LAT, and the most landward sample comprises just 23.6%. *P. stoeni* is replaced by a more diverse assemblage dominated by *T. hadai* and to a lesser extent other agglutinated species such

as *Miliammina fusca* (maximum abundance 7.3%) and *Trochammina inflata* (maximum abundance 7.0%). At the most landward of sampling stations, which corresponded to an altitude of -0.53 m TP, *T. hadai* reaches its maximum abundance of 45.8%. Although calcareous taxa were very rare in the subtidal transect at Akkeshi-ko, in the two most landward samples, *c.* 13.5% of the assemblage was composed of *Ammonia* spp.

Mochiruppu (Figure 4.7)

The salt marsh at Mochiruppu was sampled along three transects. Transects A and C encompassed mostly salt marsh (except the four lowest samples on transect A which were tidal flat). Across much of the study site is a small salt marsh cliff approximately 0.5 m in height between MLLW and MSL. Where the cliff was not present, it was possible to sample the tidal flat to marsh transition (transect B), which was not recorded in the other transects. The site is also dissected by roads that meant that not all transects extend across equal parts of the marsh.

Transect A, located to the north of the site, extends upwards from tidal flat (-0.07 m TP) to freshwater swamp (+0.6 m TP). The profile has a step that separates the low marsh from the unvegetated tidal flat. Foraminifera were only recorded to a maximum elevation of +0.24 m TP, above which no tests were present. The tidal flat is dominated by *Ammobaculities* spp., *M. fusca* and *B. pseudomacrescens*. The latter makes up 38.3% of the assemblage at the seaward edge of the transect, dropping off substantially on the marsh sections of the transects (generally < 5%). The first sample on the low marsh above the cliff is dominated by *M. fusca.* Although present over much of the transect, *M. fusca* greatly increases in abundance on the first station on the low marsh (84.1%). The most landward sample is characterised by the dominance of *Pseudothurammina limnetis* which is only present at the top of the salt marsh, together with other agglutinated taxa including *J. macrescens* (24.5%) and *Haplophragmoidies* spp. (12.3%). *S. lobata* and *T. inflata* show clear ecological niches on transect A, preferring to live on the low marsh between elevations of 0.03 to 0.19 m TP. Most of the specimens were found to be dead at the time of collection, typically > 95%.

Transect B is in the east of the marsh and extends across a similar range to Transect A but lacks a step between the tidal flat and the low marsh. The transect is dominated by three key taxa; *B. pseudomacrescens*, *Haplophragmoides*. spp and *J. macrescens* and shows limited species variance. *M. fusca* is found predominantly on the tidal flat, reaching a maximum abundance of 20.5%. The main change in foraminiferal assemblages is a decline in frequencies of *J. macresens* that occurs above *c*. 0.12 m TP. Although the majority of tests were found to be dead at the time of collection, a significant proportion (*c.* 30%) were alive around the tidal flat/low marsh transition.

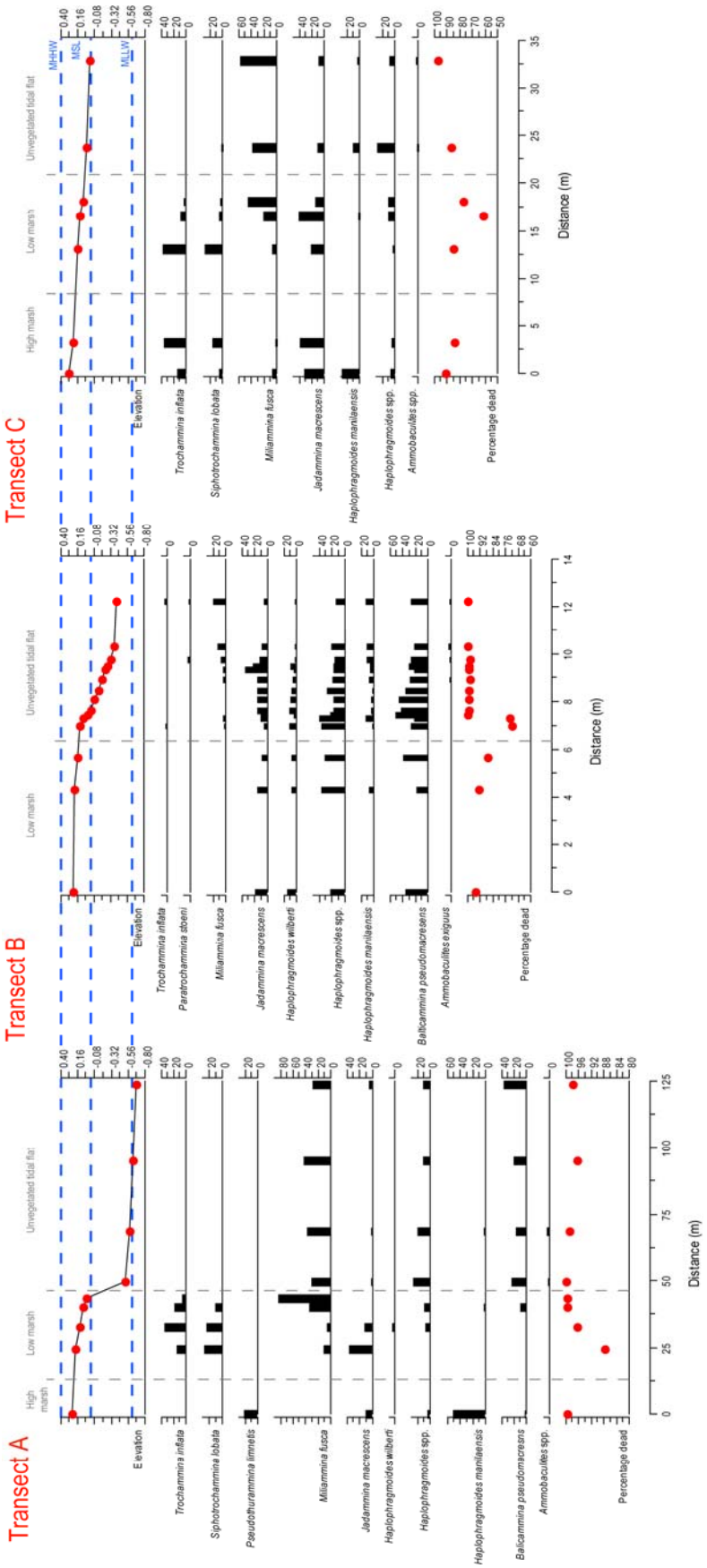

Figure 4.7 Foraminiferal distributions (in %) for the dominant species at Mochiruppu (transects A, B, and C).

Transect C is in the north-west of the study site and extends from low marsh to freshwater upland. Three agglutinated species dominate the assemblage, *M. fusca* and *T. inflata*, and *J. macrescens.* *T. inflata* dominates for the three most landward samples, peaking at 38.1% around 0.2 m TP, closely corresponding to the distribution of *S. lobata* that reaches its maximum abundance of 28.4% at roughly the same elevation. For the rest of the transect *M. fusca* increases in dominance, reaching 60.9% at the most seaward location. On transect C, most of the assemblage was found to be dead, although, similarly to transect B, a peak in the alive component (39%) in the middle of the transect (around the low marsh) was noted.

Furen-ko (Figure 4.8)

I collected 18 samples for analysis from the marsh at Furen-ko. This large marsh has many tidal channels and samples were collected from different environments along a 900 m transect that extends from unvegetated tidal flat to freshwater swamp. *M. fusca* and *Ammobaculities* spp. dominate the unvegetated tidal flat. *B. pseudomacrescens* is present over much of the marsh (typically between 40-60%), with particular dominance across the higher parts of the marsh (*c.* 70%). Whilst the majority of specimens were dead at the time of collection, a significant percentage (25%) were stained live at the back of the marsh, compared to ~0% at the seaward edge of the transect.

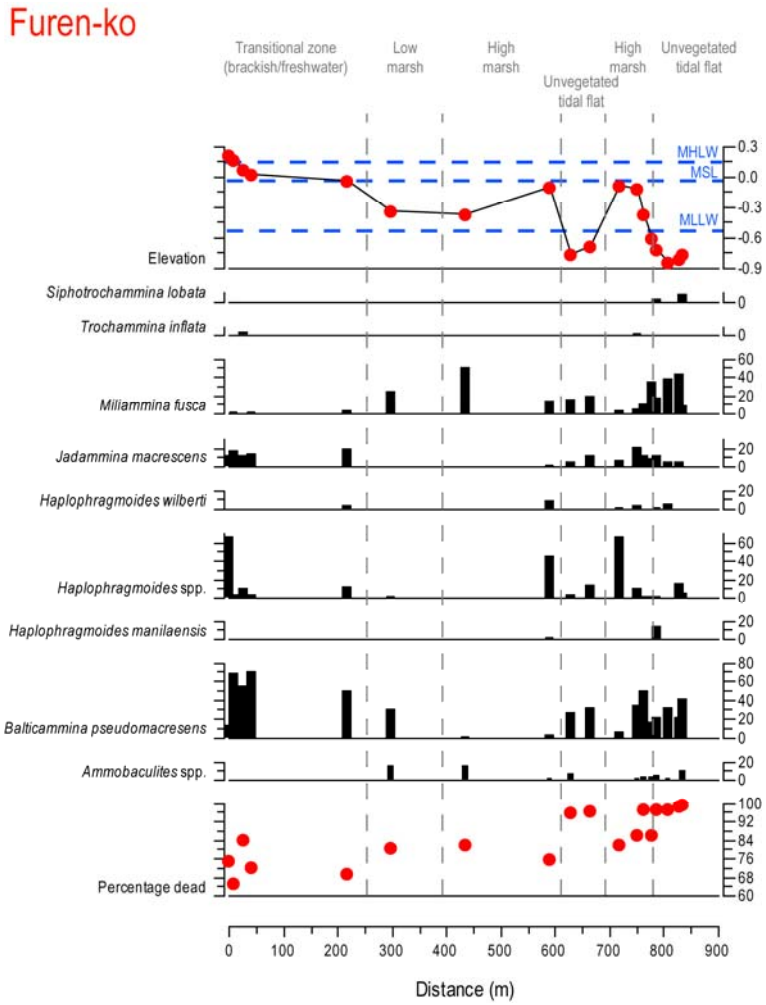

Figure 4.8 Foraminiferal distributions (in %) for the dominant species (> 5%) at Furen-ko.

Tofutsu-ko (Figure 4.9)

As noted above, the salinity at this site is very low compared with the majority of other sample sites. In a survey of nine contemporary samples extending from the tidal flat to freshwater marsh, only five contained foraminifera. Below MHHW, *Ammobaculities* spp. dominates the assemblage but above *c*. 0.36 m TP frequencies fall and are replaced by a mixed assemblage comprising *H. wilberti* and *M. fusca*. The transect samples contain the highest frequencies of live tests from all of the marshes sampled on Hokkaido, reaching a maximum of 43% total tests (*H. wilberti* and *M. fusca*) on the high marsh. The sampling date occurred during neap tides and there were no noteworthy storms or tidal surges during the weeks immediately preceding sample collection. It is possible that these high frequencies simply record a local bloom.

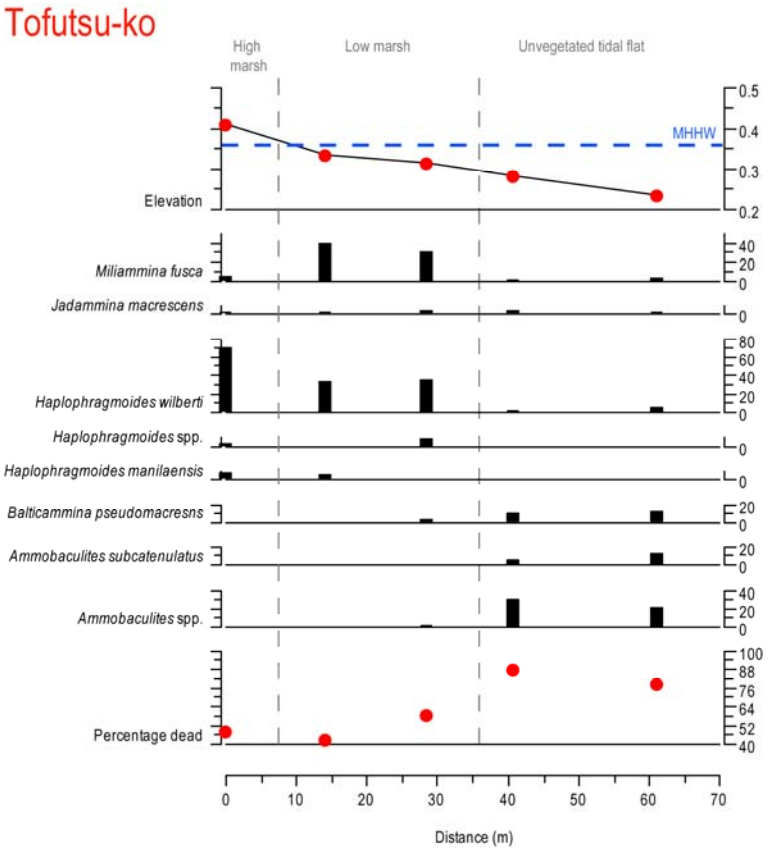

Figure 4.9 Foraminiferal distributions (in %) for the dominant species at Tofutsu-ko.

Saroma-ko (Figure 4.10)

One transect of 13 samples extends from 0.06 m to -0.77 m TP, including tidal flat to freshwater environments. Twelve of the samples contained foraminifera. The tidal flat is dominated by *A. exiguus* and *Ammobaculities* spp., with abundant *M. fusca* which become the dominant species in the low marsh (84.0%). Above MHHW the assemblage changes to one rich in frequencies of *J. macrescens* and *B. pseudomacrescens*. This assemblage is augmented in the highest sample by a dramatic rise in frequencies of *H. manilaensis* (83.1%). *S. lobata* and *T. inflata* are present on the lower reaches of the high marsh, where *B. pseudomacrescens* also reaches a maximum (peak abundance 90.8%). Most of the foraminifera were dead towards the seaward edge of the transect (typically >95%), however a significant proportion of specimens towards the back of the marsh were found to be alive (52.7 – 65.4%).

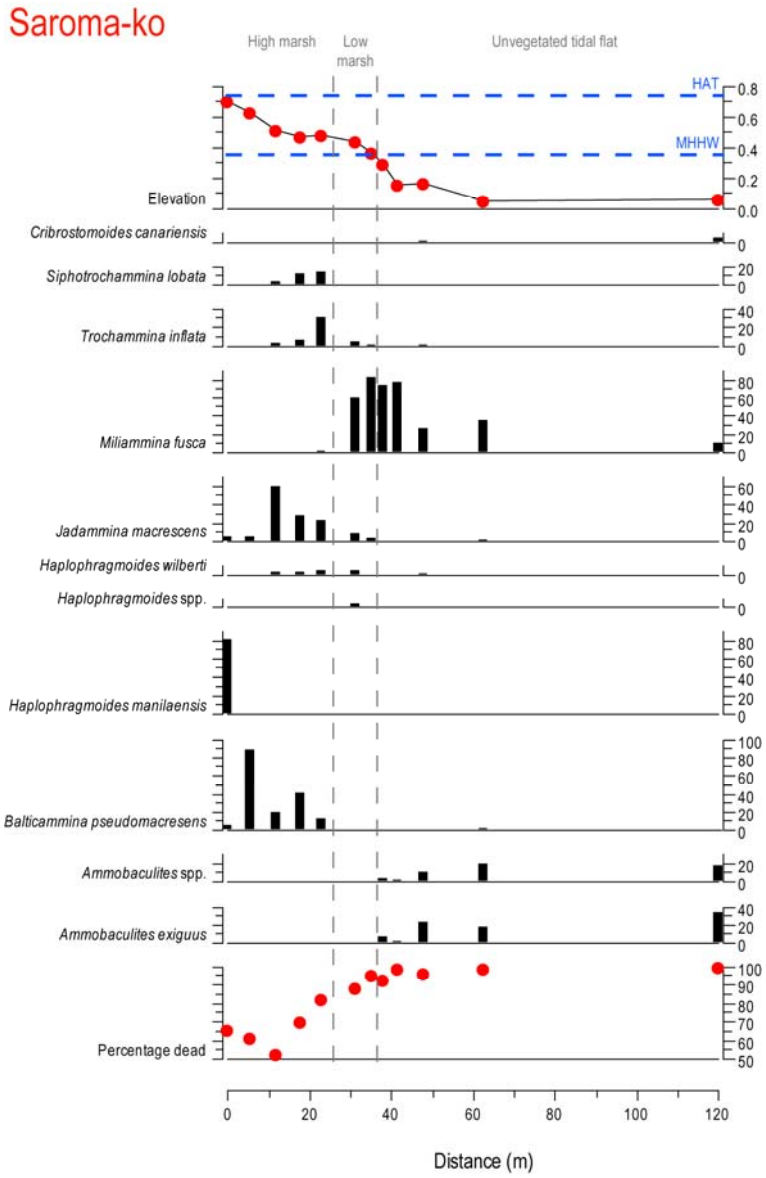

Figure 4.10 Foraminiferal distributions (in %) for the dominant species at Saroma-ko.

Sarfutsu-toh (Figure 4.11)

This is the second low salinity marsh sampled. The sampling transect comprises 20 samples, of which 13 contained sufficient foraminifera for counting, and extends from tidal flat (-0.1 m TP) to high marsh (0.7 m TP). The tidal-flat samples are dominated by high frequencies of *M. fusca* compared with the other study sites (*c*. 80%). The low-marsh transition is marked by a rise in occurrence of first *Ammonia* spp. and then *B. pseudomacresens*. The macrophyte vegetation is poorly zoned at this site because of the limited salinity range. However, at higher sample sites the foraminiferal assemblage changes to be more dominated by frequencies of *B. psuedomacrescens* and *H. manilaensis*. The highest sample contains a mixed assemblage of *B. psuedomacrescens*, *H. wilberti* and *M. fusca*.

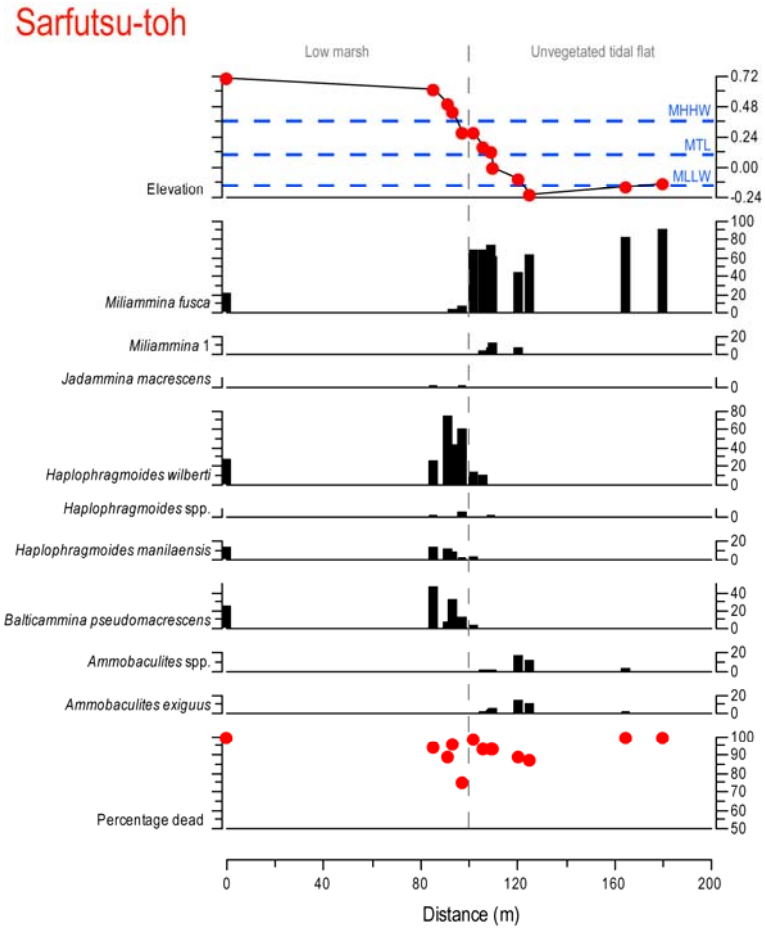

Figure 4.11 Foraminiferal distributions (in %) for the dominant species at Sarfutsu-toh.

4.4.2 Elevation-dependent ecological zones on Hokkaido

Having presented the basic contemporary foraminiferal data, I now explore using numerical techniques the extent to which the observed distributions are zoned by altitude, since this is the key variable of interest in RSL reconstruction. Although there is variability between the sites, visual interpretation of the species distribution plots described above suggests that a relationship exists between biological turnover and altitude, with certain species occupying particular areas of the intertidal zone compared with those found at lower elevations. For example, at most of the study sites the high marsh is characterised by high frequencies of *J. macrescens*, *H. manilaensis* and *B. pseudomacrescens*, the low marsh by *M. fusca* and the tidal flats by *Ammobaculities* spp. The subtidal zone is typified by high frequencies of *P. stoeni* and *T. hadai*.

In an attempt to quantify the nature of the vertical distributions at each site, two multivariate techniques are now employed that are common to foraminiferal transfer function models (Horton and Edwards, 2006): unconstrained cluster analysis and detrended correspondence analysis (DCA: Hill and Gauch, 1980). Each model is applied to the contemporary foraminiferal data from each field site to explore whether the data are

suitable for transfer function development. For this and all subsequent statistical analysis, samples that have counts of less than 40 individuals are removed. In addition, in all of the following analyses I use only dead counts. This is because analysis of two shallow sediment cores showed that there is no significant infaunal element to the near surface foraminiferal assemblages (see Section 4.5.4).

Akkeshi-ko

Cluster analysis and DCA identify two zones (Figure 4.12): zone AK-I (samples 1-12, -1.90 m to -0.90 m TP, characterised by *P. stoeni*) and zone AK-II (samples 13-16, range -0.53 to -0.82 m TP, characterised by *T. hadai* and *C. canariensis*).

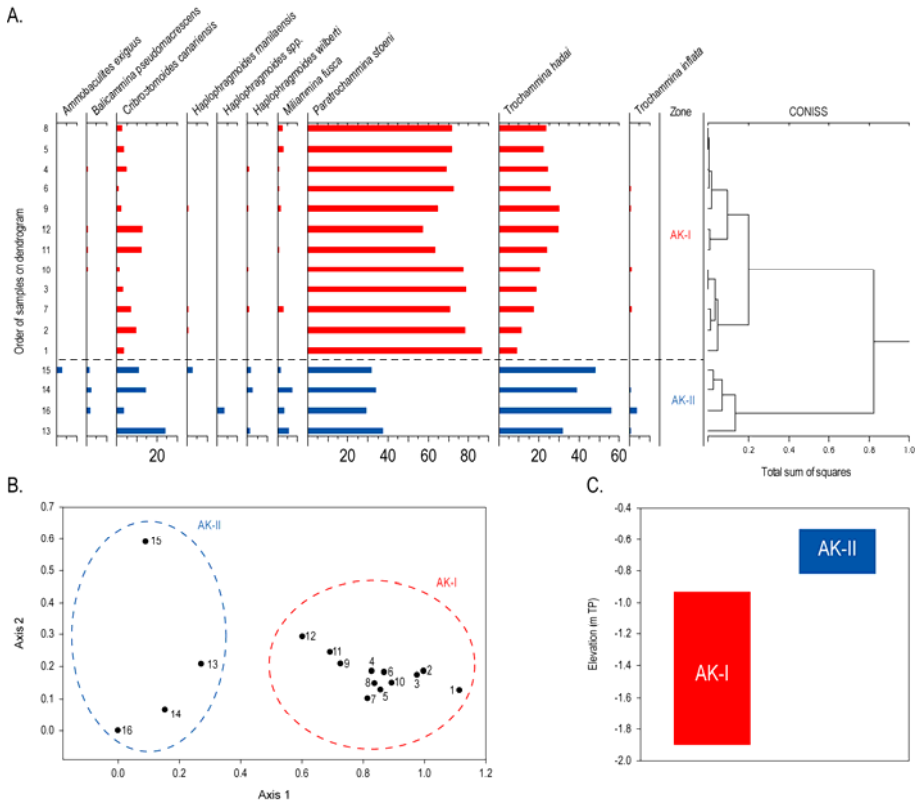

Figure 4.12 (A) Summary of foraminiferal distributions and unconstrained cluster analysis based on unweighted Euclidean distance, (B) DCA zones and (C) summary of elevation-dependent zones using cluster analysis results from contemporary transects from Akkeshi-ko. In this and following graphs, only samples with counts greater than 40 individuals and species that contribute at least 5% of the dead assemblage are included.

Mochiruppu

Cluster analysis and DCA identify three zones in Transect A and two zones in Transects B and C (Figure 4.13A-B). Differences in the sampling elevation between transects means that when the data are combined into a single dataset, cluster analysis identifies four clusters (Figure 4.13C) for the full dataset. The lowest most cluster (M-I; -0.67 – 0.08 m TP) comprises tidal-flat and low-marsh samples from transects A and C which is dominated by a mixed assemblage comprising *M. fusca*, *Ammobaculities* spp. and *B. pseudomacrescens*. Zone M-II (-0.41 – 0.23 m TP) includes all samples from transect B suggesting that this transect samples a different environment to the other two transects. At Mochiruppu it wasn't possible to sample the entire low-marsh elevation range in Transects A and C because of cliffs on the lower edge of the marsh (Figure 4.13D). Transect B was situated where there was no cliff and focuses on the elevation range missing from the other transects, explaining why the samples from this transect cluster together (M-II). The upper most zones are slightly different in terms of their foraminiferal composition. Zone M-III comprises just one sample (MA9; 0.24 m TP) that was dominated by *H, maniliaensis* and *P. limnetis* foraminifera, whereas zone M-IV has a wider elevational range (0.14 – 0.28 m TP) and contains a more diverse assemblage of *J. macrescens*, *S. lobata* and *T. inflata.*

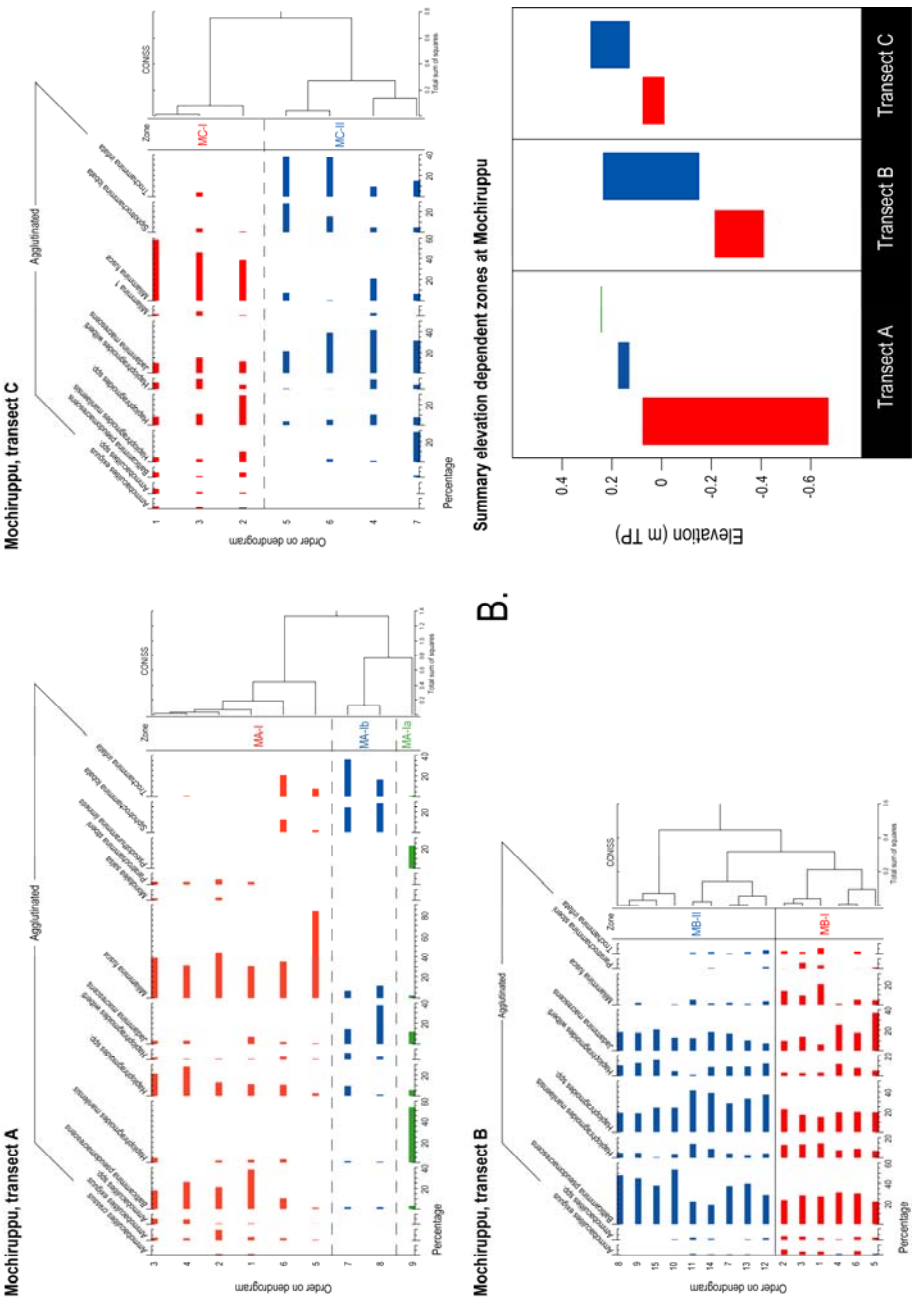

Figure 4.13 Intra-site variability of foraminifera at Mochiruppu. A) Summary of foraminiferal distributions and unconstrained cluster analysis for three transects at Mochiruppu based on unweighted Euclidean distance, (B) summary of elevation-dependent zones using cluster analysis results.

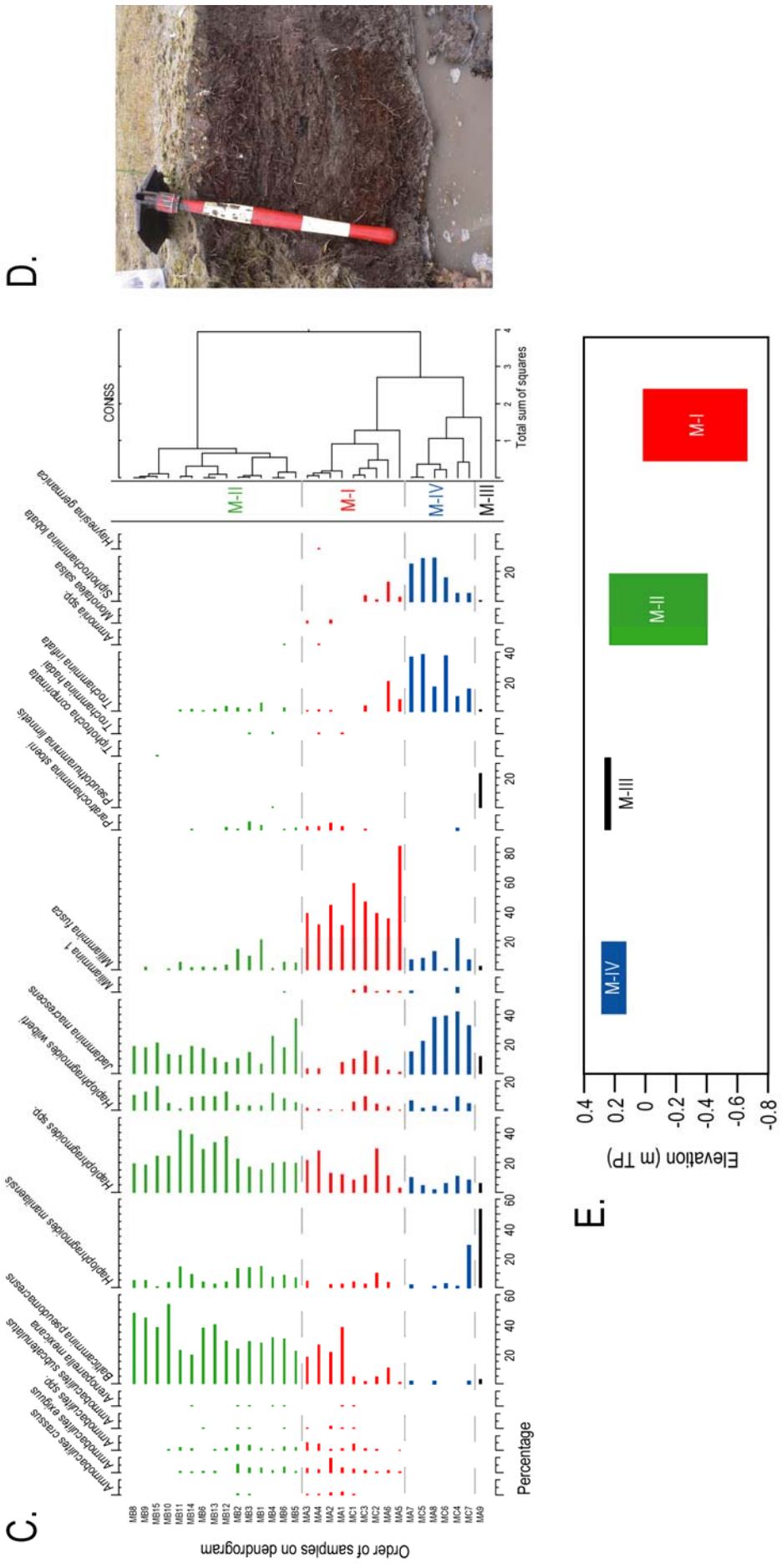

Figure 4.13 (continued) (C) Summary of foraminiferal distributions and unconstrained cluster analysis for combined data from Mochiruppu based on unweighted Euclidean distance, and summary elevation-dependent zones using cluster analysis results, (D) Photo of cliff in Mochiruppu marsh, (E) Elevational dependent zonation for all transects at Mochiruppu.

Furen-ko

Based on unconstrained cluster analysis and DCA the Furen-ko foraminifera can be divided into three zones (Figure 4.14C). When combined with cluster analysis, DCA zonations can be identified on the basis of their unique composition of foraminifera. Zone FK-I (range 0.15-0.87 m TP, characterised by *B. pseudomacrescens*, *M. fusca* and *A. exiguus*), Zone FK-II (range 0.63-1.12 m TP, characterised by *B. pseudomacrescens*), and zone FK-III (range 0.93-1.22 m TP, characterised by *Haplophragmoides* spp.).

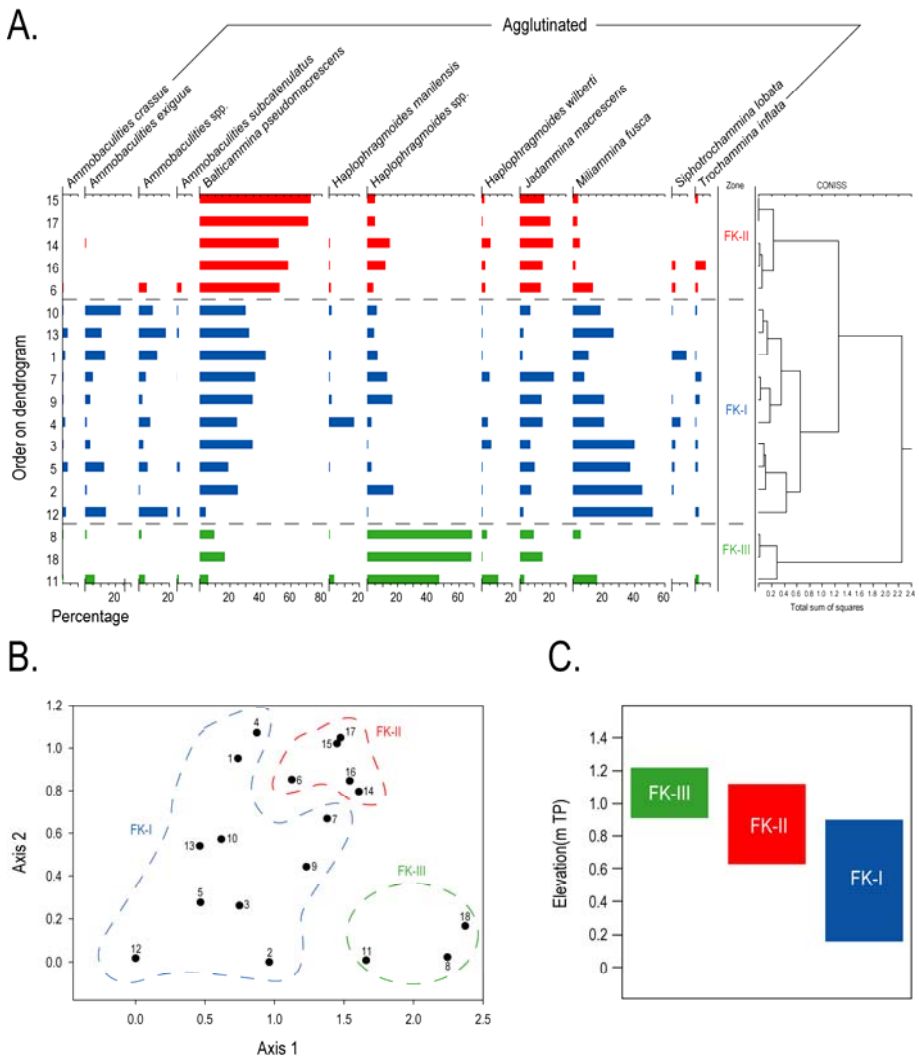

Figure 4.14 (A) Summary of foraminiferal distributions and unconstrained cluster analysis based on unweighted Euclidean distance, (B) DCA zones and (C) summary of elevation-dependent zones using cluster analysis results from contemporary transects from Furen-ko.

Tofutsu-ko

Based on unconstrained cluster analysis and DCA the limited foraminiferal data from Tofutsu-ko can be divided into two zones (Figure 4.15). Zone TF-I comprises two samples (range 0.24 m to 0.28 m TP, characterised by *Ammobaculities*. spp. and *A. exiguus*) and zone TF-II (range 0.3-0.42 m TP, characterised by *H. wilberti* and *M. fusca*).

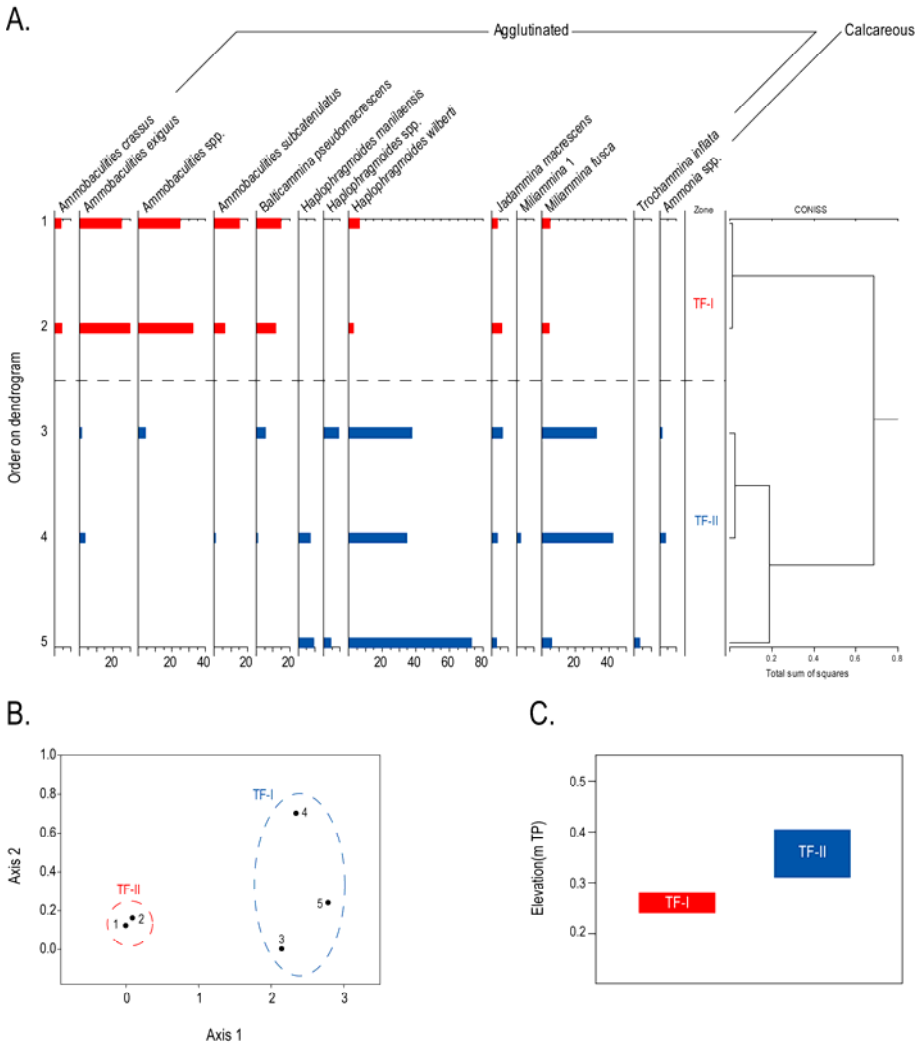

Figure 4.15 (A) Summary of foraminiferal distributions and unconstrained cluster analysis based on unweighted Euclidean distance, (B) DCA zones and (C) summary of elevation-dependent zones using cluster analysis results from contemporary transects from Tofutsu-ko.

Saroma-ko

Based on unconstrained cluster analysis and DCA the foraminiferal data from Saroma-ko can be divided into three zones (Figure 4.16). Zone SK-I (range 0.07-0.44 m TP, characterised by *Miliammina* 1 and *A. exiguus*), zone SK-IIa (range 0.47-0.65 m TP, characterised by *J. macrescens* and *B. pseudomacrescens*) and one sample making up zone SK-IIb (0.7 m TP, dominated by *H. manileansis*).

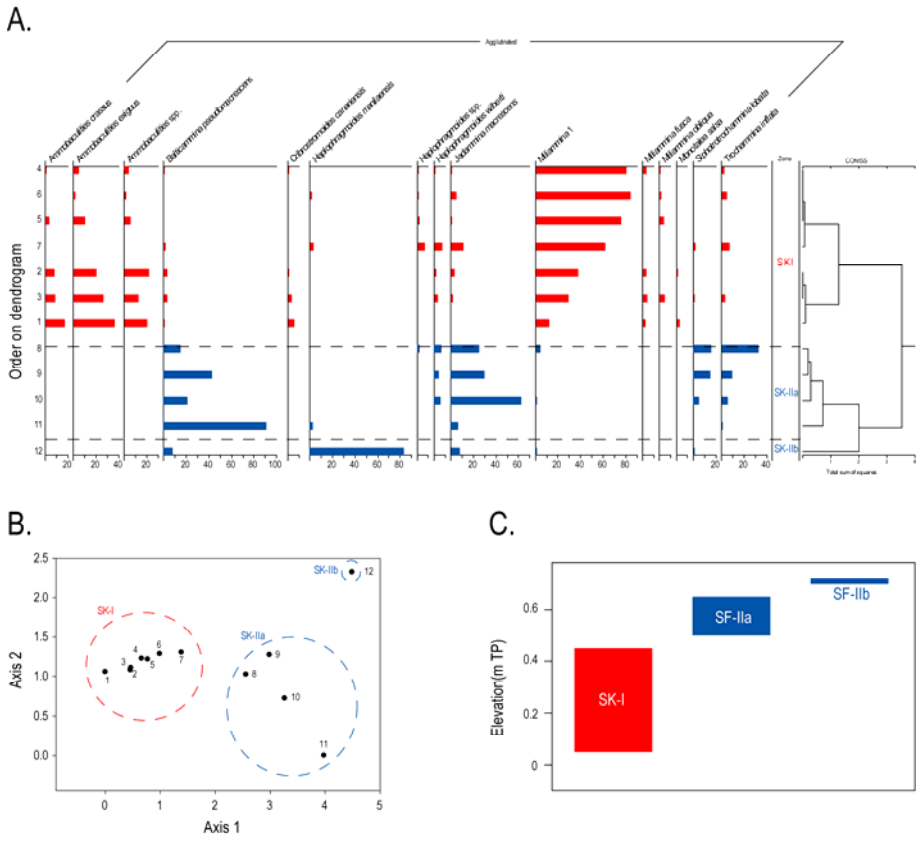

Figure 4.16 (A) Summary of foraminiferal distributions and unconstrained cluster analysis based on unweighted Euclidean distance, (B) DCA zones and (C) summary of elevation-dependent zones using cluster analysis results from contemporary transects from Saroma-ko.

Sarfutsu-toh

Based on unconstrained cluster analysis the Sarfustu-toh foraminifera can be divided into two zones (Figure 4.17A). Zone SF-I comprises eight samples from between -0.15-0.28 m TP, and Zone SF-II comprises five samples between 0.3-0.7 m TP. A similar division of the dataset is apparent from DCA analysis, with the same samples in SF-I and SF-II occupying distinct and mutually exclusive ordination space (Figure 4.17B). On this basis, it is possible to divide the Sarfutsu-toh assemblage into two zones as described above (Figure 4.17C).

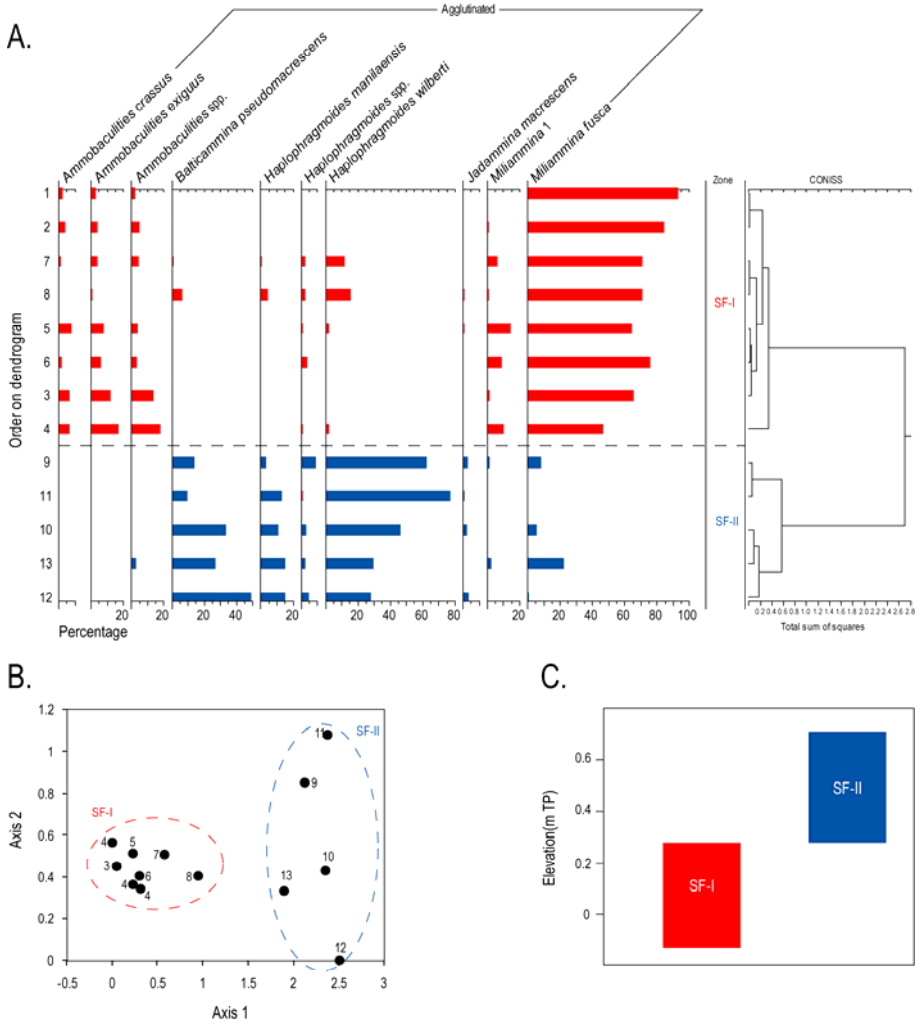

Figure 4.17 (A) Summary of foraminiferal distributions and unconstrained cluster analysis based on unweighted Euclidean distance, (B) DCA zones and (C) summary of elevation-dependent zones using cluster analysis results from contemporary transects from Sarfutsu-toh.

In Figure 4.18 I present the individual zonations for all of the study sites. This shows that each transect can be divided into a maximum of three zones but that the elevation of these zones differs and indeed overlaps. Despite this, the DCA analysis indicates that the data are potentially suitable for use in transfer functions, although it is obvious at this stage that there is a degree of variability both within (e.g. Mochiruppu) and between different marshes. The marshes of Hokkaido do display a significant level of zonation with elevation and there are some clear trends which are observable. *J. macrescens* is consistently observed in the upper part of the high marsh, *B. pseudomacrescens* is found across a wide range of elevations, *T. inflata* is generally observed in mid- to low-marsh environments and *P. stoeni* occurs in low marsh/tidal flat and particularly subtidal settings. Generally above MHHW *Haplophragmoides* dominates, although the specific species varies between the marshes. The two marshes with the most significant freshwater influence, Tofutsu-ko and Sarfutsu-toh are dominated by *H. wilberti* whereas the other sites comprise *H. manilaensis* at the highest elevations. Some sites have unique environmental conditions and are

consequently dominated by certain taxa. For example, the most landward samples on the Mochiruppu transects show a distinct composition. *P. limnetis* is exclusively found on transect A, whereas *H. manilaensis* dominates on transect C. The only site that differs in terms of its *Haplophragmoides* composition is Furen-ko which typically has very small, undifferentiated *Haplophragmoides.* spp. on the salt marsh/freshwater transition. Around MHHW *B. pseudomacrescens* and *J. macrescens* tend to dominate, with the latter being found generally at higher elevations. This is in stark contrast to those British salt marshes that comprise a near monospecific abundance of *J. macrescens* at the most landward sample (Horton and Edwards, 2006). Around MHLW, *T. inflata* and *S. lobata* occupy a tight elevational range in most of the marshes, typically between 70 and 100 SWLI units. The lowest-most intertidal zone in all of the salt marshes comprises a mixed assemblage dominated by *A. crassus, A. exiguus, Ammobaculities* spp. and *M. fusca.* Between the marshes there appears to be a significant level of variability in the quantities of these species. *M. fusca* is dominant at Sarfutsu-toh below MTL, whereas at Tofutsu-ko, *Ammobaculities* spp. is found in greatest numbers.

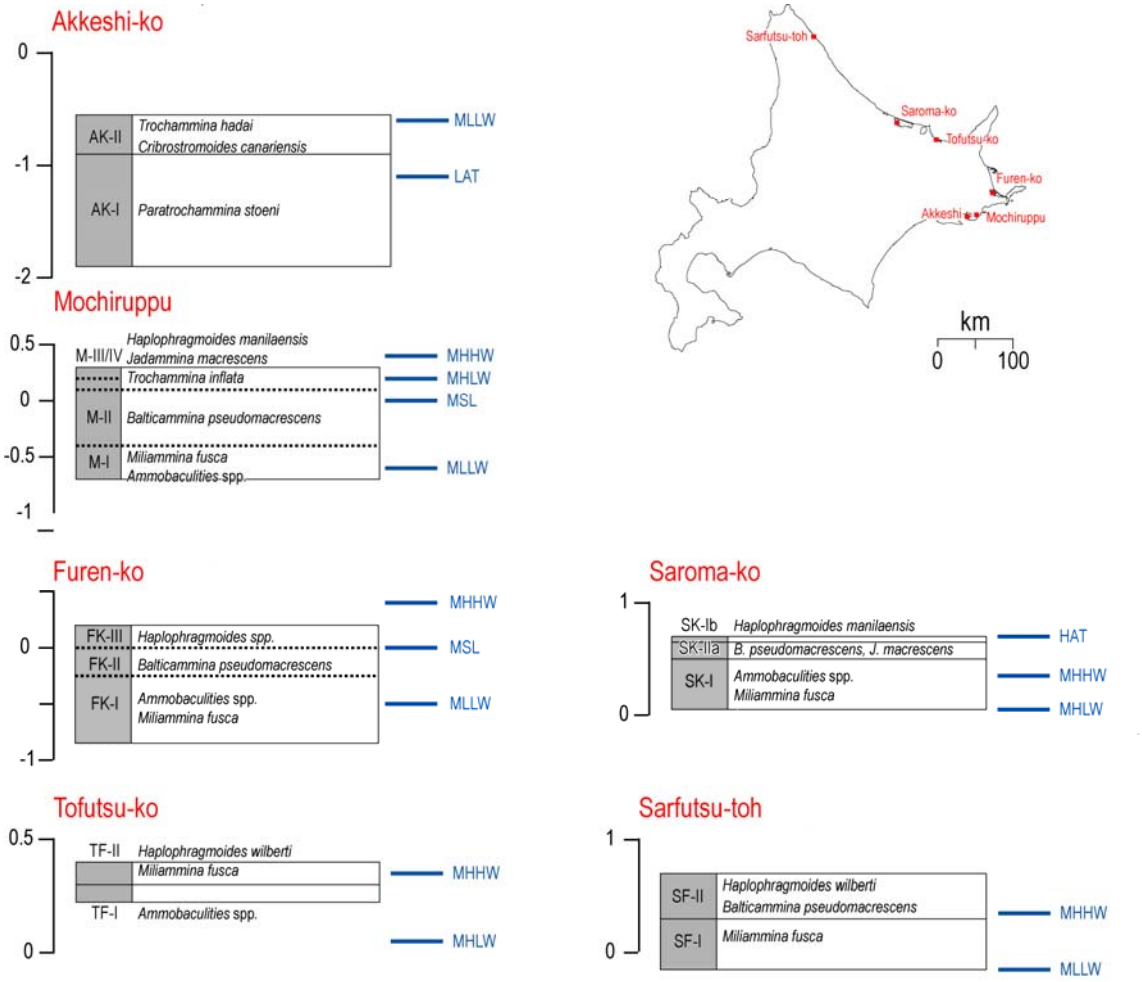

Figure 4.18 Summary of foraminiferal zonation for marshes of Hokkaido plotted against metres TP. Dashed lines represent overlapping zones. Tidal levels at each individual salt marsh are also shown.

Two species dominate the intertidal flat assemblages in all marshes on the eastern and northern coastlines of Hokkaido, *Ammobaculities* (typically *A. exiguus* and *A. crassus*) and *M. fusca.* *Ammobaculities* species are useful to distinguish tidal-flat and low-marsh conditions, and have been observed on the marshes of Virginia (Spencer, 2000; Vance *et al.*, 2006) and North Carolina (Horton and Culver, 2008; Kemp *et al.*, 2009a; Kemp *et al.*, 2009b). *M. fusca* is also a species indicative of low intertidal conditions, although there appears to be considerable variability in abundance between sites. At Sarfutsu-toh, *M. fusca* was the dominant species below MHHW, however in the other Hokkaido salt marshes *A. exiguus* and *A. crassus* dominate the most seaward sample stations, and *M. fusca* tends to prefer higher elevations. *M. fusca* also showed relatively large variability in its ecological preference between the two transects studied by Scott *et al*. (1996). On transect 1, although found at higher quantities at the seaward edge of the transect, the distribution of *M. fusca* is widespread over much of the marsh, reaching between 40 to 60%. In comparison, on transect 2, *M. fusca* was spatially restricted to higher elevations. *M. fusca* is ubiquitous worldwide, being found in low-marsh settings with salinity ranges up to 35 ppt (Murray, 1991). In the UK, *M. fusca* is a middle- to low-marsh species, occurring around or below MHWST in an assemblage also comprising calcareous taxa (Horton and Edwards, 2006). A similar zone has been noted in many temperate salt marshes around the world (Coles, 1977; Coles and Funnell, 1981; Gehrels, 1994; Horton and Culver, 2008; Patterson, 1990; Scott and Medioli, 1980; Scott *et al.*, 1990; Scott and Medioli, 1978; Smith *et al.*, 1984), as well as mangrove environments in tropical locations (Woodroffe *et al.*, 2005; Woodroffe, 2009).

The dominance of agglutinated taxa on tidal-flat and low-marsh environments in Hokkaido, is in stark contrast to European and North American marshes where high concentrations of calcareous species dominate (e.g. Gehrels *et al.*, 2001; Horton and Edwards, 2006; Murray, 1971; Phleger, 1970). Calcareous species generally are absent, or present in very low quantities, confirming the analysis of Scott *et al*. (1996) who identified no calcareous species in his study of foraminifera in Nemuro Bay. Due to the low calcareous counts it is difficult to reconcile the live/dead balance of contemporary foraminifera. Where sufficient samples are analysed, Akkeshi-ko illustrates the absence of live taxa in the total assemblage (> 90% of the calcareous assemblage are dead), whereas in Furen-ko the picture is reversed and more live foraminifera are found (averaging live populations of *c.* 65%, but reaching a maximum of 93% for *Ammonia* spp.). Generally the dead assemblage is broadly comparable with the live assemblage; however other factors including local blooms in foraminifera may temporally unbalance this relationship (e.g. Furen-ko).

There appears to be a general lack of dead calcareous foraminifera in intertidal foraminiferal studies in the Pacific (e.g. Hawkes *et al.*, In Press; Scott *et al.*, 1996). The

shell protoplasm of calcareous tests are affected by acidic conditions (Bradshaw, 1968; Green *et al.*, 1993) through increases in hydrogen sulphide production attributable to the changes in the concentration of carbonic acid or bicarbonate (Berkeley *et al.*, 2007). These processes confine the foraminifera to a narrow pH window, below which low abundance and diversity (Phleger, 1970) and/or dissolution (etching) of the tests (Boltovskoy and Wright, 1976) becomes apparent. Hawkes *et al.* (In Press) found organic test linings in their surface samples, which are attributed to the dissolution of calcareous species due to taphonomic and laboratory analysis (Edwards and Horton, 2000), however the marshes in this study contained none. The relatively neutral pH observed on the marshes of Hokkaido (see Section 4.3 and Figure 4.5) suggest dissolution may not be significant. Furthermore, calcareous taxa may naturally occur in very low abundances in these sites rather than being poorly preserved. This could possibly be due to the relative isolation on the Hokkaido marshes, limiting the diversity and abundance of calcareous taxa on tidal-flat and low-marsh environments. Furthermore, due to the low abundance of calcareous foraminifera, the effects of post-depositional change are less significant than on European and North American marshes which comprise higher abundances.

Low diversity of calcareous taxa is mirrored in the agglutinated assemblages. Scott *et al*. (1996) observed a similar pattern to this study in relation to the dominance of a few taxa over wide environmental gradients, most significantly *M. fusca*, and *Trochammina macrescens*. As discussed previously (see Section 3.2.4), *T. macrescens* comprises *B. pseudomacrescens* and *J. macrescens.* On transect 1 in Scott *et al*. (1996), there appears to be considerable variability in the percentage of *T. macrescens*. Stations located in the same vegetation zone (and at similar elevations) display vastly different abundance percentages (ranging from 0 to 80%); suggesting factors other than elevation play a dominant role in controlling the distribution of foraminifera along this transect. On transect 2, *T. macrescens* is considerably more abundant, reaching percentages of 75 to 100% for all but the most landward of samples. Despite considerable variability between transects, *B. pseudomacrescens* and *J. macrescens* typically dominate the tidal-flat and low-marsh environments in this study. Elsewhere, *B. pseudomacrescens* is found in the high marsh in a range of locations from around the Pacific (Hawkes *et al.*, In Press; Patterson *et al.*, 2004; Riveiros *et al.*, 2007), the circum-Atlantic (Edwards *et al.*, 2004; Gehrels and van de Plassche, 1999; Horton and Edwards, 2006), and elsewhere in Europe (Alve and Murray, 1999). Throughout the intertidal zone on the marshes of Hokkaido *J. macrescens* is found in significant numbers. *J. macrescens* are more commonly associated with high marsh floral zones, where a near monospecific assemblage dominates the marsh-to-upland transition (Gehrels, 1994; Scott and Medioli, 1980; Scott and Medioli, 1978). The presence of such an assemblage composition may be site-specific (Edwards *et al.*, 2004), although its narrow altitudinal range may also be missed during sampling (Patterson, 1990; Scott

and Leckie, 1990). Other studies support the Hokkaido analysis and find *J. macrescens* lower in the tidal frame on the middle and low marsh (Hawkes *et al.*, In Press; Murray and Alve, 1999; Southall *et al.*, 2006).

Some species appear to have a ubiquitous distribution along the marsh while other species have tighter elevational control. Specifically, *H. manilaensis* is often found at the top of the marsh. Scott *et al*. (1996) noted that *H. manilaensis* dominates the brackish/freshwater transition in his study of Hokkaido salt marshes, as it does elsewhere (de Rijk, 1995). Although found at high-marsh elevations in this study, *H. manilaensis* was also found to live throughout the intertidal zone in agreement with studies in Oregon where it is found in the middle marsh floral zone (Hawkes *et al.*, In Press). More generally *H.* spp. and *Haplophragmoides* spp. (all species) are found to be the dominant species in many high-marsh settings in temperate salt marshes around the world (Barbosa *et al.*, 2005; de Rijk and Troelstra, 1997; Gehrels and van de Plassche, 1999; Gehrels *et al.*, 2001; Guilbault *et al.*, 1996; Horton and Culver, 2008; Kemp *et al.*, 2009b; Massey *et al.*, 2006b). *T. inflata* also displayed significant elevational zonation, although absent from Scott *et al*.'s (1996) transect 1, on transect 2 this species reached peak abundances of *c.* 30% in the lower marsh in their study. *T. inflata* and *H. manilaensis* were the only species in Scott *et al*.'s (1996) study to exhibit a preference for lower and higher elevations respectively, which is similar to the pattern observed in other locations (Collins *et al.*, 1995; Scott *et al.*, 1996). *T. inflata* has been identified in marshes of varying salinities (Murray, 1991), on the Pacific seaboard (Guilbault *et al.*, 1995; Guilbault *et al.*, 1996; Hawkes *et al.*, 2005; Hawkes *et al.*, In Press; Jennings and Nelson, 1992; Nelson and Kashima, 1993; Patterson *et al.*, 1999; Scott *et al.*, 1996) and in temperate marshes elsewhere (e.g Hayward *et al.*, 2004; Horton and Edwards, 2006; Massey *et al.*, 2006a; Murray, 1971; Scott and Medioli, 1978). Elevation-dependent zones are typically poorer on marshes that display lower salinity variability (typically less than 10‰), which comprises Tofutsu-ko and Sarfutsu-toh, and plant species that were largely freshwater such as those on the marshes of Louisiana (Scott *et al.*, 1991). Other authors also observe differences in species composition between elevation-dependent zones located at different sites, which they attribute to variable salinity regimes between study sites (Kemp *et al.*, 2009b)

These trends observed as part of this thesis are generally in line with the findings of Scott *et al*. (1995), who found just ten species of foraminifera in their analysis in Nemuro Bay. They noted that *Ammotium salsum*, *Tiphotrocha comprimata*, *Ammobaculities.* spp., and *H. wilberti* were not present or rare. By studying more marshes and examining foraminifera over wider environmental gradients, I have been able to detect *Ammobaculities.* spp., and *H. wilberti* in much higher quantities. These taxa are generally not as abundant in Pacific Rim marshes when compared to those circum-Atlantic marshes, which typically display a

more diverse assemblage composition (Horton and Edwards, 2006; Scott *et al.*, 1996). Scott *et al*. (1996) hypothesised that this may be due to the isolation of the marshes from the main migratory waterfowl flyways which is considered the most important dispersal mechanism for marsh foraminifera. Although Hokkaido has some important wetland areas, there is a lack of habitats on the mainland that in turn attracts fewer waterfowl.

The results from my analysis confirm the general distribution of agglutinated foraminifera found across temperate salt marshes worldwide (e.g. Edwards *et al.*, 2004; Horton and Edwards, 2006; Scott *et al.*, 1996; Southall *et al.*, 2006) and also in Hokkaido (Scott *et al.*, 1995). Unlike other temperate marshes, Hokkaido has very limited calcareous foraminifera and therefore the lowest-most intertidal zone is dominated by agglutinated taxa, such as *Ammobaculities.* spp. and *M. fusca.*

4.4.3 Canonical correspondence analysis (CCA)

Cluster analysis and DCA indicated that individual salt marshes on Hokkaido display an elevation-dependent zonation, therefore I have combined the individual study sites into a regional training set to test the applicability of this hypothesis using multivariate analysis. CCA of foraminiferal and environmental data from all six Hokkaido salt-marsh sites have been used to extract synthetic environmental gradients. These gradients were the basis for illustrating the different habitat preferences (niches) of taxa via an ordination diagram. The eigenvalues for CCA axis 1 (0.638) and axis 2 (0.244) explain 25.2% of the variance in the foraminiferal data and 84.5% of the species-environment relationship (Table 4.1). The unexplained (74.8%) proportion of the total variance may be due to other factors (e.g. temperature, dissolved oxygen, or due to variations in the positioning of the transects). The unexplained percentage could also be due to large amounts of stochastic variation. However it is similar to other biological variables that have large numbers of samples with zero values (Zong and Horton, 1999) and replicates analysis undertaken elsewhere in the Pacific (Riveiros *et al.*, 2007).

Table 4.1 Summary of CCA results from foraminiferal assemblages taken from six salt marshes on Hokkaido.

Axes	1	2	3	4	Total inertia
Eigenvalues:	0.638	0.244	0.107	0.035	3.497
Species-environment correlations:	0.854	0.692	0.59	0.484	
Cumulative percentage variance					
of species data:	18.2	25.2	28.3	29.3	
of species-environment relation:	61.1	84.5	94.7	98.1	
Sum of all unconstrained eigenvalues					3.497
Sum of all canonical eigenvalues					1.043

The arrows on the CCA biplots (Figure 4.19) represent the direction of the maximum variation of the measured environmental variables, the length of which is proportional to the relative importance in explaining the variance recorded in the foraminiferal data. Intra-set correlations of environmental variables with axes one, show that SWLI, salinity and % clay vary primarily along axis 1, while pH and LOI show a joint correlation with axes 1 and 2. As such, CCA axis 1 reflects a major gradient from land to sea; sampling stations located low in the tidal frame plot to the right (low SWLI, barren vegetation, high pH and relatively coarse grain size). Figure 4.19A shows the sample-environment biplot for all 95 samples (see figure caption for colour key). The green circles representing the 16 sampling stations from Akkeshi-ko are clustered together on right-hand side of the graph. Conversely, the high-marsh and upland environments plot on the left (high elevations, dense vegetation cover, low pH and relatively fine grain size), where the highest sampling stations from each of the salt marsh transects can be found.

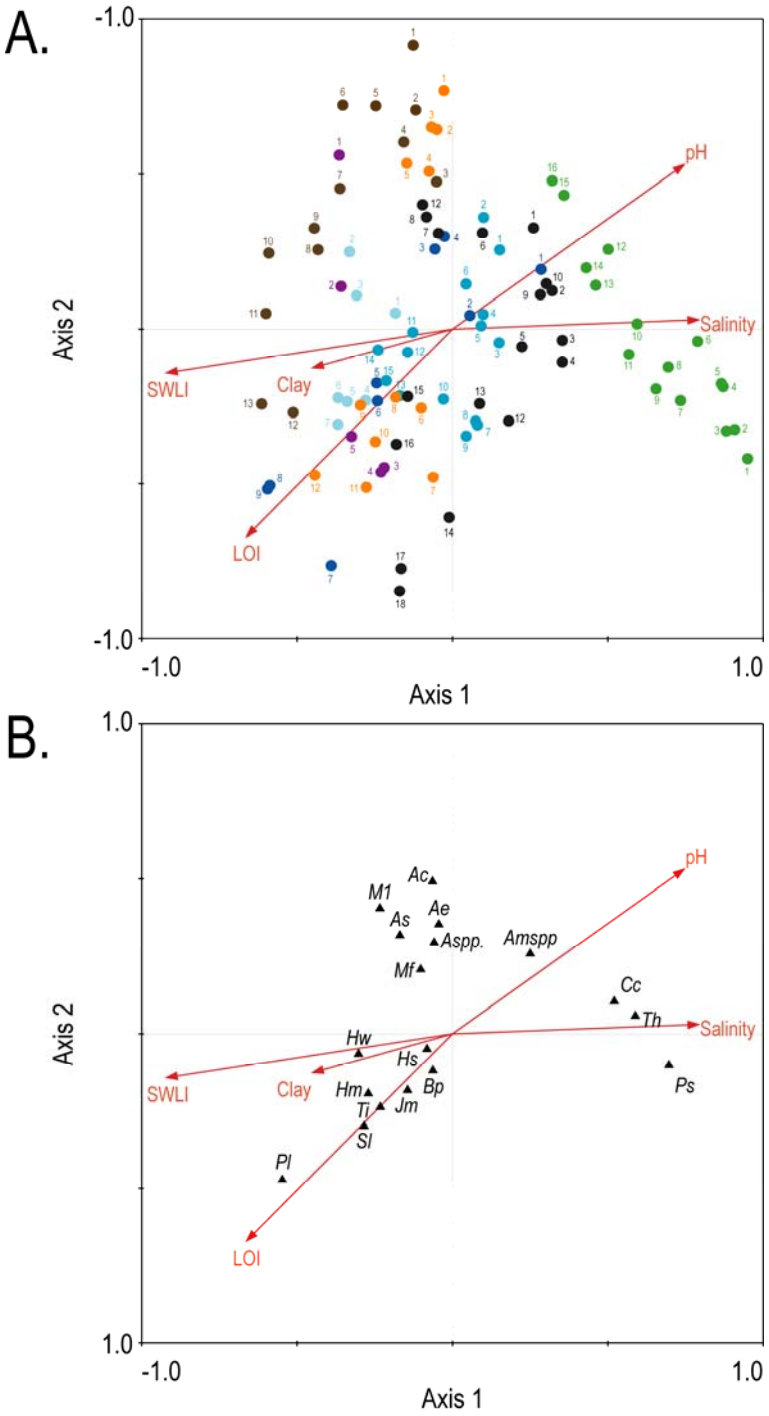

Figure 4.19 The CCA biplots of the Hokkaido site data showing (A) foraminiferal sample-environment and (B) species-environment. The colours represent each individual salt marsh; Akkeshi-ko (green); Mochiruppu (A, royal blue; B, medium blue; C, light blue); Furen-ko (black); Tofutsu-ko (purple); Saroma-ko (orange); Sarfutsu-toh (brown). Species abbreviations; Ac, *Ammobaculites crassus*; Ae, *Ammobaculites exiguus*; Aspp, *Ammobaculites* spp.; As, *Ammobaculites subcatenulatus*; Bp, *Balticammina pseudomacrescens*; Hm, *Haplophragmoides manilaensis*; Hs; *Haplophragmoides* spp.; Hw, *Haplophragmoides wilberti*; Jm, *Jadammina macrescens*; M1, *Miliammina* 1; Mf, *Miliammina fusca*; Ps, *Paratrochammina stoeni*; Pl, *Pseudothurammina limnetis*; Th; *Trochammina hadai*; Ti; *Trochammina inflata*; Amspp, *Ammonia* spp.; Sl, *Siphotrochammina lobata*; Cc; *Cribrostomoides canariensis*. Environmental abbreviations; LOI, loss on ignition.

On the species-environment biplot, the position of species is projected perpendicularly onto environmental arrows. This approximates the weighted average optima of the individual taxa along each environmental variable and is valuable to ascertain the environmental preference of specific species (Horton and Edwards, 2006). Taxa preferring higher elevations (including species such as *S. lobata*, *P. limnetis*, and *H. manilaensis*) are situated to the left whereas those taxa indicative of lower elevations such as *P. Stoeni*, *T. hadai* and *C. canariensis* are located to the right.

The five environmental variables account for 25.2% of the explained variance in the foraminiferal data (Table 4.1 and Figure 4.19) and partial CCAs (Figure 4.20) demonstrate that the total explained variance is composed of 16% SWLI, 12% salinity, 12% pH, 11% LOI and 6% clay. Monte Carlo permutation tests (p = 0.05, 499 permutations under reduced model) indicate that all of these variables, except for pH, account for a statistically significant portion of the total variance in the foraminiferal data.

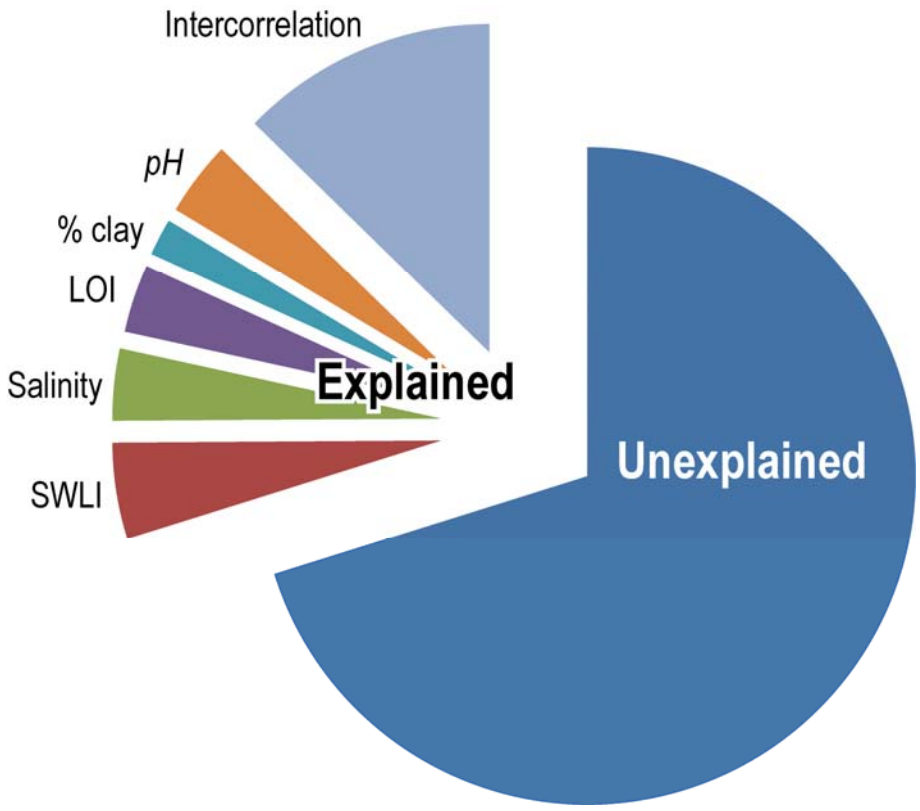

Figure 4.20 Pie chart showing the total variation (in %) of the Hokkaido foraminiferal training set in unexplained and explained portions. The explained proportion of the variance highlights the unique contributions of SWLI, salinity, pH, loss on ignition, % clay and the intercorrelation among gradients. The environmental variable not explaining a statistically significant proportion of variance using Monte Carlo permutation tests (499 unrestricted permutations) is highlighted in italics (i.e. pH).

The CCA and partial CCA results presented in this thesis indicate that the Hokkaido marshes display a less significant relationship with elevation compared to other marshes in north-west Europe and North America (Table 4.2). This may in part be due to a large amount of stochastic variation (e.g. Horton *et al.*, 2006), or another factor which could not be quantified (e.g. temporal variability; Horton and Edwards, 2003). However, the large amount of explained variance seems to be, in part, a function of the number of samples within the training set. A larger training set suggests more spatial heterogeneity and thus more unexplained variation, and a weaker relationship to elevation. Where multiple sites have been studied (Horton and Culver, 2008; Sawai *et al.*, 2004; Woodroffe, 2006), the strength of the relationship between the microfossils and the environmental variables is reduced. Although the CCA results presented in this thesis seem low compared to other studies, given the geomorphological and physiographic variability between the six salt marsh environments, the between-site variation in foraminiferal composition seems understandable.

Table 4.2 Comparison of CCA and partial CCA results between this and other microfossil-based studies.

Microfossil	Location	No. of samples	CCA explained (%)	Partial CCAs (of total explained variation)		Reference
				Elevation	Salinity	
F	Cowpen Marsh, UK		76	32	13	Horton and Edwards (2006)
F	North Carolina, USA	47	57	14	6	Horton and Culver (2008)
F	Nehalem River, Oregon, USA[1]	17	78	30	2	Hawkes et al. (In Press)
F	Queensland, Australia	76	61	12.5	7	Woodroffe (2006)
F	Hokkaido, Japan	95	25	4	3	This study
D	British Isles	88	22	5	-	Zong and Horton (1999)
D	Hokkaido, Japan		20	3	3	Sawai et al. (2004)
D	North Carolina, USA	46	31	6	3	Horton et al. (2006)

Where, F refers to foraminiferal-based studies, and D refers to diatom-based studies.

This analysis supports the hypothesis that foraminiferal dead assemblages from *all* the six salt marshes on Hokkaido's eastern and northern coastlines are related to SWLI and therefore tidal submergence. Elevation, acting as a proxy for the duration and frequency of intertidal exposure plays a dominant role in controlling the distribution of foraminifera, and thus transfer functions developed for SWLI are both appropriate and statistically valid. There are two important cautionary points which should be addressed. Firstly, there is a high degree of intercorrelation amongst the environmental variables suggesting the elevational gradient cannot be considered completely independent (Horton and Edwards, 2006). The interplay between the different environmental factors, which are primarily linked to the frequency of tidal flooding, implies the distribution of foraminiferal assemblages

across the intertidal zone is likely to be jointly affected by many linear or non-linear related factors (Bé, 1977; Buzas, 1968; Buzas *et al.*, 1977).

4.4.4 Infaunal foraminifera

Most studies assume intertidal foraminifera are primarily epifaunal, and take surface samples from the top 0-1 cm accordingly (e.g. de Rijk, 1995; Gehrels, 1994; Hawkes *et al.*, 2005; Horton *et al.*, 2006; Jennings and Nelson, 1992; Patterson *et al.*, 2004). This narrow surface sample better represents sub-surface assemblages as very low numbers of infaunal foraminifera are present below the top 2 cm and the distribution of species downcore is unaffected (Culver and Horton, 2005). However, Rose Bengal stained agglutinated foraminifera have been found at depths up to 50 cm and 60 cm in some North American marshes (Hippensteel *et al.*, 2000; Saffert and Thomas, 1998). My training set is comprised of surficial (0-1cm deep) samples, but if foraminifera live below this depth and constitute a significant proportion of total foraminifera at depth, their presence will affect sea-level reconstructions (Culver and Horton, 2005). When live foraminifera travel down the sediment column and assimilate with fossil assemblages, these assemblages no longer reflect the environment before they were buried.

In the low-marsh core from Akkeshi-ko (Figure 4.21) live foraminifera (*Haplophragmoides spp., H. wilberti, J. macrescens* and *T. inflata)* constitute *c.* 22.5% of the total assemblage in the surface sample (0-1 cm), but the percentage abundance of these live species decreases rapidly down core below 9 cm depth, falling to very low abundances at 19 cm depth.

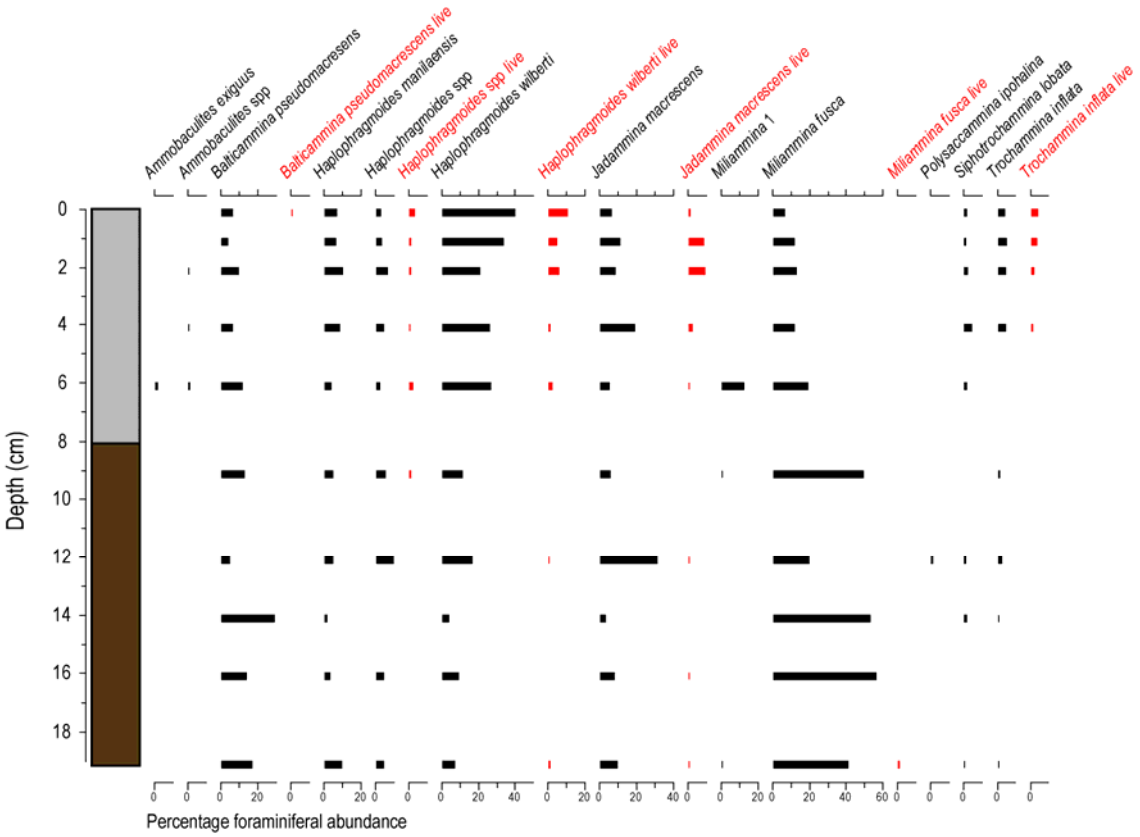

Figure 4.21 Relative abundance of taxa comprising greater than 5% in low-marsh core at Akkeshi-ko, eastern Hokkaido. Red bars indicate live specimens at the time of collection, black bars indicate dead foraminifera.

In the Akkeshi-ko high-marsh core (Figure 4.22), a larger number of foraminifera are found live below the marsh surface. *H manileansis*, *H. wilberti* and *Haplophragmoides* spp all appear to live infaunally. The top 0-1 cm surface sample comprised 28.9% live specimens, decreasing to 11.1% in the 12-13 cm sample. Although generally mirroring the relative proportions of the dead assemblage, some taxa were found alive in the core in disproportionally large percentages. For example, the count at 9 cm depth was made up of live *H. manileansis* (13 %), *Haplophragmoides* spp. (9 %) and *H. wilberti* (2 %).

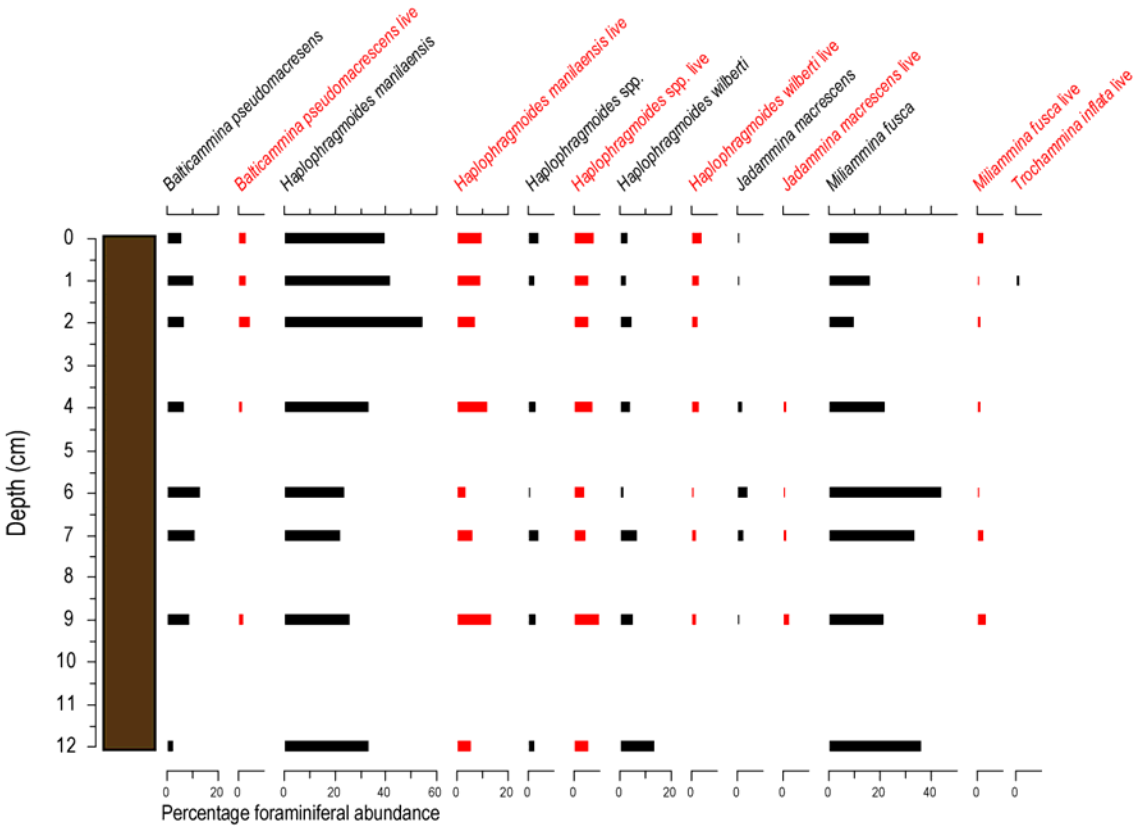

Figure 4.22 Relative abundance of taxa comprising greater than 5% in high-marsh core at Akkeshi-ko, eastern Hokkaido. Red bars indicate live specimens at the time of collection, black bars indicate dead foraminifera.

The results of this suggest that live foraminifera on the low marsh and high marsh at Akkeshi-ko are predominantly epifaunal. Infaunal foraminifera do not constitute a significant percentage of counts in the low-marsh environment. The percentage of live foraminifera at depth can be as much as 24% in the high-marsh environment (Figure 4.22), which may cause some blurring in the relative abundance of some species, particularly *Haplophragmoides* which are found in significant quantities to 9 cm. Since the infaunal *Haplophragmoides* population is different from the surficial sample on the high marsh, the reconstruction of former sea levels based on *Haplophragmoides* is complex as quantitative RSL predictions may artificially imply a higher palaeosurface elevation than that experienced. A thicker modern surface sample (0-10 cm) did not comprise species absent or under-represented in the 0-1 cm section, which has been noted elsewhere (Ozarko *et al.*, 1997; Patterson *et al.*, 1999). The results of this investigation suggest that the assemblages of foraminifera found in the 0-1 cm interval largely do broadly represent the deeper infaunal assemblages. Although there is some variability in certain taxa which may blur the signal of sea-level change derived from older marsh deposits, a larger 0-10 cm surficial sample would be unsuitable due to the focus in this thesis on interseismic land deformation and the need for high-resolution analysis.

4.5 NUMERICAL ANALYSES

I now explore the potential of the contemporary foraminiferal data described above for the development of transfer functions to reconstruct RSL histories for the study sites. The first stage in this exercise is to construct a training set based on the contemporary foraminiferal data. Variations in tidal range between sites mean it is necessary to standardise the elevation of the samples from the six study sites to a common datum. This is achieved by converting each sample elevation to a standardised water level index (SWLI, after Horton 1999), as detailed in Chapter Three.

I start by comparing the elevation of the macrophyte vegetation zones observed in each of my study sites, analysed relative to a standard water level (Figure 4.23). Although these boundaries were identified subjectively, there is a reasonably strong agreement between sites indicating that the SWLI transformation is robust in most cases. Thus, the upper limit of tidal flat and lower limit of low marsh (generally) occurs between *c*. 80-100 SWLI, around MHHW. This finding is in accordance with the observations made at each sample site. Equally, the transition from salt marsh to freshwater swamp also occurs at a broadly similar SWLI of *c*. 120-140.

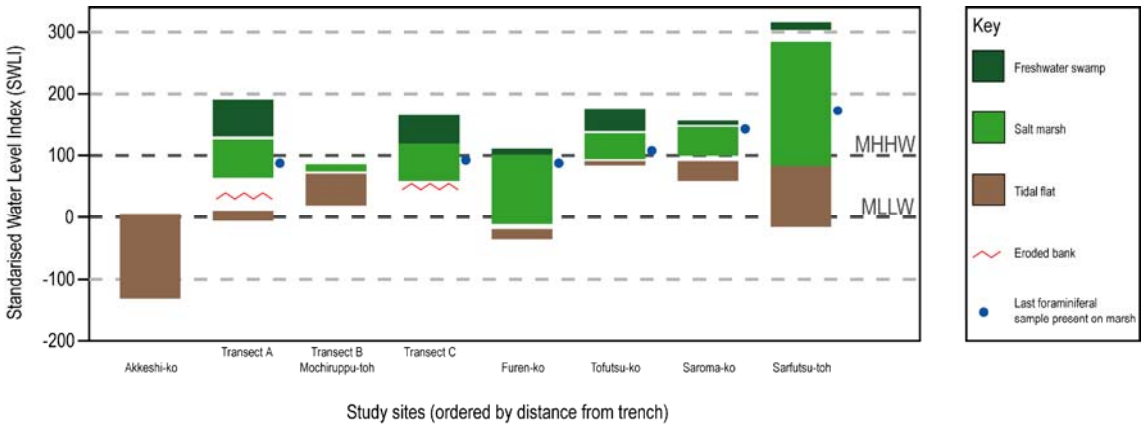

Figure 4.23 Summary vegetation zones from the six sites investigated in this study.

The one exception to this overall pattern is Sarfutsu-toh where the transition from salt marsh to freshwater swamp extends considerably higher in SWLI units compared to the other sites. There is no obvious explanation for this deviation. SWLI reconstructions at high elevations are sensitive to small changes in the assumed elevation of MHHW and the tidal data for this site are partly based on extrapolation from elsewhere. At this site I have estimated MHHW to be 0.36 m TP, based on comparison with the secondary port of Hama-Onishibetsu, located 2 km away (see Section 3.2.4 for details). There is no obvious reason to doubt this value since this is the height of MHHW along much of this coast. The SWLI

calculation for this site is also dependent on my assumption that the tidal range at this site is 0.50 m, the lowest for the six sites studied. If this is incorrect, then the resulting SWLI reconstructions, especially for the top and the bottom of the range of environmental samples, will change. However, given the general pattern of tidal variability along this coast, this factor is also unlikely to be the cause of the differences observed. Even if the tidal range were 1.0 m, which would be greater than that recorded at any of the five other sites, this would result in a lowering of the salt-marsh/freshwater swamp transition from SWLI 306 to only 203. The site would still be anomalous.

The site at Sarfutsu-toh is different to the other marshes studied. Its assemblage of foraminifera is dominated by *M. fusca* that extend to 0.72 m TP, well above MHHW (0.36 m TP) (Figure 4.23). The salinity data indicate that the sample site is much fresher than elsewhere (2 psu) and the transition from the salt-marsh macrophytes to the freshwater swamp occurs at 1.28 m TP, which is also well above MHHW. The site has a narrow tidal inlet with a low tidal range and it is possible that limited exchange of waters between ocean and the back-barrier area elevates water levels and also reduces salinity (although data to support this hypothesis are lacking). Whatever the exact cause for the differences observed here, it is clear that the contemporary data from this site are different to those from the other sites studied, especially towards the upper part of the intertidal zone. For this reason, in the statistical analyses of the foraminiferal data that follow, this data is treated with a degree of caution.

4.5.1 Local versus regional training sets

There is debate in the literature as to whether it is better to use locally derived training sets, constructed and applied from the same study marsh, or regional training sets that combine data from several sites (see, for example, Horton and Edwards (2006)). Table 4.3 illustrates examples of the number of microfossil samples, and the distance over which they were collected. Some authors undertake detailed local sampling, whilst others, in their pursuit of regional training sets adopt a wider geographical sampling area. The debate centres on whether the range of contemporary samples at any single site is likely to be representative of all the past environments recorded in the fossil stratigraphy. A smaller training set is inevitably prone to more errors, associated with a smaller range of modern analogues, and an under-representation of variability (Griffith and Amrhein, 1997; Horton and Edwards, 2006).

Table 4.3 Examples of training set numbers, with approximate area over which training function encompasses.

Location	Number of samples in modern training set	Number of marshes studied	Area covered (km)	Reference
Sisimiut, West Greenland	74	3	2.5	Woodroffe and Long (2009)
Outer Banks, North Carolina	47	3	80	Horton and Culver (2008), Kemp *et al*. (2009a)
UK and Ireland	203	14	800	Horton and Edwards (2006)
Alaska	154	3	120	Zong *et al*. (2003), Hamilton and Shennan (2005)
Great Barrier Reef coastline	62	2		Woodroffe (2009)
South-west England	85	2	16	Massey *et al*. (2006a)
Hokkaido, Japan	95	6	500	This study

On passive coastal margins, where RSL and intertidal environments may have changed little during the last few millennia, the use of a local training set is intuitively attractive since it should encompass the full range of environmental conditions encountered in the past. To put this another way, it is probable under this scenario that the fossil environment will result in good 'matching analogues' with the contemporary data. However, Hokkaido is located on an active plate boundary, containing salt marshes that have recorded multiple abrupt changes in RSL and accompanying shifts in shoreline position and coastal configuration. Moreover, recent human impacts have significantly altered the geomorphology of the coastline (e.g. Atwater *et al.*, 2004). As a result, it is highly likely that the environments recorded today at any single site will not completely replicate the environments recorded in even relatively recently deposited stratigraphic sequences. For this reason, I chose to construct a regional training set that combines data from six sample sites. There is an additional practical point here which is that the development of local training sets is a highly time intensive process, requiring typically 50 or more samples from each contemporary site. This was beyond the scope of this thesis which instead sought to develop a wider understanding of the distribution of foraminifera across this little studied coastline.

4.5.2 Species response curves

The first stage of transfer function development is to determine whether to use linear- or unimodal-based numerical techniques (ter Braak and Prentice, 1988). To this end, the combined dataset (and various sub-sections of the data – see Section 4.5.3) was analysed initially by DCA to estimate the lengths of the compositional gradients in each dataset. First gradient lengths less than two standard deviation units suggest that the data are behaving in a linear response, whereas gradients that are more than 2.5 standard deviation units imply that much more of the data fit a unimodal trend. Table 4.4 lists the DCA axis 1 gradients for the Hokkaido dataset. Despite some individual taxa occurring across much of the marsh, there appears to be sufficient biological turnover in taxa to ensure that all

subsequent analyses are based on an underlying unimodal species-response model (Birks, 1995; ter Braak, 1986), namely CCA (Section 4.4.3), and WA-PLS regression (ter Braak and Juggins, 1993). This conclusion stands whether Sarfutsu-toh is included or not in the training set (Table 4.4).

Table 4.4 DCA axis 1 gradients for training sets developed in this thesis.

Training set	Regional	Regional, no subtidal	Regional, no Sarfutsu-toh
DCA Axis 1	4.917	3.979	4.873

4.5.3 Transfer function development

There are some important decisions to be taken when developing a transfer function, notably which samples and species to include in the training set. Removing outliers from the training set may improve model precision by reducing RMSEP, but the resulting model may then not properly reflect the ecological variability in the contemporary and fossil datasets. Equally, there may be good reasons to reduce the number of samples in a training set, for example in cases where data from one site are clearly anomalous compared to the majority of other data due to local site specific factors. These are judgements that must be made when considering all of the data available to the analyst.

In the following analysis I explore the potential of three different transfer function models that use data from all of the six study sites. I then re-run these models using data from only five of the sample sites, removing the observations from Sarfutsu-toh for reasons discussed above, to assess whether this significantly improves model performance.

The 'All data' Model

The first model developed incorporates all the foraminiferal data from the six sites (eight transects in total, only taxa with counts that are greater than 40). The training set includes 95 samples, 27 species and extends across a SWLI range of -129.7 to 170.9 (Figure 4.24). This includes data from subtidal and intertidal environments. I present the 'All data' model with taxa plotted against SWLI in Figure 4.25. From this model, it is apparent that some taxa have more clearly defined species optima and tolerance than others and that some have well defined unimodal distributions whereas others are more linear.

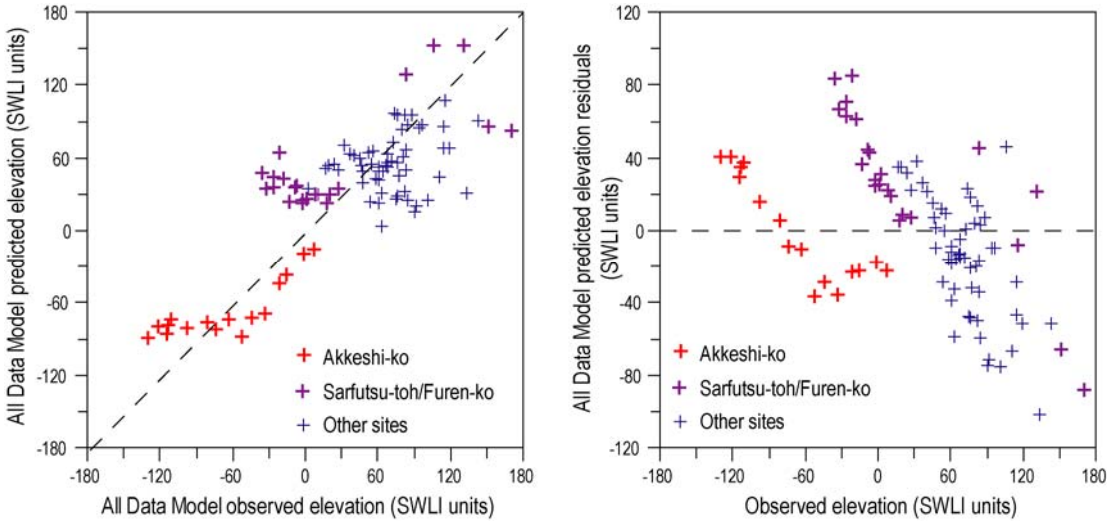

Figure 4.24 Observed versus predicted elevation and elevation residuals (predicted-observed) using the ''All data'' model.

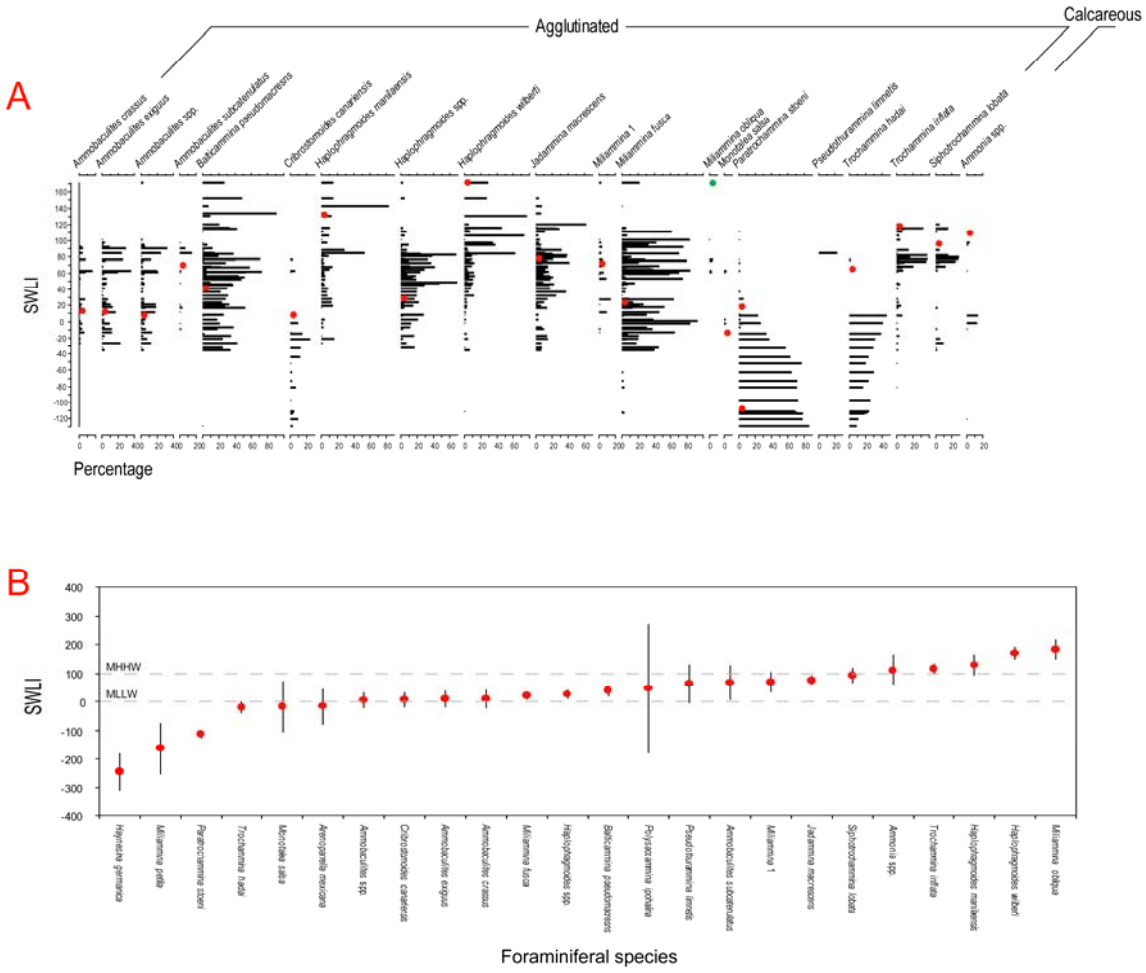

Figure 4.25 Optima and tolerances of foraminiferal species in ''All data'' model predicted by WA-PLS component 1 (with bootstrapping). (A) contemporary foraminiferal data plotted against SWLI units. Red dots refer to the species optima as predicted by the 'All data' model, and green circle indicates species optima above the range of SWLIs displayed. (B) shows the optima and tolerances of all the species in the 'All data' model.

4.5.4 'Pruned' Model

As a second stage of analysis, I now extract from the training set five samples and three species which are clearly defined outliers within the 'All data' training set. My justification for doing so is as follows. Large biological data sets comprising samples from a broad range of geomorphological and physiographical environments invariably contain some samples that may show a poor relationship to SWLI. For these samples, environmental factors other than elevation (such as salinity) may be dominant in driving the assemblage, alternatively transport or diagenesis may have altered the composition of the original assemblage. These outliers may strongly affect the transfer function coefficients and have a detrimental effect on the models' predictive ability (Birks *et al.*, 1990; Gasse *et al.*, 1997).

There are various methods to remove outliers from training sets. One involves screening samples with an absolute residual (observed minus predicted) greater than the standard deviation of SWLI in the training set (Horton and Edwards, 2006; Jones and Juggins, 1995). In this study this value is 65.06 SWLI and results in the removal of 11 samples, or nearly 12% of the training set. This 'Pruned A' model improves the r^2 and RMSEP from 0.65 and 40.02 SWLI (at component 2) respectively in the 'All data' model to 0.77 and 31.54 SWLI (at component 2) (Table 4.5).

Table 4.5 Summary statistics for all models in this thesis using a WA-PLS transfer function with three components. Component 2 generally provides the minimum adequate model.

Model	Comp No.	No. of samples	R^2_{boot}	Average bias	Maximum bias	$RMSEP_{boot}$	% change in RMSEP
All data	1	95	0.61	1.28	77.31	41.21	-
	2	95	0.65	2.33	51.51	40.02	-2.90
	3	95	0.65	2.29	53.35	41.37	+3.38
Pruned A	1	84	0.72	0.88	53.43	33.58	-
	2	84	0.77	1.81	37.62	31.54	-6.08
	3	84	0.77	1.92	32.39	32.12	+1.84
Pruned B	1	87	0.70	1.04	53.20	34.42	-
	2	87	0.75	2.37	35.87	32.92	-4.35
	3	87	0.75	2.41	36.18	33.59	+2.06
Pruned, no subtidal	1	69	0.32	2.30	72.98	39.74	-
	2	69	0.36	3.22	68.70	39.77	+0.06
	3	69	0.33	3.59	75.34	43.69	+9.86
All data, no SF*	1	82	0.62	1.39	76.18	40.40	-
	2	82	0.64	4.01	88.25	41.30	+2.22
	3	82	0.63	4.10	101.36	43.57	+5.50
Pruned B, no SF	1	76	0.73	1.24	65.61	34.07	-
	2	76	0.76	3.59	66.32	33.64	-1.25
	3	76	0.76	3.69	73.68	34.98	+3.97

* SF; Sarfutsu-toh

An alternative method of removing outliers involves deleting samples with an absolute residual greater than one quarter of the total range of the SWLI gradient (Gasse *et al.*, 1997; Woodroffe, 2009). In this study this value is 75.16 SWLI and results in the removal of 8 samples, 8% of the training set. This 'Pruned B' model has an improved r^2 and RMSEP of 0.75 and 35.87 SWLI at Component 2 respectively (Table 4.5).

Both approaches result in a significant improvement in model performance. However, given the relatively small number of samples in the overall training set, and the small difference in model performance, my preference is to minimise the number of samples removed by using the 'Pruned B' model. Figure 4.26 shows a plot of the observed versus predicted for the 'Pruned B' model. This plot still illustrates some non-linearity, especially at the lower end of the training set that comprises the subtidal samples from Akkeshi-ko (Figure 4.26).

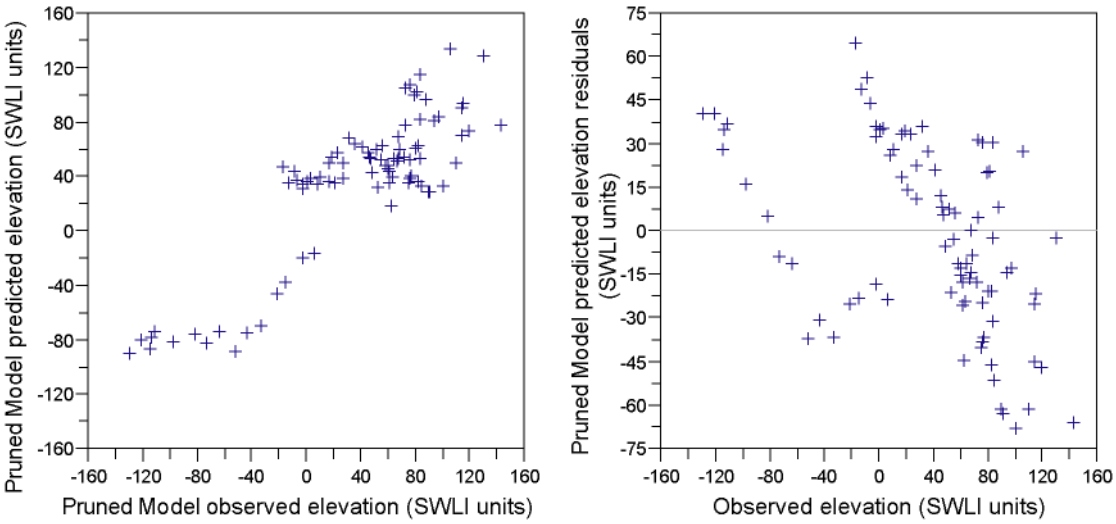

Figure 4.26 Observed versus predicted elevation and elevation residuals using the 'Pruned B' model.

The fossil foraminiferal data described later in this thesis contain some assemblages that have little resemblance to the contemporary samples collected from subtidal environments below LAT (approximately -50 SWLIs). In addition, although the CONISS and Cluster analysis detailed in Section 4.4.2 shows that there is a statistical difference between subtidal and tidal flat samples, there is no obvious trend within the subtidal samples with respect to elevation. This is apparent from the plot of the observed versus predicted for the 'All data' model (Figure 4.24). For this reason, I now remove 10 subtidal samples from the Pruned model, which is the best model using the whole environmental gradient. This reduces the length of the environmental gradient by 75%, from 271 to 168 SWLI and results in an r^2 and RMSEP of 0.36 and 39.77 SWLI at Component 2 respectively. The decline in r^2 is reflective of a shortening in the environmental gradient.

The effect of removing the Sarfutsu-toh data

As noted above, the contemporary foraminiferal data from Sarfutsu-toh differ significantly from those from the other salt-marsh sites, occurring at anomalous elevations with respect to tidal datums and with restricted assemblage diversity. For this reason, I have opted to re-run the 'All data' and 'Pruned B' models, this time excluding the 13 samples from this site. The results (Table 4.5) indicate that their removal has a limited impact on overall model performance, with a marginal reduction in the r^2 and RMSEP compared with the models that include data from all sites.

Model evaluation

An important step in model evaluation is to compare the results of different models when they are applied to the fossil sediment sequences. For example, a model developed from a particular sub-set of the contemporary training data may appear at this stage to be most

suitable, based on summary statistical measures detailed in Table 4.5, but may be inappropriate when applied to fossil sediments due to a lack of contemporary analogues.

There are some observations that are appropriate at this stage. First, as a general rule, transfer function model training sets should not be overly-tuned by removing taxa and samples unless there are very good reasons to do so. In the analyses above, I believe that there are good reasons to remove a small number of obvious outliers, as indicated by the significant model improvement that is seen in the 'Pruned' compared with the 'All data' models. Of the two 'Pruned' models, my preference is for the model that minimises samples lost from the training set ('Pruned model B'). The 'No Subtidal' model is intuitively attractive since the removed samples are all from one site, they have a weak zonation with respect to elevation and they are not common in the fossil sequences. Their removal results in a significant shortening of the environmental gradient and a deterioration in model performance. However, the 10 samples removed from the lower end of the training set include low frequencies of a number of important taxa that occur at higher elevations. Transfer function model performance is sensitive to such abbreviations and, where possible, the full ranges of the taxa should be retained in the models (Woodroffe, 2009). These points argue against the adoption of the 'No Subtidal' model. Finally, the exclusion of the contemporary data from Sarfutsu-toh has only a minor impact on model performance and is therefore considered unnecessary.

In summary, at this stage in the analysis, my preferred model is the 'Pruned B' model. This strikes a balance between judicious pruning of the training set to remove obvious outliers, whilst also retaining a reasonably large training set that extends across a sufficiently long environmental gradient to include the full distributions of as many taxa as possible. Further evaluation of these different models is completed in the following Chapter, where the different models are applied to fossil assemblages for RSL reconstruction.

4.6 CONCLUSION

This chapter presents the results of the analysis of the contemporary salt-marsh environments from six field sites in Hokkaido. The main conclusions from the work are:

- The studied salt marshes show a distinct vertical zonation based on analysis of a range of physical and biological data. The marsh- and tidal-flat environments are typically fine-grained (silty-clays), low energy depositional environments in protected coastal settings. Organic content is generally low on the tidal flat but rises across the marsh to reach a maximum of *c*. 90% LOI on the high marsh and in

the freshwater swamp. Salinity decreases with elevation at most sample sites, although at two sites (Tofutsu-ko and Sarfutsu-toh) significant freshwater input and limited tidal mixing result in considerably lower salinity compared to elsewhere.

- A training set comprising 95 contemporary samples of foraminifera and 27 species collected from the six study sites is developed for RSL reconstruction. As a first stage of analysis, CONISS and DCA demonstrate the existence of statistically significant vertical zonations at each of the study sites although there is not a single pattern common to all sites. This reflects local site variability in terms of depositional conditions.
- Individual marshes typically support 2/3 foraminiferal zones comprising a tidal flat or low marsh zone, dominated by *Ammobaculities*. spp. and *M. fusca* and then a high zone dominated by *Haplophragmoides*. spp. (typically *H. wilberti*) or *J. macrescens*. In two of the marshes, a near monospecific assemblage of *H. manileansis* is found at the brackish/freshwater transition.
- DCA demonstrates that the training set is suitable for transfer function development using WA-PLS. Elevations are standardised to account for tidal variability between sites using the SWLI methodology. Four transfer function models are developed and assessed; an 'All data' model, two 'Pruned' models (A and B) in which selected outlier samples are removed, and a 'Non Subtidal' model which excludes samples forming below LAT.
- Model performance is variable, largely reflecting differences in the length of the environmental gradient and the number of taxa included. A careful consideration of the relative merits of each model suggests that the preferred model at this stage in analysis is the 'Pruned B' model, which removes obvious outliers whilst retaining a significant number of samples and taxa. This model has an r^2 of 0.75 which shows a strong positive correlation between assemblage change and elevation and a relatively small RMSEP of 32.92 SWLI at Component 2.

The following Chapter presents the fossil core foraminifera and applies the transfer functions developed here to reconstruct past RSL change from the study site marshes.

CHAPTER FIVE

Results II – Fossil Environments and Relative Sea-level Reconstruction

5.1 INTRODUCTION

In Chapter Four, I presented the results of the contemporary data analysis from my six field sites. At each of these sites I also conducted a lithostratigraphical investigation of the near-surface sediments, focussing on the upper 1-2 m of the stratigraphic record to encompass the last several centuries of sedimentation. In each case, I collected one or more sample cores from the study site which I returned to Durham University for detailed laboratory analysis. This work included analysis of a range of physical properties, namely percentage LOI and grain size, as well as age determination through gamma spectrometry (^{210}Pb and ^{137}Cs dating). Finally, I analysed sample cores for their fossil foraminifera in order to reconstruct palaeomarsh elevation and RSL change during the interseismic period of the last earthquake cycle using the transfer function models developed in Chapter Four. In this latter work I use three models ('All Data', 'Pruned B' and 'No Subtidal').

The objectives of this Chapter are to:

- Present the lithostratigraphic data from the study sites;
- To report the results of the physical properties examined from the sample cores;
- To detail the age models developed for each sample core;
- To describe the foraminifera from the sample cores;
- To combine the above data and apply the transfer functions developed in Chapter Four to reconstruct RSL change at five study sites.

5.2 THE FOSSIL ENVIRONMENTS AND RSL HISTORY OF THE HOKKAIDO SALT MARSHES

In this section, I present field and laboratory results for each of the field sites in turn, starting with Mochiruppu on the Pacific south coast of Hokkaido and then working progressively to the north. Each section includes a new site map that shows core locations;

some are generated from LandSat, and others from Google Earth to maximise image resolution.

5.2.1 Mochiruppu

The stratigraphy of the Mochiruppu salt marsh has previously been examined by Sawai *et al*. (2004b) who completed a 150 m long transect of cores in the west of the basin and used diatom data from a sample core to reconstruct land- and sea-level movements during the last *c.* 500 years (Figure 5.1). In a more recent paper, Sawai *et al*. (2009) collected two large Geoslice sample cores from *c.* 300 m east of this original transect. These cores contained 17 thin (typically 20 cm thick) tsunami layers deposited in a 4 m stratigraphic sequence that accumulated in the last 6,000 cal. yrs.

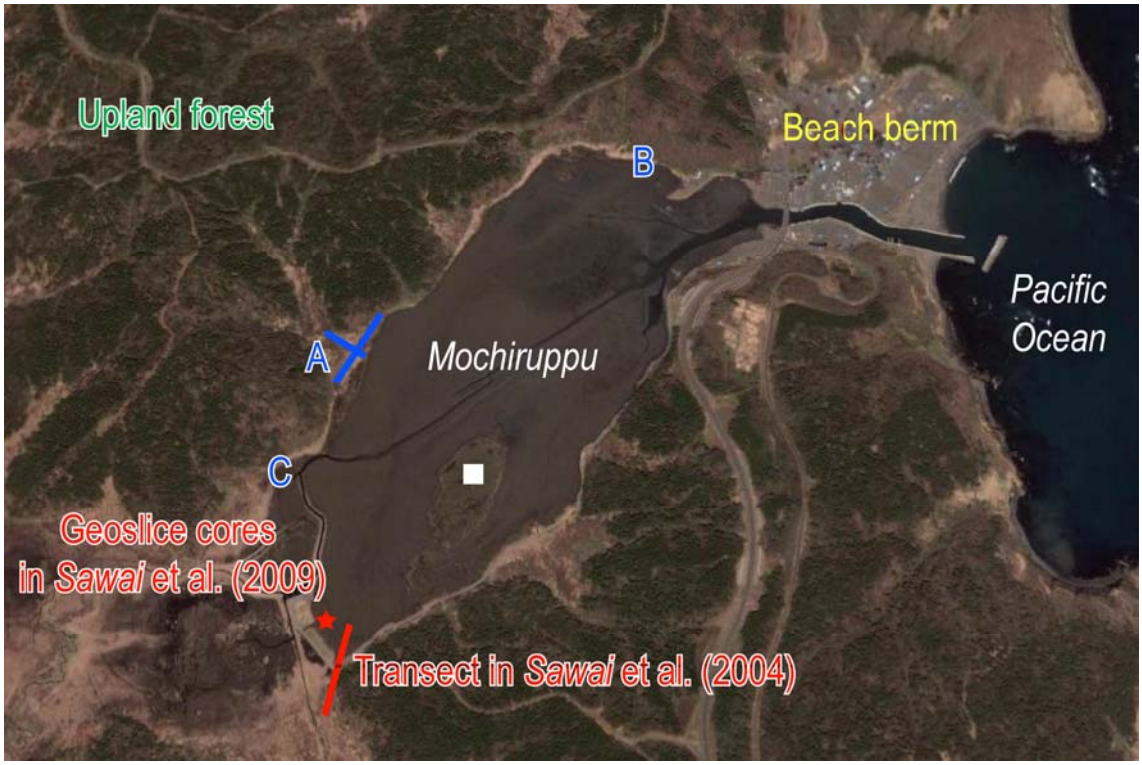

Figure 5.1 Site map of Mochiruppu, showing locations of transects completed in this and previous studies. Blue letters refer to locations of modern sampling stations, blue lines show location of transects studied in this thesis (Southern side), and white square shows location of core studied on the northern side of the marsh in this thesis. Image from Google Earth.

I resampled the Mochiruppu site in order to use the near-surface sedimentary record to calibrate the tide-gauge record from Kushiro and Hanasaki which are the longest tide records from Hokkaido and are located within *c.* 50 km of the sample site. To achieve this, I collected two sample cores (cores Mochiruppu North and South respectively), one located close to the original Sawai *et al*. (2004b) transect to compare my foraminiferal reconstruction with the existing diatom record, and a second from the northern part of the

basin in order to assess within-site variability in reconstructed RSL (Figure 5.1). A second objective was to extend these shallow records back in time to provide information on RSL changes during the current interseismic period.

Mochiruppu North

The Sawai *et al*. (2004b) stratigraphy from the west of the basin is broadly similar to that recorded from Akkeshi-ko, although with some important differences. As at Akkeshi-ko, the near-surface stratigraphy comprises interbedded peats, muddy peats and mud (Figure 5.2A). There are two peat beds separated by a thick unit of mud that contains a prominent muddy sand interpreted as a tsunami deposit dating from *c.* AD 1650 (its precise age is uncertain). The lower of the two peats is *c.* 5 cm thick whereas the main upper peat is *c.* 30 cm thick and extends close to the present surface where it is capped by a thin deposit of mud, presumably deposited during the recent rise in RSL recorded by the 20th century tide-gauge records.

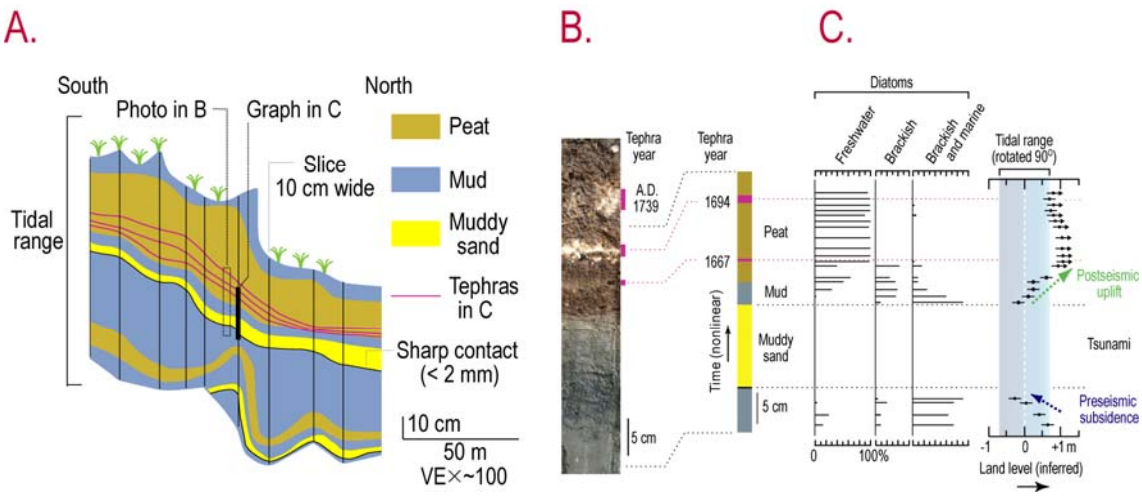

Figure 5.2 Litho- and biostratigraphy recorded by Sawai *et al*. (2004b) at Mochiruppu. (A). Lithostratigraphy of area; (B) photograph of the upper part of the Mochiruppu stratigraphic sequence including the three tephras; and (C) diatom-based RSL reconstruction from the Mochiruppu core.

Three tephras occur towards the base of the upper peat and can be traced laterally between cores across a distance of *c.* 150 m. They are the same three tephras recorded by Sawai (2001) from Akkeshi-ko, dating from AD 1667, AD 1694 and AD 1739 (Figure 5.2B). A sample core was collected by these authors from a mid-transect location and analysed for its diatom content. The diatoms from this sequence are interpreted by Sawai *et al*. (2004b) as providing evidence for initially rapid emergence following the tsunami, during the middle and late part of the 17th century. The uplift is estimated to be *c.* 1 m and to have been largely complete within 30 years. The record is essentially the same as that described from Akkeshi-ko by Atwater *et al*. (2004), but this time with only one emergence.

In this study, I collected a replicate short sample core (Core Mochiruppu North) from the same location of the Sawai *et al*. (2004b) diatom study using a small Geosclice corer (Figure 5.1; core location given by white square). The sample core is 0.77 m in length, comprises twelve stratigraphic units (Table 5.1) and corresponds to the upper sediments identified by Sawai *et al*. (2004b) (Figure 5.2C). The base of the core contains the upper of the three tephras, Ta-a, dated to AD 1739.

Table 5.1 Lithostratigraphy of the sample core from Mochiruppu North described using the Troels-Smith (1955) scheme of stratigraphic notation.

0 - 2.5	Ag3, As2, Th2+	1 0 0 2	Dark grey silty clay with some herbaceous material.
2.5 – 16	$Th^2$2, Ag1. As1, Sh+	2 0 0 2 1	Reddish brown herbaceous peat with silt and clay.
16 - 18.5	Ag2, As1, Th^2+, Sh+	1 0 0 2 0	Brown silty clay with organics.
18.5 – 26	$Th^2$2, Ag1. As1, Sh+	3 0 0 2 0	Reddish brown herbaceous peat with silt and clay.
26 - 28.5	Ag2, As2, Sh+,	1 0 0 2 1	Grey clayey-silt with occasional organics.
28.5 – 31	$Th^2$2, Ag1. As1, Sh+	3 0 0 2 1	Reddish brown herbaceous peat with silt and clay.
31 - 32.5		Lim. sup.	Light grey tephra.
32.5 – 33.5	$Th^2$2, Ag1. As1, Sh+	3 0 0 2 1	Reddish brown herbaceous peat with silt and clay.
33.5 – 36.5		Lim. sup.	Very pale brown tephra.
36.5 – 36.8	$Th^2$2, Ag1. As1, Sh+	3 0 0 2 1	Reddish brown herbaceous peat with silt and clay. Very pale brown (10YR 8/3) pumice between 36.5 and 36.8 cm.
36.8 – 37.8	$Th^2$2, Ag1. As1, Sh+	2 0 0 2 1	Reddish brown herbaceous peat with silt and clay.
37.8 – 77	Gmin3, Ag1, Th2+	1 0 0 2 1	Dark grey fine sands with silts and some organics.

Laboratory analysis

The results of the laboratory analyses are presented in Figure 5.3.

The grain-size data (Figure 5.3) show that the core material comprises a sand silt with a trace of clay, with overall little change up-profile. Percentage LOI data are available for the upper 30 cm of sediment and shows a lower peak at *c.* 40% LOI at 28 cm, and a second broader peak between 22-16 cm, after which values remain steady before declining in the upper most samples above *c.* 6 cm.

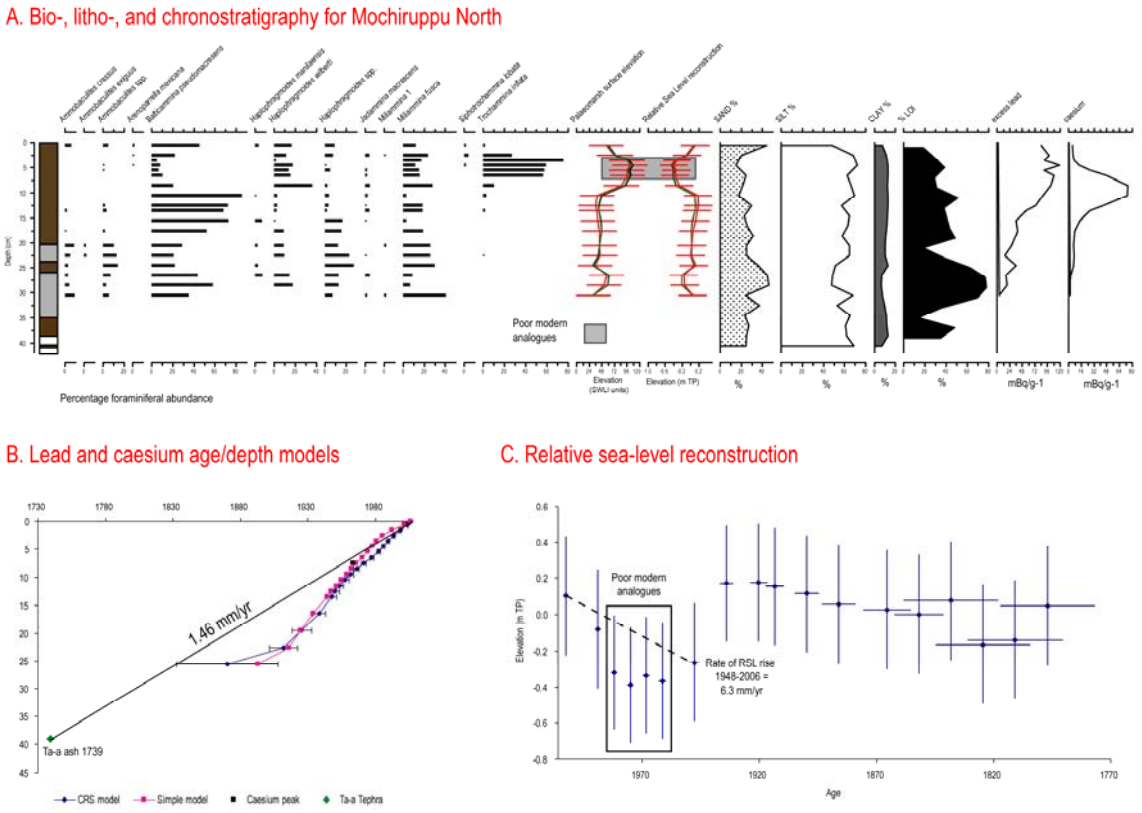

Figure 5.3 Litho-bio-, and chronostratigraphical analysis at Mochiruppu North (A) Foraminifera assemblages, RSL (black = all data model, red = pruned model, green = no subtidal model), % Loss on Ignition, particle size data and excess ^{210}Pb and caesium profiles for the Mochiruppu North core. Core lithology – brown – turfa peat, grey – organic mud, white – tephra horizons. (B) ^{210}Pb age/depth models using the CRS and Simple models, with the 1964 caesium peak highlighted (in black). Sediment accumulation rates used in (C) are based on 1.46 mm/yr which is derived from the 1739 tephra at 39 cm. (C) RSL reconstruction for this core using the pruned transfer function model.

I counted 18 samples for foraminifera, with samples collected a 2 cm intervals between 32 cm and the present surface, focussing on the interval of core containing ^{210}Pb as a guide to the 20th century part of the sequence (Figure 5.3). Overall, the sequence is dominated by *B. pseudomacrescens*, *Haplophragmoides* spp., *H. wilberti*, *M. fusca* and *T. inflata*. The main change in assemblage is the rise in frequencies of *T. inflata* above 6 cm, coinciding with the decrease in LOI. The change in fauna towards the top of the sequence, from a *B. pseudomacrescens* and a *M. fusca* mixed assemblage to one dominated by *T. inflata* implies a fall in sea level. In comparison to *B. pseudomacrescens* which is found over much of the unvegetated tidal flat, *T. inflata* has a tight ecological niche on the low marsh. The decrease in *T. inflata* in the top 5 cm of the core, and the re-establishment of a more mixed assemblage indicates the palaeomarsh surface elevation has decreased in the very recent past.

A chronology for the sample core is provided by linear extrapolation back to the 1739 tephra, which corresponds also to the clear caesium peak at a depth of 7.5 cm (Figure 5.3). Although there is close similarity between the CRS and Simple model age/depth profiles and the peak in caesium, I have chosen to rely solely on the tephra age which is clearly evident throughout Mochiruppu.

I now apply the three transfer function models developed in Chapter Four to the foraminiferal data in order to reconstruct palaeomarsh surface elevation (converting the SWLI values to local elevation in m TP), using the age model described above to provide an absolute chronology. The RSL reconstruction is very similar between models. During the early part of the 19th century, the three lowest foraminiferal samples suggest RSL fell from *c.* 0.10 m MTL to *c.* -0.20 m MTL, before rising again to a maximum of *c.* 0.20 m MTL by *c.* 1960. An abrupt fall in RSL occurred at around 1930, from *c.* 0.20 m to -0.20 m MTL. This corresponds to an increase in the frequencies of *T. inflata* in the sample core. This assemblage has poor modern analogues in the contemporary foraminiferal training set, but the evidence for a fall in RSL is clear, as indicated by the change observed from samples at 8 cm and 6 cm which have good modern analogues and are therefore reliable reconstructions. There followed, from the mid-twentieth century onwards, an overall rise in RSL to present. This is associated with a near-surface decline in percentage LOI and an increase in the sand content of the lithostratigraphic record (Figure 5.3).

Mochiruppu South

At Mochiruppu South I sampled two transects of 18 cores completed at approximately 10 m intervals in a transect of 150 and 80 m in length respectively (Figure 5.4). The first transect presented runs parallel to the modern shoreline; and comprises stratigraphy similar to that recorded on the other side of the bay, however the more detailed stratigraphic plots shown below highlight the two silty units found above the tephra's which are thought to represent earthquakes during the 20th century. The lithostratigraphy reveals a silty unit (which overlies the sand of tsunami origin mentioned in Sawai *et al*. (2004b), above which two distinct tephra's can be seen, which are thought to correlate with the 1694 and 1739 eruptions. The rest of the cores then report a thick sequence of peat, punctuated by two distinct more clastic units which are thought to be associated with land-level change following 20th century earthquakes. These units which can be traced laterally through all the cores are overlain by an organic mud, the present surface of the low marsh which these cores are sampled from. The second of the transects was sampled to understand how the units are traced with distance from the main basin. Those cores located close to the seaward edge of transect record the same stratigraphy as the previous transect, with the tephra's and silty units in the upper section of the peat. With distance from the trench, the

units narrow, and the tsunami sand found in Sawai *et al*. (2004b) appears in the core stratigraphy, overlain by tephra which correlated with those in the late 17th and early 18th centuries. I collected a sample core from the location of core 9 (M05/1/9) for laboratory analysis, which comprises two silty units in a predominantly peat matrix. The sample core is 0.66 m in length, and comprises twelve stratigraphic units (Table 5.2).

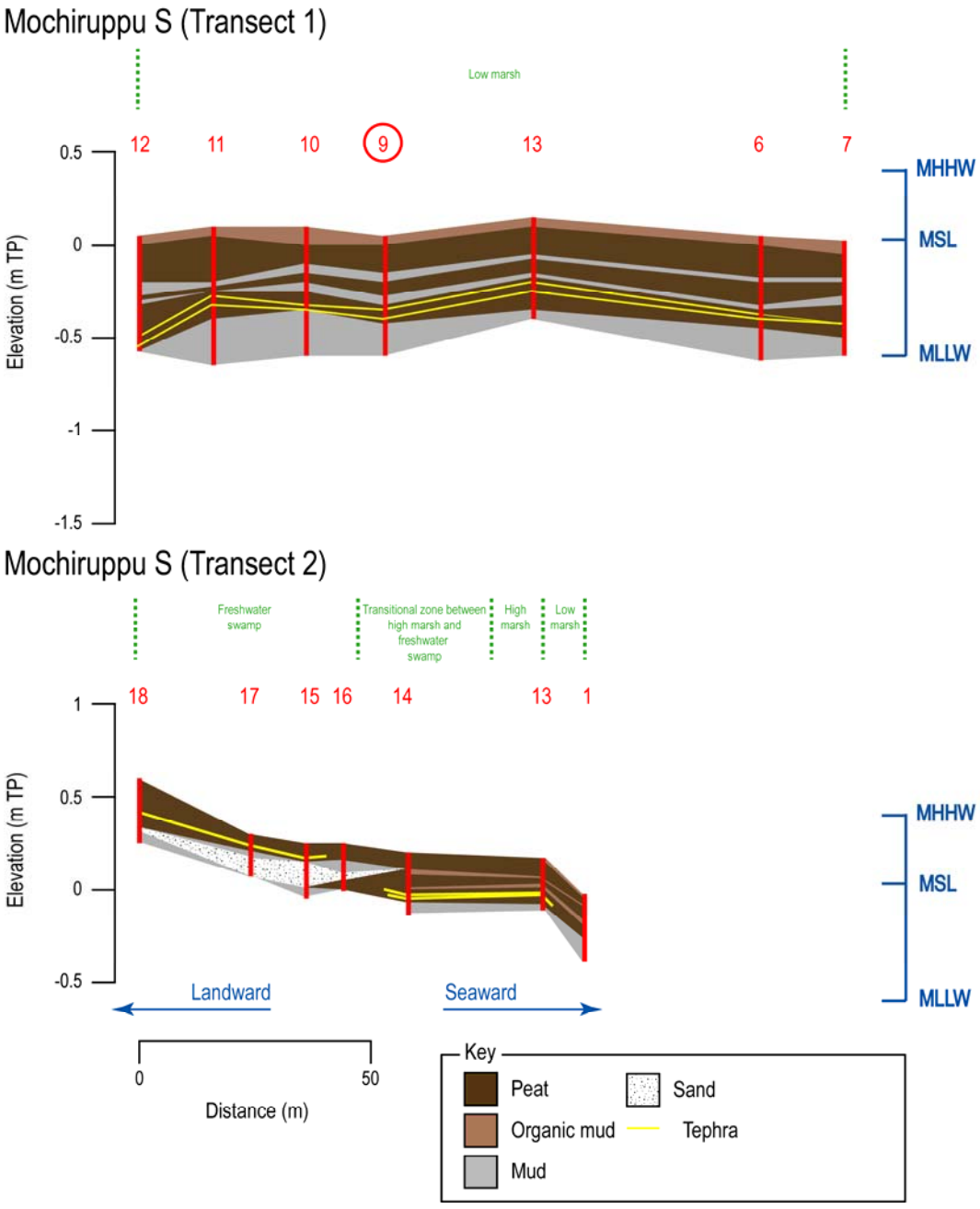

Figure 5.4 Core stratigraphy for Mochiruppu South. In this and subsequent site stratigraphies from Hokkaido, red bars show location of cores, with important tidal levels shown with respect to national datum (m TP). Also shown is a brief faunal zonation summary for each transect. Numbers in red represent core identification. Circled number shows core chosen for analysis.

Laboratory analysis

The sample core is 0.66 m long and its lithology is detailed in Table 5.2. The sample is a peat with two muddy units at 21-24 cm and 33-36 cm, with two tephras at the base of the core which are assumed to be the 1739 Ta-a and 1694 Ko-c2 horizons. No grain size analyses were completed on the core.

Table 5.2 Lithostratigraphy of the sample core from Mochiruppu South described using the Troels-Smith (1955) scheme of stratigraphic notation.

0 – 2	Ag1+, Sh1, $Th^2$1, As1	4 0 2 0	Dark reddish grey organic mud.
2 – 6	Sh2, $Th^3$1, Ag1, As+	3 0 2 0 2	Dusky red well humified organics with silt and clay.
6 – 21	$Th^2$2, Ag1, As1	3 0 2 0 0	Reddish brown well humified peat.
21 – 24	$Th^2$2, Ag1++, As1	2 0 2 0 0	Dark reddish grey muddy organic layer, with herbaceous material throughout.
24 – 33	$Th^2$2, Ag1, As1	3 0 2 0 2	Well humified organics with silt and clay. Rhizome roots found at 24 – 26 cm.
33 – 36.5	Ag2, As1, Sh1, Th^2+	2 0 2 0 1	Reddish grey muddy organic layer with some roots and stems. Clear bottom boundary.
36.5 – 39	Sh2+, $Th^3$1, Ag1, As+	3 0 2 0 3	Dark reddish brown well humified organics with silt and clay.
39 – 42		Lim. sup. 1	Tephra.
42 – 43	Sh2, $Th^3$1, Ag1, As+	3 0 2 0 2	Dark reddish brown well humified organics with silt and clay and some tephra.
43 – 45		Lim. sup. 2	Tephra.
45 – 47	Sh2, $Th^3$1, Ag1, As+	3 0 2 0 2	Dark reddish brown well humified organics with silt and clay. Pummice found at 47 cm.
47 - 66	Ag2, As1, Gmin1, Th^3+	2 0 2 0 0	Grey silty clay with herbaceous root and stem fragments and some sand.

I counted 19 foraminiferal samples in order to reconstruct RSL change and analysed the core for ^{210}Pb and ^{137}Cs (Figure 5.5). The foraminiferal assemblage is dominated by *B. pseudomacrescens*, *Haplophragmoides* spp., *H. wilberti*, *M. fusca* and, above *c.* 10 cm depth, *T. inflata*. The broad structure of the record is similar to that recorded in Mochiruppu North. The gradual change from *B. pseudomacrescens*, to *Haplophragmoides*, and then to *T. inflata* implies the gradual rise in palaeosurface elevation toward the top of the core. The increase in the unvegetated tidal-flat dominated species of *M. fusca* at 12 and 2 cm suggests sea level has increased, most markedly towards the very top of the core.

A chronology for the sample core is provided by linear extrapolation back to the 1739 tephra, found at a depth of 31 cm. The caesium profile does not display a clear peak, and the lead profile seems to be truncated at the top of the sequence, and therefore sedimentation rates are based solely on the tephra, yielding an average sedimentation rate of 1.16 mm/yr.

I now apply the three transfer function models to the foraminiferal data in order to reconstruct palaeomarsh surface elevation, using the age model described above to provide an absolute chronology. The RSL reconstruction differs between models, with the

'No Subtidal' model predicting higher elevations compared with the 'All Data' and 'Pruned' models. The record spans the last 170 years, and shows RSL falling slightly from *c.* 0.3 m MTL at *c.* 1850 to 0 m MTL by the middle of the twentieth century. RSL then fell quickly to *c.* -0.4 m MTL before rising by an equivalent amount to present at a rate of *c.* 7.95 mm yr. As in Mochiruppu North, there are some near-surface samples with poor modern analogues that should be interpreted with care, particularly the *T. inflata* assemblage.

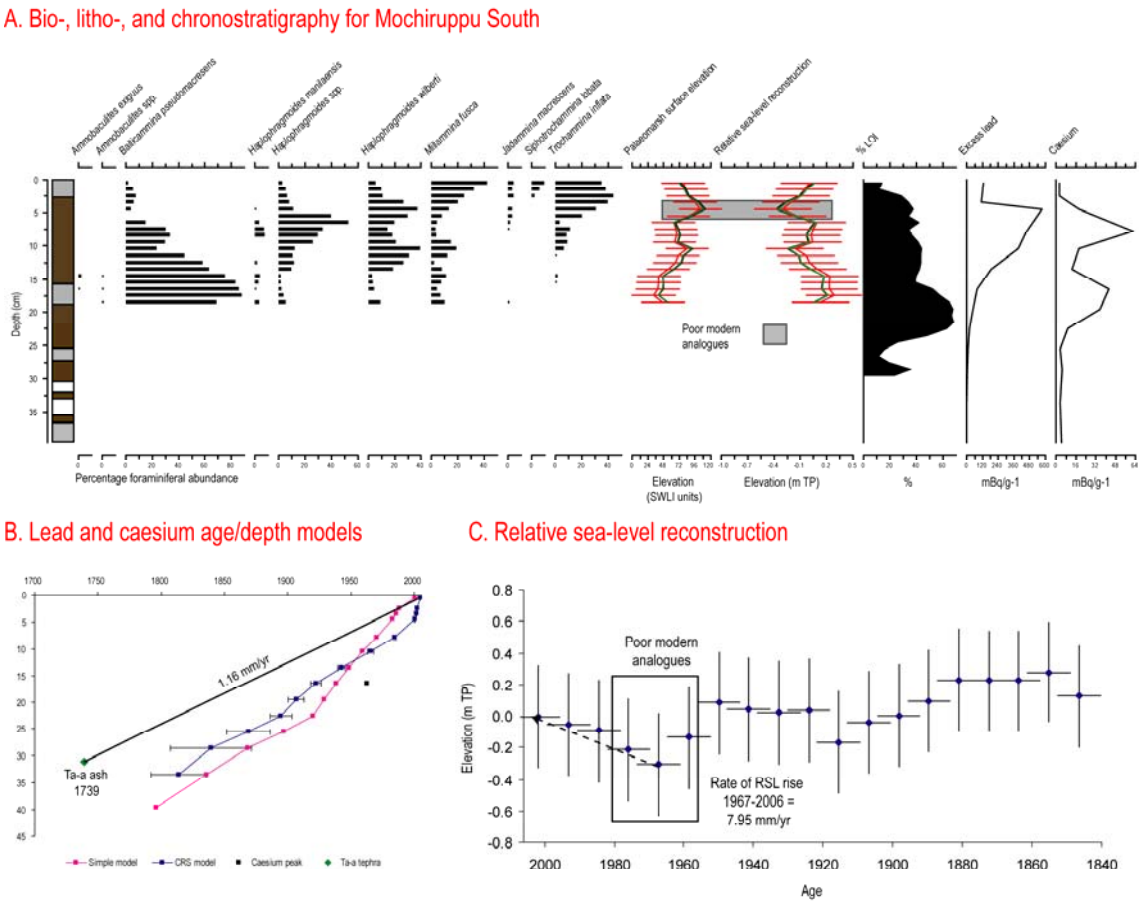

Figure 5.5 Litho-bio-, and chronostratigraphical analysis at Mochiruppu South. (A) Foraminifera assemblages, RSL reconstructions (black = all data model, red = pruned model, green = no subtidal model), % Loss on Ignition and excess ^{210}Pb and caesium profiles for the Mochiruppu South core. Core lithology – brown = turfa peat, grey = organic mud, white = tephra horizon. (B) ^{210}Pb age/depth models using the CRS and Simple models, with the 1964 Caesium peak highlighted. Sediment accumulation rates used in (C) are based on extrapolation from the surface to the 1739 tephra found at 31 cm. (C) RSL reconstruction for this core using the pruned transfer function model and the 1.16 mm yr sedimentation rate.

5.2.2 Furen-ko

Furen-ko is the first of the sites studied in this thesis on the Okhotsk Sea. The site has previously been studied by Atwater *et al*. (2004) who worked in the north-west of the area (Figure 5.6), and also Ohira (2004) who studied the sediments of the Furen River to assess

Late Holocene sea-level change. The Atwater *et al*. (2004) study, which was close to my sampling site, comprised three lithostratigraphic transects known as Yausubetsu (north and south) and Kimura respectively.

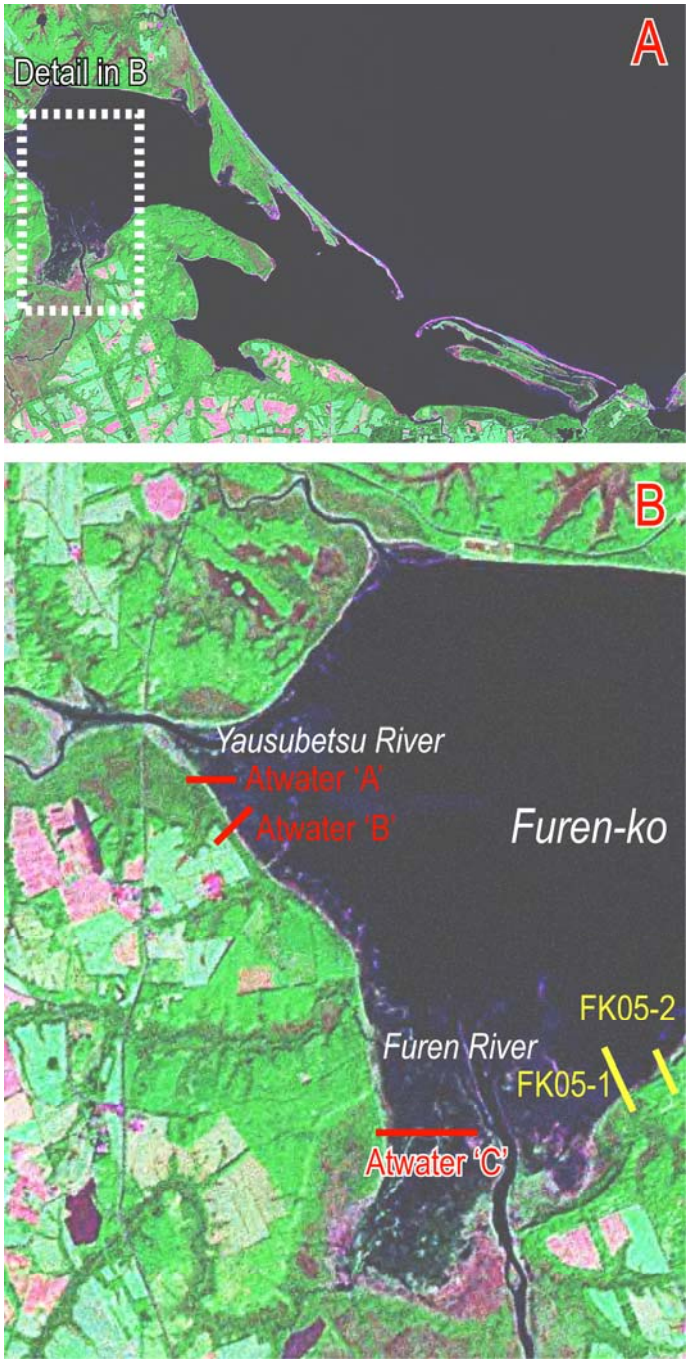

Figure 5.6 Site map showing location of transects studied at Furen-ko during this study (in yellow) and in Atwater *et al*. (2004); where (A) is Yasubetsu-north; (B) is Yasubetsu-south and (C) is Kimura. Landsat image from https://zulu.ssc.nasa.gov/mrsid/

The lithostratigraphy at each of the Atwater *et al*. (2004) transects comprises peat, muddy peat and peaty mud which overlies generally coarse sand or, in the more seaward cores, mud (Figure 5.7). The undulating nature of the sand surface is suggestive of a series of

ridges and berms that were likely spits and beaches during the 17th century (Atwater *et al*., 2004). The seaward transition from sand to mud in these lower sediments rules out a tsunami origin for this sand. The overlying organic-rich deposits drape this surface in an isochronous (or near isochronous) contact, suggesting that tidal sand or mudflats emerged from the sea at the same time as a result of tectonic processes. The authors argue that this type of stratigraphic architecture cannot be created through normal sedimentary processes of estuarine infilling and must record abrupt emergence. Although this site featured in the Atwater *et al*. (2004) model of emergence associated with the 17th century earthquake, no biostratigraphy was presented from the study site.

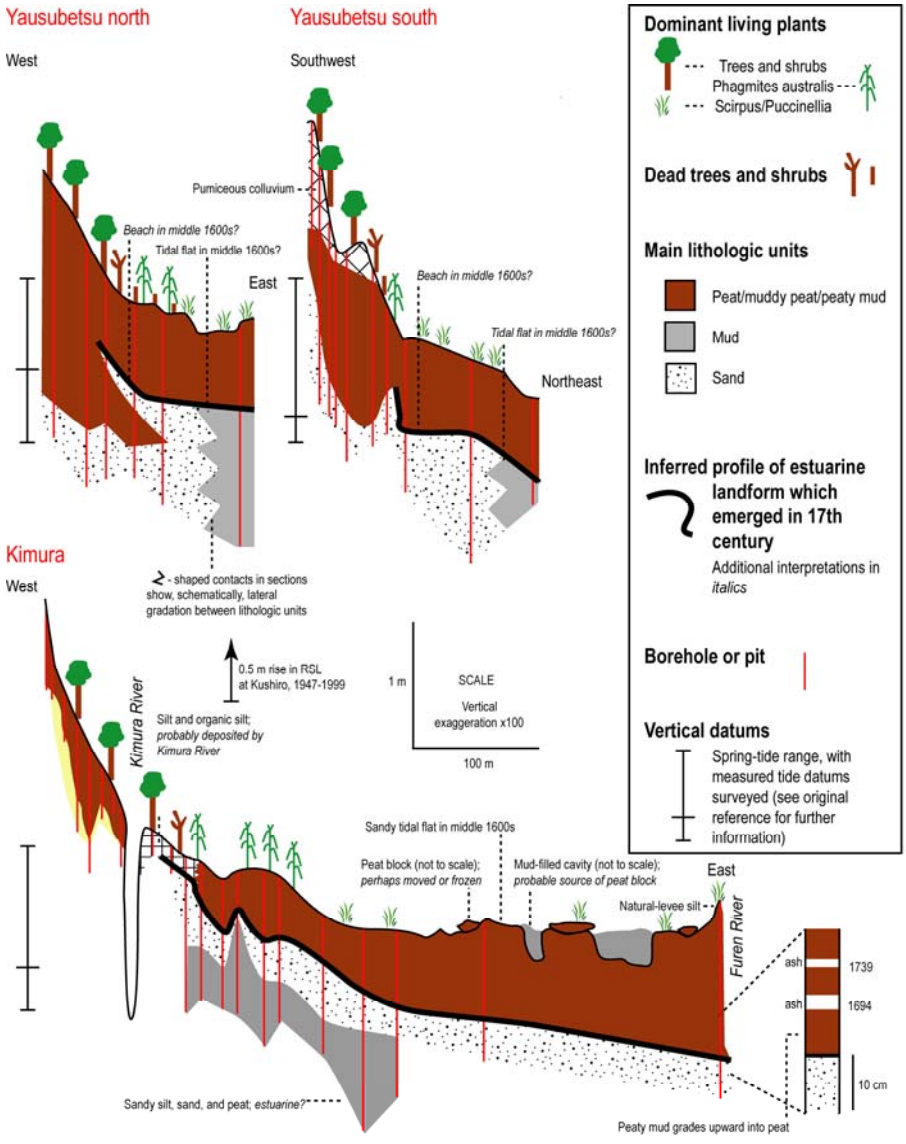

Figure 5.7 Stratigraphy at three lithostratigraphic transects known as Yausubetsu (north and south) and Kimura at Furen-ko (Atwater *et al*., 2004).

I completed two transects of boreholes adjacent to the Furen River (Figure 5.6). The lithostratigraphy is relatively complex, comprising intercalated peats, sands and organic

muds. Transect 1 is located closest to the Furen River and samples the stratigraphy over the marsh and into the freshwater swamp at the back of the marsh. The upper units are dominated by a thick sequence of peat, within which the tephras previously identified at Mochiruppu can be seen. Below the peat, a thick sequence of sands can be identified which fine landward. This widespread sand unit lies above an organic mud and turfa peat unit. Towards the bottom of the cores, a sand unit can be identified, which lies above a more organic mud unit which is found in core 2. The second transect lies broadly parallel to the other Furen transect and comprises just 12 m between the low marsh and freshwater swamp. In its seaward end it records a similar stratigraphy of sand overlain by peat. Towards the back of the marsh, the stratigraphy is more complex. The sand unit becomes shallower, and a more complex stratigraphy of intercalated peat and organic mud units is found. The present marsh geomorphology is dominated by a beach ridge which comprises the sandy and gravel material found in the most of the cores. This beach ridge has migrated over the Late Holocene, and in the most landward locations it is reasonable to hypothesise that detailed intertidal stratigraphies that have built up behind the beach ridge may be capable of recording detailed sea-level change over the last earthquake cycle. More specifically, turfa peat units are overlain sharply by clastic-dominated sediments which may indicate coseismic subsidence. The stratigraphies are detailed in Figure 5.8 (transect 2).

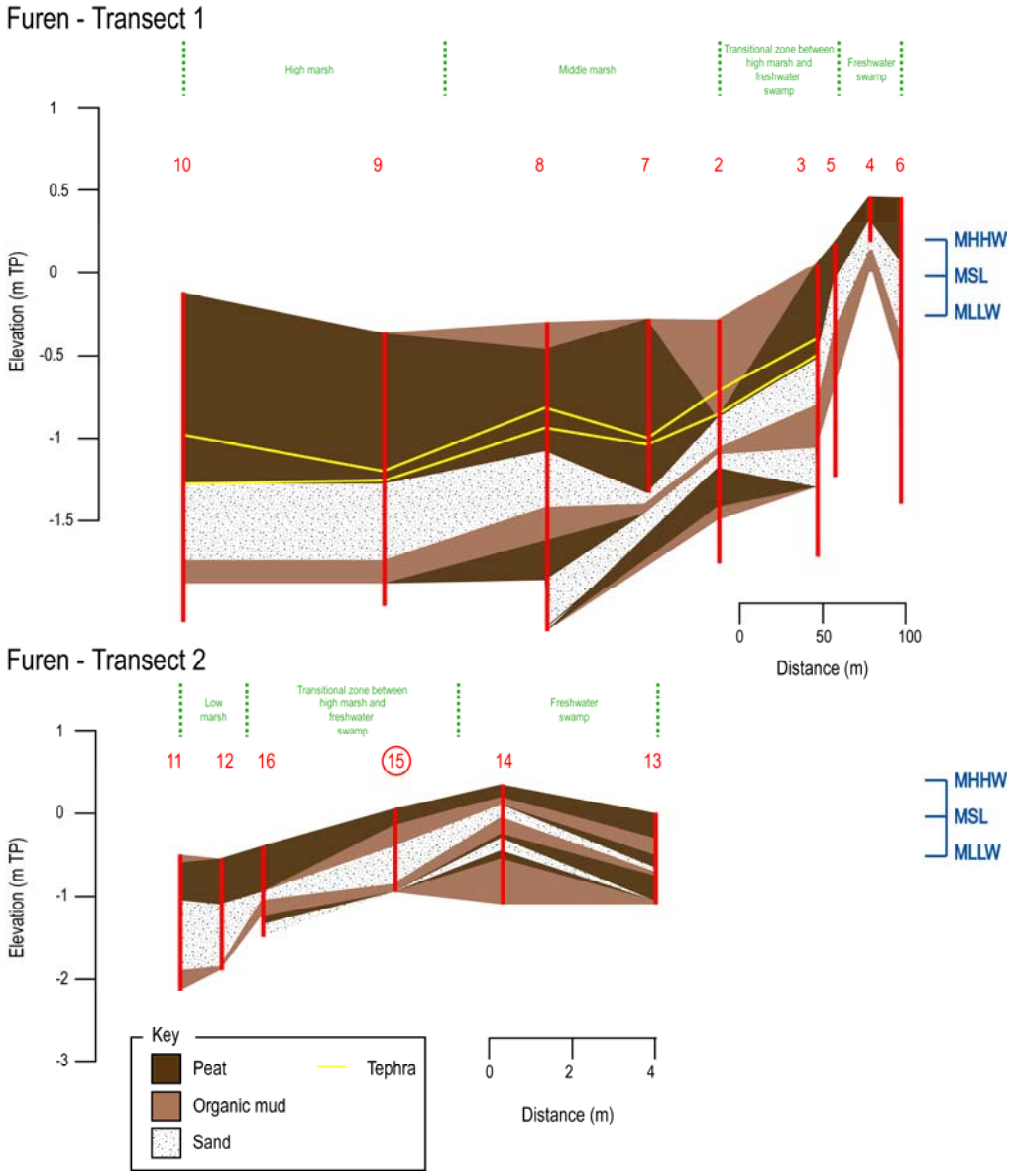

Figure 5.8 Core stratigraphy for Furen-ko.

I collected one sample core from the study area (Figure 5.6) to develop a chronology of RSL changes in the last 200-300 years of interseismic period. The core provides a further opportunity to compare the reconstructed RSL changes with tide-gauge data from Hanasaki.

Laboratory analysis

The sample core lithology is detailed in Table 5.3. The sample is peat in the uppermost section with two tephras, the upper believed to be either the Ta-a 1739 or the 1694 Ko-c2 eruption. The lower tephra is assumed to be Ta-b 1667 ash. No percentage LOI or grain size analyses were completed on the core.

Table 5.3 Lithostratigraphy of the sample core from Furen-ko described using the Troels-Smith (1955) scheme of stratigraphic notation.

0 – 9	Ag2, Sh2, Th^{3}+	3 0 2 0	Medium brown silty peat with sand trace with some herbaceous roots.
9 – 19	SC		Sediment lost (most probably peaty silt).
19 – 27	Sh3, Ag1	4 0 2 0	Dark brown peaty silt.
27 – 34		3 0 2 0 0	Dark brown peaty silt, less well decomposed. Pummice tephra at 30 cm.
34 – 38		Lim. Sup. 1	Tephra (very diffused in the sediment).
38 – 43	Ag2, Sh2	2 0 2 0 1	Silty peat with tephra.
43 – 44		Lim. Sup. 1	Tephra.
44 – 49	Gmin4	3 0 2 0 1	Tephra with some sand.
49 – 77	Gmin4, Sh+	3 0 2 0 0	Dark grey sand. Coarsens to 70 cm, fines to 73 cm, and then coarsens again until 77 cm.
77 – 83	Gmin2, Gmaj1, Th+	3 0 2 0 0	Light reddish brown fine sand with some gravel (7 – 10 mm). Some organics.
83 - 90	Gmin4, Sh+	3 0 2 0 0	Dark grey sand.
87 – 92	Ag2, Sh2	4 0 2 0 1	Black very well decomposed silty peat.
92 - 102	Ag2, As1, Th^{1}1	3 0 2 0 1	Medium grey silty clay with occasional modern rhizomes.

I counted 14 foraminiferal samples in order to reconstruct RSL change and analysed the core for ^{210}Pb and ^{137}Cs (Figure 5.9). The foraminiferal assemblage is dominated by *B. pseudomacrescens*, *Haplophragmoides* spp., *H. wilberti* and, above *c.* 4 cm depth, *T. inflata*. For much of the sequence, there is a dominance of *B. pseudomacrescens* and *Haplophragmoides* spp., however both of these species are found ubiquitously over much of the marsh implying sea level did not significantly vary over the period. However, the dramatic rise in *T. inflata* recorded in the top three samples suggest sea level has dropped toward the present.

The sample core was analysed for ^{210}Pb and ^{137}Cs but the results are not clear; there is no consistent decline in the former and the latter peak at the base of the sample core. Fortunately, the 1739 tephra can be traced in this core, and this is solely used to calculate the sedimentation rate of 1.27 mm/yr.

I now apply the three transfer function models to the foraminiferal data in order to reconstruct palaeomarsh surface elevation, using the age model described above to provide an absolute chronology. The RSL reconstructions are similar for each model. The record spans all of the 20th century and shows RSL fluctuating gently around present throughout the record, although the uppermost two samples suggest rapid RSL fall since the mid 1990s. The latter sample should be treated with caution though, due to a poor matching analogue. The rise in frequencies of *T. inflata* in the core is similar to that observed in Mochiruppu and probably records a recent rise in RSL (not the fall predicted by the transfer function).

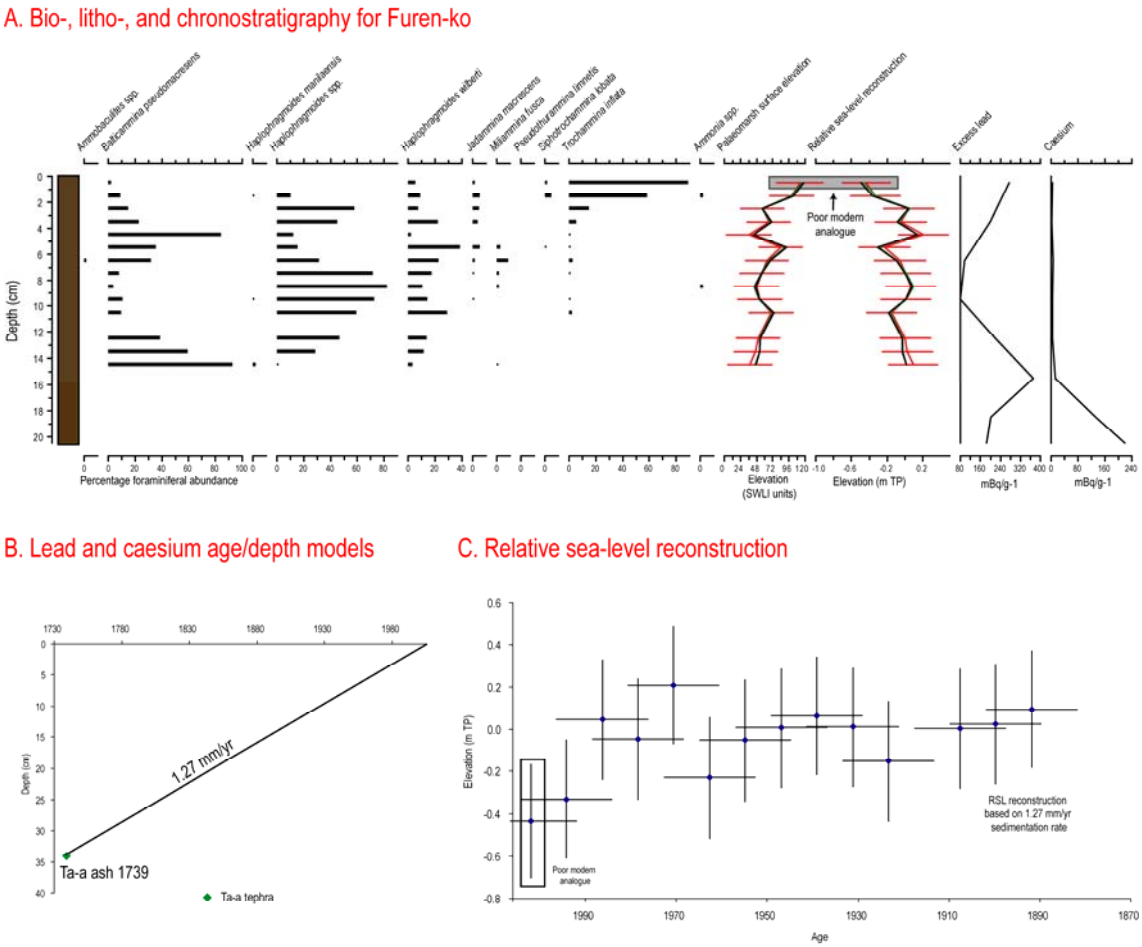

Figure 5.9 Litho-bio-, and chronostratigraphical analysis at Furen-ko. A. Foraminifera assemblages, relative sea-level reconstructions (black = all data model, red = pruned model, green = no subtidal model), B. Excess ^{210}Pb and caesium profiles for the Furen-ko core. Core lithology – brown = turfa peat. (b) Lead and caesium age/depth model. As the profiles of lead and caesium were unreliable, a 1.27 mm/yr sedimentation rate was calculated from the 1739 Ta-a ash. (c) RSL reconstruction for this core, using the pruned transfer function model and the 1.27 mm yr sedimentation rate.

5.2.3 Tohoro

This is the last of my four sites located in south-east Hokkaido, and is the only site where modern sampling for foraminifera was not undertaken. There have been no previous stratigraphic investigations at the site. The location of the core transects completed in 2004 and 2005 are shown in Figure 5.10.

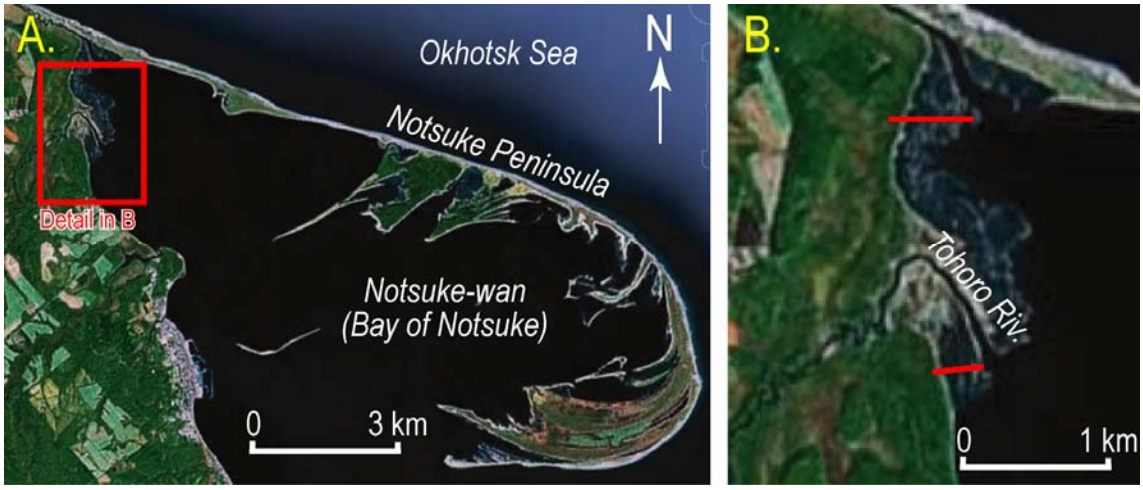

Figure 5.10 Site map showing location of transects studied Tohoro during this study. Images taken from Google Earth (northernmost transect is '1', and the southernmost transect, around the mouth of the Tohoro River is '2').

The first transect sampled the tidal-flat to upland sediments of Tohoro (Figure 5.11). Below a surface layer of mud, a thick sequence of peat is found, which is punctuated by two tephras and a mud unit found in cores 4 to 12. Below this mud unit, a thick sequence of sands and gravels is found. Towards the landward edge of the marsh, the coarse sands and gravels fine, and the sequence is dominated by more muddy units which comprise a sharp upper boundary.

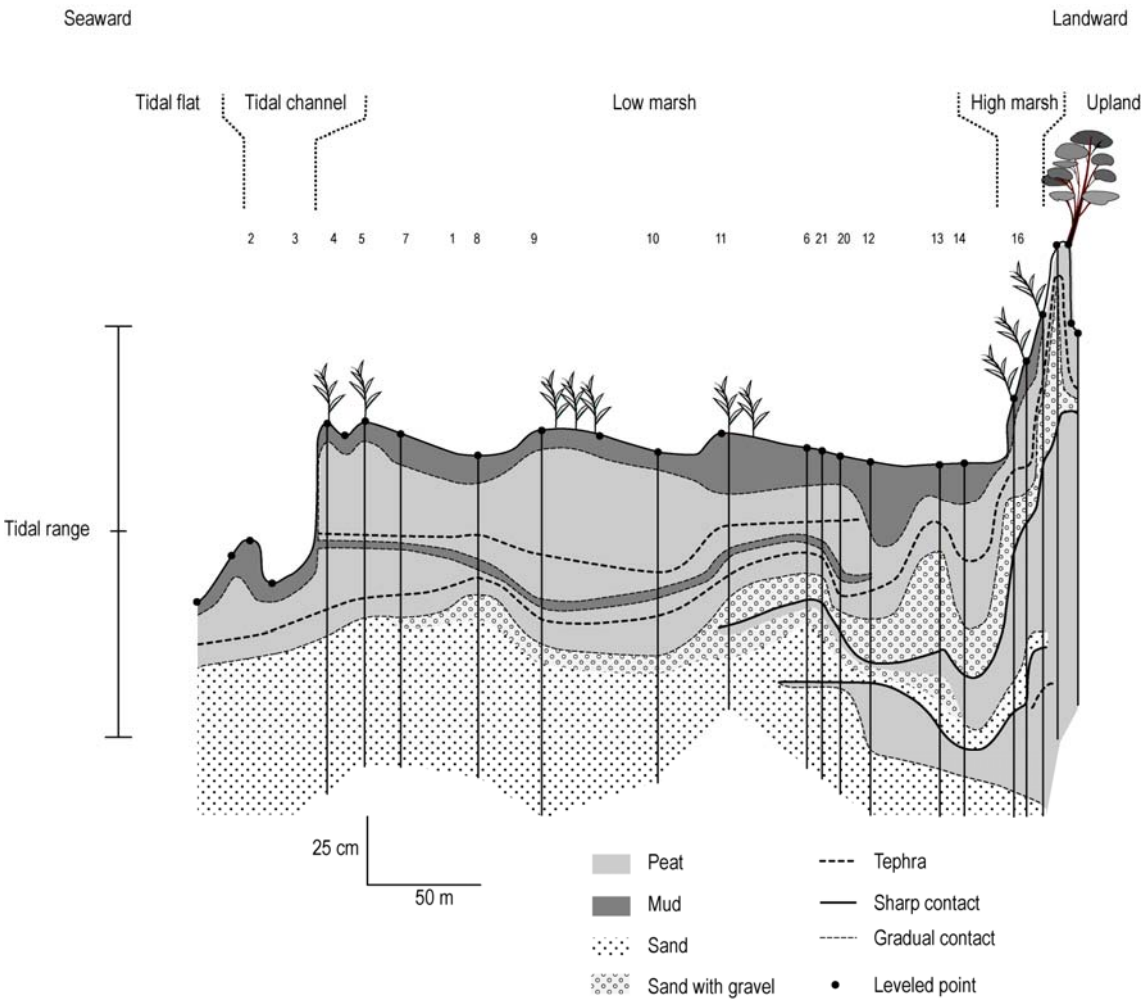

Figure 5.11 Stratigraphy at Tohoro (transect 1) in relation to tidal frame (Yuki Sawai *pers. comm*.).

The second transect (Figure 5.12) comprising approximately 350 m is dominated by mud/organic mud, found particular in those landward cores. The upper sediments of the seaward edge of the transect proved difficult to sample, however were most probably peat. Underlying the mud/organic mud, a turfa peat is identified which is found above an organic mud with comprises much sand. Below this, a coarse sand and gravel unit was identified which often proved difficult to sample.

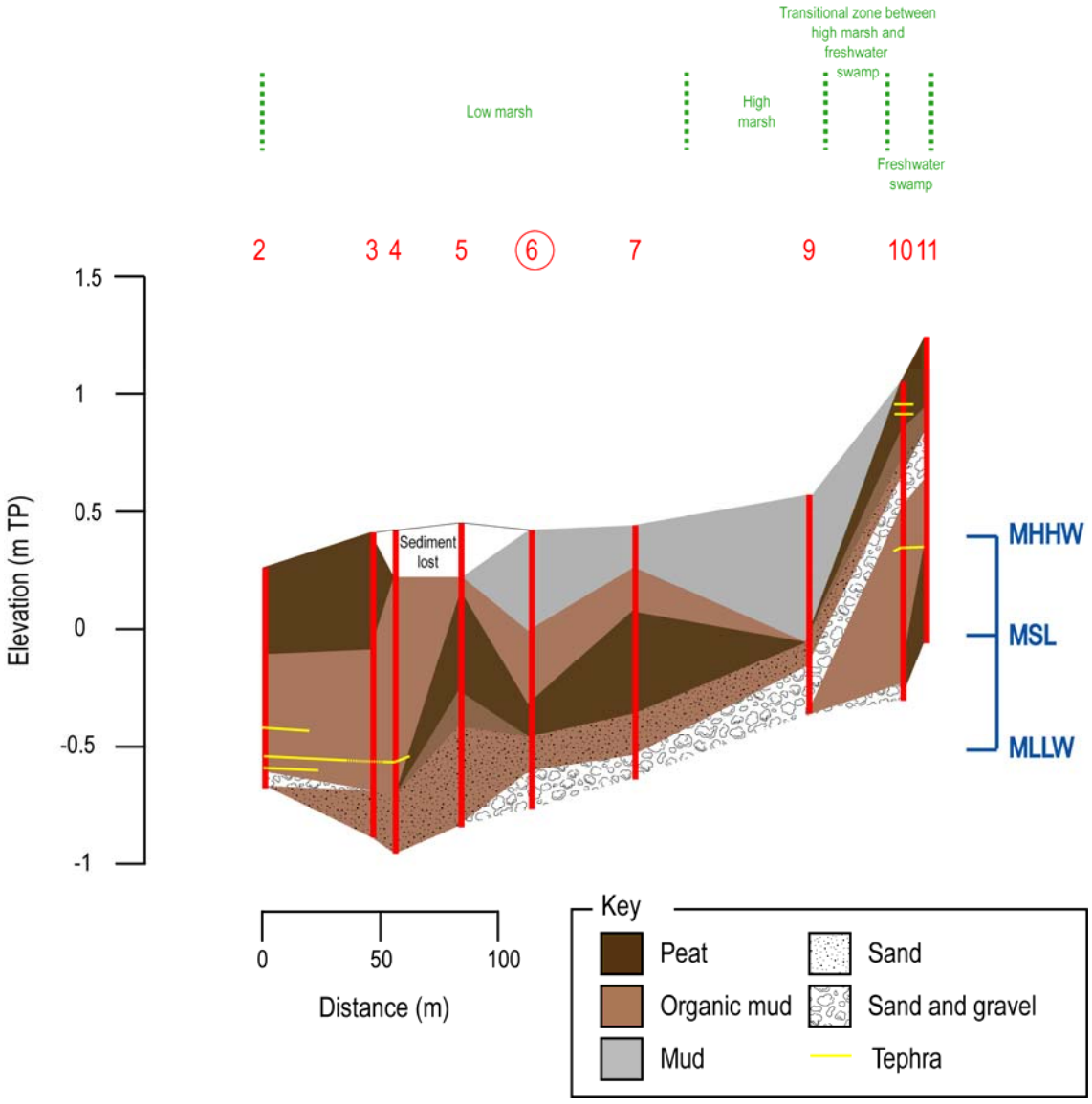

Figure 5.12 Stratigraphy at Tohoro, transect 2.

I collected one sample core from the study area to develop a chronology of RSL changes in the last 200-300 years of interseismic period. Most of the stratigraphy of Tohoro is complicated by a series of large channels which dissect the marsh, and the organic mud which is found in many of the cores may provide evidence for channel migration and not sea-level change. Consequently, core 6 was identified for detailed bio- and lithostratigraphical analysis. The focus of investigation was on the interseismic period from the 18th century onwards.

Laboratory analysis

The sample core lithology is detailed in Table 5.4; the sediments comprise peat that is overlain at 42 cm by a muddy peat which extends to surface. I analysed the sample core for % LOI, foraminifera as well as ^{210}Pb and ^{137}Cs (Figure 5.13). The percentage LOI data show little change up-core with values remaining stable at *c.* 20-25%.

Table 5.4 Lithostratigraphy of the sample core from Tohoro described using the Troels-Smith (1955) scheme of stratigraphic notation.

0 – 19	Ag2+, As1, $Th^1$1, Sh+,	3 0 2 0-	Very dark grey silty clay with organic material including some visible root and stem fragments.
19 – 42.5	Ag2, As1, Sh1, Th1+	2 0 2 0 0	Brown silty mud with trace of organic fragments throughout.
42.5 - 74	Ag2, Sh1, As1, Th^1+	3 0 2 0 0	Dark brown silty organic mud, with root and stem fragments throughout. Pummice tephra found at 62-3 cm.
74 - 89	$Th^2$2, Sh1, Ag1	3 0 2 0 1	Dark reddish brown poorly decomposed turfa peat. Possibly more muddy unit between 78 – 82 cm. Possibly tephra at 85 – 89 cm.
89 - 104	Ag2, As1, Gmin1, Th22 Gmaj+	3 0 2 0 0	Silty clay with fine sand and mud and some gravel.
104 - 120	Gmaj2, Gmin1, As1, Th^2+	3 0 2 0 0	Fine sand and gravel in silty matrix, with occasional root and stem fragments.

I analysed 25 samples for foraminifera from the sample core (Figure 5.13). The lower part of the sequence, between 46-32 cm, is dominated by an assemblage rich in frequencies of *B. psuedomacrescens,* although importantly frequencies of *M. fusca* start to rise at 34 cm. There is a break in the sample core at 30 cm, however close inspection of the core suggests no considerable change in stratigraphy. However no foraminifera were recorded at this elevation which may possibly elude to a local process. Above this level, *M. fusca* dominates the assemblage as frequencies of *B. pseudomacrescens* fall. The upper part of the sequence sees frequencies of first *H. wilberti* and then *B. pseudomacrescens* rise and then fall. The highest samples, above 6 cm, see a return to dominance of *M. fusca*. This suggests that the upper sequence, dominated by *M. fusca*, records a period of sea-level fall, however the peak in *H. wilberti* (a species found in marsh environments) around 12 cm implies a short-lived oscillation in sea level.

A chronology for the sample core is provided by tephra found at the base of the core. Although the tephra cannot be assigned to a particular date, its stratigraphic position suggests it was deposited in 1694 or 1739. Therefore, I have averaged these two dates, and assigned a sedimentation rate of 2.14 mm/yr. ^{210}Pb and ^{137}Cs results are ambiguous and therefore are not used. There is no peak in ^{137}Cs, which actually has its maximum values towards the base of the core. Moreover, the ^{210}Pb fails to reach background concentration levels, despite sampling to a depth of 24 cm.

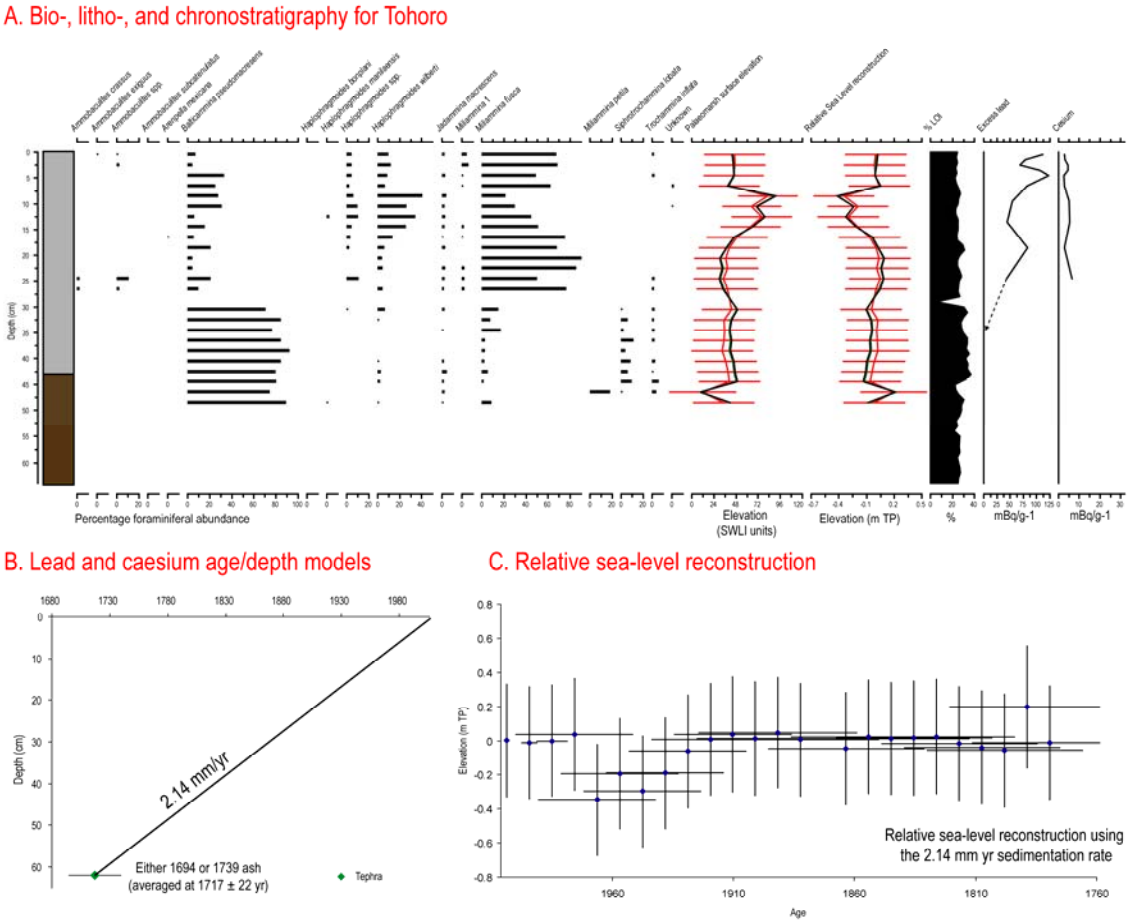

Figure 5.13 Litho-, bio-, and chronostratigraphical analysis at Tohoro (A) Foraminifera assemblages, RSL reconstructions (black = all data model, red = pruned model, green = no subtidal model), % Loss on Ignition data, excess ^{210}Pb and caesium profiles for the Tohoro core. Core lithology: brown = turfa peat, grey = organic mud. (B) The ^{210}Pb and ^{137}Cs profiles are unreliable, and therefore the sedimentation rate for Tohoro is based on the tephra (which is either the 1694 or 1739 ash layer) found at 61 cm. (C) RSL reconstruction for this core using the pruned transfer function model and the 2.14 mm/yr sedimentation rate.

I now apply the three transfer function models to the foraminiferal data in order to reconstruct palaeomarsh surface elevation, using the age model described above to provide an absolute chronology. The record spans the 19th and 20th centuries and shows RSL broadly stable and close to 0 m MTL between *c.* 1780 and 1910, before falling to *c.* -0.35 m MTL and then rising abruptly to 0 m MTL again towards the top of the sequence.

5.2.4 Tofutsu-ko

This is the first of the northern sites studied in this thesis. No previous research has been undertaken at this site regarding recent RSL changes in the last few centuries.

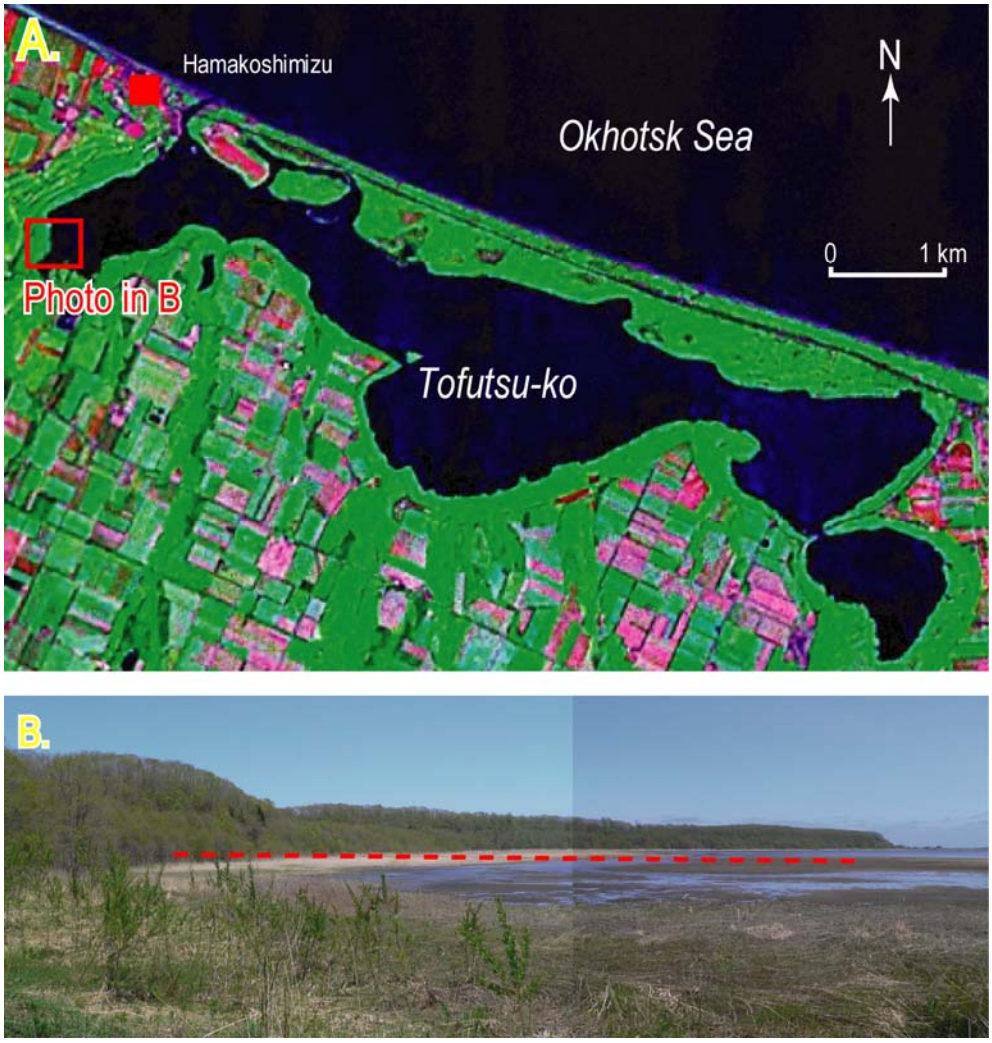

Figure 5.14 Site map showing location of transects studied Tofutsu-ko during this study.

I completed one transect of nine boreholes from the west of the study area (Figure 5.15). The cores penetrated to a maximum depth of *c.* 2 m below marsh surface. The lithostratigraphy comprises three main units; a lower coarse sand recorded in the landward cores (cores 6-9) which is overlain by a finer-grained silt sand with rare shells that is extensive across the entire width of the transect (Figure 5.15). This grades upwards into an organic-rich peat which varies in composition between a muddy peat in the seaward cores and an organic-rich turfa peat in the higher, more landward cores.

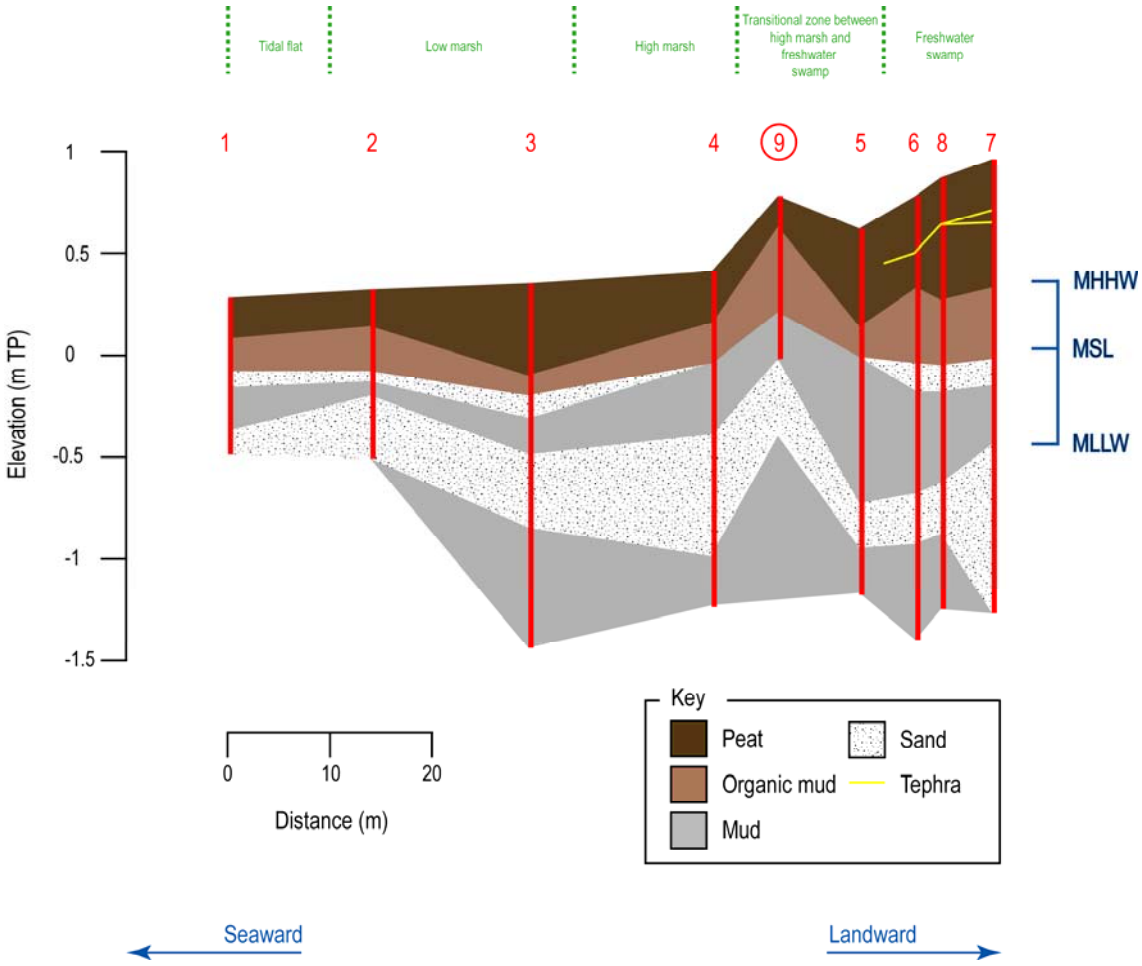

Figure 5.15 Stratigraphy at Tofutsu-ko.

Within these units there are two other deposits of note. First, within the lower silt-sand unit is a distinct thin coarse sand deposit at *c.* -0.2 m TP. This deposit fines in a landward direction and thins. It is recorded in all cores apart from core 8 which failed to penetrate to sufficient depth. The second minor unit is a prominent tephra recorded in the two landward cores (cores 7 and 8) at a depth of *c.* 40-80 cm below marsh surface. This tephra is coarse-grained and contains distinct pumice. Based on the descriptions given in Sawai *et al*. (2001) and Atwater *et al*. (2004), I correlate this tephra to the AD 1667 Ta-b ash (Furukawa *et al.*, 1997).

I collected one sample core for laboratory analysis, from the position of core 9 (TF06/1/9). This shallow core extended through the uppermost organic rich silts to a depth of *c.* 0.5 m and was sampled to provide a record of postseismic RSL changes during the last several centuries.

Laboratory analysis

The sample core lithology is detailed in Table 5.5. Percentage LOI data show an abrupt up-core change from relatively low percentages of *c.* 10% between 60-36 cm, to high (and

rising) values above this level of between 40-80%. Maximum percentage LOI values are at the core top.

Table 5.5 Lithostratigraphy of the sample core from Tofutsu-ko described using the Troels-Smith (1955) scheme of stratigraphic notation.

Depth	Colour	TS code	Description
0 - 15	2.5 YR N3/	$Th_3$3, Sh1, Ag+ 420 -	Dark reddish grey herbaceous peat with some organic material and trace of silt.
15 - 36	5YR 2.5/1	$Th^2$1, Sh1, Ag2 3200	Black herbaceous peaty-silt with visible root and stem fragments with some well decomposed organic material. Increasing silt with depth.
36 – 57	7.5 YR 3/2	Sh1, Ag2, As1, Gmin+ 3200	Dark brown silty organic material with trace of fine sand.
57 - 80	10 YR 3/2	As2, Ag2 2200	Very dark greyish brown silty clay.

I counted 16 samples for foraminfera (Figure 5.16). The lower samples are dominated by frequencies of *A. exiguus* and *Ammobaculities* spp. but above 36 cm there is a pronounced change in assemblage as the assemblage becomes dominated by *M. fusca* and *H. bonplani*. A single spike in frequencies of *A. exiguus* and *Ammobaculites* spp. occurs at 16 cm, and above this the assemblage shifts to one dominated by *H. wilberti* and *Haplophragmoides* spp. that extends to the present surface. The switch from *Ammobaculites* to a more varied assemblage comprising *Haplophragmoides* and *M. fusca* suggests palaeosurface marsh elevation rose towards the top of the sequence. Although counts are low at the top of the core, the fall in *H. wilberti*, and associated rise in *M. fusca* suggests sea level has risen in the very recent past.

A chronology for the sample core is provided by ^{210}Pb and ^{137}Cs. There is no tephra ash at Tofutsu-ko, and therefore the chronology is developed primarily on the caesium peak at 9 cm. The uppermost samples were high in water content and as a result I had to combine the uppermost 3 samples for the 'surface' ^{210}Pb and ^{137}Cs value (samples 0-2 cm, 2-4 cm and 4-6 cm, combined and plotted at 5 cm depth in Figure 5.16). Since the caesium peak and Simple model are in close agreement, a linear rate of sedimentation of 1.95 mm/yr through the 1964 peak is calculated, which largely follows the sedimentation rate predicted by the Simple model.

I now apply the three transfer function models to the foraminiferal data in order to reconstruct RSL change using the age model described above to provide an absolute chronology. The RSL reconstructions are broadly similar between models and show that MTL changed little in the lower part of the profile, remaining stable at *c.* 0.7 m TP between 1770 and the early part of the twentieth century. The pronounced increase in the percentage of LOI at *c.* 30 cm depth occurs shortly after a significant change in foraminiferal assemblage, with a rise in the frequencies of *M. fusca* - but there is no

associated change in reconstructed RSL using the transfer function. This is surprising, although there are good matching analogues for this part of the core.

By the mid-twentieth century, RSL fell to *c.* 0.1 m MTL. The highest sample in the sequence, at *c.* 4 cm depth, reconstructs an anomalously high RSL value of *c.* 0.7 m MTL. This is because the assemblage contains high frequencies of *Haplophragmoides* spp. and *H. wilberti*. The foraminiferal preservation in the top of the core is very poor, indeed samples above and below this level contained no foraminifera at all (this reflects the high surface elevation of the sample core (0.78 m TP) which is *c.* 0.15 m above HAT). The count in the highest sample was *c.* 120, but the reconstructed MTL value is *c.* 0.7 m above the level of the ground surface. For these reasons, I ignore this uppermost sample in the RSL reconstruction and conclude that MTL has remained close to present throughout the 20th century.

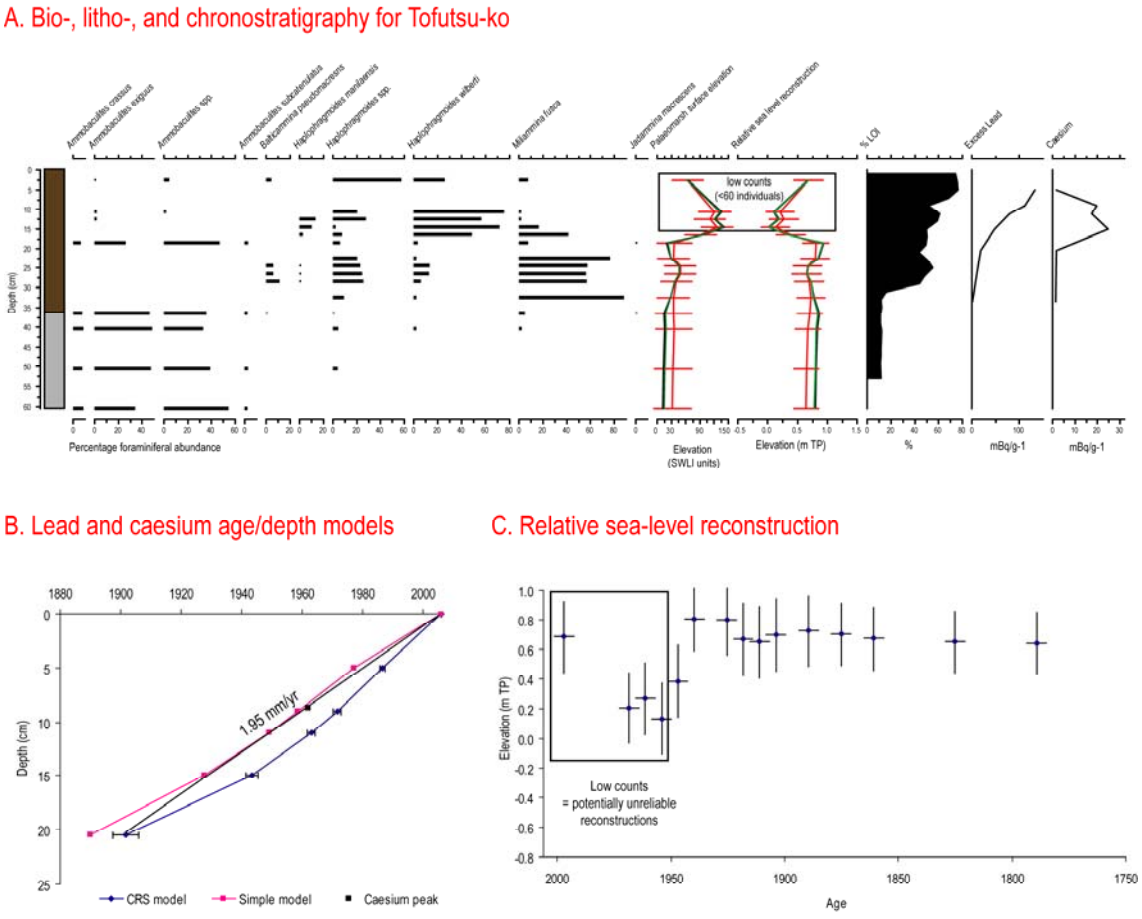

Figure 5.16 Litho-, bio-, and chronostratigraphical analysis at Tofutsu-ko (A) Foraminifera assemblages, RSLl reconstructions (black = all data model, red = pruned model, green = no subtidal model), % Loss on Ignition data, excess ^{210}Pb and caesium profiles for the Tofutsu-ko core. Core lithology – brown = turfa peat, grey = organic mud. (b) ^{210}Pb age/depth models using the CRS and Simple models, with the 1964 Caesium peak highlighted. Sediment accumulation rates used in (C) are based on the caesium peak at 9 cm, which is in close agreement with the Simple model. (C) RSL reconstruction for this core using the pruned transfer function model and the 1.95 mm yr sedimentation rate.

5.2.5 Sarfutsu-toh

This is the most northerly of the sites studied in this thesis. No previous work has been completed on this marsh (Figure 5.17).

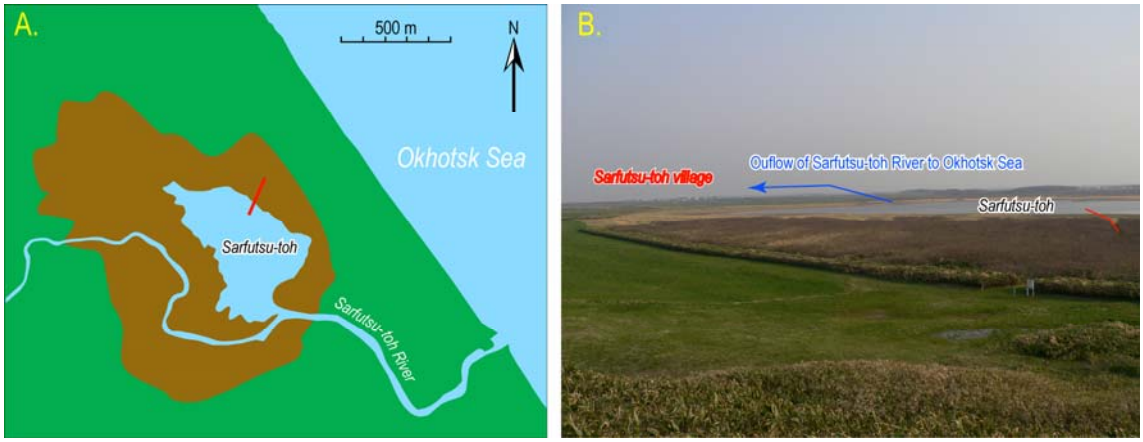

Figure 5.17 Site map showing location of transects studied Sarfutsu-toh during this study.

I sunk a transect of 10 cores extending from the upland towards the sea, sampling unconsolidated sediments to a depth of between 1-2 m (Figure 5.18). The seaward cores ended in a grey mud containing shells (cores 1-6) and the landward cores in coarse sands (cores 6-10). These sediments are overlain by a sequence of organic muds and then peats which thicken and increase their organic content in a landwards direction. No distinct muddy beds occur within the lithostratigraphy but a distinct tephra can be traced within the peat in cores 10-8 and at the junction between the muddy peat and peat in core 7. The origin and age of this tephra is not known.

I collected a 0.58 m long sample core from the location of core 1 for laboratory analysis.

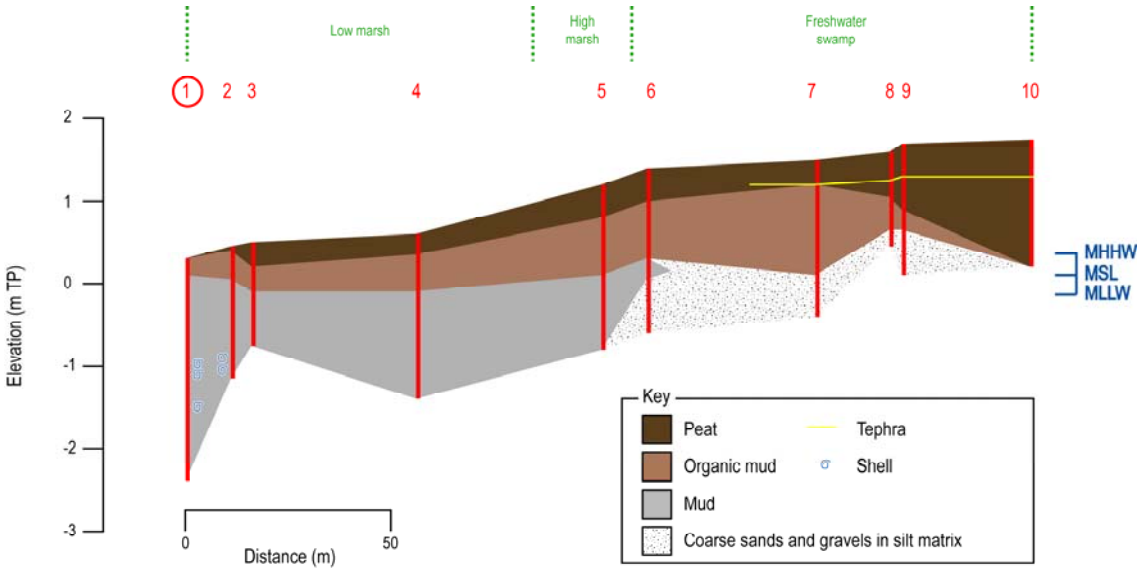

Figure 5.18 Stratigraphy at Sarfutsu-toh.

Laboratory analyses

The stratigraphy of the sample core is detailed in Table 5.6. Grain-size data show that the minerogenic component of the sample is dominated by silt with lesser quantities of both sand and clay (Figure 5.19). There is little variability up-core. The precentage LOI is also stable throughout the lower part of the sequence at levels of *c.* 20%, only rising above 6 cm to *c.* 50% in the surface sample.

Table 5.6 Lithostratigraphy of the sample core from Sarfutsu-toh described using the Troels-Smith (1955) scheme of stratigraphic notation.

0 – 2.5	10YR 3/1	Sh2, Ag2, As+	4 0 2 0 -	Very dark grey well humified silt with much organic matter.
2.5 – 18	5YR 5/1	Ag2, $Th^3$1, As1, Sh+	2 0 2 0 0	Gray silty clay with visible organic fragments. Modern rhizomes at 18 cm.
18 – 200	5YR 6/1	Ag2, As2, Th+, Dh+, test.(moll)+	3 0 2 0 0	Gray silty clay with modern rhizomes (at 27 and 33 cm). Animal burrows found at 59 – 62 and 72 – 80 cm. Occasional woody stalks. Shells found at 124, 140 and 180 cm.

I counted 24 samples for foraminiferal analysis (Figure 5.19). The lower part of the sequence is dominated by *M. fusca*, with the exception of a single spike in values of *M. petila* at 36 cm. The *M. fusca* assemblage is replaced gradually above *c.* 16 cm by a more mixed assemblage as frequencies of *H. wilberti* and then *B. pseudomacrescens* rise. The dominance of *M. fusca*, particularly below 20 cm, suggests that for much of the core, sea-level has been relatively constant. The dominance of a more mixed assemblage towards the top of the sequence comprising *H. wilberti* and *B. pseudomacrescens* amongst others implies palaeomarsh surface elevation has increased.

Samples from above 40 cm were analysed for ^{210}Pb and ^{137}Cs (Figure 5.19) and age models developed using both the CRS and Simple models. The ^{137}Cs peak appears low in the sequence compared to where the ^{210}Pb data would predict it, irrespective of the age model used. Therefore the chronology for the Sarfutsu-toh core is derived from a linear sedimentation rate through the caesium peak at 15.5 cm, giving a rate of approximately 2.7 mm/yr.

The reconstructed RSL shows MTL rose from *c.* 1720 to 1900, from *c.* -0.1 m TP to *c.* 0.40 m TP. Although there are occasional small oscillations in RSL after this date, overall there is little change in MTL throughout the record, with the uppermost sample suggesting RSL was *c.* 0.1 m MTL in the mid 1990s. Overall, the record over the last 300 years is one of generally stable RSL with minor fluctuations in RSL that largely fall within the error of the reconstructions.

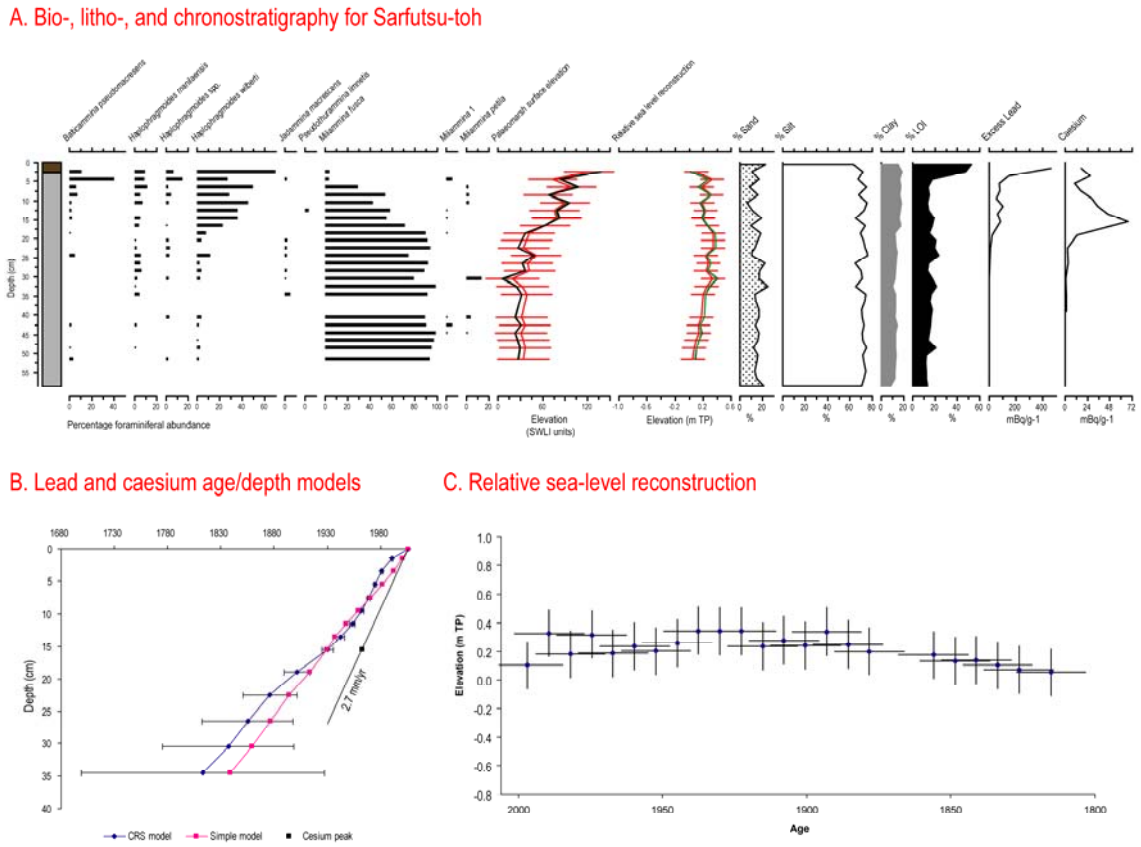

Figure 5.19 Litho-, bio-, and chronostratigraphical analysis at Sarfutsu-toh (A) Foraminifera assemblages, RSL reconstructions (black = all data model, red = pruned model, green = no subtidal model), % Loss on Ignition data, excess ^{210}Pb and caesium profiles for the Sarfutsu-toh core. Core lithology – brown = turfa peat, grey = organic mud. (B) ^{210}Pb age/depth models using the CRS and Simple models, with the 1964 Caesium peak highlighted. Sediment accumulation rate used in (C) is based on the caesium peak at 15.5 cm. (C) RSL for this core using the pruned transfer function model and the 2.7 mm yr sedimentation rate.

5.3 CONCLUSION

This chapter presents the results of the fossil investigations completed at five sample sites in north-east Hokkaido. The main conclusions are:

- A combination of litho-, bio- and chronostratigraphic data have been collected from five salt marshes in north-east Hokkaido. The sediment sequences are generally short, less than 30 cm in most instances, and span the last 300 years of sedimentation or less.
- Fossil foraminifera are well preserved in most of the sample cores, although their frequencies are more varied in those deposits formed close to the freshwater/high marsh. Consideration of individual sequences indicates that the assemblages are

typically dominated by a relatively small number of taxa, namely *B. pseudomacrescens*, *Haplophragmoides* spp., *H. wilberti* , *T. inflata* and *A. exiguus*.

- ^{210}Pb and ^{137}Cs data, together with the most recent visible tephra provide a chronology for most of the sites. Down-core migration of radionuclides is suspected in several of the records. Typical sedimentation rates in the sample cores, generally collected from high-marsh locations, is 1.8 – 2.2 mm yr. Most of the sample cores extend through the 20th century and the longest records span from *c.* 1700 to present, covering much of the current interseismic period.
- I apply the three transfer functions developed in Chapter Four to the fossil sequences to reconstruct RSL changes during the last 100-300 yrs. The models result in similar RSL predictions which gives confidence in their use. However, for the reasons outlined in Chapter Four, my preferred model in subsequent analysis of these data is the 'Pruned B' model.
- Overall, the reconstructions suggest that RSL has changed little during the study period, although there is a tendency for RSL fall in the more northerly sites. There is no evidence for individual earthquake-related RSL change in most of the records, demonstrating the relative insensitivity of the methods used to small-scale (decimeter) changes in RSL. In some samples, especially those close to the present surface, I observe poor matching analogue situations which mean that the reconstructions at these levels should be treated with caution. However, these problems do not mean that the data cannot be used to infer patterns of RSL change since they are often associated with other stratigraphic evidence such as up-core changes in percentage LOI. For this reason, in subsequent analyses I retain the identification of 'poor modern analogue' samples in my analyses.

CHAPTER SIX

Discussion

6.1 INTRODUCTION

This chapter discusses the key issues tackled in this thesis that relate to reconstructing patterns of land- and sea-level movements in Hokkaido over a range of timescales. The majority of data generated in this thesis relate to the current interseismic period, thereby partly bridging the gap between the geodetic (tide gauge, GPS and repeat levelling) observations of the 20th century and the reconstruction of postseismic transient uplift following the AD 1650 earthquake in the south-east of Hokkaido (Atwater *et al.*, 2004; Sawai *et al.*, 2004b).

It is helpful at this stage to revisit the main research objectives addressed by this work, which help form the structure of this chapter.

I. My first objective is to reconstruct patterns of RSL change during the current interseismic period in order to test whether the chronic subsidence recorded by 20th century tide gauges on the Pacific coast of Hokkaido is typical of the full interseismic period. A key focus remains to compare the development of new chronologies of RSL change established from my selected salt-marsh sites to assess spatial and temporal variability.

II. A second objective is to relate the reconstructed records to what we know from recent direct observations from tide gauge, repeat levelling and GPS data. Using tide-gauge data I focus in particular on the most detailed records available, from 1979-2007, but I also critically assess previous interpretations of the historic sea-level records from Kushiro and Hanasaki on the Pacific coast that have underpinned models of interseismic subsidence in the area.

III. Thirdly, I explore how short-term (decadal to century-scale) rates of RSL change compare with longer-term records relating to the mid- to late-Holocene using the sea-level database I have collated for Hokkaido, which I further extend to the late

Pleistocene with the use of previously published data regarding the raised marine terraces of the region.

The chapter concludes by evaluating both existing patterns of RSL change in Hokkaido and the factors driving them. In particular, I explore the implications of the new findings of this research for our understanding of the seismic and non-seismic controls on RSL change over short- and long-timescales.

6.2 RSL CHANGES IN HOKKAIDO DURING THE CURRENT INTERSEISMIC PERIOD

In Chapter Five, I detail the results of the microfossil-based transfer function reconstructions of RSL change from five field sites. The emphasis is on examining the trends extending back to close to the end of the well-documented post-earthquake transient uplift event (Sawai *et al.* (2004b); Atwater *et al.* (2004)). In the following discussion, I acknowledge from the outset that the reconstructions derived from salt-marsh sediments are weighted primarily in relation to sedimentation rates derived from tephra with known dates (where possible), supported where there is a clear caesium peak in the fossil stratigraphy, and only thirdly if reliable ^{210}Pb profiles are available. Independent dating controls such as pollution markers and the use of 'bomb spike' calibration and high-precision AMS ^{14}C analyses (Marshall et al., 2007) would strengthen the resolution of the records. Without such techniques, the dates described in the following section must be viewed with caution. Although for the most part the pattern of the records will be valid (where there are good modern analogues), the exact timing of specific events could vary.

Before comparing the records from the individual sites and linking these with the other datasets there is an important internal calibration exercise that involves comparing the two salt-marsh reconstructions from Mochiruppu to assess intra-site variability in reconstructions.

6.2.1 Intra-site variability in interseismic RSL change

Previous research at Mochiruppu by Sawai *et al*. (2004b) reported four samples analysed for their diatom content from the uppermost sediments that accumulated during the current interseismic phase (Figure 5.2). This small dataset suggests that MTL changed little following the postseismic transient uplift event. Though limited to a few samples, the diatom data contradict the chronic subsidence recorded from the 20th century tide gauges.

I have analysed two cores from Mochiruppu to assess intra-site variability within RSL reconstructions and to enable comparison with the Pacific coast tide-gauge records (Figure 5.3 and Figure 5.5). Both datasets exhibit strong chronologies provided by clear tephras evident in the core. At both sites the age models are in broad agreement and suggest a sedimentation rate during the 20th century of *c*. 1.16 to 1.46 mm/yr. The lithostratigraphy of both sample cores is consistent; with a peat that contains two main muddy units (Mochiruppu South has an additional thin surface muddy unit). The detailed structure of the microfossil diagrams also show a reasonable degree of coherence, notably the up-core decline in frequencies of *B. pseudomacrescens* and the associated rise in frequencies of *T. inflata.*

A comparison of the reconstructed RSL records also shows a reasonable degree of agreement between the records (Figure 6.1). Both show a fall in RSL around 1960-1970, from slightly above present MTL to *c*. -0.3 to -0.4 m below present, with a minimum reached in the early 1980s after which RSL rose quickly to present. The average rates of RSL rise to present vary from *c*. 6 mm yr to *c*. 8 mm yr, calculated from 1950 and 1970 respectively. The data show a clear trend of RSL falling after *c*. 1950 to a minimum in the early 1980s and then rising to present, although individual reconstructions have height uncertainties of *c*. ± 0.30 m and consequently should not be over-interpreted. The older parts of the record from Mochiruppu North suggest little change in RSL during the 19th century.

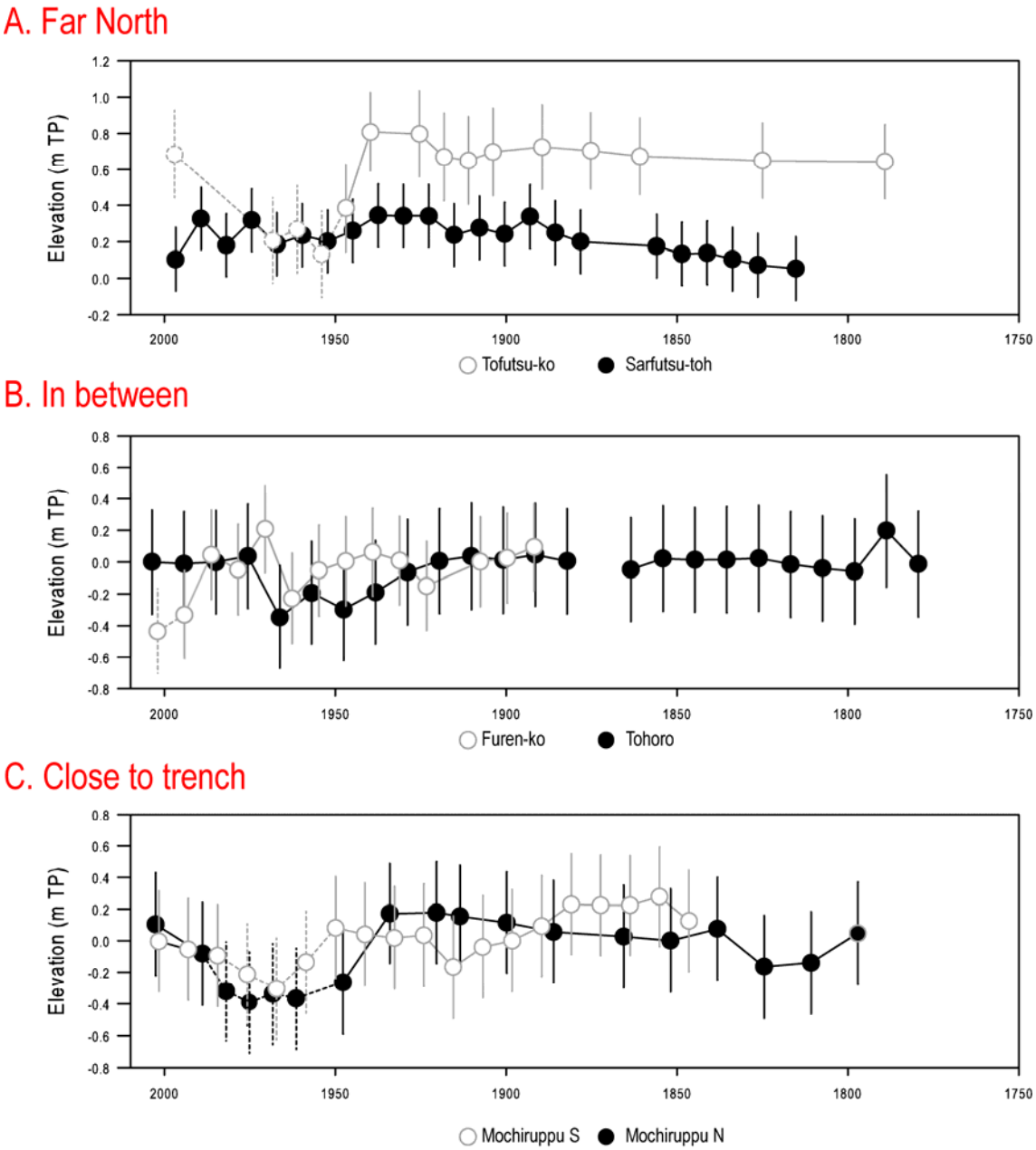

Figure 6.1 Comparison of salt marsh reconstructed RSL from the six study sites in Hokkaido. A small number of samples from the post-1980 period have poor modern analogues (see Chapter Five, these are identified by a dashed line on the vertical error bars).

The foraminiferal-based records from Mochiruppu identify negligible net RSL change during the 150-200 year interval that they cover. This is significant since it demonstrates that the subsidence of the later part of the 20th century is not necessarily typical of the entire interseismic period, at least at this site. The records also show that rates of RSL change are variable within the current interseismic period with evidence of rapid rises and falls. This finding is particularly important given the limited temporal extent of GPS, whilst the repeat levelling surveys are typically conducted too infrequently (3-4 times in the last century) to resolve significant multi-decadal variability (Yokoyama, 1987).

It is important to note that some of these variations may reflect non-seismic processes, notably variations in oceanographic factors including possible changes in the rate of eustatic sea-level rise.

6.2.2 Comparison with the Kushiro and Hanasaki tide gauge records

Continuing the analysis of the Mochiruppu datasets, I now compare the reconstructions directly to the raw tide-gauge data derived from the long tidal records observed at Kushiro and Hanasaki. Before plotting the data it is important to consider several points regarding these records and their previous interpretation.

As noted above, many authors cite the records from both these sites as indicating persistent subsidence during the 20th century on Hokkaido's Pacific coast. This trend of subsidence is similar to that suggested by repeat levelling surveys during the 20th century (Yokoyama, 1987) and also by vertical motions determined by GPS stations (e.g. Aoki and Scholz, 2003), which show maximum rates of subsidence along this coast and reduced rates to the north (see below).

The record from Kushiro (Figure 6.2) clearly indicates RSL rise from 1947 to the present at an average rate of *c*. 9.5 mm per year, although the rate of rise has not been constant (Atwater *et al.*, 2004; Ozawa *et al.*, 2004); there was a period of relatively slow RSL rise from the mid-1970s to the mid-1980s and a period of faster rise from the mid-1980s to present. The Hanasaki record (Figure 6.3) is more varied and does not register the same rapid rate of RSL rise as observed at Kushiro. Furthermore, the Hanasaki record indicates an abrupt rise in RSL at 1994 associated with the 8.1 M_w Kuril islands earthquake and resultant tsunami. Although the long-term average equates to a RSL rise of 13.5 mm per year, the two segments of the Hanasaki II record, either side of this event, only a slight upward trend.

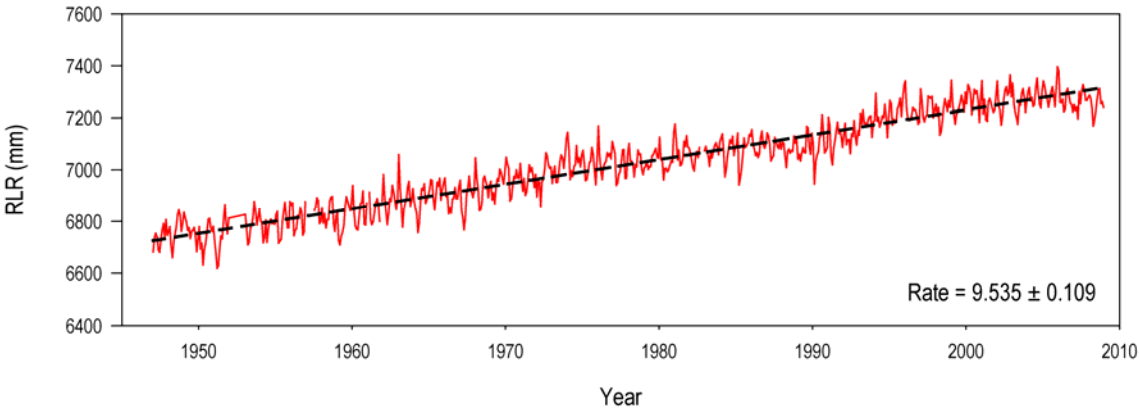

Figure 6.2 Kushiro tide gauge record from 1947-2008.

The differences between the Kushiro and Hanasaki time series are significant but have not been discussed in previous salt-marsh studies that generally assume that both records provide evidence of continuous subsidence throughout the 20th century. In fact, neither record spans the full 20th century and at best they provide trend data from the second half of this century; Kushiro (1947-2008), Hanasaki (1957-1977 and 1983-2008). Moreover, the Kushiro record indicates high overall rates of RSL rise whereas the Hanasaki record indicates little recent change aside from the abrupt shift at 1994. A linear rate through the Hanasaki II record yields an apparent rate of 13.5 mm per yr, whereas rates calculated before and after the 1994 event remain approximately stable.

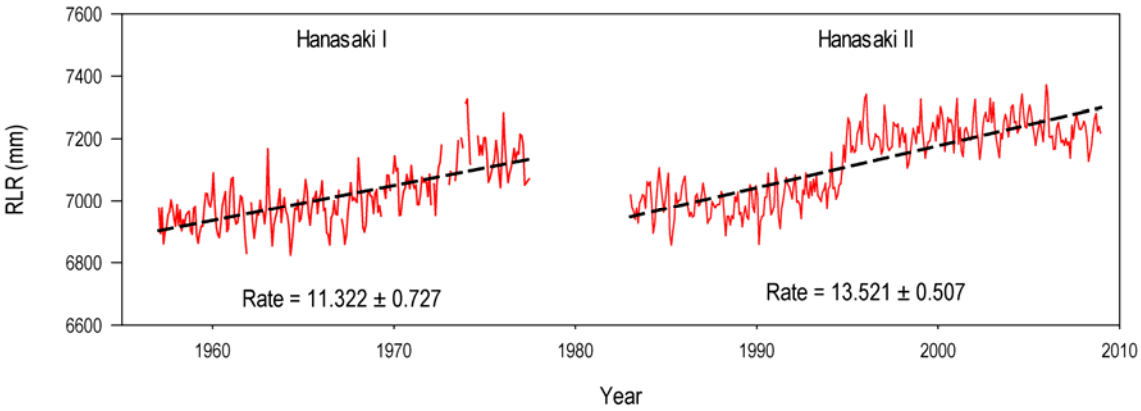

Figure 6.3 Hanasaki I and II tide gauge records from 1957-1977 and 1983-2008.

The cause of the Kushiro RSL rise is assumed to be interseismic subsidence, but limited consideration has been given to other local processes that may influence the tide gauge. Yokoyama (1987) acknowledged the potential effects of local compaction and cryoturbation, although he assumed that they were too local and too small scale to explain the regional subsidence patterns apparent in the south-east part of Hokkaido.

A consideration of the Kushiro station's location immediately raises questions regarding its stability since it is located on the mouth of a large river delta, positioned over a thick sequence of unconsolidated sediments that are likely to experience compaction through time (Yokoyama, 1987). The Kushiro coastal plain has also experienced surface subsidence as a result of extensive coal mining associated with the opening of the main Kushiro mine in 1920 (it closed in 2002). The Kushiro area is underlain by one of Japan's most important coal reserves, which originally formed in a tensional fore-arc basin of Tertiary age (Fujii, 1989). Mining has been completed under the land and more recently extensively under the sea, with the main mine shaft in Kushiro city itself. Measurements taken between 1926-1950 show peak surface subsidence of up to 1 m within a decade of mining activity (Jeremic, 1985). Although such high values cannot be sustained for long periods, since they relate to the rapid closure of mine voids, it is possible that mining induced subsidence as well as sediment compaction may have contributed to the high rate

of RSL rise recorded by the Kushiro site, especially during the earlier part of the century when mining was under the land surface.

In Figure 6.4 I plot the reconstructed RSL records from Mochiruppu North and Mochiruppu South with the tide-gauge records from Kushiro and the most recent part of the Hanasaki series.

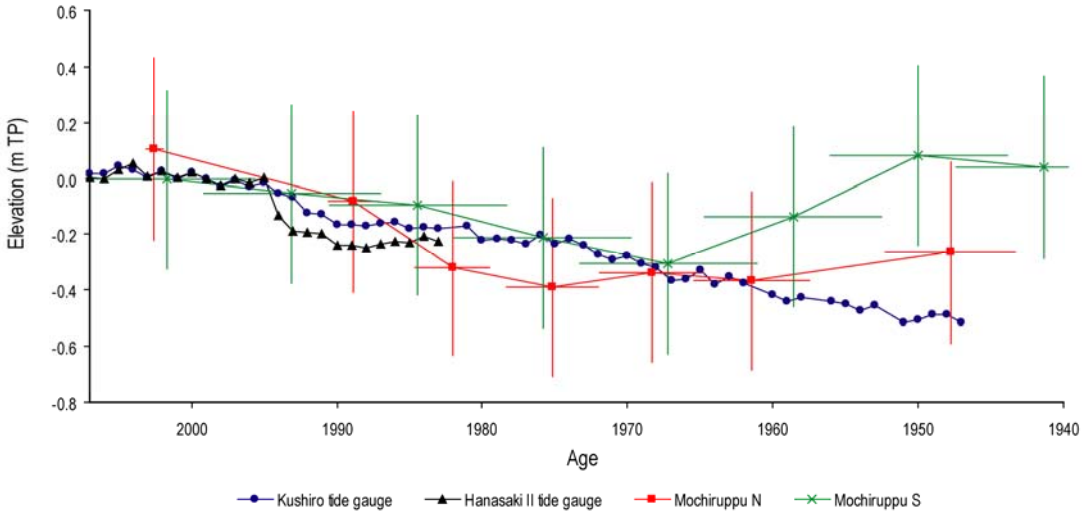

Figure 6.4 RSL records from the Mochiruppu North and South salt marsh cores alongside the raw tide gauge records from Kushiro and Hanasaki II.

Figure 6.4 shows that the observations and reconstructions are in agreement between the present day and around the early 1980s with both tide gauge time series recording a strongly upwards trend in MTL. The salt-marsh reconstructions are slightly higher than those observed by the tide-gauge stations although they overlap when the former's age and altitude errors are taken into consideration. Around the 1960s/1970s, the records differ. The Mochiruppu North reconstruction matches (within error) the tide-gauge data from Kushiro for all of the record, whereas the foraminiferal reconstruction from Mochiruppu South does not, significantly around the 1960s.

The comparison between tide-gauge observations and sea-level reconstructions is limited by the fact that the Hanasaki record is not continuous and thus cannot provide an independent assessment of the Kushiro tidal record prior to *c*. 1970, when the reconstructions and observations diverge. The reason for this divergence remains unconfirmed, although repeat levelling data (see below) strongly suggest subsidence and RSL rise characterised much of the 20th century (Yokoyama, 1987)

6.2.3 Salt marsh trends in RSL change recorded in Hokkaido

I now compare the data from my other sites in Hokkaido in order to assess spatial and temporal patterns of sea-level change. I subdivide the analysis into two groups, first the records from Tohoro and Furen-ko and then those from the northerly sites at Sarfutsu-toh and Tofutsu-ko (Figure 6.1).

The Tohoro reconstruction extends back to approximately the 19th century and shows little change in RSL until AD 1900 when RSL falls gradually from close to 0 m TP to reach a minimum in the 1960s at *c*. -0.4 m TP. Then the RSL record shows a sharp rise to close to its present position before stabilising. The shorter duration Furen-ko reconstruction also shows a fall in RSL to a minimum during the 1960s, although the most recent sample from this site has a poor matching analogue and should be considered with caution. Overall, the records from these two sites are similar, showing little net RSL change during the last 200 and 100 years respectively. It should be noted that a reliable age model exists for neither site and consequently the precise timing of the fluctuations identified above remains uncertain.

The reconstructions from the northerly pair of sites place RSL above present for most of the periods on record. The Sarfutsu-toh and Tofutsu-ko time series are some of the longest reconstructions in this thesis and extend back to the 18th century. The oldest records show little RSL change until after the mid-20th century when there is a fall in RSL at Tofutsu-ko from *c*. 0.80 m TP to 0.20 m TP. The uppermost reconstructions from this site have poor matching analogues and should be treated with caution. The Tofutsu-ko record plots sea level consistently above that from Sarfutsu-toh during the 18th and 19th centuries, with a consistent vertical offset of *c*. 0.60 m. The latter records relatively stable RSL throughout the last three centuries with no net change.

Several conclusions can be drawn from these reconstructions and their comparison. Firstly, it is notable that all of the reconstructions show little net RSL change during the last 100-300 years, with maximum fluctuations of 0.8 m and consequently there is no overall rise or fall in RSL, which remains within *c*. ± 0.20 m of present MTL. This implies that either there is no net deformation over this interval or that any deformation is countered by changes in eustatic sea level during the equivalent interval. Allowing for a 1-2 mm rise in eustatic sea-level during the 20th century, one would expect to see a gradual rise in RSL of *c*. 0.10 to 0.20 m during this interval. That this is not seen, suggests that there is a slight net uplift at all of the sample sites during this interval, of the order of a few decimetres.

The apparent stability of the RSL reconstructions, at least during the early (pre-1900) part of the records from three sites (Sarfutsu-toh, Tofutsu-ko and Tohoro) indicates that chronic

subsidence recorded by recent tide-gauge records has not typified the present interseismic period. The GPS and repeat levelling data (see below) suggest that the Pacific coast subsidence does not extend northwards beyond the Tohoro area and so confirm this conclusion.

Secondly, there is a clear difference in the data from Sarfutsu-toh compared with the other reconstructions. This site is located close to an area of rapid uplift, indicated by the elevation of the Pleistocene marine terraces along this part of the Hokkaido coast (see below). However, the rate of RSL at this site was close to zero between AD 1700-1900 indicating that episodic uplift, as oppose to gradual deformation, was controlling RSL change at this site.

Thirdly, the pattern of change during the 20th century contrasts with the preceding two centuries by having a greater variability in rate of RSL change, both in individual records and when comparisons are made between the sites. For example, RSL at Mochiruppu reached a minimum in the mid-1960s before rising rapidly to present, in contrast to Tohoro and Furen-ko RSL where the opposite patterns were recorded during this interval. Given the uncertainties in the age models for the latter sites, the significance of the exact timing of these variations needs to be treated with caution. However, regardless of the age models used, the more recent records indicate a more varied spatial and temporal RSL pattern than that experienced during earlier periods.

Finally, it is not possible to resolve abrupt changes in RSL associated with decimetre-scale uplift caused by 20th century earthquakes in the RSL reconstructions. It is possible that the rapid fall in RSL recorded in Tofutsu-ko in the early 20th century is related to the AD 1894 earthquake, although this is the only site that records a significant change in RSL at this time. The fluctuating RSL from the middle of the 20th century onwards at the more southerly sites may record vertical land motions associated with the 1952 and 1973 earthquakes but the resolution of existing dating models is not sufficient to draw definite conclusions as to whether these correlations are real or an artefact of age models.

In summary, I find no evidence for persistent subsidence during the current interseismic period on the Pacific facing sites studied here. Although there is recent rapid RSL rise in the sites closest to the trench (Mochiruppu), this is a relatively short-lived phenomenon and cannot have persisted during the last several centuries. Such high rates of RSL (7-11 mm per year) would be unlikely to permit the formation of metre-thick sequences of near surface salt marsh and freshwater peat observed at this site. Trends in RSL are generally more stable in the northern two field sites and I note an increase in the amplitude and frequency of RSL change during the latter part of the 20th century compared with earlier

decades and centuries. The changes are not synchronous in either timing or tendency between sites in Hokkaido suggesting that they may have a tectonic origin and that patterns of interseismic land motions are not constant.

6.2.4 Assessment of the viability of the transfer function technique in microtidal environments and back barrier environments

The sites investigated in Hokkaido were mainly coastal lakes and lagoons, separated from the sea by narrow barriers of land. These locations may be considered as unsuitable locations for sea-level research as their relationship with elevation is unclear. These enclosed features are primarily shielded from direct exposure to ocean waves (Oertel, 2005), and may form as a result of the upbuilding of shoals and bars (de Beaumont, 1845), the embayment of interior shores by spit progration (Gilbert, 1885) or and the inundation of lowland areas by sea-level rise (McGee, 1890). Coastal lagoons are different from estuaries because of their circulation characteristics, and this has important implications for their use in transfer function reconstructions.

Compared to estuaries, which are generally more open, back barrier environments can support a mosaic of different foraminiferal communities controlled by the physical and geochemical characteristics of each habitat zone (Woo et al., 1997). Spatial and temporal variations in salinity and tidal regime influence the precise composition and elevation of vertical assemblage zones (de Rijk, 1995b, a; de Rijk and Troelstra, 1997). Extensive marsh surfaces show a wide differentiation of facies, such as levees, unvegetated spots and pond holes (de Rijk and Troelstra, 1997), and these different sub-environments give rise to diverse foraminiferal assemblages. In their study of the Albemarle-Pamlico estuarine system of North Carolina, Kemp et al. (2009b) identified seven principal biozones of salt-marsh foraminifera reflecting salinity regimes caused by the current configuration of barrier-island inlets. However local variability in microfossil assemblages is not limited to back-barrier environments. On the west coast of Greenland, differences in diatom assemblages and organic content between sites (which are likely the result of tidal range variations) render a local training set more appropriate for palaeoenvironmental reconstruction than a regional one (Woodroffe and Long, in press).

The complicated hydrodynamic regime of back-barrier environments requires that the common assertion that elevation is a suitable surrogate for flooding frequency be tested. However, compared with the studies described above, the Hokkaido barrier environments are typically very small, and the topography of the marshes remarkably constant. Detailed intra-site comparisons were beyond the scope of this thesis (which focused primarily on developing a training set applicable over a wide spatial setting), but

foraminiferal assemblages over the six study marshes were broadly comparable (see Section 4.5.2), and multivariate analysis suggested that these are indeed related to elevation and therefore tidal inundation and flooding frequency (see Section 4.5.3).

One big advantage of the Hokkaido coast for transfer function development is the fact that the area is microtidal since this means that absolute vertical are typically small. In a similar study using foraminifera in the microtidal Outer Banks of Northern Carolina (where the difference between MHHW and MLLW was around 0.4 m), Kemp et al. (2009a) observed a vertical error (RMSEP) in their transfer function of just 4.2 cm. Assemblages of foraminifera on microtidal environments typically display a weaker relationship to elevation compared to macrotidal areas (such as the Cowpen Marsh, UK; Horton, 1999). The small vertical range of the samples studied, which reflects the low elevation and limited spatial extent of the vegetated marsh surface (Horton and Edwards, 2006), gives rise to a few species being dominant over much of the marsh (e.g. *B. pseudomacrescens*). Although one effect of this is to lower the predictive ability of the transfer function (the 'r^2'), this is mitigated to some degree by the predicted errors which are typically small.

6.3 COMPARISON OF SALT MARSH RSL RECORDS WITH OTHER GEODETIC TIMESERIES

6.3.1 Tide-gauge data

There are nine tide-gauge stations around the coast of Hokkaido recording RSL change through part of the last 100 years (Figure 6.5 and Figure 6.6A to C). In order to compare the same duration of records at each station I analyse the period between 1979-2007 at each tide-gauge station for linear trends in the data. The RSL trend in the tide-gauge data is calculated by correcting for seasonal, pressure and oceanographic effects, as detailed in Chapter Three (Section 3.3.3). As described above, the tide gauges of Kushiro and Hanasaki show the greatest rate of RSL rise around Hokkaido but all other sites apart from Urakawa on the southern tip also show RSL rise (Figure 6.5; Figure 6.6A to C). Some sites record a RSL rise in excess of the probable global eustatic contribution during the period *c*. 1.8 mm yr (Douglas, 1997) calculated for Wakkanai and Abashiri on the North coast (Figure 6.6A). Elsewhere the rate of RSL rise is largely comparable with the eustatic contribution during this period.

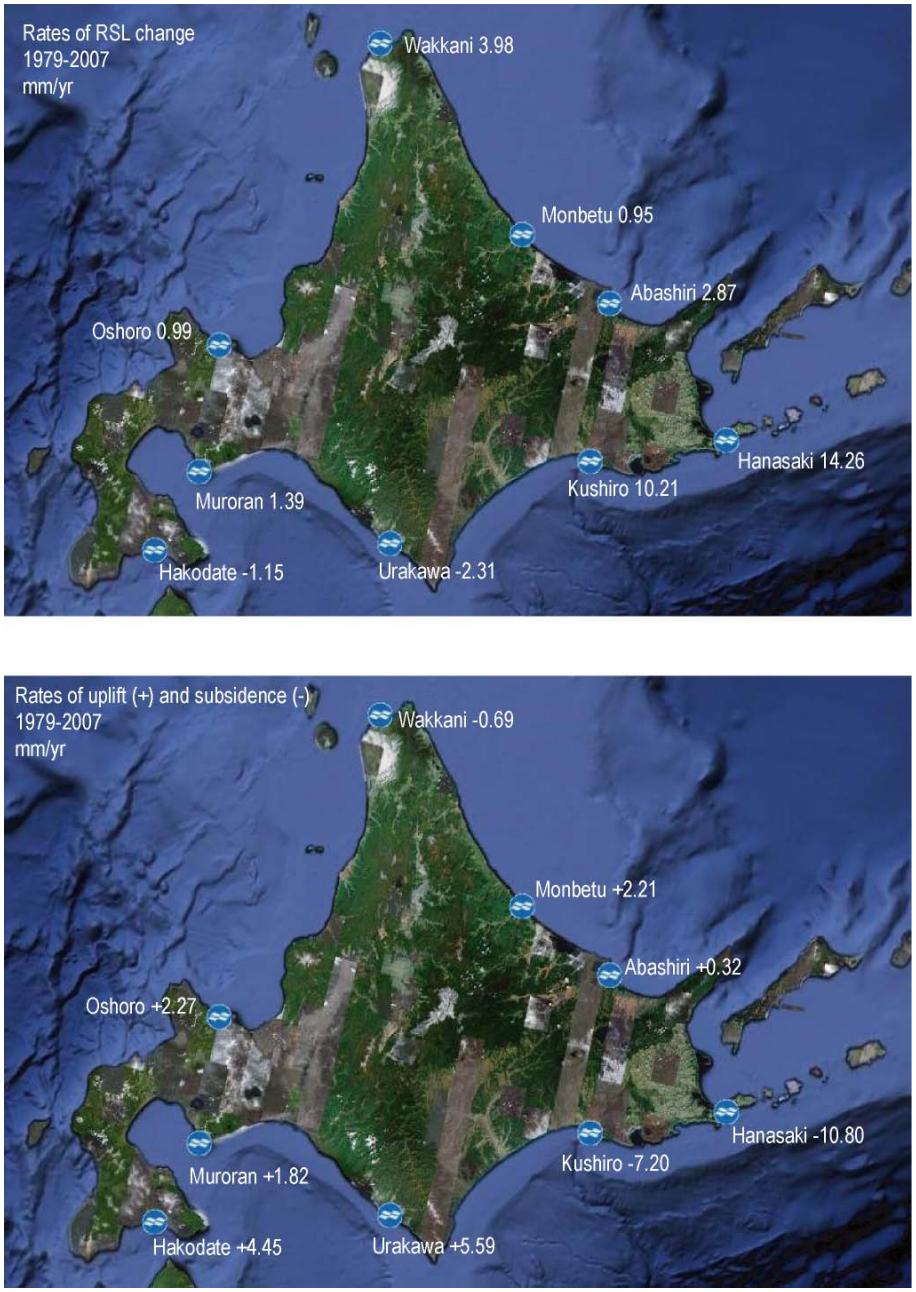

Figure 6.5 Tide-gauge stations around Hokkaido showing a rate of RSL rise between 1979-2007 (top pane) and the rate of tectonic uplift (+) and subsidence (-) during the same period (lower pane). The uplift/subsidence rate is calculated by correcting the tide-gauge data for eustasy and long term GIA effects (see Chapter Three for details of the methods used).

When the tide-gauge records are corrected for the eustatic and GIA contributions (using corrections described in Chapter Three) the linear rate between 1979-2007 should approximate to tectonic movements over the period; henceforth this concordance is referred to as 'tectonic RSL'. The data in the lower pane of Figure 6.5 and Figure 6.6A-C) show these corrected values for each tide gauge on Hokkaido. Kushiro and Hanasaki are undergoing the most subsidence, as I would expect given the rate of RSL rise during the period. All other sites apart from Wakkanai on the northern tip show tectonic uplift during this period.

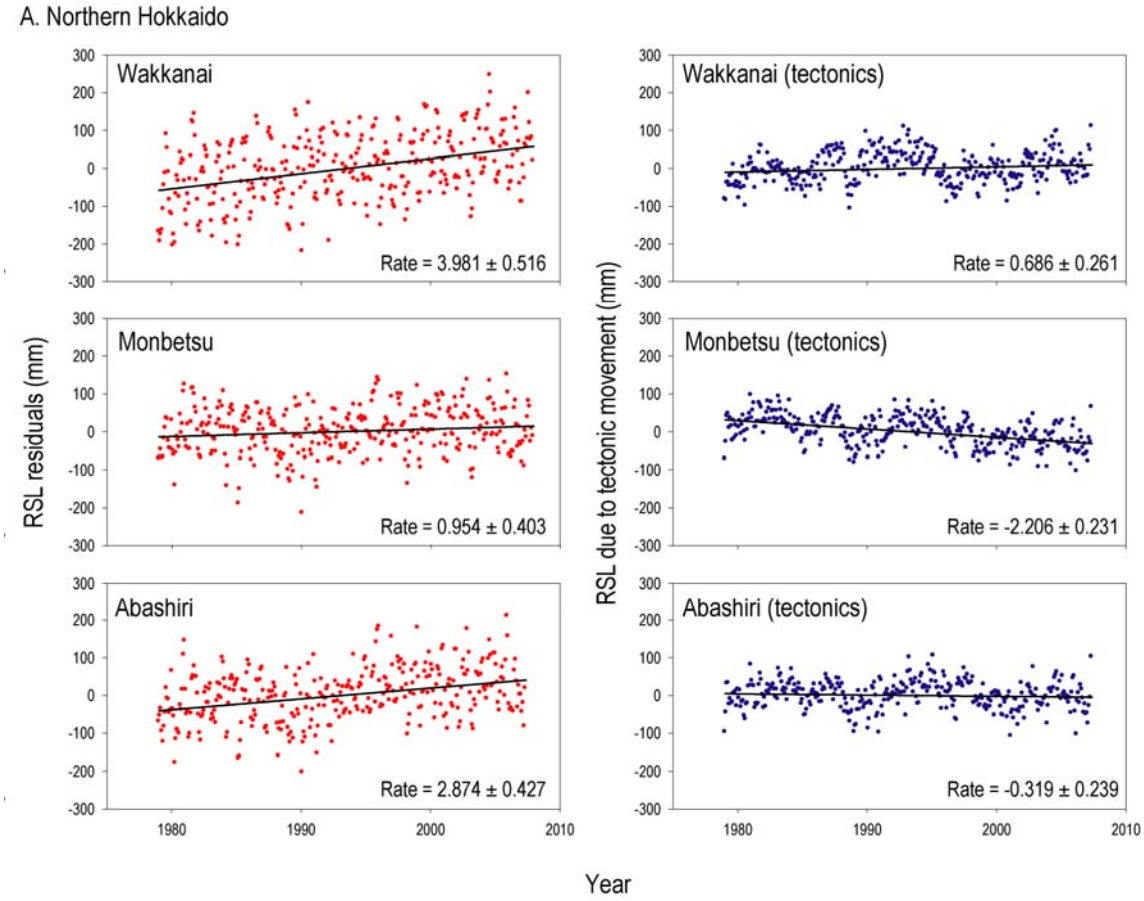

Figure 6.6 Tide-gauge analysis showing RSL and RSL attributable to tectonic movement. (A) Data from Wakkanai, Monbetsu and Abashiri tide gauges on the northern Hokkaido coastline. On this and subsequent figures, on the left is RSL data, on the right is tectonic RSL during the period 1979-2007. The RSL data is corrected for seasonal, pressure and oceanographic variations. Tectonic RSL is corrected for these, plus eustasy and GIA movements.

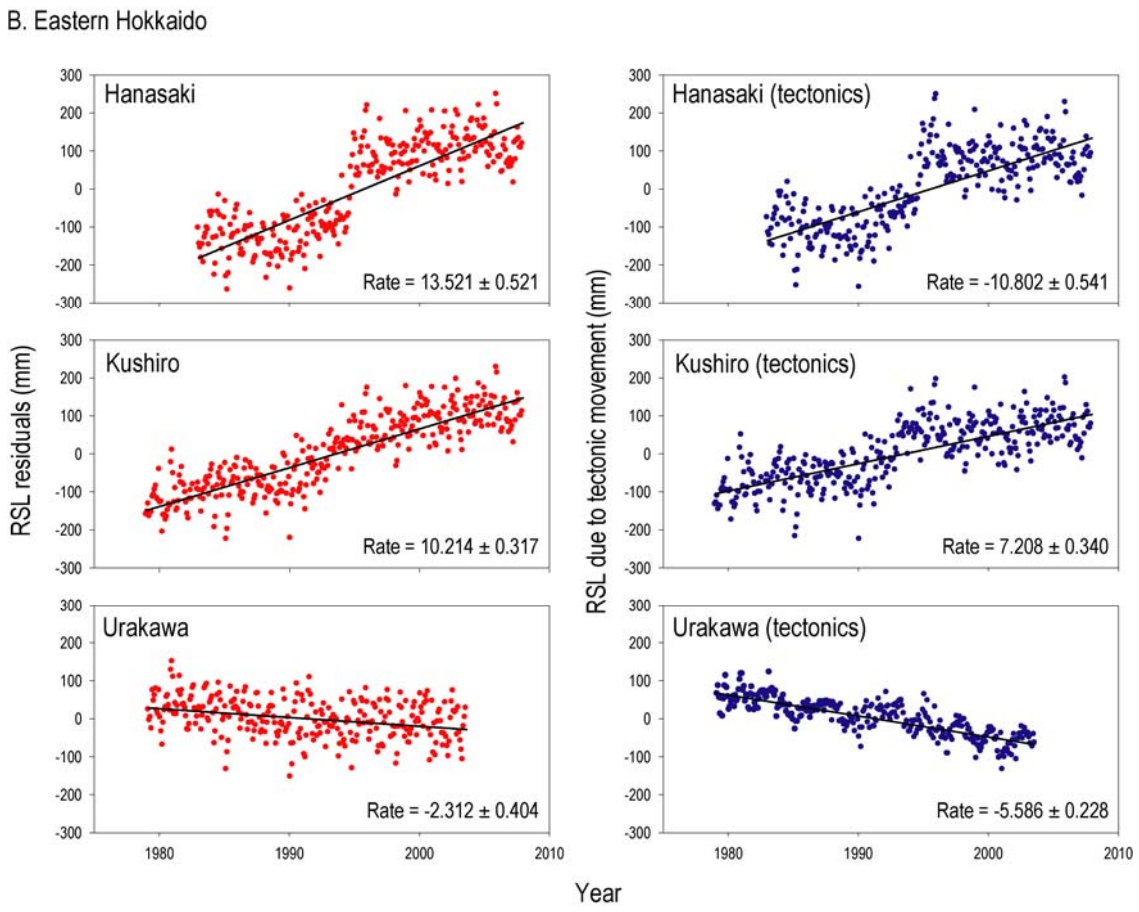

Figure 6.6 (B) Data from Hanasaki, Kushiro and Urakawa tide gauges on the east Hokkaido coast.

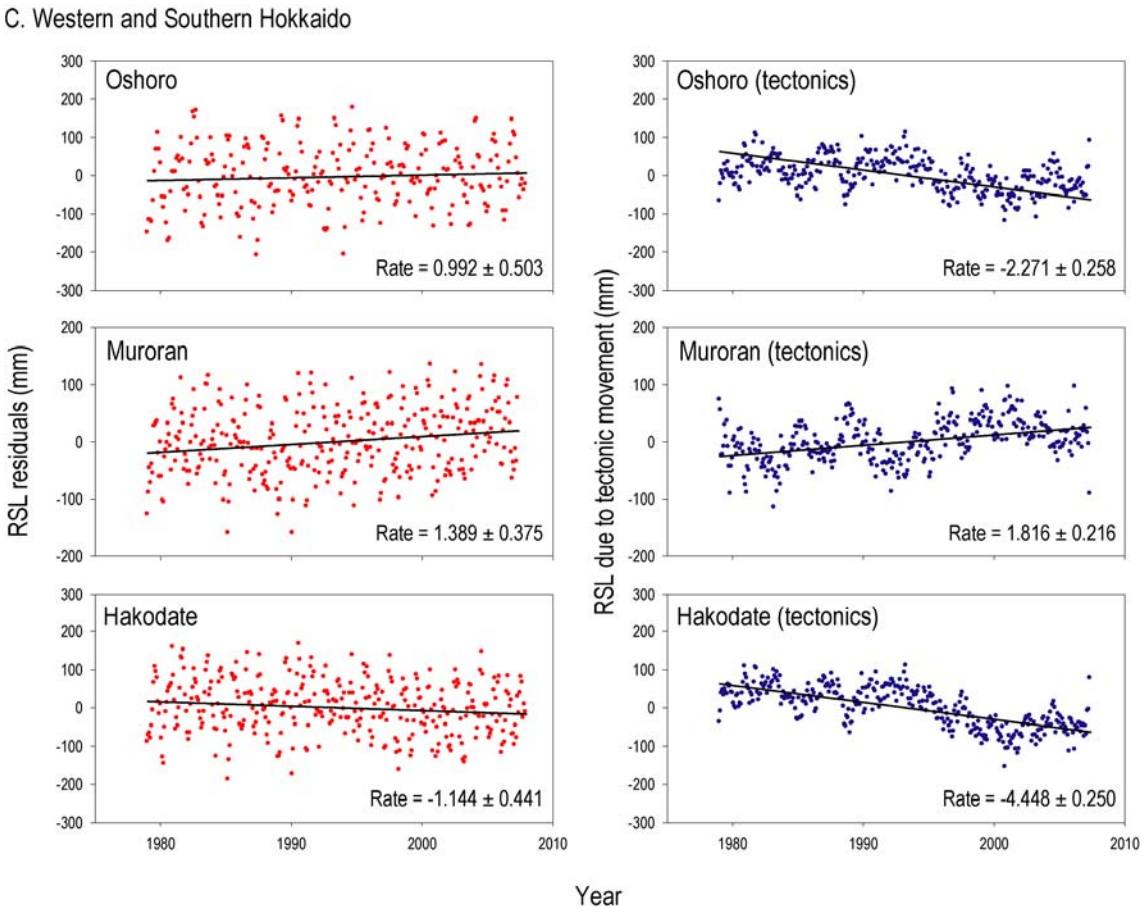

Figure 6.6 (C) Data from Oshoro, Muroran and Hakodate tide gauges on the southern and south-western Hokkaido coast.

There are distinct small-scale fluctuations within the tectonic RSL plots that are common to different tide gauges (Figure 6.6A-C). This appears to be an artefact of the eustatic correction procedure, which extrapolates 30 years of tide gauge data from many sites in the north-eastern Pacific ocean basin to deduce the amount of eustatic sea-level rise during the 20th century (Jevrejeva *et al.*, 2006). Figure 6.7a shows the residuals in the tectonic RSL plots for the northern Hokkaido coast sites from 1979-2007 compared to the residuals in the eustatic component over this period. There is a trend in the residuals that parallels the trend in the eustatic residuals but that is not apparent in an equivalent plot of RSL data uncorrected for eustasy (Figure 6.7b). This overprinting suggests that the true eustatic contribution in Hokkaido during this period is different to that produced by a basin-wide analysis of tide-gauge records (Jevrejeva *et al*., 2006, A. Grinstead *pers. comm*).

Fitting a linear trend line to the interseismic RSL plots would be inappropriate if these records are overprinted by the eustatic correction applied. Conversely, applying a fixed 1.8 mm yr global eustatic correction to the tide-gauge data would also be wrong, since we know that local eustatic changes do not equate to the global average through time (Milne and Mitrovica, 2008). Eustatic sea-level rise is likely to have changed during the 1979-2007 period, but has probably been less variable than eustatic correction suggests.

However without an alternative method to estimate and subtract the eustatic signal from tide-gauge records, I use the Jevrejeva *et al*. (2006) correction whilst acknowledging that this may have some impact on the linear rate of tectonic movement calculated from each tide-gauge record.

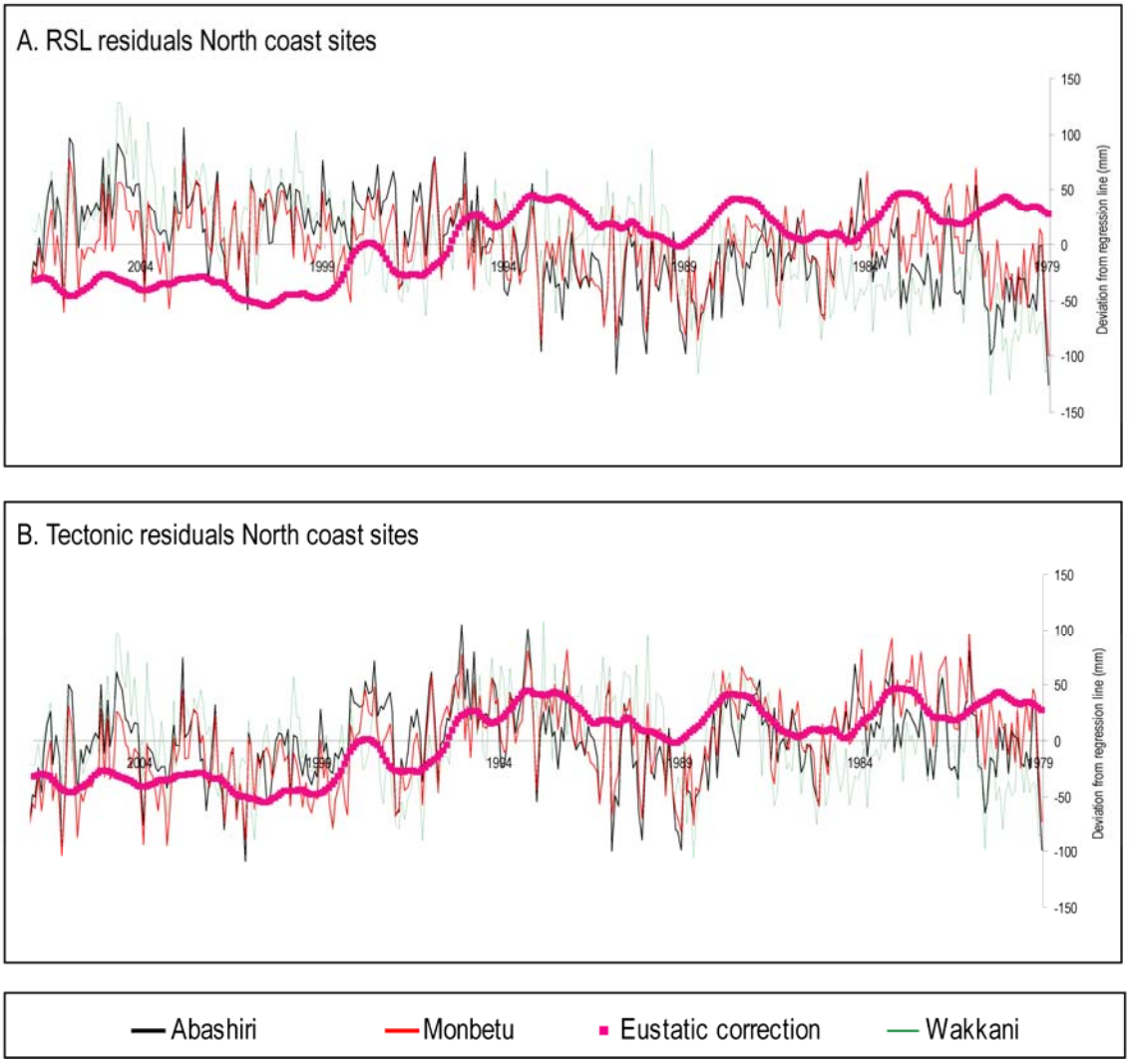

Figure 6.7 RSL and tectonic residuals around Hokkaido (A) Residuals around the linear trend line in the tide-gauge tectonic RSL data (eustatic and GIA correction applied) for three sites on the northern Hokkaido coast, plotted with residuals in the Japan-specific eustatic contribution during the period 1979-2007. (B) residuals around the linear trend line in the tide-gauge RSL data (no eustatic or GIA correction applied) for three sites on the northern Hokkaido coast, plotted with the residuals in the Japan-specific eustatic contribution during the period 1979-2007.

6.3.2 Repeat levelling and GPS record

Repeat levelling and triangulation surveys provide direct observations of land motion during the last 100 years in north-east Hokkaido. Yokoyama (1987) provides an analysis of data since 1910 and notes that rates of vertical deformation vary in time and space although certain large-scale features are apparent. The most important observation is that there is a

general sinking of the land to the south of the study area (Figure 6.8), with contours of subsidence approximately parallel in an east-west direction. Rates of subsidence are highest in the south and decrease gradually in a northerly direction to *c*. 0.05 m towards Sarfutsu-toh (Figure 6.8). These rates have changed through time; the region of peak subsidence narrowed and decreased in rate between 1970-1975 (Yokoyama, 1987).

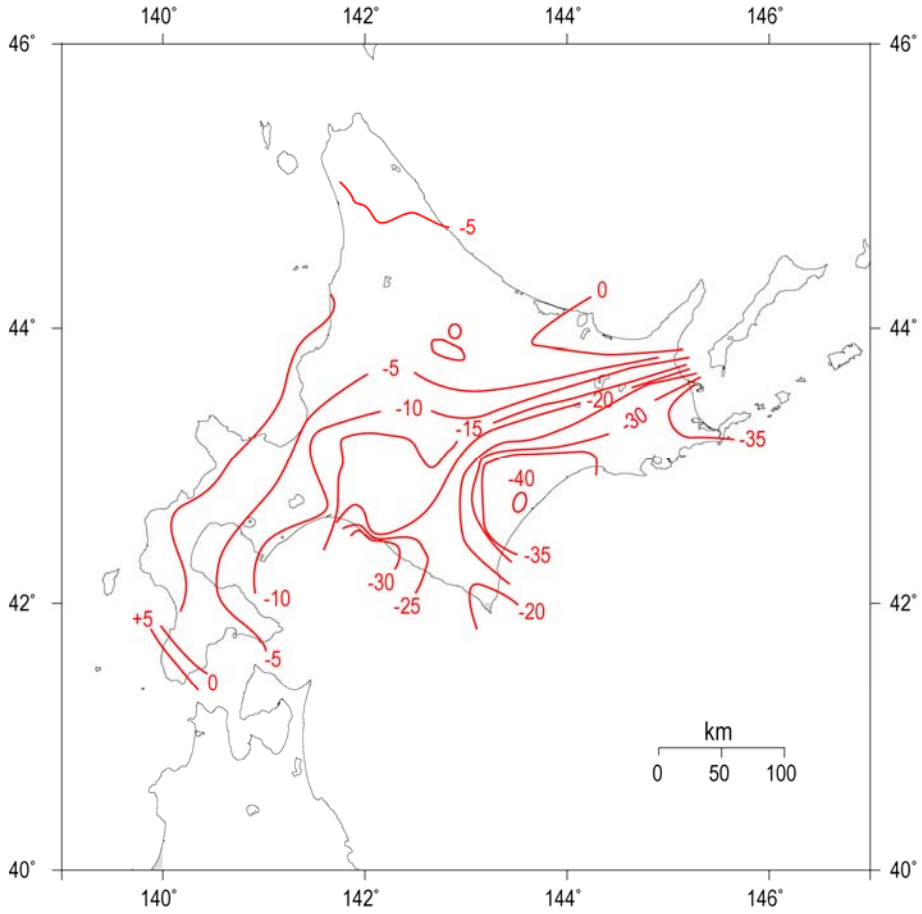

Figure 6.8 Land subsidence (in cm) in south-east Hokkaido derived from repeat levelling between 1900-1950 (Yokoyama, 1987).

It is important to note that these data record average land-level changes during the period of survey and do not isolate the specific effects of individual earthquakes nor for the effects of human-induced subsidence. Despite the above, these spatial patterns are in agreement with the spatial trends observed in my reconstructed RSL records. Thus, RSL in the north of the study area has been above present for the majority of the last few centuries, whereas the general trend of RSL rise in this interval is greatest in the more southerly areas.

The trend of subsidence between 1920-1970 does not match the RSL reconstructions from Mochiruppu, Tohoro and Furen-ko, each of which indicate RSL fall during this interval. The RSL reconstructions record changes in eustatic sea-level and other oceanographic factors, so the rates are not directly comparable between these reconstructions. However,

assuming that the geodetic data are correct, and that subsidence persisted between 1920-1970, the data imply that either the RSL reconstructions are wrong or that there was a strong fall in RSL due to eustatic and oceanographic factors during this interval.

Japan has one of the densest arrays of GPS networks in the world with many stations installed in recent years across Hokkaido. These data have been analysed previously by several workers in order to examine the horizontal and vertical dimension of crustal deformation in the last decade as part of wider regional analyses of land motions across Japan (e.g. Ito *et al.*, 2000; Aoki and Scholz, 2003; Nishimura *et al.*, 2004; El-Fiky and Kato, 2006). The earliest GPS receivers that provide useful data regarding vertical deformation of Hokkaido date from the mid-1990s. Ito *et al*. (2000) invert GPS data collected between April 1996 and March 1998 measured by 161 GPS stations across Japan and demonstrated that horizontal plate velocities are highest in the immediate coastal region of the Pacific. These rates decline along the Okhotsk Sea coast (Figure 6.9).

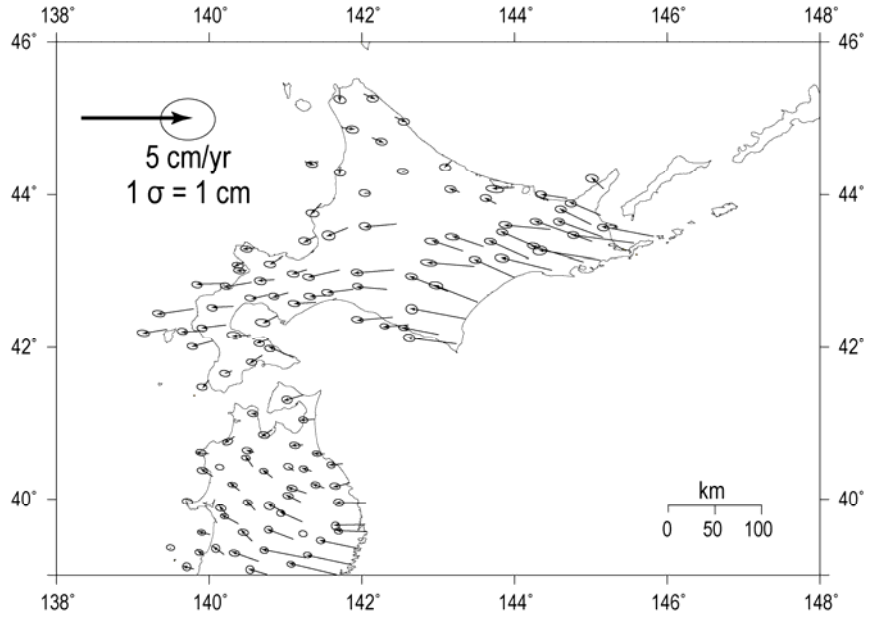

Figure 6.9 Horizontal rates of land motion in north-east Japan and Hokkaido based on GPS data from Ito *et al*. (2000).

Ito *et al*. (2000) also calculate absolute vertical motions, calibrating their GPS data to 12 tide-gauge stations. This analysis indicated that peak vertical motions (subsidence) occur along the Pacific coast of Hokkaido with lower values along the Okhotsk Sea (Figure 6.10). High uplift rates are also indicated along the Sea of Japan.

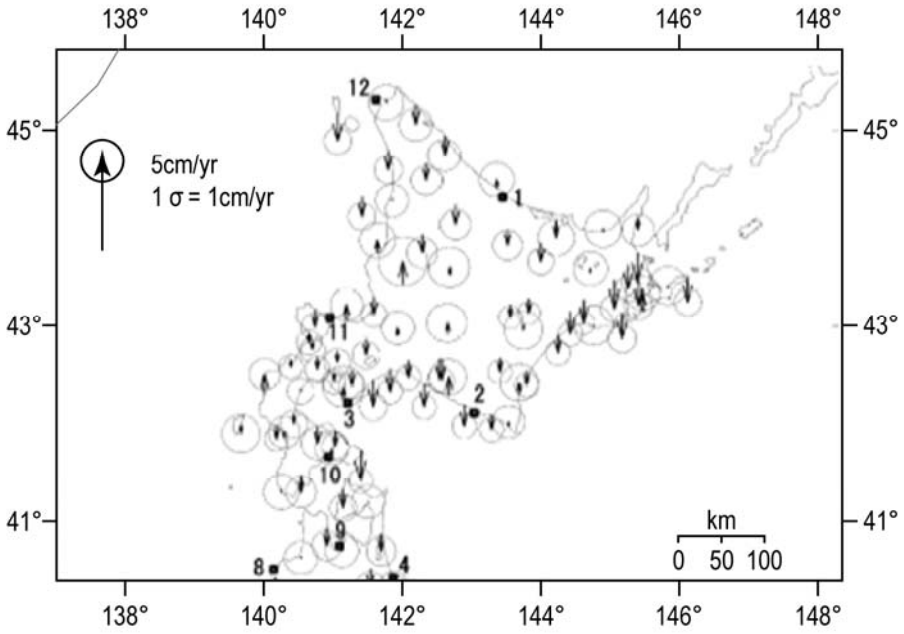

Figure 6.10 Vertical land motions based on analysis of GPS data (Ito *et al.*, 2000). The confidence ellipses represent 1 sigma uncertainties. The upward and downward vectors represent uplift and subsidence respectively.

Aoki and Scholz (2003) present an analysis of vertical motions using GPS data from 1996-1999 across Japan. The authors use a screened total of 502 GPS stations that are processed to give velocity measurements relative to the Tsukuba tide gauge (Japan Sea coast), which is assumed to be in a region of stability being located distant to the plate boundary. The analysis also identifies an area of rapid subsidence on the Pacific coast of Hokkaido (Figure 6.11), with rates of *c*. 2-4 mm yr (± 2 mm yr). The authors noted that the data fail to define any uplift in this area, reflecting that the coastline of Hokkaido lies too far from the trench to resolve the vertical component of interplate coupling.

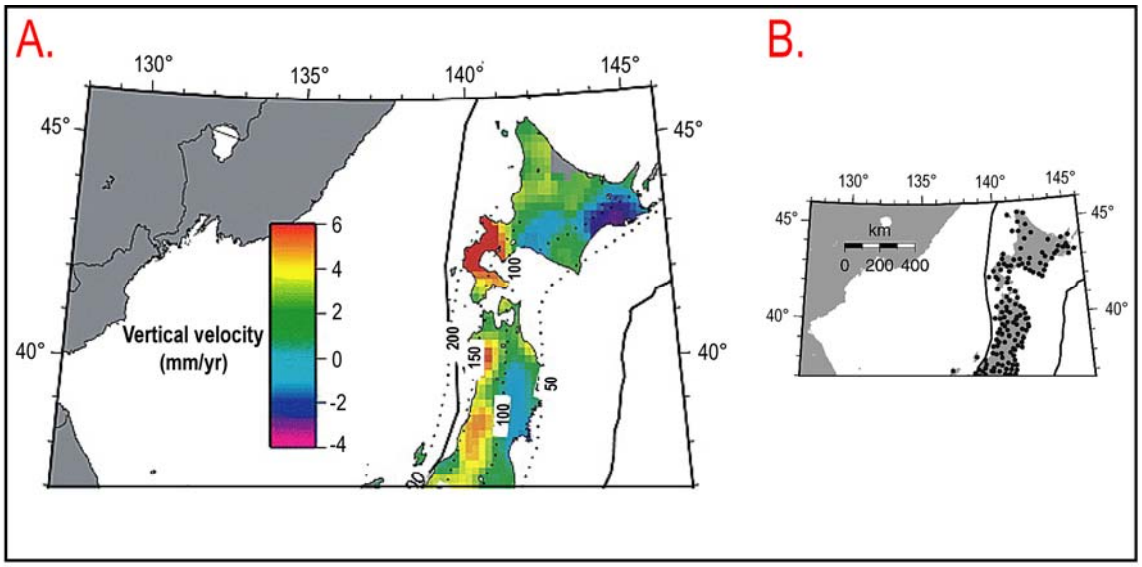

Figure 6.11 Rates of vertical land motion inferred from GPS data (A), with insert (B) showing the location of GPS station used in the analysis from Hokkaido and northern Honshu (after Aoki and Scholz, 2003).

In summary, previously published GPS analysis from Hokkaido agree with the general pattern defined by repeat levelling surveys during the 20th century, with peak subsidence focussed on the Pacific coast between Kushiro and the Hanasaki tide-gauge stations (which are an important source of data for this study). The surveys suggest that a transition from subsidence to slight uplift occurs in the region of the Shiretoko Peninsula. The Aoki and Scholz (2003) analysis suggests that there is slight subsidence in the Saroma-ko region but in general there is no evidence for significant differential uplift patterns along the Okhotsk coast.

My re-analysis of selected tide-gauge data demonstrates that the general pattern of uplift and subsidence agrees with that from previous GPS-based studies. The two tide-gauge sites (Kushiro and Hanasaki), from which the term 'chronic subsidence' has been derived, show significant subsidence both in GPS and tide-gauge records. The northern coast sites of Abashiri and Monbetsu show uplift in both the tide-gauge and GPS records, although the most northerly site of Wakkanai shows mild subsidence (-0.69 mm yr) in the tide-gauge record. Other studies provide conflicting rates of change ranging from uplift of *c*. 2 mm yr (Aoki and Scholtz, 2003) to subsidence of -8 mm yr (Ito *et al*., 2000). In the south east of Hokkaido my tide-gauge analysis agrees with uplift shown by Aoki and Scholtz (2003), but the magnitude is greater in their analyses.

6.4 HOLOCENE RSL RECORDS FROM HOKKAIDO

This thesis has assembled the first rigorous review of sea-level data from around the Hokkaido coastline from both published and unpublished records (Appendix E). As discussed in Chapter Three, the sea-level data is divided into six regional areas (see Figure 6.12). The database compiled consists of 82 sea-level index points (57 Primary, 25 Secondary) quantitatively related to a past tide level together with an error estimate and a further 116 data points that provide limits on the maximum and minimum elevation of RSL. In many regions, the form of the Holocene sea-level trend is constrained by both terrestrial and marine limiting dates, illustrating their importance for sea-level reconstructions. Further, the temporal distribution of the index points is very uneven; only 24% of the index points and limiting dates are older than 6,000 cal yr BP. There remains a critical need to extend the fossil reconstructions into the early Holocene. Nevertheless, a review of the best quality data indicates that all areas of Hokkaido have experienced a stable or slightly falling RSL during the late Holocene (last *c*. 3,000 cal. yrs).

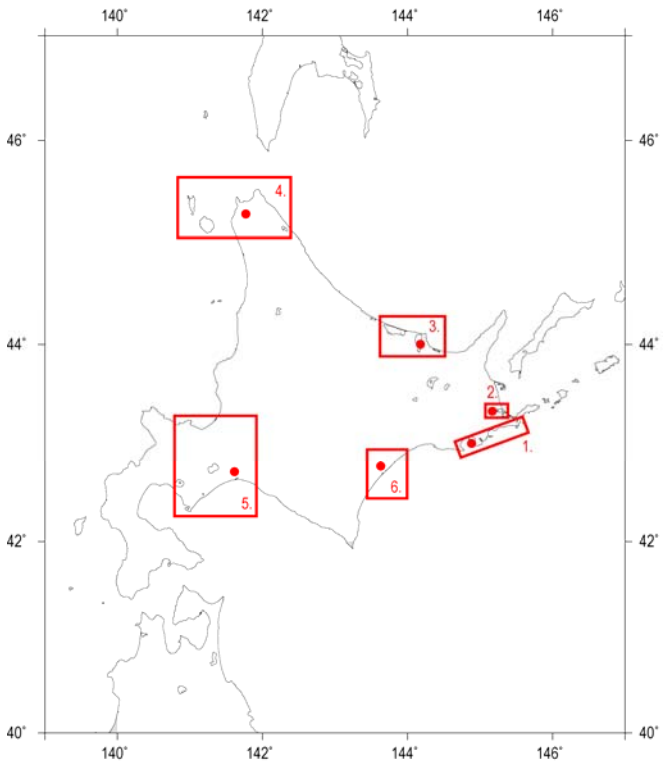

Figure 6.12 Map showing location of sites used for Holocene RSL reconstruction and GIA model predictions (red circles). 1 = Akkeshi-Mochiruppu, 2 = Furen-ko, 3 = Abashiri, 4 = Sarubetsu – N. Hokkaido, 5 = Tokachi, 6 = Isikara Lowlands.

In Figure 6.13 I present a comparison of the RSL data from the sites closest to those studied using salt-marsh sediments in this thesis (Figure 6.12). No site, even those located

on the Pacific coast, record a continually rising trend in RSL during this interval. Despite the poor quality of the data, this observation is important since it means that the recent subsidence observed by various geodetic data in south-east Hokkaido cannot have persisted for long because they would otherwise have caused continually rising sea level during the late Holocene.

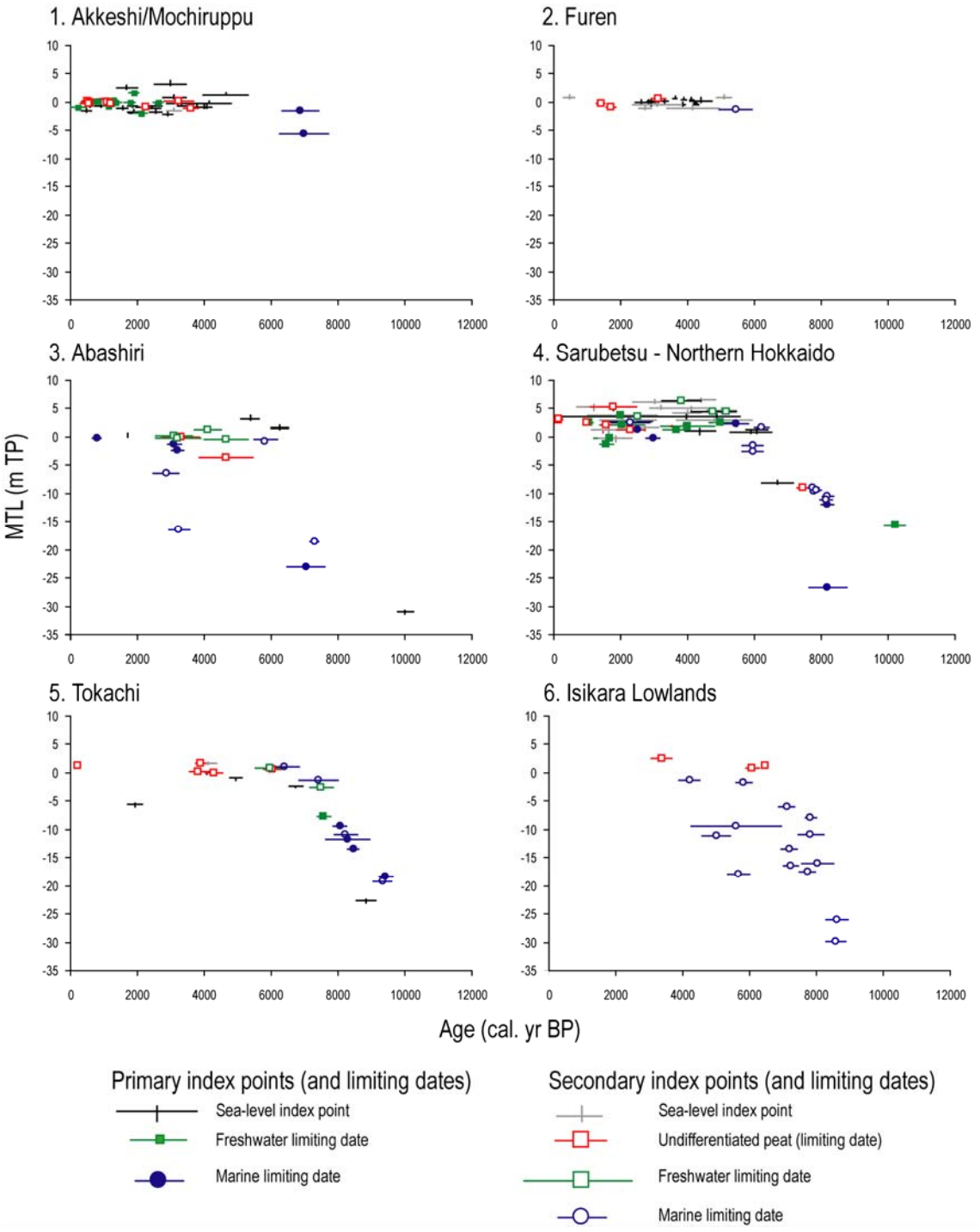

Figure 6.13 Age/altitude plots of Holocene RSL change from Hokkaido.

The Ishikawa Lowland stretches between Sapporo on the Japan Sea coast of Hokkaido to Muroran in the south of Hokkaido, situated on the Pacific coast. Previous research that

contributes to the age/altitude plot comes from the Isikara Plain (Matsushita, 1979), the Yufutsu Plain (Ikeda *et al*., 1995), Tomakomai (Arakawa, 1994, 1997) and the Toyohira River (Daimaru, 1989). Although there has been a considerable amount of data from the region, it is generally not suitable for rigorous sea-level assessment. There are no primary sea-level index points and only four freshwater limiting dates (undifferentiated peat), with a further 13 marine limiting points. No microfossil material is available for this region. Unfortunately samples tend to be taken from the middle of stratigraphic units and this limits their ability to constrain sea level. There are no index points from the Isikara Lowlands during the last 2,000 cal. yrs. Overall, the data suggest that MTL was at or close to present MTL by *c*. 6,000 cal. yr BP, which is similar to the pattern observed elsewhere on Hokkaido.

The area around Akkeshi-ko, extends south to Kushiro (Kumano *et al*., 1990b), through Akkeshi-ko (Kumano *et al*., 1990a; Sawai, 2001), to Onnetoh (Sawai *et al.*, 2002; Sawai and Nasu, 2005) on the Nemuro Peninsula. The data demonstrate that MTL was essentially stable through the last 4,000 cal. yrs. A small number of data points plot above present MTL but these generate outliers to the majority of data. The Akkeshi-ko RSL data comprises 27 validated sea-level index points (only one of which is classed as a secondary index points), eight undifferentiated peat samples and two freshwater limiting dates which restrict RSL to a maximum and an additional 18 marine limiting dates. The material dated is younger than that from the Ishikawa Lowland, with a particular concentration over the past 4 ka yrs reflecting the aim of the studies to evaluate land level change over the late Holocene. In comparison to other sites around Hokkaido, detailed biostratigraphical data exist for several index points and clear elevational data is provided.

An almost identical RSL history is observed at Furen-ko, on the Okhotsk Sea coast where MTL is essentially stable since 6,000 cal. yr BP. The Furen-ko sea-level observations are principally derived from the work of Ohira (2004) who investigated Holocene RSL change in the Furen-gawa lowland. Although some of the earlier papers are not referenced to m TP, his later papers include well-dated material that is suitable for use in the sea-level database. Index points typically involve 1a or 1b transitions (see Table 3.7) which were used to constrain sea-level precisely in this region. In total there are 17 index sea-level index points with defined age and altitude errors and a further four points comprising undifferentiated peat and one marine limiting data. The data from Furen-ko span the past 6 ka yrs and the data are tightly clustered to around 0 m TP over the duration of the mid- to late Holocene. As noted above, the implication from these data is that there has been no significant subsidence during this interval. Any late-Holocene subsidence would not cause the essentially stable RSL patterns that this analysis indicates; instead one would expect to see a gradient to the age/elevation distribution of the index points.

A number of studies have investigated RSL changes around the lowlands of Abashiri (Kodaira, 1996; Sato *et al.*, 1997; Atago, 1998), including at Tokoro (Umitsu, 1983; Hamano *et al.*, 1985), Tofustu-ko (Sato *et al*., 2004) and Saroma-ko (Soeda and Akamatsu, 2001). Most of the material is of limited value for RSL reconstruction, with only six high-quality, validated index points in the database (Sato *et al*., 1997) comprising peat and geochemically distinct tephra. A range of data is available for Abashiri. The majority (11 samples) are derived from index points, whilst the remaining data comes from two undifferentiated peat, four freshwater limiting dates and eight marine limiting dates (shell fragments). From the age-altitude plot it is evident that sea level has been relatively stable since the mid Holocene. The highest primary index point (1a) records a highstand at 3.24 m above present sea level approximately 6 ka years ago. However, given the quantity of secondary limiting dates available this conclusion is tentative. For much of the past 4 ka years sea level appears to have remained at around 0 m MTL.

The largest collection of sea-level data from Hokkaido is derived from studies on the northern tip of Hokkaido. This area encompasses the Sarubetsu Lowlands (Ohira, 1995; Ohira and Umitsu, 1996, 1999) on the north-west coastline, Rebun Island (Kumano *et al.*, 1990a; Akamatsu *et al.*, 1997), Kutonebetsu River Lowland (Ohira, 2000), and Kutcharo Lake (Kumano *et al*., 1990a). Peat is the most commonly dated terrestrial material, and is sometimes accompanied by a detailed biostratigraphical plot which improves the environmental interpretation substantially. *Classostrea gigas* is the often used for marine limiting dates, however the limited textual description of the material makes the assertion of *in situ* deposits problematic.

The Sarubetsu Lowlands record comprises 23 sea-level index points quantifiably related to a past tide level (15 are secondary index points). The large number of data points from this region clearly suggests that MTL was higher than present during the mid- and late-Holocene. This is the only site from Hokkaido to indicate clear evidence for such a pattern. There is a degree of scatter in the index points but MTL appears to have fallen by 2-5 m since *c*. 4,000 cal. yr BP in this region.

The final site analysed is from Tokachi in the south-east of Hokkaido. Here, a relatively limited number of index points provide useful constraints on the early Holocene rise in RSL, with MTL reaching close to present at *c*. 6,000 cal. yr BP, as elsewhere in the region. There are few data points from this point onwards but those that exist suggest little change in MTL.

The data from Tokachi is obtained from two previous studies; Fujimoto *et al*. (2003) and Ohira (2004) who undertook litho- and biostratigraphical analysis on the sediments of the Lower Tokachi River Plain. The samples, which encompass the last 9000 years, show RSL at approximately 20 m below present during the early Holocene. Sea levels stabilised during the mid-Holocene. The record comprises five sea-level index points quantifiably related to a past tide level and one secondary index point. Due to the nature of the material dated, the rest of the RSL history is based on limiting dates only. Six undifferentiated peat samples date from the middle-Holocene period, with a further eight marine limiting dates and three freshwater dates constraining sea level during the mid- to late Holocene.

This compilation of Holocene RSL data from Hokkaido challenges what has previously been reported and what might be expected given the patterns of recent land motions inferred from various geodetic data.

As noted in Chapter Two, there is widespread evidence in Japan for RSL reaching a mid-Holocene highstand and then decreasing to present, including a prominent fall at *c*. 3,000-1,500 cal. yr BP known as the Yayoi regression (Ota *et al.*, 1990). Previous Holocene RSL studies in Hokkaido have noted the presence of undated low terraces that surround Akkeshi-ko and Furen-ko that Atwater *et al*. (2004) note may correspond to a higher than present mid-Holocene level proposed by Maeda *et al*. (1992; 1994). The latter authors suggest that RSL fell gradually in the east of Hokkaido towards the tip of the Nemuro Peninsula and invoke variations in hydro-isostatic loading as the cause. Maeda *et al*. (1992) also note that RSL has changed little during the mid-and late-Holocene and conclude that vertical crustal displacement associated with the subduction of the Pacific plate seems not to have been accumulated on a timescale of 10^3-10^4 years.. This latter conclusion is supported by the analysis presented here although I am unable to identify a systematic north-south gradient to the RSL data from Hokkaido.

I explained in Chapter Three that GIA modelling provides a potentially useful means to isolate the contribution of seismic and non-seismic processes, on the grounds that the current generation of models are unable to account for seismic processes. Therefore, assuming that their predictions are reasonably reliable, differences between these and direct observations from Hokkaido might provide a measure of net vertical displacement due to seismic processes.

In Figure 6.13 I compare the GIA model predictions provided by Dr Glenn Milne (*pers. comm.*) with the observations from the six field study areas in Hokkaido. The model predictions vary little across this relatively small area and in all cases they predict MTL rising swiftly during the early Holocene to reach close to present *c*. 8,000 cal. yr BP and

then a small highstand (maximum of + 3 m above present MTL) before falling gradually to present. The predicted highstand is slightly smaller in the north of the study area compared to more southerly sites.

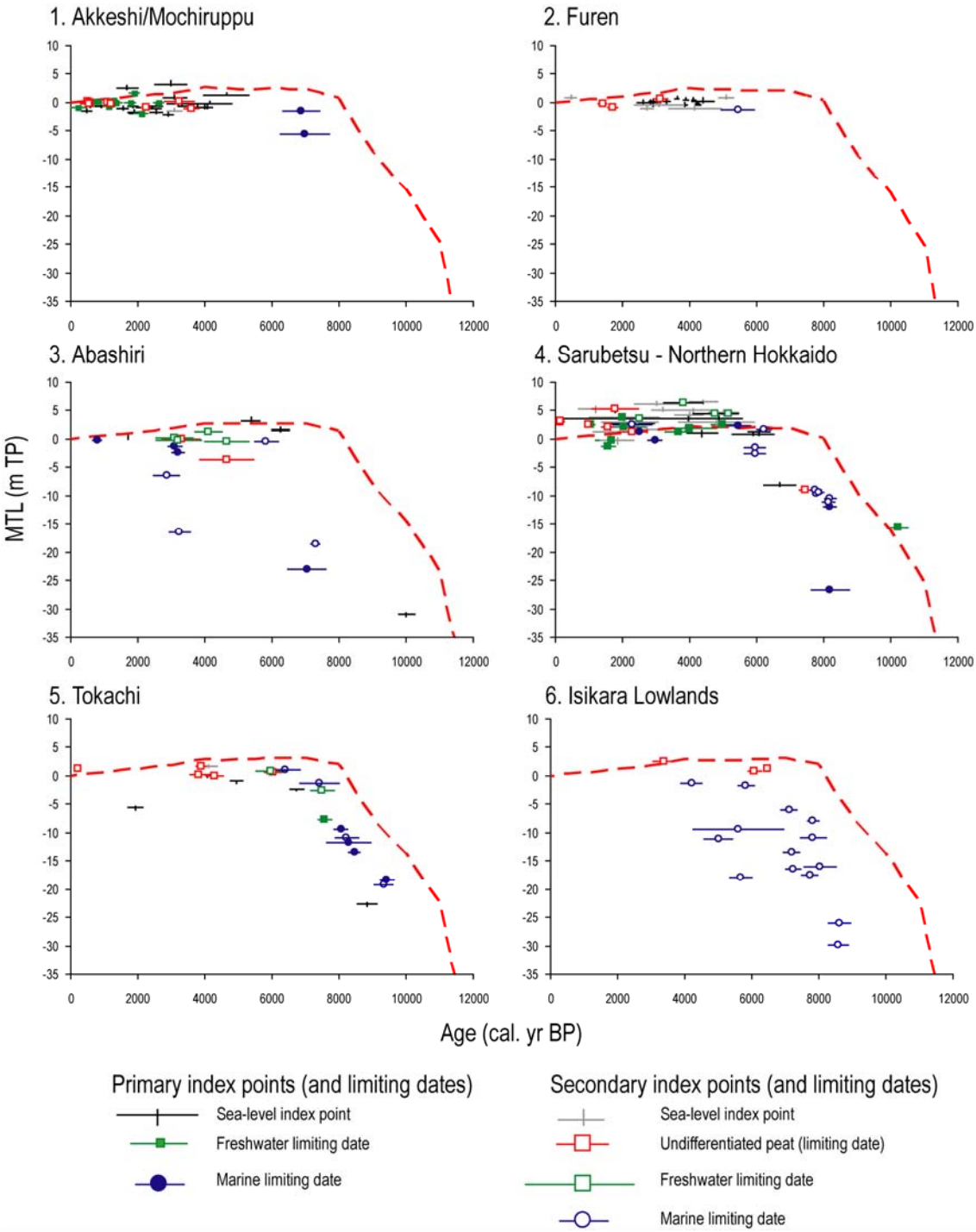

Figure 6.14 Holocene sea-level index points from the six study areas in Hokkaido, with GIA model prediction (G. Milne, *pers. comm.*). The dashed red line is the GIA model prediction.

The model predictions provide a reasonably good match to the RSL observations, although in all cases except for Sarubetsu the predictions plot 1-2 m above the observations during the mid- and late-Holocene. I use only a single model prediction and it was beyond the

scope of this study to conduct sensitivity analyses to assess model variability as a function of changing the parameters used to model the earth parameters, or the ice equivalent eustatic function. Research elsewhere (e.g. Milne *et al.*, 2005) indicates that the envelope of predictions would easily encompass the majority of the data here. For this reason, although this is an interesting exercise in demonstrating no significant mis-matches between observations and predictions and thus limited net deformation due to non-seismic processes, it is sensible not to over-interpret the differences observed.

Using the most detailed sites of Akkeshi/Mochiruppu and Sarubetsu (northern Hokkaido), I am able to evaluate in detail the local tectonic effect during the early to mid-Holocene by comparison between observations and predictions of sea-level variations (Figure 6.15). The interplay of isostatic contribution and local tectonic effects is important to assess Holocene coastal evolution in Japan, and help reconcile the recent trends presented in this thesis in the context of changes over the last few thousand years. The late-Holocene record at Akkeshi/Mochiruppu shows a relatively stable period of sea-level change over the past 4,000 years. Using just the primary index points (in black), it is evident that sea level has remained below present for most of the late Holocene. There appears to be distinct deviations from this trend at *c*. 500, 1,800 and 3,000 years BP, where sea level was much higher than present (up to 3 m at *c*. 1,800 years). However the freshwater limiting dates which typically plot above the validated sea-level index points provide evidence for repeated emergence events in the mid- to late-Holocene, which is supported in the field by sequences of clastic deposits overlain with freshwater peat deposits (Sawai, 2001; Kelsey *et al.*, 2002; Sawai *et al.*, 2002; Sawai *et al.*, 2004a; Sawai *et al.*, 2004b). Despite these emergence events, the net movement over the late Holocene seems to be relatively stable. The sea-level index points do not seem to follow the GIA model predictions, with considerable net offset noted for the mid-Holocene. A number of reasons could account for this, not least inaccuracies in the Earth and ice model used, however the discrepancy could be attributable to tectonic subsidence. The stability of the sea-level records over the Holocene period is in broad agreement with the salt marsh reconstructed RSL over the past 200 years (see 'close to trench' in Figure 6.1). There does appear to be a distinct period of a fall and rise in sea level recorded in both Mochiruppu records from the 1970s onwards, however such a short-lived interseismic change would not be discernable in the longer Holocene record presented in Figure 6.15.

The data for Northern Hokkaido (Sarubetsu) is of much poorer quality. The majority of the data comprises secondary index points. Although there is considerable scatter in the data, there appears to be relative stability in the sea-level index points, which typically plot *c*. 2 m above present for the late Holocene. In comparison to the Akkeshi/Mochiruppu data which shows evidence for emergence events, the Sarubetsu data shows no such pattern. The

freshwater limiting dates are typically within the scatter of the index points. Compared to research in Northern Europe and North America which routinely applies the consistent methods developed during IGCP projects to extract accurate sea-level index points from different palaeo-coastal environments to constrain Holocene sea-levels, research in Japan is in its infancy. The result of this is data of variable quality. However, since the majority of the data plots above the GIA model prediction, it is likely that there has been some degree of tectonic uplift. The stability of the sea-level records over the Holocene period is seen also in the salt marsh reconstructed RSL over the interseismic period (see 'far north' in Figure 6.1). Although there has been some variability, the record from Sarfutsu-toh (in red) remains remarkably stable, reflecting its distal position from the Kuril Trench.

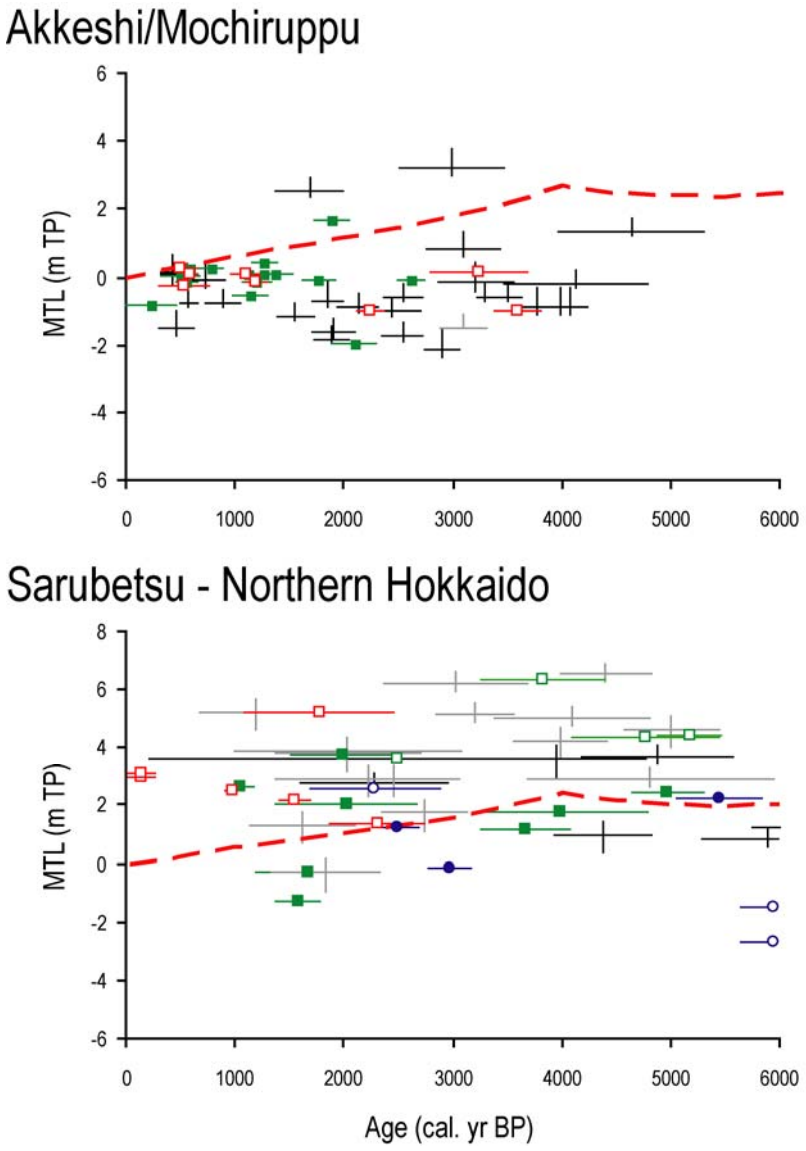

Figure 6.15 Holocene sea-level index points from Akkeshi/Mochiruppu and Sarubetsu, with GIA model prediction (G. Milne, *pers. comm.*). The dashed red line is the GIA model prediction. See Figures 6.13 and 6.14 for sea-level index points key.

6.5 PLEISTOCENE RSL RECORDS FROM HOKKAIDO

A critical question for geomorphologists remains how the short-term interseismic motion reported above translates into long-term permanent deformation that generates topographic relief. The general distribution of the Pleistocene marine terraces in Hokkaido is described in Chapter Two. As mapped by Okumura (1996), the shorelines along the Okhotsk Sea are generally parallel to each other, showing no significant north to south tilt other than the two narrow (30-40 km) zones of significant net uplift around Abashiri and the Shiretoko Peninsula that are separated by the subsiding Shari plain (Figure 6.16) (Okumura, 1996).

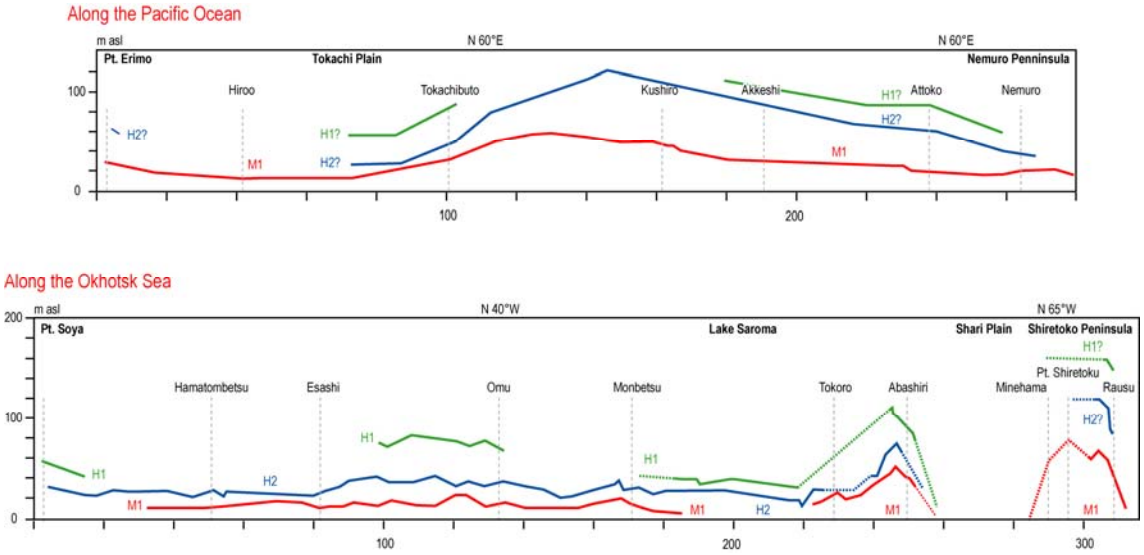

Figure 6.16 The elevation of the three main Late Pleistocene marine terraces identified in north-east Hokkaido plotted by coast (from Okumura, 1996).

The broadly parallel nature of the raised terraces provides evidence of long-term net uplift. No differential uplift other than that referred to around Abashiri and the Shiretoko Peninsula is observed over Pleistocene timescales. Along the Pacific coast of Hokkaido the pattern is more varied and there is a broad upward doming of the M1 and H2 shorelines between Tockachibuto and Akkeshi, with shorelines deformed upwards by 20-80 m compared to regions to the south and north. Okumura (1996) suggests that the deformation in Abashiri represents an uplifted zone with a North-South axis, whilst ridge uplift is also apparent for the Shiretoko Peninsula. These two uplifting zones are interpreted as the south-western part of active echelon ridges in the Kurile inner arc region. I replot the Okumura (1996) marine terrace data below in Figure 6.17.

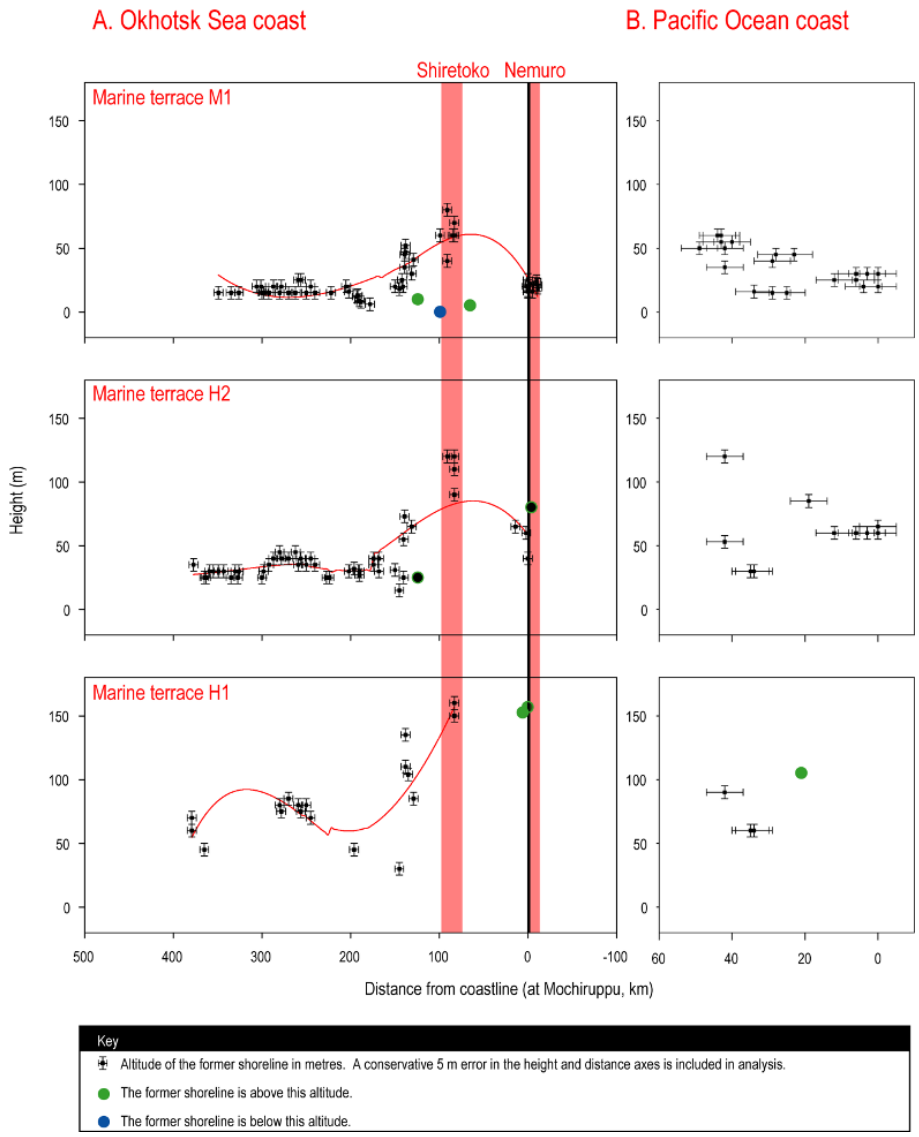

Figure 6.17 The elevation of the three main Late Pleistocene marine terraces identified in north-east Hokkaido plotted against distance from the coastline at Mochiruppu (from Okumura, 1996).

The terraces mapped by Okumura (1996) can be used to infer rates of crustal rebound once they are corrected for the changes in eustatic sea level since their formation (see Section 3.3.1) and assuming that rates of uplift have remained constant through time (Pirazzoli, 2005). I recognise that this calculation is a simplification, since it excludes the possible effects of GIA movements during the interval, changes in the gravity field and possible temporal variations in uplift.

The lowest coastal terrace in the study area is found at elevations of between 6 m and 80 m above present sea level. In Figure 6.18, I plot rates of uplift for the MIS 5e marine shoreline, correcting the original field elevations for the estimated value of eustatic sea-level at the time of formation. Uplift rates range between 0.1 mm per yr towards the

northern tip of Hokkaido to 0.6 mm yr centred on the Shiretoku Peninsula (at around 100 km from the coastline).

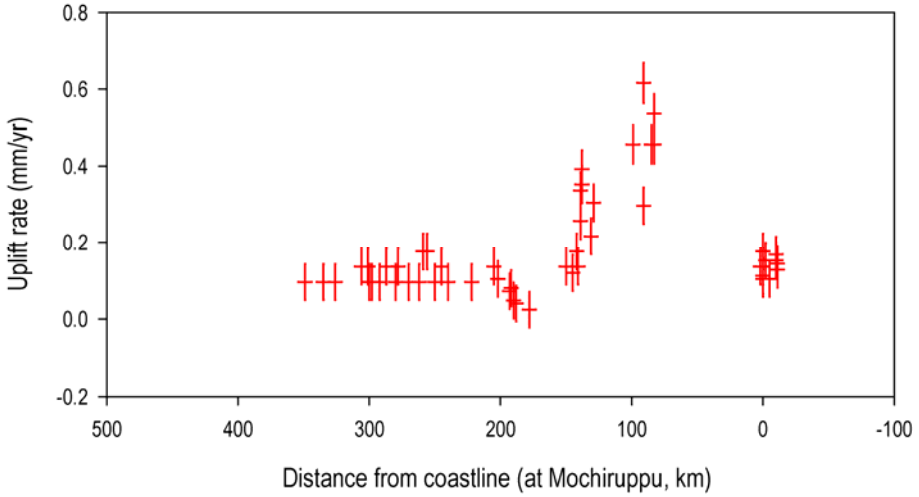

Figure 6.18 Uplift rate (and variance) for MIS 5e interglacial terrace identified in north-east Hokkaido plotted against distance from the coastline at Mochiruppu (from Okumura, 1996), with uplift calculations after Lambeck *et al*. (2004).

The horizontal wavelength of the deformation (Figure 6.17) suggests flexural bending, which may be related to volcanic loading, sediment loading (especially by the Sea of Okhotsk), or due to stresses related to subduction (which have on shorter timescales been discussed previously). Volcanic loading (Hieronymus and Bercovici, 1999; 2000) describes the process whereby magma flow feeds volcanic growth and leads to flexure caused by volcanic loads on the underlying plate. Volcanic loading should principally result in downwarping of the plate (near the volcano) and slight uplift at the flexural bulge (a ring around the volcano some 100-200km from the volcano centre).

The area of maximum deformation (correlating to uplift rates of 0.6 mm per yr) along the Hokkaido coastline correlates with an active volcanic chain that runs as an arc along the Kuril Islands and then through the Hokkaido and Honshu land masses (Figure 6.18). Many of these volcanoes are of Quaternary age (Nakano *et al.*, 2001) and their formation has caused significant regional deformation, which will have affected the elevation of the Pleistocene shorelines considered here (Figure 6.18). There are particular processes associated with active volcanoes that may influence the rates of long-term uplift in this part of the study area. Between eruptions volcanoes inflate as a result of magma ascent and refilling of the volcanic plumbing system and reservoirs. For example, observations from GPS, electro-optical distant measurements, satellite synthetic radar and levelling suggest that inflationary phases over the past 15 years have controlled vertical deformation of Mount Etna, Italy (Bonaccorso *et al*., 2005). Such inflationary behaviour could, depending on the time between eruptions, be sustained for tens, hundreds or thousands of years but

would reduce after an eruption as the height of the volcano decreases rapidly. Geological investigations indicate that there have been several major eruptions of the Shiretoko volcanoes in the last few thousand years (e.g. Naomichi, 2000) and over the course of the Pleistocene (Nakano *et al.*, 2001), but a direct link between long-term volcanic activity and deformation of the marine terraces has not previously been made.

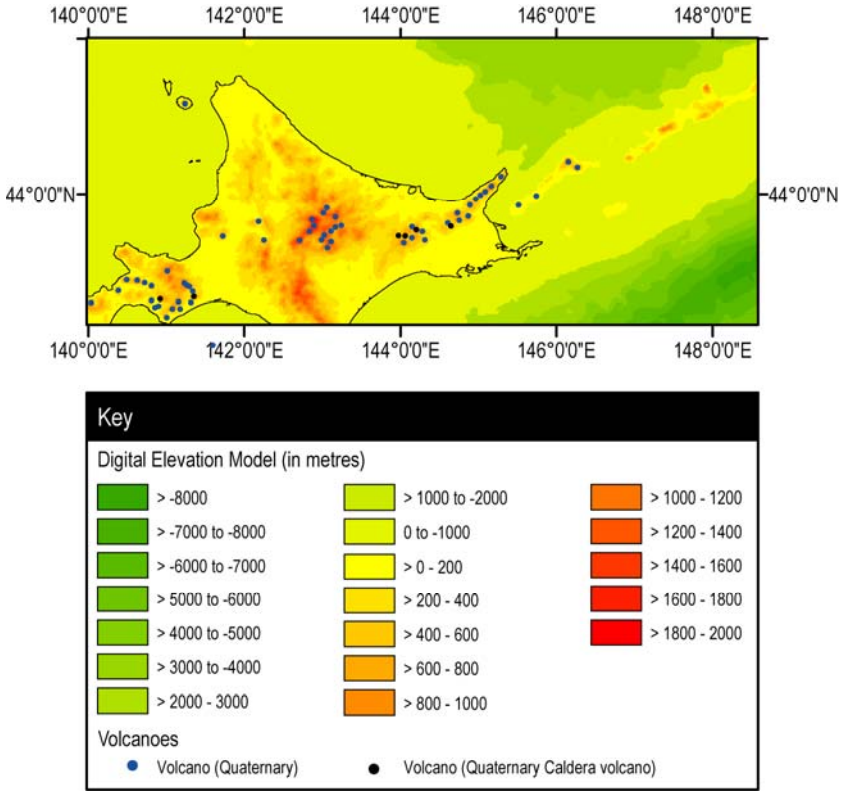

Figure 6.19 Quaternary volcanoes of north-east Hokkaido. Elevation data overlain with volcanoes active during the Quaternary (from Quaternary Volcanoes in Japan, Geological Survey of Japan; accessible via http://riodb02.ibase.aist.go.jp/strata/VOL_JP/EN/index.htm)

In summary, the Late Pleistocene marine terraces of Hokkaido record long-term uplift and RSL fall. The uplift pattern is generally uniform with the exception of two narrow uplift zones on the Okhotsk coast and a wider doming on the north Pacific coast. It is reasonable to hypothesise that these deformations are associated with tectonic activity, including the development of extensive Pleistocene volcanism in these regions. This activity is connected to the overall process of plate subduction but requires considering alongside other regional-scale deformation patterns that may accompany individual earthquake cycles.

6.6 RATES OF RSL CHANGE IN HOKKAIDO OVER DIFFERENT TIMESCALES

The various datasets discussed above provide complementary but sometimes conflicting evidence for RSL change over different timescales. It is important to pull these different strands of research together to determine whether or not the differences in time and over space can be explained, starting with the modern data and moving on to consider progressively longer time series.

All of the short-term geodetic data agree in identifying subsidence on the Pacific coast of north Hokkaido. The absolute rates determined by GPS data are *c*. -2 mm to – 4 mm ± 2 mm yr (Aoki and Scholz, 2003). My analysis of selected GPS data confirms this trend. Long-term insights into land motions are provided by the 30 yr analysis of selected tide gauge stations from Hokkaido. These also record higher rates of RSL rise in Pacific coast stations compared with records from further to the north. The salt-marsh reconstructions from Mochiruppu, the site closest to this area of subsidence, also record RSL rise since the early 1980s, indicating agreement between various direct and proxy reconstructions.

General agreement between direct measures of land and sea-level motions is also seen on the Okhotsk coast during the last few decades, with GPS and tide-gauge data indicating little spatial variability north of the Shiretoko Peninsula. Salt-marsh RSL reconstructions from Tohoro and Furen-ko differ over the last 20 years, possibly because of poor matching analogues in these younger samples as well as difficulties in developing a robust age model using ^{210}Pb and ^{137}Cs from each site.

Over the longer interval of the 20th Century, divergence between direct observations and RSL reconstructions is evident. Thus, although the repeat levelling and tide-gauge records from Kushiro and Hanasaki suggest subsidence in this interval, with the former suggesting 30-40 cm during the period 1905-1955 alone (Yokoyama, 1987), the salt-marsh RSL reconstructions suggest that RSL was actually falling or stable during this same general interval. However, it is important to note that the vertical errors in the salt-marsh reconstructions are rather large (± 0.30 m) and at the four southerly sites (at least) the variability in RSL during the 20th century could all be interpreted as falling within the errors of the reconstructions (i.e. implying that RSL changed little overall during this interval).

Extending back in time further into the pre-observation interval between 1900 and 1700, the salt-marsh reconstructions suggest that RSL was stable throughout this interval (Figure 6.1). The one clear difference between sites is the observation that data from Sarfutsu-toh

and Tofutsu-ko plot higher than the rest of the data, suggesting some net uplift in these areas (0.2 m and 0.6 m respectively).

The Holocene RSL data also show a stable trend in all time series during the last 6,000 to 4,000 cal. yrs. With the exception of the Sarubetsu dataset, all the remaining five records depict negligible (< 1 m) RSL change in this interval (Figure 6.13). One GIA model examined here predicts a slight Holocene highstand in Hokkaido, in-line with previous modelling experiments (Maeda *et al.*, 1992) and attributable to hydro-isostatic loading. The model prediction is in close agreement with the RSL observations, when appropriate uncertainties in the model are considered. No sites record net RSL rise during the Holocene, discounting the possibility of persistent net subsidence along the Pacific coast. Even the data from Abashiri, which one might expect to be elevated relative to the other time series because of its proximity to a Pleistocene uplift zone, agrees with the other data presented.

Finally, the Pleistocene terrace data suggest that the major variations in deformation are likely associated with volcanism and mountain building, certainly along the Okhotsk coast and potentially also along the northern Pacific coast. These deviations aside, the general pattern is one of remarkably similar long-term net uplift for the remaining regions of Hokkaido, irrespective of distance to the trench.

To summarise, data over different timescales regarding rates of RSL change do not reveal the strong spatial gradients that were expected at the outset of this research. The subsidence observed presently on the Pacific coast is shown to be a recent phenomenon that cannot have been sustained over century, millennial or glacial-interglacial cycles. Elsewhere, long-term uplift of the Abashiri region over Pleistocene timescales is not obviously correlated to patterns during the current interseismic period, nor over Holocene timescales. The pattern that emerges from this analysis is that there is little or no evidence for the accumulation of differential strain over either short (century-scale) or long (millennial/glacial-interglacial) timescales other than that likely associated with the thrusting beneath the Abashiri tectonic line (Okumura, 1996).

6.6.1 Land motions during the interseismic period in Hokkaido

A key focus of this study has been to examine in detail the patterns of land motions during the current interseismic period. The currently favoured model for the most recent earthquake cycle, as advocated by Sawai *et al*. (2004b), Atwater *et al*. (2004) and Kelsey *et al*. (2006) is based on analyses at Akkeshi-ko and other nearby sites in north-east Hokkaido is as follows:

- *Stage 1:* A pre-seismic rise in RSL of about 1 m in the decades to centuries before a plate-boundary earthquake.

- *Stage 2:* A large earthquake on the Kuril subduction zone at *c*. 1650, which may or may not have caused coseismic deformation. The earthquake generated a large tsunami.

- *Stage 3:* Rapid, aseismic slip and postseismic uplift (RSL fall) of at least 1 m but less than 2 m, complete within 30 years of the earthquake.

- *Stage 4:* Interseismic subsidence (RSL rise), as indicated by 20th century geodetic data (tide gauge, GPS and repeat levelling), as well as ghost forests surrounding wetlands at Onnetoh and Akkeshi-ko.

These authors argue that this four-stage model is able to resolve the often discussed mismatch between long-term uplift recorded by the Pleistocene marine terraces and chronic 20th century subsidence.

I note in Chapter Two that there have been limited palaeoecological investigations through complete earthquake cycles in Hokkaido. It is not certain, therefore, whether the model outlined above is typical of previous cycles. The one investigation completed to date, that of Sawai *et al*. (2004a), demonstrates that although coseismic (or postseismic) uplift has occurred on at least four occasions in the last 4,500 cal. yrs, the direction of land motions and associated changes in RSL during the intervening interseismic intervals is highly varied. There is evidence for falling, rising and stable RSL occurring during different cycles (including the present). This variability raises questions regarding the significance of the currently observed interseismic subsidence experienced on the Pacific coast.

The various lines of direct and proxy time series detailed earlier in this thesis demonstrate that the presently observed subsidence on the Pacific coast cannot have been a persistent feature of the current or previous interseismic periods. The evidence for this is as follows:

I. The Pleistocene marine terraces along the Pacific coast, between Kushiro and Nemuro, decline northwards. This shows that there has been long-term uplift of this coast, which is near to its maximum in the vicinity of the Kushiro tide gauge.

II. The Holocene RSL data from the Pacific coast sites studied here (the Isikara Lowlands, Akkeshi-ko/Mochiruppu and Furen-ko) all show stable RSL during the

late Holocene from *c*. 5,000-4,000 cal. yr BP onwards. The quoted rates of subsidence for the region during the 20th century are >0.5 m and, were they to be sustained over any length of time, they would rapidly exceed any inferred postseismic uplift and cause net submergence and RSL rise over millennial timescales.

III. The foraminiferal-based trends in RSL during the last 100-300 years show no evidence for net subsidence during this interval. The apparently stable RSL during this interval probably records a slight uplift to counteract the rise in 20th century eustatic sea-level.

From this discussion it is clear that the existing four-stage model of the Hokkaido earthquake deformation cycle requires revision.

A characteristic of the earthquake deformation cycle recorded elsewhere in the Pacific Northwest and Alaska is that although there are short-tem periods of rapid pre- or post-seismic RSL change, during the remaining interseismic interval rates of RSL change are broadly constant. The results presented in this thesis show that this is clearly not the case in Hokkaido. Thus, the repeat levelling survey data during the 20th century detailed by Yokoyama (1987) indicates a change in the rate of 20th century subsidence on the north Pacific coast as well as variations in the spatial pattern to this subsidence. Moreover, the foraminiferal-based RSL reconstructions presented here also indicate that the last 100 to 300 years has seen periods of faster and slower RSL change that are unlikely to be solely the product of global changes in eustatic sea-level.

In reflecting on the implications of the above, there are several critical points worth highlighting.

I. Firstly, it is highly unlikely that there is a single, repeatable, Hokkaido earthquake deformation cycle. The existing data indicate that previous cycles vary in duration (Sawai and Nasu, 2005; Sawai *et al.*, 2009) and vary in their associated patterns of land- and sea-level movements (Sawai *et al.*, 2004a).

II. Secondly, short-term geodetic data should be treated with care when being used to infer patterns over several decades or centuries. The work presented here, and that evident from repeat levelling surveys (Yokoyama, 1987), clearly shows that current deformation patterns may have been different in the past and are likely to be different in the future.

III. Thirdly, much of our understanding regarding the plate-boundary earthquakes of Hokkaido is based on detailed analysis of a number of marshes located on or close to the Pacific coast. There are no comparable studies to the north of Onnetoh (near Furen-ko) that can provide complementary information regarding patterns of RSL change during the events described thus far. This is a significant weakness to present knowledge since it is not known at present whether emergence events also affected areas to the north of the Abashiri region. This is important when considering the widespread extent of the raised Pleistocene marine terraces across this region.

IV. Fourthly, it is important that we do not ignore some of the larger-scale geomorphological features of Hokkaido and their potential impact on patterns of land deformation and RSL change over different time scales. In particular, Hokkaido is crossed by a significant chain of volcanoes, many of which have developed during the Quaternary. For example, the 20x26 km Kutcharo caldera, one of the largest calderas in north-east Hokkaido, formed as a result of a series of major eruptions between 340-30 ka. Some of the volcanoes, such as the stratovolcano Shari-Dake, located to the south of Furen-ko (Figure 6.20) are over 1,500 m high and have caused significant deformation since their formation between 0.9-0.5 Ma (Nakano *et al.*, 2001). No work to date has explored the potential for regional-scale deformation, such as that observed by the Pleistocene marine terraces associated with this wide area of significant volcanic activity.

Figure 6.20 The 1,500 m high Shari-Dake volcano of north-east Hokkaido.

6.7 CONCLUSIONS

This Chapter has examined the evidence for RSL changes over different timescales, from the very recent to the Late Pleistocene, in order to examine the evidence for RSL changes in Hokkaido. The emphasis has been on integrating evidence across timescales, with a particular focus on learning what lessons can be drawn from the exercise regarding the patterns of RSL changes during the current (and previous) interseismic period(s). My main conclusions are:

- I compare within and between site variability in reconstructed RSL since AD 1700 using a foraminiferal-based transfer function. A degree of within-site variability is apparent when attempting detailed comparisons between two records from Mochiruppu, although there is broad agreement in the overall trends especially when age and height errors are considered. Comparison with available long tide-gauge records confirm that RSL has risen sharply since the mid-1970s but there is poor agreement between these records before this date.
- Inter-site trends in RSL change during the last 300 years reveal only a small net change in RSL during this interval; long-term subsidence on the Pacific coast is not observed. Two sites to the north of Abashiri record RSL fall of between 0.2 m and 0.6 m.
- Tide-gauge records and repeat levelling data demonstrate that subsidence has occurred in the Pacific coast region during much of the 20th century, although rates and spatial patterns of change have varied. Recent submergence is confirmed by published GPS data of between -1 to -4 mm ± 2 mm along the Pacific coast, with slight uplift recorded across much of north-east Hokkaido.
- A review of Holocene sea-level trends from six regions indicates that there is little variability between records. Most record a rapid rise in RSL which reached close to present by 6,000 cal. yr BP before changing little to the present. Only at the most northerly site is there evidence for a mid-Holocene RSL highstand of between 1 to 3 m. Comparisons with a single GIA model prediction indicates good agreement between observations and model predictions, suggesting little net deformation over mid- to late-Holocene timescales.
- Pleistocene raised marine terrace data demonstrate long-term net uplift of most of the Pacific and Okhotsk Sea coasts. These terraces are locally deformed, notable in two narrow uplift zones close to Abashiri and also along the Pacific coast around Kushiro where terraces of mid-Pleistocene age occur at over 110 m above present sea level. These differences in elevation suggest that large-scale deformation

processes associated with the development of the north-east Hokkaido volcanic chain are likely to be significant influences on raised beach elevations.

- The Chapter finishes by exploring the spatial and temporal variability in RSL across the study area and reflecting on the implications of these patterns for existing models of the earthquake deformation cycle in Hokkaido. The key points to emerge from this analysis are that the recent chronic subsidence of the Pacific coast of Hokkaido is not typical of the current interseismic period, and that there is likely to be no 'typical' Hokkaido earthquake deformation cycle and that greater attention should be paid to the causes of regional scale deformation of the entire north-east of Hokkaido.

CHAPTER SEVEN

Conclusions

This chapter provides a summary of the main findings of the thesis. It is structured to mirror the main objectives of the research and highlights lessons learnt from the work and identifying areas for future research.

7.1 CONTEMPORARY FORAMINIFERA AND RSL IN HOKKAIDO

Yuki Sawai and colleagues have pioneered the application of micro- and macrofossil-techniques to reconstruct past RSL change in Hokkaido, mainly through the analysis of diatom and plant macrofossils. Apart from the preliminary investigations by Scott *et al*. (1995), no systematic analysis of the salt-marsh foraminifera of Hokkaido had been undertaken prior to the research presented here.

The contemporary salt-marsh and freshwater-swamp environments of Hokkaido are varied, reflecting differences in site configuration with respect to the open coast as well as freshwater discharge from terrestrial sources. An advantage of the study area over other regions studied for earthquake reconstruction (e.g. the Turnagain Arm, Alaska; Hamilton *et al.* 2005; Hawkes *et al*., 2005) is that the region is generally micro-tidal.

Foraminiferal assemblages were collected from the intertidal zone of five salt marshes of Hokkaido, and the subtidal environments of one. Statistical analyses indicate that the foraminiferal distributions for this region are controlled predominantly by elevation (water depth). Furthermore, the contemporary foraminiferal assemblages broadly reflect vertical floral zones based on vascular plants. Cluster analysis, supplemented with DCA, separates foraminiferal assemblages into a maximum of three zones but the elevation of these zones often differs and overlaps. At or above MHHW a high-marsh zone is evident on Hokkaido, consisting of differing abundances of *J. macrescens*, *B. pseudomacrescens* and *Haplophragmoides* species. A low marsh/tidal flat zone dominated by *Ammobaculites* species and *Miliammina fusca* is present around MLLW and an additional subtidal zone

dominated by *P. stoeni, T. hadai* and to a lesser degree *C. canariensis* was observed at Akkeshi-ko. The elevational ranges of the faunal zones are employed to identify the vertical relationship of the local environment in which the assemblage accumulated to a reference tide level.

The statistically significant relationship between elevation and the foraminiferal data was used to develop foraminiferal-based transfer functions using weighted averaging calibration and regression. A regional dataset, consisting of 95 contemporary foraminiferal samples and associated tide-level information, was compiled by combining data from all intertidal study areas. To facilitate comparisons between study areas with different tidal ranges the elevational data are expressed as a SWLI. I have explored various transfer-function models, modifying the contemporary training set to choose the optimum model for reconstruction. The foraminiferal distributions from each model show a strong and highly statistically significant relationship with SWLI (r^2 = 0.75; 'Pruned B' model). Statistical measures assessing the performance of this model suggest that reliable reconstructions of former sea levels are possible (RMSEP = 33 SWLI units). Each of the four models resulted in broadly similar reconstructions but I focus on the 'Pruned B' model which adopts a judicious approach with regard to minimising the removal of taxa and species from the contemporary training set.

7.2 RECONSTRUCTING CHANGE IN RSL IN THE CURRENT INTERSEISMIC PERIOD

Previous work in north-east Hokkaido has focussed on the coseismic and postseismic phase in sites located on or close to the Pacific coast (Atwater *et al.*, 2004; Sawai *et al.*, 2004b). However, prior to this study only limited research has been undertaken to understand RSL changes during the remainder of the current interseismic period. Existing models proposed by the above authors suggest that this interval is characterised by subsidence, reflecting in part the fact that the Pacific coast of Hokkaido lies beyond the uplift zone associated with the Kuril Trench.

I have completed the investigation of contemporary salt-marsh environments and stratigraphic investigations at six field sites, analysing shallow sample cores from five of them. In most instances, contemporary and fossil foraminiferal preservation was good and enabled the development and application of a transfer function to reconstruct past changes in RSL. I have developed, for the first time, age models for the Hokkaido fossil sequences using ^{210}Pb and ^{137}Cs. The method did not provide uniformly consistent results; at some sites the resulting age models are robust with good agreement between the two dating

methods, but more commonly the ^{210}Pb and ^{137}Cs age models differ. This suggests that there has been some post-depositional migration of radionuclides in the sediment sequences.

Despite these dating problems, I have reconstructed RSL change at each site during the last 300 years. The resulting records show that there is limited net change in RSL during the current interseismic period, that rates of RSL change vary in time and space during the current interseismic period, and that chronic subsidence observed in parts of the 20th century by tide-gauge and other geodetic data are not typical of the last 300 years. Although there are few microfossil-based studies of previous full earthquake cycles, those that do exist suggest highly varied patterns of RSL during the interseismic period between large plate-boundary earthquakes (Sawai *et al.*, 2004a).

7.3 COMPARISONS WITH OTHER TIMESCALES

An important part of this thesis is to compare rates of RSL change during the last few centuries with data obtained from recent geodetic observations (tide gauge, repeat levelling and GPS survey) as well as with Holocene and Pleistocene RSL records.

The most recent GPS data indicate rapid RSL rise on the Pacific coast, also supported by tide-gauge records. These are in agreement with the salt-marsh reconstructions from Mochiruppu during the last 20 years or so. Ghost forests at sites further north, at Furen-ko and Onnetoh, suggest recent submergence in these areas too, but this is not supported by recent RSL reconstructions using salt marsh or other methods from the former site, which show essentially stable RSL during the 20th century.

During the 20th century, repeat levelling data indicate a broad north to south increase in subsidence rates, with contours running approximately east-west across Hokkaido (Yokoyama, 1987). Although the observations are not continuous, they nevertheless show that rates of subsidence have varied during the 20th century; notably at sites close to the Pacific coast. My salt-marsh RSL reconstructions do not agree with these longer 20th century patterns. In particular, records from Mochiruppu and Furen-ko suggest that RSL fell during the early to middle part of the 20th century by *c*. 0.4 ± 0.20 m.

The salt-marsh reconstructions from the last 300 years indicate that RSL has fallen in the north of Hokkaido compared to the south. At Tofutsu-ko, reconstructed RSL is *c*. 0.6 m higher than the other records prior to *c*. AD 1920. This may reflect local uplift of this site relative to the areas to the south. However, this case aside, the dating uncertainties in the

salt-marsh reconstructions mean that it is not possible to resolve the effects of individual, decimetre-scale land motions associated with individual earthquakes observed during the historical period.

I have analysed tide-gauge data from Hokkaido, focusing on trends during the 28 year interval between 1978-2007 when the most continuous records are available. These data have been corrected for changes in atmospheric pressure, seasonal and oceanographic factors in addition to GIA and eustatic changes and show that stations closest to the trench (Kushiro and Hanasaki) experience the most subsidence. All the other sites apart from Wakkanai on the northern tip are showing tectonic uplift during this period. However, isolating tectonic signals within the tidal data proved problematic owing to the dominance of the eustatic correction.

A new database of Holocene sea-level index points provides, for the first time, validated constraints for the long-term RSL changes across Hokkaido. The screening process indicates that many of the existing 450 radiocarbon dates from Hokkaido have a weak vertical relationship to former sea level, mainly because of a lack of detailed levelling or supporting biostratigraphy. The screened database contains 198 dates and indicates that in most sites RSL has been stable during the last several thousand years, in-line with GIA model predictions for the region. Only the north of Hokkaido provides evidence for a 1 to 3 m mid-Holocene highstand.

A review of previous research on Pleistocene RSL data from Hokkaido provides long-term context for the current investigation. Raised marine terraces occur at elevations in excess of 100 m above sea level, but there are notable spatial variations in their elevation (and preservation). In particular, along the Okhotsk coast the older shorelines are deformed by two narrow zones of uplift (Tokoro-Abashiri and the Shiretoko Peninsula) separated by the subsiding Shari Plain where Pleistocene terraces are lacking, presumably below present. To the north of this area, terrace elevations are broadly horizontal and point to uniform regional uplift. The Tokoro-Abashiri uplift zone coincides with the location of one of my salt-marsh sites, Tofutsu-ko, which, as noted above, has a higher reconstructed RSL than any other site in the study area, suggesting that this recent uplift may be part of a longer-term trend.

Along the Pacific coast, the Pleistocene shorelines decrease in elevation northwards from *c*. 100 m at Akkeshi to *c*. 20 m on the tip of the Nemuro Peninsula. This trend is opposite to that suggested by the recent GPS, tide-gauge and repeat-levelling data (which shows maximum subsidence in the south, decreasing northwards) and provides further evidence

that the recent subsidence here cannot be a persistent feature of the Late Pleistocene or indeed the Holocene.

7.4 IMPLICATIONS FOR MODELS OF RSL CHANGE IN HOKKAIDO

Existing models of RSL change in Hokkaido require revision. Specifically, the model developed by Sawai *et al* (2004b) and Atwater *et al*. (2004) assumes that short-lived postseismic uplift due to aseismic slip is followed by interseismic subsidence. These authors contend that this model provides a way to reconcile the apparent contradiction between 20th century subsidence and Pleistocene and Holocene uplift. This model has been developed from the detailed analysis of the most recent emergence event on the coastal marshes close to or on the Pacific coast of Hokkaido. The model was untested (and remains so) in other sites further north along the Okhotsk Sea coast, although microfossil analyses through older uplift events at Onnetoh suggests that patterns of interseismic RSL change have varied over previous cycles (Sawai *et al.*, 2004a).

The results presented in this thesis demonstrate that short-term 20th century subsidence cannot be a persistent element of the current interseismic period. My salt-marsh RSL reconstructions reveal that there have been little or no net RSL movement during the last 300 years in north-east Hokkaido. Direct and proxy records suggest that patterns of land and RSL motions during the current interseismic period have been varied. Nevertheless, the absence of significant displacement to the Holocene RSL data suggests that there is little if any net strain accumulation across Hokkaido over this timescale.

In contrast, there is substantive evidence for long-term net uplift provided by the flights of raised marine terraces of Pleistocene age that overlook the current Pacific and Okhotsk coasts. These terraces testify to regional scale uplift of a broad nature, with more local-scale deformation in areas most strongly affected by volcanic activity and mountain building during the Late Pleistocene.

It is clear that patterns of RSL change on Hokkaido reflect a variety of processes associated with the subduction of the Pacific by the North American plate. However, it seems probable that they are not all related directly to strain accumulation and release on the plate interface, instead reflecting a combination of different forcing mechanisms that operate over different temporal and spatial scales.

7.5 LIMITATIONS OF THE CURRENT STUDY

There are several important limitations to the current study that provide useful indicators as to where future research might focus in order to address the research questions that remain unanswered regarding RSL change in Hokkaido. I address the most important of these in turn, starting with a reflection on the main focus of the thesis (the salt-marsh work) and then considering the secondary data sources before concluding with some final reflections.

Salt-marsh reconstructions: The use of transfer functions for RSL reconstruction has reinvigorated sea-level research in the last decade (e.g. Horton and Edwards, 2006). However, their use is not always straightforward, as this work has demonstrated. I chose at the outset to develop a regional training set of contemporary samples because I decided that I needed to maximise the range of contemporary environments sampled. I was also aware of the limited time available to conduct the research programme and recognised that developing multiple local training sets would not be possible if I was to explore wider spatial patterns of RSL change. However, recent research elsewhere is beginning to highlight a pressing need to develop local training sets, not least to minimise the complications that arise in converting contemporary microfossil distributions to a common SWLI datum (e.g. Woodroffe and Long, in press). It would beneficial to investigate whether the rather large RMSEP (*c*. 0.30 m) in the 'Pruned B' model might be reduced with a local rather than regional training set. Related to the above is the fact that despite sampling a wide range of environments, I still encountered important matching analogue difficulties including across the critical upper part of several sections analysed. Further close sampling of local environments might assist here.

Study sites: Some of the study sites are clearly influenced by significant freshwater discharge, in addition to potential changes in barrier dynamics (Chapter Three). I assumed here that there have been no changes in palaeotidal range, although this may not be the case given the likelihood of tidal dampening as observed elsewhere (van der Molen, 1997). Likewise, the lithostratigraphy of the sample sites is varied both within and between sites. Although I conducted three field seasons, working closely with support from Dr Sawai and colleagues from the Japanese Geological Survey, there was a limit to the amount of stratigraphic work that could be achieved. This is certainly one area of research that can be improved upon in the future.

Chronologies: The use of ^{210}Pb and ^{137}Cs is a time consuming and laborious task, and was often subject to delays caused by backlogs of samples in the well detectors. As a result, I

was not as flexible as I might have been in my dating strategy. For example, there are three well know visible tephras that I was able to identify in the field, the geochemical analyses of which would significantly contribute to our understanding of Hokkaido's chronology. In addition, although the last 300 years is challenging for radiocarbon dating, research elsewhere has shown that high-precision dating combined with wiggle-match dating and bomb-spike dating (e.g. Marshall *et al.*, 2007) can be successful in developing complementary absolute age models for the last few centuries. Future work should explore the potential of these and other dating methods, such as pollutant records as well as pollen markers. Improved age models might make it possible to identify distinct RSL changes associated with particular earthquakes in the last few centuries, especially if vertical precision is improved.

Duration of the records: The records that I reconstruct are varied in length and this is not ideal; it would have been preferable to sample more continuously throughout the present interseismic period, preferably across the last event itself. The reason for this is that when sampling in the field it was not always obvious where the most recent emergence event was recorded. Much of my sampling work was also collaborative with colleagues from the Japanese Geological Survey and so compromises were made in agreeing what material to be collected and returned to Durham University for analysis. Finally, in some of the cores the microfossils simply were not preserved at depth and this was not apparent until the material had been returned to the laboratory.

Tide-gauge records: The procedures involved in processing the tide-gauge data are complicated and require several steps to remove oceanographic and atmospheric processes. Several of the existing tide-gauge records are suspect, notably the Kushiro station that is likely to have experienced some human-induced subsidence due to sediment compaction as well as mining subsidence. The duration of the short records is often fragmented and so I was required to target a specific time interval to obtain sufficient data to enable consideration of spatial trends. Even so, the number of station records from Hokkaido is small.

Holocene RSL changes: I have discussed in depth the fact that the database of reliable RSL data from Hokkaido is limited, despite the large number of radiocarbon dates collected by previous researchers. In this light, it would be very helpful to construct a small number of detailed Holocene RSL records from selected wetland sites in the region applying well defined methodologies that are now common to the sea-level community. It would be helpful, for example, to fill in the large gap between the most northerly site studied (Sarubetsu) and Abashiri on the Okhotsk coast. Reports of small terraces surrounding the wetlands of the Akkeshi and Furen-ko sites (Atwater *et al.*, 2004) require assessing in order

to determine whether they record a mid-Holocene highstand, which remains inconclusive from the existing Holocene RSL data.

Pleistocene RSL change: The spatial distribution and ages of the Pleistocene terraces provide powerful insights into long-term deformation of the Hokkaido coastlines. The mapping work of Okumura (1996) could be extended more widely to enable larger scale analyses of these terrace elevations. Particularly, direct dating of the MIS 7 and 9 shorelines would determine the particular substage of the interglacial in which the terraces formed, enabling uplift rates to be compared over Pleistocene timescales. In addition, the role of volcanic deformation in controlling the elevation of these terraces requires further research.

CHAPTER EIGHT

References

AKAMATSU, M., SAITO, Y., IKEDA, K., YOKOTA, S., HASAKA, T., MATSUMOTO, E. and YAMAZAKI, N. 1997. Holocene natural shells beds in Rishiri and Rebun Islands in northern Hokkaido. *Bulletin of the Historical Museum of Hokkaido* 25, 1-17. [In Japanese with English abstract].

AKERS, W. H. 1971. Estuarine foraminiferal associations of the Beaufort area, North Carolina. *Tulane Studies in Geology and Paleontology* 8, 147-165.

ALLAN, R. J. and ANSELL, T. J. accepted. A new globally complete monthly historical mean sea level pressure data set (HadSLP2): 1850-2004. *Journal of Climate*.

ALLEN, J. R. L. and THORNLEY, D. M. 2004. Laser granulometry of Holocene estuarine silts: effects of hydrogen peroxide treatment. *Holocene* 14, 290-295.

ALLEY, R. B., MAROTZKE, J., NORDHAUS, W. D., OVERPECK, J. T., PETEET, D. M., JR., R. A. P., PIERREHUMBERT, R. T., RHINES, P. B., STOCKER, T. F., TALLEY, L. D. and WALLACE, J. M. 2005. Abrupt climate change. *Science* 299, 2005-2010.

ALVE, E. and MURRAY, J. W. 1999. Marginal marine environments of the Skagerrak and Kattegat: a baseline study of living (stained) benthic foraminiferal ecology. *Palaeogeography Palaeoclimatology Palaeoecology* 146, 171-193.

ALVE, E. and NAGY, J. 1986. Estuarine foraminiferal distribution in Sandebukta, a branch of the Oslo Fjord. *Journal of Foraminiferal Research* 16, 261-284.

ANDERSON, H. V. 1953. Two new species of Haplophragmoides from the Louisiana coast. *Contributions from the Cushman Foundation for Foraminiferal Research* 4, 21-22.

ANTONIOLI, F., FERRANTI, L., LAMBECK, K., KERSHAW, S., VERRUBBI, V. and DAI PRA, G. 2006. Late Pleistocene to Holocene record of changing uplift rates in southern Calabria and northeastern Sicily (southern Italy, Central Mediterranean Sea). *Tectonophysics* 422, 23-40.

AOKI, Y. and SCHOLZ, C. H. 2003. Vertical deformation of the Japanese islands, 1996-1999. *Journal of Geophysical Research-Solid Earth* 108, ETG 10-1, DOI 10.1029/2002JB002129.

ARAKAWA, T. 1994. Holocene shell beds in southern Ishikari lowlands - characteristics of 7000 yr old shell beds. *Tomakomai-shi Hakubutsukan Kenkyuu Houkoku (Research Report of the Tomakomai City Museum)* 4, 26-38. [In Japanese].

ARAKAWA, T. 1997. Characteristics and implications of Holocene shell beds - examples of Tomakomai and Muroran. *Tomakomai-shi Hakubutsukan Kenkyuu Houkoku (Research Report of the Tomakomai City Museum)* 7, 1-11 [In Japanese].

ARNAL, R. E. 1961. Limnology, sedimentation, and microorganisms of the Salton Sea, California. *Geological Society of America, Bulletin* 72, 427–478.

ASANO, K. 1951: Rotaliidae. In Stach, L. W., (Ed.), *Illustrated Catalogue of Japanese Tertiary Smaller Foraminifera*: Hosokawa Printing, 1-21.

ASCOUGH, P., COOK, G. and DUGMORE, A. 2005. Methodological approaches to determining the marine radiocarbon reservoir effect. *Progress in Physical Geography* 29, 532-547.

ATAGO, S. 1998: Holocene deposits in Abashiri River Lowland, northeastern Hokkaido. *Summaries of Researches Using AMS at Nagoya University (IX)*, Nagoya University, Japan. [In Japanese]: Dating and Materials Research Center, 140-148.

ATWATER, B. F. 1987. Evidence for great Holocene earthquakes along the outer coast of Washington state. *Science* 236, 942-944.

ATWATER, B. F., FURUKAWA, R., HEMPHILL-HALEY, E., IKEDA, Y., KASHIMA, K., KAWASE, K., KELSEY, H. M., MOORE, A. L., NANAYAMA, F., NISHIMURA, Y., ODAGIRI, S., OTA, Y., PARK, S. C., SATAKE, K., SAWAI, Y. and SHIMOKAWA, K. 2004. Seventeenth-century uplift in Eastern Hokkaido, Japan. *Holocene* 14, 487-501.

ATWATER, B. F. and HEMPHILL-HALEY, E. 1997: *Recurrence intervals for great earthquakes of the past 3500 years at northeastern Willapa Bay, Washington*: U.S. Geological Survey Professional Paper 1576.

ATWATER, B. F., YAMAGUCHI, D. K., BONDEVIK, S., BARNHARDT, W. A., AMIDON, L. J., BENSON, B. E., SKJERDAL, G., SHULENE, J. A. and NANAYAMA, F. 2001. Rapid resetting of an estuarine recorder of the 1964 Alaska earthquake. *Geological Society of America Bulletin* 113, 1193-1204.

AUSTIN, W. E. N., BARD, E., HUNT, J. B., KROON, D. and PEACOCK, J. D. 1995. The ^{14}C age of the Icelandic Vedde ash; implications for Younger Dryas marine reservoir age corrections. *Radiocarbon* 37, 53–62.

BABA, T., HIRATA, K., HORI, T. and SAKAGUCHI, H. 2006. Offshore geodetic data conducive to the estimation of the afterslip distribution following the 2003 Tokachi-oki earthquake. *Earth and Planetary Science Letters* 241, 281-292.

BANDY, O. L. 1960. The geologic significance of coiling ratios in the foraminifer Globigerina pachyderma (Ehrenberg). *Journal of Paleontology* 34, 671–681.

BARBOSA, C. F., SCOTT, D. B., SEOANE, J. C. S. and TURCQ, B. J. 2005. Foraminiferal zonations as base lines for quaternary sea-level fluctuations in south-southeast Brazilian mangroves and marshes. *Journal of Foraminiferal Research* 35, 22-43.

BARD, E., HAMELIN, B. and FAIRBANKS, R. G. 1990. U-Th Ages obtained by mass-spectrometry in corals from Barbados - sea-level during the past 130,000 years. *Nature* 346, 456-458.

BARRETO, A. M. F., BEZERRA, F. H. R., SUGUIO, K., TATUMI, S. H., YEE, M., PAIVA, R. P. and MUNITA, C. S. 2002. Late Pleistocene marine terrace deposits in northeastern Brazil: sea-level change and tectonic implications. *Palaeogeography Palaeoclimatology Palaeoecology* 179, 57-69.

BÉ, A. W. H. 1977: An ecological, zoogeographic and taxonomic review of recent planktonic Foraminifera. In Ramsay, A. T. S., (Ed.), *Oceanic Micropaleontology*, London: Academic Press, 1-100.

BERKELEY, A., PERRY, C. T., SMITHERS, S. G., HORTON, B. P. and TAYLOR, K. G. 2007. A review of the ecological and taphonomic controls on foraminiferal assemblage development in intertidal environments. *Earth-Science Reviews* 83, 205-230.

BERRYMAN, K. R. 1987: Tectonic processes and their impact on the recording of relative sea-level changes. In Devoy, R. J. N., (Ed.), *Sea Surface Studies - A Global View*, London: Croom Helm, 127-161.

BEVINGTON, P. R. and ROBINSON, D. K. 2003: *Data Reduction and Error Analysis*. New York: McGraw-Hill.

BINFORD, M. W., KAHL, J. S. and NORTON, S. A. 1993. Interpretation of ^{210}Pb profiles and verification of the CRS dating model in PIRLA project lake sediment cores. *Journal of Paleolimnology* 9, 275-296.

BIRKS, H. J. B. 1974. Numerical zonations of Flandrian pollen data. *New Phytologist* 73, 351-358.

BIRKS, H. J. B. 1986: Numerical zonation, comparison and correlation of Quaternary pollen-stratigraphical data. In Berglund, B. E., (Ed.), *Handbook of Holocene Palaeoecology and Palaeohydrology*, London: John Wiley and Sons Ltd, 743–773.

BIRKS, H. J. B. 1992. Some reflections on the application of numerical methods in Quaternary palaeoecology. *Publication of Karelian Institute, University of Joensuu* 102, 7–20.

BIRKS, H. J. B. 1995: Quantitative palaeoenvironmental reconstructions. In Maddy, D. and Brew, J. S., (Eds.), *Statistical Modelling of Quaternary Science Data*, Cambridge: Quaternary Research Association, 161-236.

BIRKS, H. J. B. and BIRKS, H. H. 1980: *Quaternary Palaeoecology*. London: Edward Arnold, p. 289.

BIRKS, H. J. B., LINE, J. M., JUGGINS, S., STEVENSON, A. C. and TER BRAAK, C. J. F. 1990. Diatom and pH reconstruction. *Philosophical Transactions of the Royal Society of London (series B, Biological Sciences)* 327, 263-278.

BLOTT, S. J. and PYE, K. 2001. Gradistat: a grain size distribution and statistics package for the analysis of unconsolidated sediments. *Earth Surface Processes and Landforms* 26, 1237-1248.

BOLTOVSKOY, E., SCOTT, D. B. and MEDIOLI, F. S. 1991. Morphological variations of benthic foraminiferal tests in response to changes in ecological parameters, a review. *Journal of Paleontology* 65, 175-185.

BOLTOVSKOY, E. and WRIGHT, R. 1976: *Recent Foraminifera*. The Hague: Junk, p. 515.

BONACCORSO, A., CIANETTI, S., GIUNCHI, C., TRASATTI, E., BONAFEDE, M. and BOSCHI, E. 2005. Analytical and 3-D numerical modelling of Mt. Etna (Italy) volcano inflation. *Geophysical Journal International* 163, 852-862.

BORCARD, D., LEGENDRE, P. and DRAPEAU, P. 1992. Partialling out the spatial component of ecological variation. *Ecology* 73, 1045-1055.

BOSCHI, E., CASAROTTI, E., DEVOTI, R., MELINI, D., PIERSANTI, A., PIETRANTONIO, G. and RIGUZZI, F. 2006. Coseismic deformation induced by the Sumatra earthquake. *Journal of Geodynamics* 42, 52-62.

BOURGEOIS, J. 2006. Earthquakes - a movement in four parts? *Nature* 440, 430-431.

BRADSHAW, J. S. 1968. Environmental parameters and marsh foraminifera. *Limnology and Oceanography* 13, 26-38.

BRADY, G. S. 1870: Foraminifera. In Brady, G. S. and Robertson, D., (Eds.), *Annals and Magazine of Natural History*, 273-306.

BRIGGS, R. W., SIEH, K., MELTZNER, A. J., NATAWIDJAJA, D., GALETZKA, J., SUWARGADI, B., HSU, Y. J., SIMONS, M., HANANTO, N., SUPRIHANTO, I., PRAYUDI, D., AVOUAC, J. P., PRAWIRODIRDJO, L. and BOCK, Y. 2006. Deformation and slip along the Sunda Megathrust in the great 2005 Nias-Simeulue earthquake. *Science* 311, 1897-1901.

BRONK RAMSEY, C. 1995. Radiocarbon calibration and analysis of stratigraphy: the OxCal Program. *Radiocarbon* 37, 425-430.

BRÖNNIMAN, P. and ZANINETTI, L. 1979. Paratrochammina stoeni, n. sp., a new Trochamminid (Foraminiferida) from recent mangrove swamp sediments of Viti Levu, Fuji, with remarks on S Atlantic and S Pacific mangrove foraminifera. *Notes du Laboratoire de Paléontologie de l'Université de Genève* 4, 51-55.

BRÖNNIMANN, P., LUTZE, G. F. and WHITTAKER, J. E. 1989. *Balticammina pseudomacrescens*, a new brackish water trochamminid from the western Baltic Sea, with remarks on the wall structure. *Meyniana* 41, 167-177.

BRÖNNIMANN, P. and WHITTAKER, J. E. 1988. The trochamminaceous test and the taxonomic criteria used in the classification of the superfamily Trochamminacea. *Abhandlungen der Geologischen Bundesanstalt* 41, 23–39.

BRÖNNIMANN, P., WHITTAKER, J. E. and ZANINETTI, L. 1992. Brackish water foraminifera from mangrove sediments of southwestern Viti Levu, Fiji Islands, southwest Pacific. *Revue de Paléobiologie* 11, 13-65.

BROOKS, A. 2007: Late Devensian and Holocene Relative Sea-Level Change around Ireland. Unpublished PhD thesis, Trinity College Dublin.

BROOKS, A. and EDWARDS, R. J. 2006. The development of a sea-level database for Ireland. *Irish Journal of Earth Science* 24, 13-27.

BROOKS, A. J., BRADLEY, S. J., EDWARDS, R. J., MILNE, G. A., HORTON, B. P. and SHENNAN, I. 2006. Postglacial relative sea-level observations from Ireland and their role in glacial rebound modelling. *Journal of Quaternary Science* 23, 175 - 192.

BUZAS, M. A. 1968. On the spatial distribution of foraminifera. *Contributions of the Cushman Foundation for Foraminiferal Research* 19, 1-11.

BUZAS, M. A., SMITH, R. K. and BEEM, K. A. 1977. Ecology and systematics of foraminifera in two Thalassia habitats, Jamaica, West Indies. *Smithsonian Contributions to Paleobiology* 31, 139 p.

CISTERNAS, M., ATWATER, B. F., TORREJON, F., SAWAI, Y., MACHUCA, G., LAGOS, M., EIPERT, A., YOULTON, C., SALGADO, I., KAMATAKI, T., SHISHIKURA, M., RAJENDRAN, C. P., MALIK, J. K., RIZAL, Y. and HUSNI, M. 2005. Predecessors of the giant 1960 Chile earthquake. *Nature* 437, 404-407.

CLAGUE, J. J. and BOBROWSKY, P. T. 1999. The geological signature of great earthquakes off Canada's West Coast. *Geoscience Canada* 26, 1-15.

CLARK, J. A., FARRELL, W. E. and PELTIER, W. R. 1978. Global changes in postglacial sea level: a numerical calculation. *Quaternary Research* 9, 265-287.

COCHRAN, U., HANNAH, M., HARPER, M., VAN DISSEN, R., BERRYMAN, K. and BEGG, J. 2007. Detection of large, Holocene earthquakes using diatom analysis of coastal sedimentary sequences, Wellington, New Zealand. *Quaternary Science Reviews* 26, 1129-1147.

COHEN, S. C. and FREYMUELLER, J. T. 2001. Crustal uplift in the south central Alaska subduction zone: new analysis and interpretation of tide gauge observations. *Journal of Geophysical Research-Solid Earth* 106, 11259-11270.

COLES, B. P. L. 1977: The Holocene foraminifera and palaeogeography of central Broadland. Unpublished PhD thesis, University of East Anglia, Norwich.

COLES, B. P. L. and FUNNELL, B. M. 1981. Holocene palaeoenvironments of Broadland, England. *Special Publication of the International Association of Sedimentologists* 5, 123-131.

COLLINS, E. S., SCOTT, D. B., GAYES, P. T. and MEDIOLI, F. S. 1995. Foraminifera in Winyah Bay and North Inlet marshes, South Carolina; relationship to local pollution sources *The Journal of Foraminiferal Research* 25, 212-273.

COX, N. J. 2006. Speaking Stata: in praise of trigonometric predictors. *Stata Journal* 6, 561-579.

CULVER, S. J. and HORTON, B. P. 2005. Infaunal marsh foraminifera from the Outer Banks, North Carolina, USA. *Journal of Foraminiferal Research* 35, 148-170.

CUNDY, A. B. and CROUDACE, I. W. 1996. Sediment accretion and recent sea-level rise in the Solent, southern England: inferences from radiometric and geochemical studies. *Estuarine Coastal and Shelf Science* 43, 449-467.

CUNDY, A. B., KORTEKAAS, S., DEWEZ, T., STEWART, I. S., COLLINS, P. E. F., CROUDACE, I. W., MAROUKIAN, H., PAPANASTASSIOU, D., GAKI-PAPANASTASSIOU, P., PAVLOPOULOS, K. and DAWSON, A. 2000. Coastal wetlands as recorders of earthquake subsidence in the Aegean: a case study of the 1894 Gulf of Atalanti earthquakes, central Greece. *Marine Geology* 170, 3-26.

CUNDY, A. B. S., I.S. 2004. Dating recent colluvial sequences with ^{210}Pb and ^{137}Cs along an active fault scarp, the Eliki Fault, Gulf of Corinth, Greece *Tectonophysics* 386, 147-156.

CUSHMAN, J. A. and BRÖNNIMANN, P. 1948. Additional new species of arenaceous Foraminifera from the shallow waters of Trinidad. *Contributions from the Cushman Laboratory for Foraminiferal Research* 24, 37-42.

CUSHMAN, J. A. and MCCULLOCH, I. 1939. A report on some arenaceous Foraminifera. *Alan Hancock Pacific Expedition* 6, 113 p.

D'ORBIGNY, A. D. 1839: Foraminifères des iles Canaries. In Barker-Webb, P. and Berthelot, S., (Eds.), *Historie Naturelle des Iles Canaries*, Paris: Béthune, 119-146.

DAIMARU, H. 1989. Holocene evolution of the Toyohira River alluvial fan and distal floodplain, Hokkaido, Japan. *Geographical Review of Japan (Chirigaku hyoron)* 62A, 589-603. [In Japanese with English abstract].

DAVIS, J. L., MITROVICA, J. X., SCHERNECK, H. G. and FAN, R. 1999. Investigations of Fennoscandian glacial isostatic adjustment using modern sea level records. *Journal of Geophysical Research-Solid Earth* 104, 2733-2747.

DAWSON, A. G., LONG, D. and D.E., S. 1988. The Storegga Slides: evidence from eastern Scotland for a possible tsunami. *Marine Geology* 82, 271–276.

DE BEAUMONT, L. E. 1845: Septieme lechón. In Bertrand, P., (Ed.), *Lecons de geologie pratique*, Paris: Bertrand, 221–252.

DE RIJK, S. 1995a: Agglutinated Foraminifera as indicators of salt marsh development in relation to late Holocene sea-level rise (Great Marshes at Barnstable, Massachusetts). Amsterdam: Free University, 188 p.

DE RIJK, S. 1995b. Salinity control on the distribution of salt marsh Foraminifera (Great Marshes, Massachusetts). *Journal of Foraminiferal Research* 25, 156-166.

DE RIJK, S. and TROELSTRA, S. R. 1997. Saltmarsh foraminifera from the Great Marshes, Massachusetts: environmental controls. *Palaeogeography, Palaeoclimatology, Palaeoecology* 130, 81-112.

DEMETS, C. 1992. Oblique convergence and deformation along the Kuril and Japan Trenches. *Journal of Geophysical Research-Solid Earth* 97, 17615-17625.

DONNELLY, J. P. and WOODRUFF, J. D. 2007. Intense hurricane activity over the past 5,000 years controlled by El Niño and the West African monsoon. *Nature* 447, 465-468.

DOUGLAS, B. C. 1997. Global sea rise: a redetermination. *Surveys in Geophysics* 18, 279-292.

DRAGERT, H., WANG, K. L. and JAMES, T. S. 2001. A silent slip event on the deeper Cascadia subduction interface. *Science* 292, 1525-1528.

DUBLIN-GREEN, C. O. 1992: Benthic foraminiferal ecology and sediment distribution in the Bonny River, Niger Delta. Unpublished PhD Dissertation, University of London.

DUCHEMIN, G. F., JORISSEN, F. J., REDIOS, F. and DEBENAY, J.-P. 2005. Foraminiferal microhabitats in a high marsh: consequences for reconstructing past sea levels. *Palaeogeography, Palaeoclimatology, Palaeoecology* 226, 167-185.

DUTTON, A., BARD, E., ANTONIOLI, F., ESAT, T. M., LAMBECK, K. and MCCULLOCH, M. T. 2009. Phasing and amplitude of sea-level and climate change during the penultimate interglacial. *Nature Geoscience* 2, 355-359.

EDWARDS, R. and HORTON, B. 2006. Developing detailed records of relative sea-level change using a foraminiferal transfer function: an example from North Norfolk, UK. *Philosophical Transactions of the Royal Society A: Mathematical, Physical and Engineering Sciences* 364, 973-991.

EDWARDS, R. J. and HORTON, B. P. 2000. Reconstructing relative sea-level change using UK salt-marsh foraminifera. *Marine Geology* 169, 41-56.

EDWARDS, R. J., VAN DE PLASSCHE, O., GEHRELS, W. R. and WRIGHT, A. J. 2004a. Assessing sea-level data from Connecticut, USA, using a foraminiferal transfer function for tide level. *Marine Micropaleontology* 51, 239-255.

EDWARDS, R. J., WRIGHT, A. and VAN DE PLASSCHE, O. 2004b. Surface distributions of salt-marsh foraminifera from Connecticut, USA: modem analogues for high-resolution sea level studies. *Marine Micropaleontology* 51, 1-21.

EHRENBERG, G. C. 1840a: Eine weitere Erlauterung des Organismus mehrerer in Berlin lebend beobachteter Polythalamien der Nordsee. Bericht über die zu Bekanntmachung geeigneten Verhandlungen der Königlichen Preussischen Akademie der Wissenschaften zu Berlin. 18-23.

EHRENBERG, G. C. 1840b. Über noch Jetze zahlreich lebende Thierarten der Kreidebildung und den Organismus der Polythalamien: Physikalische Mathematische Abhandlungen der Königlichen Akademie der Wissenschaften zu Berlin. 81-174.

EISENHAUER, A., ZHU, Z. R., COLLINS, L. B., WYRWOLL, K. W. and EICHSTATTER, R. 1996. The last interglacial sea level change: new evidence from the Abrolhos islands, west Australia. *Geologische Rundschau* 85, 606-614.

EL-FIKY, G. and KATO, T. 2006. Secular crustal deformation and interplate coupling of the Japanese Islands as deduced from continuous GPS array, 1996-2001 *Tectonophysics* 422, 1-22.

FERRANTI, L., ANTONIOLI, F., MAUZ, B., AMOROSI, A., PRA, G. D., MASTRONUZZI, G., MONACO, C., ORRU, P., PAPPALARDO, M., RADTKE, U., RENDA, P., ROMANO, P., SANSO, P. and VERRUBBI, V. 2006. Markers of the last interglacial sea-level high stand along the coast of Italy: tectonic implications. *Quaternary International* 145, 30-54.

FLÜCK, P., HYNDMAN, R. D. and WANG, K. 1997. Three-dimensional dislocation model for great earthquakes of the Cascadia subduction zone. *Journal of Geophysical Research-Solid Earth* 102, 20539-20550.

FRIEDMAN, G. M. 1979. Differences in size distributions of populations of particles among sands of various origins. *Sedimentology* 26, 3–32.

FUJII, K. 1989: Structural control on sedimentation of coal-bearing formations in Japan. In Taira, A. and Masuda, F., (Eds.), *Sedimentary Facies in the Active Plate Margin*, Tokyo: Terrapub, 675-688.

FUJIMOTO, K., OHIRA, A., KAWASE, K., ISHIZUKA, S., SHICHI, K. and ADACHI, H. 2003. Bulk density and carbon content rate of alluvium in the Lower Tokachi River Plain, northern Japan. *Journal of the Nanzan Academic Society. Natural Science and Health and Physical Education* 11, 57-73. [In Japanese with English abstract].

FUJITA, H., IGARASHI, Y., HOTES, S., TAKADA, M., INOUE, T. and KANEKO, M. 2009. An inventory of the mires of Hokkaido, Japan - their development, classification, decline, and conservation. *Plant Ecology* 200, 9-36.

FURUKAWA, R., YOSHIMOTO, M., YAMAGATA, K., WADA, K. and UI, T. 1997. Did Hokkaido Komagatake volcano erupt in 1694? - reappraisal of the eruptive ages of 17-18th centuries in Hokkaido. *Kazan* 42, 269-279 [In Japanese with English abstract].

GALLUP, C. D., CHENG, H., TAYLOR, F. W. and EDWARDS, R. L. 2002. Direct determination of the timing of sea level change during Termination II. *Science* 295, 310-313.

GASSE, F., BARKER, P., GELL, P. A., FRITZ, S. C. and CHALIEA, F. 1997. Diatom-inferred salinity in palaeolakes: an indirect tracer of climate change *Quaternary Science Reviews* 16, 547-563.

GEHRELS, W. R. 1994. Determining relative sea-level change from salt-marsh foraminifera and plant zones on the Coast of Maine, USA. *Journal of Coastal Research* 10, 990-1009.

GEHRELS, W. R. 2007: Sea level studies: Microfossil reconstructions. In Elias, S., (Ed.), *Encyclopaedia of Quaternary Sciences*, Amsterdam: Elsevier, 3015-3023.

GEHRELS, W. R., MILNE, G. A., KIRBY, J. R., PATTERSON, R. T. and BELKNAP, D. F. 2004. Late Holocene sea-level changes and isostatic crustal movements in Atlantic Canada. *Quaternary International* 120, 79-89.

GEHRELS, W. R., ROE, H. M. and CHARMAN, D. J. 2001. Foraminifera, testate amoebae and diatoms as sea-level indicators in UK saltmarshes: a quantitative multiproxy approach. *Journal of Quaternary Science* 16, 201-220.

GEHRELS, W. R. and VAN DE PLASSCHE, O. 1999. The use of Jadammina macrescens (Brady) and Balticammina pseudomacrescens Brönnimann, Lutze and Whittaker (Protozoa: Foraminiferida) as sea-level indicators. *Palaeogeography, Palaeoclimatology, Palaeoecology* 149, 89-101.

GEOGRAPHICAL SURVEY INSTITUTE. 1997: *The National Atlas of Japan*. Tokyo: Japan Map Centre.

GILBERT, G. K. 1885: Lake Bonneville. U.S. Geological Survey, Monograph 1, 438.

GOLDBERG, E. D. 1963: Geochronology with ^{210}Pb: Radioactive Dating. *IAEA, November 19-23, 1962*, Vienna, 121-131.

GOLDSTEIN, S. T., G.T., W. and KUHN, R. M. 1995. Microhabitats of salt marsh foraminifera: St. Catherines Island, Georgia, USA. *Micropaleontology* 26, 17-29.

GOLDSTEIN, S. T. and HARBEN, E. B. 1993. Taphofacies implications of infaunal foraminiferal assemblages in a Georgia saltmarsh, Sapelo Island. *Micropaleontology* 39, 55-62.

GOLDSTEIN, S. T. and WATKINS, G. T. 1998. Elevation and the distribution of salt-marsh foraminifera, St. Catherine's Island, Georgia: a taphonomic approach. *Palaios* 13, 570-580.

GORBARENKO, S. A., CHEKHOVSKAYA, M. P. and SOUTHON, J. R. 1998. About the paleoenvironment of the central part of Okhotsk Sea during the Last Glaciation and the Holocene. *Oceanology* 38, 305–308. [In Russian].

GORSHKOV, G. S., editor. 1974: *Atlas of the Oceans: the Pacific Ocean*. Moscow: Defence Department.

GREEN, M. A., ALLER, R. C. and ALLER, J. Y. 1993. Carbonate dissolution and temporal abundances of foraminifera in Long-Island Sound sediments. *Limnology and Oceanography* 38, 331-345.

GRIFFITH, D. A. and AMRHEIN, C. G. 1997: *Multivariate Statistical Analysis for Geographers* Upper Saddle River, N.J.: Prentice Hall, p. 345.

GUILBAULT, J. P., CLAGUE, J. J. and LAPOINTE, M. 1995. Amount of subsidence during a late Holocene earthquake - evidence from fossil tidal marsh foraminifera at Vancouver-Island, west-coast of Canada. *Palaeogeography Palaeoclimatology Palaeoecology* 118, 49-71.

GUILBAULT, J. P., CLAGUE, J. J. and LAPOINTE, M. 1996. Foraminiferal evidence for the amount of coseismic subsidence during a late Holocene earthquake on Vancouver Island, west coast of Canada. *Quaternary Science Reviews* 15, 913-937.

GVOZDEVA, I. G., GORBARENKO, S. A., RAKOV, V. A., LUTAENKO, K. A., SHORNIKOV, E. I. and MIKISHIN, Y. A. 1997: The paleoenvironment of the Primorye in the Middle and Late Holocene according to complex study of the Shkotovo outcrop. Vladivostok: Pacific Oceanographical Institute., 32. [In Russian].

HADA, Y. 1936. Studies on the Foraminifera of brackish waters. I. Hijirippu and Mochirippu Lakes. *Zoological Magazine* 48, 847-860 [In Japanese].

HAEMET-AHTI, L., AHTI, T. and KOPONEN, T. 1974. A scheme of vegetation zones for Japan and adjacent regions *Annales Botanici Fennici* 11, 59-88.

HALL, M. E. 1999: Some archaeological thoughts on AMS dating. *Proceedings of the International Workshop on Frontiers in Accelerator Mass Spectrometry*, January 6-8, 1999, Tsukuba and Sakura (Japan): National Institute for Environmental Studies and National Museum of Japanese History, 174 - 193.

HAMANO, Y., MAEDA, Y., MATSUMOTO, E. and KUMANO, S. 1985. Holocene sedimentary history of some coastal plains in Hokkaido, Japan. III. Transition of diatom assemblages in Tokoro along the Okhotsk Sea. *Japanese Journal of Ecology* 35, 307-316.

HAMILTON, S. and SHENNAN, I. 2005a. Late Holocene great earthquakes and relative sea-level change at Kenai, southern Alaska. *Journal of Quaternary Science* 20, 95-111.

HAMILTON, S. and SHENNAN, I. 2005b. Late Holocene relative sea-level changes and the earthquake deformation cycle around upper Cook Inlet, Alaska. *Quaternary Science Reviews* 24, 1479-1498.

HAMILTON, S., SHENNAN, I., COMBELLICK, R., MULHOLLAND, J. and NOBLE, C. 2005. Evidence for two great earthquakes at Anchorage, Alaska and implications for multiple great earthquakes through the Holocene. *Quaternary Science Reviews* 24, 2050-2068.

HAMILTON, S. L. 2003: Late Holocene relative sea-level changes and earthquakes around the upper Cook Inlet, Alaska, USA. Unpublished PhD thesis, University of Durham.

HAWKES, A., D., SCOTT, D. B., LIPPS, J. H. and COMBELLICK, R. 2005. Evidence for possible precursor events of megathrust earthquakes on the west coast of North America. *GSA Bulletin* 117, 996-1008.

HAWKES, A. D., BIRD, M., COWIE, S., GRUNDY-WARR, C., HORTON, B. P., HWAI, A. T. S., LAW, L., MACGREGOR, C., NOTT, J., ONG, J. E., RIGG, J., ROBINSON, R., TAN-MULLINS, M., SA, T. T., YASIN, Z. and AIK, L. W. 2007. Sediments deposited by the 2004 Indian Ocean Tsunami along the Malaysia-Thailand Peninsula. *Marine Geology* 242, 169-190.

HAWKES, A. D., HORTON, B. P., NELSON, A. R. and HILL, D. F. In Press. The application of intertidal foraminifera to reconstruct coastal subsidence during the giant Cascadia earthquake of AD 1700 in Oregon, USA. *Quaternary International*.

HAYNES, J. R. 1973. Cardigan Bay recent foraminifera (Cruises of the R. V. Antur, 1962-1964). *Bulletin of the British Museum (Natural History, Zoology series)* Supplement 4, 1-245.

HAYWARD, B. W., COCHRAN, U., SOUTHALL, K., WIGGINS, E., GRENFELL, H. R., SABAA, A., SHANE, P. R. and GEHRELS, R. 2004a. Micropalaeontological evidence for the Holocene earthquake history of the eastern Bay of Plenty, New Zealand, and a new index for determining the land elevation record. *Quaternary Science Reviews* 23, 1651-1667.

HAYWARD, B. W., HOLZMANN, M., GRENFELL, H. R., PAWLOWSKI, J. and TRIGGS, C. M. 2004b. Morphological distinction of molecular types in Ammonia - towards a taxonomic revision of the world's most commonly misidentified foraminifera. *Marine Micropaleontology* 50, 237-271.

HAYWARD, B. W., SCOTT, G. H., GRENFELL, H. R., CARTER, R. and LIPPS, J. H. 2004c. Techniques for estimation of tidal elevation and confinement (similar to salinity) histories of sheltered harbours and estuaries using benthic foraminifera: examples from New Zealand. *Holocene* 14, 218-232.

HEARTY, P. J., HOLLIN, J. T., NEUMANN, A. C., O'LEARY, M. J. and MCCULLOCH, M. 2007. Global sea-level fluctuations during the Last Interglaciation (MIS 5e). *Quaternary Science Reviews* 26, 2090-2112.

HEMPHILL-HALEY, E. 1995. Intertidal diatoms from Willapa Bay, Washington: application to studies of small-scale sea-level changes. *Northwest Science* 69, 29-45.

HERON-ALLEN, E. and EARLAND, A. 1930. Miliammina, a new siliceous genus. *Journal of the Royal Microscopic Society of London* 50, 38-45.

HIERONYMUS, C. F. and BERCOVICI, D. 1999. Discrete alternating hotspot islands formed by interaction of magma transport and lithospheric flexure. *Nature* 397, 604-607.

HIERONYMUS, C. F. and BERCOVICI, D. 2000. Non-hotspot formation of volcanic chains: control of tectonic and flexural stresses on magma transport. *Earth and Planetary Science Letters* 181, 539-554.

HILL, M. O. and GAUCH, H. G. 1980. Detrended correspondence analysis - an improved ordination technique. *Plant Ecology* 42, 47-58.

HINTON, A. C. 1995. Holocene tides of The Wash, UK: the influence of water-depth and coastline-shape changes on the record of sea-level change. *Marine Geology* 124, 87-111.

HIPPENSTEEL, S. P., MARTIN, R. E., NIKITINA, D. and PIZZUTO, J. E. 2000. The formation of Holocene marsh foraminiferal assemblages, middle Atlantic Coast, USA:

implications for the Holocene sea-level change. *Journal of Foraminiferal Research* 30, 272-298.

HIRATA, K., GEIST, E., SATAKE, K., TANIOKA, Y. and YAMAKI, S. 2003. Slip distribution of the 1952 Tokachi-Oki earthquake (M 8.1) along the Kuril Trench deduced from tsunami waveform inversion. *Journal of Geophysical Research-Solid Earth* 108, 16.

HOGG, A. G., HIGHAM, T. F. G. and DAHM, J. 1998. ^{14}C dating of modern marine and estuarine shellfish. *Radiocarbon* 40, 975–984.

HONDA, R., AOI, S., MORIKAWA, N., SEKIGUCHI, H., KUNUGI, T. and FUJIWARA, H. 2004. Ground motion and rupture process of the 2003 Tokachi-oki earthquake obtained from strong motion data of K-NET and KiK-net. *Earth Planets and Space* 56, 317-322.

HORTON, B. P. 1999. The contemporary distribution of intertidal foraminifera of Cowpen Marsh, Tees Estuary, UK: implications for studies of Holocene sea-level changes. *Palaeogeography, Palaeoclimatology, Palaeoecology* 149 127-149.

HORTON, B. P., CORBETT, R., CULVER, S. J., EDWARDS, R. J. and HILLIER, C. 2006. Modern saltmarsh diatom distributions of the Outer Banks, North Carolina, and the development of a transfer function for high resolution reconstructions of sea level. *Estuarine, Coastal, and Shelf Science* 69, 381-394.

HORTON, B. P. and CULVER, S. J. 2008. Modern intertidal foraminifera of the Outer Banks, North Carolina, USA, and their applicability for sea-level studies. *Journal of Coastal Research* 24, 1110-1125.

HORTON, B. P., CULVER, S. J., HARDBATTLE, M. I. J., LARCOMBE, P., MILNE, G. M., MORIGI, C., WHITTAKER, J. E. and WOODROFFE, S. A. 2007. Reconstructing Holocene sea-level change for the Great Barrier Reef using subtidal foraminifera. *Journal of Foraminiferal Research* 37, 327-343.

HORTON, B. P. and EDWARDS, R. J. 2003. Seasonal distributions of foraminifera and their implications for sea-level studies. *Special Publication - Society for Sedmentary Geology* 75, 21-30.

HORTON, B. P. and EDWARDS, R. J. 2005. The application of local and regional transfer functions to the reconstruction of Holocene sea levels, north Norfolk, England. *Holocene* 15, 216-228.

HORTON, B. P. and EDWARDS, R. J. 2006: Quantifying Holocene Sea Level Change Using Intertidal Foraminifera: Lessons from the British Isles. *Cushman Foundation For Foraminiferal Research, Special Publication*, p. 97.

HORTON, B. P., EDWARDS, R. J. and LLOYD, J. M. 1999a. A foraminiferal-based transfer function: implications for sea-level studies. *Journal of Foraminiferal Research* 29, 117-129.

HORTON, B. P., EDWARDS, R. J. and LLOYD, J. M. 1999b. Reconstruction of former sea levels using a foraminiferal-based transfer function. *Journal of Foraminifera Research* 29, 117-129.

HORTON, B. P., EDWARDS, R. J. and LLOYD, J. M. 1999c. UK intertidal foraminiferal distributions: implications for sea-level studies. *Marine Micropaleontology* 36, 205-223.

HORTON, B. P., EDWARDS, R. J. and LLOYD, J. M. 2000: Implications of a microfossil based transfer function in Holocene sea level studies. In Shennan, I. and Andrews, J. E., (Eds.), *Holocene Land-ocean Interaction and Environmental Change Around the Western North Sea*, London: Geological Society Special Publication, 41-54.

HORTON, B. P., LARCOMBE, P., WOODROFFE, S. E., WHITTAKER, J. E., WRIGHT, M. W. and WYNN, C. 2003. Contemporary foraminiferal distributions of the Great Barrier Reef coastline, Australia: implications for sea-level reconstructions. *Marine Geology* 3320, 1-19.

HORTON, B. P., WHITTAKER, J. E., THOMSON, K. H., HARDBATTLE, M. I. J., KEMP, A., WOODROFFE, S. A. and WRIGHT, M. R. 2005. Contemporary foraminiferal distributions, Wakatobi National Park, Southeast Sulawesi, Indonesia. *Journal of Foraminiferal Research* 35, 1-14.

HSU, Y. J., SIMONS, M., AVOUAC, J. P., GALETZKA, J., SIEH, K., CHLIEH, M., NATAWIDJAJA, D., PRAWIRODIRDJO, L. and BOCK, Y. 2006. Frictional afterslip following the 2005 Nias-Simeulue earthquake, Sumatra. *Science* 312, 1921-1926.

HU, Y., WANG, K., HE, J., KLOTZ, J. and KHAZARADZE, G. 2004. Three-dimensional viscoelastic finite element model for postseismic deformation of the great 1960 Chile earthquake. *Journal of Geophysical Research-Solid Earth* 109, B12403, DOI:10.1029/2004JB003163.

HUGHEN, K. A., BAILLIE, M. G. L., BARD, E., BECK, J. W., BERTRAND, C. J. H., BLACKWELL, P. G., BUCK, C. E., BURR, G. S., CUTLER, K. B., DAMON, P. E., EDWARDS, R. L., FAIRBANKS, R. G., FRIEDRICH, M., GUILDERSON, T. P., KROMER, B., MCCORMAC, G., MANNING, S., RAMSEY, C. B., REIMER, P. J., REIMER, R. W., REMMELE, S., SOUTHON, J. R., STUIVER, M., TALAMO, S., TAYLOR, F. W., VAN DER PLICHT, J. and WEYHENMEYER, C. E. 2004. Marine04 marine radiocarbon age calibration, 0-26 cal kyr BP. *Radiocarbon* 46, 1059-1086.

HYDROGRAPHIC AND OCEANOGRAPHIC DEPARTMENT. 2006: *Tide Tables - Japan and its vicinities*. Tokyo: Japan Coast Guard, p. 431.

HYNDMAN, R. D. and PEACOCK, S. M. 2003. Serpentinization of the forearc mantle. *Earth and Planetary Science Letters* 212, 417-432.

HYNDMAN, R. D. and WANG, K. 1993. Thermal constraints on the zone of major thrust earthquake failure - the Cascadia Subduction Zone. *Journal of Geophysical Research-Solid Earth* 98, 2039-2060.

IKEDA, Y., HASAKA, T. and MURASE, T. 1995. Holocene sediments and topography of the Yufutsu plain in Hokkaido. *Bulletin of the Geological Survey of Japan* 46, 283-300. [In Japanese with English abstract].

IMBRIE, J. and KIPP, N. G. 1971: A new micropaleontological method for quantitative paleoclimatology: application to a Late Pleistocene Caribbean core. In Turekian, K. K., (Ed.), *The Late Cenozoic Glacial Ages*, New Haven, U.S: Yale University Press, 71-181.

IPCC. 2007: *Climate Change 2007: The Physical Science Basis. Contribution of Working Group I to the Forth Assessment Report of the Intergovernmental Panel on Climate Change*. New York: Cambridge University Press. Accessible at http://www.ipcc.ch/index.htm.

ITO, T., YOSHIOKA, S. and MIYAZAKI, S. 2000. Interplate coupling in northeast Japan deduced from inversion analysis of GPS data. *Earth and Planetary Science Letters* 176, 117-130.

ITOH, Y., ISHIYAMA, T. and NAGASAKI, Y. 2005. Deformation mode in the frontal edge of an arc-arc collision zone: subsurface geology, active faults and paleomagnetism in southern central Hokkaido, Japan. *Tectonophysics* 395, 81-97.

JANKAEW, K., ATWATER, B. F., SAWAI, Y., CHOOWONG, M., CHAROENTITIRAT, T., MARTIN, M. E. and PRENDERGAST, A. 2008. Medieval forewarning of the 2004 Indian Ocean tsunami in Thailand. *Nature* 455, 1228-1231.

JENNINGS, A. E. and NELSON, A. R. 1992. Foraminiferal assemblage zones in Oregon tidal marshes-relation to marsh floral zones and sea-level. *Journal of Foraminifera Research* 22, 13-29.

JENNINGS, A. E., NELSON, A. R., SCOTT, D. B. and ARAVENA, J. C. 1995. Marsh foraminiferal assemblages in the Valdivia Estuary, South-Central Chile, relative to vascular plants and sea-level. *Journal of Coastal Research* 11, 107-123.

JEVREJEVA, S., GRINSTED, A., MOORE, J. C. and HOLGATE, S. 2006. Nonlinear trends and multiyear cycles in sea level records. *Journal of Geophysical Research-Oceans* 111, C09012, DOI:10.1029/2005JC003229.

JEVREJEVA, S., MOORE, J. C., GRINSTED, A. and WOODWORTH, P. L. 2008. Recent global sea level acceleration started over 200 years ago? *Geophysical Research Letters* 35, L08715, DOI:10.1029/2008GL033611.

JONASSON, K. and PATTERSON, R. T. 1992. Preservation potential of marsh benthic foraminifera from the Fraser River Delta, British Columbia. *Micropaleontology* 38, 289–301.

JONES, G. A. and KUZMIN, Y. V. 1995: Radiocarbon dating of the “thermophilous” mollusks from the Peter the Great Gulf coast using accelerator mass spectrometry. In Kuzmin, Y. V., (Ed.), *Complex studies of the Holocene sections of Peter the Great Gulf coast (Sea of Japan)*, Vladivostok Pacific Institute of Geography, 34-38 p. [In Russian with English abstract].

JONES, G. D. and ROSS, C. A. 1979. Seasonal distribution of foraminifera in Samish Bay, Washington. *Journal of Paleontology* 53, 245-257.

JONES, M., PETCHEY, F., GREEN, R., SHEPPARD, P. and PHELAN, M. 2007. The marine ΔR for Nenumbo (Solomon Islands): a case study in calculating reservoir offsets from paired sample data. *Radiocarbon* 49, 95-102.

JUGGINS, S. 2006: C2 Version 1.4. Newcastle Upon Tyne.

KASAHARA, K. 1975. Aseismic faulting following the 1973 Nemuro-Oki earthquake, Hokkaido, Japan (a possibility). *Pure and Applied Geophysics* 113, 127-139.

KASAHARA, K. and KATO, T. 1981. Aseismic faulting following the 1973 Nemuro-Oki earthquake, Hokkaido, Japan (a retrospective study). *Pure and Applied Geophysics* 119, 392-403.

KATO, T. 1983. Secular and earthquake-related vertical crustal movements in Japan as deduced from tidal records (1951-1981). *Tectonophysics* 97, 183-200.

KAZUKA, T. 2002. Structure of the foreland fold-and-thrust belt, Hidaka Collision Zone, Hokkaido, Japan: Re-processing and re-interpretation of the JNOC seismic reflection profiles 'Hidaka' (H91-2 and H91-3). *Bulletin of the Earthquake Research Institute, University of Tokyo* 77, 97-109 [In Japanese].

KEIGWIN, L. D. 1998. Glacial-age hydrography of the far northwest Pacific Ocean. *Paleoceanography* 13, 323-339.

KELSEY, H., SATAKE, K., SAWAI, Y., SHERROD, B., SHIMOKAWA, K. and SHISHIKURA, M. 2002: Late Holocene repeated rapid coastal uplift in eastern Hokkaido. *Annual Report on Active Fault and Paleoearthquake Researches*: Geological Survey of Japan/AIST, vol. 2, pp. 223-233 [In Japanese with English abstract].

KELSEY, H., SATAKE, K., SAWAI, Y., SHERROD, B., SHIMOKAWA, K. and SHISHIKURA, M. 2006. Recurrence of postseismic coastal uplift, Kuril subduction zone, Japan. *Geophysical Research Letters* 33, L13315, DOI:10.1029/2006GL026052.

KEMP, A. C., HORTON, B. P., CORBETT, R., CULVER, S. J., EDWARDS, R. J. and PLASSCHE, O. 2009a. The relative utility of foraminifera and diatoms for reconstructing late Holocene sea-level change in North Carolina, USA. *Quaternary Research* 71, 9-21.

KEMP, A. C., HORTON, B. P. and CULVER, S. J. 2009b. Distribution of modern salt-marsh foraminifera in the Albemarle – Pamlico Estuarine System of North Carolina, USA: implications for sea-level research. *Marine Micropaleontology* 72, 222-238.

KENNETT, D. J., INGRAM, B. L., ERLANDSON, J. M. and WALKER, P. 1997. Evidence for temporal fluctuations in marine radiocarbon reservoir ages in the Santa Barbara Channel, Southern California. *Journal of Archaeological Science* 24, 1051-1059.

KIDSON, C. 1986: Sea-level changes in the Holocene. In van de Plaasche, O., (Ed.), *Sea-level Research: Manual for the Collection and Evaluation o*, Norwich: Geobooks, 27-64.

KIDSON, C. and HEYWORTH, A. 1978. Holocene eustatic sea level change. *Nature* 273, 748-750.

KIMURA, G. 1994. The latest Cretaceous-early Paleogene rapid growth of accretionary complex and exhumation of high pressure series metamorphic rocks in northwestern Pacific margin. *Journal of Geophysical Research* 99, 22147-22164.

KIMURA, G. and TAMAKI, K. 1985: Tectonic framework of the Kuril arc since its initiation In Nasu, N., Uyeda, S., Kushiro, I., Kobayashi, K. and Kagami, H., (Eds.), *Formation of Active Ocean Margins*, Tokyo: Terra Publishing, 641-676.

KITAZATO, H. 1994. Foraminiferal microhabitats in four marine environments around Japan. *Micropaleontology* 24, 29-41.

KOAZE, T., NOGAMI, M., ONO, Y. and HIRAKAWA, K., editors. 2003: *Regional Geomorphology of the Japanese Islands*. Volume 2. Geomorphology of Hokkaido. Tokyo: University of Tokyo Press.

KODAIRA, E. 1996. Holocene palaeoenvironmental reconstruction in the Shari area. *Bulletin of the Shiretoko Museum* 17, 1-16. [In Japanese].

KOIKE, K. and MACHIDA, H. 2001: *Atlas of Quaternary Marine Terraces in the Japanese Islands*. Tokyo: University of Tokyo Press, p. 105.

KOJIMA, S. 1979. Biogeoclimatic zones of Hokkaido Island, Japan. *The Journal of the College of Liberal Arts, Toyama University (Natural Science)* 12, 97-141.

KOMATSU, M., MIYASHITA, S., MAEDA, J., OSANAI, Y. and TOYOSHIMA, T. 1983: Disclosing of a deepest section of continental-type crust up-thrust as the final collision of arcs in Hokkaido, North Japan. In Hashimoto, M. and Uyeda, S., (Eds.), *Accretion Tectonics in the Circum-Pacific Regions*, Tokyo: Terra Publishing, 149-165.

KOMATSU, M., OSANAI, Y., TOYOSHIMA, T. and MIYASHITA, S. 1989: Evolution of the Hidaka metamorphic belt, Northern Hokkaido, North Japan. In Daly, J. S., Cliff, R. A. and Yardley, B. W. D., (Eds.), *Evolution of Metamorphic Belts*, London: Geological Society, 487-493.

KOMSOMOLSKY, G. V. and SIRYK, I. M., editors. 1967: *The Atlas of the Sakhalin District*. Moscow: Main Administration of Geodezy and Cartography.

KOSHIMIZU, S. and IKUSHIMA, J. 1989. Fission track dating of the Older Kutcharo pyroclastic flow (Furume welded tuff) in eastern Hokkaido, Japan. *Journal of the Geological Survey of Japan* 95, 77-79.

KUMANO, S., IHIRA, M., KUROMI, M., MAEDA, Y., MATSUMOTO, E., NAKAMURA, T., MATSUSHIMA, T., SATO, H. and MATSUDA, I. 1990a. Holocene sedimentary history of some coastal plains in Hokkaido, Japan. V. Sedimentary history of Kushu Lake and Akkeski. *Ecological Research* 5, 277-289.

KUMANO, S., IHIRA, M., MAEDA, Y., YAMAUCHI, M., MATSUMOTO, E. and MATSUDA, I. 1990b. Holocene sedimentary history of some coastal plains in Hokkaido, Japan. IV. Diatom assemblages in the sediments from Kushiro Moor. *Ecological Research* 5, 221-235.

KUZMIN, Y. V., BURR, G. S., GORBUNOV, S. V., RAKOV, V. A. and RAZJIGAEVA, N. G. 2007. A tale of two seas: Reservoir age correction values (R, [Delta]R) for the Sakhalin Island (Sea of Japan and Okhotsk Sea). *Nuclear Instruments and Methods in Physics Research Section B: Beam Interactions with Materials and Atoms* 259, 460-462.

KUZMIN, Y. V., BURR, G. S. and JULL, A. J. T. 2001. Radiocarbon reservoir correction ages in the Peter the Great Gulf, Sea of Japan, and eastern coast of the Kunashir, Southern Kuriles (northwestern Pacific). *Radiocarbon* 43, 477-481.

LAJOIE, K. R. 1986: Coastal Tectonics. In Wallace, R. E., (Ed.), *Active Tectonics*, Washington D.C.: National Academy of Science, National Academy Press, 95-124.

LALLEMAND, S. and JOLIVET, L. 1986. Japan Sea - a pull-apart basin. *Earth and Planetary Science Letters* 76, 375-389.

LAMBECK, K., ANTONIOLI, F., PURCELL, A. and SILENZI, S. 2004. Sea-level change along the Italian coast for the past 10,000 yr. *Quaternary Science Reviews* 23, 1567-1598.

LAMBECK, K., ESAT, T. M. and POTTER, E. K. 2002. Links between climate and sea levels for the past three million years. *Nature* 419, 199-206.

LARSEN, C. F., ECHELMEYER, K. A., FREYMUELLER, J. T. and MOTYKA, R. J. 2003. Tide gauge records of uplift along the northern Pacific-North American plate boundary, 1937 to 2001. *Journal of Geophysical Research-Solid Earth* 108.

LEONARD, L. J., HYNDMAN, R. D. and MAZZOTTI, S. 2004. Coseismic subsidence in the 1700 great Cascadia earthquake: coastal estimates versus elastic dislocation models. *Geological Society of America Bulletin* 116, 655-670.

LI, H. and YANG, S. L. 2009. Trapping effect of tidal marsh vegetation on suspended sediment, Yangtze Delta. *Journal of Coastal Research* 25, 915–924.

LONG, A. J. 1992. Coastal responses to changes in sea level in the East Kent Fens and southeast England. *Proceedings of the Geologists' Association* 103, 187-199.

LONG, A. J., INNES, J. B., KIRBY, J. R., LLOYD, J. M., RUTHERFORD, M. M., SHENNAN, I. and TOOLEY, M. J. 1998. Holocene sea-level change and coastal evolution in the Humber estuary, eastern England: an assessment of rapid coastal change. *Holocene* 8, 229-247.

LONG, A. J., INNES, J. B., SHENNAN, I. and TOOLEY, M. J. 1999: Coastal stratigraphy: a case study from Johns River, Washington. In Jones, A. P., Tucker, M. E. and Hart, J. K., (Eds.), *The Description and Analysis of Quaternary Stratigraphic Field Sections*: Quaternary Research Association, 267-286.

LONG, A. J. and SHENNAN, I. 1994. Sea-level changes in Washington and Oregon and the earthquake deformation cycle. *Journal of Coastal Research* 10, 825-838.

LONG, A. J. and SHENNAN, I. 1998. Models of rapid relative sea-level change in Washington and Oregon, USA. *Holocene* 8, 129-142.

LUISE, G. and HEINZ, H. 1997: Migration of Cesium-137 in typical soils of North Germany ten years after the Chernobyl accident. *Journal of Plant Nutrition and Soil Science* 160, 81-83.

MACHIDA, H., ARAI, F., MIYAUCHI, T. and OKUMURA, K. 1987. Toya Ash - a widespread Late Quaternary time-marker in northern Japan. *The Quaternary Research (Daiyonki-Kenkyu)* 26, 129-145 [In Japanese with English abstract].

MAEDA, J. 1986. Origin of Hidaka metamorphic zone, spreading of the Kuril basin, collision of Eurasian and North American plates. *Monography of the Association of the Geological Collaboration of Japan* 31, 459-473 [In Japanese with English abstract].

MAEDA, Y., MATSUDA, I., NAKADA, M., MATSUSHIMA, Y., MATSUMOTO, K. and SATO, T. 1994. Holocene sea-level change along the Okhotsk Sea in Hokkaido, Japan: on the theoretical and observational values of the high sea-level stand. *Bulletin of the Yamagata University, Natural Sciences* 13, 205-229. [In Japanese with English abstract].

MAEDA, Y., NAKADA, M., MATSUMOTO, E. and MATSUDA, I. 1992. Crustal tilting derived from Holocene sea-level observations along the east-coast of Hokkaido in Japan and upper mantle rheology. *Geophysical Research Letters* 19, 857-860.

MAKAROVIC, B. 1973. Progressive sampling for digital terrain models. *ITC Journal* 3, 397–416.

MARSHALL, W. A., GEHRELS, W. R., GARNETT, M. H., FREEMAN, S. P. H. T., MADEN, C. and XU, S. 2007. The use of 'bomb spike' calibration and wiggle-matched high-precision AMS ^{14}C analyses to date salt-marsh sediments deposited during the past three centuries. *Quaternary Research* 68, 325-337.

MASSEY, A. C., GEHRELS, W. R., CHARMAN, D. J. and WHITE, S. V. 2006a. An intertidal foraminifera-based transfer function for reconstructing Holocene sea-level change in southwest England. *Journal of Foraminiferal Research* 36, 215-232.

MASSEY, A. C., PAUL, M. A., GEHRELS, W. R. and CHARMAN, D. J. 2006b. Autocompaction in Holocene coastal back-barrier sediments from south Devon, southwest England, UK. *Marine Geology* 226, 225-241.

MATERA, N. J. and LEE, J. J. 1972. Environmental factors affecting the standing crop of foraminifera in sublittoral and psammolittoral communities of a Long Island saltmarsh. *Marine Biology* 14, 89–103.

MATSUSHITA, K. 1979. Buried topography and the upper Pleistocene-Holocene deposits of the Ishikura coastal plain, Hokkaido, north Japan. *The Quaternary Research (Daiyonki-Kenkyu)* 18, 69-78. [In Japanese with English abstract].

MAZZOTTI, S., DRAGERT, H., HENTON, J., SCHMIDT, M., HYNDMAN, R., JAMES, T., LU, Y. A. and CRAYMER, M. 2003. Current tectonics of northern Cascadia from a decade of GPS measurements. *Journal of Geophysical Research-Solid Earth* 108, B12, DOI:10.1029/2003JB002653.

MAZZOTTI, S., LE PICHON, X., HENRY, P. and MIYAZAKI, S. 2000. Full interseismic locking of the Nankai and Japan-west Kurile subduction zones: an analysis of uniform elastic strain accumulation in Japan constrained by permanent GPS. *Journal of Geophysical Research-Solid Earth* 105, 13159-13177.

MCCULLOCH, D. S. and BONILLA, M. G. 1970: Effects of the earthquake of March 27, 1964, on the Alaska Railroad. *U.S. Geological Survey Professional Paper 545-D*, D1-D161.

MCGEE, W. J. 1890. Encroachments of the sea. *Forum*, 437-499.

MELBOURNE, T. I., WEBB, F. H., STOCK, J. M. and REIGBER, C. 2002. Rapid postseismic transients in subduction zones from continuous GPS. *Journal of Geophysical Research-Solid Earth* 107, B10, ETG10.1-ETG10.10.

MELTZNER, A. J., SIEH, K., ABRAMS, M., AGNEW, D. C., HUDNUT, K. W., AVOUAC, J. P. and NATAWIDJAJA, D. H. 2006. Uplift and subsidence associated with the great Aceh-Andaman earthquake of 2004. *Journal of Geophysical Research-Solid Earth* 111, B02407, DOI:10.1029/2005JB003891.

MICHURIN, A. N. and FUKS, V. R. 1988: Geografiya i Praktika [Geography and Practice]. In Seliverstov, Y. P. and Chistobaev, A. I., (Eds.), Leningrad: Nauka Publications, 209 [In Russian].

MILNE, G. A., LONG, A. J. and BASSETT, S. E. 2005. Modelling Holocene relative sea-level observations from the Caribbean and South America. *Quaternary Science Reviews* 24, 1183-1202.

MILNE, G. A. and MITROVICA, J. X. 2008. Searching for eustasy in deglacial sea-level histories. *Quaternary Science Reviews* 27, 2292-2302.

MITROVICA, J. X., MILNE, G. A. and DAVIS, J. L. 2001. Glacial isostatic adjustment on a rotating earth. *Geophysical Journal International* 147, 562-578.

MIURA, S., SUWA, Y., HASEGAWA, A. and NISHIMURA, T. 2004. The 2003 M8.0 Tokachi-Oki earthquake - how much has the great event paid back slip debts? *Geophysical Research Letters* 31, L05613, DOI:10.1029/2003GL019021.

MIYAZAKI, S., LARSON, K. M., CHOI, K. H., HIKIMA, K., KOKETSU, K., BODIN, P., HAASE, J., EMORE, G. and YAMAGIWA, A. 2004. Modeling the rupture process of the 2003 September 25 Tokachi-Oki (Hokkaido) earthquake using 1-Hz GPS data. *Geophysical Research Letters* 31, L21603, DOI:10.1029/2004GL021457.

MONTAGU, G. 1808: *Supplement to Testacea Britannica*. Exeter: S. Woolmer, p. 183.

MORISHIMA, M. and CHIJI, M. 1952. Foraminiferal thanatocoenoses of Akkeshi Bay and its vicinity. *Memoir of the College of Science, University of Kyoto (series B)* 22, 113-117.

MORIWAKE, N. 2005: Information Sheet on Ramsar Wetlands (RIS): Tofutsu-ko. Gland, Switzerland: Ramsar, p. 7.

MUHS, D. R., KENNEDY, G. L. and ROCKWELL, T. K. 1994. Uranium-series ages of marine terrace corals from the Pacific coast of North-America and implications for Last-Interglacial sea-level history. *Quaternary Research* 42, 72-87.

MURRAY, J. W. 1968. The living foraminifera of Christchurch Harbour, England. *Micropaleontology* 14, 83–96.

MURRAY, J. W. 1971. Living foraminiferids of tidal marshes: a review. *Journal of Foraminiferal Research* 1, 153-161.

MURRAY, J. W. 1979: *British Nearshore Foraminiferids*. London: Academic Press, p. 62.

MURRAY, J. W. 1982. Benthic foraminifera: the validity of living, dead or total assemblages for the interpretation of palaeoecology *Journal of Micropalaeontology* 1, 137-140.

MURRAY, J. W. 1991: *Ecology and Palaeoecology of Benthic Foraminifera* Harlow: Longman Scientific and Technical, p. 397.

MURRAY, J. W. 2000. JFR comment: the enigma of the continued use of total assemblages in ecological studies of benthic foraminifera. *Journal of Foraminiferal Research* 30, 244-245.

MURRAY, J. W. and ALVE, E. 1999. Natural dissolution of modern shallow water benthic foraminifera: taphonomic effects on the palaeoecological record. *Palaeogeography, Palaeoclimatology, Palaeoecology* 146, 195-209.

NAKANO, S., YAMAMOTO, T., IWAYA, T., ITOH, J. and TAKADA, A. 2001: Quaternary Volcanoes of Japan. National Institute of Advanced Science and Technology, Geological Survey of Japan.

NAOMICHI, M. 2000. Eruptive History of Rausudake volcano during the last 2200 years. *Bulletin of the Volcanological Society of Japan* 45, 75-85.

NELSON, A. R. 2007: Sea-levels, late Quaternary: tectonic locations. In Elias, S., (Ed.), *The Encyclopaedia of the Quaternary*, Amsterdam: Elsevier, 3072-3087.

NELSON, A. R. and KASHIMA, K. 1993. Diatom zonation in Southern Oregon tidal marshes relative to vascular plants, foraminifera, and sea-level. *Journal of Coastal Research* 9, 673-697.

NELSON, A. R., KELSEY, H. M. and WITTER, R. C. 2006. Great earthquakes of variable magnitude at the Cascadia subduction zone. *Quaternary Research* 65, 354-365.

NELSON, A. R., OTA, Y., UMITSU, M., KASHIMA, K. and MATSUSHIMA, Y. 1998. Seismic or hydrodynamic control of rapid late-Holocene sea-level rises in southern coastal Oregon, USA? *Holocene* 8, 287-299.

NELSON, A. R., SAWAI, Y., JENNINGS, A. E., BRADLEY, L. A., GERSON, L., SHERROD, B. L., SABEAN, J. and HORTON, B. P. 2008. Great-earthquake paleogeodesy and tsunamis of the past 2000 years at Alsea Bay, central Oregon coast, USA. *Quaternary Science Reviews* 27, 747-768.

NELSON, A. R., SHENNAN, I. and LONG, A. J. 1996. Identifying coseismic subsidence in tidal-wetland stratigraphic sequences at the Cascadia subduction zone of western North America. *Journal of Geophysical Research - Solid Earth* 101, 6115-6135.

NIIDA, K. and KITO, N. 1986. Cretaceous arc-trench systems in Hokkaido. *Monographs of the Associationof the Geological Collaboration of Japan* 31, 379-402 [In Japanese with English abstract].

NISHIMURA, T., HIRASAWA, T., MIYAZAKI, S., SAGIYA, T., TADA, T., MIURA, S. and TANAKA, K. 2004. Temporal change of interplate coupling in northeastern Japan during 1995-2002 estimated from continuous GPS observations *Geophysical Journal International* 157, 901-916.

NOMURA, R. and SETO, K. 1992: Benthic foraminifera from brackish lake Nakanoumi, San-in district, southwestern Honshu, Japan. In Ishizaki, K. and Saito, T., (Eds.), *Centenary of Japanese Micropaleontology*, Tokyo: Terra Scientific Publishing Company, 227-240.

ODAMAKI, M. and IWAMOTO, K. 1999: Currents and Tidal Observations by the Hydrographic Department of Maritime Safety Agency, off the Okhotsk Coast of Hokkaido. *Proceedings of the Second PICES Workshop on the Okhotsk Sea and Adjacent Areas*, 149-152.

OERTEL, G. F. 2005: Coastal lakes and lagoons. In Schwartz, M., (Ed.), *Encyclopaedia of Coastal Science (Encyclopaedia of Earth Sciences).* New York: Springer-Verlag 263-266.

OHIRA, A. 1995. Holocene evolution of peatland and palaeoenvironmental changes in the Sarubetsu Lowland, Hokkaido, northern Japan. *Geographical Review of Japan (Chirigaku hyoron)* 68A, 695-712.

OHIRA, A. 2000. Late Holocene peatland development in the Kutonebetsu River Lowland, northern Hokkaido, Japan. *Memoirs of the Faculty of Education and Culture, Miyazaki University (Natural Science)* 3, 1-11. [In Japanese with English abstract].

OHIRA, A., FUJIMOTO, K. and ADACHI, H. 2004. Relative sea-level changes in Furen-gawa Lowland, eastern Hokkaido. Research reports of Grants-in-Aid for Scientific

Research from the Japanese Ministry of Education, Science and Culture (Project number 13308004), 55-66. [In Japanese].

OHIRA, A. and UMITSU, M. 1996. Late Holocene geomorphic development of the costal alluvial lowlands of northern Hokkaido. *Journal of Geography* 105, 500-503. [In Japanese].

OHIRA, A. and UMITSU, M. 1999. Holocene relative sea-level changes and geomorphic development in the riverine coastal plain around Lake Ohnuma, northern Hokkaido, Japan. *Geographical Review of Japan (Chirigaku hyoron)* 72A, 536-555. [In Japanese with English abstract].

OHIRA, A., UMITSU, M. and HAMADE, S. 1993: Paleoenvironmental changes of small alluvial lowlands by the Lake Furen, Hokkaido, during the middle an late Holocene. *Summaries of Researches Using AMS at Nagoya University*, Nagoya University, Japan: Dating and Materials Research Center, 4-8. [In Japanese]

OHIRA, A., UMITSU, M. and HAMADE, S. 1994. Late Holocene development of peatlands in small alluvial lowlands around Lake Furen, eastern Hokkaido, Japan. *The Quaternary Research (Daiyonki-Kenkyu)* 33, 45-50. [In Japanese].

OHKUSHI, K., UCHIDA, M., AOKI, K., YONEDA, M., IKEHARA, K., MINOSHIMA, K., KAWAHATA, H., TADA, R., MURAYAMA, M. and SHIBATA, Y. 2007. Radiocarbon marine reservoir ages in the northwestern Pacific off Hokkaido Island, Japan, during the last deglacial period. *Radiocarbon* 49, 963-968.

OKUMURA, K. 1996. Tephrochronology, correlation, and deformation of marine terraces in Eastern Hokkaido, Japan. *Geographical Report of Tokyo Metropolitan University* 31, 19-26.

OTA, Y. and MACHIDA, H., editors. 1987: *Quaternary sea-level changes in Japan*. Basil: The Institute of British Geographers Special Publication Series 20, Blackwell.

OTA, Y. and OMURA, A. 1991. Late Quaternary shorelines in the Japanese Islands. *The Quaternary Research (Daiyonki-Kenkyu)* 30, 175-186.

OTA, Y., UMITSU, M. and MATSUSHIMA, Y. 1990. Recent Japanese research on relative sea level changes in the Holocene and related problems: review of studies between 1980 and 1988. *Quaternary Research (Daiyonki-Kenkyuu)* 29, 31-48. [In Japanese with English anstract].

OVERPECK, J. T., WEBB, T. and PRENTICE, I. C. 1985. Quantitative interpretation of fossil pollen spectra: dissimilarity coefficients and the method of modern analogs. *Quaternary Research* 23, 87-108.

OZARKO, D. L., PATTERSON, R. T. and WILLIAMS, H. F. L. 1997. Marsh foraminifera from Nanaimo, British Columbia: infaunal habitat and taphonomic implications. *Journal of Foraminiferal Research* 27, 51–68.

OZAWA, S., HASHIMOTO, M. and TADA, T. 1997. Vertical crustal movements in the coastal areas of Japan estimated from tidal observations. *Bulletin of the Geographical Survey Institute* 43, 1-22.

OZAWA, S., KAIDZU, M., MURAKAMI, M., IMAKIIRE, T. and HATANAKA, Y. 2004. Coseismic and postseismic crustal deformation after the M-w 8 Tokachi-oki earthquake in Japan. *Earth Planets and Space* 56, 675-680.

PATTERSON, R. T. 1990. Intertidal benthic foraminiferal biofacies on the Fraser River delta, British Columbia; modern distribution and paleoecological importance. *Micropaleontology* 36, 229-244.

PATTERSON, R. T., GEHRELS, W. R., BELKNAP, D. F. and DALBY, A. P. 2004. The distribution of salt marsh foraminifera at Little Dipper Harbour New Brunswick, Canada: applicable transfer functions in sea-level research. *Quaternary International* 120, 185-194.

PATTERSON, R. T., GUILBAULT, J.-P. and CLAGUE, J. J. 1999. Taphonomy of tidal marsh foraminifera: implications of surface sample thickness for high-resolution sea-level studies. *Palaeogeography, Palaeoclimatology, Palaeoecology* 149, 199-211.

PAUL, M. A. and BARRAS, B. F. 1998. A geotechnical correction for post-depositional sediment compression: examples from the Forth Valley, Scotland. *Journal of Quaternary Science* 13, 171-176.

PELTIER, W. R. 2004. Global glacial isostasy and the surface of the ice-age earth: the ice-5G (VM2) model and grace. *Annual Review of Earth and Planetary Sciences* 32, 111-149.

PELTIER, W. R., SHENNAN, I., DRUMMOND, R. and HORTON, B. 2002. On the postglacial isostatic adjustment of the British Isles and the shallow viscoelastic structure of the Earth. *Geophysical Journal International* 148, 443-475.

PETRUCCI, F., MEDIOLI, F. S., SCOTT, D. B., PIANETTI, F. A. and CAVAZZINI, R. 1983. Evaluation of the usefulness of foraminifera as sea level indicators in the Venice Lagoon (N Italy). *Acta Naturae Ateneo Parmense* 19, 63–77.

PHLEGER, F. B. 1960: *Ecology and Distribution of Recent Foraminifera*. Balitmore: Johns Hopkins Press, p. 297.

PHLEGER, F. B. 1970. Foraminiferal populations and marine marsh processes. *Limnology and Oceanography* 15, 522-534.

PHLEGER, F. B. 1977: Soils of marine marshes. In Chapman, V. J., (Ed.), *Wet Coastal Ecosystems*, Amsterdam: Elsevier, 69-77.

PHLEGER, F. B. and WALTON, W. R. 1950. Ecology of marsh and bay foraminifera, Barnstable, Massachusetts. *American Journal of Science* 248, 274-294.

PIRAZZOLI, P. A. 1991: *World Atlas of Holocene Sea-Level Changes*. Amsterdam: Elsevier, p. 300.

PIRAZZOLI, P. A. 2005: Marine Terraces. In Schwartz, M. L., (Ed.), *Encyclopaedia of Coastal Science* Dordrecht, The Netherlands Springer, p. 612.

PIRAZZOLI, P. A., RADTKE, U., HANTORO, W. S., JOUANNIC, C., HOANG, C. T., CAUSSE, C. and BEST, M. B. 1991. Quaternary raised coral-reef terraces on Sumba-Island, Indonesia. *Science* 252, 1834-1836.

PLAFKER, G. 1969: Tectonics of the March 27, 1964 Alaska earthquake. *U. S. Geological Survey Professional Paper 543-I*, 1-74.

PLAFKER, G. 1972. Alaskan earthquake of 1964 and Chilean earthquake of 1960 - implications for arc tectonics. *Journal of Geophysical Research* 77, 901-925.

PLAFKER, G. and SAVAGE, J. C. 1970. Mechanism of the Chilean earthquakes of May 21 and 22, 1960. *Geological Society of America Bulletin* 81, 1001-1030.

POLLITZ, F. F., BURGMANN, R. and BANERJEE, P. 2006a. Post-seismic relaxation following the great 2004 Sumatra-Andaman earthquake on a compressible self-gravitating Earth. *Geophysical Journal International* 167, 397-420.

POLLITZ, F. F., NYST, M., NISHIMURA, T. and THATCHER, W. 2006b. Inference of post-seismic deformation mechanisms of the 1923 Kanto earthquake. *Journal of Geophysical Research-Solid Earth* 111, B05408, DOI:10.1029/2005JB003901.

PRENTICE, I. C. 1980. Multidimensional scaling as a research tool in quaternary palynology: a review of theory and methods *Review of Palaeobotany and Palynology* 31, 71-104.

PREUSS, H. 1979: Progress in computer evaluation of sea-level data within the IGCP project no. 61. In Suguio, K., Fairchild, T. R., Martin, L. and Flexor, J., (Eds.), *International Symposium on coastal evolution in the Quaternary, September 11-18, 1978*, Sao-Paulo, Brazil, 104-134.

PUGH, D. T. 2004: *Changing Sea Levels: Effects of Tides, Weather, and Climate*. Cambridge: Cambridge University Press, p. 265.

PYE, K. and BLOTT, S. J. 2004. Particle size analysis of sediments, soils and related particulate materials for forensic purposes using laser granulometry. *Forensic Science International* 144, 19-27.

RABENHORST, M. C. 1988. Determination of organic and carbonate carbon in calcareous soils using dry combustion. *Soil Science Society of America Journal* 52, 965-969.

RAHMSTORF, S. 2007. A semi-empirical approach to projecting future sea-level rise *Science* 315, 368-370.

REAVIE, E. D., HALL, R. I. and SMOL, J. P. 1995. An expanded weighted-averaging model for inferring past total phosphorus concentrations from diatom assemblages in eutrophic British Columbia (Canada) lakes. *Journal of Paleolimnology* 14, 49-67.

REID, H. F. 1910: *The Mechanics of the Earthquake*. Washington D.C.: Carnegie Institution of Washington, p. 192.

REIMER, P. J., BAILLIE, M. G. L., BARD, E., BAYLISS, A., BECK, J. W., BERTRAND, C. J. H., BLACKWELL, P. G., BUCK, C. E., BURR, G. S., CUTLER, K. B., DAMON, P. E., EDWARDS, R. L., FAIRBANKS, R. G., FRIEDRICH, M., GUILDERSON, T. P., HOGG, A. G., HUGHEN, K. A., KROMER, B., MCCORMAC, G., MANNING, S., RAMSEY, C. B., REIMER, R. W., REMMELE, S., SOUTHON, J. R., STUIVER, M., TALAMO, S., TAYLOR, F. W., VAN DER PLICHT, J. and WEYHENMEYER, C. E. 2004. INTCAL04 terrestrial radiocarbon age calibration, 0-26 cal kyr BP. *Radiocarbon* 46, 1029-1058.

REIMER, P. J. and REIMER, R. W. 2001. A marine reservoir correction database and on-line interface. *Radiocarbon* 43, 461-463.

RITCHIE, J. C. and MCHENRY, J. R. 1990. Application of radioactive fallout cesium-137 for measuring soil erosion and sediment accumulation rates and patterns: a review. *Journal of Environmental Quality* 19, 215-233.

RIVEIROS, N. V., BABALOLA, A. O., BOUDREAU, R. E. A., PATTERSON, R. T., ROE, H. M. and DOHERTY, C. 2007. Modern distribution of salt marsh foraminifera and thecamoebians in the Seymour-Belize Inlet Complex, British Columbia, Canada. *Marine Geology* 242, 39-63.

ROBBINS, J. A. 1978: Geochemical and geophysical applications of radioactive lead. In Nriagu, J. O., (Ed.), *Biogeochemistry of lead in the environment*: Elsevier, 285-393.

ROHLING, E. J., GRANT, K., BOLSHAW, M., ROBERTS, A. P., SIDDALL, M., HEMLEBEN, C. and KUCERA, M. 2009. Antarctic temperature and global sea level closely coupled over the past five glacial cycles. *Nature Geoscience* 2, 500-504.

RONGVED, L. and FRASIER, J. T. 1958. Displacement discontinuity in the elastic half-space. *Journal of Applied Mechanics* 25, 25–128.

ROSTAMI, K., PELTIER, W. R. and MANGINI, A. 2000. Quaternary marine terraces, sea-level changes and uplift history of Patagonia, Argentina: comparisons with predictions of the ICE-4G (VM2) model of the global process of glacial isostatic adjustment. *Quaternary Science Reviews* 19, 1495-1525.

SAFFERT, H. and THOMAS, E. 1998. Living foraminifera and total populations in salt marsh peat cores: Kelsey marsh (Clinton, CT) and the Great Marshes (Barnstaple, MA). *Marine Micropaleontology* 33, 175-202.

SAKAGUCHI, Y. 1959. The coastal movement of Hokkaido in the Latest Geological Age. *Geographical Review of Japan* 32, 401-431. [In Japanese with English abstract].

SAKAKIBARA, M., NIIDA, K., TODA, H., KITO, N., KIMURA, G., TAJIKA, J., KATO, T., YOSHIDA, A. and THE RESEARCH GROUP OF THE TOKORO BELT. 1986. Nature and tectonic history of the Tokoro Belt *Monographs of the Association of the Geological Collaboration of Japan* 31, 173-187.

SASAKI, K., OMURA, A., MIWA, T., TSUJI, Y., MATSUDA, H., NAKAMORI, T., IRYU, Y., YAMADA, T., SATO, Y. and NAKAGAWA, H. 2006. Th-230/U-234 and C-14 dating of a lowstand

coral reef beneath the insular shelf off Irabu Island, Ryukyus, southwestern Japan. *Island Arc* 15, 455-467.

SATAKE, K. 2004. Detection of Kuril subduction-zone earthquakes from remote historic records in Honshu, Japan, between 1656 and 1867. *Annals of Geophysics* 47, 369-378.

SATAKE, K. and ATWATER, B. F. 2007. Long-term perspectives on giant earthquakes and tsunamis at subduction zones. *Annual Review of Earth and Planetary Sciences* 35, 349–374.

SATAKE, K., HIRATA, K., YAMAKI, S. and TANIOKA, Y. 2006. Re-estimation of tsunami source of the 1952 Tokachi-oki earthquake. *Earth Planets and Space* 58, 535-542.

SATAKE, K., NANAYAMA, S., YAMAKI, Y., TANIOKA, Y. and HIRATA, K. 2005. Variability among tsunami sources in the 17th–21st centuries along the southern Kuril Trench. *Advances in Natural and Technological Hazards Research* 23, 157–170.

SATAKE, K., SHIMAZAKI, K., TSUJI, Y. and UEDA, K. 1996. Time and size of a giant earthquake in Cascadia inferred from Japanese tsunami records of January 1700. *Nature* 379, 246-248.

SATO, H., IHIRA, M., MATSUDA, I. and KUMANO, S. 1997. Diatom assemblages and sedimentary environments during the mid- to late-Holocene in the Mokoto site along the Okhotsk Sea in Hokkaido, Japan. *Diatom* 13, 193-199.

SATO, H., MATSUDA, I., KATOH, S. and MATSUBARA, T. 2004. Holocene sedimentary environments and relative sea levels at a site along the coast of Lake Tofutsu in the eastern part of Hokkaido, Japan. *The Quaternary Research (Daiyonki-Kenkyu)* 43, 447-455. [In Japanese with English abstract].

SAUNDERS, J. B. 1957. Trochamminidae and certain Lituolidae (Foraminifera) from the recent brackish-water sediments of Trinidad, British West Indies. *Miscellaneous Collections* 134, 16 p.

SAUNDERS, J. B. 1958. Recent foraminifera of mangrove swamps and river estuaries and their fossil counterparts in Trinidad. *Micropaleontology* 4, 79-92.

SAVAGE, J. C. 1983. A dislocation model of strain accumulation and release at a subduction zone. *Journal of Geophysical Research* 88, 4984-4996.

SAVAGE, J. C. and THATCHER, W. 1992. Interseismic deformation at the Nankai Trough, Japan, subduction zone. *Journal of Geophysical Research-Solid Earth* 97, 11117-11135.

SAWAI, Y. 2001. Episodic emergence in the past 3000 years at the Akkeshi estuary, Hokkaido, northern Japan. *Quaternary Research* 56, 231-241.

SAWAI, Y. 2002. Evidence for 17th-century tsunamis generated on the Kuril-Kamchatka subduction zone, Lake Tokotan, Hokkaido, Japan. *Journal of Asian Earth Sciences* 20, 903-911.

SAWAI, Y., HORTON, B. P. and NAGUMO, T. 2004a. The development of a diatom-based transfer function along the Pacific coast of eastern Hokkaido, northern Japan - an aid in paleoseismic studies of the Kuril subduction zone. *Quaternary Science Reviews* 23, 2467-2483.

SAWAI, Y., KAMATAKI, T., SHISHIKURA, M., NASU, H., OKAMURA, Y., SATAKE, K., THOMSON, K. H., MATSUMOTO, D., FUJII, Y., KOMATSUBARA, J. and AUNG, T. T. 2009. Aperiodic recurrence of geologically recorded tsunamis during the past 5500 years in eastern Hokkaido, Japan. *Journal of Geophysical Research* 114, B01319, DOI:10.1029/2007JB005503.

SAWAI, Y. and MISHIO, W. 1998. Marine transgressions and regressions over the last 3000 years in Akkeshi Moor, Hokkaido, northern Japan. *The Quaternary Research (Daiyonki-Kenkyuu)* 37, 1–12. [In Japanese with English abstract].

SAWAI, Y. and NASU, H. 2005. A 4500-year record of emergence events at Onnetoh, Hokkaido, northern Japan, reconstructed using plant macrofossils. *Marine Geology* 217, 49-65.

SAWAI, Y., NASU, H. and YASUDA, Y. 2002. Fluctuations in relative sea-level during the past 3000 yr in the Onnetoh estuary, Hokkaido, northern Japan. *Journal of Quaternary Science* 17, 607-622.

SAWAI, Y., SATAKE, K., KAMATAKI, T., NASU, H., SHISHIKURA, M., ATWATER, B. F., HORTON, B. P., KELSEY, H. M., NAGUMO, T. and YAMAGUCHI, M. 2004b. Transient uplift after a 17th Century earthquake along the Kuril subduction zone. *Science* 306, 1918-1920.

SCHELLMANN, G. and RADTKE, U. 2004. A revised morpho- and chronostratigraphy of the Late and Middle Pleistocene coral reef terraces on Southern Barbados (West Indies). *Earth-Science Reviews* 64, 157-187.

SCHULTE, E. E. and HOPKINS, B. G. 1996: Estimation of organic matter by weight loss-on-ignition. In Magdoff, F. R., Tabatai, M. A. and Hanlon, E. A., (Eds.), *Soil organic matter: Analysis and interpretation*, Madison, Wisconsin: Soil Science Society of America (SSSA) 21–31.

SCOTT, D. B. 1976. Brackish-water foraminifera from southern California and description of Polysaccammina ipohalina n. gen., n. sp. . *The Journal of Foraminiferal Research* 6.

SCOTT, D. B. 1986: Foraminifera as sea-level indicators. In van de Plassche, P., (Ed.), *Sea-level Research: A Manual for the Collection and Evaluation of Data*, Norwich: GEO Books, 435-456.

SCOTT, D. B., COLLINS, E. S., DUGGAN, J., ASIOLI, A., SAITO, T. and HASEGAWA, S. 1996. Pacific rim marsh foraminiferal distributions: implications for sea-level studies. *Journal of Coastal Research* 12, 850-861.

SCOTT, D. B., HASEGAWA, S., SAITO, T., ITO, K. and COLLINS, E. 1995. Marsh foraminiferal and vegetation distributions in Nemuro Bay wetland areas, eastern Hokkaido.

Transactions and Proceedings of the Palaeontological Society of Japan, N.S. 180, 282-295.

SCOTT, D. B. and MEDIOLI, F. S. 1980a. Living vs. total foraminifera populations: their relative usefulness in paleoecology. *Journal of Paleontology* 54, 814-831.

SCOTT, D. B. and MEDIOLI, F. S. 1980b. Quantitative studies of marsh foraminifera distribution in Nova Scotia: implications for sea-level studies. *Journal of Foraminifera Research Special Publication* 17, 1-58.

SCOTT, D. B., MEDIOLI, F. S. and SCHAFER, C. T. 2001: *Monitoring in Coastal Environments Using Foraminifera and Thecamoebian Indicators*. Cambridge: Cambridge University Press, p. 177.

SCOTT, D. B., SCHNACK, E. J., FERRERO, L., ESPINOSA, M. and BARBOSE., C. F. 1990: Recent marsh foraminifera from the east coast of South America: comparison to the Northern Hemisphere. In Hemleben, C., Kaminski, M. A., Kuhnt, W. and Scott, D. B., (Eds.), *Paleoecology, Biostratigraphy, Paleoceanography and Taxonomy of Agglutinated Foraminifera*, Dordrecht, The Netherlands: Kluwer Academic Press, 717–738.

SCOTT, D. B., SUTER, J. R. and KOSTERS, E. C. 1991. Marsh foraminifera and arcellaceans of the lower Mississippi Delta: controls on spatial distributions. *Micropaleontology* 37, 373-392.

SCOTT, D. K. and LECKIE, R. M. 1990. Foraminiferal zonation of Great Sippwissett salt marsh (Falmouth, Massachusetts). *Journal of Foraminiferal Research* 20, 248-266.

SCOTT, D. S. and MEDIOLI, F. S. 1978. Vertical zonations of marsh foraminifera as accurate indicators of former sea-levels. *Nature* 272, 528-531.

SEN GUPTA, B. K. 1999: Foraminifera in marginal marine environments In Sen Gupta, B. K., (Ed.), *Modern Foraminfera*, Dordrecht: Kluwer Academic Publishers, 141-159.

SHACKLETON, N. J., BERGER, A. and PELTIER, W. R. 1990. An alternative astronomical calibration of the lower Pleistocene timescale based on ODP Site 677. *Transactions of the Royal Society of Edinburgh* 81, 251–261.

SHAW, J., GAREAU, P. and COURTNEY, R. C. 2002. Palaeogeography of Atlantic Canada 13–0 kyr. *Quaternary Science Reviews* 21, 1861-1878.

SHENNAN, I. 1982. Interpretation of Flandrian sea-level data from the Fenland, England. *Proceedings of the Geologists Association* 93, 53-93.

SHENNAN, I. 1986. Flandrian sea-level changes in the Fenland. II: Tendencies of sea-level movement, altitudinal changes, and local and regional factors. *Journal of Quaternary Science* 1, 155-179.

SHENNAN, I. 1989. Holocene crustal movements and sea-level changes in Great Britain. *Journal of Quaternary Science* 4, 77-89.

SHENNAN, I. 1994: Data synthesis: altitudinal trends. In Waller, M. P., (Ed.), *The Fenland Project, Number 9: Flandrian Environmental Change in Fenland, East Anglian Archaeology*, 53-60.

SHENNAN, I. and HAMILTON, S. 2006. Coseismic and pre-seismic subsidence associated with great earthquakes in Alaska. *Quaternary Science Reviews* 25, 1-8.

SHENNAN, I. and HORTON, B. 2002. Holocene land- and sea-level changes in Great Britain. *Journal of Quaternary Science* 17, 511-526.

SHENNAN, I., INNES, J. B., LONG, A. J. and ZONG, Y. Q. 1995. Holocene relative sea-level changes and coastal vegetation history at Kentra-Moss, Argyll, Northwest Scotland. *Marine Geology* 124, 43-59.

SHENNAN, I., LAMBECK, K., FLATHER, R., HORTON, B., MCARTHUR, J., INNES, J., LLOYD, J., RUTHERFORD, M. and WINGFIELD, R. 2000a. Modelling western North Sea palaeogeographies and tidal changes during the Holocene. *Geological Society, London, Special Publications* 166, 299-319.

SHENNAN, I., LAMBECK, K., HORTON, B. P., INNES, J. B., LLOYD, J. M., MCARTHUR, J. J. and RUTHERFORD, M. M. 2000b: Holocene isostasy and relative sea-level changes on the east coast of England. In Shennan, I. and Andrews, J., (Eds.), *Holocene land-ocean interaction and environmental change around the North Sea*, London: Geological Society, 275-298.

SHENNAN, I., LONG, A. J., RUTHERFORD, M. M., GREEN, F. M., INNES, J. B., LLOYD, J. M., ZONG, Y. and WALKER, K. J. 1996. Tidal marsh stratigraphy, sea-level change and large earthquakes. 1. A 5000 year record in Washington, USA. *Quaternary Science Reviews* 15, 1023-1059.

SHENNAN, I., LONG, A. J., RUTHERFORD, M. M., INNES, J. B., GREEN, F. M. and WALKER, K. J. 1998. Tidal marsh stratigraphy, sea-level change and large earthquakes - II: submergence events during the last 3500 years at Netarts Bay, Oregon, USA. *Quaternary Science Reviews* 17, 365-393.

SHENNAN, I., PELTIER, W. R., DRUMMOND, R. and HORTON, B. 2002. Global to local scale parameters determining relative sea-level changes and the post-glacial isostatic adjustment of Great Britain. *Quaternary Science Reviews* 21, 397-408.

SHENNAN, I., SCOTT, D. B., RUTHERFORD, M. and ZONG, Y. Q. 1999. Microfossil analysis of sediments representing the 1964 earthquake, exposed at Girdwood Flats, Alaska, USA. *Quaternary International* 60, 55-73.

SHENNAN, I., TOOLEY, M. J., DAVIS, M. J. and HAGGART, B. A. 1983. Analysis and interpretation of Holocene sea-level data. *Nature* 302, 404-406.

SHENNAN, I. and WOODWORTH, P. L. 1992. A comparison of Late Holocene and 20th-century sea-level trends from the UK and North-Sea region. *Geophysical Journal International* 109, 96-105.

SHERIDAN, M. F., WOHLETZ, K. H. and DEHN, J. 1987. Discrimination of grain-size sub-populations in pyroclastic deposits. *Geology* 15 367–370.

SHERROD, B. L. 2001. Evidence for earthquake-induced subsidence about 1100 yr ago in coastal marshes of southern Puget Sound, Washington. *Geological Society of America Bulletin* 113, 1299-1311.

SHERROD, B. L., BUCKNAM, R. C. and LEOPOLD, E. B. 2000. Holocene relative sea level changes along the Seattle fault at Restoration Point, Washington. *Quaternary Research* 54, 384-393.

SHIMAZAKI, K. 1972. Focal mechanism of a shock at the northwestern boundary of the pacific plate: extensional feature of the oceanic lithosphere and compressional feature of the continental lithosphere. *Physics of The Earth and Planetary Interiors* 6, 397-404.

SHIMAZAKI, K. 1974. Pre-seismic crustal deformation caused by an underthrusting oceanic plate, in eastern Hokkaido, Japan. *Physics of The Earth and Planetary Interiors* 8, 148-157.

SHIMAZAKI, K. and NAKATA, T. 1980. Time-predictable recurrence mode for large earthquakes. *Geophysical Research Letters* 4, 279–282.

SHIRASAWA, K., LEPPARANTA, M., SALORANTA, T., KAWAMURA, T., POLOMOSHNOV, A. and SURKOV, G. 2005. The thickness of coastal fast ice in the Sea of Okhotsk. *Cold Regions Science and Technology* 42, 25-40.

SHISHIKURA, M., ECHIGO, T. and KANEDA, H. 2007. Marine reservoir correction for the Pacific coast of central Japan using ^{14}C ages of marine molluscs uplifted during historical earthquakes. *Quaternary Research* 67, 286-291.

SIDDALL, M., BARD, E., ROHLING, E. J. and HEMLEBEN, C. 2006. Sea-level reversal during Termination II. *Geology* 34, 817-820.

SIEH, K. 1996. The repetition of large-earthquake ruptures. *Proceedings of the National Academy of Sciences* 93, 3764-3771.

SMITH, D. A., SCOTT, D. B. and MEDIOLI, F. S. 1984. Marsh foraminifera in the Bay of Fundy: modern distribution and application to sea-level determinations. *Atlantic Geology* 20, 127-142.

SOEDA, Y. 2002. Distribution characteristics of diatoms in Lake Tofutsu along the coast of Okhotsk Sea. *Bulletin of the Historical Museum of Hokkaido* 30, 27-38. [In Japanese with English abstract].

SOEDA, Y. and AKAMATSU, M. 2001. Sea-level change from the 10th to 17th centuries around Lake Saroma, eastern Hokkaido. *The Quaternary Research (Daiyonki-Kenkyu)* 40, 423-430. [In Japanese with English abstract].

SOUTHALL, K. E., GEHRELS, W. R. and HAYWARD, B. W. 2006. Foraminifera in a New Zealand salt marsh and their suitability as sea-level indicators. *Marine Micropaleontology* 60, 167-179.

SOUTHON, J. R., RODMAN, A. O. and TRUE, D. 1995. A comparison of marine and terrestrial radiocarbon ages from northern Chile. *Radiocarbon* 37, 389-393.

SPENCER, R. S. 2000. Foraminiferal assemblages from a Virginia salt marsh, Phillips Creek, Virginia *The Journal of Foraminiferal Research* 30, 143-155.

STEKETEE, J. A. 1958. On Volterra's dislocations in a semi-infinite elastic medium. *Canadian Journal of Physics* 36, 192-205.

STIRLING, C. H., ESAT, T. M., LAMBECK, K. and MCCULLOCH, M. T. 1998. Timing and duration of the Last Interglacial: evidence for a restricted interval of widespread coral reef growth. *Earth and Planetary Science Letters* 160, 745-762.

STIRLING, C. H., ESAT, T. M., MCCULLOCH, M. T. and LAMBECK, K. 1995. High-precision U-series dating of corals from Western-Australia and implications for the timing and duration of the Last Interglacial. *Earth and Planetary Science Letters* 135, 115-130.

STUIVER, M. and BRAZIUNAS, T. F. 1993. Modelling atmospheric ^{14}C influences and ^{14}C ages of marine samples to 10000 BC. *Radiocarbon* 35, 137-191.

STUIVER, M., PEARSON, G. W. and BRAZIUNAS, T. F. 1986. Radiocarbon age calibration of marine samples back to 9000 cal yr BP. *Radiocarbon* 28, 980-1021.

SUGIHARA, K., NAKAMORI, T., IRYU, Y., SASAKI, K. and BLANCHON, P. 2003. Holocene sea-level change and tectonic uplift deduced from raised reef terraces, Kikai-jima, Ryukyu Islands, Japan. *Sedimentary Geology* 159, 5-25.

SUMMERFIELD, M. A. 1991: *Global Geomorphology: An Introduction to the Study of Landforms*. London/New York: Longman/Wiley, p. 537.

SZABO, B. J., LUDWIG, K. R., MUHS, D. R. and SIMMONS, K. R. 1994. Th-230 ages of corals and duration of the Last Interglacial sea-level high stand on Oahu, Hawaii. *Science* 266, 93-96.

SZKORNIK, K., GEHRELS, W. R. and KIRBY, J. R. 2006. Salt-marsh diatom distributions in Ho Bugt (western Denmark) and the development of a transfer function for reconstructing Holocene sea-level changes. *Marine Geology* 235, 137-150.

TADA, K. and NISHIHAMA, Y. 1988: Studies about lake water in Lake Saroma, Hokkaido: Reports of Hokkaido Abashiri Fisheries Experimental Station. 209-213 [In Japanese].

TAKAHASHI, H., NAKAO, S., OKAZAKI, N., KOYAMA, J., SAGIYA, T., ITO, T., OHYA, F., SATO, K., FUJITA, Y., HASHIMOTO, M., HOSO, Y., KATO, T., IINUMA, T., FUKUDA, J., MATSUSHIMA, T., KOHNO, Y. and KASAHARA, M. 2004. GPS observation of the first month of postseismic crustal deformation associated with the 2003 Tokachi-oki earthquake

(M-JMA 8.0), off southeastern Hokkaido, Japan. *Earth Planets and Space* 56, 377-382.

TAKATA, H., TAKAYASU, K. and HASEGAWA, S. 2006. Foraminifera in an organic-rich, brackish-water lagoon, Lake Saroma, Hokkaido, Japan. *Journal of Foraminiferal Research* 36, 44-60.

TAKEI, T., MINOURA, K., TSUKAWAKI, S. and NAKAMURA, T. 2002. Intrusion of a branch of the Oyashio Current into the Japan Sea during the Holocene. *Paleoceanography* 17, 1039, DOI:1010.1029/2001PA000666.

TAMURA, T., MURAKAMI, F., NANAYAMA, F., WATANABE, K. and SAITO, Y. 2008. Ground-penetrating radar profiles of Holocene raised-beach deposits in the Kujukuri strand plain, Pacific coast of eastern Japan. *Marine Geology* 248, 11-27.

TAMURA, T., NANAYAMA, F., SAITO, Y., MURAKAMI, F., NAKASHIMA, R. and WATANABE, K. 2007. Intra-shoreface erosion in response to rapid sea-level fall: depositional record of a tectonically uplifted strand plain, Pacific coast of Japan. *Sedimentology* 54, 1149-1162.

TANIOKA, Y., HIRATA, K., HINO, R. and KANAZAWA, T. 2004. Slip distribution of the 2003 Tokachi-oki earthquake estimated from tsunami waveform inversion. *Earth, Planets and Space* 56, 373-376.

TANIOKA, Y., SATAKE, K. and HIRATA, K. 2007: Recurrence of recent large earthquakes along the Southernmost Kurile-Kamchatka subduction zone,. In Eichelberger, J., Gordeev, E., Kasahara, M., Izbekov, P. and Lees, J. M., (Eds.), *Volcanism and Subduction: The Kamchatka Region*, Washington, D.C.: American Geophysical Union, 145-152.

TER BRAAK, C. J. F. 1986. Canonical correspondence analysis: a new eigenvector for multivariate gradient analysis. *Ecology* 67, 1167-1179

TER BRAAK, C. J. F. 1987. The analysis of vegetation-environment relationships by canonical correspondence-analysis. *Vegetatio* 69, 69-77.

TER BRAAK, C. J. F. and JUGGINS, S. 1993. Weighted averaging partial least-squares regression (WA-PLS) - an improved method for reconstructing environmental variables from species assemblages. *Hydrobiologia* 269, 485-502.

TER BRAAK, C. J. F. and PRENTICE, I. C. 1988. A theory of gradient analysis. *Advances in Ecological Research* 18, 271-317.

TER BRAAK, C. J. F. and ŠMILAUER, P. 2002: *CANOCO reference manual and CanoDraw for Windows user's guide: software for canonical community ordination (version 4.5)*. Wageningen, The Netherlands: Biomteris, p. 500.

TER BRAAK, C. J. F. and VERDONSCHOT, P. F. M. 1995. Canonical correspondence analysis and related multivariate methods in aquatic ecology. *Aquatic Sciences* 57, 225-289.

THATCHER, W. 1984. The earthquake deformation cycle at the Nankai Trough, southwest Japan. *Journal of Geophysical Research* 89, 3087-3101.

THATCHER, W. 1989. Earthquake recurrence and risk assessment in circum-Pacific seismic gaps. *Nature* 341, 432-434.

THATCHER, W. and RUNDLE, J. B. 1984. A viscoelastic coupling model for the cyclic deformation due to periodically repeated earthquakes at subduction zones. *Journal of Geophysical Research* 89, 7631-7640.

THOMAS, A. L., HENDERSON, G. M., DESCHAMPS, P., YOKOYAMA, Y., MASON, A. J., BARD, E., HAMELIN, B., DURAND, N. and CAMOIN, G. 2009: Penultimate deglacial sea-level timing from uranium/thorium dating of Tahitian corals. *Science* 324, 1186-1189.

THOMPSON, W. G., SPIEGELMAN, M. W., GOLDSTEIN, S. L. and SPEED, R. C. 2003. An open-system model for U-series age determinations of fossil corals. *Earth and Planetary Science Letters* 210, 365-381.

THOMSON, K. H. 2004: The development of foraminiferal and lithostratigraphical-based transfer functions as an aid in the palaeoseismic study of the Kuril subduction zone. Unpublished MSc thesis, Royal Holloway (University of London), p. 70.

TOBIN, R., SCOTT, D. B., COLLINS, E. S. and MEDIOLI, F. S. 2005. Infaunal benthic foraminifera in some North American marshes and their influence on fossil assemblages. *Journal of Foraminiferal Research* 35, 130-147.

TODD, R. and BRÖNNIMANN, P. 1957. Recent Foraminifera and Thecamoebina from the eastern Gulf of Paria. *Cushman Foundation For Foraminiferal Research, Special Publication* 3, p. 43.

TOKUI, Y. 1989. Volcanic eruptions and their effects on human activity, in Hokkaido, Japan. *Annals of Ochanomizu Geographical Society* 30, 27-33 [In Japanese].

TOOLEY, M. J. 1978: *Sea-level Changes in North-west England during the Flandrian Stage*. Oxford: Clarendon Press, p. 232.

TOOLEY, M. J. 1982. Sea-level changes in northern England. *Proceedings of the Geologists' Association* 93, 43-51.

TROELS-SMITH, J. 1955. Karakterisering of løse jordarter (Characterization of unconsolidated sediments). *Danmarks Geologiske Undersøgelse* 4, 38-73.

TURNEY, C. S. M. and BROWN, H. 2007. Catastrophic early Holocene sea level rise, human migration and the Neolithic transition in Europe. *Quaternary Science Reviews* 26, 2036-2041.

TZEDAKIS, P. C., ANDRIEU, V., DE BEAULIEU, J.-L., CROWHURST, S., FOLLIERI, M., HOOGHIEMSTRA, H., MAGRI, D., REILLE, M., SADORI, L., SHACKLETON, N. J. and WIJMSTRA, A. 1997. Comparison of terrestrial and marine records of changing climate of the last 500,000 years. *Earth and Planetary Science Letters* 150, 171-176.

UCHIO, T. 1962. Influence of the River Shinano on foraminifera and sediment grain size distribution. *Seto Marine Biological Laboratory Publications* 10, 363–393.

ULM, S. 2002. Marine and estuarine reservoir effects in central Queensland, Australia: Determination of Delta R values. *Geoarchaeology* 17, 319-348.

UMITSU, M. 1983: Chusekisou in Tokoro and Abashiri lowlands (post LGM deposits in Tokoro and Abashiri lowlands). Research reports of Grants-in-Aid for Scientific Research from the Japanese Ministry of Education, Science and Culture. Project number 57380021, 57-62. [In Japanese].

VAN DE PLASSCHE, O. 1986: *Sea-level Research: A Manual for the Collection and Evaluation of Data*. Norwich: Geobooks, p. 617.

VAN DER MOLEN, J. 1997: Tides in a Salt-Marsh (Great Marshes, Barnstable, Cape Cod, USA). PhD thesis, Vrije Universiteit (Free University), Amsterdam, p.104.

VANCE, D. J., CULVER, S. J., CORBETT, D. R. and BUZAS, M. A. 2006. Foraminifera in the Albemarle Estuarine System, North Carolina: distribution and recent environmental change. *The Journal of Foraminiferal Research* 36, 15-33.

VERDONCK, D. 2005. An inverse dislocation model of surface deformation in western Washington. *Tectonophysics* 395, 179-191.

VIGNY, C., SIMONS, W. J. F., ABU, S., BAMPHENYU, R., SATIRAPOD, C., CHOOSAKUL, N., SUBARYA, C., SOCQUET, A., OMAR, K., ABIDIN, H. Z. and AMBROSIUS, B. A. C. 2005. Insight into the 2004 Sumatra-Andaman earthquake from GPS measurements in southeast Asia. *Nature* 436, 201-206.

WALTON, W. R. 1952. Techniques for the reconstruction of living foraminifera. *Contributions of the Cushman Foundation for Foraminiferal Research* 3, 56-60.

WANG, K., HU, Y., BEVIS, M., KENDRICK, E., SMALLEY, R. and LAURIA, E. 2007. Crustal motion in the zone of the 1960 Chile earthquake: detangling earthquake-cycle deformation and forearc-sliver translation. *Geochemistry Geophysics Geosystems* 8, Q10010, DOI:10.1029/2007GC001721.

WANG, K., WELLS, R., MAZZOTTI, S., HYNDMAN, R. D. and SAGIYA, T. 2003. A revised dislocation model of interseismic deformation of the Cascadia subduction zone. *Journal of Geophysical Research-Solid Earth* 108, 2026, DOI:10.1029/2001JB001227.

WARD, G. K. and WILSON, S. R. 1978. Procedures for comparing and combining radiocarbon age determinations: a critique. *Archaeometry* 20, 19-31.

WARREN, A. D. 1957. Foraminifera of the Buras-Scofield Bayou Region, southeast Louisiana. *Contributions from the Cushman Foundation for Foraminiferal Research* 3, 56-60.

WILLIAMS, H. F. L., HUTCHINSON, I. and NELSON, A. R. 2005. Multiple sources for late-Holocene tsunamis at Discovery Bay, Washington State, USA. *Holocene* 15, 60-73.

WOO, H. J., CULVER, S. J. and OERTEL, G. F. 1997. Benthic foraminiferal communities of a barrier-lagoon system, Virginia, USA. *Journal of Coastal Research* 13, 1192-1200.

WOODROFFE, S. 2006: Holocene relative sea-level change in north Queensland, Australia. Unpublished PhD thesis, Durham University.

WOODROFFE, S. A. 2008. Recognising subtidal foraminiferal assemblages: implications for quantitative sea-level reconstructions using a foraminifera-based transfer function. *Journal of Quaternary Science* 24, 215 - 223.

WOODROFFE, S. A. 2009. Recognising subtidal foraminiferal assemblages: implications for quantitative sea-level reconstructions using a foraminiferal-based transfer function. *Journal of Quaternary Science* 24, 215-223.

WOODROFFE, S. A., HORTON, B. P., LARCOMBE, P. and WHITTAKER, J. E. 2005. Intertidal mangrove foraminifera from the central Great Barrier Reef shelf, Australia: implications for sea-level reconstruction. *Journal of Foraminiferal Research* 35, 259-270.

WOODROFFE, S. A. and LONG, A. J. 2009. Salt marshes as archives of recent sea level change in West Greenland. *Quaternary Science Reviews* 28, 1750-1761.

WOODROFFE, S. A. and LONG, A. J. In press. Reconstructing recent relative sea-level changes in West Greenland: local diatom-based transfer functions are superior to regional models. *Quaternary Science Reviews*.

WRIGHT, A. L., WANG, Y. and REDDY, K. R. 2008. Loss-on-ignition method to assess soil organic carbon in calcareous everglades wetlands. *Communications in Soil Science and Plant Analysis* 39, 3074-3083, DOI 10.1080/00103620802432931|PII 00103620905629812.

YAGI, Y., KIKUCHI, M. and NISHIMURA, T. 2003. Co-seismic slip, post-seismic slip, and largest aftershock associated with the 1994 Sanriku-haruka-oki, Japan, earthquake. *Geophysical Research Letters* 30, 2177, DOI:10.1029/2003GL018189.

YOKOYAMA, I. 1987. Vertical displacements in the eastern part of Hokkaido revealed by geodetic data. *Geophysical Bulletin of Hokkaido University, Sapporo, Japan* 49, 31-43 [In Japanese with English abstract].

YOKOYAMA, Y., NAKADA, M., MAEDA, Y., NAGAOKA, S., OKUNO, J., MATSUMOTO, E., SATO, H. and MATSUSHIMA, Y. 1996. Holocene sea-level change and hydro-isostasy along the west coast of Kyushu, Japan. *Palaeogeography, Palaeoclimatology, Palaeoecology* 123, 29-47.

YONEDA, M., HIROTA, M., UCHIDA, M., UZAWA, K., TANAKA, A., SHIBATA, Y. and MORITA, M. 2001. Marine radiocarbon reservoir effect in the western North Pacific observed in archaeological fauna. *Radiocarbon* 43, 465-471.

YONEDA, M., SHIBATA, Y., MORITA, M., HIROTA, M., SUZUKI, R., UZAWA, K., OHSHIMA, N. and DODO, Y. 2004. Interspecies comparison of marine reservoir ages at the Kitakogane

shell midden, Hokkaido, Japan. *Nuclear Instruments & Methods in Physics Research Section B-Beam Interactions with Materials and Atoms* 223-24, 376-381.

YONEDA, M., TANAKA, A., SHIBATA, Y., MORITA, M., UZAWA, K., HIROTA, M. and UCHIDA, M. 2002. Radiocarbon marine reservoir effect in human remains from the Kitakogane Site, Hokkaido, Japan. *Journal of Archaeological Science* 29, 529-536.

YONEDA, M., UNO, H., SHIBATA, Y., SUZUKI, R., KUMAMOTO, Y., YOSHIDA, K., SASAKI, T., SUZUKI, A. and KAWAHATA, H. 2007. Radiocarbon marine reservoir ages in the western Pacific estimated by pre-bomb molluscan shells. *Nuclear Instruments and Methods in Physics Research Section B: Beam Interactions with Materials and Atoms* 259, 432-437.

YOSHIDA, S. 1954. Studies on the Foraminifera of brackish waters. III. The Foraminifera of Lake Saroma. *Science Reports of the University of Tokyo Education, section C, Geology, Mineralogy, Geography* 3, 149-158 [In Japanese].

ZAZO, C. 1999. Interglacial sea levels. *Quaternary International* 55, 101-113.

ZONG, Y., SHENNAN, I., COMBELLICK, R. A., HAMILTON, S. L. and RUTHERFORD, M. M. 2003. Microfossil evidence for land movements associated with the AD 1964 Alaska earthquake. *Holocene* 13, 7-20.

ZONG, Y. Q. and HORTON, B. P. 1999. Diatom-based tidal-level transfer functions as an aid in reconstructing Quaternary history of sea-level movements in the UK. *Journal of Quaternary Science* 14, 153-167.

APPENDIX A

Foraminiferal Taxonomy

Original references to salt-marsh taxa identified to species level.

Species	Citation
Ammoastuta inepta	*Ammoastuta ineptus* Cushman and McCulloch (1939), p. 89, pl. 7, fig. 6.
Ammobaculites crassus	*Ammobaculites crassus* Warren (1957), p. 32, pl. 3, figs. 5-7.
Ammobaculites exiguss	*Ammobaculites exiguss* Cushman and Brönnimann (1948), p. 38, pl. 7, figs 7,8.
Ammobaculites subcatenulatus	*Ammobaculites subcatenulatus* Warren (1957), p. 32, pl. 3, figs. 11-13.
Ammonia aberdoveyensis	*Ammonia aberdoveyensis* Haynes (1973), p. 184, pl. 18, fig. 15.
Arenoparrella mexicana	*Trochammina inflata* (Montagu) var. mexicana Kornfeld, 1931: p.86
Balticammina pseudomacrescens	*Balticammina pseudomacrescens* Brönnimann *et al*. (1989), p. 169, pl. 1-3.
Cribrostromoides canariensis	*Nonionina canariensis* d'Orbigny (1839), p. 128, pl. 2, figs. 33, 34.
Haplophragmoides bonplandi	*Haplophragmoides bonplandi* Todd and Brönnimann (1957), p. 23, pl. 3, fig. 2.
Haplophragmoides manilaensis	*Haplophragmoides manilaensis* Anderson (1953), p. 22, pl. 4, fig. 7.
Haplophragmoides wilberti	*Haplophragmoides manilaensis* Anderson (1953), p. 21, pl. 4, fig. 7.
Haynesina germanica	*Nonion germanicum* Ehrenberg (1840), p. 23, illustrated in Ehrenberg (1840), pl. 2, figs. 1a-g.
Haynesina germanica	*Nonionina germanica* Ehrenberg (1840), p. 23 [figured in Ehrenberg (1840), pl. 2, figs. 1a-g].
Jadammina macrescens	*Trochammina inflata* (Montagu) var. macrescens

	Brady (1870), p. 290, pl. 11, figs. 5a-c.
Miliammina fusca	*Quinqueloculina fusca* Brady (1870), p. 47, pl. 11, figs. 2,3.
Miliammina obliqua	*Miliammina obliqua* Heron-Allen and Earland (1930), pl. V, figs. 9-14.
Miliammina petila	*Miliammina petila* Saunders (1958), p. 88, pl. 1, fig. 15.
Monotalea salsa	*Monotalea salsa* Brönnimann *et al*. (1992) p. 32, fig. 75.
Paratrochammina stoeni	*Paratrochammina stoeni* Brönniman and Zaninetti (1979) [figured in Brönniman *et al*. (1992), pl. 4, figs. 5-6.
Polysaccammina ipohalina	*Polysaccammina ipohalina* Scott (1976), p. 318, pl. 2, figs. 1-4.
Pseudothurammina limnetis	*Thurammina* (?) *limnetis*, Scott and Medioli (1980), p. 43, 44, pl. 1, figs. 1-3.
Siphotrochammina lobata	*Siphotrochammina lobata* Saunders (1957), p. 3, pl. 9, figs. 1, 2
Tiphotrocha comprimata	*Trochammina comprimata* Cushman and Brönnimann (1948), p. 41, pl. 8, figs. 1-3.
Trochammina hadai	*Trochammina hadai* Uchio (1962), p. 387, 388, pl. 18, fig. 9.
Trochammina inflata	*Nautilus inflatus* Montagu (1808), p. 81, pl. 18, fig. 3.

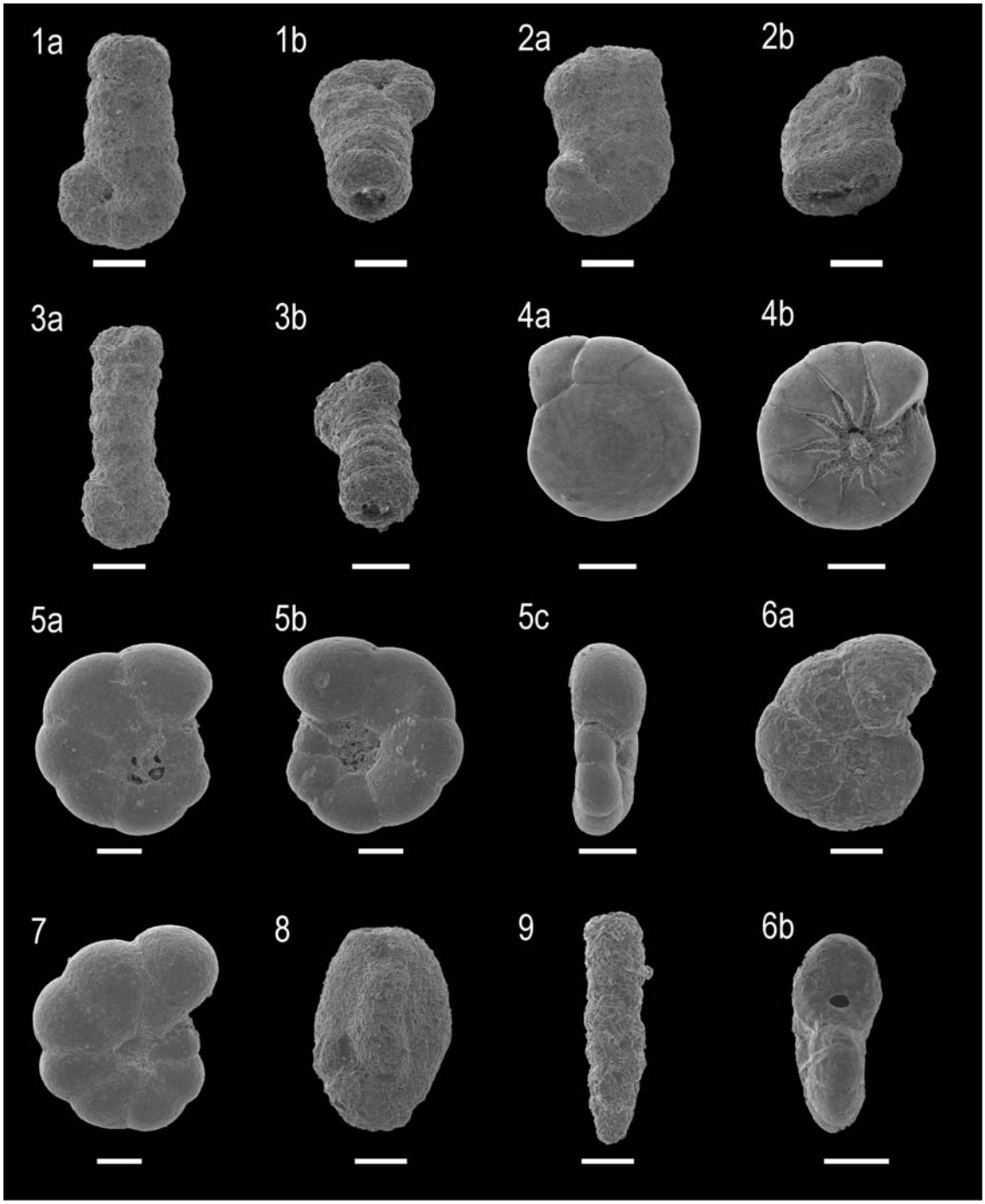

Plate 1. Scale bar = 100 µm. 1. *Ammobaculites crassus* (a. side view, b. oblique aperture view), 2. *Ammobaculites exiguss* (a. side view, b. oblique aperture view); 3. *Ammobaculites subcatenulatus* (a. side view, b. oblique aperture view); 4. *Ammonia aberdoveyensis* (a. spiral view, b. umbilical view); 5. *Balticammina pseudomacrescens* (a. spiral view, b, umbilical view, c, side view); 6. *Cribrostromoides canariensis* (a. side view, b. edge view); 7. *Haplophragmoides manilaensis* (side view); 8. *Miliammina fusca* (side view); 9. *Monotalea salsa* (side view).

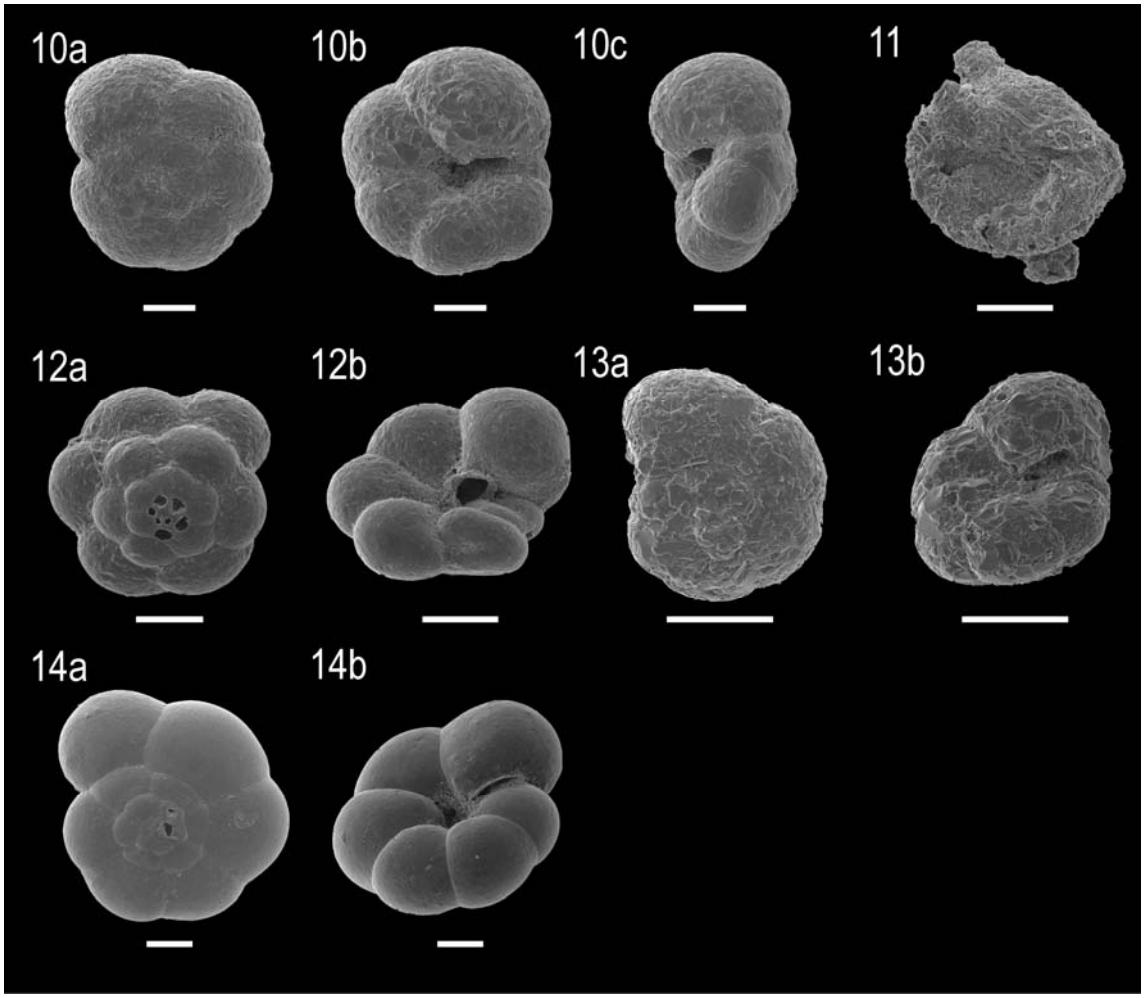

Plate 2. Scale bar = 100 µm. 10. *Paratrochammina stoeni* (a. spiral view, b. umbilical view, c. side view); 11. *Pseudothurammina limnetis* (oblique side view); 12. *Siphotrochammina lobata* (a. spiral view, b. oblique umbilical view); 13. *Trochammina hadai* (a. spiral view, b. oblique umbilical view); 14. *Trochammina inflata* (a. spiral view, b. oblique umbilical view).

APPENDIX B

Modern Foraminiferal Data

The tables that follow display modern foraminiferal counts from the six salt marshes studied in this thesis, as well as the two short cores from Akkeshi-ko which were used to investigate the infaunal foraminifera. The tables record raw counts, with **blue** numbers representing foraminifer dead, and **red** numbers indicating foraminifer which were found alive at the time of collection.

Infaunal cores

Akkeshi-ko (Low marsh infaunal core)	0-1		1-2		2-3		4-5		6-7		9-10		12-13		14-15		16-17		19-20	
Species																				
Ammobaculites crassus									2											
Ammobaculites exiguus						1		1		5		2								
Ammobaculites spp.						2		3		4										
Ammobaculites subcatenulatus										1										
Arenapella mexicana					1		1	1		1				2						1
Balticammina pseudomacrescens	3	17		8		21	1	17	1	33	1	34		6	1	78		37	1	34
Haplophragmoides manilaensis		18	1	14		22		22		12		13		6	1	5		10	1	19
Haplophragmoides spp.	9	8	3	7	3	15	2	12	7	7	4	15		11		2	1	12		9
Haplophragmoides wilberti	28	100	10	68	13	46	4	65	7	73	1	30	1	19	2	12		25	3	15
Jadammina macrescens	4	17	18	23	20	19	6	47	3	16	2	16	1	35		10	3	22	2	20
Miliammina 1										34		3				1				2
Miliammina fusca		17		24		28		30	1	53	1	129		22	1	143	1	146	3	81
Polysaccammina ipohalina								1						2						
Pseudothurammina limnetis							1													
Siphotrochammina lobata	1	5	1	3	1	6	1	11		6	1			2	1	6				2
Trochammina inflata	11	11	8	11	5	11	4	12	1	2	2	5		3	1	3				2
Total foraminifera counted	249		199		214		242		269		259		110		267		257		195	
Percentage dead	77.51		79.40		79.91		91.74		92.57		95.37		98.18		97.38		98.05		94.87	

Akkeshi-ko (High marsh infaunal core)	0-1		1-2		2-3		4-5		6-7		7-8		9-10		12-13	
Species																
Balticammina pseudomacrescens	8	14	8	28	12	18	4	19	1	33	2	31	3	14		1
Haplophragmoides manilaensis	24	94	25	112	20	145	32	91	9	59	18	63	21	40	2	12
Haplophragmoides spp.	18	10	16	7	15	1	20	8	11	2	14	12	15	5	2	1
Haplophragmoides wilberti	10	7	8	7	7	12	9	11	3	4	6	20	3	8		5
Jadammina macrescens	1	3	1	3	2	1	4	5	3	10	5	7	4	2		
Miliammina fusca	6	37	3	43	4	27	4	60	3	110	7	96	6	33		13
Miliammina 1												1				
Siphotrochammina lobata		1		1		1			1			2				
Trochammina inflata	1	1	4	1		1	1	1		1						
Total foraminifera counted	235		267		266		269		250		284		154		36	
Percentage dead	71.06		75.66		77.44		72.49		87.60		81.69		66.23		88.89	

Modern foraminiferal data

Akkeshi-ko	1	2	3	4	5	6	7	8	9	10	11	12	13	14	15	16
Species																
Ammobaculites exiguus															2	
Ammobaculites spp.														1		
Balticammina pseudomacrescens	1			1						1	1	1		4	1	1
Cribrostomoides canariensis	16	22	8	12	7	2	1 14	5	5	3	28	30	45	28	8	2
Haplophragmoides manilaensis		1					1		1						2	
Haplophragmoides spp.																1 2
Haplophragmoides wilberti				2			1		1	1			2	1 5	1	
Miliammina fusca				2	6	1	6	1 5	3		1		1 10	3 14	1	2
Paratrochammina stoeni	16 404	8 180	5 223	10 170	8 146	4 160	12 141	22 152	12 139	5 195	3 145	3 135	1 70	1 65	1 23	2 17
Trochammina hadai	10 43	2 26	53	7 60	3 45	2 57	10 34	7 50	2 65	1 51	55	70	1 59	75	35	1 33
Trochammina inflata						1	2		1	2			1	1	1	1 5
Ammonia spp.	3	2													11	1 10
Elphidium spp.	1															
Total foraminifera counted	**493**	**241**	**289**	**264**	**215**	**227**	**222**	**242**	**229**	**259**	**233**	**239**	**190**	**198**	**86**	**78**
Percentage dead	**94.93**	**95.85**	**98.27**	**93.56**	**94.88**	**97.36**	**89.64**	**87.60**	**93.89**	**97.68**	**98.71**	**98.74**	**98.42**	**97.47**	**98.84**	**92.31**
Elevation (m TP)	-1.90	-1.81	-1.74	-1.71	-1.73	-1.57	-1.41	-1.33	-1.23	-1.12	-1.04	-0.93	-0.82	-0.75	-0.62	-0.53
pH	8.05	8.18	8.11	8.46	8.46	8.55	7.80	7.99	7.64	8.01	7.66	8.41	7.95	8.01	8.41	8.41
LOI (%)	4.92	4.82	5.72	4.60	4.51	3.28	3.91	4.03	4.09	2.92	3.96	3.10	3.87	3.86	2.60	2.46
Porew ater salinity	34	34	34	35	34	34	34	34	34	34	34	34	34	34	34	34
Clay (%)	0.00	0.00	0.00	0.00	0.00	0.00	0.00	0.00	0.00	0.00	0.00	0.00	0.00	0.00	0.00	0.00
Silt (%)	88.41	89.04	90.64	87.42	89.21	80.03	87.21	94.28	85.89	68.24	68.49	66.23	64.52	57.69	43.27	40.82
Sand (%)	11.59	10.96	9.36	12.58	10.79	19.97	12.79	5.72	14.11	31.76	31.51	33.77	35.48	42.31	56.73	59.18
Distance (m)	0.00	200.50	322.10	792.50	803.80	866.10	965.60	1043.50	1124.30	1181.10	1241.00	1263.40	1336.30	1388.90	1432.70	1466.60

Mochiruppu (Transect A)	1		2		3		4		5		6		7		8		9	
Species																		
Ammobaculites crassus		5		3		1		1										
Ammobaculites exiguus		9		24		5		5		1		4						
Ammobaculites spp.		3		2		10		11		1								
Ammobaculites subcatenulatus		1		3		1												
Arenoparrella mexicana		1																
Balicammina pseudomacrescens		108	1	53		34		65		4		27	1	3		4		7
Haplophragmoides manilaensis		7		5		8						8		3		2	1	122
Haplophragmoides spp.		33		31		40		69		8		27	2	20		3		13
Haplophragmoides wilberti		1		1		3		2		1		6	1	13	3	6		
Jadammina macrescens	1	21				6		8		3		6	1	30	15	98		26
Miliammina 1										1		2		1				
Miliammina fusca	3	86	6	109		73	1	77		281	1	87		14		31		5
Monotalea salsa				5		3												
Paratrochammina stoeni	1	6	1	11		4		5										
Pseudothurammina limnetis																		52
Siphotrochammina lobata										8		31	1	52	7	75		1
Trochammina hadai		1						1										
Trochammina inflata				1		1		3		26		51	2	77	11	42		2
Ammonia spp.	1		1		2			1										
Haynesina germanica								1										
Total foraminifera counted	**288**		**257**		**191**		**250**		**334**		**250**		**221**		**297**		**229**	
Percentage dead	**97.9**		**96.5**		**99.0**		**99.6**		**100.0**		**99.6**		**96.4**		**87.9**		**99.6**	

Elevation (m TP)	-0.67	-0.62	-0.57	-0.52	0.03	0.08	0.14	0.19	0.24
pH	7.7	7.5	7.8	7.9	7	6.9	6.7	6.4	6.7
LOI (%)	7.6	6.71	6.63	7.09	32.52	30.31	70.81	58.49	72.82
Porewater salinity	26	30	25	26	26	30	16	10	4
Clay (%)	3.03	45.5	48.4	41.6	51.3	55.4	65.2	74.8	65.5
Silt (%)	17.92	54.94	58.65	56.21	64.83	63.35	72.45	77.52	71.8
Sand (%)	79.06	36.39	32.37	36.42	26	26.05	16.41	9.83	19.93
Distance (m)	0	28.38	55.1	74.13	80.11	83.54	90.98	99.14	123.75

Mochiruppu (Transect B)	1		2		3		4		5		6		7		8		9		10		11		12		13		14		15	
Species																														
Ammobaculites crassus				2		1																								
Ammobaculites exiguus		9		13		8		4		3		10		2								2				2		1		
Ammobaculites spp.		4		9		8		2		6		7								1		4		3		1		2		
Ammobaculites subcatenulatus				1		1						1		1																
Arenoparrella mexicana				1	1	1		1	1			1																1		
Balticammina pseudomacrescens		71		55		71		83		60		81		94		100		105		76		44		51	1	93	1	35		94
Haplophragmoides manilaensis		37		30		33		19		18		23		10		10		11		5	5	27	5	7		6		16		2
Haplophragmoides spp.		39		52		42	1	52		53	1	54		72		40		43		34	50	81	45	66	24	77	9	70	5	60
Haplophragmoides wilberti		8		8		7		31		14	1	21		23		22		30		7	12	2	7	22	7	22	1	16	5	40
Jadammina macrescens		16		23		35		66		100	2	47		42	1	38	1	41		18	1	24	11	13	1	24	3	33	2	51
Miliammina 1												1																		
Miliammina fusca		53		32		23		3		12		14	1	5				5		1	1	10		6		3		3		
Paratrochammina stoeni		8		1		14				4		1												3				1		
Pseudothurammina limnetis								1																						
Tiphotrocha comprimata																														1
Trochammina hadai						1		2																						
Trochammina inflata		14		6	2	4						6		1							1	2	1	6		4		3		
Ammonia spp.												1																		
Total foraminifera counted	**259**		**233**		**252**		**265**		**271**		**271**		**251**		**211**		**236**		**142**		**266**		**246**		**265**		**195**		**260**	
Percentage dead	**100.00**		**100.00**		**98.81**		**99.62**		**99.63**		**98.52**		**99.60**		**99.53**		**99.58**		**100.00**		**73.68**		**71.95**		**87.55**		**92.82**		**95.38**	

Elevation (m TP)	-0.41	-0.37	-0.32	-0.28	-0.24	-0.19	-0.15	-0.08	-0.04	0.01	0.08	0.12	0.17	0.21	0.23
pH	7.42	7.76	7.18	7.32	7.14	6.97	6.99	7.02	6.94	6.95	6.8	6.68	6.65	6.98	7
LOI (%)	6.63	10.55	18.92	20.96	20.88	13.36	37.67	41.36	45.10	42.83	34.79	37.35	47.99	50.40	57.37
Porewater salinity	26	24	28	25	25	23	25	25	23	20	15	15	13	10	10
Clay (%)	5.96	7.83	11.07	10.24	8.6	5.9	13.46	9.29	9.64	10.67	7.57	8.56	10.21	11.91	9.31
Silt (%)	43.68	56.69	69.43	72.15	72.28	60.26	66.52	71.96	73.17	64.66	54.95	59.91	63.28	67.55	70.04
Sand (%)	50.36	35.48	19.49	17.61	19.12	33.84	20.02	18.73	17.19	24.68	37.48	31.53	26.5	20.54	20.64
Distance (m)	0	1.88	2.45	2.73	2.89	3.31	3.76	4.11	4.59	4.75	4.9	5.22	6.59	7.9	12.23

Mochiruppu (Transect C)	1		2		3		4		5		6		7	
Species														
Ammobaculites crassus		1												
Ammobaculites exiguus		6		1		3								
Ammobaculites spp.		11		2		3								
Ammobaculites subcatenulatus		1												
Arenoparrella mexicana		1												
Balticammina pseudomacrescens		12		15		3								3
Haplophragmoides manilaensis	2	10	3	31	3	6	2	1				5		53
Haplophragmoides spp.		21	3	91	17	25	33	15		8		11		14
Haplophragmoides wilberti	1	15	18	13	12	21	7	13		2		1		8
Jadammina macrescens	4	25	14	36	26	34	43	60	12	46	8	80	10	59
Miliammina 1		4	1	2	2	9		4						
Miliammina fusca		151	7	122	6	105	4	30	3	16		1	1	12
Paratrochammina stoeni						1		1						
Siphotrochammina lobata				2		8		7	2	61	3	32	1	9
Trochammina inflata						9	3	14	22	82	27	77	6	27
Total foraminifera counted	**265**		**361**		**293**		**237**		**254**		**245**		**203**	
Percentage dead	**97.36**		**87.26**		**77.47**		**61.18**		**84.65**		**84.49**		**91.13**	

Elevation (m TP)	-0.01	0.04	0.08	0.13	0.17	0.22	0.28
pH	6.9	6.7	6.9	6.2	6.5	6.9	6.8
LOI (%)	32.05	27.07	38.84	46.94	55.99	67.99	72.75
Porewater salinity	13	5	5	5	3	0	0
Clay (%)	17.08	17.67	16.3	14.25	19.92	18.99	16.95
Silt (%)	75.07	76.2	78.41	79.45	76.09	79.38	77.81
Sand (%)	7.85	6.13	5.29	6.3	3.99	1.63	5.24
Distance (m)	0	9.18	14.84	16.34	19.82	29.65	32.91

Furen-ko	1		2		3		4		5		6		7		8		9		10		11		12		13		14		15		16		17		18	
Species																																				
Ammoastuta inepta																									1											
Ammobaculites crassis		4				1		4		8		2		2		1		1		2		1	1	4	3	6										
Ammobaculites exiguus		31		2		7		2	5	27				12		2		8	5	61	2	11	12	25	6	20		1								
Ammobaculites spp.		30		2		7		17	7	13		13		11	2	5		6		24		8	10	35	14	34	1									
Ammobaculites subcatenulatus										4		8		1						2		2		3	1	2										
Arenoparrella mexicana				2		2				1								4		2		1									2	4				
Balticammina pseudomacrescens		105		62	3	80		55	1	41	2	128	3	89	7	24		82		79	1	11		7		62	37	92	16	46	21	129	45	123	8	31
Haplophragmoides manilaensis		3						36		1		2		1		1		3		4	1	6						1				1				
Haplophragmoides spp.		17		42		1		6	4	6	1	10	6	32	23	173		38		16	48	89		1	2	8	7	26	3	3	6	26	2	9	36	130
Haplophragmoides wilberti		1		2		15		9		1		6	2	13	1	9				2	1	20		1		1	1	10		1		5	1	1		1
Jadammina macrescens		5	1	18		16		33	3	22	3	33	26	55	20	23	2	33		18	4	5		4	1	4	25	38	5	10	9	33	37	35	19	28
Miliammina 1						1				3						1		1						1	1	2										
Miliammina fusca		24	1	113	2	93	4	45	14	82		32		18		12	4	48	5	47	1	30	15	97	18	50	4	8		2		3	4	5		
Miliammina petila								2																												
Paratrochammina stoeni				1										1																						
Polysaccammina ipohalina																		1																		
Pseudothurammina limnetis																		1														1				1
Siphotrochammina lobata		23		2		4		12		3		5						1		1												4	1			
Trochammina inflata		1				4		1		4		5		10				7		4		4		4						1	2	15				
Ammonia spp.							2		12	2							4						12	1	14		4	1	24		2	1				
Haynesina germanaca			4	2			2	1	2	1							5	1		2			5	2	1				3						
Total foraminifera counted	**244**		**248**		**236**		**226**		**250**		**250**		**282**		**304**		**240**		**272**		**246**		**220**		**235**		**251**		**87**		**261**		**263**		**254**	
Percentage dead	**100.00**		**99.19**		**97.88**		**98.23**		**86.40**		**97.60**		**86.88**		**82.57**		**97.50**		**96.32**		**76.42**		**82.73**		**80.85**		**70.12**		**72.41**		**84.67**		**65.78**		**75.20**	

Elevation (m TP)	0.24	0.19	0.16	0.29	0.40	0.63	0.90	0.91	0.32	0.24	0.91	0.64	0.67	0.97	1.03	1.08	1.18	1.22
pH	7.98	7.95	7.70	7.86	7.39	8.04	7.84	7.60	7.86	7.82	7.62	7.22	6.91	6.95	6.94	6.38	6.18	6.08
LOI (%)	8.20	15.74	18.40	26.49	22.20	22.66	30.16	23.90	17.11	12.60	22.75	38.89	34.89	73.26	55.10	56.81	79.85	84.77
Porewater salinity	18.0	19.5	20.0	23.5	19.0	18.5	16.0	15.0	21.5	20.5	14.0	20.5	16.0	10.0	7.5	5.0	4.0	3.0
Clay (%)	3.45	4.93	4.90	5.35	7.21	6.40	6.57	6.87	5.43	4.83	6.87	6.70	8.73	4.97	7.73	6.81	6.13	3.64
Silt (%)	44.07	69.86	65.70	67.30	75.73	67.08	69.66	76.01	64.85	58.45	76.67	78.43	88.00	62.04	92.12	93.18	78.82	70.01
Sand (%)	52.48	25.21	29.40	27.35	17.06	26.52	23.77	17.12	29.72	36.72	16.46	14.87	3.28	32.98	0.15	0.01	15.05	26.35
Distance (m)	0.00	6.34	24.82	48.00	57.06	71.52	82.35	114.76	168.13	204.44	244.83	397.31	534.66	616.97	793.06	805.75	823.90	833.48

Tofutsu-ko	1		2		3		4		5	
Species										
Ammobaculites crassus	4	8	3	12						
Ammobaculites exiguus	15	48	14	77		2	1	4		
Ammobaculites spp.	5	48	11	84	3	6				
Ammobaculites subcatenulatus	19	29	4	17				1		
Balticammina pseudomacrescens	3	29		31	8	8		1		
Haplophragmoides manilaensis				1			4	8	8	6
Haplophragmoides spp.					5	13			6	3
Haplophragmoides wilberti	2	13	1	8	42	52	70	38	52	47
Jadammina macrescens	1	7		16	12	9	5	4		2
Miliammina 1	1	5		1				3		
Miliammina fusca	1	10		11	27	45	61	46	2	4
Trochammina inflata										2
Ammonia spp.						2	1	4		
Total foraminifera counted	**248**		**291**		**234**		**251**		**132**	
Percentage dead	**79.44**		**88.66**		**58.55**		**43.43**		**48.48**	

Elevation (m TP)	0.24	0.28	0.31	0.34	0.41
pH	7.42	6.32	6.91	6.88	7.01
LOI (%)	29.91	33.66	79.87	82.68	85.49
Porewater salinity	5.00	5.00	5.50	4.00	0.00
Clay (%)	7.68	7.62	3.51	1.26	2.15
Silt (%)	73.38	73.78	62.96	31.79	54.49
Sand (%)	18.95	18.60	33.52	66.95	43.35
Distance (m)	0.00	14.13	28.54	40.87	61.18

Sarama-ko	1		2		3		4		5		6		7		8		9		10		11		12	
Species																								
Ammobaculites crassus		25		17		16		1	3	8														
Ammobaculites exiguus		55		43	1	53		7	7	26		4												
Ammobaculites spp.		30		47		25		5	8	13		6												
Ammobaculites subcatenulatus		2		2		1																		
Arenoparrella mexicana												1		1				1		2		1		
Balticammina pseudomacrescens		1		6		5		1						1	7	27	24	79	39	31	86	157	10	6
Cribrostomoides canariensis		9		2		6		1																
Haplophragmoides manilaensis											1	5		3								3	34	69
Haplophragmoides spp.								2	1	4	8	4	4	8	2	4								
Haplophragmoides wilberti				4		7		1		1	2	1		8	1	12	1	8	10	8				
Jadammina macrescens			1	6		2		1		2	5	20	6	13	9	48	47	54	72	93	24	11		6
Miliammina fusca		18	1	81	3	58	1	125	1	201	2	353		73	1	8				1				1
Miliammina obliqua		3		6	2	8		5				1												
Monotalea salsa		4		3																				
Paratrochammina stoeni		2		1		2		1			1	4		1										
Polysaccammina ipohalina														1										
Miliammina 1						9		1		10		4	1											
Siphotrochammina lobata						1								2	2	30	1	27	1	7				1
Trochammina hadai						3		2																
Trochammina inflata					2	6		3			2	18	4	8	18	63	5	17	13	8		1		
Ammonia spp.		2																						
Total foraminifera counted	**151**		**220**		**210**		**157**		**285**		**442**		**134**		**232**		**264**		**285**		**283**		**127**	
Percentage dead	**100.00**		**99.09**		**96.19**		**99.36**		**92.98**		**95.25**		**88.81**		**82.76**		**70.45**		**52.63**		**61.13**		**65.35**	

Elevation (m TP)	0.06	0.05	0.17	0.16	0.29	0.37	0.45	0.48	0.48	0.52	0.63	0.70
pH	8.35	8.1	5	7.84	7.74	6.74	6.92	6.81	6.71	6.9	6.69	5.6
LOI (%)	4.98	6.11	8.96	12.92	14.48	42.05	66.25	57.28	61.49	75.68	83.57	68.45
Porewater salinity	30	30	30	30	30	30	26	19.5	14	12.5	13	6.5
Clay (%)	8.21	14.53	7.64	12.53	12.97	14.76	3.77	2.24	11.1	2.67	2.74	5.11
Silt (%)	52.71	84.1	56.89	81.33	84.3	70.37	27.89	8.91	55.1	19.1	31.72	42.79
Sand (%)	47.29	15.9	43.11	18.67	15.7	29.63	72.11	91.09	44.9	80.9	68.28	57.21
Distance (m)	0	5.56	12.06	17.75	23.01	31.16	35.27	38.08	41.75	47.8	62.55	119.83

Sarfutsoh-toh	1		2		3		4		5		6		7		8		9		10		11		12		13	
Species																										
Ammobaculites crassus		5		10	5	15	5	16	4	20	1	5		2												
Ammobaculites exiguus		7		10	6	29	13	42	4	20	6	20	2	9		1										
Ammobaculites spp.		6		12	21	32	7	44	6	10	5	10	4	10												1
Ammobaculites subcatenulatus						1		3				1														
Balticammina pseudomacrescens												1		2	1	16	10	28	3	96	6	29	4	85		11
Cribrostomoides canariensis				2		3																				
Haplophragmoides manilaensis														1		11		6		30		39	2	26		6
Haplophragmoides spp.							3	1	1	2	3	11	2	6		6	8	18	1	8	1	2		8		1
Haplophragmoides wilberti							1	4		5		1	3	29	2	39	29	130	3	133	27	237	3	48		12
Haynesina germanica			1																							
Jadammina macrescens										1						2		6		6	1	2		6		
Miliammina 1				2		3		24		37		29	1	15		1		3								1
Miliammina fusca		253		226	1	156		115	3	169	7	250	5	177		181	22	17	4	16				1		9
Miliammina petila		1		5								2														
Monotalea salsa				1																						
Pseudothurammina limnetis												2														
Total foraminifera counted	**272**		**269**		**272**		**278**		**282**		**354**		**268**		**260**		**277**		**300**		**344**		**183**		**41**	
Percentage dead	**100.00**		**99.63**		**87.87**		**89.57**		**93.62**		**93.79**		**93.66**		**98.85**		**75.09**		**96.33**		**89.83**		**95.08**		**100.00**	

Elevation (m TP)	-0.13	-0.15	-0.21	-0.09	0.00	0.13	0.16	0.28	0.28	0.44	0.51	0.62	0.71
pH	8.35	7.7	7.65	7.55	7.64	7.37	6.84	6.6	6.84	6.25	6.33	6.68	6.48
LOI (%)	6.07	5.9	14.71	12.78	12.56	14.86	21.81	35.09	35.88	37.91	55.34	88.28	88.2
Porewater salinity	2	0	0	0	0	0	0	0	0	0	0	0	0
Clay (%)	18.89	13.99	16.86	14.79	8.26	7.63	9.28	4.30	1.98	0.00	3.00	82.42	69.19
Silt (%)	71.82	78.07	73.69	76.79	80.95	81.43	78.90	82.21	83.08	81.66	80.22	15.87	25.96
Sand (%)	9.29	7.94	9.45	8.42	10.78	10.94	11.83	13.48	14.94	18.34	16.79	1.70	4.85
Distance (m)	0.0	85.3	91.5	93.3	97.6	101.8	105.8	109.1	109.7	120.6	124.9	164.8	180.2

APPENDIX C

Fossil Lithostratigraphic Data

The fossil lithostratigraphic data is listed on the attached CD.

APPENDIX D

Fossil Foraminiferal Data

Mochiruppu (North)	0-1	2-3	4-5	6-8	8-9	10-11	12-13	14-15	16-17	18-19	20-21	22-23	24-25
Species													
Ammobaculites crassus	2	2											
Ammobaculites exiguus	3	2		1								1	1
Ammobaculites spp.	3	5		1									5
Ammobaculites subcatenulatus		1											
Arenmpella mexicana						1			1				
Balicammina pseudomacrescens	19	12	53	65	71	81	15	22	5	68	6	6	10
Haplophragmoides manilaensis					1		5						
Haplophragmoides spp.	11	12	7	6	15	25	27	6	3	7	1	1	5
Haplophragmoides bonplani	2	1			1								
Haplophragmoides wilberti	26	31	14	17	103	68	90	36	13	20	5	6	
Jadammina macrescens	6	1	4	2	10	6	7	3	1	8	1	4	1
Miliammina fusca	182	185	79	161	54	77	117	72	72	225	120	126	24
Miliammina 1	12	16	2	3			1	2	1	2	1	3	1
Trochammina inflata	4	2	3			1						1	1
Unknown					4	3	2			1			
Total foraminifera counted	**270**	**270**	**162**	**256**	**259**	**262**	**264**	**141**	**96**	**331**	**134**	**148**	**48**

Mochiruppu (South)	0-1	2-3	3-4	4-5	5-6	6-7	8-9	10-11	12-13	13-14	15-16	17-18	20-21	22-23	24-25	26-27	28-29	30-31
Species																		
Ammobaculites crassus	4				1				2	4		2	25	11	1	2	3	10
Ammobaculites exiguus				1									5	5				
Ammobaculites spp.	3			2	2			1	4	8		3	30	31	5	5	2	6
Ammobaculites subcatenulatus													2	1	1			
Arenepella mexicana	1	1		2														
Balticammina pseudomacrescens	30	18	11	20	14	25	55	208	193	174	120	91	84	50	8	31	46	40
Haplophragmoides bonplandi	3	6		2	4			8	7	4	26	25	36	53	8	6	10	8
Haplophragmoides manilaensis	2					1		2	1		10	1	6	1	1	5		
Haplophragmoides spp.	3			1	6	1	6	1	1		1	2		2	2	3		
Haplophragmoides wilberti	11	9	4	43	30	38	98	6	7	6	2	16	27	23		10	14	
Jadammina macrescens		3	1		3	4	11	5	3	10	2	1		2		3		2
Miliammina 1		1			1	1						1	4	1				2
Miliammina fusca	8	19	40	28	33	39	75	6	49	46	4	33	75	62	11	6	5	46
Siphotrochammina lobata	1	3	1	4		1												
Trochammina inflata	1	22	175	148	126	142	27	7	2	4				2				
Total foraminifera counted	**67**	**82**	**232**	**251**	**220**	**252**	**272**	**244**	**269**	**256**	**165**	**175**	**294**	**244**	**37**	**71**	**80**	**114**

Furen-ko	0-1	1-2	2-3	3-5	4-5	5-6	6-7	7-8	8-9	9-10	10-11	12-13	13-14	14-15
Species														
Ammobaculites spp.				1			3							
Balticammina pseudomacrescens	4	14	24	46	161	84	71	16	10	25	25	100	98	148
Haplophragmoides bonplandi				1	6	3	4	1					1	1
Haplophragmoides manilaensis		2								2				3
Haplophragmoides spp.	1	16	94	90	17	33	66	144	219	173	156	121	46	1
Haplophragmoides wilberti	10	14	12	45	4	91	51	35	28	34	76	35	19	5
Jadammina macrescens	3	8	8	7	1	13	4	2	1	2				
Miliammina fusca		1	1	1		6	19	3	4				1	2
Pseudothurammina limnetis						1								
Siphotrochammina lobata	3	7				3								
Trochammina inflata	171	90	24	11	2	3	6	2		3	5	2		
Ammonia spp.		3				1			5			1		
Total foraminiferal counted	**192**	**155**	**163**	**202**	**191**	**238**	**224**	**203**	**267**	**239**	**262**	**259**	**165**	**160**

Tohoro	0-1	2-3	4-5	6-7	8-9	10-11	12-13	14-15	16-17	18-19	20-21	22-23	24-25	26-7	30-31	32-33	34-35	36-37	38-39	40-41	42-43	44-45	46-47	48-49
Species																								
Ammobaculites crassus	2	2										1	1	3	1									
Ammobaculites exiguus	3	2		1											1									
Ammobaculites spp.	3	5		1									5	3	2									
Ammobaculites subcatenulatus		1																						
Arenpelia mexicana						1			1										2		1		1	
Balticammina pseudomacrescens	19	12	53	65	71	81	15	22	5	68	6	6	10	14	213	251	223	240	287	227	214	214	225	221
Haplophragmoides bonplani	2	1			1																			
Haplophragmoides manilaensis					1		5																	2
Haplophragmoides spp.	11	12	7	6	15	25	27	6	3	7	1	1	5	1	3	1	2				2			1
Haplophragmoides wilberti	26	31	14	17	103	68	90	36	13	20	5	6		6	20	3	2	1	1	3	7	5	2	2
Jadammina macrescens	6	1	4	2	10	6	7	3	1	8	1	4	1	2	7		3		1	4	12	4	6	2
Miliammina 1	12	16	2	3			1	2	1	2	1	3	1	3										
Miliammina fusca	182	185	79	161	54	77	117	72	72	225	125	126	24	112	45	22	50	8	8	5	14	4		21
Miliammina petila																							55	
Siphrotrochammina lobata					1										3	17	6	31	12	23	16	25	3	
Trochammina inflata	4	2	3			1						1	1	2	7	5	6	6	1	7	3	15	11	
Unknown				4		3	2			1				1										
Total foraminifera counted	**270**	**270**	**162**	**260**	**256**	**262**	**264**	**141**	**96**	**331**	**139**	**148**	**48**	**147**	**302**	**299**	**292**	**286**	**312**	**269**	**269**	**267**	**303**	**249**

Tofutsu-ko	2-3	10-11	12-13	14-15	16-17	18-19	22-23	24-25	26-27	28-29	32-33	36-37	40-41	50-51	60-61
Species															
Ammobaculites crassus						8						16	15	10	18
Ammobaculites exiguus	1	1	1			32					1	100	88	66	74
Ammobaculites spp.	5	1			1	57	1				1	77	60	54	118
Ammobaculites subcatenulatus						3						4	1	4	4
Balicammina pseudomacrescens	5							13	13	26	1	2	1		
Haplophragmoides bonplani							52	43	53	55	16		1		
Haplophragmoides manilaensis			8	5	4		1	2	3	2					
Haplophragmoides spp.	68	12	17	1	11	7		8	3	4	7	2	7	5	
Haplophragmoides wilberti	31	45	35	35	74	4	5	29	29	13	5	1	4		
Jadammina macrescens						1	1			1		2			1
Miliammina 1						1						1			1
Miliammina fusca	9	1	1	8	63	9	195	128	129	131	221	10	4	1	1
Total foraminifera counted	**119**	**60**	**62**	**49**	**153**	**122**	**255**	**223**	**230**	**232**	**252**	**215**	**181**	**140**	**217**

Sarfutsoh-toh	2-3	4-5	6-7	8-9	10-11	12-13	14-15	16-17	18-19	20-1	22-23	24-5	26-28	28-29	30-31	32-33	34-5	40-41	42-43	44-45	46-47	48-49	51-2
Species																							
Ammobaculites spp.																			1				
Balticammina pseudomacrescens	28	111	16	16	4	4	7	2	3			11	2		2				1		1	1	2
Haplophragmoides manilaensis	24	24	31	11	18		15	11	1	3	1	12	13	18	5	2	3		1			1	
Haplophragmoides spp.	18	40	5	10	5	2		3		6	2	6	1	2	5			2					1
Haplophragmoides wilberti	187	74	135	65	120	95	107	63	18	9		27	6	11	6	1		3	1		2	2	1
Jadammina macrescens	1	5						1		5	1	4	2	5	2		3				1		
Miliammina 1		14	1			3	3		2									1	3	2	1		
Miliammina fusca	10	9	79	122	112	152	163	197	207	236	59	173	252	278	198	242	60	73	54	227	155	72	54
Miliammina petila	1		5	5	5		2								33	1		3		2			
Pseudothurammina limnetis						8	1																
Total foraminifera counted	**269**	**277**	**272**	**229**	**264**	**264**	**298**	**277**	**231**	**259**	**63**	**233**	**276**	**314**	**251**	**246**	**66**	**82**	**61**	**231**	**160**	**76**	**58**

APPENDIX E

Sea-level Database

1 INTRODUCTION

In Chapter Three I outline the construction of a database of Holocene sea-level index points and explain the main criteria used in its development. Here I provide further explanation of certain key fields and present the database in full.

The Hokkaido sea-level database has up to 70 fields detailing key parameters such as location, altitude, age together with other essential information on the nature of the dated material and its indicative meaning. This material derives from a series of publications, mainly in Japanese, which have a varied quality of index points related to the thrust of the original publication. The database is included in full at the end of this section.

2 DEFINITION OF KEY FIELDS

2.1 Altitude

The altitude of all samples relate to national datum in Japan (m TP). Where altitudinal information was unavailable, best estimates relied on finding approximate elevations using 1:50,0000 scale maps provided by the Geographical Survey Institute (http://watchizu.gsi.go.jp/), with an arbitrary error of ± 1m.

The elevation of index and limiting points within the core are subject to further errors relating to measurement, sampling density and levelling. These differ to the values associated with my own fieldwork (see Table 3.4) and are detailed below in Table 1.

Table 1 Quantitative estimates of various altitudinal error sources (after Shennan, 1982; 1986; Woodroffe, 2006; Brooks, 2007).

Source of error	Estimated total elevation error (m)
Measurement of depth using hand corer[1]	1% of core depth
Sampling density[2]	
1 bore hole/2m^2	± 0.06
1 bore hole/5400m^2	± 0.14
95% confidence level	± 0.30
Levelling error	± 0.05
Bench mark to national datum (m TP)	± 0.05

[1] Depth error is used as a percentage of the sample depth, to avoid unnecessary bias introduced through using a standardised error (usually 0.05 m).
[2] An accurate assessment of the depth of a stratigraphic boundary is dependent upon the roughness of the ground surface and the sample density (Makarovic, 1973). Shennan (1986) advocates a sampling density equal to a 30 m grid to avoid errors in the region of 0.30 m.

In addition to altitudinal errors described above, the error term on the reference water level for the index and limiting dates are subject to other error terms associated with the indicative range and the thickness of sample as detailed in Chapter Three of the main thesis.

2.2 Age (calibration methods)

Terrestrial samples

Radiocarbon dates were calibrated using Oxcal (www.c14.arch.ox.ac.uk/oxcal.html - Bronk Ramsey, 1995) with the InCal04 (Reimer *et al.*, 2004) calibration curves using a laboratory multiplier of 1 and 95% confidence limits. For marine-limiting dates involving shell material an assessment of the marine reservoir effect is critical to constrain ages from shell material, which comprise approximately 20% of the Hokkaido database. A preliminary assessment of the marine reservoir effect around Hokkaido shows distinct variability, necessitating a more detailed evaluation of the available literature which follows below.

Marine reservoir age

The marine reservoir effect (defined as R value) represents the difference of conventional radiocarbon age between the atmosphere and the surface seawater (Stuiver and Braziunas, 1993). In contrast to the global distribution of atmospheric ^{14}C which is almost uniform, seawater ^{14}C concentration varies markedly geographically due to climatic and oceanographic conditions. Whilst the global ocean reservoir age, R, averages around 400 ^{14}C years, regional variations (ΔR) can be significant. Polar waters exhibit greater reservoir ages (ΔR *c*. +400 to 800 ^{14}C yrs) than equatorial waters (ΔR *c*. 0 ^{14}C y) (Austin *et al.*, 1995). Empirical studies from specific geographic locations allow for the quantification of ΔR. The atmospheric testing of nuclear bombs in the 1950s and early 1960s meant the disturbance of the natural equilibrium of global ^{14}C distribution. Therefore the ΔR value is evaluated

from ^{14}C measurements of known-age marine samples formed before the early 1950s (when the effects of atmospheric testing was negligible or nil, i.e. the pre-bomb period).

The determination of reservoir ages for the Northwest Pacific is inadequate for the purposes of palaeoceanography and archaeology (Keigwin, 1998; Kuzmin *et al.*, 2001). Furthermore, the regional results as listed in the Marine Reservoir Correction Database (http://calib.qub.ac.uk/marine/) by Reimer and Reimer (2001) are based on too few studies necessitating a re-evaluation of the literature to more accurately quantity ΔR for the area surrounding Hokkaido. This part of the northern Pacific has a complicated regime of ocean currents (Figure 1) and there are a lack of reliable known-age marine specimens collected alive (Yoneda *et al.*, 2007). The relative inflow of colder surface waters from the high latitudes, which have been subject to gas exchange with the atmosphere, and the amount of mixing with deeper, unexposed ocean layers controls the reservoir age of the Hokkaido surface waters. Hokkaido is situated at the tip of Japan, at the southern-most latitude at which sea ice forms on the Okhotsk Sea coast. Consequently, the ocean circulation is complex. The Oyashio, East Sakhalin and Liman Current transport cold, dense water from the northern Pacific, Okhotsk Sea and Sea of Japan/Tartar Strait to the northern and eastern coastlines of Hokkaido, which is met by the relative warmer waters of the Soya Warm, Tsushima Warm and Tsugaru Warm Current. The reservoir age therefore varies around Hokkaido, due to the interaction of the different currents and necessitates 'coastline specific' corrections to avoid erroneous values assigned to specific shell dates within the database.

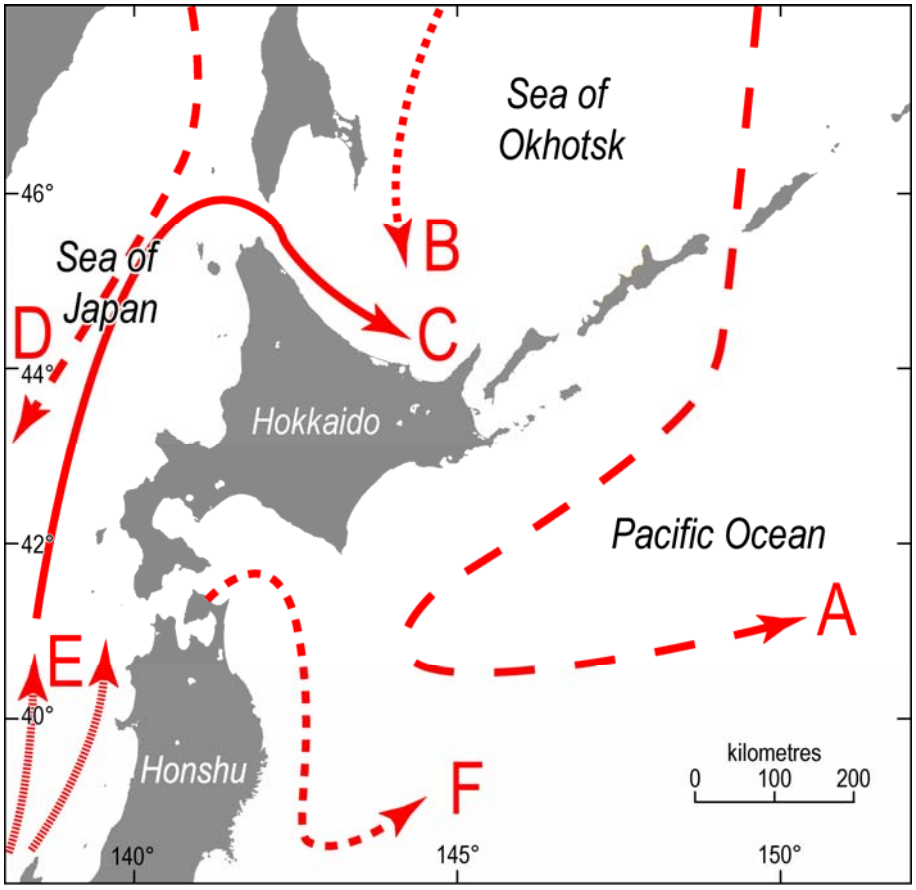

Figure 1 Oceanographic currents dominant around Hokkaido. Arrows show the flow of the following currents; A, Oyashio Current; B, East Sakhalin Current; C, Soya Warm Current; D, Liman Current; E; Tsushima Warm Current and F, Tsugaru Warm Current. After Yoneda *et al*. (2007).

Recalibrating dates (where necessary) using the most recent calibration curves enables comparison of published data analysed over the last decade. There are three main approaches to quantify the marine reservoir effect; (a) using tephra isochrones (present onshore/offshore); (b) using known-age samples (from the pre-bomb period or from the palaeo record – e.g. Shishikura *et al*. (2007)); and (c) using paired marine and terrestrial samples. Previous studies from Hokkaido and the surrounding area employ all three methods, the last of which Ascough *et al*. (2005) suggest to be the most promising approach to constraining changes over the last 5,000 cal. yr BP. Whilst other marine reservoir dates are available for the region, either the publication is untraceable (Hall, 1999), or the origin or geographical positioning of the samples is unknown (Gvozdeva *et al.*, 1997; Gorbarenko *et al.*, 1998). Table 2 describes the methodology followed to calculate the marine reservoir corrections for known-age and paired samples. Whereas there is one standard methodology for dealing with samples of known-age, there are three methods to calculate ΔR for paired samples. The first two assume that the paired marine and terrestrial samples are treated as relating to isochronous events. Southon *et al*. (1995) calculates both a terrestrial and marine age, whereas Stuiver and Braziunas (1993) use a simplified approach calculating ΔR for each marine/terrestrial pair using the modelled marine

radiocarbon age versus the atmospheric calibration data. A third, Bayesian approach (Jones *et al.*, 2007) allows uncertainty in the temporal relationships between paired samples to be incorporated in the calibration process, however the software is not currently available. Instead, I assess the stratigraphic context of the burial deposits to limit erroneous ΔR calculations.

Table 2 Methods used to recalibrate the marine reservoir effect using known age, and paired samples.

Known age samples from museum or analogue samples. After Stuiver and Braziunas (1993)	Paired samples. After Stuiver and Braziunas (1993)
Calculation of the atmospheric age and the surface ocean modelled age uses interpolation between the calendar ages in the InCal04 (Reimer *et al.*, 2004) and Marine04 (Hughen *et al.*, 2004) datasets respectively, where age is determined from the calculation 1950 minus the calendar date. The reservoir age (R) is then the radiocarbon age of the shell minus the atmospheric age. Then, the correction value (ΔR) is equal to: $\Delta R = t - t_m$ Where; t = the radiocarbon age of the shell; t_m = is the marine model age. The error on ΔR does not include the uncertainty in the curve as this is incorporated in the calibration process, however for calculating R the uncertainty is expressed as the square root of sum of squares of the curve error and the shell age error.	Calculation of ΔR for each marine/terrestrial pair uses the modelled marine radiocarbon age versus the atmospheric calibration data. The intersection of the terrestrial radiocarbon age (plus and minus one standard deviation) with the calibration data is used to calculate a maximum and minimum marine age model. The correction value (ΔR) is then: $\Delta R = t - (\frac{t_o^{max} - t_o^{min}}{2})$ Where; t = the radiocarbon age of the shell; t_o = is the marine model age and max and min represent a maximum and minimum model marine age (i.e. the mid-point of the marine model age). The error in ΔR includes the reported error in the shell age and the spread in the model marine age

Hokkaido displays considerable variability in ΔR between the northern, eastern, southern and western coastlines with the marine reservoir effect deviating significantly from the pre-industrial global mean reservoir correction of 400 years (Table 3). A total of 40 dates were recalibrated, with the most data having been collated from the northern (13) and southern (15) Hokkaido coastline. The marine reservoir values show considerable variability for ΔR from just 17 ± 30 ^{14}C years for a *Spisula sakhalinensis* mollusc found in the early twenty-first century on the western coastline (Kuzmin *et al.*, 2007), to 2,625 ± 179 ^{14}C years for a paired *Neogloboquadrina pachyderma*/tephra date from a core in the north-west Pacific found in Late Devensian sediments (Ohkushi *et al.*, 2007). These differences are due to the differing ocean circulation systems which surround the island. In essence warmer surface currents are generally associated with reduced reservoir ages, whereas regions where deep waters are upwelled, show greater reservoir ages (Ascough *et al.*, 2005).

Table 3 Summary of ΔR values from around the Hokkaido coast, calibrated with InCal2004 (Reimer *et al.*, 2004) and Marine2004 (Hughen *et al.*, 2004).

Region	Class	Year of collection (where appropriate)	Age	±	ΔR[1]	±	Reference
Northern Hokkaido (Sea of Okhotsk)							
Svobodnaya, Sakhalin	*Swiftopectan swifti*	1906	869	35	420	35	Yoneda *et al.* (2007)
Gulf of Aniva, Sakhalin	*Pseudocardium sybillae*	1906	826	35	377	35	Yoneda *et al.* (2007)
Makarov	*Mizuhopecten yessoensis*	*c.* 1905-1945[2]	960	30	507	30	Kuzmin *et al.* (2007)
Davydov Cape	*Callista brevisiphonata*	*c.* 1905-1945	1150	30	697	30	Kuzmin *et al.* (2007)
Uda River mouth	*Swiftopectan swifti*	*c.* 1905-1945	985	30	532	30	Kuzmin *et al.* (2007)
Porechye	*Spisula sakhalinensis*	*c.* 1905-1945	920	30	467	30	Kuzmin *et al.* (2007)
Ustinovka-8 site, Russian Far East	Charcoal ascribed to terrestrial and marine origins using δ13C, δ15N and C:N.		4300 4960	45 45	302	50	Kunikita *et al.* (2007)
Kunashir Island, Kurile Islands, Northwest Pacific	*Spisula sakhalinensis*	1900-1945	950	40	497	40	Kuzmin *et al.* (2001)
Kunashir Island, Kurile Islands, Northwest Pacific	*Swiftopectan swifti*	1900-1945	800	45	347	45	Kuzmin *et al.* (2001)
Kunashir Island, Kurile Islands, Northwest Pacific	*Neptunea bulbaceae*	1900-1945	895	45	442	45	Kuzmin *et al.* (2001)
Kunashir Island, Kurile Islands, Northwest Pacific	*Mizuhopecten yessoensis*	1900-1945	915	40	462	40	Kuzmin *et al.* (2001)
Kunashir Island, Kurile Islands, Northwest Pacific	*Crepidula grandis*	1900-1945	725	40	272	40	Kuzmin *et al.* (2001)
Kunashir Island, Kurile Islands, Northwest Pacific	*Spisula sakhalinensis*	1900-1945	670	45	217	45	Kuzmin *et al.* (2001)
Eastern Hokkaido (northern Pacific Ocean)							
Zeleny Island (Lesser Kuriles, Habomai group)	*Mizuhopecten yessoensis*	*c.* 1905-1945	790	25	337	25	Kuzmin *et al.* (2007)
Zeleny Island (Lesser Kuriles, Habomai group)	*Mizuhopecten yessoensis*	*c.* 1905-1945	830	35	377	35	Kuzmin *et al.* (2007)
Yuri Island (Lesser Kuriles, Habomai group)	*Mizuhopecten yessoensis*	*c.* 1905-1945	805	50	352	50	Kuzmin *et al.* (2007)
Shikotan Island, Hokkaido	*Tridonta borealis*	1904	939	36	489	36	Yoneda *et al.* (2007)
Northwest Pacific (eastern Hokkaido)	*Neogloboquadrina pachyderma*	12 cm above tephra	13730	100	675	166	Ohkushi *et al.* (2007)[4]
	Tephra (Towada-Hachinohe)		12650	106			
Northwest Pacific (eastern Hokkaido)	*Neogloboquadrina pachyderma*	3 cm below tephra	15680	120	2625	179	Ohkushi *et al.* (2007)[4]
	Tephra (Towada-Hachinohe)		12650	106			
Southern Hokkaido (southern Pacific Ocean)							
Hakodate, Hokkaido	*Monodontga neritoides*	1899	490	34	35	34	Yoneda *et al.* (2007)
Kitakogane	Deer (*Cervus nippon*)	Early Jomon	4820	20	491	56	Yoneda *et al.* (2001; 2002)
	Fur Seal (*Callorhinus ursinus*)		5680	15			
Kitakogane	Deer (*Cervus nippon*)	Early Jomon	4820	20	338	67	Yoneda *et al.* (2002; 2004)[3]
	Scallop		5527	40			
Kitakogane	Deer (*Cervus nippon*)	Early Jomon	4820	20	372	57	Yoneda *et al.* (2002; 2004)[3]
	Porpoise		5561	18			
Kitakogane	Deer (*Cervus nippon*)	Early Jomon	4820	20	340	81	Yoneda *et al.* (2002; 2004)[3]
	Sea lion		5529	61			
Takasago	Deer (*Cervus nippon*)	Middle Jomon	3670	26	298	60	Yoneda *et al.* (2001)
	Fur Seal (*Callorhinus ursinus*)		4297	33			
Minami Usu 6	Deer (*Cervus nippon*)	Zoku-Jomon	2228	21	454	63	Yoneda *et al.* (2001)
	Fur Seal (*Callorhinus ursinus*)		3029	20			
Minami Usu 7	Deer (*Cervus nippon*)	Satsumon	749	19	390	19	Yoneda *et al.* (2001)
	Fur Seal (*Callorhinus ursinus*)		1534	15			
Oyakotsu	Deer (*Cervus nippon*)	Ainu	882	47	374	73	Yoneda *et al.* (2001)
	Fur Seal (*Callorhinus*		1649	24			

	ursinus)						
Northwest Pacific (southern Hokkaido)	*Neogloboquadrina pachyderma*	4 cm above tephra	13330	100	780	172	Ohkushi *et al.* (2007)[4]
	Tephra (Nigorikawa)		12145	134			
Northwest Pacific (southern Hokkaido)	*Neogloboquadrina pachyderma*	5 cm below tephra	13430	90	880	167	Ohkushi *et al.* (2007)[4]
	Tephra (Nigorikawa)		12145	134			
Northwest Pacific (southern Hokkaido)	*Neogloboquadrina pachydermam*	4 cm above tephra	13260	90	710	167	Ohkushi *et al.* (2007)[4]
	Tephra (Nigorikawa)		12145	134			
Northwest Pacific (southern Hokkaido)	*Neogloboquadrina pachyderma*	43 cm below tephra	13190	80	640	162	Ohkushi *et al.* (2007)[4]
	Tephra (Nigorikawa)		12145	134			
Northwest Pacific (southern Hokkaido)	Mixed foraminiferal assemblage	12 cm above tephra	14150	60	1600	153	Ohkushi *et al.* (2007)[4]
	Tephra (Towada-Hachinohe)		12650	106			
Northwest Pacific (southern Hokkaido)	*Neogloboquadrina pachyderma*	0 cm below tephra	14480	90	1930	167	Ohkushi *et al.* (2007)[4]
	Tephra (Towada-Hachinohe)		12650	106			
Western Pacific (Sea of Japan)							
Peter the Great Gulf, Sea of Japan	*Yoldia johanni*	1932	505	45	47	45	Kuzmin (2001)
Peter the Great Gulf, Sea of Japan	*Crassostrea gigas*	1880-1900	500	40	36	40	Kuzmin (2001)
Tomari, Sakhalin	*Spisula sakhalinensis*	*c*. 1905-1945	470	30	17	30	Kuzmin *et al.* (2007)
Ostrovki, Sakhalin	*Spisula sakhalinensis*	*c*. 1905-1945	520	30	67	30	Kuzmin *et al.* (2007)
Ilyinsky, Sakhalin	*Spisula sakhalinensis*	*c*. 1905-1945	660	30	207	30	Kuzmin *et al.* (2007)
Otaru, Hokkaido	*Glycymeris yessoensis*	1899	490	34	35	34	Yoneda *et al*. (2007)
Peter the Great Gulf, Sea of Japan	*Anadara inaequivalvis*		4340	35	485	68	Jones and Kuzmin (1995)
	Juglans mandshurica		3535	45			
Peter the Great Gulf, Sea of Japan	*Crassostrea gigas*		6600	55	22	88	Jones and Kuzmin (1995)
	Conifer bark		6195	60			

[1] For paired samples, calculation of ∆R was undertaken by P. Reimer (Queens University, Belfast).
[2] For dates with a range of calendar ages, I used the average age and uncertainty/error for that period (following P. Reimer, *pers. comm.*).
[3] The dates reported in Yoneda *et al*. (2004) use the same deer dates with different marine species to evaluate interspecies comparison of marine reservoir ages at the Kitakogane shell midden. As the marine and terrestrial species used are from a range of possible samples (where *n* is 8 - 30), the different combinations of species are all evaluated here.
[4] The tephra ages in Ohkushi *et al*. (2007) use two terrestrial ^{14}C dates. A pooled mean, using the methodology of Ward *et al*. (1978), an option in CALIB program (www.calib.org) is used.

The eastern and southern coastlines of Hokkaido display the widest range of ΔR values around the island (Figure 2). Although the majority of the marine reservoir ages fit between 400 and 700 ^{14}C yrs, some very old material is dated between 1,600 and 2,625 ^{14}C yrs, which relate to the Late Devensian samples from the northern Pacific reported by Ohkushi *et al*. (2007). In comparison the northern and western coastlines display less scatter, the six western Hokkaido mollusc samples collected during the late 20th and early 21st century in particular are tightly scattered, with the majority having ΔR values falling between 17 to 67 ^{14}C yrs.

Figure 2 Box plots (with outliers visible) showing ΔR median and interquartile range for the Hokkaido coastline (data taken from Table 3).

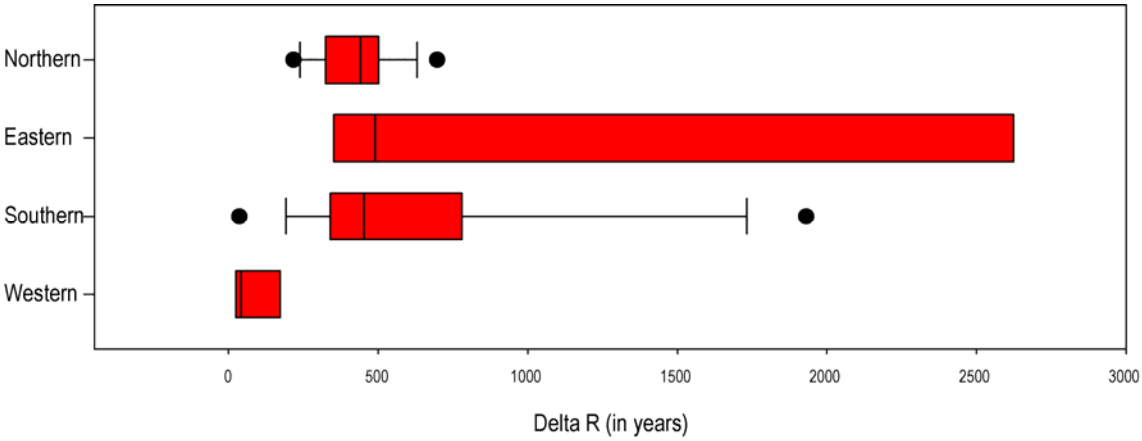

The variability in the marine reservoir correction around the island of Hokkaido is a product of the different oceanographic conditions prevalent at any one time. The northern Hokkaido coastline has some of the highest ΔR signatures around the island, between 200 and 700 ^{14}C years. Here, two currents are dominant – the East Sakhalin Current which flows from the north-western part of the Okhotsk Sea, and the Soya Warm Current which flows via the La Perouse Strait as a branch of the Tsushima current (Komsomolsky and Siryk, 1967). The relatively old ΔR values found around the island suggest the dominance of the colder current bringing ^{14}C-depleted waters from the high-latitude Okhotsk sea coast. Slow ventilation of these colder waters serves to lower the reservoir age recorded by the molluscs which reside in these waters, and have subsequently been analysed. In eastern Hokkaido, the ΔR signatures are also large, responding to the Oyashio cold current with normal ocean water salinity of 35‰ strongly affecting the regional conditions (Gorshkov, 1974; Kuzmin *et al.*, 2001). The southern coastline of Hokkaido is affected by the Oyashio Current and the Tsugaru Warm Current, the higher reservoir ages found in this area (particularly during the Late Devensian period) suggest there are seasonal inversions of Oyashio waters along the eastern and southern coastline of Hokkaido (Michurin and Fuks, 1988), and during the Holocene these intrusions moved even further south, through the Tsugaru Strait to the Sea of Japan (Takei *et al.*, 2002). On the western coastline of Hokkaido, the Sea of Japan is dominated by the Tsushima warm current and the Soya Warm Current (Kuzmin *et al.*, 2001). Two cold currents, Shrenk (Primorskoye) and North Korean, also flow into the Sea of Japan. The coastal waters of the Peter the Great Gulf are under the strong influence of cold Shrenk current, originated in the Amur River estuary with quite low salinity, about 10‰ (Gorshkov, 1974; Kuzmin *et al.*, 2001). Different currents influence the ΔR of specific regions, and the changing oceanographic regime following the last glacial maximum suggests a temporal dimension in the marine reservoir effect.

The global average marine reservoir offset of approximately 400 radiocarbon years is variable both in space and time, dependent upon local oceanic and climatic conditions in a specific location. As Earth's climate improved following the last deglaciation, ocean circulation has responded to this forcing, suggesting temporally variability in ΔR over the Holocene period. In their research from the Santa Barbara Channel, Kennet *et al*. (1997) observed large-scale fluctuations (*c*. 650 yrs) during the late Holocene, and smaller-scale fluctuations (*c*. 210 yrs) during the late to mid Holocene suggesting unique ΔR values for different periods of time. ^{14}C years do not correspond directly to calendar years, and therefore the terrestrial pairs of samples have been calibrated using Oxcal program (Bronk Ramsey, 1995) and the InCal04 calibration curve (Reimer *et al.*, 2004), and plotted by coastline to display the variability of the marine reservoir effect over time (Figure 3). Whilst too few data points are available to quantify the effect of the temporal variability in the marine reservoir effects around Hokkaido, particularly the paucity of data available around the start of the Holocene, it can broadly be seen Late Devensian ΔR ages are considerably older than their Holocene counterparts. Around Hokkaido, Ohkushi *et al*. (2007) determine the marine reservoir effect by comparing onshore/offshore isochrones, estimating the surface water reservoir age (not ΔR) during the Bølling-Allerød period to be more than 200 yr higher than the Holocene values of ~800 yr. The older deglacial ages are attributed to active upwelling of deep water during the last deglaciation and the mixing of 'older' deep water with 'younger' surface waters.

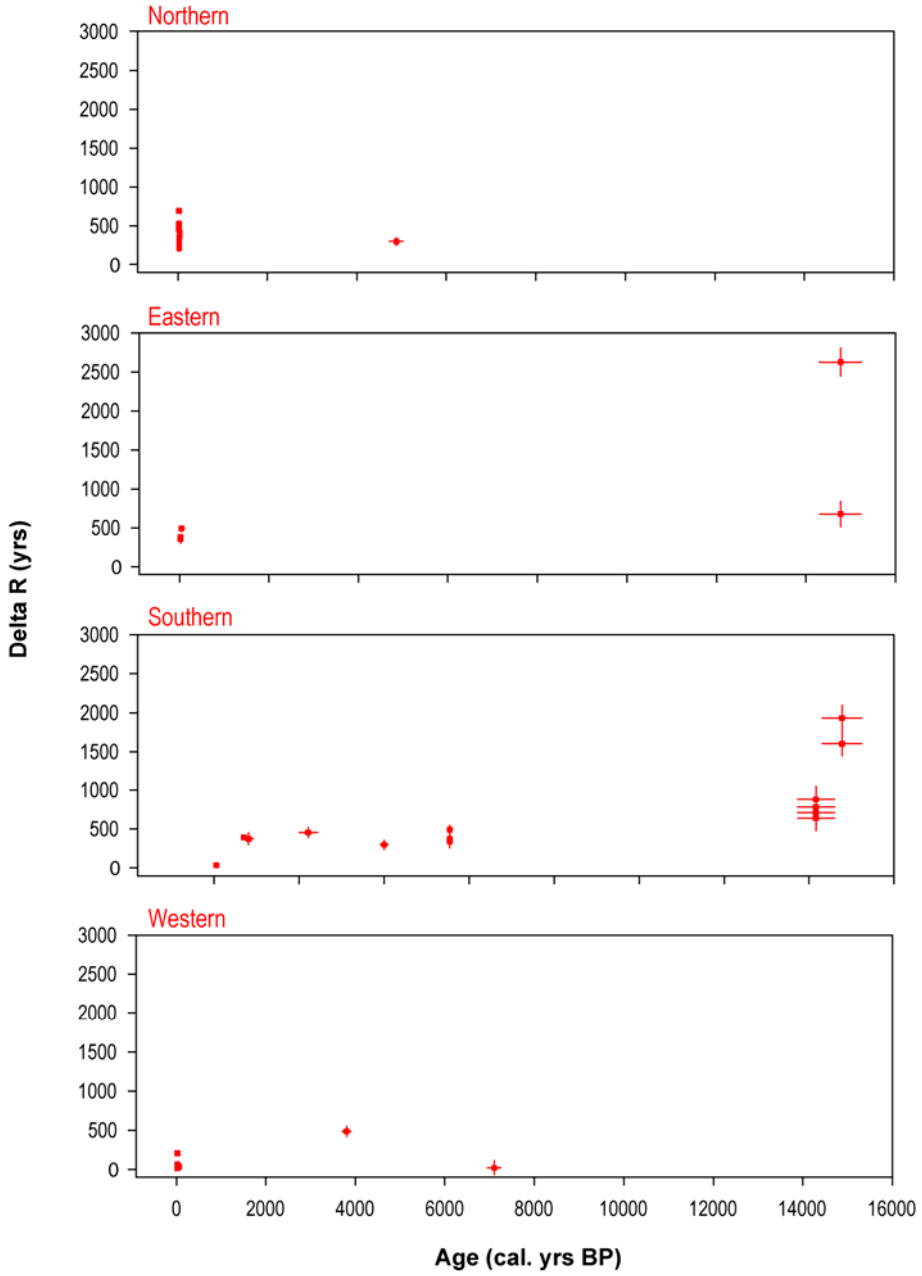

Figure 3 ΔR versus midpoint of two-sigma calibrated age range of terrestrial samples for the northern, eastern, southern and western coastlines of Hokkaido. The vertical error bar represents the uncertainty in ΔR and the horizontal bars represent the spread in the calibrated age range. To allow comparison between areas, the scaling of the axes remains the same.

The marine reservoir correction around northern Hokkaido is mainly dominated by twenty-first century mollusc specimens, with ΔR values between 217 and 697 ^{14}C years. Some variability could be due to the range of species dated; however the older samples are from historic rubbish dumps for which the shells precise origin may not be accurately assessed. The only mid-Holocene sample gives a date of 301 ± 50 ^{14}C years which fits between the early 21st century values. The ΔR samples from the eastern coast are either from the 21st century or the Late Devensian. The most recent samples record lower corrections,

whereas the tephra/foraminiferal samples display greater variability. The foraminifera from the 675 ± 166 ΔR sample were found 12 cm above the tephra, and the 2,625 ± 179 sample 3 cm below the tephra, suggesting an under and over estimation respectively. Temporal variability is best observed in samples found on the southern coastline. From the data points a linear or exponential trend may be observed. Using linear regression, the 15 samples have an r^2 of 0.571. The slope of the regression is 0.07 ± 0.02. This trend suggests a time dependency in delta R, which would most probably become stronger as three of the ages clustered around 700 ^{14}C yrs are from foraminifera above the tephra, and the 1,600 ^{14}C yrs date should be younger as the foraminifera are found 12 cm above the tephra. The ΔR values from the western coastline are limited to the late 20th century and early 21st century, but the dates are generally low and well clustered.

The wide range of reservoir ages for the eastern and southern coastlines are affected greatly by the Late Devensian samples reported by Ohkushi *et al*. (2007). During colder periods, the ventilation rate of the deep oceans was slowed considerably leading to higher reservoir ages, which have since fallen as the Earth's climate has improved. The database presented in this thesis is limited mainly to the Holocene period, for which the sea-level data for the region is mainly concentrated. The Late Devensian results skew the ∆R dates for the southern and eastern coastlines. For that reason, only Holocene ∆R samples are included in subsequent analysis. Two samples are removed from along the eastern coastline, and six samples along the southern coastline. As such the samples are considerably more tightly scattered and are more likely to represent the shell samples in the sea-level database. Although there still statistical scatter within the marine reservoir ages for the different coastlines, it is desirably to have a single value which is then used in the subsequent database analysis. The regional ∆R have different uncertainties, therefore a weighted average (as opposed to an arithmetic mean) is used which assumes parent distributions with the same mean but with different standard deviations.

The weighted mean ∆R for each coastline is listed in Table 4. For the samples remaining after selective rejection of material on the eastern and southern coastlines, the ∆R values are 455 ± 36, 398 ± 28, 332 ± 48 and 75 ± 31 ^{14}C yrs, with an empirical standard deviation (or 'scatter') in the data of between 70 and 130 ^{14}C yrs. The uncertainty in ∆R derives from the reported error in the shell age and the spread in the model marine age. The standard deviation in the weighted mean, based on the variance in ∆R values ('sigma scatter'), is larger than the standard deviation based on the reported error from the spread in the model marine age ('sigma mean'), and is quoted for all Hokkaido coastlines.

Table 4 Summary of ΔR values around the Hokkaido coast, where n is equal to the number of samples, the ΔR is the weighted mean.

Region	n (all)1	ΔR2	Error3	Standard deviation of Holocene subset (standard deviation of all values)1
Northern Hokkaido	13	455.9	36.2	126.1
Eastern Hokkaido	4 (6)	380.2	34.4	69.0 (898.6)
Southern Hokkaido	9 (15)	331.9	48.2	130.0 (506.7)
Western Hokkaido	8	161.8	54.5	161.8

1 The numbers in parenthesis refer to the full suite of reservoir ages listed in Table 3.
2 Following Bevington and Robinson (2003:57), the most probable value for the weighted average (μ') is:

$$\mu' = \frac{\sum(x_i / \sigma_i^2)}{\sum(1/\sigma_i^2)}$$

Where, each data point (xi) in the sum is weighted inversely by its own variance σ_i^2.
3 To calculate the uncertainty of the mean σ (termed sigma mean), a general formulae for the error in the weighted mean is calculated:

$$\sigma_\mu = \sqrt{\frac{1}{\sum(1/\sigma_i^2)}}$$

To find the error in the estimate μ' of the mean, a weighted average variance of the data is calculated (Bevington and Robinson, 2003:58):

$$\sigma^2 = \frac{\sum w_i \left(x_i - \mu'\right)^2}{\sum w_i} \times \frac{N}{N-1}$$

Where, wi is the weights (derived from 1/ΔR uncertainity). The deviation in the unweighted mean (√σ2) or 'scatter' sigma is calculated following Stuiver *et al*. (1986).

Calculating a precise marine reservoir signature for a region is complicated by a series of factors, relating to the spatial and temporal context of the sample. The marine reservoir effect is quantified with reference to marine creatures, which may have unique ΔR signatures which is a function of their migratory or lifestyle pattern. Analysis of the reservoir ages of fur seal remains found in the Kitakogane shell midden on Hokkaido's southern coastline suggest these migratory animals have significantly larger reservoir age offset than sedentary species (including porpoise, sea lion and scallop found at the same site) due to their seasonal migration between the North Pacific and the Sea of Okhotsk (Yoneda *et al.*, 2004) which display larger reservoir ages. Even marine molluscs are susceptible to ΔR variability depending on the species, habitat and/or substrate (e.g. Hogg *et al.*, 1998). Furthermore, from research in central Queensland, Ulm (2002) indentifies variability of ΔR, suggesting estuary-specific patterns of variation input and exchange with the open ocean. Although, the choice of species as well as the temporal and spatial setting determines ΔR, a detailed methodology following best practise is presented here and allows for a more accurate approximation of the marine reservoir effect around the Hokkaido coastline.

3 SEA-LEVEL DATABASE

The new sea-level database used to constrain Holocene sea levels in Hokkaido, applying the consistent methodology developed previously and discussed in Chapter Three (and this Appendix) is presented below. The data is organised by site, and presented graphically in Chapter Six. The type of index point is listed in code form, where P represents Primary Index Points and S represents Secondary Index Points. The subsequent number following P or S describes the nature of the index point (i.e. 1a or 1b). IM, represents indicative meaning and is listed for primary and secondary sea-level index points (as upper and lower RSL error estimates).

Site 1: Akkeshi/Mochiruppu

Type of index point	Site	Location		Dated material	^{14}C date			Calibrated yr BP		Reconstruction			Reference
		Lat.	Long.		Laboratory code (where available)	Age	Error	From	To	RSL	IM (upper)	IM (lower)	
P/1a	Kushiro Moor	43.10	144.49	Peat	JGS 271	2860	180	3465	2504	3.23	0.54	0.24	Kumano *et al.* (1990b)
P/1a	Kushiro Moor	40.11	144.35	Peat	JGS 268	2930	150	3440	2762	0.82	0.54	0.24	Kumano *et al.* (1990b)
P/1a	Kushiro Moor	43.08	144.39	Peat	JGS 270	3040	140	3557	2869	-0.14	0.54	0.30	Kumano *et al.* (1990b)
P/1a	Onnetoh	43 12	145 33	Cone scale of *Picea glehnii*	Wk-9727	400	50	522	316	0.09	0.57	0.28	Sawai *et al.* (2004a)
P/1a	Onnetoh	43.21	145.51	Bulk peat (coarse fraction)	GrN-25704	3500	45	3890	3642	-0.87	0.55	0.21	Sawai and Nasu (2005)
P/1a	Onnetoh	43.21	145.51	Bulk peat (fine fraction)	GrN-25755	3650	35	4086	3878	-0.87	0.55	0.21	Sawai and Nasu (2005)
P/1a	Onnetoh	43.21	145.51	Stones of *Sambucus sieboldiana* var. *miquelii*	Wk-9728	3720	50	4234	3914	-0.87	0.55	0.21	Sawai and Nasu (2005)
P/1a	Chiraikaribetsu Lowland	43.10	144.96	Leaf	GrrA-7420	780	60	900	568	-0.10	0.55	0.21	Sawai (2001)
P/1a	Chiraikaribetsu Lowland	43.08	144.96	Leaf	GrrA-7397	2750	70	3060	2746	-2.12	0.55	0.22	Sawai (2001)
P/1a	Chiraikaribetsu Lowland	43.10	144.94	Leaf	GrrA-7402	440	70	623	310	-1.52	0.55	0.21	Sawai (2001)
P/1a	Onnetoh	43.21	145.51	Small bulk peat	Wk-8055	1900	60	1988	1709	-0.69	0.55	0.21	Sawai *et al.* (2002)
P/1b	Kushiro Moor	40.11	144.35	Peat	JGS 269	3690	220	4789	3474	-0.18	0.38	0.15	Kumano *et al.* (1990b)
P/1b	Kushiro Moor	40.11	144.35	Peat	JGS 267	1760	140	1994	1372	2.53	0.38	0.15	Kumano *et al.* (1990b)
P/1b	Toya River	43.05	144.49	Peat	JGS 119	4090	240	5302	3974	1.35	0.38	0.15	Ihira *et al.* (1985)
P/1b	Onnetoh	43.21	145.51	Bulk peat (coarse fraction)	GrN-25703	2470	60	2717	2360	-0.58	0.39	0.14	Sawai and Nasu (2005)
P/1b	Onnetoh	43.21	145.51	Bulk peat (fine fraction)	GrN-25754	3080	35	3374	3215	-0.58	0.39	0.14	Sawai and Nasu (2005)
P/1b	Onnetoh	43.21	145.51	Seeds	Wk-9730	3270	60	3636	3380	-0.58	0.39	0.14	Sawai and Nasu (2005)
P/1b	Onnetoh	43.21	145.51	Seeds of *Carex* sp.	Wk-10385	540	60	655	502	-0.77	0.39	0.14	Sawai *et al.* (2002)
P/1b	Onnetoh	43.21	145.51	Leaf of *Picea glehnii* and seeds	Wk-9724	2360	60	2702	2183	-1.02	0.39	0.14	Sawai *et al.* (2002)
P/1b	Onnetoh	43.21	145.51	Cone scale of *Picea glehnii*	Wk-9727	400	50	522	316	0.16	0.39	0.14	Sawai *et al.* (2002)
P/1b	Onnetoh	43.21	145.51	Seeds of *Polygonum*	Wk-9723	1950	60	2041	1730	-1.85	0.39	0.14	Sawai *et al.* (2002)
P/1b	Chiraikaribetsu Lowland	43.10	144.96	Leaf	GrrA-7395	1950	70	2096	1718	-1.64	0.39	0.14	Sawai (2001)
P/1b	Chiraikaribetsu Lowland	43.10	144.96	Leaf	GrrA-7400	2120	70	2315	1946	-0.88	0.39	0.14	Sawai (2001)
P/1b	Chiraikaribetsu Lowland	43.10	144.95	Leaf	GrrA-7393	980	70	1052	737	-0.75	0.39	0.14	Sawai (2001)
P/1b	Chiraikaribetsu Lowland	43.10	144.95	Leaf	GrrA-7394	1660	70	1721	1392	-1.15	0.39	0.14	Sawai (2001)
P/1b	Chiraikaribetsu Lowland	43.10	144.95	Leaf	GrrA-7401	2470	70	2724	2357	-1.75	0.39	0.14	Sawai (2001)
P/3	Onnetoh	43 12	145 33	Leaf of *Osmunda cinnamomea*	Wk-9884	1360	60	1389	1153	0.4			Sawai *et al.* (2004a)

P/3	Onnetoh	43 12	145 33	Seeds of *Polygonum* sp.	Wk-9726	1950	60	2041	1730	1.705			Sawai *et al.* (2004a)
P/3	Onnetoh	43.21	145.51	Leaves *Picea glehnii*, stone of *Sambucus sieboldiana* var. *miquelii*, seeds of *Polygonum* sp., and seeds of *Carex* sp.	Wk-9731	795	50	894	661	0.2695			Sawai and Nasu (2005)
P/3	Onnetoh	43.21	145.51	Bulk peat (coarse fraction)	GrN-25726	500	45	635	485	0.2675			Sawai and Nasu (2005)
P/3	Onnetoh	43.21	145.51	Bulk peat (fine fraction)	GrN-25705	820	40	893	673	0.2675			Sawai and Nasu (2005)
P/3	Onnetoh	43.21	145.51	Bulk peat (coarse fraction)	GrN-25727	1180	60	1261	968	0.08			Sawai and Nasu (2005)
P/3	Onnetoh	43.21	145.51	Bulk peat (fine fraction)	GrN-25778	1360	30	1338	1186	0.08			Sawai and Nasu (2005)
P/3	Onnetoh	43.21	145.51	Seeds of *Carex* sp. And *Gramineae* sp.	Wk-9729	1458	80	1536	1189	0.08			Sawai and Nasu (2005)
P/3	Onnetoh	43.21	145.51	Bulk peat (coarse fraction)	GrN-25702	1840	60	1920	1614	-0.0765			Sawai and Nasu (2005)
P/3	Onnetoh	43.21	145.51	Bulk peat (fine fraction)	GrN-25779	2530	35	2747	2488	-0.0765			Sawai and Nasu (2005)
P/3	Onnetoh	43.21	145.51	Leaf of *Osmunda cinnamomea*	Wk-9884	1360	60	1389	1153	0.4			Sawai *et al.* (2002)
P/3	Chiraikaribetsu Lowland	43.10	144.96	Leaf	GrrA-7390	590	70	669	515	0.257			Sawai (2001)
P/3	Chiraikaribetsu Lowland	43.10	144.96	Leaf	GrrA-7392	1300	70	1331	1063	-0.143			Sawai (2001)
P/3	Chiraikaribetsu Lowland	43.10	144.95	Leaf	GrrA-7415	500	110	668	314	0.04			Sawai (2001)
P/3	Chiraikaribetsu Lowland	43.10	144.95	Leaf	GrrA-7417	1230	80	1293	979	-0.56			Sawai (2001)
P/3	Chiraikaribetsu Lowland	43.08	144.96	Leaf	GrrA-7419	510	60	654	466	-0.114			Sawai (2001)
P/3	Chiraikaribetsu Lowland	43.10	144.94	Leaf	GrrA-7411	230	60	461	-4	-0.806			Sawai (2001)
P/3	Chiraikaribetsu Lowland	43.10	144.94	Wood	GrrA-7421	2070	60	2299	1886	-1.944			Sawai (2001)
P/4	Aikappu Cape	43 01	144 51	Mollusc shells		6240	220	7726	6259	-5.50			Kumano *et al.* (1990b)
P/4	Toya River	43 3 13	144 27 31	*Tapes philippinarum*	JGS 143	6420	260	7430	6335	-1.44			Ihira *et al.* (1985)
S/1b	Onnetoh	43.21	145.51	Small bulk peat	Wk-8053	2930	60	3319	2888	-1.50	0.39	-0.03	Sawai *et al.* (2002)
S/2	Aikappu Cape	44 01	145 51	Peat	JGS-170	3070	180	3688	2797	0.15			Kumano *et al.* (1990b)
S/2	Onnetoh	43.21	145.51	Leaf of *Picea glehnii* and seeds	Wk-9723	520	70	664	339	0.255			Sawai *et al.* (2002)
S/2	Onnetoh	43.21	145.51	Leaf of *Picea glehnii* and seeds	Wk-9725	1170	50	1239	965	0.075			Sawai *et al.* (2002)
S/2	Onnetoh	43.21	145.51	Small bulk peat	Wk-8054	2260	60	2360	2117	-0.97			Sawai *et al.* (2002)
S/2	Onnetoh	43.21	145.51	Leaf of *Ericaceae*	Wk-9722	590	40	655	534	0.06			Sawai *et al.* (2002)
S/2	Onnetoh	43.21	145.51	Twig *of Ledum palustre* var. *diversipilosum*?	Wk-9732	1290	40	1297	1095	-0.165			Sawai *et al.* (2002)
S/2	Onnetoh	43.21	145.51	Small bulk peat	GrA-7415	550	140	766	299	-0.26			Sawai *et al.* (2002)
S/2	Onnetoh	43.21	145.51	Small bulk peat	GrA-7393	3310	80	3811	3374	-1.01			Sawai *et al.* (2002)

Site 2: Furen

Type of index point	Site	Location		Dated material	^{14}C date			Calibrated yr BP		Reconstruction			Reference
		Lat.	Long.		Laboratory code (where available)	Age	Error	From	To	RSL	IM (upper)	IM (lower)	
P/1a	Furen-gawa	43.25	145.20	Peat		2630	200	3320	2185	0.01	0.44	0.21	Ohira (1993)
P/1a	Furen-gawa	43.25	145.20	Peat	NU-1564	4235	70	4965	4569	-0.32	0.39	0.10	Ohira *et al.* (2004)
P/1a	Furen-gawa	43.25	145.20	Peat	NU-1565	3855	90	4519	3987	-0.51	0.39	0.10	Ohira *et al.* (2004)
P/1a	Furen-gawa	47.27	149.22	Peat	NU-1645	3620	70	4147	3721	0.62	0.39	0.09	Ohira *et al.* (2004)
P/1b	Furen-gawa	43.25	145.20	Peat		2820	310	3817	2160	-0.04	0.44	0.21	Ohira *et al.* (2004)
P/1b	Nemuro Peninsula	43.38	145.67	Peaty mud	JGS210	4400	330	5888	4151	0.27	0.46	0.26	Ohira *et al.* (2004)
P/1b	Furen-gawa	43.25	145.20	Peat	NU-1563	4120	60	4830	4446	0.51	0.40	0.12	Ohira *et al.* (2004)
P/1b	Furen-gawa	43.25	145.20	Peat	NU-1641	4240	75	4972	4533	-0.38	0.39	0.10	Ohira *et al.* (2004)
P/1b	Furen-gawa	44.27	146.22	Organic clay	NU-1643	2900	85	3327	2845	0.13	0.38	0.80	Ohira *et al.* (2004)
P/1b	Furen-gawa	44.27	146.22	Peaty clay	NU-1644	3315	90	3825	3365	0.13	0.56	0.41	Ohira *et al.* (2004)
P/1b	Furen-gawa	44.27	146.22	Peat	NU-1646	3890	75	4522	4090	0.40	0.39	0.10	Ohira *et al.* (2004)
P/1b	Furen-gawa	44.27	146.22	Clayey peat	NU-1647	4410	85	5290	4850	0.28	0.39	0.10	Ohira *et al.* (2004)
S/1a	Furen-gawa	44.27	146.22	Peat	NU-1568	2650	55	2919	2548	-1.04	0.54	0.36	Ohira *et al.* (2004)
S/1a	Furen-gawa	43.23	145.18	Clayey peat	NU-1650	430	75	623	306	0.81	0.54	0.09	Ohira *et al.* (2004)
S/1b	Furen-gawa	43.25	145.20			2920	300	3829	2353	-0.46	0.44	0.22	Ohira *et al.* (2004)
S/1b	Furen-gawa	43.25	145.20			3730	300	4957	3365	-0.99	0.44	0.22	Ohira *et al.* (2004)
S/1b	Furen-gawa	43.23	145.18	Peat	NU-1651	4440	75	5291	4869	0.79	0.39	0.09	Ohira *et al.* (2004)
S/2	Furen-gawa	43.27	145.22	Peaty clay	NU-1566	1470	65	1518	1289	-0.315			Ohira *et al.* (2004)
S/2	Furen-gawa	43.27	145.22	Clay with peaty sand	NU-1567	1785	55	1861	1563	-0.965			Ohira *et al.* (2004)
S/2	Furen-gawa	43.27	145.22	Peaty clay	NU-1642	2945	70	3332	2893	0.675			Ohira *et al.* (2004)
S/4	Nemuro Peninsula	43.38	145.67	*Mya arenaria oonogai*	JGS142	5190	200	5933	4953	-1.27			Ohira *et al.* (2004)

Site 3: Abashiri

Type of index point	Site	Location		Dated material	^{14}C date			Calibrated yr BP		Reconstruction			Reference
		Lat.	Long.		Laboratory code (where available)	Age	Error	From	To	RSL	IM (upper)	IM (lower)	
P/1a	Lake Mokoto	43.92	144.39	Peat	Gak-17502	4720	90	5646	5089	3.24	0.55	0.18	Sato *et al.*, (1997)
P/1a	Lake Mokoto	43.92	144.39	Peat	Gak-17503	5490	110	6496	5995	1.49	0.55	0.18	Sato *et al.*, (1997)
P/1a	Saroma-ko	44.15	143.71	Tephra (above decomposed peat)	N/A			1694	0	0.08	0.55	0.18	Soeda and Akamatsu (2001)
P/1a	Lake Mokoto	43.92	144.39	Peat	Gak-17502	4720	90	5646	5089	3.24	0.55	0.18	Sato *et al.*, (1997)
P/1b	Tokoro	43.85	144.09	Silt containing peat	KL-449	8970	80	10253	9780	-31.01	0.36	0.47	Hamano *et al.* (1985)
P/1b	Lake Mokoto	43.92	144.39	Peat	Gak-17503	5490	110	6496	5995	1.69	0.36	0.10	Sato *et al.*, (1997)
P/4	Tokoro	43.85	144.09	Clay (contained within a bed of *Ostrea* sp.)	KL-451	6210	280	7612	6469	-22.96			Hamano *et al.* (1985)
P/4	Lake Tofutsu	43.94	144.35	Batillaria cumingii	Beta-98291	1290	60	915	658	-0.19			Sato *et al.* (2004)
P/4	Lake Tofutsu	43.94	144.35	*Trapezium liratum*	Beta-124742	3320	60	3300	2899	-1.36			Sato *et al.* (2004)
P/4	Lake Tofutsu	43.94	144.35	*Crassostrea gigas*	Beta-98871	3410	60	3380	3005	-2.29			Sato *et al.* (2004)
S/2	Tokoro	43.85	144.09		KL-443	4100	290	5455	3841	-3.585			Hamano *et al.* (1985)
S/2	Tokoro	43.85	144.09	Wood stems	JGS-120	3050	240	3866	2735	-0.025			Hamano *et al.* (1985)
S/3	Abashiri River Lowland	43.90	144.15	Peat	NUTA-3996	2930	210	3639	2541	0.12			Atago (1998)
S/3	Abashiri River Lowland	43.89	144.14	Peat	NUTA-3994	3020	250	3879	2544	-0.3			Atago (1998)
S/3	Abashiri River Lowland	43.88	144.14	Peat	NUTA-3518	3720	140	4507	3696	1.29			Atago (1998)
S/3	Abashiri River Lowland			Peat	NUTA-3995	4110	230	5300	3990	-0.4			Atago (1998)
S/4	Abashiri River Lowland	43.92	144.15	Shell fragment	NUTA-3743	3120	140	3244	2480	-6.48			Atago (1998)
S/4	Abashiri River Lowland	43.92	144.15	Shell fragment	NUTA-3744	3460	110	3551	2955	-16.43			Atago (1998)
S/4	Abashiri River Lowland	43.92	144.15	Shell fragment	NUTA-3745	6830	50	7415	7175	-18.68			Atago (1998)
S/4	Tokoro River Lowland	46.08	144.07	Shell	TH-855	5840	+140/-150	6169	5485	-0.46			Umitsu (1983)

Site 4: Sarubetsu

Type of index point	Site	Location		Dated material	^{14}C date			Calibrated yr BP		Reconstruction			Reference
		Lat.	Long.		Laboratory code (where available)	Age	Error	From	To	RSL	IM (upper)	IM (lower)	
P/1a	Sarobetsu Lowland	45.12	141.73	Peat	NUTA-2078	1970	290	2460	1093	5.24	0.45	0.63	Ohira *et al.*, (1995)
P/1a	Sarobetsu Lowland	45.12	141.73	Peat	NUTA-2628	3920	160	4825	3930	0.99	0.45	0.64	Ohira *et al.*, (1995)
P/1a	Kutcharo Lake	45.15	142.25	Peat	KL-157	5340	140	6408	5754	1.24	0.45	0.63	Kumano *et al.* (1984)
P/1a	Lake Ohnuma	45.35	141.79	Peat	NUTA-3009	3610	170	4416	3485	3.62	0.45	0.63	Ohira *et al.*, (1995)
P/1b	Sarobetsu Lowland	45.12	141.73	Wood	NUTA-2202	2250	280	2949	1610	2.74	0.37	0.28	Ohira *et al.* (1995)
P/1b	Sarobetsu Lowland	45.12	141.73	Peat	NUTA-2629	5110	270	6498	5290	0.84	0.38	0.28	Ohira *et al.*, (1995)
P/1b	Kushu Lake, Rebun Island	45.43	141.03	Peat	NUTA-708	5810	210	7170	6208	-8.14	0.38	0.29	Kumano *et al.* (1990a)
P/1b	Lake Ohnuma	45.35	141.79	Wooden fragments	NUTA-3734	4260	230	5567	4182	3.7	0.37	0.28	Ohira and Umitsu (1996)
P/3	Sarobetsu Lowland	45.11	141.29	Peat	Beta-81018 Geo-95-0070	1130	50	1173	938	2.6			Ohira *et al.*, (1995)
P/3	Sarobetsu Lowland	45.12	141.73	Peat	NUTA-2181	1960	240	2675	1374	2.04			Ohira *et al.* (1995)
P/3	Sarobetsu Lowland	45.12	141.73	Peat	NUTA-2182	3540	270	4785	3209	1.79			Ohira *et al.*, (1995)
P/3	Kushu Lake, Rebun Island	45.12	141.73	Peat	NUTA-2627	3380	160	4085	3265	1.19			Kumano *et al.* (1990a)
P/3	Kushu Lake, Rebun Island	42.43	141.03	Plant remains	NUTA-709	1660	80	1778	1375	-1.28			Kumano *et al.* (1990a)
P/3	Kutcharo Lake	42.43	141.03	Plant remains	NUTA-707	1700	210	2145	1185	-0.28			Kumano *et al.* (1984)
P/3	Kutcharo Lake	46.15	143.25	Peat	KL-155	4350	100	5304	4646	2.44			Kumano *et al.* (1984)
P/3	Kutcharo Lake	46.15	143.25	Peat	KL-166	2000	190	2457	1520	3.74			Kumano *et al.* (1984)
P/3	Lake Ohnuma	46.15	143.25	Peat	N-3992	9050	100	10504	9897	-15.56			Ohira *et al.*, (1995)
P/4	Kushu Lake, Rebun Island	47.00	143.72	Wood	NUTA-2744	7340	270	8760	7620	-26.76			Kumano *et al.* (1990a)
P/4	Kutcharo Lake	45.43	141.03	Plant remains	NUTA-710	7370	100	8379	8005	-11.96			Kumano *et al.* (1984)
P/4	Sarobetsu Lowland	45.43	141.76	*Mercenaria stimpsoni*	Beta-81013	2790	70	2693	2291	1.24			Ohira *et al.*, (1995)
P/4	Kucharo Lake	45.11	142.35	*Tapes* bed	GaK-3082	5170	150	5835	5060	2.24			Sekiya and Kumano (1983)
P/4	Kucharo Lake	44.11	144.01	Shell	KL-299	3220	60	3161	2773	-0.16			Sekiya and Kumano (1983)
S/1a	Sarobetsu Lowland	45.12	141.69	Peat	NUTA-2183	1970	450	3075	1000	3.89	0.45	0.63	Ohira *et al.* (1995)
S/1a	Sarobetsu Lowland	45.12	141.69	Peat	NUTA-2201	1980	280	2704	1373	3.79	0.45	0.63	Ohira *et al.* (1995)
S/1a	Sarobetsu Lowland	45.08	141.68	Peat	NUTA-2198	1860	230	2340	1334	-0.31	0.45	0.63	Ohira *et al.* (1995)
S/1a	Sarobetsu Lowland	45.09	141.74	Peat	NUTA-2199	1230	250	1690	681	5.24	0.45	0.63	Ohira *et al.* (1995)

S/1a	Lake Ohnuma	45.35	141.79	Peat	NUTA-4250	2170	360	3064	1379	2.9	0.45	0.63	Ohira and Umitsu (1996; 1999)
S/1a	Lake Ohnuma	45.35	141.79	Peat	NUTA-3735	3610	160	4414	3558	4.25	0.45	0.63	Ohira and Umitsu (1996; 1999)
S/1a	Lake Ohnuma	45.35	141.79	Peat	NUTA-3736	2640	150	3140	2348	1.74	0.45	0.63	Ohira and Umitsu (1996; 1999)
S/1a	Lake Ohnuma	45.35	141.79	Peat	NUTA-3010	4360	140	5440	4569	4.63	0.45	0.63	Ohira and Umitsu (1996)
S/1a	Lake Ohnuma	45.35	141.79	Peat	NUTA-3156	2400	130	2755	2150	2.91	0.45	0.63	Ohira and Umitsu (1996)
S/1a	Lake Ohnuma	45.35	141.79	Peat	NUTA-2746	1640	210	2105	1145	1.31	0.45	0.63	Ohira and Umitsu (1996)
S/1b	Sarobetsu Lowland	46.09	141.74	Peat	NUTA-2200	4270	450	5939	3690	2.89	0.37	0.28	Ohira *et al.* (1995)
S/1b	Kutonebetsu River Lowland	45.32	141.65	Peat	NUTA-4248	3640	250	4800	3384	5.02	0.37	0.27	Ohira (2000)
S/1b	Kutonebetsu River Lowland	45.32	141.66	Peat	NUTA-4247	2910	260	3689	2366	6.21	0.37	0.27	Ohira (2000)
S/1b	Kutonebetsu River Lowland	45.32	141.66	Peat	NUTA-4244	3940	150	4827	3986	6.52	0.37	0.28	Ohira (2000)
S/1b	Kutonebetsu River Lowland	45.32	141.64	Peat	NUTA-4930	2900	70	3559	2856	5.16	0.37	0.28	Ohira (2000)
S/2	Sarobetsu Lowland	45.12	141.73	Peat	NUTA-2078	1970	290	2460	1093	5.24	0.45	0.63	Ohira *et al.*, (1995)
S/2	Rebun Island	46.19	142.72	Peat	NUTA-2633	2240	180	2739	1874	1.34			Akamatsu *et al.* (1997)
S/2	Rebun Island	45.11	141.29	Peat	Beta-81022 Geo-95-0074	50	40	262	24	2.97			Akamatsu *et al.* (1997)
S/2	Rebun Island	45.11	141.29	Peat	Beta-81021 Geo-95-0073	1050	40	1059	915	2.48			Akamatsu *et al.* (1997)
S/2	Rebun Island	45.11	141.29	Peat	Beta-81020 Geo-95-0072	1630	50	1691	1403	2.13			Akamatsu *et al.* (1997)
S/2	Rebun Island	45.11	141.29	*Classostrea gigas*	Beta-81017 Geo-95-0069	7000	80	7597	7281	-9.07			Akamatsu *et al.* (1997)
S/2	Rebun Island	45.11	141.29	Peat	Beta-81019 Geo-95-0071	70	40	268	18	3.09			Akamatsu *et al.* (1997)
S/3	Kutonebetsu River Lowland	45.35	141.79	Peat	NUTA-2747	4210	230	5450	4098	4.37			Ohira (2000)
S/3	Tonbetsu River Lowland	45.32	141.66	Wood	NUTA-4245	3450	210	4401	3250	6.37	0.37	0.28	Fang *et al.* (1998)
S/3	Tonbetsu River Lowland	45.06	142.32	Peat	NUTA-5651	4540	95	5468	4878	4.44			Fang *et al.* (1998)
S/3	Tonbetsu River Lowland	45.08	142.36	Peat	NUTA-5652	4780	220	4780	220	3.64			Fang *et al.* (1998)
S/4	Sarobetsu Lowland	45.11	142.41	Peat	NUTA-5654	2260	250	2876	1696	2.54			Ohira *et al.* (1995)
S/4	Rebun Island	47.15	144.25	Tapes japonica	N-3991	5890	90	6450	5999	1.64			Akamatsu *et al.* (1997)
S/4	Rebun Island	45.11	141.29	*Classostrea gigas*	Beta-84267 Geo-95-1040	7390	60	7938	7655	-9.67			Akamatsu *et al.* (1997)
S/4	Rebun Island	45.11	141.29	*Classostrea gigas*	Beta-81016 Geo-95-0068	7790	70	8356	8020	-10.37			Akamatsu *et al.* (1997)
S/4	Rebun Island	45.11	141.29	*Classostrea gigas*	Beta-81015 Geo-95-0067	7330	70	7910	7590	-9			Akamatsu *et al.* (1997)
S/4	Rebun Island	45.11	141.29	*Classostrea gigas*	Beta-84266 Geo-95-1039 CAMS	7450	60	7989	7694	-9.45			Akamatsu *et al.* (1997)

S/4	Rebun Island	45.11	141.29	*Classostrea gigas*	Beta-84266 Geo-95-1039 CAMS	7450	60	7989	7694	-9.45			Akamatsu *et al.* (1997)
S/4	Lake Ohnuma	45.11	141.29	*Classostrea gigas*	Beta-81014 Geo-95-0066	7770	80	8339	7975	-11.16			Ohira and Umitsu (1999)
S/4	Kucharo Lake	45.15	142.25	*Ostrea* bed	GaK-3083	5610	130	6248	5650	-1.46			Ohshima *et al.* (1972) and Maeda *et al.* (1994)
S/4	Kuetoi, Soya Strait	44.11	144.01	Shell	KL-300	3400	85	3416	2941	-2.66			Arakawa and Yamazaki (1998)

Site 5: Tokachi

Type of index point	Site	Location		Dated material	^{14}C date			Calibrated yr BP		Reconstruction			Reference
		Lat.	Long.		Laboratory code (where available)	Age	Error	From	To	RSL	IM (upper)	IM (lower)	
P/1a	Tokachi Lowlands	42.40	143.38	Plant	Beta-155906	5890	40	6830	6634	-2.36	0.09	0.25	Ohira (2003)
P/1a	Tokachi Lowlands	42.40	143.38	Peat	Beta-155908	3710	40	4220	3926	0.13	0.10	0.28	Ohira (2003)
P/1b	Tokachi Lowlands	42.40	143.38	Plant	Beta-125461	1990	40	2043	1830	-5.65	0.32	0.42	Ohira (2003)
P/1b	Tokachi Lowlands	42.40	143.38	Wood	Beta-125465	8290	30	8986	8690	-22.65	0.26	0.51	Ohira (2003)
P/1b	Tokachi Lowlands	42.40	143.38	Peat	Beta-155907	4360	40	5040	4849	-0.98	0.09	0.24	Ohira (2003)
P/3	Tokachi Lowlands	42.40	143.38	Wood	Beta-124739	6700	60	7668	7468	-7.77			Ohira (2003)
P/4	Tokachi Lowlands	42.40	143.38	Shell	Beta-124740	7820	150	8606	7955	-11.77			Ohira (2003)
P/4	Tokachi Lowlands	42.40	143.38	Shell	Beta-125462	7600	40	8166	7954	-9.4			Ohira (2003)
P/4	Tokachi Lowlands	42.40	143.38	Shell	Beta-125463	7990	30	8545	8365	-13.4			Ohira (2003)
P/4	Tokachi Lowlands	42.40	143.38	Shell	Beta-125464	8770	40	9528	9330	-18.4			Ohira (2003)
S/1b	Tokachi Lowlands	42.40	143.38	Peat	Beta-144516	3760	40	4242	3985	1.72	0.10	0.24	Ohira (2003)
S/2	Tokachi Lowlands	42.40	143.38	Peat	Beta-144515	5250	30	6178	5925	0.57			Ohira (2003)
S/2	Tokachi Lowlands	42.40	143.38	Peat	Beta-144517	3590	30	3979	3831	1.78			Ohira (2003)
S/2	Tokachi Lowlands	42.40	143.38	Peat	Beta-144519	5200	50	6178	5769	0.84			Ohira (2003)
S/2	Tokachi Lowlands	42.40	143.38	Plant	Beta-155909	3890	40	4423	4159	-0.1			Ohira (2003)
S/2	Tokachi Lowlands	42.40	143.38	Plant	Beta-155910	3550	40	3965	3705	0.12			Ohira (2003)
S/2	Tokachi Lowlands	42.40	143.38	Tephra (Ta-c)				211	211	1.35			Ohira (2003)
S/3	Tokachi Lowlands	42.72	143.66	Peat	Beta-163462	5160	70	6177	5734	0.9			Fujimoto *et al.* (2003)
S/3	Tokachi Lowlands	42.71	143.66	Plant remains	Beta-163465	6620	100	7669	7325	-2.6			Fujimoto *et al.* (2003)
S/4	Tokachi Lowlands	42.40	143.38	Shell	Beta-163466	7790	70	8400	8070	-10.88			Fujimoto *et al.* (2003)
S/4	Tokachi Lowlands	42.40	143.38	Shell	Beta-163467	8680	50	9478	9200	-19.13			Fujimoto *et al.* (2003)
S/4	Pashikuru-numa	43.92	144.01	*Crassostrea gigas*	N-3990	5950	95	6608	6180	1.1			Matsushima (1982)
S/4	Kushiro Moor	43.08	144.43	*Scapharca sachalinensis*	GaK-14231	6910	150	7711	7134	-1.4			Matsushima and Yamashiro (1992)
P/1a	Tokachi Lowlands	42.40	143.38	Plant	Beta-155906	5890	40	6830	6634	-2.36	0.09	0.25	Ohira (2003)
P/1a	Tokachi Lowlands	42.40	143.38	Peat	Beta-155908	3710	40	4220	3926	0.13	0.10	0.28	Ohira (2003)

Site 6: Ishikari Lowlands

Type of index point	Site	Location		Dated material	^{14}C date			Calibrated yr BP		Reconstruction			Reference
		Lat.	Long.		Laboratory code (where available)	Age	Error	From	To	RSL	IM (upper)	IM (lower)	
S/2	Toyohira River	43.09	141.38	Peat	KSU-1291	5700	25	6550	6410	1.34			Daimaru (1989)
S/2	Toyohira River	43.11	141.36	Peat	HR-068	5270	90	6283	5894	0.84			Daimaru (1989)
S/2	Yufutsu Plain	42.72	141.71	Peat		3160	120	3688	3063	2.56			Ikeda *et al.* (1995)
S/3	Tomakomai	43.19	141.31	*Dosinia japonica*	N-6659	7190	115	7963	7500	-17.44			Arakawa (1994; 1997)
S/3	Tomakomai	42.64	141.31	*Mya arenaria oonogai*	N-6092	6680	95	7469	7024	-16.39			Arakawa (1994; 1997)
S/3	Tomakomai	42.64	141.73	*Callithaca adamsi*	N-6620	6620	110	7435	6930	-13.44			Arakawa (1994; 1997)
S/3	Tomakomai	42.64	141.31	*Mya arenaria oonogai*	N-6091	6540	95	7362	6874	-5.99			Arakawa (1994; 1997)
S/3	Tomakomai	42.64	141.31	*Crassostrea gigas*	N-6090	5380	90	6062	5590	-1.79			Arakawa (1994; 1997)
S/3	Tomakomai	42.64	141.73	*Corbicula japonica*	N-6657	4070	95	4494	3906	-1.34			Arakawa (1994; 1997)
S/3	Muroran	42.35	140.95	*Mya arenaria oonogai*	NUTA-2866	7970	100	8863	8287	-29.94			Arakawa (1997)
S/3	Muroran	42.35	140.95	*Crassostrea gigas*	NUTA-2872	7990	130	8961	8275	-25.94			Arakawa (1997)
S/3	Muroran	42.35	140.95	*Crassostrea gigas*	I-17,135	7500	230	8516	7579	-15.94			Arakawa (1997)
S/3	Muroran	42.32	140.98	*Crassostrea gigas*	I-17,334	7315	60	7989	7675	-7.94			Arakawa (1997)
S/3	Muroran	42.35	140.95	*Patinopecten yessoensis* (Hotategai)	I-17,137	4950	130	5987	5329	-17.94			Arakawa (1997)
S/3	Yufutsu Plain	42.75	141.69	*Crassostrea gigas*		7280	190	8211	7454	-10.94			Ikeda *et al.* (1995)
S/3	Ishikari Coastal Plain	43.15	141.25	Shell	GaK-5787	4920	560	6960	4262	-9.44			Matsushita (1979)
S/3	Ishikari Coastal Plain	43.15	141.25	Shell	GaK-5955	4410	160	5432	4578	-11.16			Matsushita (1979)